Characteristics of Environmental Data Layers for Use in Species Distribution Modelling in the Gulf of St. Lawrence

L. Beazley, C. Lirette, J. Sabaniel, Z. Wang, A. Knudby, and E. Kenchington

Ocean and Ecosystem Sciences Division
Maritimes Region
Fisheries and Oceans Canada

Bedford Institute of Oceanography
P.O. Box 1006
Dartmouth, Nova Scotia
Canada B2Y 4A2

2016

Canadian Technical Report of Fisheries and Aquatic Sciences 3154

Fisheries and Oceans Canada Pêches et Océans Canada

Canada

Canadian Technical Report of Fisheries and Aquatic Sciences

Technical reports contain scientific and technical information that contributes to existing knowledge but which is not normally appropriate for primary literature. Technical reports are directed primarily toward a worldwide audience and have an international distribution. No restriction is placed on subject matter and the series reflects the broad interests and policies of Fisheries and Oceans Canada, namely, fisheries and aquatic sciences.

Technical reports may be cited as full publications. The correct citation appears above the abstract of each report. Each report is abstracted in the data base *Aquatic Sciences and Fisheries Abstracts*.

Technical reports are produced regionally but are numbered nationally. Requests for individual reports will be filled by the issuing establishment listed on the front cover and title page.

Numbers 1-456 in this series were issued as Technical Reports of the Fisheries Research Board of Canada. Numbers 457-714 were issued as Department of the Environment, Fisheries and Marine Service, Research and Development Directorate Technical Reports. Numbers 715-924 were issued as Department of Fisheries and Environment, Fisheries and Marine Service Technical Reports. The current series name was changed with report number 925.

Rapport technique canadien des sciences halieutiques et aquatiques

Les rapports techniques contiennent des renseignements scientifiques et techniques qui constituent une contribution aux connaissances actuelles, mais qui ne sont pas normalement appropriés pour la publication dans un journal scientifique. Les rapports techniques sont destinés essentiellement à un public international et ils sont distribués à cet échelon. Il n'y a aucune restriction quant au sujet; de fait, la série reflète la vaste gamme des intérêts et des politiques de Pêches et Océans Canada, c'est-à-dire les sciences halieutiques et aquatiques.

Les rapports techniques peuvent être cités comme des publications à part entière. Le titre exact figure au-dessus du résumé de chaque rapport. Les rapports techniques sont résumés dans la base de données *Résumés des sciences aquatiques et halieutiques.*

Les rapports techniques sont produits à l'échelon régional, mais numérotés à l'échelon national. Les demandes de rapports seront satisfaites par l'établissement auteur dont le nom figure sur la couverture et la page du titre.

Les numéros 1 à 456 de cette série ont été publiés à titre de Rapports techniques de l'Office des recherches sur les pêcheries du Canada. Les numéros 457 à 714 sont parus à titre de Rapports techniques de la Direction générale de la recherche et du développement, Service des pêches et de la mer, ministère de l'Environnement. Les numéros 715 à 924 ont été publiés à titre de Rapports techniques du Service des pêches et de la mer, ministère des Pêches et de l'Environnement. Le nom actuel de la série a été établi lors de la parution du numéro 925.

Canadian Technical Report of
Fisheries and Aquatic Sciences 3154

2016

CHARACTERISTICS OF ENVIRONMENTAL DATA LAYERS FOR USE IN SPECIES DISTRIBUTION MODELLING IN THE GULF OF ST. LAWRENCE

by

L. Beazley, C. Lirette, J. Sabaniel, Z. Wang, A. Knudby, and E. Kenchington

Ocean and Ecosystem Sciences Division
Maritimes Region
Fisheries and Oceans Canada
Bedford Institute of Oceanography
P. O. Box 1006
Dartmouth, N.S.
Canada B2Y 4A2

© Her Majesty the Queen in Right of Canada, 2016.
Cat. No. Fs97-6/3154E-PDF ISBN 978-0-660-04442-2 ISSN 1488-5379

Correct citation for this publication:

Beazley, L., Lirette, C., Sabaniel, J., Wang, Z., Knudby, A., and Kenchington, E. 2016. Characteristics of Environmental Data Layers for Use in Species Distribution Modelling in the Gulf of St. Lawrence. Can. Tech. Rep. Fish. Aquat. Sci. 3154: viii + 357p.

TABLE OF CONTENTS

ABSTRACT vii
RÉSUMÉ viii
INTRODUCTION 1
MATERIALS AND METHODS 2
Study Area 2
Data Sources 3
Global Ocean Reanalyses and Simulations (GLORYS) 3
Sea Surface Chlorophyll *a* 5
Primary Production 6
World Ocean Database 2013 (WOD13) 8
Spatial Interpolation Methods 10
Data Exploration and Model Fitting 10
Assessment of Model Performance 11
RESULTS 14
Temperature 14
Bottom Temperature Mean 14
Bottom Temperature Minimum 17
Bottom Temperature Maximum 20
Bottom Temperature Range 23
Bottom Temperature Average Minimum 26
Bottom Temperature Average Maximum 29
Bottom Temperature Average Range 32
Surface Temperature Mean 35
Surface Temperature Minimum 38
Surface Temperature Maximum 41
Surface Temperature Range 44
Surface Temperature Average Minimum 47
Surface Temperature Average Maximum 50
Surface Temperature Average Range 53
Salinity 56
Bottom Salinity Mean 56
Bottom Salinity Minimum 59
Bottom Salinity Maximum 62
Bottom Salinity Range 65
Bottom Salinity Average Minimum 68
Bottom Salinity Average Maximum 71
Bottom Salinity Average Range 74
Surface Salinity Mean 77
Surface Salinity Minimum 80
Surface Salinity Maximum 83
Surface Salinity Range 86
Surface Salinity Average Minimum 89

Surface Salinity Average Maximum 92
Surface Salinity Average Range 95
Current Speed 98
Bottom Current Mean 98
Bottom Current Minimum 101
Bottom Current Maximum 104
Bottom Current Range 107
Bottom Current Average Minimum 110
Bottom Current Average Maximum 113
Bottom Current Average Range 116
Surface Current Mean 119
Surface Current Minimum 122
Surface Current Maximum 125
Surface Current Range 128
Surface Current Average Minimum 131
Surface Current Average Maximum 134
Surface Current Average Range 137
Maximum Mixed Layer Depth 140
Maximum Spring Mixed Layer Depth 140
Maximum Summer Mixed Layer Depth 143
Maximum Fall Mixed Layer Depth 146
Maximum Winter Mixed Layer Depth 149
Maximum Average Spring Mixed Layer Depth 152
Maximum Average Summer Mixed Layer Depth 155
Maximum Average Fall Mixed Layer Depth 158
Maximum Average Winter Mixed Layer Depth 161
Bottom Shear 164
Bottom Shear Mean 164
Bottom Shear Minimum 167
Bottom Shear Maximum 170
Bottom Shear Range 173
Bottom Shear Average Minimum 176
Bottom Shear Average Maximum 179
Bottom Shear Average Range 182
Sea Surface Chlorophyll *a* 185
MODIS Case I Spring Chlorophyll *a* Mean 185
MODIS Case I Spring Chlorophyll *a* Minimum 188
MODIS Case I Spring Chlorophyll *a* Maximum 191
MODIS Case I Spring Chlorophyll *a* Range 194
MODIS Case I Summer Chlorophyll *a* Mean 197
MODIS Case I Summer Chlorophyll *a* Minimum 200
MODIS Case I Summer Chlorophyll *a* Maximum 203
MODIS Case I Summer Chlorophyll *a* Range 206
MODIS Case I Fall Chlorophyll *a* Mean 209
MODIS Case I Fall Chlorophyll *a* Minimum 212
MODIS Case I Fall Chlorophyll *a* Maximum 215

MODIS Case I Fall Chlorophyll *a* Range 218
MODIS Case I Annual Chlorophyll *a* Mean 221
MODIS Case I Annual Chlorophyll *a* Minimum 224
MODIS Case I Annual Chlorophyll *a* Maximum 227
MODIS Case I Annual Chlorophyll *a* Range 230
MERIS Case II Spring Chlorophyll *a* Mean 233
MERIS Case II Spring Chlorophyll *a* Minimum 236
MERIS Case II Spring Chlorophyll *a* Maximum 239
MERIS Case II Spring Chlorophyll *a* Range 242
MERIS Case II Summer Chlorophyll *a* Mean 245
MERIS Case II Summer Chlorophyll *a* Minimum 248
MERIS Case II Summer Chlorophyll *a* Maximum 251
MERIS Case II Summer Chlorophyll *a* Range 254
MERIS Case II Fall Chlorophyll *a* Mean 257
MERIS Case II Fall Chlorophyll *a* Minimum 260
MERIS Case II Fall Chlorophyll *a* Maximum 263
MERIS Case II Fall Chlorophyll *a* Range 266
MERIS Case II Annual Chlorophyll *a* Mean 269
MERIS Case II Annual Chlorophyll *a* Minimum 272
MERIS Case II Annual Chlorophyll *a* Maximum 275
MERIS Case II Annual Chlorophyll *a* Range 278
Primary Production 281
Spring Primary Production Mean 281
Spring Primary Production Minimum 284
Spring Primary Production Maximum 287
Spring Primary Production Range 290
Spring Primary Production Average Minimum 293
Spring Primary Production Average Maximum 296
Spring Primary Production Average Range 299
Summer Primary Production Mean 302
Summer Primary Production Minimum 305
Summer Primary Production Maximum 308
Summer Primary Production Range 311
Summer Primary Production Average Minimum 314
Summer Primary Production Average Maximum 317
Summer Primary Production Average Range 320
Annual Primary Production Mean 323
Annual Primary Production Minimum 326
Annual Primary Production Maximum 329
Annual Primary Production Range 332
Annual Primary Production Average Minimum 335
Annual Primary Production Average Maximum 338
Annual Primary Production Average Range 341
Dissolved Oxygen and Nutrients 344
Dissolved Oxygen 344
Phosphate 347

Silicate..... 350
ACKNOWLEDGMENTS 353
REFERENCES 354

ABSTRACT

Beazley, L., Lirette, C., Sabaniel, J., Wang, Z., Knudby, A., and Kenchington, E. 2016. Characteristics of Environmental Data Layers for Use in Species Distribution Modelling in the Gulf of St. Lawrence. Can. Tech. Rep. Fish. Aquat. Sci. 3154: viii + 357p.

Species distribution modelling is often employed to predict the distribution of a species in unsampled areas based on its species-environment relationship in sampled areas, and is becoming a more widely used tool in the management of fisheries resources and benthic ecosystems. Continuous surfaces of environmental data are necessary in order to predict over the entire spatial domain of the model. There are growing numbers of online sources of environmental data assembled for the purpose of habitat classification or species distribution modelling. However, the data hosted on these sites is often on differing spatial scales. Such data are often spatially interpolated to provide continuous surfaces that can be used for modelling at all spatial scales. In this report we provide detailed information on 113 environmental variables for the Gulf of St. Lawrence that have been obtained from a broad range of data sources and spatially interpolated using geostatistical methods. For each variable we document the underlying data distribution and relevant diagnostics of the interpolation models, and present the final interpolated surface. These interpolated layers have been compiled in a common (raster) format and archived at the Bedford Institute of Oceanography. The information detailed in this report will help future users of these layers make informed decisions on which variables are appropriate for their modelling needs.

RÉSUMÉ

Beazley, L., Lirette, C., Sabaniel, J., Wang, Z., Knudby, A., and Kenchington, E. 2016. Characteristics of Environmental Data Layers for Use in Species Distribution Modelling in the Gulf of St. Lawrence. Can. Tech. Rep. Fish. Aquat. Sci. 3154: viii + 357p.

La modélisation de la répartition des espèces est souvent utilisée pour prédire l'aire de répartition d'une espèce dans les zones non échantillonnées en fonction de la relation entre l'environnement et cette espèce dans les zones échantillonnées. Cet outil est de plus en plus souvent utilisé dans le cadre de la gestion des ressources halieutiques et des écosystèmes benthiques. Les surfaces continues des données environnementales sont nécessaires afin d'émettre des prévisions pour le domaine spatial entier du modèle. Il y a un nombre croissant de sources de données environnementales compilées en ligne aux fins de classification de l'habitat ou de modélisation de la répartition des espèces. Cependant, les données qui se trouvent sur ces sites se retrouvent souvent sur des échelles spatiales différentes. Ces données font souvent l'objet d'une interpolation spatiale pour fournir des surfaces continues qui peuvent être utilisées pour la modélisation à toutes les échelles spatiales. Dans ce rapport, nous fournissons des renseignements détaillés sur les 113 variables environnementales pour le golfe du Saint-Laurent qui ont été obtenues à partir d'une vaste gamme de sources de données et de méthodes géostatistiques interpolées sur le plan spatial. Pour chaque variable, nous documentons la répartition des données sous-jacentes et les diagnostics pertinents pour les modèles de répartition et nous présentons la surface interpolée finale. Ces couches d'interpolation de données ont été compilées dans un format commun (trame) et archivées à l'Institut océanographique de Bedford. Les renseignements détaillés dans le présent rapport aideront les futurs utilisateurs de ces couches à prendre des décisions éclairées sur les variables qui sont appropriées pour répondre à leurs besoins en modélisation.

INTRODUCTION

Species distribution modelling (SDM) is a tool that utilizes spatially explicit environmental data to predict the distribution of a response variable in unsampled areas. Continuous surfaces for each environmental variable are necessary in order to predict across the spatial domain of the model, and to extract point data for each response datum so that the final data matrix will be fully populated. The creation of continuous surfaces allows analysts to work with predictor variables in locations where data was not collected at the time of sampling. Predictor variables may themselves be from direct measurements, modelled outputs, temporal averages, and derivations. These variables are typically collected at different spatial and temporal resolutions, and are often spatially interpolated to provide continuous surfaces that can be used for predictive modelling at all spatial scales.

Continuous interpolated surfaces produced at high resolution often show very detailed spatial variation, implying that the surfaces are very precise. However, spatial interpolation methods are affected by sample size, sampling design and data quality properties, and variation within the data has very large impacts on the performance of the spatial interpolators (Li and Heap, 2008). There are over 60 methods to choose from, including geostatistical interpolators (e.g., kriging), non-geostatistical interpolators (e.g., inverse distance weighting, natural neighbours, nearest neighbours), and methods that combine both (Li and Heap, 2008).

The Estuary and Gulf of St. Lawrence is considered one of the largest and most productive estuarine/marine ecosystems in the world (Dufour and Ouellet, 2007). The physical oceanography of this region has been previously described (see Dufour and Ouellet (2007) and De Vernal et al. (2011)). Dutil et al. (2011) provide a thorough description of environmental variables compiled for use in habitat classification in the Gulf of St. Lawrence. The variables compiled were aspects of salinity, temperature, dissolved oxygen, depth, slope, and variability in landscape and sediments. They created a grid over the study area made up of 100 km^2 cells (10 km x 10 km) and performed interpolations to extract values for each variable. For depth, slope, and bottom temperature and salinity, they used a non-geostatistical interpolation method, natural neighbours (Sibson, 1981), and calculated the mean, minimum, and maximum as well as their standard deviation for each grid cell. Similar dissolved oxygen data were interpolated by a co-kriging method with depth as the co-variable. The resulting grid cell statistics were derived from interpolated data in all cases. The cells were then classified into a smaller number of units using different methods for each variable. Although each grid cell has an associated standard deviation in this approach, it is derived from the interpolated points and there is no quantitative assessment of the quality of the underlying data or interpolations. Consequently, we felt the need to create new interpolated surfaces for use in SDM which examine in greater detail the distribution of underlying data and the associated error. We recognize that different interpolation methods will have different optimal data requirements and we refrain from making any decision on their usage. However, we have examined the variables for use in geostatistics using ordinary kriging by selecting relevant diagnostics for that purpose. Herein we provide detailed information on 113 environmental variables that have been interpolated for potential use in species distribution models for the Gulf of St. Lawrence.

MATERIALS AND METHODS

Study Area

The Gulf Region, one of DFO's six administrative regions across Canada, was used as the boundary for the construction of environmental variables in this report. The boundary was drawn 5 km from all land points and covers 196,494 km^2 based on a NAD 1983 UTM Zone 20N projection.

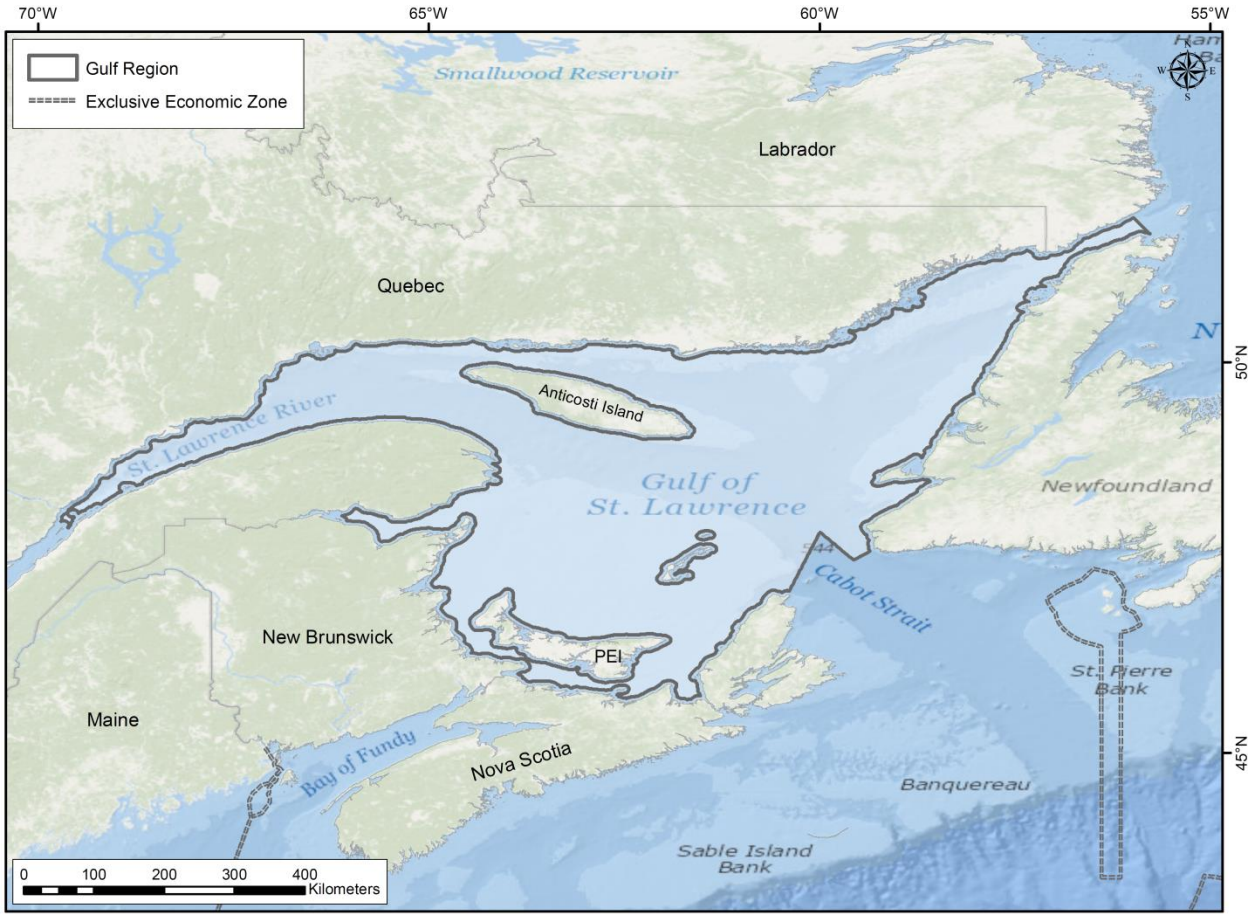

Fig. 1. DFO's Gulf Region administrative boundary (grey polygon) used for creating interpolated surfaces of environmental variables in the Gulf of St. Lawrence. A 5 kilometre buffer was added around all land points.

Data Sources

Global Ocean Reanalyses and Simulations (GLORYS)

Data for surface and bottom temperature, salinity, current speed, and mixed layer depth were extracted from the Global Ocean Reanalyses and Simulations (GLORYS2V1). GLORYS2V1 is a numerical ocean general circulation model reanalysis product with ¼° horizontal resolution (approximately 18 km in the Gulf of St. Lawrence; Fig. 2) that aims to provide the mean and time-varying state of the oceanic states with a focus on capturing variation of meso-scale eddies (http://www.mercator-ocean.fr/eng/science/GLORYS). This reanalysis product is a model run with data assimilation – designed to reproduce the ocean state. GLORYS assimilates satellite altimetry data, sea surface temperature data, temperature and salinity data from ARGO (www.argo.net), and ship-based CTD data. The assimilation of the satellite altimetry data allows the product to represent reliable information on ocean eddies. This product covers the period of January 1993 to December 2011. We extracted data on bottom and surface temperature, salinity and current velocity (calculated from current vectors U and V). Mixed layer depth (m), defined as the depth at which the potential density (σ_θ) in the upper layer changes by 0.01 kg m^{-3} relative to the ocean surface density (at z= 0.5 m), was also extracted from GLORYS. Bottom shear stress was calculated from current vectors obtained from GLORYS using the following equation:

$$\tau_b = 3.5 \times 10^{-3} \times \rho \times U \times \sqrt{(U^2 + 0.02)}$$

Where ρ is the density of sea water and U is the speed of near-bottom currents.

Seabed depth ('bottom') used in the data processing is a modelled depth based on the closest point to the seabed in the z level model product. The z vertical levels grid uses partial cells parameterization to realistically represent ocean bathymetry (Ferry et al., 2012). Surface is a constant measure and spans 1 vertical metre of water beginning at 0.5 metres below true sea surface level.

For each variable, two different sets of statistics were created from the GLORYS2V1 monthly data. First, the absolute minima, maxima, and range were calculated for each variable by taking the minimum and maximum values across all months and years at each location. Range was calculated as the difference between these values at each location. In this report these variables are denoted as Minimum/Maximum/Range. These 'absolute' variables are likely reflective of anomalous events over the time period. The second dataset was created by calculating the average minima, maximum and range by taking the minimum and maximum values at each location across all months within a year, and averaging across years. These variables are denoted as Average Minimum/Maximum/Range in this report, and are likely more representative of long-term oceanographic conditions in the region. Finally, the mean of each variable was calculated by averaging the values at each location across all months and years, and is denoted as the Mean in this report. For mixed layer depth, statistics were compiled quarterly to derive spring (April - June), summer (July - September), fall (October - December) and winter (January - March)

variables. Zero values in the current and shear data, which were falsely generated from a model topography issue, were removed prior to calculating the statistics.

Caveat for GLORYS variables

Bottom temperature values derived from the GLORYS model were abnormally low in some shallow (coastal) portions of the Gulf study extent, particularly in the Strait of Belle Isle and south of Anticosti Island. This is likely caused by the data assimilation scheme of the model. Interpolation/extrapolation is required in some areas where observed quantities are sparse, which may lead to the occurrence of these erroneous values. This problem affects mainly the absolute minimum temperature quantity, and therefore caution should be taken when using this variable in species distribution models for these areas. To ensure good congruence between modelled bottom temperature values from GLORYS and observed temperature values, mean bottom temperature derived from GLORYS was statistically compared to bottom temperature values extracted from CTD casts collected during DFO research vessel groundfish trawl surveys conducted in the Gulf Region between 2006 and 2011. Only data from August and September over the 5-year time period were compared. Spearman's rank correlation analysis revealed good congruence between the modelled mean bottom temperature and the measured CTD values (Spearman's ρ = 0.839).

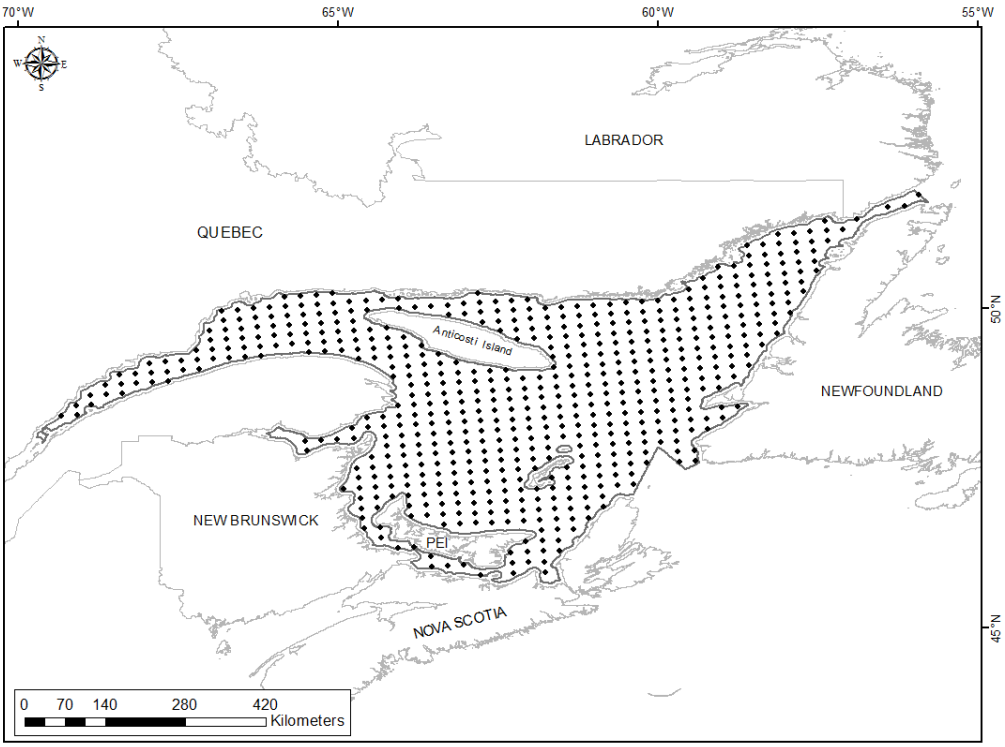

Fig. 2. Distribution of point data extracted from the GLORYS2V1 model from 1993 to 2011 for the Gulf Region. Point data have a native resolution of ¼°.

Sea Surface Chlorophyll *a*

Sea surface chlorophyll *a* data were derived from Aqua-MODIS (Moderate Resolution Imaging Spectroradiometer) Case I and MERIS (Medium Resolution Imaging Spectrometer) were processed by the Remote Sensing Unit at the Bedford Institute of Oceanography (RSU-BIO). In deep oceanic waters, optical properties are dominated by phytoplankton and the observed spectral features in the reflected light can be directly related to chlorophyll *a* concentration (Moses et al., 2009). These waters are referred to as Case I waters. In Case I waters, spectral algorithms that use reflectances in the blue green regions of the spectrum have shown to accurately estimate chl-*a* concentration. In contrast, most inland, estuarine, and coastal waters that are rich in suspended solids and dissolved organic matter are referred to as Case II waters. The optical properties of Case II waters are therefore not dominated by phytoplankton, and spectral algorithms based on reflectance in the red and near-infrared spectral regions are typically used to estimate chl-*a* concentration (Moses et al., 2009). Generally, Case I chlorophyll calculations should not be used for Case II waters. In the study extent used in this report, the Northumberland Strait and Gulf of St. Lawrence estuary are considered Case II. Coastal waters less than 30 m deep are also considered Case II, however, these waters are generally excluded due to the 5-km land buffer. We therefore recommend the use of MERIS Case II chlorophyll *a* variables for species distribution modelling in the Gulf Region, but provide MODIS Case I in addition to MERIS Case II to suit the specific needs of the data modeller.

Daily MODIS (Aqua Level-2) data from 2002 to 2012 were downloaded from NASA's OceanColor Web (http://oceandata.sci.gsfc.nasa.gov/]). Composite images were displayed in raster format with a resolution of 2 km. Individual passes of MERIS Case II (*algal_2*) at a 1 km resolution were downloaded from the European Space Agency (ESA) and displayed in raster format with a resolution of 2 km. Data from 2003 to 2011 were used. Individual passes were filtered to eliminate extreme outliers using the median of a 3 x 3 pixel matrix (ENVI-IDL). The native resolution of the point data for both MODIS Case I and MERIS Case II chlorophyll *a* data are shown in Fig. 3.

Annual and seasonal averages were computed for the MODIS Case I and MERIS Case II datasets. Seasons were delimited by the following 'day of year' ranges: days 91 – 181 (spring), 182 – 273 (summer), and 274 – 365 (fall). These seasonal delimitations capture the peak of the spring and fall phytoplankton blooms in most areas of the Gulf. Alternate seasonal ranges could be considered that would fully capture the spring phytoplankton bloom in all areas of the study extent (see Fuentes-Yaco et al. 2013 for a review of the temporal range of the spring and fall phytoplankton blooms in this region). Winter chlorophyll was considered inconsequential to the benthos and was not included in this report. The minimum, maximum and range values for each season (except winter) and annually were derived from these using the 'Cell Statistics' tool in ArcMap's Spatial Analyst toolbox. Zero and N/A values in the chlorophyll data were removed prior to calculating the statistics.

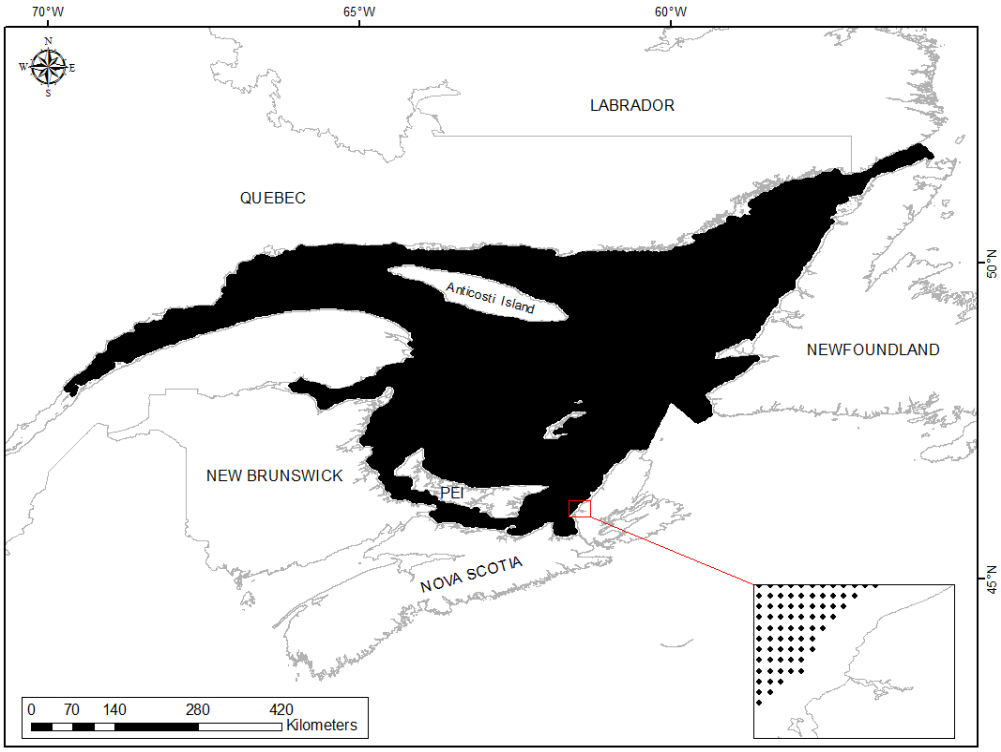

Fig. 3. Distribution of sea surface chlorophyll *a* (both MODIS Case I and MERIS Case II) point data (spring, summer, fall and annual) for the Gulf Region. Point data have a native resolution of 2 km.

Primary Production

Primary production was calculated following the method of Platt et al. (2008) using software developed by the RSU-BIO and the Department of Oceanography at Dalhousie University. The calculation of primary production requires input from multiple sources. Monthly mean surface chlorophyll *a* and photosynthetically active radiation (PAR) was obtained from NASA's Sea-viewing Field-of-view Sensor (SeaWiFS) Level 3, 9-km global coverage (reprocessing R2010.0; Feldman and McClain, 2012). Sea surface temperature (SST) was obtained from NOAA PathFinder version 5.2 data and was reprocessed from its native resolution of 4000 m^2 $pixel^{-1}$ to match the spatial and temporal resolution of chlorophyll data. Monthly images of total cloud fraction data used in the model were obtained in November 2014 from MYD08_M3, a monthly aggregation of MYD35, collection 51 (ftp://ladsweb.nascom.nasa.gov/allData/51/MYD08_M3/). The *in situ* parameters, such as photosynthetic performance, chlorophyll *a*, sea surface temperature, and water depth originate from ship-based observations made by DFO's Atlantic Zone Monitoring Program (AZMP; http://www.bio.gc.ca/science/monitoring-monitorage/azmp-pmza-en.php). Reliability of the resulting primary production data is therefore unknown for areas outside the AZMP region. The model described in Platt et al. (2008) results in pixel-by-pixel depth-integrated net primary production (mg C m^{-2} day^{-1}) calculated for the 15 day of each month from September 2006 to September 2010. Like the GLORYS2V1-derived variables,

monthly values for primary production allowed for the calculation of both ‘absolute’ and ‘average’ minima, maxima, and range quantifications. However, for some months and years no data was available (see Table 1), therefore only spring (April – June), summer (July – Sept.), and annual layers were created. For the creation of these variables, we ensured that each point location across the study extent had at least two months of data in each of the five years contributing to the quantifications. Summer and annual surfaces showed nearly full coverage across the Gulf Region, whereas a portion of the St. Lawrence River estuary is not covered in the spring as these are locations with less than one month of data contributing across the 5-year data period.

Table 1. Contributing months to each of the 5 years of data for the primary production dataset. The √ indicates that data exists for this month. Note however that even though data exists for a particular month, each point location across the Gulf Region study extent may not have observation data.

Season	Month	2006	2007	2008	2009	2010	Total number of years
	January	√	√		√	√	4
	February	√	√		√	√	4
	March	√	√		√	√	4
	April	√	√	√	√	√	5
Spring	**May**	√	√	√		√	4
	June	√	√	√	√	√	5
	July	√	√		√	√	4
Summer	**August**	√	√	√	√	√	5
	September	√	√	√		√	4
	October	√	√	√		√	4
	November	√		√	√	√	4
	December			√	√	√	3

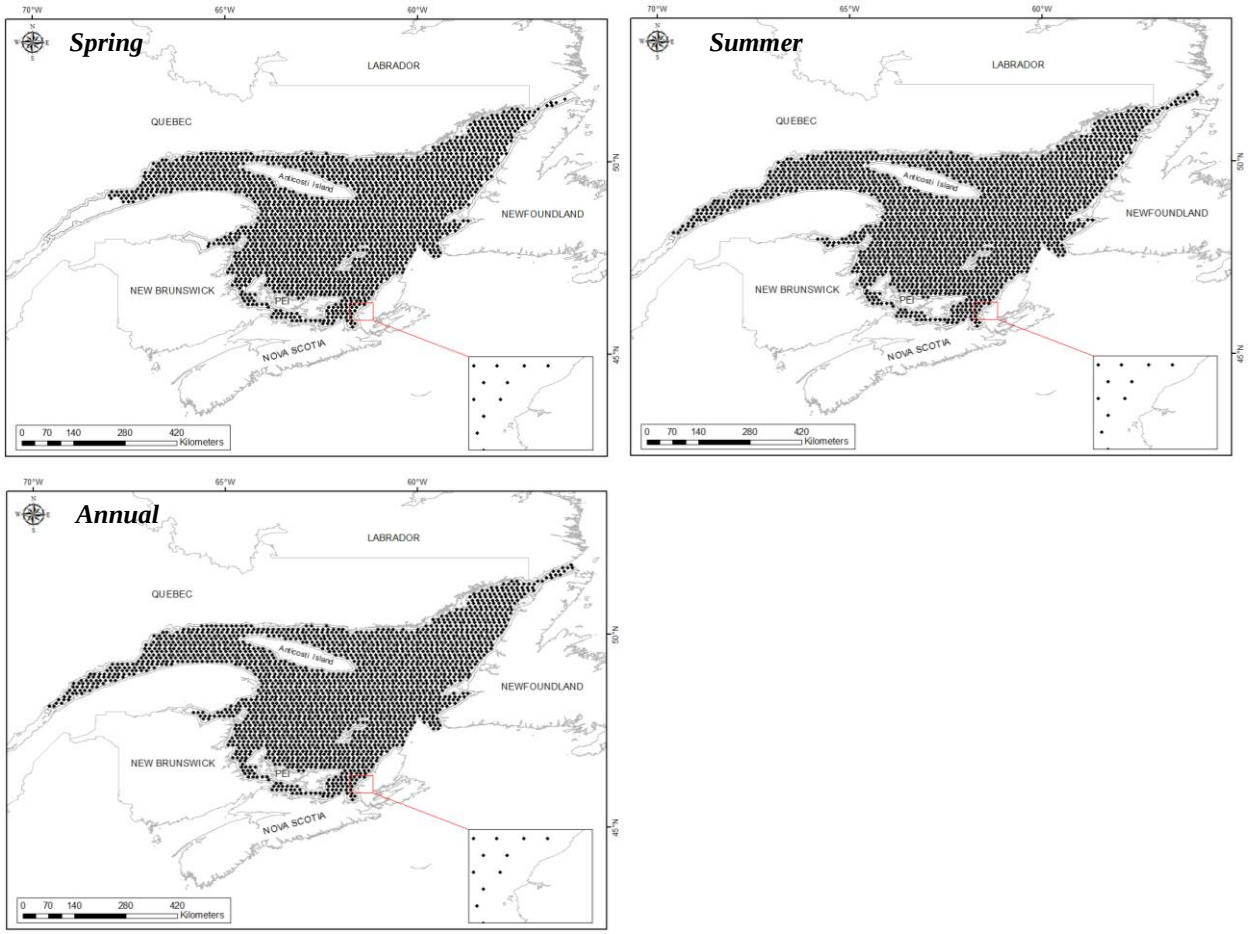

Fig. 4. Distribution of spring, summer, and fall primary production point data from 2006 to 2010 for the Gulf Region. Point data have a native resolution of 9 km.

World Ocean Database 2013 (WOD13)

Dissolved oxygen and nutrients (nitrate, phosphate, and silicate) were extracted from the World Ocean Database 2013 (WOD13) (https://www.nodc.noaa.gov/OC5/WOD13/; Boyer et al., 2013) produced by the US National Oceanographic Data Center (NODC) Ocean Climate Laboratory (OCL). WOD13 houses ocean profile and plankton measurement data submitted by individual scientists and institutional, national, and regional data centres with the goal of providing a centralized source for large-scale oceanographic data and metadata that has been formatted in a similar way. Data in WOD13 are organized under four different operational definitions: profile, cast, station, and cruise. Each data value and profile in WOD13 are associated with their own quality control flag. Data collected in a similar manner are further grouped together into 11 different datasets.

The data were queried from the WODselect retrieval system (https://www.nodc.noaa.gov/OC5/SELECT/dbsearch/dbsearch.html) using user-specified search criteria under the following four categories: geographic coordinates, observation dates, dataset,

and measured variables. Nutrient data were queried from the Ocean Station Data (OSD) dataset from the period of 2006 to 2011 (although note that there were no data records for the Gulf Region from the year 2008). The OSD dataset groups together bottle (Nansen and Niskin) and bucket data, plankton data, and low resolution CTD and expendable CTD (XCTD) data, and is the only dataset in WOD13 that contains nutrient data. Only data collected within the top 10 metres of water and with the highest quality control flag ('Accepted') were used. Data records for each nutrient showed good coverage over the Gulf Region (see Fig. 5). Although nitrate was extracted from WOD13 for the above time period, there were too few records within the Gulf Region to interpolate. In the event where more than one value was measured at a single location, the data values were averaged.

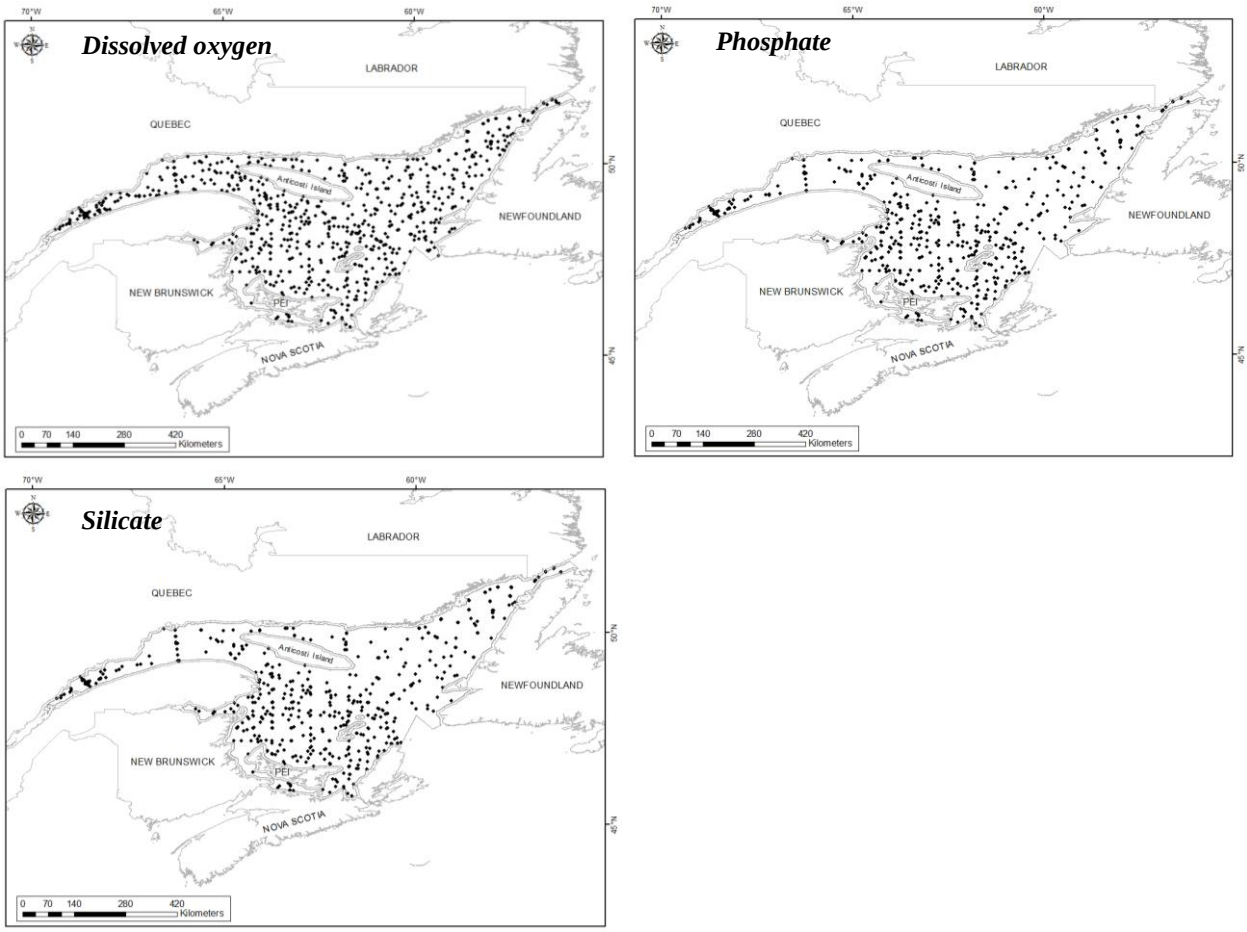

Fig. 5. Distribution of dissolved oxygen, phosphate, and silicate point data from 2006 to 2011 extracted from WOD13 for the Gulf Region. The spatial distribution of the data is not uniform across the study extent.

Spatial Interpolation Methods

Data Exploration and Model Fitting

Kriging is a family of geostatistical estimators used to interpolate spatial data. It is a generalized least-square regression technique that allows for spatial prediction in unsampled locations by accounting for the spatial dependence between observed data (Goovaerts, 2000). Spatial dependence is captured by constructing an empirical semivariogram that shows the average semivariance between points by the distance between them. A semivariogram model is then fit to the points forming the empirical semivariogram, and predictions are generated for unmeasured locations based on a weighted average of neighbouring data and their spatial arrangement (Johnston et al., 2001).

Within the kriging family a number of different methods exist including but not limited to, ordinary kriging, universal kriging, and simple kriging. For this report, we chose ordinary kriging as the method of spatial interpolation as it assumes that the mean is unknown prior to modelling and approximately constant (stationary) only in the local neighbourhood of each estimation point and not over the entire data domain (Li and Heap, 2008; Krivoruchko, 2011). Thus ordinary kriging with a local search neighbourhood already accounts for trends in the data (Li and Heap, 2008).

Ordinary kriging as a geostatistical interpolator does not require the data to follow a normal distribution (Krivoruchko, 2011). However, the generation of quantile and probability maps using ordinary kriging does require the data to meet this assumption (Krivoruchko, 2011). Transformation of highly skewed data prior to ordinary kriging may result in improved estimates and prediction errors, particularly if the dataset is small and contains outliers (Kravchenko and Bullock, 1999). If a variable shows positive skewness, the confidence limits on the variogram are wider than normal resulting in higher variance (Robinson and Metternicht, 2006; Yamamoto, 2007). Thus, data are often transformed prior to spatial interpolation in order to improve the calculation of statistics and weighted averages (Yamamoto, 2007). Transformation of the data results in estimates on a different scale than the original data, and so it is necessary to back-transform the kriging estimates to their original scale prior to creating the interpolation surface. However, for logarithmic transformation, back-transformation through exponentiation results in exaggerated interpolation-related errors, with extreme errors being the worst affected (Goovaerts, 1997; Robinson and Metternicht, 2006).

We assessed the distributional properties of all variables by examining histograms and summary statistics generated in the ‘Explore Data’ option in ArcMap’s Geostatistical Analyst package. These were reviewed to detect anomalous data points and to visually assess departures from a normal distribution (skewness, kurtosis) in advance of conducting geostatistics. Normal Q-Q plots were then constructed to compare the distribution of the data against a standard normal (Gaussian) distribution. The data values are ordered and cumulative distribution values are calculated as (i– 0.5)/n for the ith ordered value out of n total values. If the data values are normally distributed they will form a perfect line at 45 degrees to the origin. Data values that fell

above and below the reference line were mapped to identify any spatial trend in the departure from normality.

For those variables showing high skewness or bimodality in the histogram, and/or large deviations from the reference line (particularly in the centre of the data, not the tails) of the Q-Q plot, we examined the effect of variable back-transformation on the prediction errors. We compared prediction errors (see Assessment of Model Performance section below for details) generated by log-transforming the data within the ordinary kriging routine in ArcMap's Geostatistical Analyst package, to those generated from data that were log-transformed outside the ArcMap forum (and thus, were not back-transformed in ArcMap). We found that variables back-transformed in ArcMap had poor prediction errors compared to logarithmic data that were not back-transformed. Therefore, to avoid biased prediction errors, we chose not to transform our data prior to interpolation. Instead, for those variables that displayed non-normality, the data were interpolated using two different methods: 1) inverse distance weighting, or IDW, and 2) ordinary kriging without transformation. Unlike kriging, IDW predicts values at unmeasured locations only by weighting them based on their distance to the prediction location; thus semivariograms are not used and spatial dependence is not taken into account. IDW is non-parametric and is often recommended for data that do not fit the assumptions required for kriging (Shepard, 1968).

Following Gunstra and van Auken (2007), the performance of IDW and ordinary kriging models were evaluated by comparing their overall mean prediction and root-mean-square errors. The model with errors closest to zero was considered to be optimal. We found that ordinary kriging with no transformation consistently produced errors that were closer to zero compared to those produced by IDW. The smoothness of the resulting prediction surfaces produced using each interpolation method was also used as an indicator of model performance. Visual examination revealed that the surfaces produced using ordinary kriging were consistently smoother than those produced by IDW. Therefore, we chose ordinary kriging without transformation as the final interpolation method.

Ordinary kriging models were created using all default settings in the Geostatistical Analyst wizard. Default settings are a stable semivariogram model type and a circular search neighbourhood with 4 sectors that capture a minimum of 2 and a maximum of 5 neighbours. The optimization function was set for each model, which determines the optimal partial sill, nugget, lag size, and number of lags based on the model range.

Assessment of Model Performance

Model performance was examined by performing cross-validation, a process where each data point is removed in turn from the model and predicted by the remaining data points. Geostatistical Analyst provides several graphical summaries of the cross validation results, including a scatterplot of the measured versus predicted values (called the Prediction plot), a scatterplot of the residuals of the measured values versus the predicted values (Error plot), a standardized error plot, which shows measured values subtracted from the predicted values and

divided by the estimated kriging standard errors, and finally a Q-Q plot, which shows the quantiles of the difference between the predicted and measured values and the corresponding quantiles from a standard normal distribution to assess the normality of the error distributions. Of these, we show only the Prediction plot in the report, although all plots were visually assessed. In the Prediction plot, a horizontal relationship indicates that the model has no information content. With autocorrelation and a good geostatistical model, the relationship between the measured and predicted values should be 1:1.

Also provided by cross validation are five prediction error statistics used for performance evaluation (see Table 2). The overall mean error represents the difference between the measured and predicted values, and should be near zero if the prediction errors are unbiased (i.e., centred on the measured values). However, this value depends on the scale and units of the data, therefore it is better to assess the standardized prediction errors, which are given as prediction errors divided by their prediction standard errors. The mean (standardized mean) of these should also be near zero. If the average standard error is close to the root mean square prediction error, variability in the predictions has been correctly assessed. The root mean square standardized error should be close to one. If the average standard error is greater than the root mean square prediction error, or if the standardized root mean square prediction error is less than one, then the variability of predictions has been overestimated. If the average standard error is less than the root mean square prediction error or if the standardized root mean square prediction error is greater than one, then the variability of predictions has been underestimated. In summary, a good geostatistical model has an overall mean and standardized mean near zero, a small root mean square prediction error that is approximately equal to the average standard error, an average standard error approximately equal to the root mean square prediction error, and a standardized root mean square prediction error close to one (Johnston et al., 2001). These five prediction error statistics are provided for each variable and are assessed against the rules in Table 2 to provide an overall assessment of model performance.

Table 2. Prediction error statistics rules used to assess performance of ordinary kriging models.

Prediction error	**Rule**
Overall Mean Error	Close to 0
Root Mean Square Prediction Error	Close to 0 and approximately equal to the average standard error
Standardized Mean	Close to 0
Standardized Root Mean Square Prediction Error	Close to 1
Average Standard Error	Approximately equal to the root mean square prediction error

Finally, model performance was assessed through visual examination of a standard error map. A standard error map quantifies the uncertainty of the prediction and is calculated by taking the square root of the kriging variances. If the data comes from a normal distribution, the true value will be within ± 2 times the prediction standard errors about 95% of the time (Johnston et al., 2001). These maps were used to determine whether there was any spatial pattern in the error distribution.

During the assessment of model performance, we noted that data with a poor underlying distribution did not always result in poor cross validation statistics during the interpolation process. For instance, ordinary kriging on some variables displaying a bimodal distribution (e.g., Bottom Temperature Mean) produced a good fit between measured and predicted values and good to excellent cross validation statistics, suggesting the ordinary kriging is robust to non-normality. Similarly, a model displaying a good fit between measured and predicted values often showed poor cross validation statistics, particularly a higher-than-expected standardized root mean square error, indicating that variability in the predictions has been underestimated.

RESULTS

Temperature

Both surface and bottom temperatures have biological relevance to benthic invertebrates. Temperature directly influences the rates of activities associated with feeding such as pumping, filtration and digestion, movement, and growth. Temperature can also influence larval duration and timing of metamorphosis (Vance, 1973). Surface water temperature can influence primary and secondary production and hence benthic food supply. Temperature, along with salinity, can be used to indicate water mass structure.

Bottom Temperature Mean

This variable displayed a bimodal distribution prior to modeling (Table 3, Fig. 6). The data were greater than predicted by a normal distribution at the smallest values and less than predicted at the highest values (Fig. 7). Centre values also deviated from the reference line. These areas of under- and over-prediction showed little spatial pattern over the region (Fig. 7).

The semivariogram showed autocorrelation present in the data (Fig. 8). The kriged model showed good cross-validation statistics (Table 4) indicating that the model was good at prediction despite the distribution of the underlying data. The error map showed low error and no strong spatial pattern over the spatial extent although error was highest along the coast (Fig. 9). The kriged surface is presented in Fig. 10.

Table 3. Distributional properties of Bottom Temperature Mean (°C).

Property	Value
Number of Observations	606
Minimum	-0.097
Maximum	7.139
Mean	2.391
Median	2.127
Standard Deviation	2.203
Skewness	0.112
Kurtosis	1.479

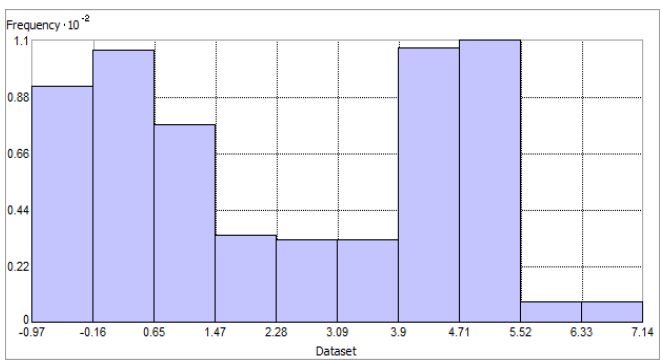

Fig. 6. Distribution of Bottom Temperature Mean (°C). Histogram was illustrated using 10 bins. Y axis is shown at 10^{-2}.

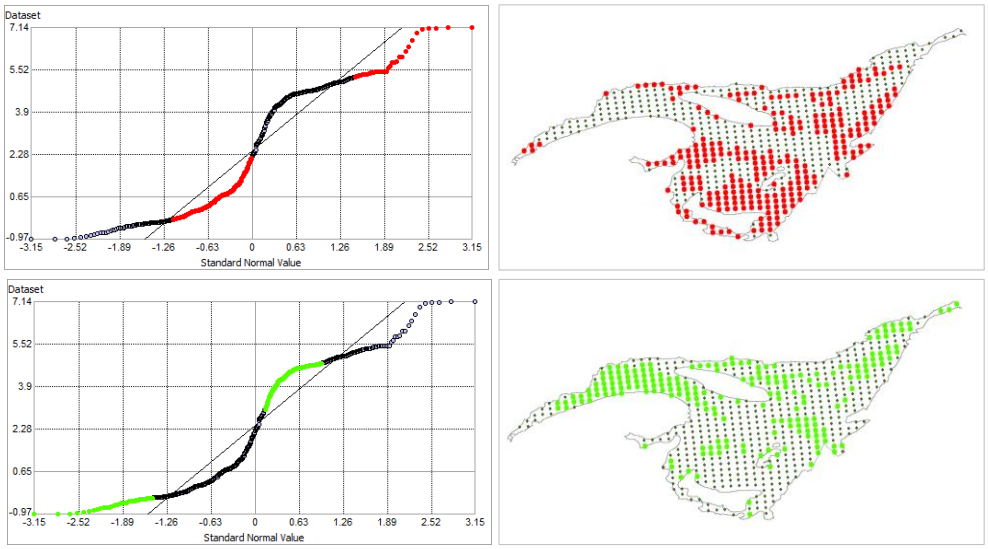

Fig. 7. Normal Q-Q plot for data values of Bottom Temperature Mean (°C). Points falling under (top right panel) and over (bottom right panel) the reference line are mapped.

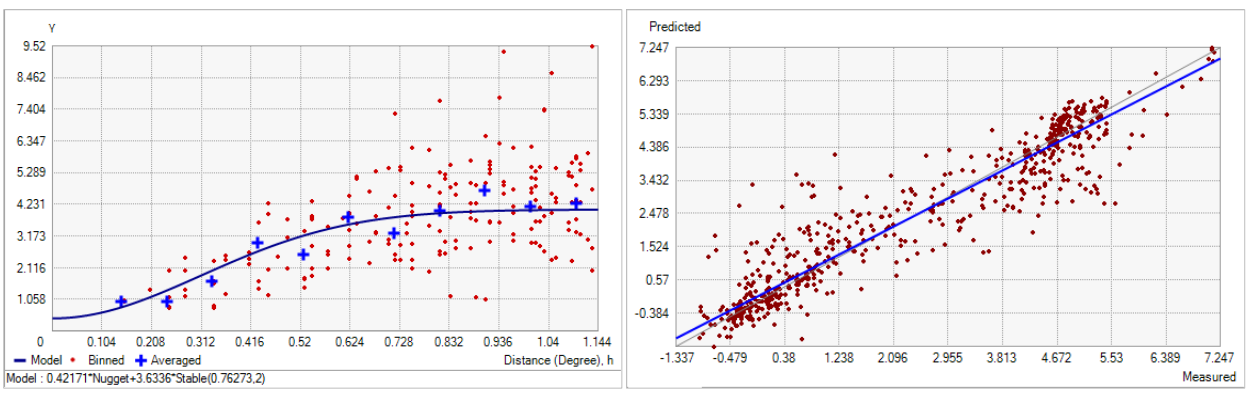

Fig. 8. Left panel: Semivariogram of Bottom Temperature Mean (°C). Binned values are shown as red dots; average points are shown as blue crosses; the model fit to the averaged values is shown as a blue line. Lag size: 0.962 degrees; number of lags: 12; Parameter: 1.583; Range: 7.700 degrees; Partial Sill: 3.405. Right panel: Scatterplot of predicted values versus observed values for the model of Bottom Temperature Mean (°C).

Table 4. Results of cross-validation of the kriged model for the Bottom Temperature Mean (°C).

Prediction error	**Value**
Number of Observations	606
Overall Mean Error	0.005
Root Mean Square Prediction Error	0.777
Standardized Mean	0.003
Standardized Root Mean Square Prediction Error	0.909
Average Standard Error	0.863

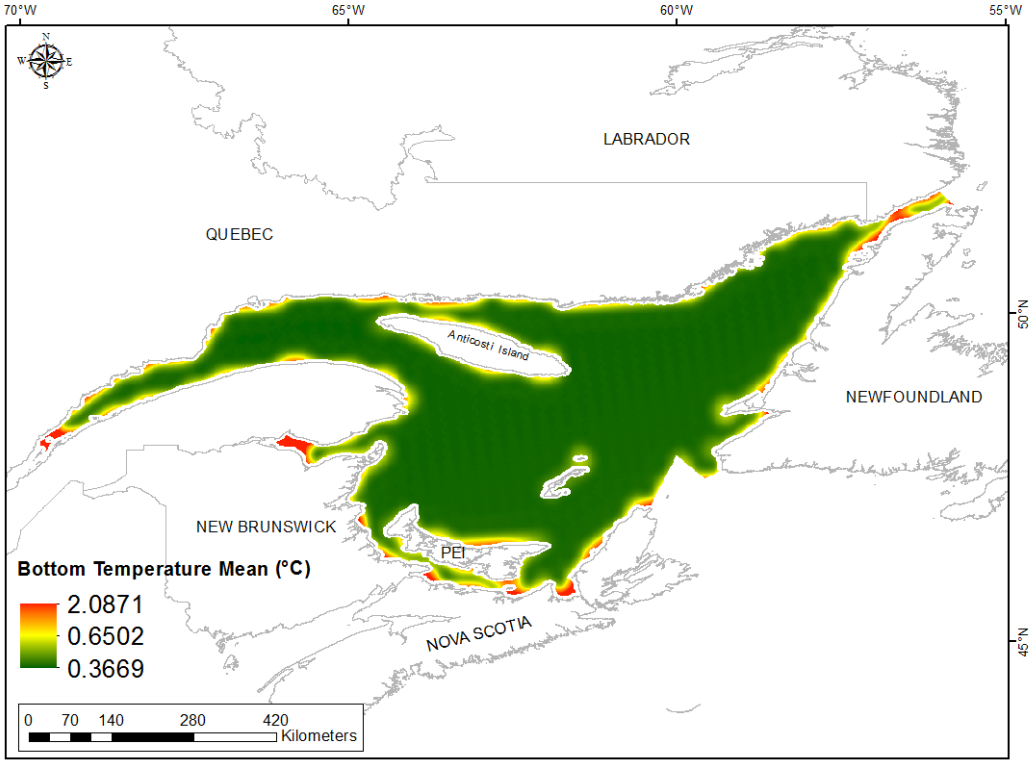

Fig. 9. Prediction standard error surface of Bottom Temperature Mean (˚C).

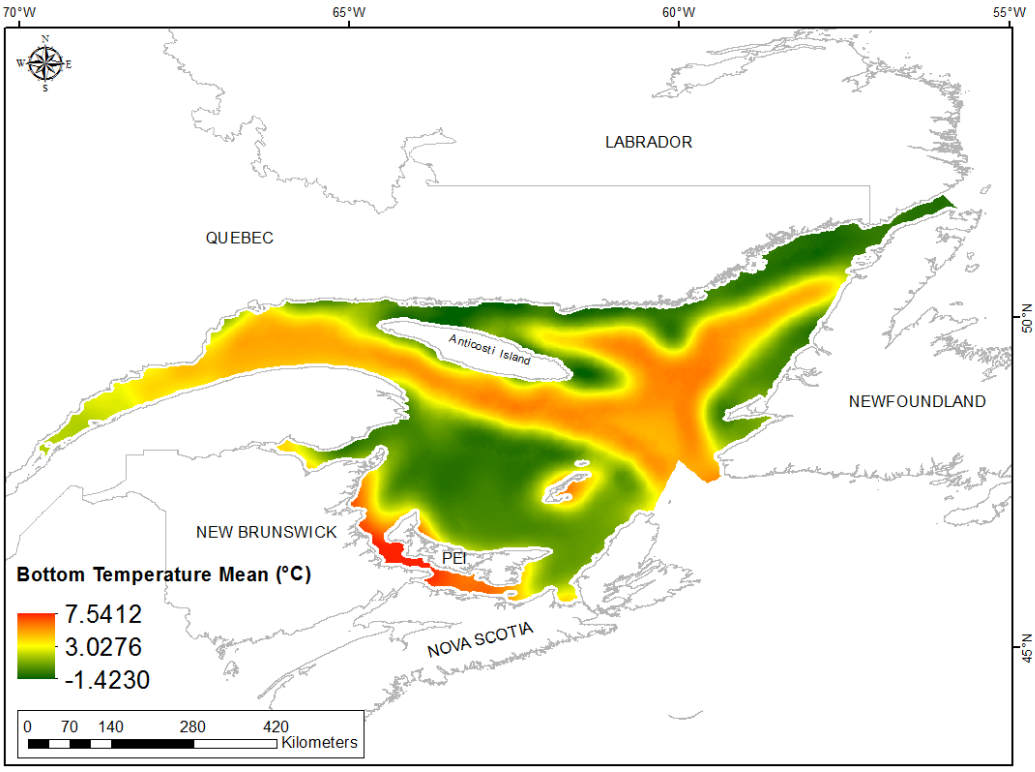

Fig. 10. Interpolated prediction surface of Bottom Temperature Mean (˚C).

Bottom Temperature Minimum

This variable displayed a bimodal distribution prior to modeling (Table 5, Fig. 11). The data were greater than predicted by a normal distribution at the smallest values and less than predicted at the highest values (Fig. 12). Centre values also deviated from the reference line. These areas of under- and over-prediction showed little spatial pattern over the region (Fig 12).

The semivariogram showed autocorrelation present in the data (Fig. 13). The kriged model showed good cross-validation statistics (Table 6) indicating that the model was good at prediction despite the distribution of the underlying data. The error map showed low error and no strong spatial pattern over most of the spatial extent although error was highest along the coast (Fig. 14). The kriged surface is presented in Fig. 15.

Table 5. Distributional properties of Bottom Temperature Minimum (°C).

Property	Value
Number of Observations	606
Minimum	-5.782
Maximum	4.933
Mean	0.013
Median	-1.137
Standard Deviation	2.932
Skewness	0.148
Kurtosis	1.611

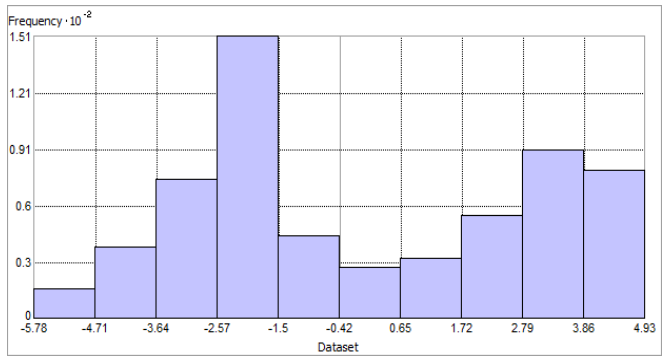

Fig. 11. Distribution of Bottom Temperature Minimum (°C). Histogram was illustrated using 10 bins. Y axis is shown at 10^{-2}.

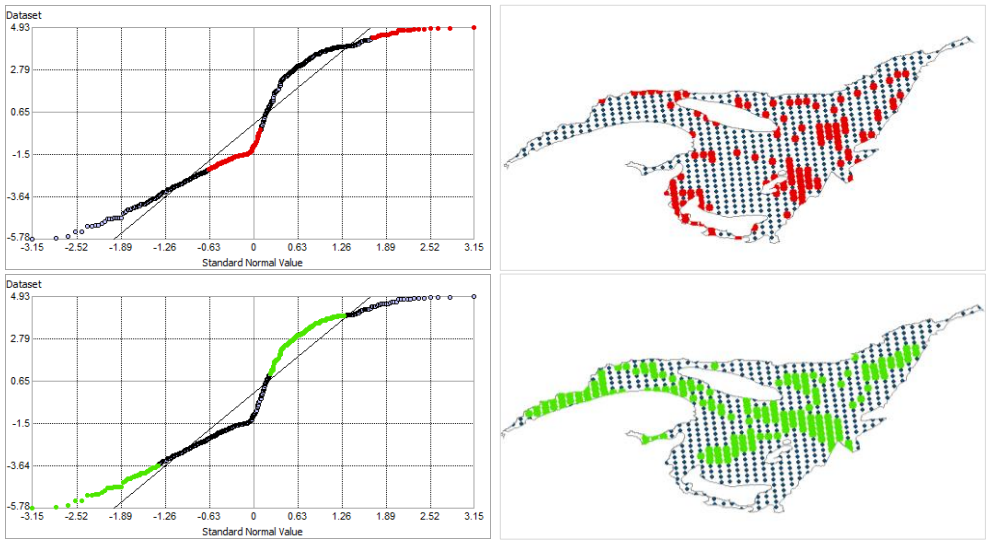

Fig. 12. Normal Q-Q plot for data values of Bottom Temperature Minimum (°C). Points falling under (upper panel) and over (bottom panel) the reference line are mapped.

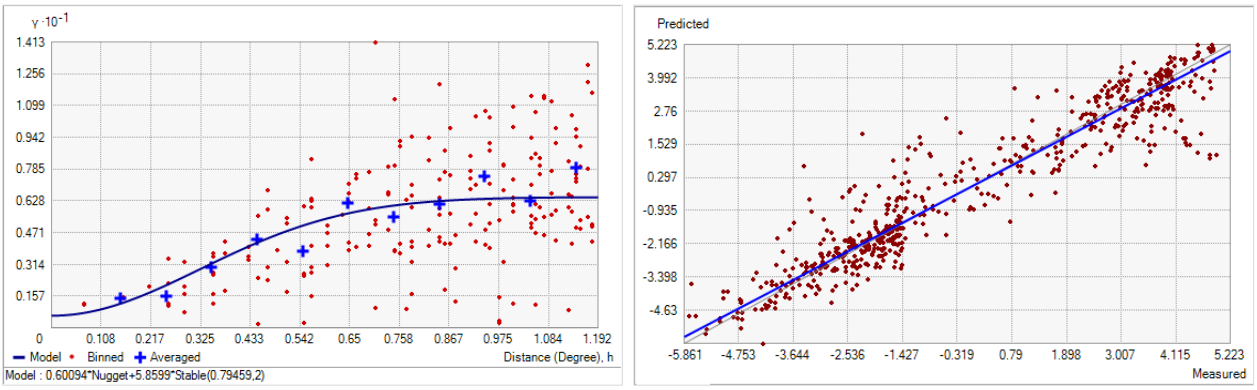

Fig. 13. Left panel: Semivariogram of Bottom Temperature Minimum (°C). Binned values are shown as red dots; average points are shown as blue crosses; the model fit to the averaged values is shown as a blue line. Lag size: 0.099 degrees; number of lags: 12; Parameter: 2; Range: 0.795 degrees; Partial Sill: 5.860. Right panel: Scatterplot of predicted values versus observed values for the model of Bottom Temperature Minimum (°C).

Table 6. Results of cross-validation of the kriged model for the Bottom Temperature Minimum (°C).

Prediction error	**Value**
Number of Observations	606
Overall Mean Error	0.013
Root Mean Square Prediction Error	0.947
Standardized Mean	0.006
Standardized Root Mean Square Prediction Error	0.943
Average Standard Error	1.023

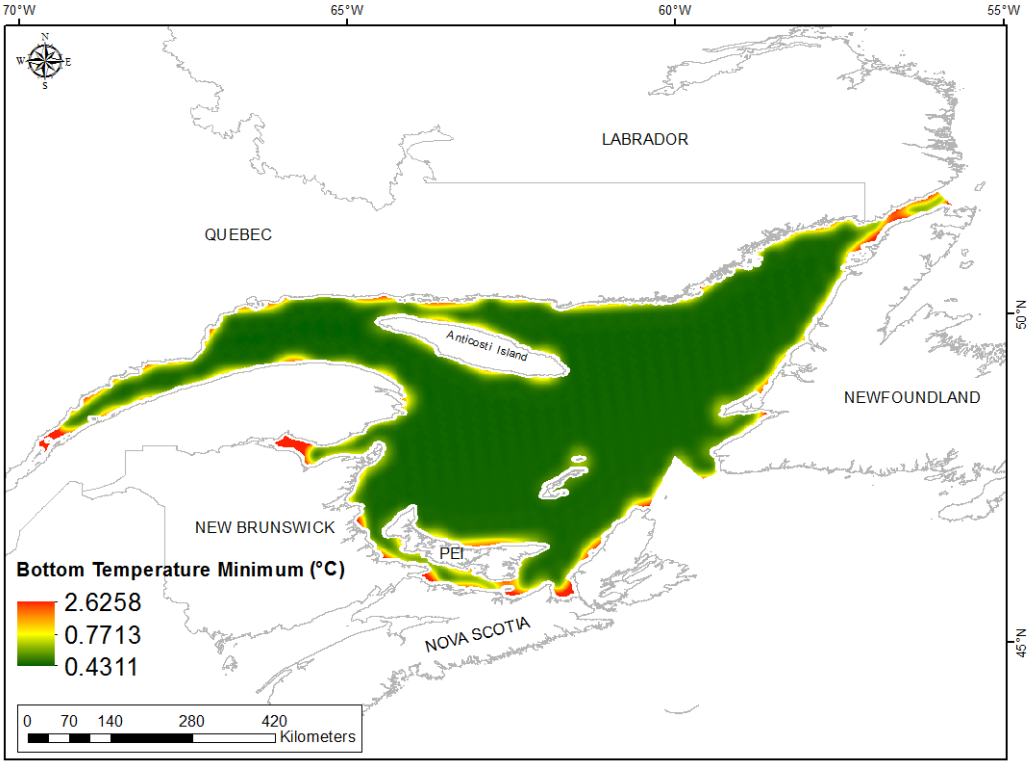

Fig. 14. Prediction standard error surface of Bottom Temperature Minimum (˚C).

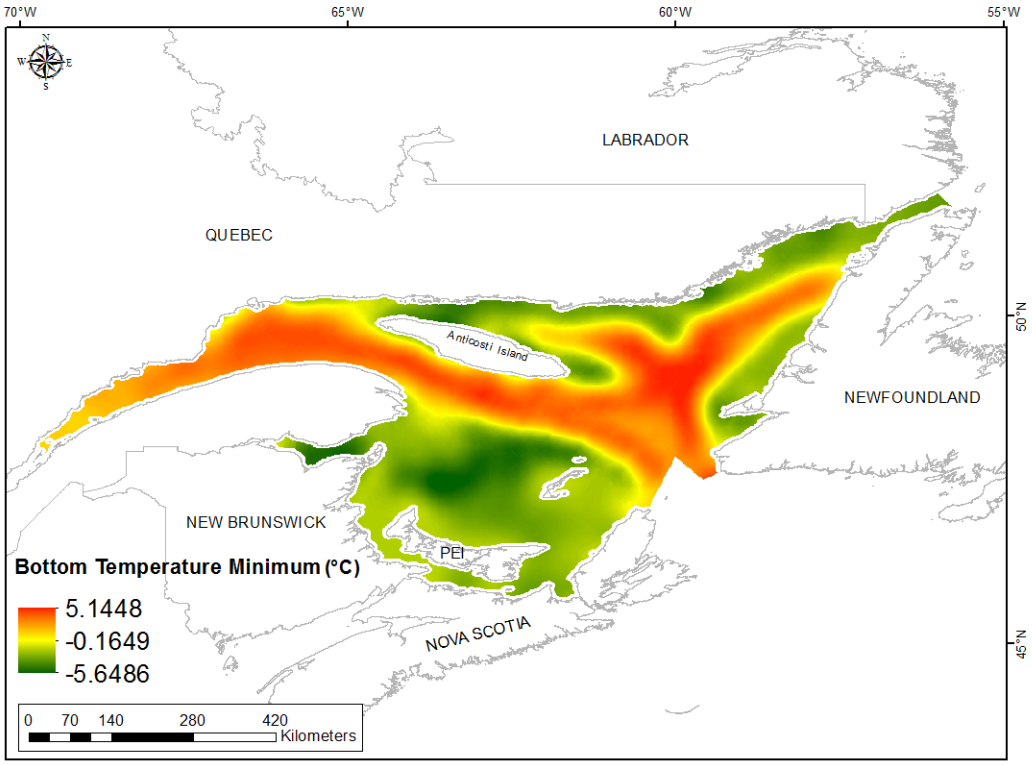

Fig. 15. Interpolated prediction surface of Bottom Temperature Minimum (˚C).

Bottom Temperature Maximum

This variable displayed a right-skewed distribution prior to modeling (Table 7, Fig. 16). At both of the tails the actual data were greater than predicted by a normal distribution while the mid-range of the data was under-predicted (Fig. 17). These data points were somewhat spatially cohesive with specific areas of over- and under-prediction. The area of over-prediction was in the channel and upper reaches of the estuary in addition to the Northumberland Strait and an area east of Anticosti Island (Fig. 17).

The semivariogram showed very weak autocorrelation present in the data (Fig. 18). The kriged model showed good cross-validation statistics (Table 8) indicating that it was good at prediction. The error map showed low error and no strong spatial pattern over the spatial extent although error was highest along the coast (Fig. 19). The kriged surface is presented in Fig. 20.

Table 7. Distributional properties of Bottom Temperature Maximum (°C).

Property	Value
Number of Observations	606
Minimum	0.891
Maximum	19.465
Mean	5.103
Median	5.026
Standard Deviation	3.092
Skewness	2.535
Kurtosis	11.201

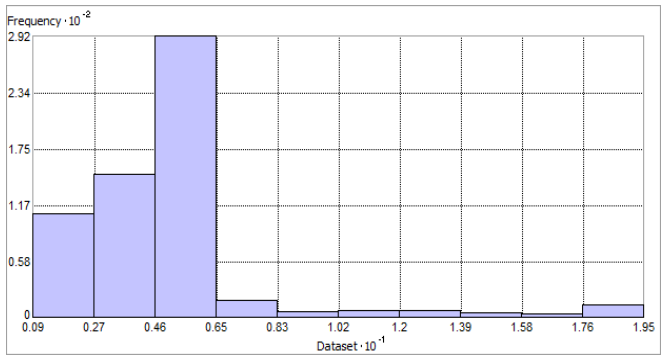

Fig. 16. Distribution of Bottom Temperature Maximum (°C). Histogram was illustrated using 10 bins. X axis shown at 10^{-1}; Y axis is shown at 10^{-2}.

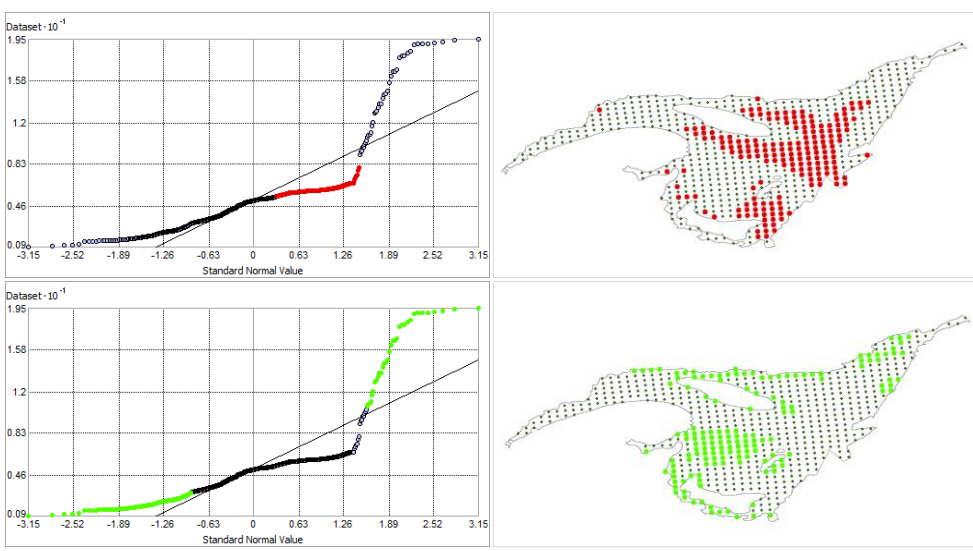

Fig. 17. Normal Q-Q plot for data values of Bottom Temperature Maximum (°C). Points falling under (upper panel) and over (bottom panel) the reference line are mapped.

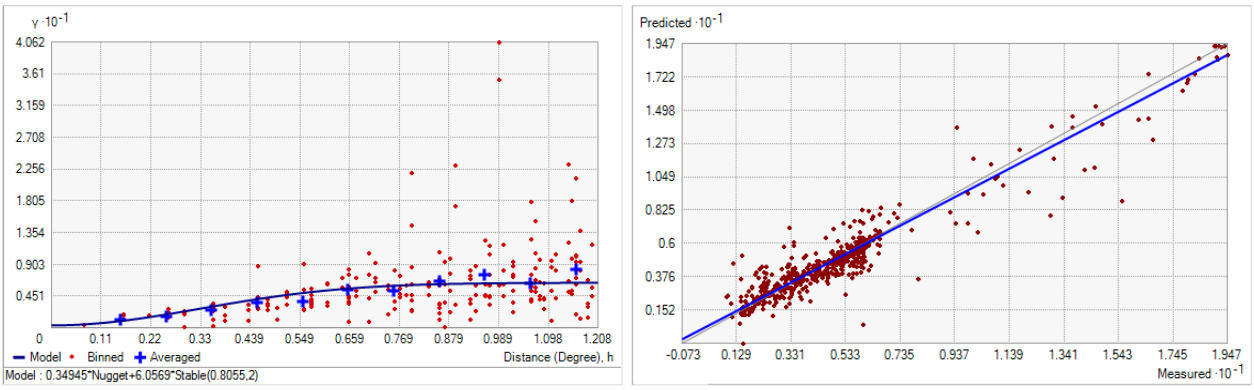

Fig. 18. Left panel: Semivariogram of Bottom Temperature Maximum (°C). Binned values are shown as red dots; average points are shown as blue crosses; the model fit to the averaged values is shown as a blue line. Lag size: 0.101 degrees; number of lags: 12; Parameter: 2; Range: 0.806 degrees; Partial Sill: 6.057. Right panel: Scatterplot of predicted values versus observed values for the model of Bottom Temperature Maximum (°C).

Table 8. Results of cross-validation of the kriged model for the Bottom Temperature Maximum (°C).

Prediction error	**Value**
Number of Observations	606
Overall Mean Error	-0.024
Root Mean Square Prediction Error	0.970
Standardized Mean	-0.015
Standardized Root Mean Square Prediction Error	1.146
Average Standard Error	0.824

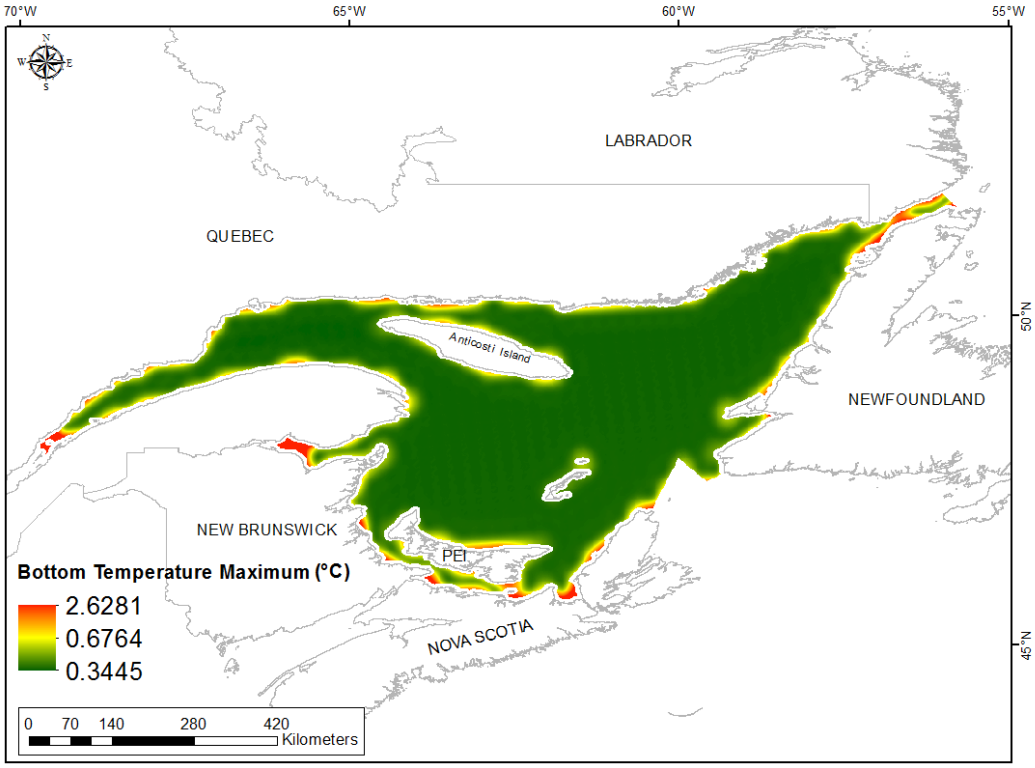

Fig. 19. Prediction standard error surface of Bottom Temperature Maximum (˚C).

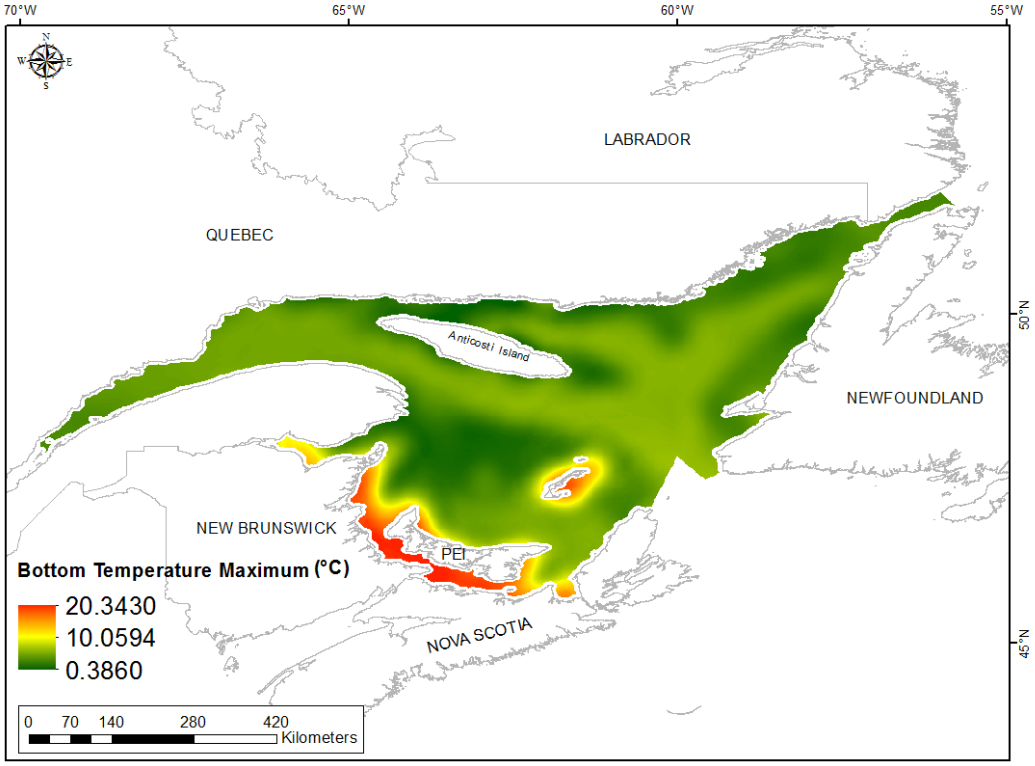

Fig. 20. Prediction prediction surface of Bottom Temperature Maximum (˚C).

Bottom Temperature Range

This variable displayed a right-skewed and kurtotic distribution prior to modeling (Table 9, Fig. 21). At both of the tails the actual data were greater than predicted by a normal distribution while there was an area of under-prediction at mid-range values (Fig. 22). These data points were somewhat spatially cohesive with specific areas of over- and under-prediction (Fig. 22).

The semivariogram showed weak autocorrelation present in the data (Fig. 23). The kriged model showed fair cross-validation statistics (Table 10) indicating fair model performance. The error map showed low error and no strong spatial pattern over the spatial extent although error was highest along the coast (Fig. 24). The kriged surface is presented in Fig. 25.

Table 9. Distributional properties of Bottom Temperature Range (°C).

Property	Value
Number of Observations	606
Minimum	1.061
Maximum	21.227
Mean	5.090
Median	4.083
Standard Deviation	3.867
Skewness	2.059
Kurtosis	7.990

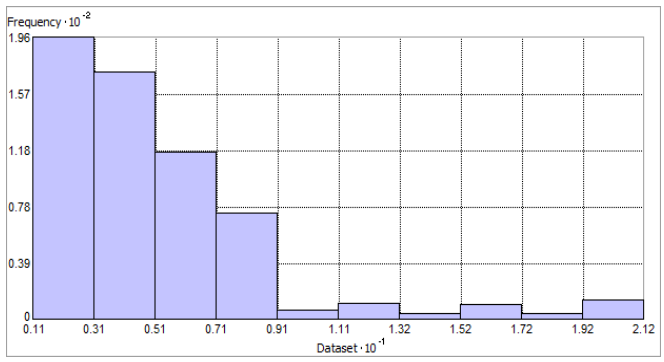

Fig. 21. Distribution of Bottom Temperature Range (°C). Histogram was illustrated using 10 bins. X axis shown at 10^{-1}; Y axis is shown at 10^{-2}.

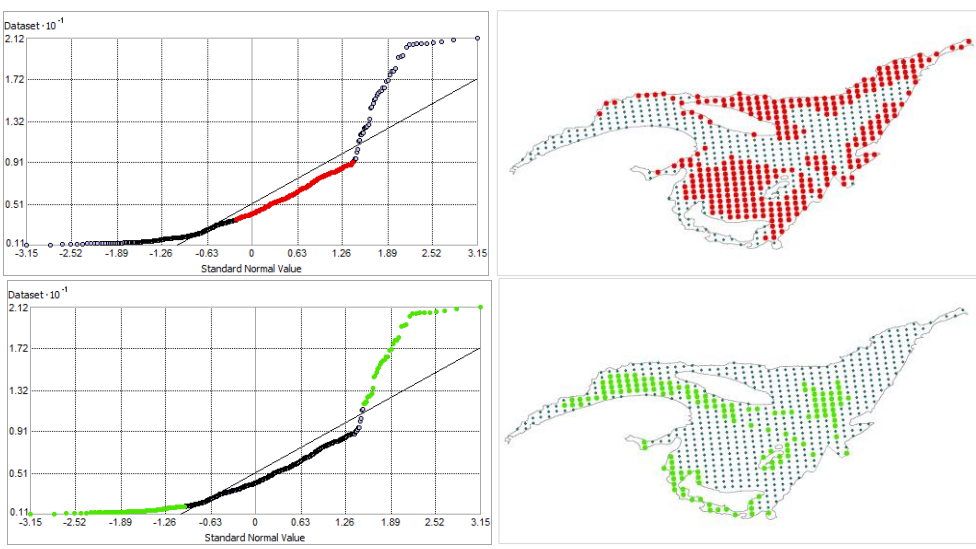

Fig. 22. Normal Q-Q plot for data values of Bottom Temperature Range (°C). Points falling under (upper panel) and over (bottom panel) the reference line are mapped.

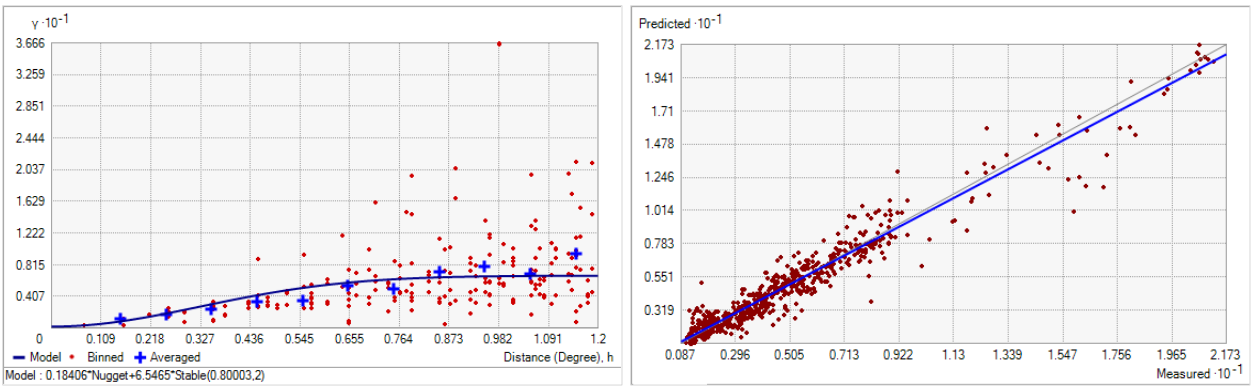

Fig. 23. Left panel: Semivariogram of Bottom Temperature Range (°C). Binned values are shown as red dots; average points are shown as blue crosses; the model fit to the averaged values is shown as a blue line. Lag size: 0.100 degrees; number of lags: 12; Parameter: 2; Range: 0.800 degrees; Partial Sill: 6.547. Right panel: Scatterplot of predicted values versus observed values for the model of Bottom Temperature Range (°C).

Table 10. Results of cross-validation of the kriged model for the Bottom Temperature Range (°C).

Prediction error	**Value**
Number of Observations	606
Overall Mean Error	-0.041
Root Mean Square Prediction Error	0.961
Standardized Mean	-0.031
Standardized Root Mean Square Prediction Error	1.423
Average Standard Error	0.662

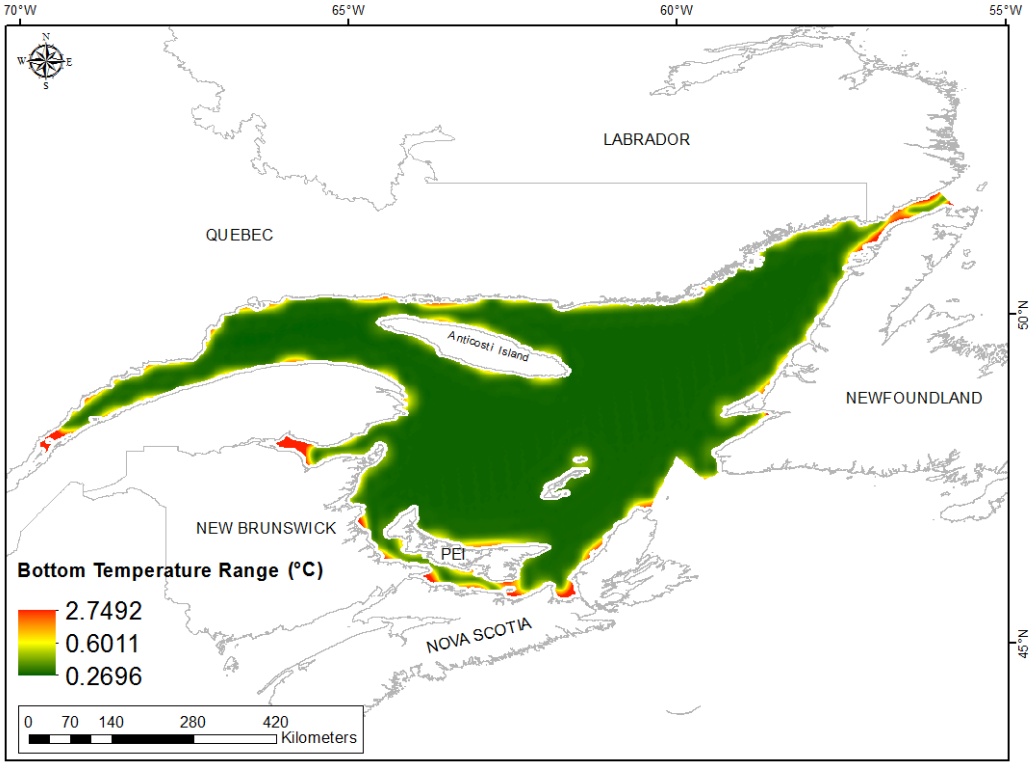

Fig. 24. Prediction standard error surface of Bottom Temperature Range (˚C).

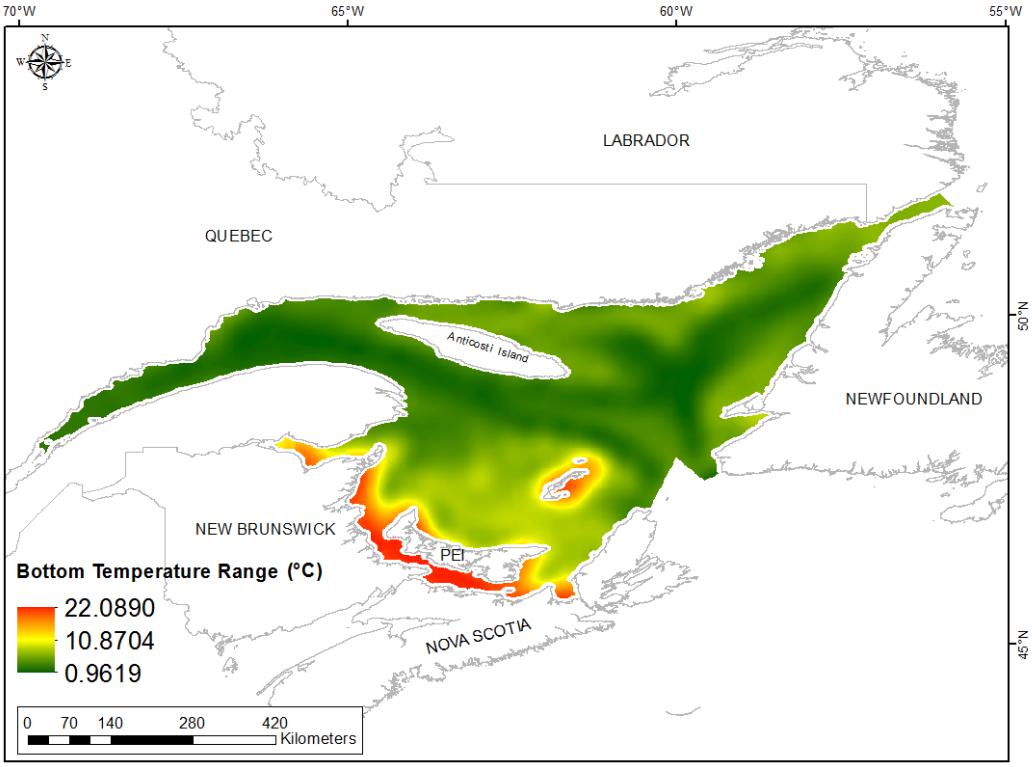

Fig. 25. Interpolated prediction surface of Bottom Temperature Range (˚C).

Bottom Temperature Average Minimum

This variable displayed a bimodal distribution prior to modeling (Table 11, Fig. 26). The data were lower than predicted by a standard normal distribution in the lower to mid-data range and in the extreme high values and higher than predicted at the smallest values and in the upper to mid-data range (Fig. 27). These areas of under- and over-prediction showed little spatial pattern over the region (Fig. 27).

The semivariogram showed moderate autocorrelation present in the data (Fig. 28). The kriged model showed good cross-validation statistics (Table 12) indicating that it was good at prediction. The error map showed low error and no strong spatial pattern over the spatial extent although error was highest along the coast (Fig. 29). The kriged surface is presented in Fig. 30.

Table 11. Distributional properties of Bottom Temperature Average Minimum (°C).

Property	Value
Number of Observations	606
Minimum	-2.714
Maximum	5.267
Mean	1.131
Median	-0.097
Standard Deviation	2.628
Skewness	0.272
Kurtosis	1.356

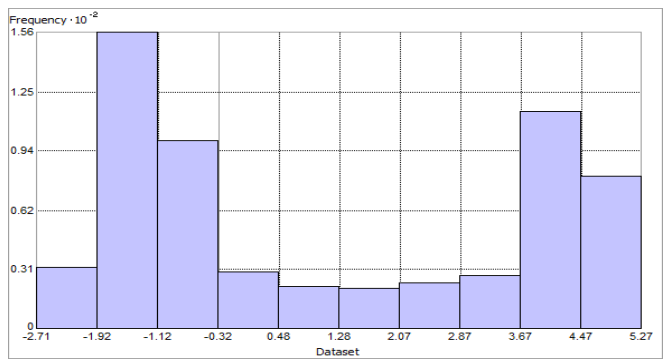

Fig. 26. Distribution of Bottom Temperature Average Minimum (°C). Histogram was illustrated using 10 bins. Y axis is shown at 10^{-2}.

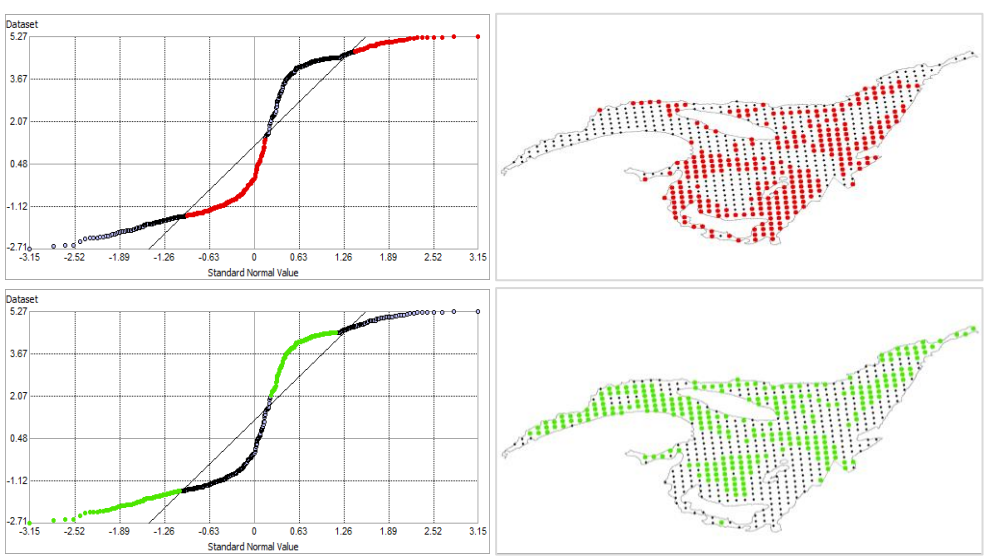

Fig. 27. Normal Q-Q plot for data values of Bottom Temperature Average Minimum (°C). Points falling under (top right panel) and over (bottom right panel) the reference line are mapped.

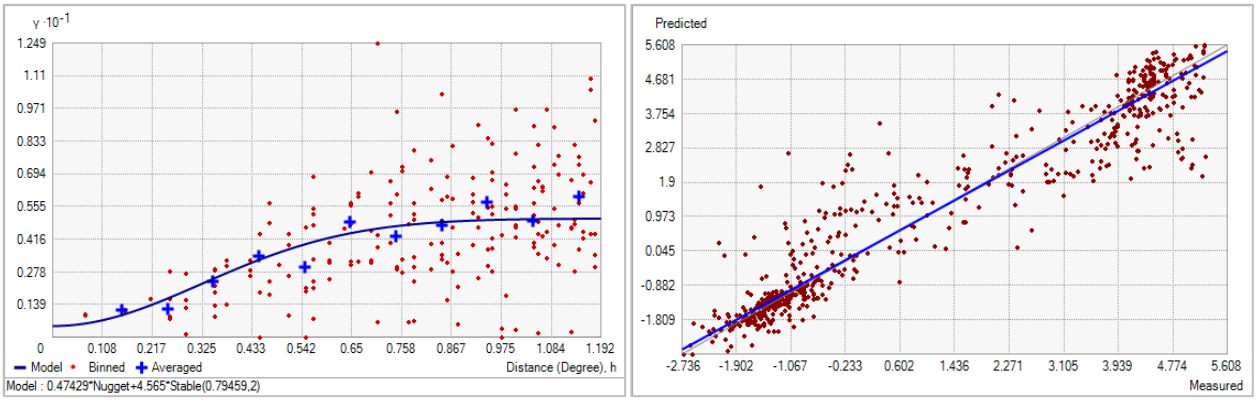

Fig. 28. Left panel: Semivariogram of Bottom Temperature Average Minimum (°C). Binned values are shown as red dots; average points are shown as blue crosses; the model fit to the averaged values is shown as a blue line. Lag size: 0.099 degrees; number of lags: 12; Parameter: 2; Range: 0.795 degrees; Partial Sill: 4.565. Right panel: Scatterplot of predicted values versus observed values for the model of Bottom Temperature Average Minimum (°C).

Table 12. Results of cross-validation of the kriged model for the Bottom Temperature Average Minimum (°C).

Prediction error	**Value**
Number of Observations	606
Overall Mean Error	0.016
Root Mean Square Prediction Error	0.794
Standardized Mean	0.009
Standardized Root Mean Square Prediction Error	0.892
Average Standard Error	0.908

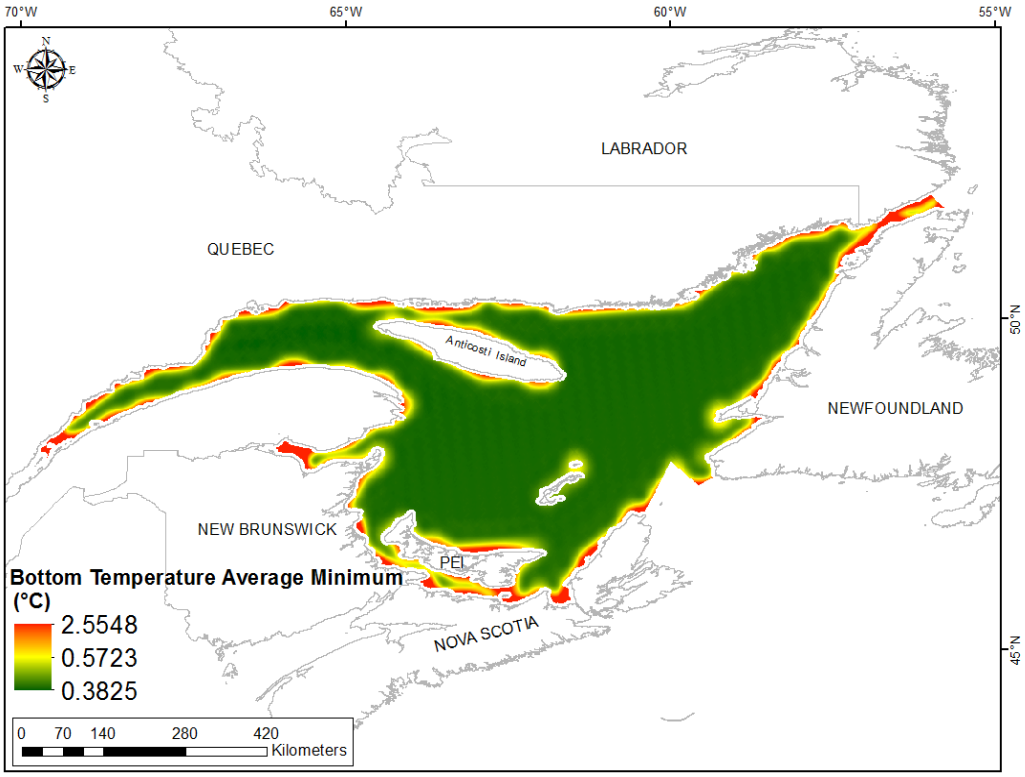

Fig. 29. Prediction standard error surface of Bottom Temperature Average Minimum (˚C).

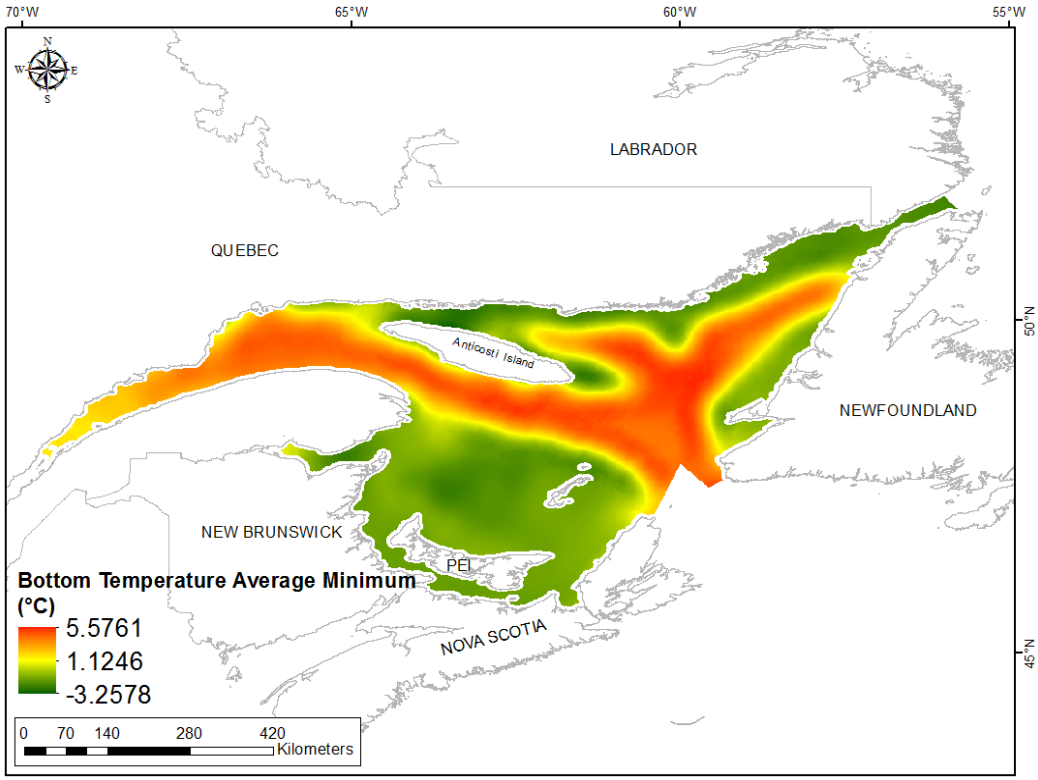

Fig. 30. Interpolated prediction surface of Bottom Temperature Average Minimum (˚C).

Bottom Temperature Average Maximum

This variable displayed a right-skewed and kurtotic distribution prior to modeling (Table 13, Fig. 31). The data were higher than predicted by a standard normal distribution at the tails of the distribution and under-predicted through the upper-mid-range of the data (Fig. 32). These data points were somewhat spatially cohesive with specific areas of over- and under-prediction with the former more extensive than the latter (Fig. 32).

The semivariogram showed weak autocorrelation present in the data (Fig. 33). The kriged model showed good cross-validation statistics (Table 14) indicating that it was good at prediction. The error map showed low error and no strong spatial pattern over the spatial extent although error was highest along the coast (Fig. 34). The kriged surface is presented in Fig. 35.

Table 13. Distributional properties of Bottom Temperature Average Maximum (°C).

Property	Value
Number of Observations	606
Minimum	-0.019
Maximum	18.417
Mean	3.841
Median	3.533
Standard Deviation	3.040
Skewness	2.341
Kurtosis	10.759

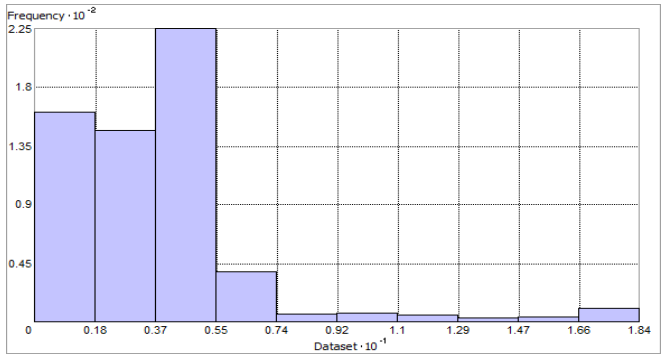

Fig. 31. Distribution of Bottom Temperature Average Maximum (°C). Histogram was illustrated using 10 bins. X axis shown at 10^{-1}; Y axis is shown at 10^{-2}.

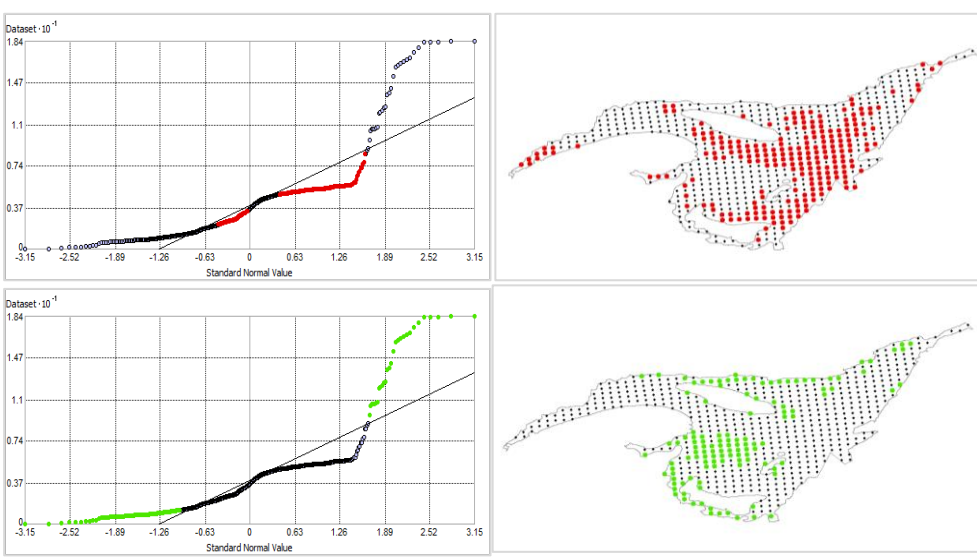

Fig. 32. Normal Q-Q plot for data values of Bottom Temperature Average Maximum (°C). Points falling under (upper panel) and over (bottom panel) the reference line are mapped.

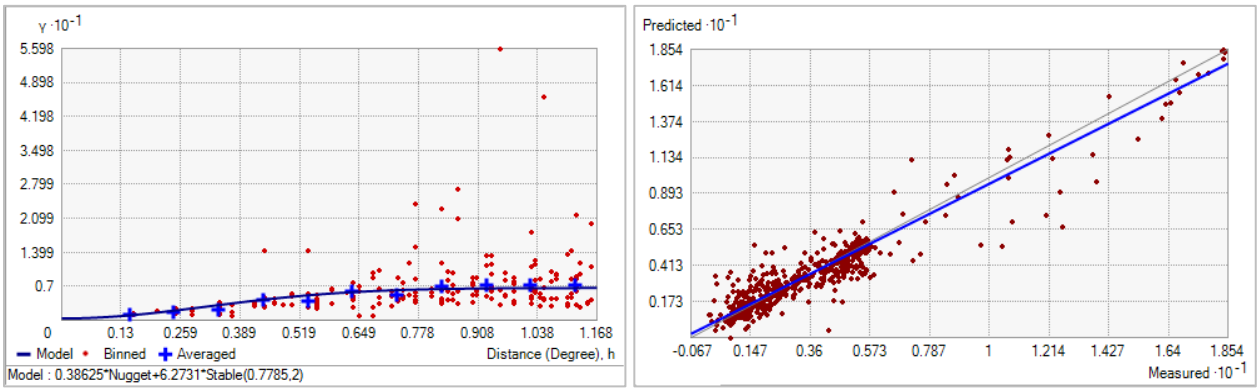

Fig. 33. Left panel: Semivariogram of Bottom Temperature Average Maximum (°C). Binned values are shown as red dots; average points are shown as blue crosses; the model fit to the averaged values is shown as a blue line. Lag size: 0.097 degrees; number of lags: 12; Parameter: 2; Range: 0.778 degrees; Partial Sill: 6.273. Right panel: Scatterplot of predicted values versus observed values for the model of Bottom Temperature Average Maximum (°C).

Table 14. Results of cross-validation of the kriged model for the Bottom Temperature Average Maximum (°C).

Prediction error	**Value**
Number of Observations	606
Overall Mean Error	-0.025
Root Mean Square Prediction Error	0.989
Standardized Mean	-0.019
Standardized Root Mean Square Prediction Error	1.104
Average Standard Error	0.878

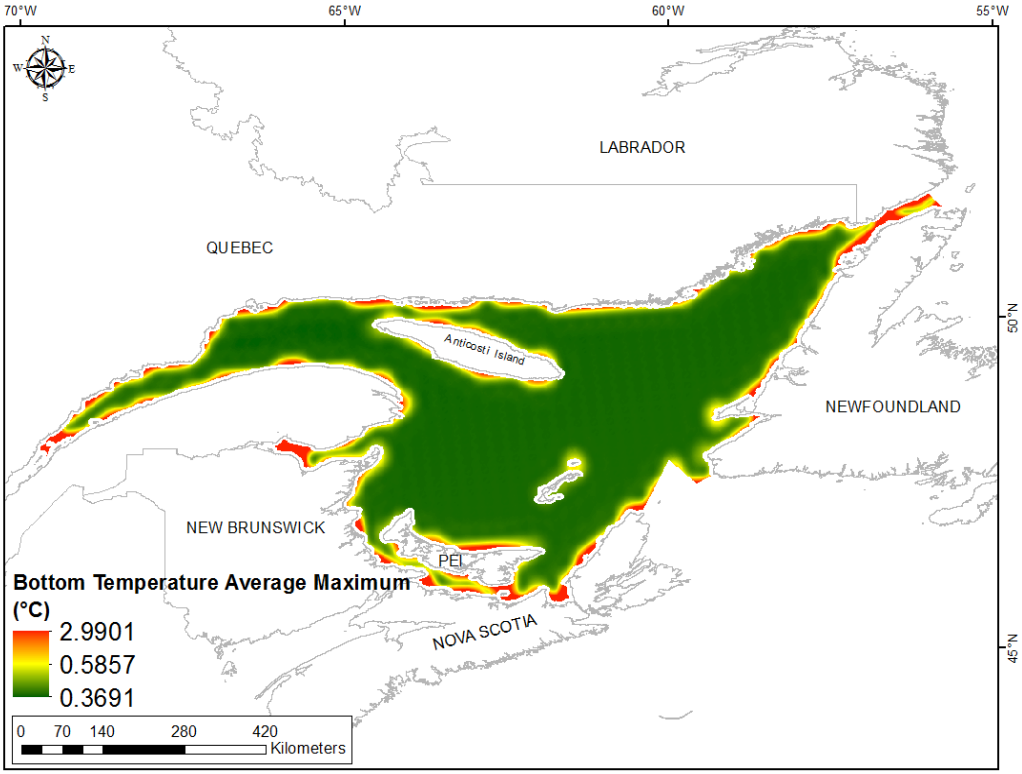

Fig. 34. Prediction standard error surface of Bottom Temperature Average Maximum (˚C).

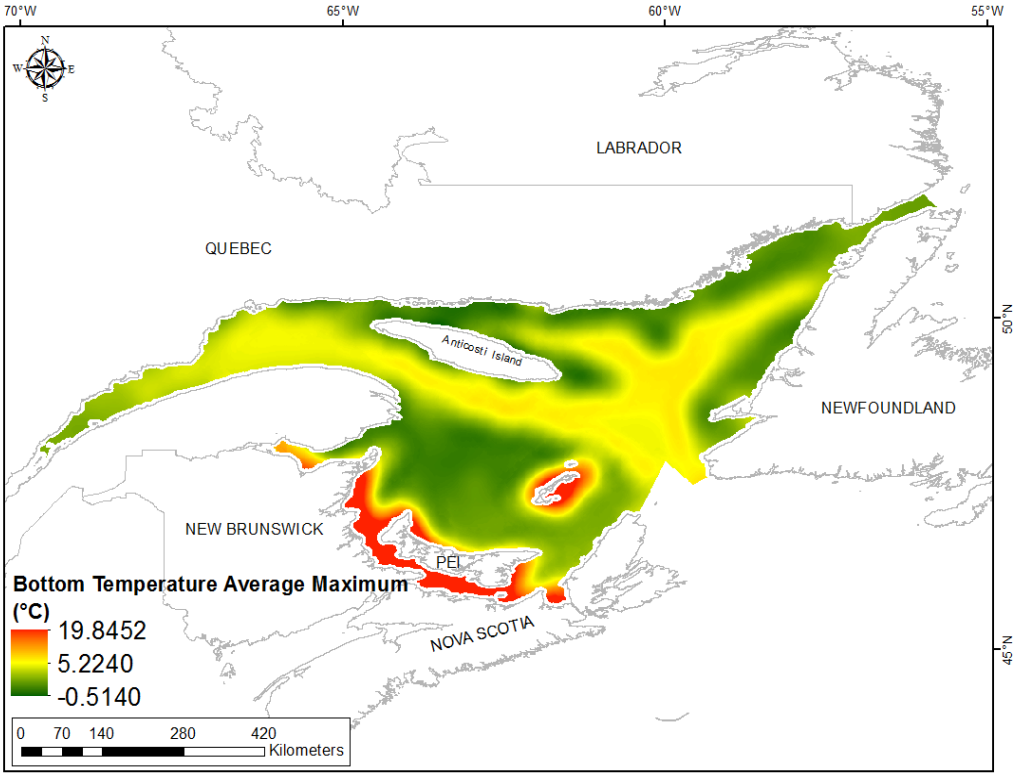

Fig. 35. Interpolated prediction surface of Bottom Temperature Average Maximum (˚C).

Bottom Temperature Average Range

This variable displayed a highly right-skewed and kurtotic distribution prior to modeling (Table 15, Fig. 36). The data were higher than predicted by a standard normal distribution at the tails and lower than predicted through the mid-range of the data (Fig. 37). These data points were somewhat spatially cohesive with specific areas of over- and under-prediction (Fig. 37).

The semivariogram showed weak autocorrelation present in the data (Fig. 38). The kriged model showed fair cross-validation statistics (Table 16). The error map showed low error and no strong spatial pattern over the spatial extent although error was highest along the coast (Fig. 39). The kriged surface is presented in Fig. 40.

Table 15. Distributional properties of Bottom Temperature Average Range (°C).

Property	Value
Number of Observations	606
Minimum	-2.544
Maximum	17.008
Mean	1.451
Median	0.775
Standard Deviation	2.957
Skewness	3.464
Kurtosis	16.089

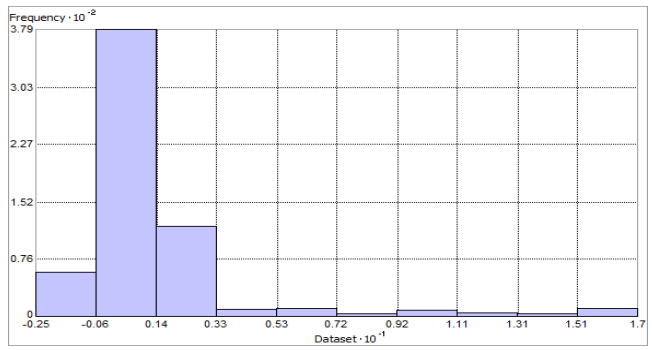

Fig. 36. Distribution of Bottom Temperature Average Range (°C). Histogram was illustrated using 10 bins. X axis shown at 10^{-1}; Y axis is shown at 10^{-2}.

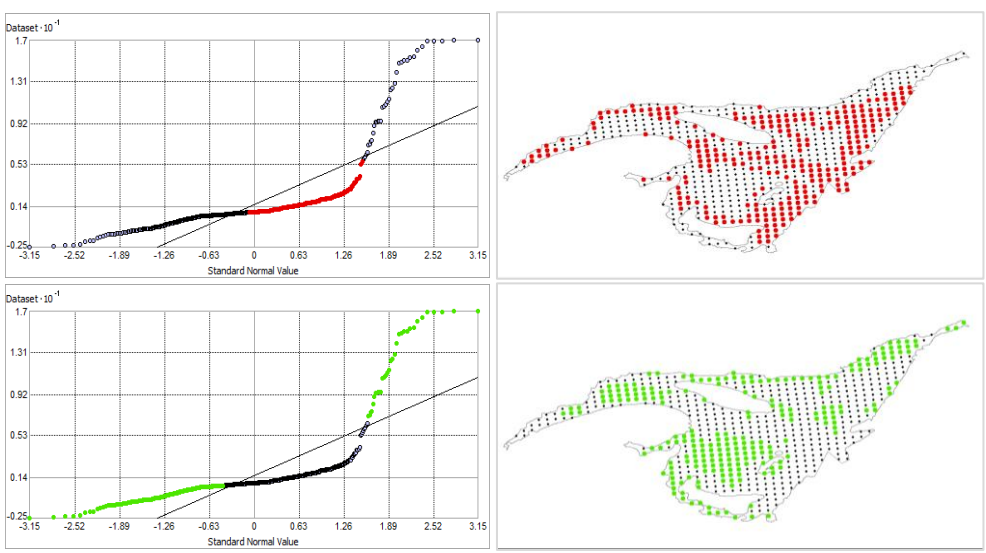

Fig. 37. Normal Q-Q plot for data values of Bottom Temperature Average Range (°C). Points falling under (upper panel) and over (bottom panel) the reference line are mapped.

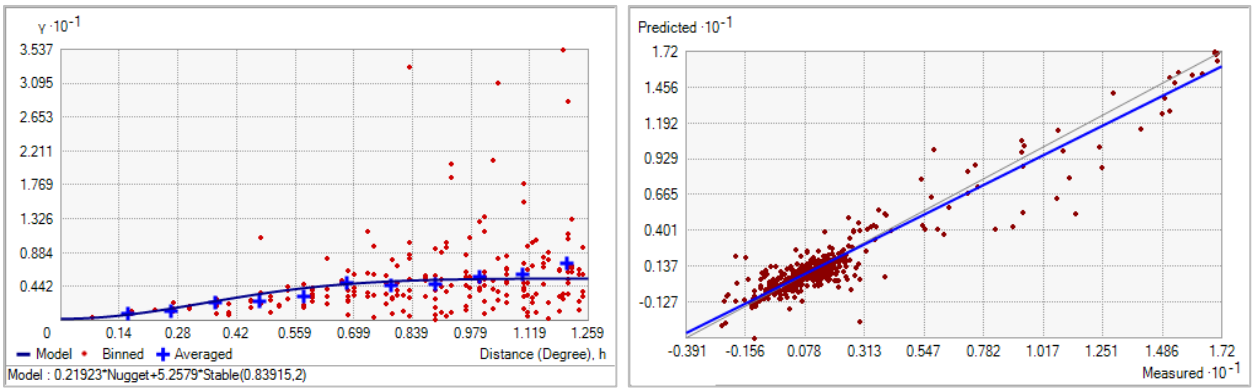

Fig. 38. Left panel: Semivariogram of Bottom Temperature Average Range (°C). Binned values are shown as red dots; average points are shown as blue crosses; the model fit to the averaged values is shown as a blue line. Lag size: 0.105 degrees; number of lags: 12; Parameter: 2; Range: 0.839 degrees; Partial Sill: 5.258. Right panel: Scatterplot of predicted values versus observed values for the model of Bottom Temperature Average Range (°C).

Table 16. Results of cross-validation of the kriged model for the Bottom Temperature Average Range (°C).

Prediction error	**Value**
Number of Observations	606
Overall Mean Error	-0.034
Root Mean Square Prediction Error	0.923
Standardized Mean	-0.026
Standardized Root Mean Square Prediction Error	1.328
Average Standard Error	0.662

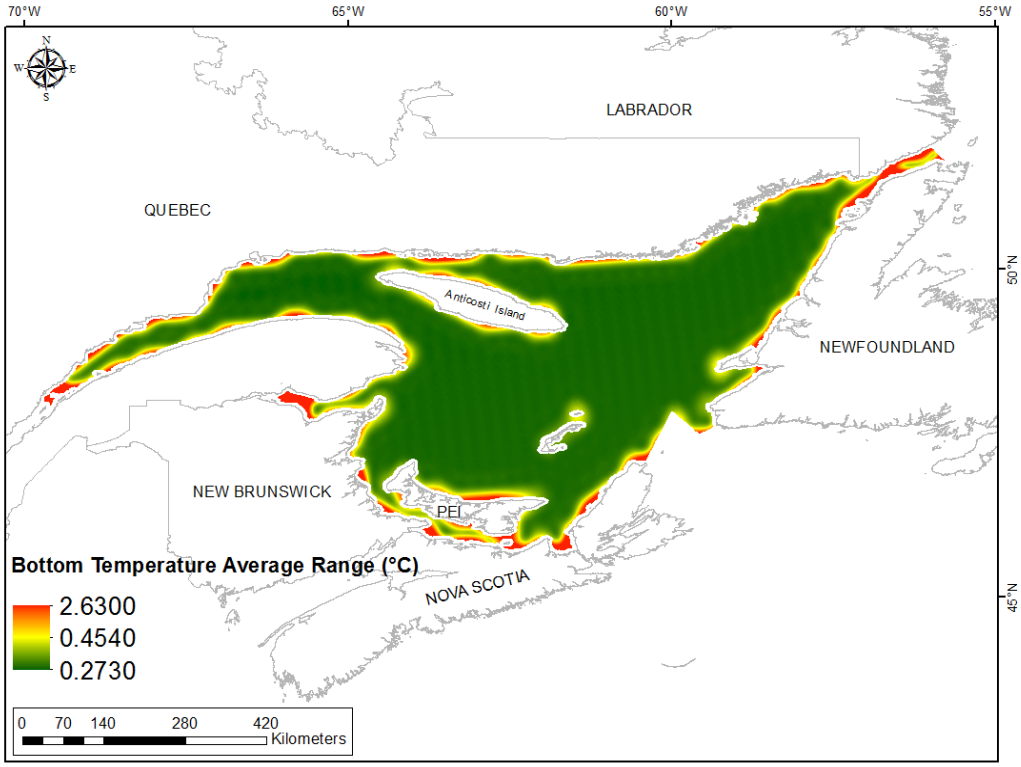

Fig. 39. Prediction standard error surface of Bottom Temperature Average Range (˚C).

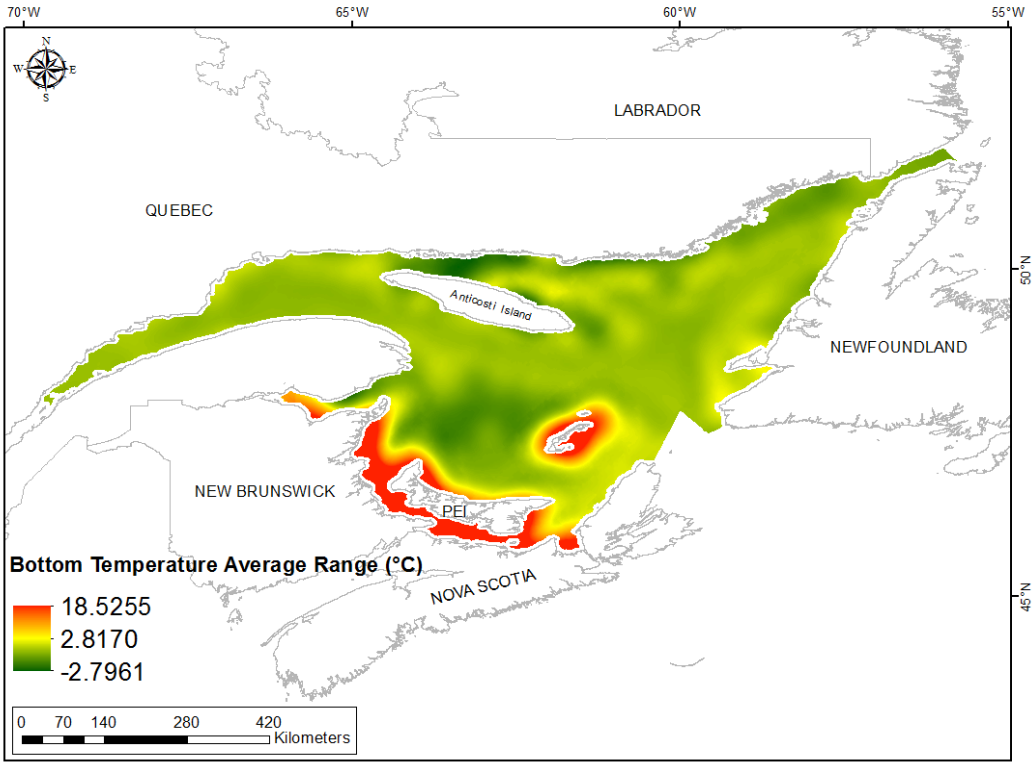

Fig. 40. Interpolated prediction surface of Bottom Temperature Average Range (˚C).

Surface Temperature Mean

This variable displayed a near-normal distribution prior to modeling (Table 17, Fig. 41), with slight deviation from a standard normal distribution at the lowest and highest data values (Fig. 42). These data points were spatially cohesive with isolated areas of over- and under-prediction near the coast (Fig. 42).

The semivariogram showed weak autocorrelation present in the data but an excellent fit between the predicted and measured values (Fig. 43). The kriged model showed good cross-validation statistics (Table 18) indicating that it was good at prediction. The error map showed a 'bullseye' pattern with error increasing with distance from data points (Fig. 44). The kriged surface is presented in Fig. 45.

Table 17. Distributional properties of Surface Temperature Mean (°C).

Property	Value
Number of Observations	606
Minimum	2.674
Maximum	7.611
Mean	5.695
Median	5.601
Standard Deviation	0.833
Skewness	0.082
Kurtosis	2.612

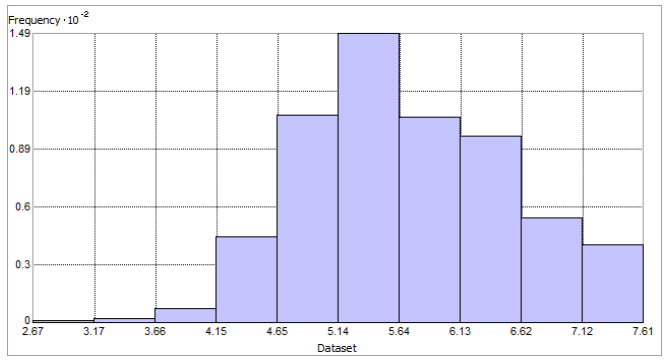

Fig. 41. Distribution of Mean Surface Temperature (°C). Histogram was illustrated using 10 bins. Y axis is shown at 10^{-2}.

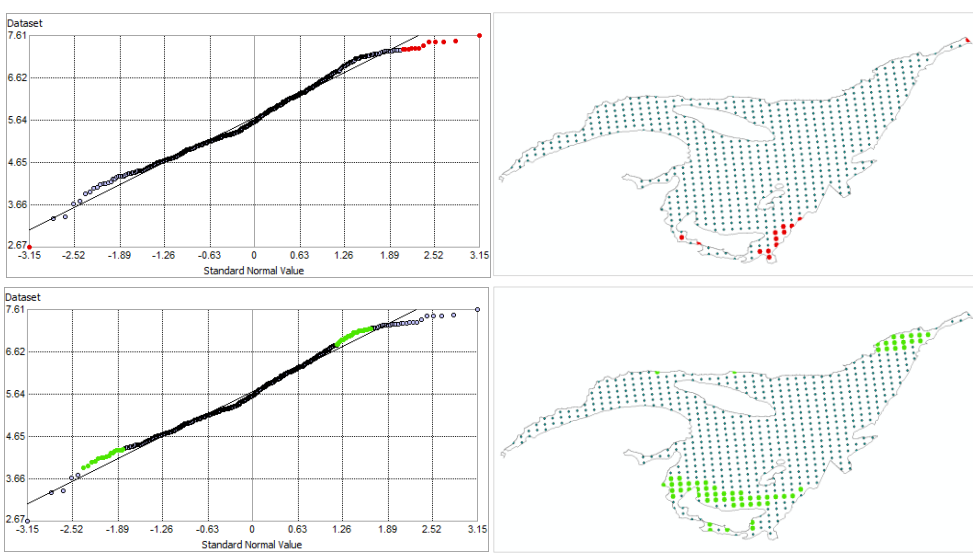

Fig. 42. Normal Q-Q plot for data values of Surface Temperature Mean (°C). Points falling under (upper panel) and over (bottom panel) the reference line are mapped.

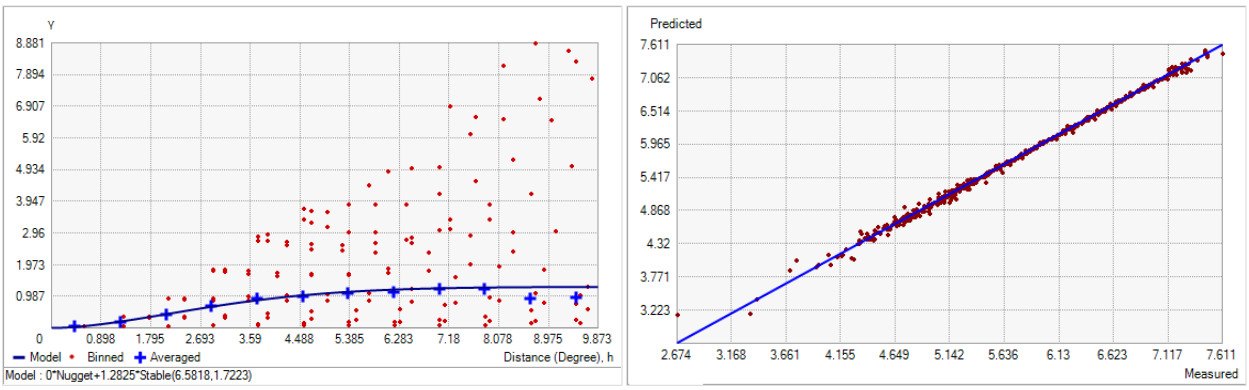

Fig. 43. Left panel: Semivariogram of Surface Temperature Mean (°C). Binned values are shown as red dots; average points are shown as blue crosses; the model fit to the averaged values is shown as a blue line. Lag size: 0.823 degrees; number of lags: 12; Parameter: 2; Range: 6.582 degrees; Partial Sill: 1.282. Right panel: Scatterplot of predicted values versus observed values for the model of Surface Temperature Mean (°C).

Table 18. Results of cross-validation of the kriged model for the Surface Temperature Mean (°C).

Prediction error	**Value**
Number of Observations	606
Overall Mean Error	5.080×10^{-4}
Root Mean Square Prediction Error	0.045
Standardized Mean	-0.003
Standardized Root Mean Square Prediction Error	0.773
Average Standard Error	0.048

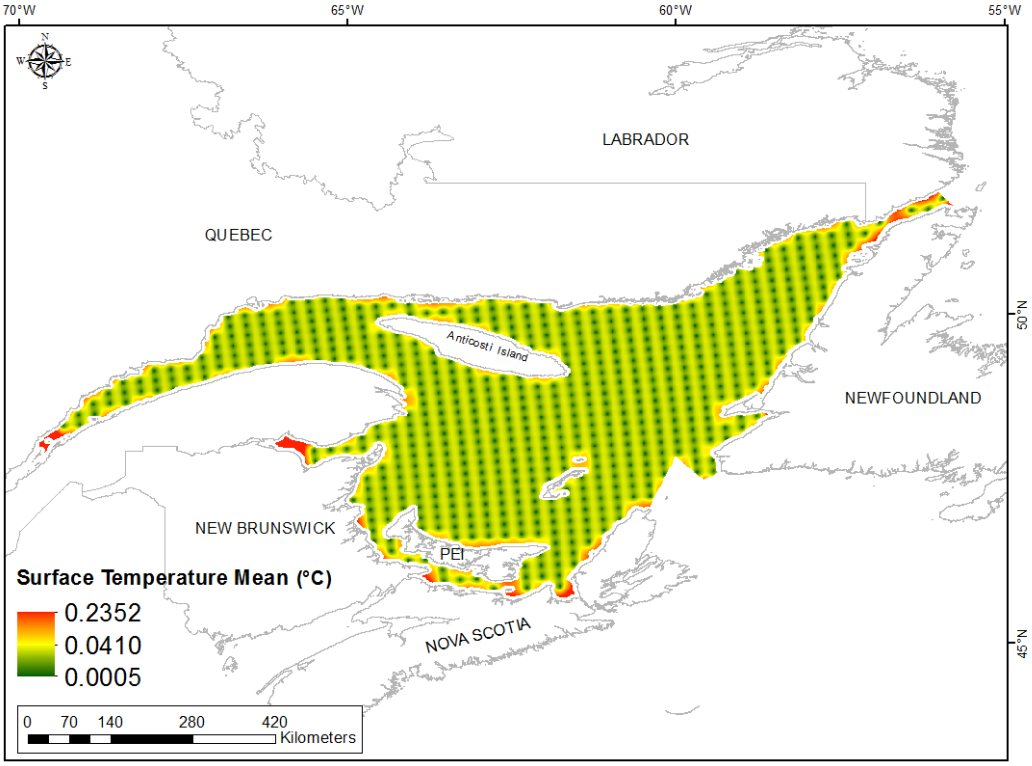

Fig. 44. Prediction standard error surface of Surface Temperature Mean (˚C).

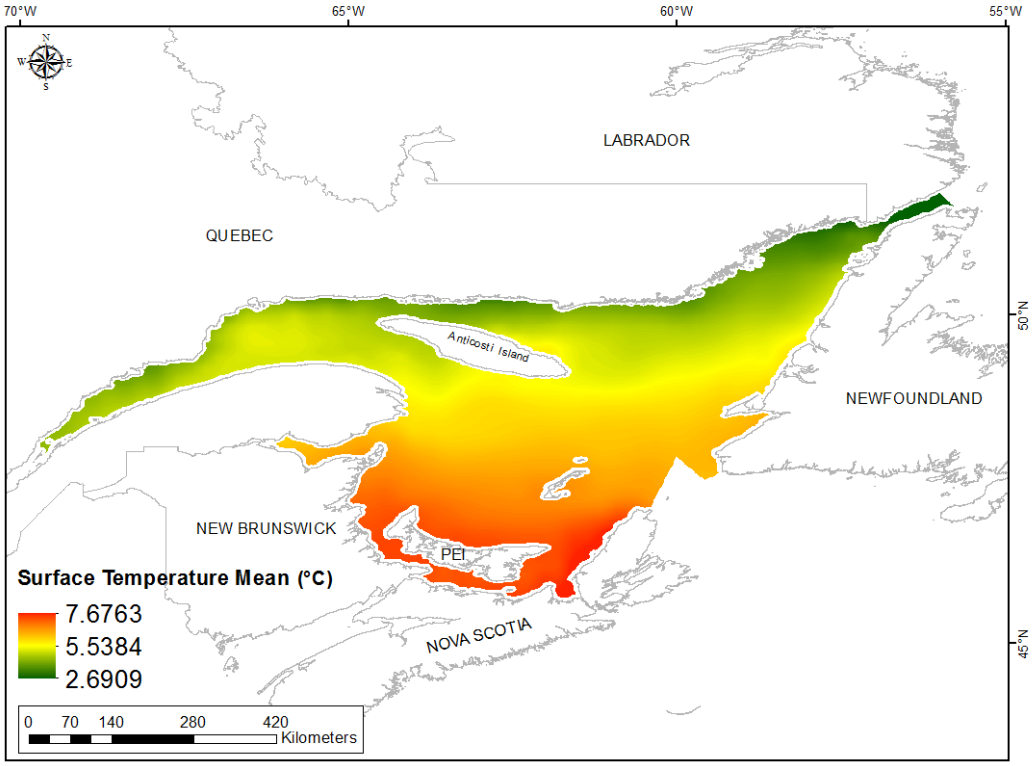

Fig. 45. Interpolated prediction surface of Surface Temperature Mean (˚C).

Surface Temperature Minimum

This variable displayed a near-normal distribution prior to modeling (Table 19, Fig. 46). The Q-Q plot showed only slight deviations from a normal distribution (Fig. 47). These data points were spatially cohesive with very small areas of over- and under-prediction (Fig. 47), with the former being more prevalent.

The semivariogram showed moderate autocorrelation present in the data (Fig. 48). The kriged model showed good cross-validation statistics (Table 20) indicating that it was good at prediction. The error map showed low error and no strong spatial pattern over the spatial extent although error was highest along the coast (Fig. 49). The kriged surface is presented in Fig. 50.

Table 19. Distributional properties of Surface Temperature Minimum (°C).

Property	Value
Number of Observations	606
Minimum	-1.894
Maximum	-1.269
Mean	-1.606
Median	-1.598
Standard Deviation	0.116
Skewness	0.101
Kurtosis	2.762

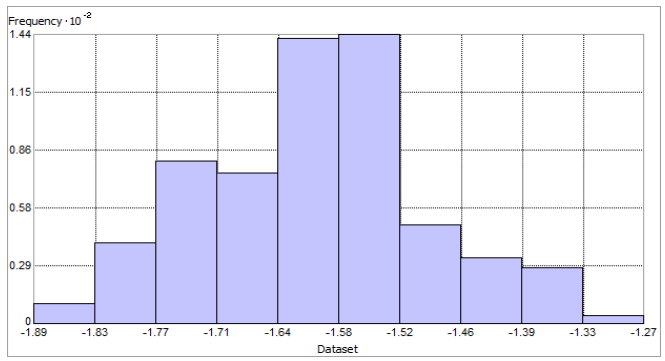

Fig. 46. Distribution of Surface Temperature Minimum (°C). Histogram was illustrated using 10 bins. Y axis is shown at 10^{-2}.

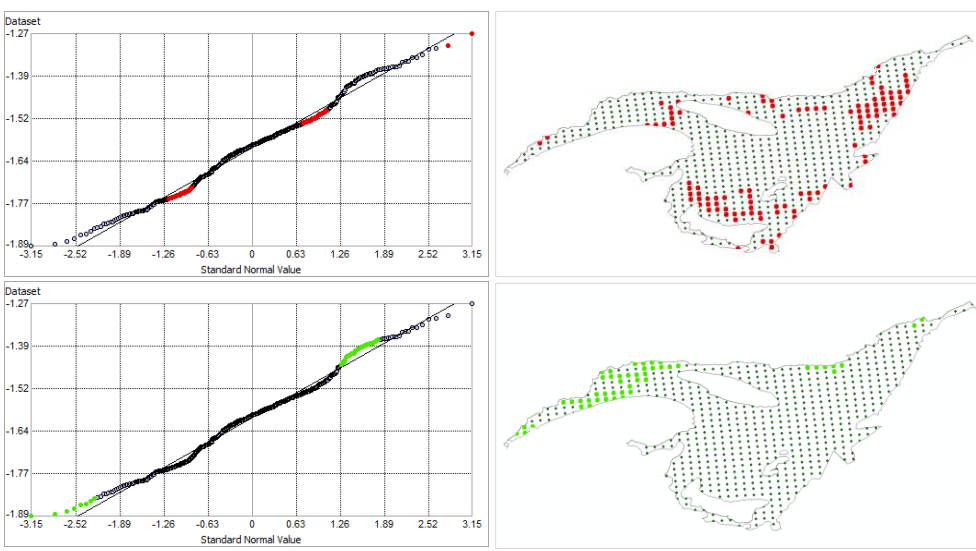

Fig. 47. Normal Q-Q plot for data values of Surface Temperature Minimum (°C). Points falling under (upper panel) and over (bottom panel) the reference line are mapped.

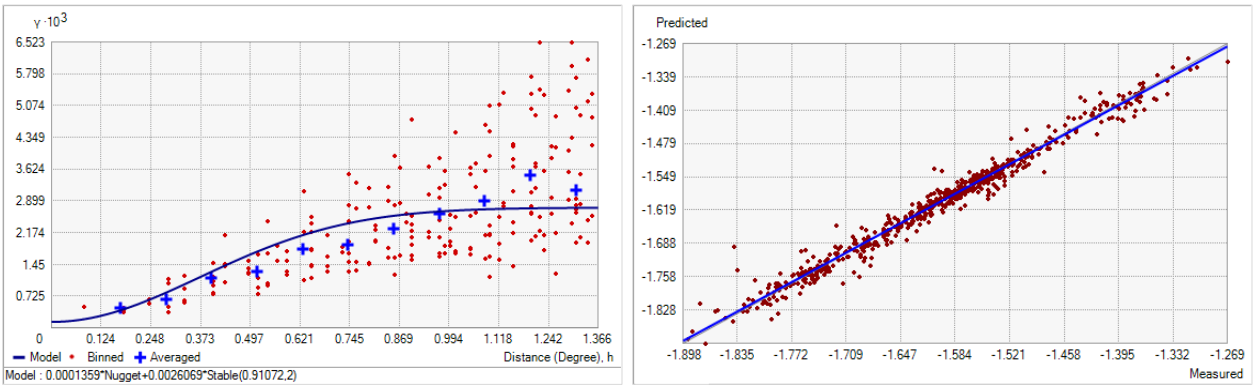

Fig. 48. Left panel: Semivariogram of Surface Temperature Minimum (°C). Binned values are shown as red dots; average points are shown as blue crosses; the model fit to the averaged values is shown as a blue line. Lag size: 0.114 degrees; number of lags: 12; Parameter: 2; Range: 0.911 degrees; Partial Sill: 0.003. Right panel: Scatterplot of predicted values versus observed values for the model of Surface Temperature Minimum (°C).

Table 20. Results of cross-validation of the kriged model for the Surface Temperature Minimum (°C).

Prediction error	**Value**
Number of Observations	606
Overall Mean Error	2.486×10^{-4}
Root Mean Square Prediction Error	0.019
Standardized Mean	0.004
Standardized Root Mean Square Prediction Error	1.147
Average Standard Error	0.015

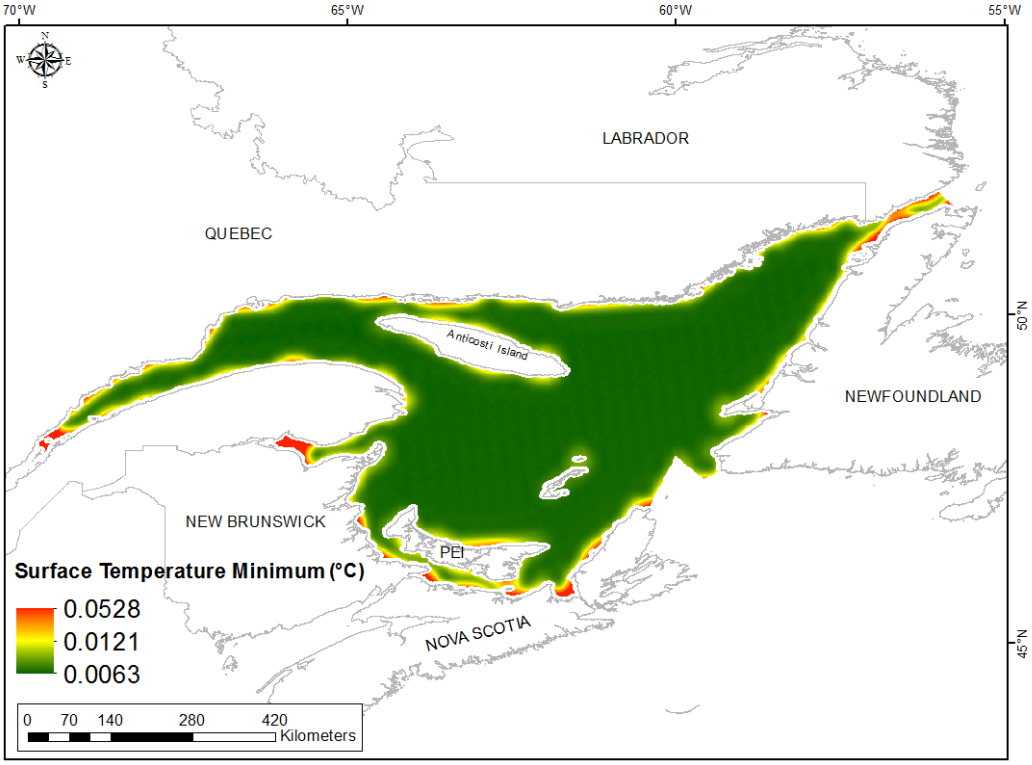

Fig. 49. Prediction standard error surface of Surface Temperature Minimum (˚C).

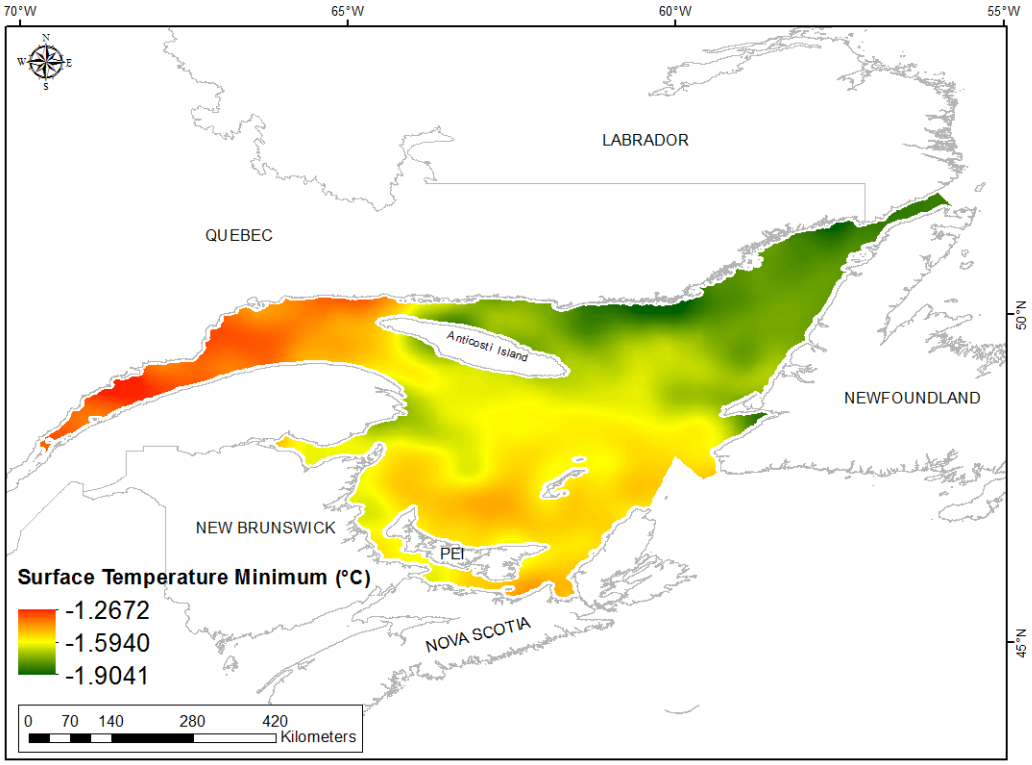

Fig. 50. Interpolated prediction surface of Surface Temperature Minimum (˚C).

Surface Temperature Maximum

This variable displayed a plateau-like distribution with outlying data in the lower range (Table 21, Fig. 51). The Q-Q plot showed only slight deviations from a normal distribution, particularly at the tails (Fig. 52). These data points were spatially cohesive with small areas of over- and under-prediction (Fig. 52).

The semivariogram showed weak autocorrelation present in the data and there was an excellent predictive fit (Fig. 53). The kriged model showed excellent cross-validation statistics (Table 22). The error map showed a 'bullseye' pattern with error increasing with distance from data points (Fig. 54). The kriged surface is presented in Fig. 55.

Table 21. Distributional properties of Surface Temperature Maximum (°C).

Property	Value
Number of Observations	606
Minimum	12.595
Maximum	20.372
Mean	17.532
Median	17.657
Standard Deviation	1.319
Skewness	-0.190
Kurtosis	2.174

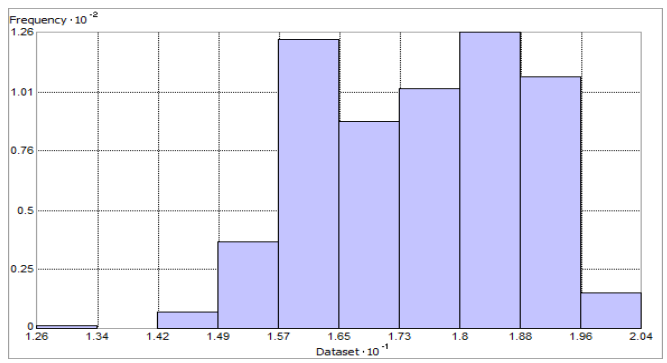

Fig. 51. Distribution of Surface Temperature Maximum (°C). Histogram was illustrated using 10 bins. Y axis is shown at 10^{-2}.

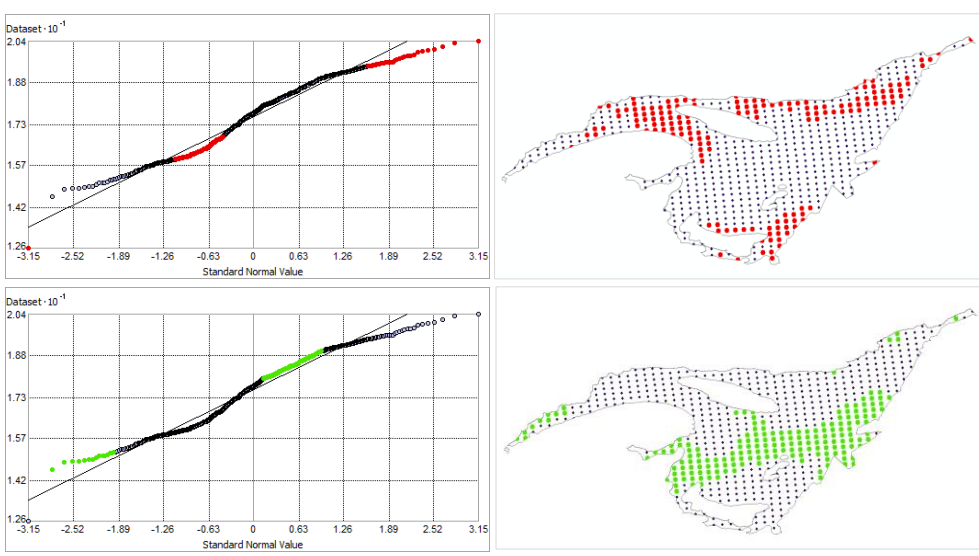

Fig. 52. Normal Q-Q plot for data values of Surface Temperature Maximum (°C). Points falling under (upper panel) and over (bottom panel) the reference line are mapped.

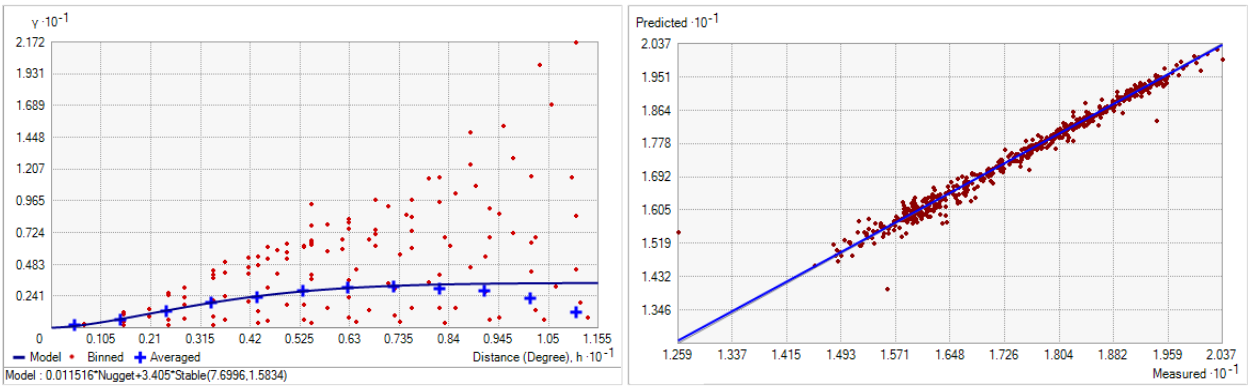

Fig. 53. Left panel: Semivariogram of Surface Temperature Maximum (°C). Binned values are shown as red dots; average points are shown as blue crosses; the model fit to the averaged values is shown as a blue line. Lag size: 0.962 degrees; number of lags: 12; Parameter: 2; Range: 7.700 degrees; Partial Sill: 3.405. Right panel: Scatterplot of predicted values versus observed values for the model of Surface Temperature Maximum (°C).

Table 22. Results of cross-validation of the kriged model for the Surface Temperature Maximum (°C).

Prediction error	**Value**
Number of Observations	606
Overall Mean Error	3.379×10^{-4}
Root Mean Square Prediction Error	0.202
Standardized Mean	-0.002
Standardized Root Mean Square Prediction Error	0.981
Average Standard Error	0.167

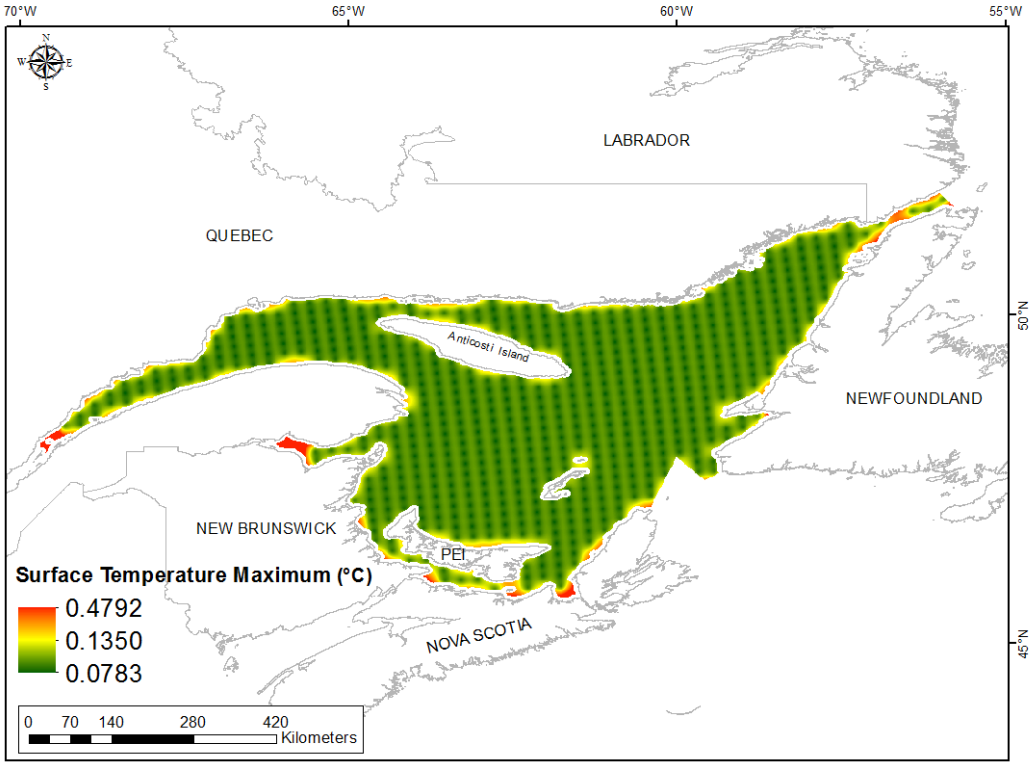

Fig. 54. Prediction standard error surface of Surface Temperature Maximum (˚C).

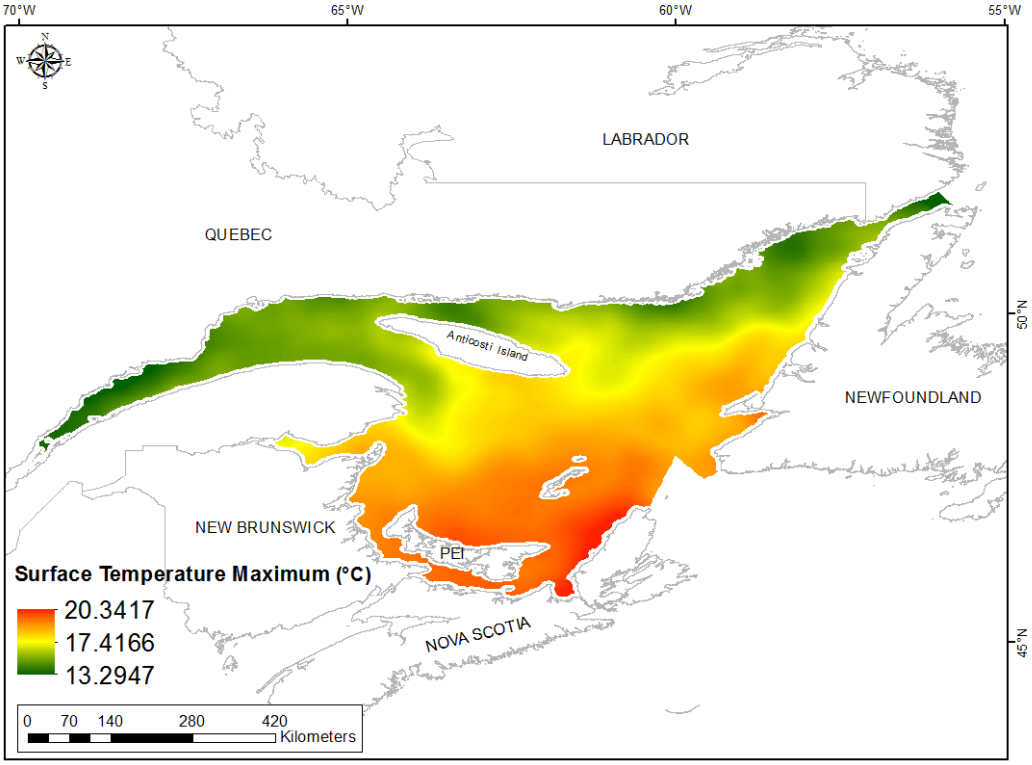

Fig. 55. Interpolated prediction surface of Surface Temperature Maximum (˚C).

Surface Temperature Range

This variable displayed a plateau-like distribution prior to modeling (Table 23, Fig. 56). The data deviated slightly from a normal distribution, particularly at the tails (Fig. 57). These data points were spatially cohesive with specific areas of over- and under-prediction (Fig. 57).

The semivariogram showed weak autocorrelation present in the data and there was an excellent predictive fit (Fig. 58). The kriged model showed excellent cross-validation statistics (Table 24). The error map showed a 'bullseye' pattern with error increasing with distance from data points (Fig. 59). The kriged surface is presented in Fig. 60.

Table 23. Distributional properties of Surface Temperature Range (°C).

Property	Value
Number of Observations	606
Minimum	14.404
Maximum	21.940
Mean	19.138
Median	19.332
Standard Deviation	1.312
Skewness	-0.293
Kurtosis	2.253

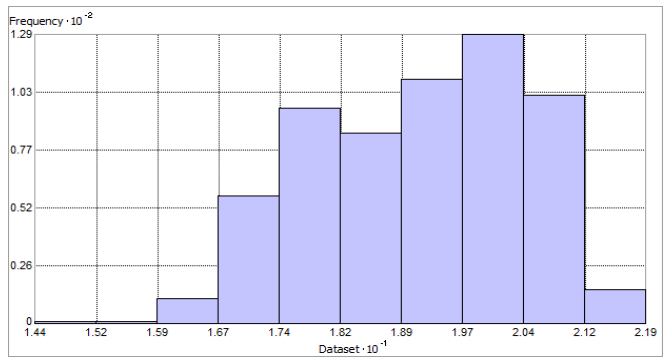

Fig. 56. Distribution of Surface Temperature Range (°C). Histogram was illustrated using 10 bins. X axis shown at 10^{-1}; Y axis is shown at 10^{-2}.

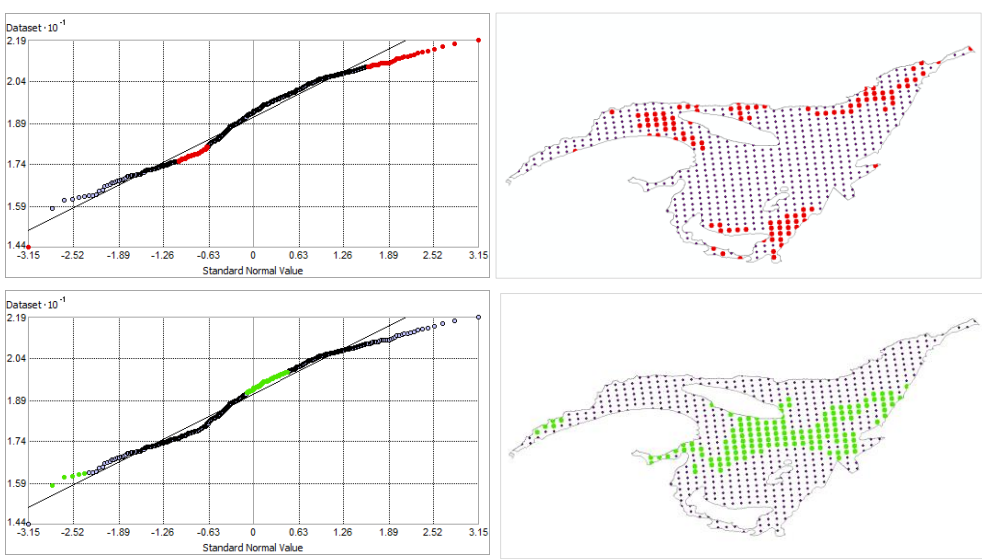

Fig. 57. Normal Q-Q plot for data values of Surface Temperature Range (°C). Points falling under (upper panel) and over (bottom panel) the reference line are mapped.

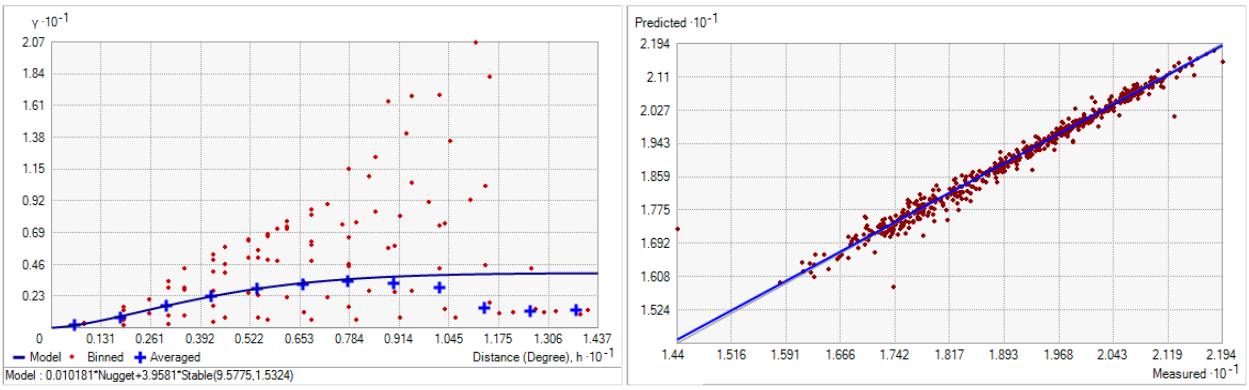

Fig. 58. Left panel: Semivariogram of Surface Temperature Range (°C). Binned values are shown as red dots; average points are shown as blue crosses; the model fit to the averaged values is shown as a blue line. Lag size: 1.197 degrees; number of lags: 12; Parameter: 1.532; Range: 9.577 degrees; Partial Sill: 3.958. Right panel: Scatterplot of predicted values versus observed values for the model of Surface Temperature Range (°C).

Table 24. Results of cross-validation of the kriged model for the Surface Temperature Range (°C).

Prediction error	**Value**
Number of Observations	606
Overall Mean Error	7.321×10^{-5}
Root Mean Square Prediction Error	0.205
Standardized Mean	-0.002
Standardized Root Mean Square Prediction Error	1.006
Average Standard Error	0.165

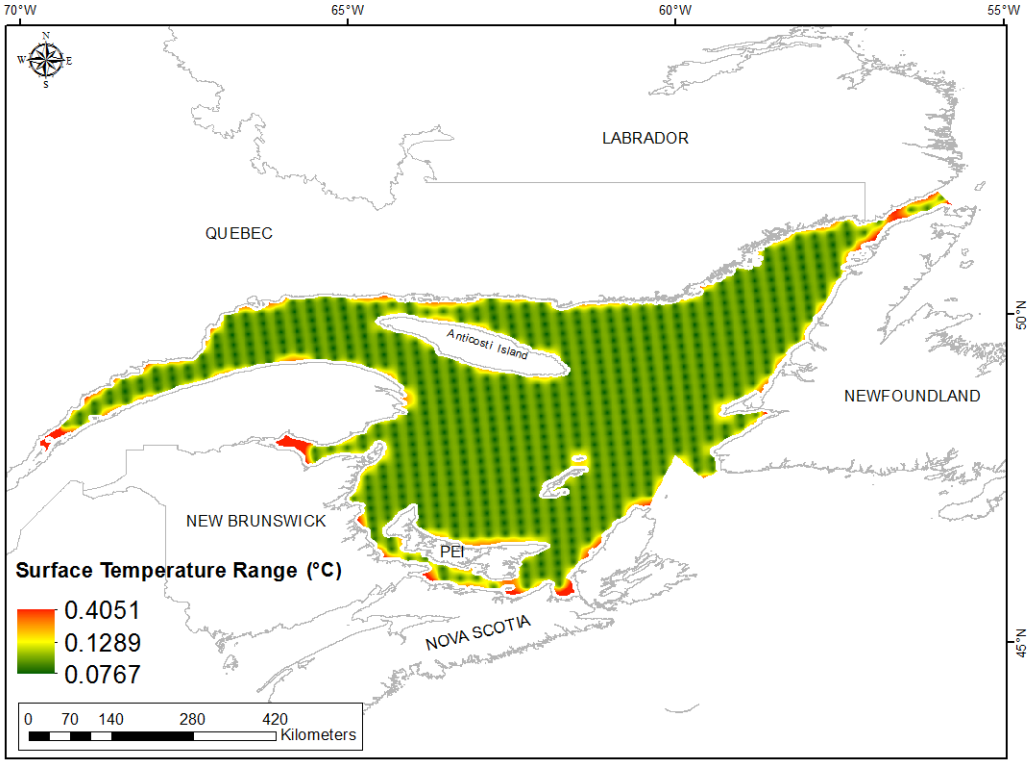

Fig. 59. Prediction standard error surface of Surface Temperature Range (˚C).

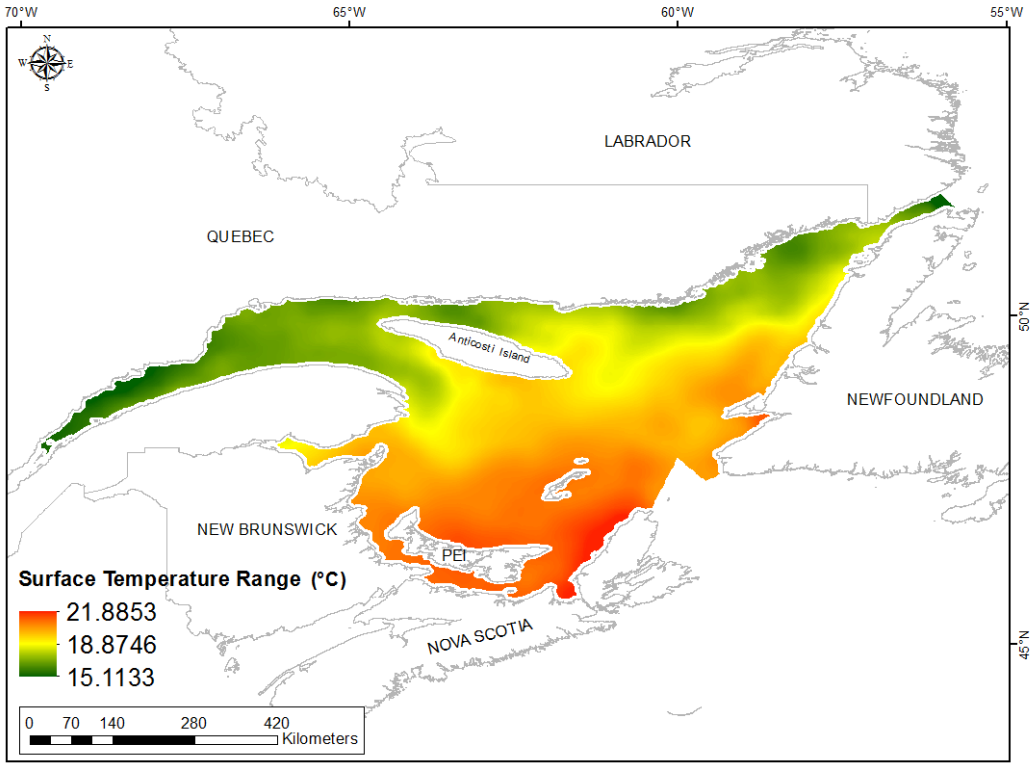

Fig. 60. Interpolated prediction surface of Surface Temperature Range (˚C).

Surface Temperature Average Minimum

This variable displayed a right-skewed distribution prior to modelling (Table 25, Fig. 61). This skewness was evident in the Q-Q plot where the upper data range showed deviation from the reference line (Fig. 62). These data points were spatially cohesive with specific areas of over-prediction and two small areas of under-prediction (Fig. 62).

The semivariogram showed moderate autocorrelation present in the data and there was an excellent predictive fit (Fig. 63). However, the model showed poor cross-validation statistics (Table 26). The standardized root mean square was greater than 1 indicating that variability in the predictions has been underestimated. The error map showed low error and no strong spatial pattern over the spatial extent although error was highest along the coast (Fig. 64). The kriged surface is presented in Fig. 65.

Table 25. Distributional properties of Surface Temperature Average Minimum (°C).

Property	Value
Number of Observations	606
Minimum	-1.680
Maximum	-0.481
Mean	-1.312
Median	-1.321
Standard Deviation	0.157
Skewness	0.760
Kurtosis	5.745

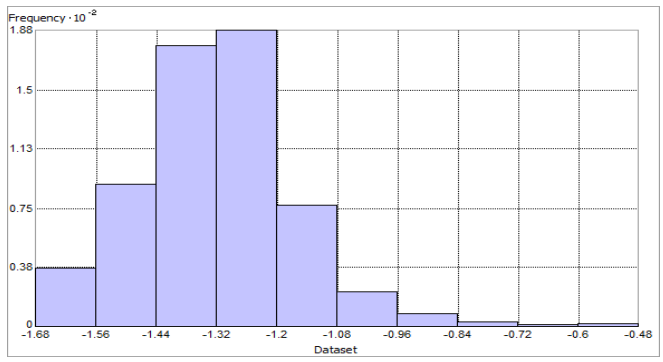

Fig. 61. Distribution of Surface Temperature Average Minimum (°C). Histogram was illustrated using 10 bins. Y axis is shown at 10^{-2}.

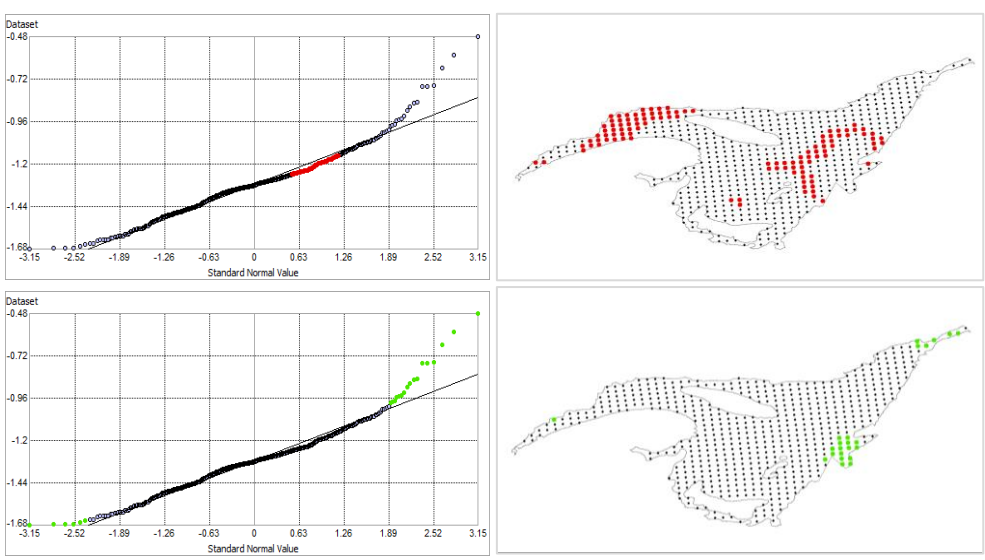

Fig. 62. Normal Q-Q plot for data values of Surface Temperature Average Minimum (°C). Points falling under (upper panel) and over (bottom panel) the reference line are mapped.

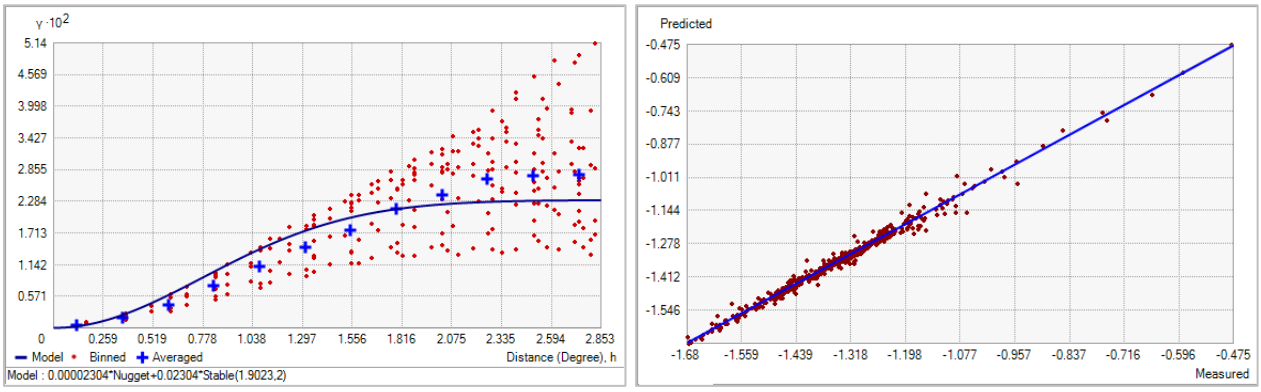

Fig. 63. Left panel: Semivariogram of Surface Temperature Average Minimum (°C). Binned values are shown as red dots; average points are shown as blue crosses; the model fit to the averaged values is shown as a blue line. Lag size: 0.238 degrees; number of lags: 12; Parameter: 2; Range: 1.902 degrees; Partial Sill: 0.023. Right panel: Scatterplot of predicted values versus observed values for the model of Surface Temperature Average Minimum (°C).

Table 26. Results of cross-validation of the kriged model for the Surface Temperature Average Minimum (°C).

Prediction error	**Value**
Number of Observations	606
Overall Mean Error	2.426×10^{-4}
Root Mean Square Prediction Error	0.017
Standardized Mean	0.011
Standardized Root Mean Square Prediction Error	2.542
Average Standard Error	0.006

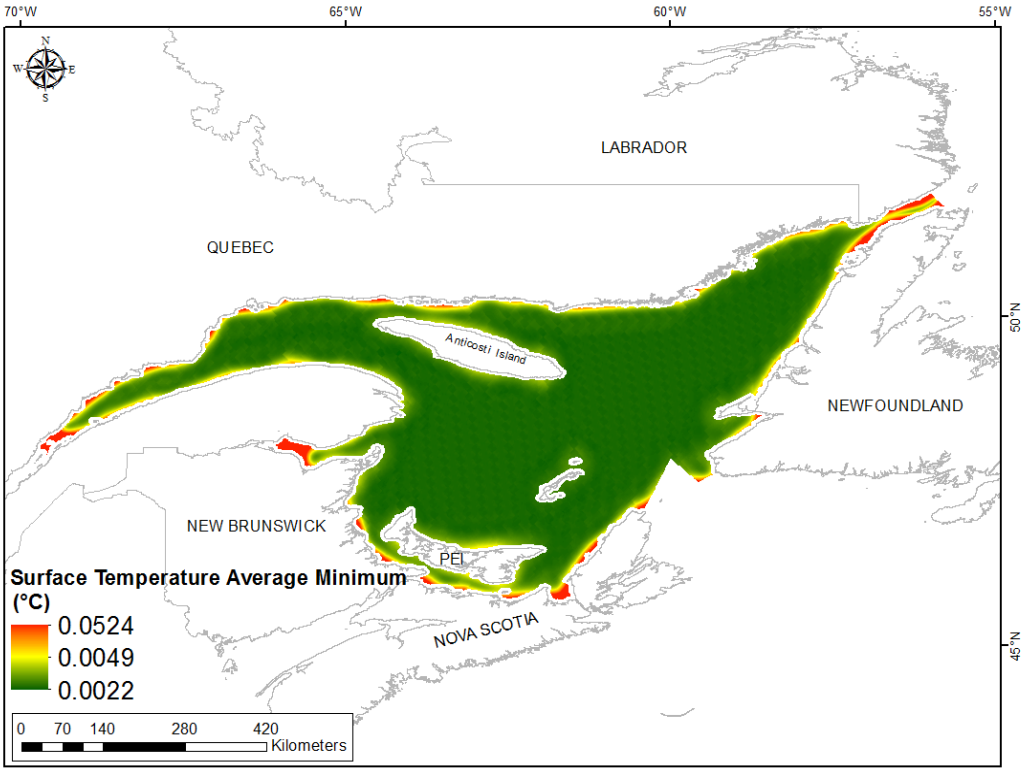

Fig. 64. Prediction standard error surface of Surface Temperature Average Minimum (˚C).

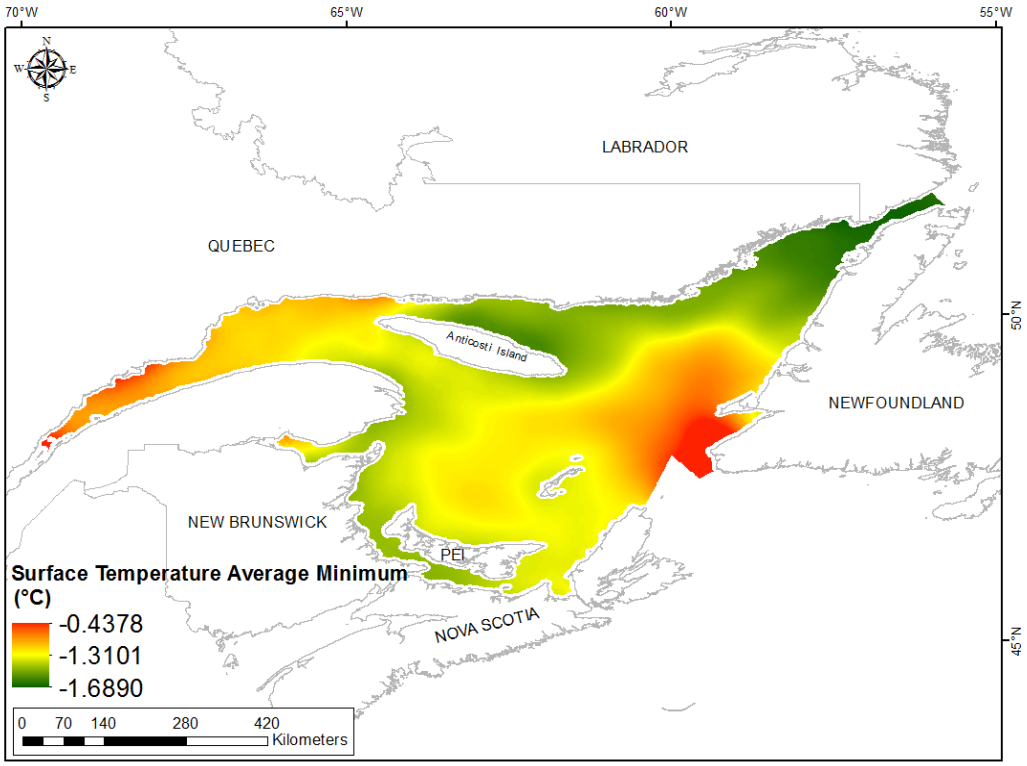

Fig. 65. Interpolated prediction surface of Surface Temperature Average Minimum (˚C).

Surface Temperature Average Maximum

This variable displayed a plateau-like distribution prior to modeling (Table 27, Fig. 66). The data showed only slight deviations from a standard normal distribution with the lower tail being higher than predicted and the upper tail being lower than predicted by a normal distribution (Fig. 67). These data points were spatially cohesive with specific areas of over-and under-prediction with the latter being more extensive (Fig. 67).

The semivariogram showed weak autocorrelation present in the data but excellent predictive fit (Fig. 68). However, the model showed poor cross-validation statistics (Table 28). The standardized root mean square was greater than 1 indicating that variability in the predictions has been underestimated. The error map showed low error and no strong spatial pattern over the spatial extent but was higher along the coast (Fig. 69). The kriged surface is presented in Fig. 70.

Table 27. Distributional properties of Surface Temperature Average Maximum (°C).

Property	Value
Number of Observations	606
Minimum	10.400
Maximum	19.186
Mean	15.956
Median	16.055
Standard Deviation	1.591
Skewness	-0.194
Kurtosis	2.237

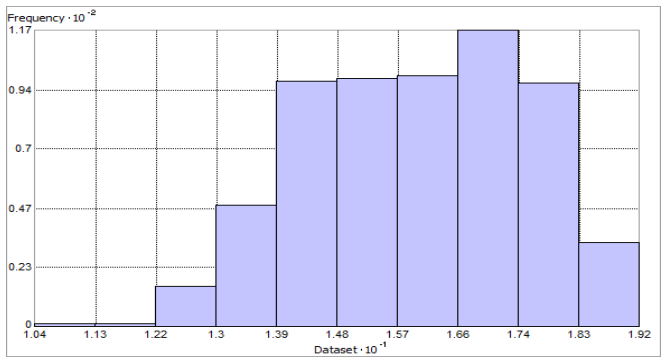

Fig. 66. Distribution of Surface Temperature Average Maximum (°C). Histogram was illustrated using 10 bins. X axis is shown at 10^{-1}; Y axis is shown at 10^{-2}.

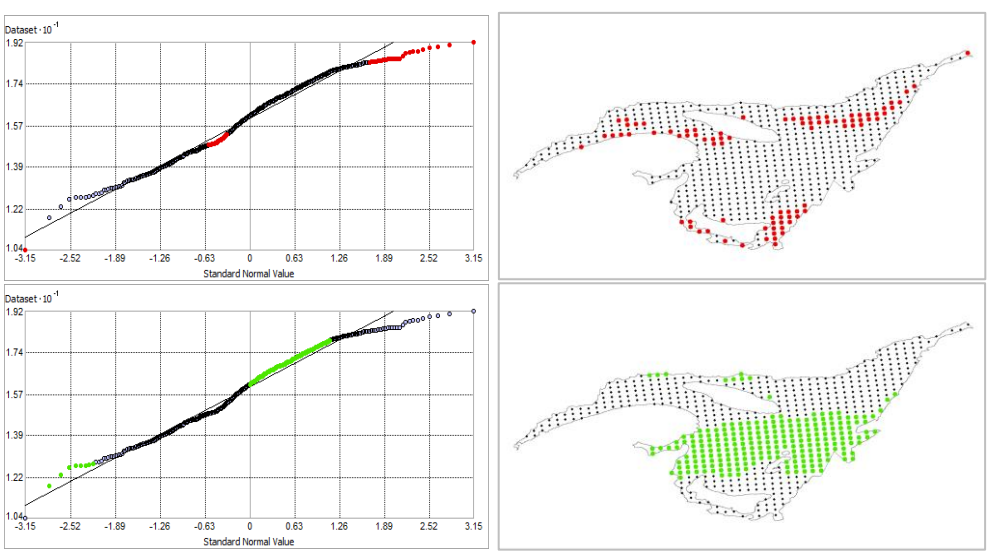

Fig 67. Normal Q-Q plot for data values of Surface Temperature Average Maximum (°C). Points falling under (upper panel) and over (bottom panel) the reference line are mapped.

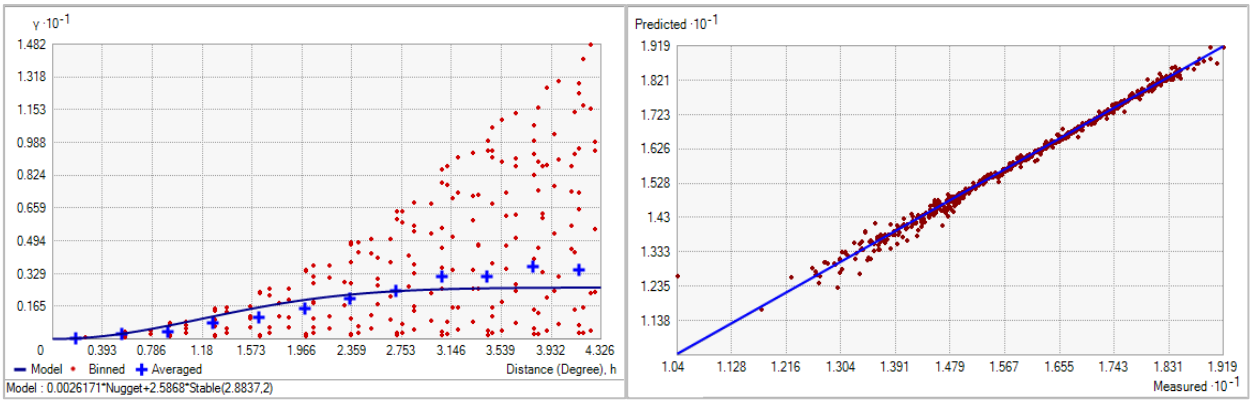

Fig. 68. Left panel: Semivariogram of Surface Temperature Average Maximum (°C). Binned values are shown as red dots; average points are shown as blue crosses; the model fit to the averaged values is shown as a blue line. Lag size: 0.360 degrees; number of lags: 12; Parameter: 2; Range: 2.883 degrees; Partial Sill: 2.587. Right panel: Scatterplot of predicted values versus observed values for the model of Surface Temperature Average Maximum (°C).

Table 28. Results of cross-validation of the kriged model for the Surface Temperature Average Maximum (°C).

Prediction error	**Value**
Number of Observations	606
Overall Mean Error	1.802×10^{-3}
Root Mean Square Prediction Error	0.152
Standardized Mean	-0.012
Standardized Root Mean Square Prediction Error	1.959
Average Standard Error	0.060

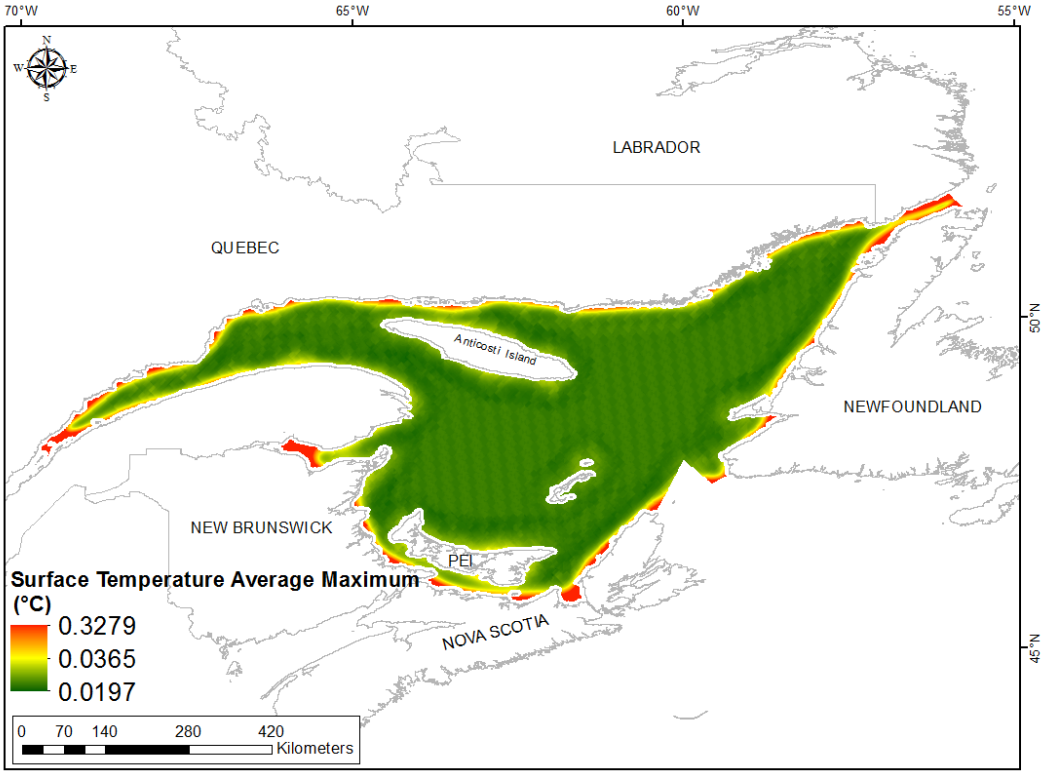

Fig. 69. Prediction standard error surface of Surface Temperature Average Maximum (˚C).

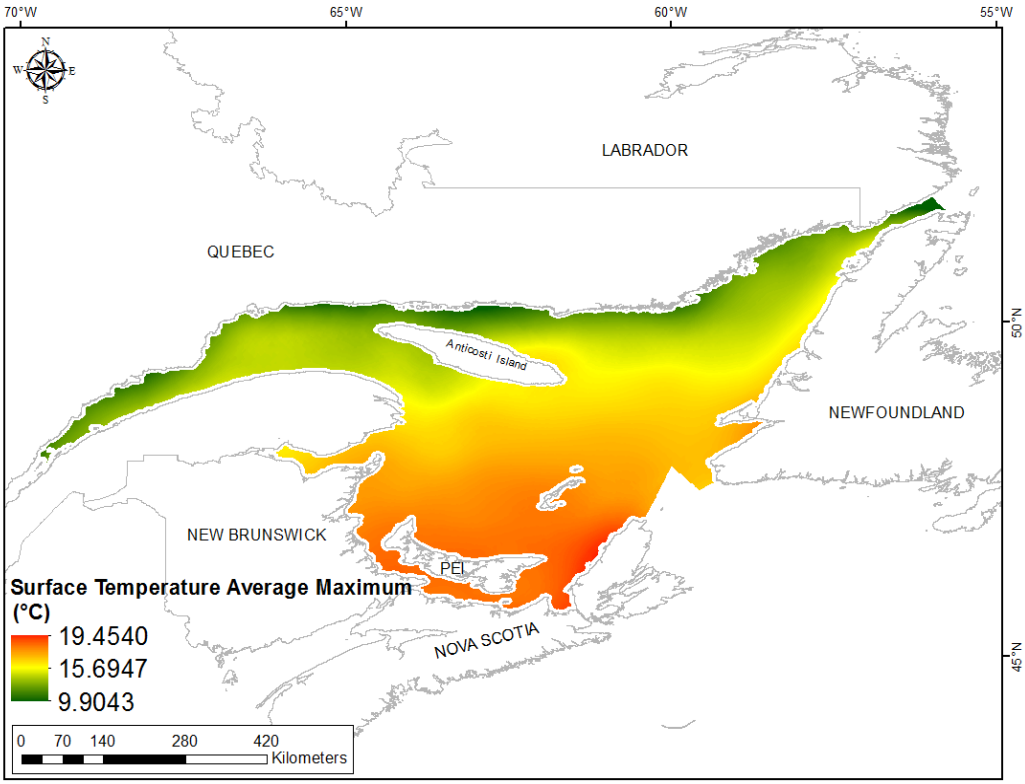

Fig. 70. Interpolated prediction surface of Surface Temperature Average Maximum (˚C).

Surface Temperature Average Range

This variable displayed a plateau-like distribution prior to modeling (Table 29, Fig. 71). The data deviated slightly from a normal distribution with the lower and upper tails being over- and under-predicted (Fig. 72). These data points were spatially cohesive with specific areas of over- and under-prediction with the latter being more extensive (Fig. 72).

The semivariogram showed weak autocorrelation present in the data and there was an excellent predictive fit (Fig. 73). However, the model showed poor cross-validation statistics (Table 30). The standardized root mean square was greater than 1 indicating that variability in the predictions has been underestimated. The error map showed low error and no strong spatial pattern over the spatial extent but was higher along the coast (Fig. 74). The kriged surface is presented in Fig. 75.

Table 29. Distributional properties of Surface Temperature Average Range (°C).

Property	Value
Number of Observations	606
Minimum	8.752
Maximum	17.888
Mean	14.770
Median	14.639
Standard Deviation	1.634
Skewness	-0.242
Kurtosis	2.193

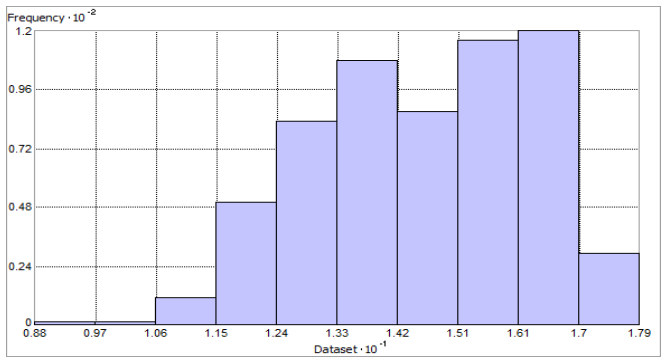

Fig. 71. Distribution of Surface Temperature Average Range (°C). Histogram was illustrated using 10 bins. X axis is shown at 10^{-1}; Y axis is shown at 10^{-2}.

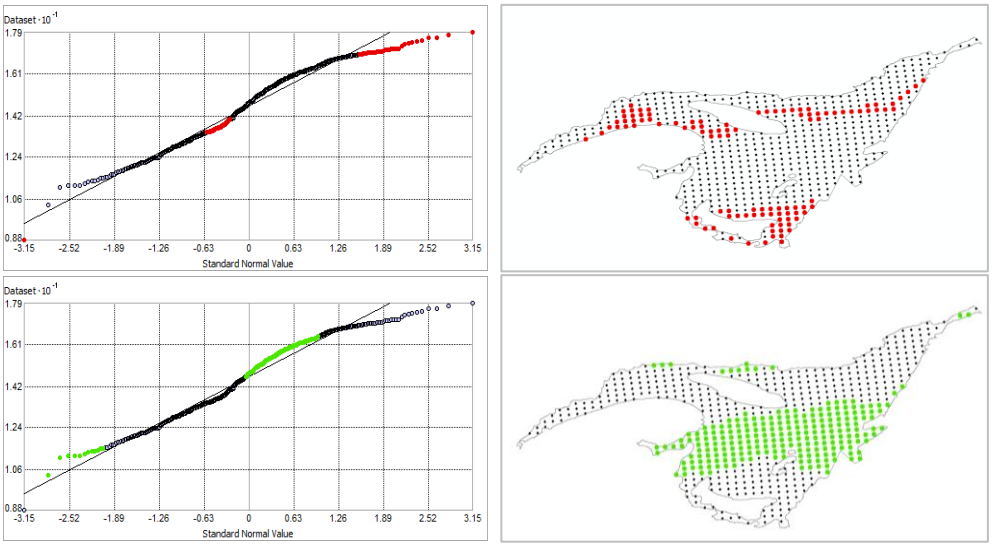

Fig. 72. Normal Q-Q plot for data values of Surface Temperature Range (°C). Points falling under (upper panel) and over (bottom panel) the reference line are mapped.

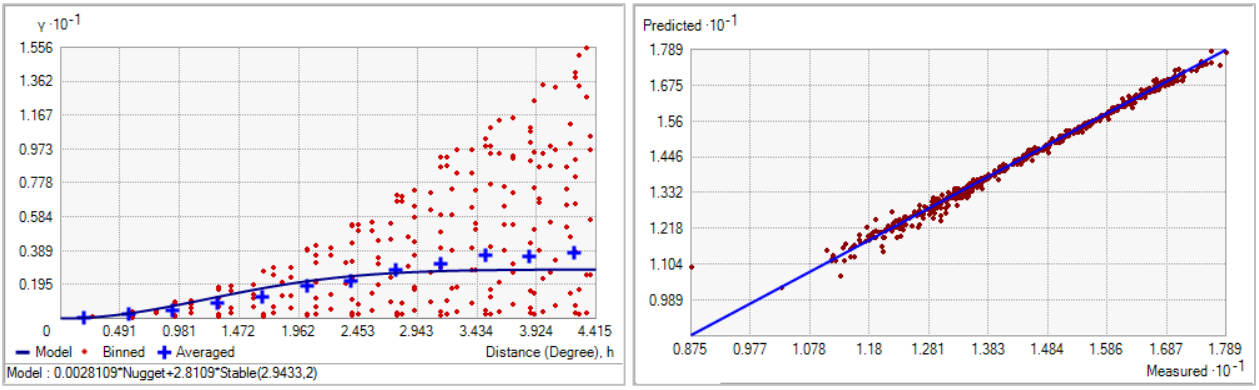

Fig. 73. Left panel: Semivariogram of Surface Temperature Average Range (°C). Binned values are shown as red dots; average points are shown as blue crosses; the model fit to the averaged values is shown as a blue line. Lag size: 0.368 degrees; number of lags: 12; Parameter: 2; Range: 2.943 degrees; Partial Sill: 2.811. Right panel: Scatterplot of predicted values versus observed values for the model of Surface Temperature Average Range (°C).

Table 30. Results of cross-validation of the kriged model for the Surface Temperature Average Range (°C).

Prediction error	**Value**
Number of Observations	606
Overall Mean Error	1.639×10^{-3}
Root Mean Square Prediction Error	0.148
Standardized Mean	-0.014
Standardized Root Mean Square Prediction Error	1.846
Average Standard Error	0.062

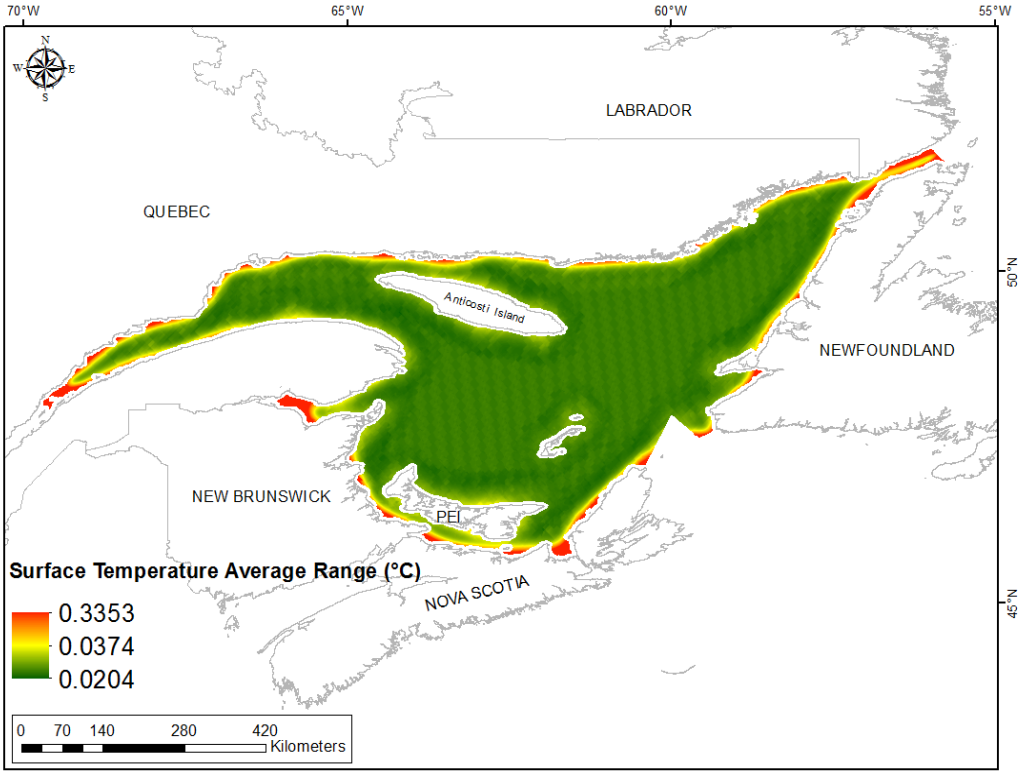

Fig. 74. Prediction standard error surface of Surface Temperature Average Range (˚C).

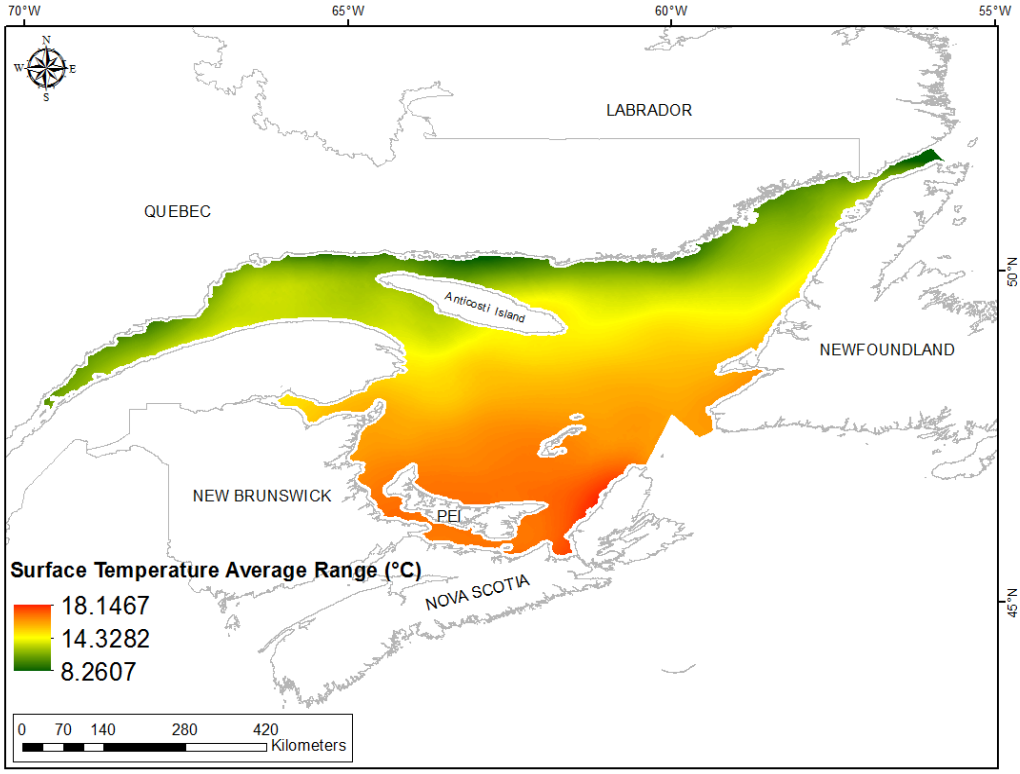

Fig. 75. Interpolated prediction surface of Surface Temperature Average Range (˚C).

Salinity

Salinity influences osmoregulation (control of osmosis and diffusion) and is a very important determinant of species distribution. Salinity also strongly influences the rate at which inorganic particles settle in response to changes in flocculation of the clay mineral kaolinite (Sutherland et al., 2014). This is particularly important in estuaries and deltas where clay minerals mix with marine waters.

Bottom Salinity Mean

This variable displayed a left-skewed distribution prior to modeling (Table 31, Fig. 76). The data deviated strongly from a normal distribution with lower and upper values falling under the reference line (Fig. 77). Mid-range values were slightly higher than predicted by a normal distribution. These data points were spatially cohesive with specific areas of over-prediction found in the eastern end of the Laurentian Channel and in the Northumberland Strait (Fig. 77).

The semivariogram showed moderate autocorrelation present in the data and there was a good predictive fit (Fig. 78). The kriged model showed fair cross-validation statistics (Table 32). The error map showed low error and no strong spatial pattern over the spatial extent but was slightly higher in the Gulf of St. Lawrence estuary and Chaleur Bay (Fig. 79). The kriged surface is presented in Fig. 80.

Table 31. Distributional properties of Bottom Salinity Mean.

Property	Value
Number of Observations	606
Minimum	26.087
Maximum	34.802
Mean	32.782
Median	32.976
Standard Deviation	1.780
Skewness	-1.321
Kurtosis	5.072

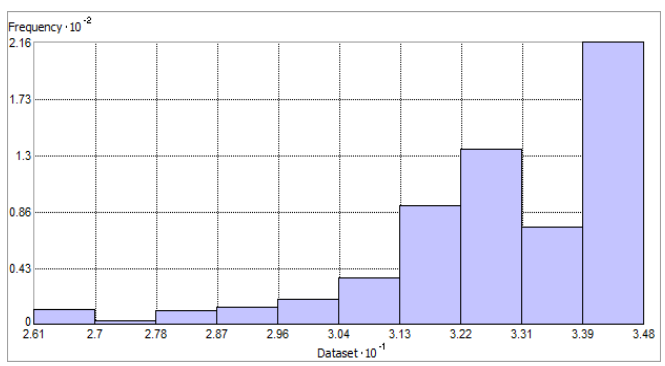

Fig. 76. Distribution of Bottom Salinity Mean. Histogram was illustrated using 10 bins. X axis shown at 10^{-1}; Y axis is shown at 10^{-2}.

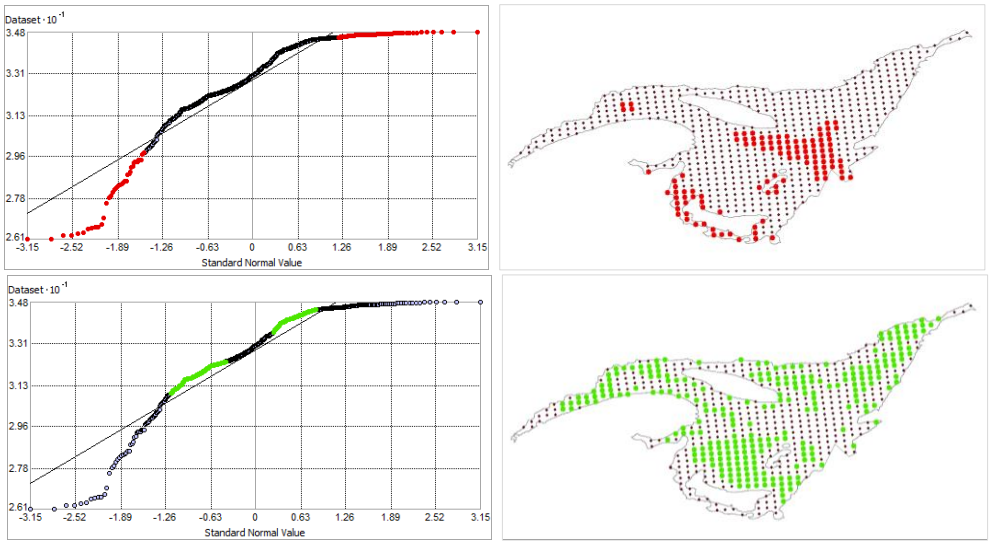

Fig. 77. Normal Q-Q plot for data values of Bottom Salinity Mean. Points falling under (upper panel) and over (bottom panel) the reference line are mapped.

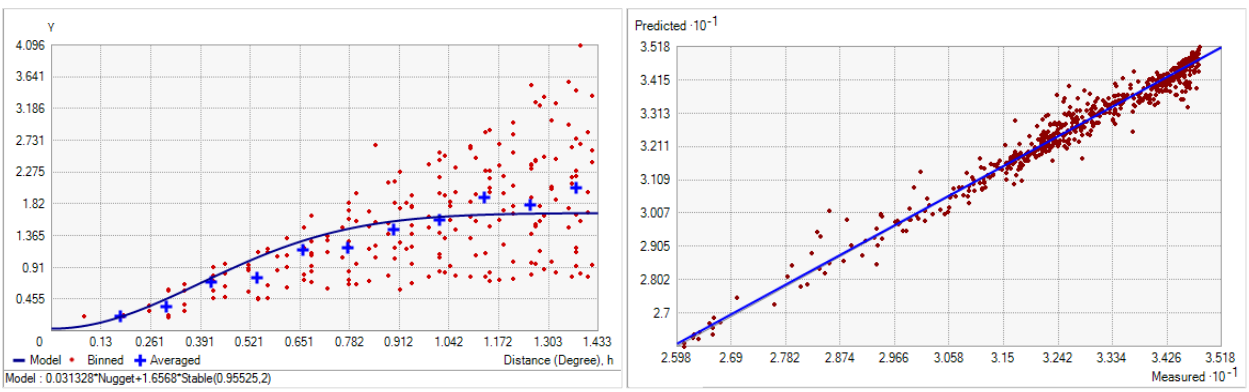

Fig. 78. Left panel: Semivariogram of Bottom Salinity Mean. Binned values are shown as red dots; average points are shown as blue crosses; the model fit to the averaged values is shown as a blue line. Lag size: 0.119 degrees; number of lags: 12; Parameter: 2; Range: 0.955 degrees; Partial Sill: 1.657. Right panel: Scatterplot of predicted values versus observed values for the model of Bottom Salinity Mean.

Table 32. Results of cross-validation of the kriged model for the Bottom Salinity Mean.

Prediction error	**Value**
Number of Observations	606
Overall Mean Error	0.016
Root Mean Square Prediction Error	0.329
Standardized Mean	0.035
Standardized Root Mean Square Prediction Error	1.313
Average Standard Error	0.254

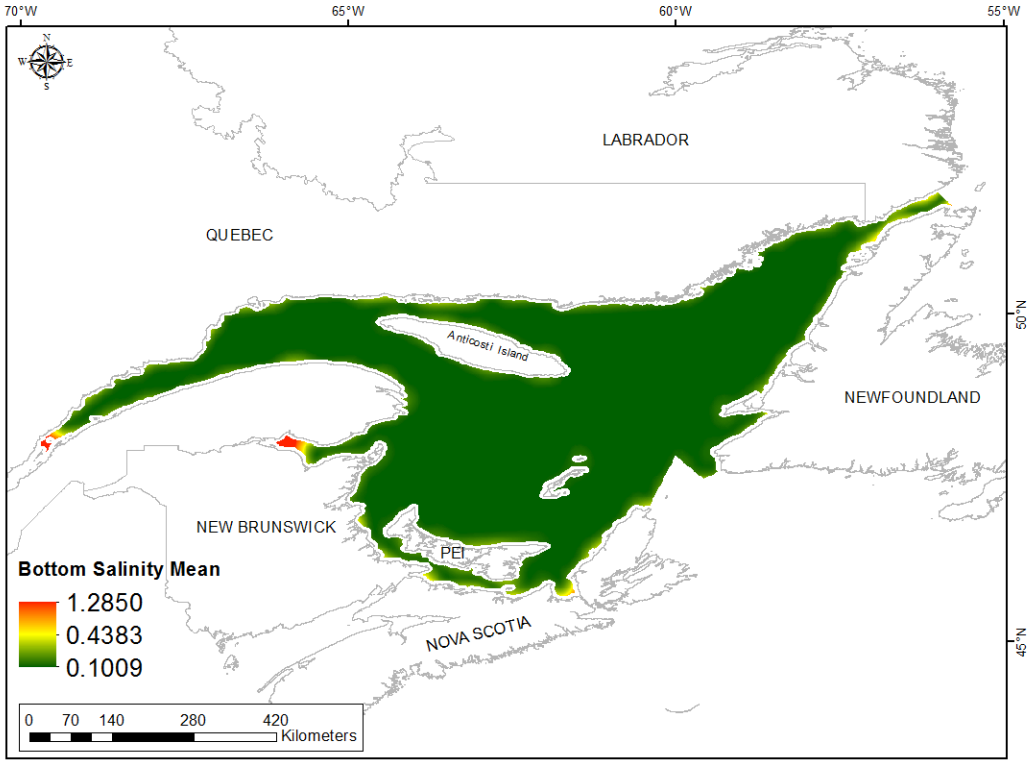

Fig. 79. Prediction standard error surface of Bottom Salinity Mean.

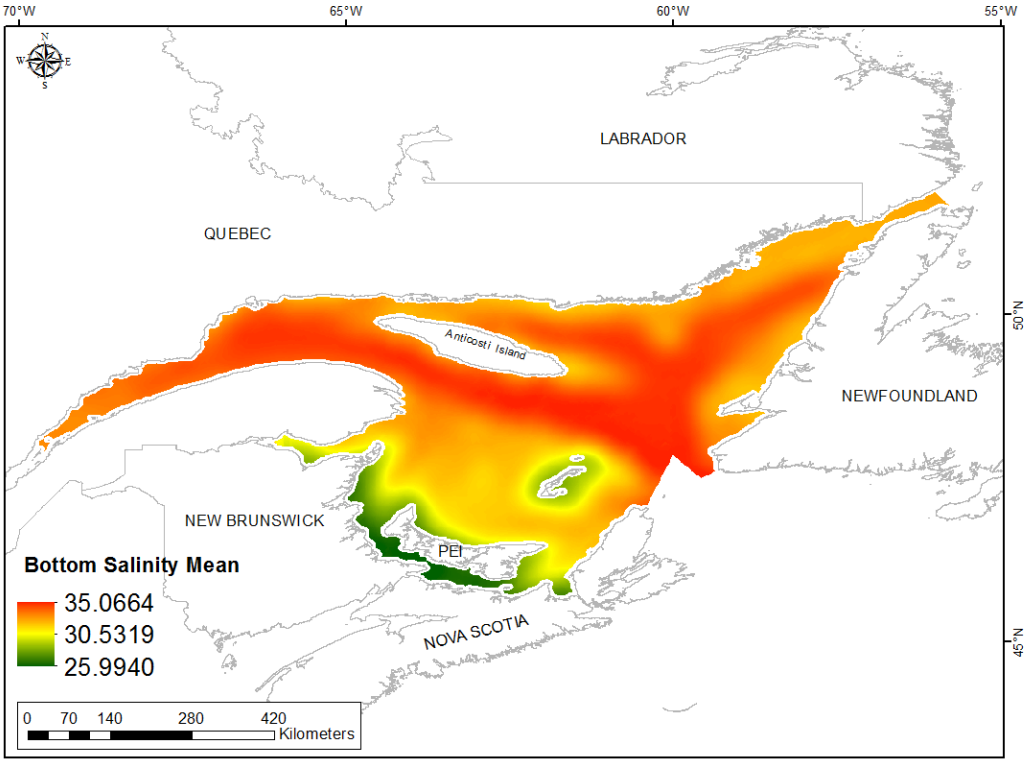

Fig. 80. Interpolated prediction surface of Bottom Salinity Mean.

Bottom Salinity Minimum

This variable displayed a left-skewed distribution prior to modeling (Table 33, Fig. 81). The data were lower than predicted by a normal distribution at low and high values (Fig. 82). Mid-range values were slightly higher than the reference line. These data points were spatially cohesive with specific areas of under-prediction found in the eastern end of the Laurentian Channel and in the Northumberland Strait with large areas of over-prediction (Fig. 82).

The semivariogram showed moderate autocorrelation present in the data and there was a good predictive fit (Fig. 83). The kriged model showed good cross-validation statistics (Table 34) indicating that it was good at prediction. The error map showed low error and no strong spatial pattern over the spatial extent but was slightly higher in the Gulf of St. Lawrence estuary and Chaleur Bay (Fig. 84). The kriged surface is presented in Fig. 85.

Table 33. Distributional properties of Bottom Salinity Minimum.

Property	Value
Number of Observations	606
Minimum	23.438
Maximum	34.541
Mean	31.990
Median	32.421
Standard Deviation	2.345
Skewness	-1.260
Kurtosis	4.398

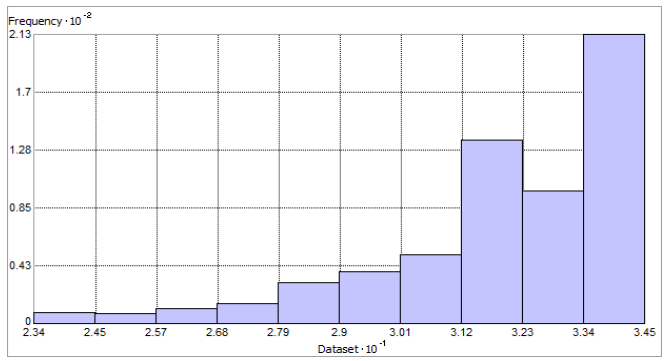

Fig. 81. Distribution of Bottom Salinity Minimum. Histogram was illustrated using 10 bins. X axis shown at 10^{-1}; Y axis is shown at 10^{-2}.

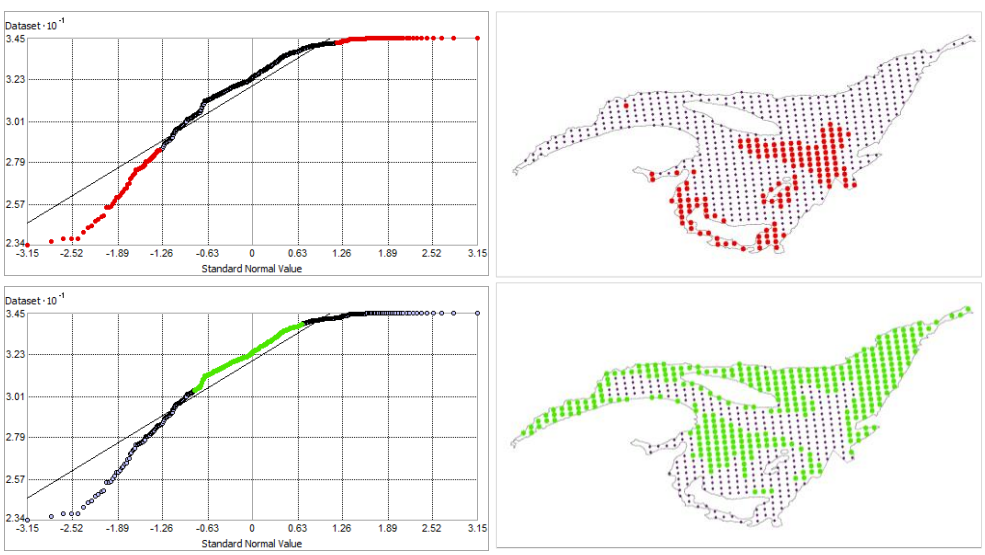

Fig. 82. Normal Q-Q plot for data values of Bottom Salinity Minimum. Points falling under (upper panel) and over (bottom panel) the reference line are mapped.

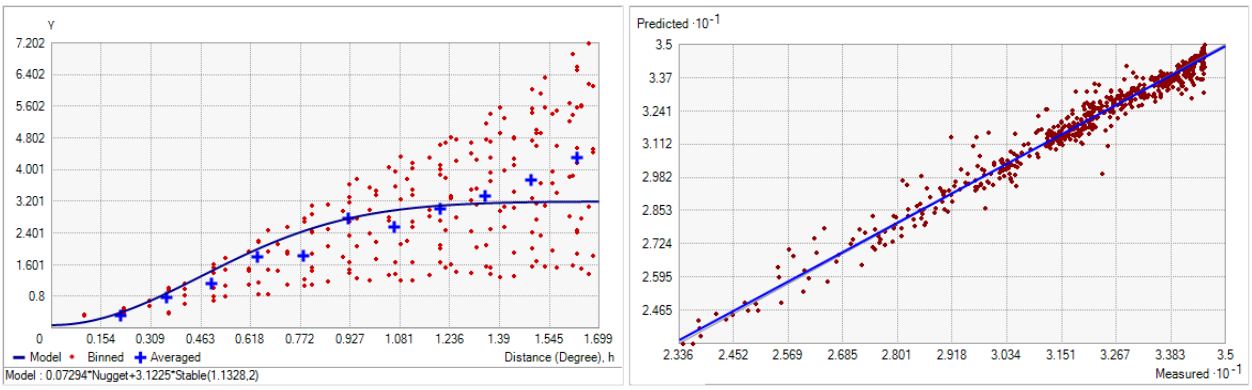

Fig. 83. Left panel: Semivariogram of Bottom Salinity Minimum. Binned values are shown as red dots; average points are shown as blue crosses; the model fit to the averaged values is shown as a blue line. Lag size: 0.142 degrees; number of lags: 12; Parameter: 2; Range: 1.133 degrees; Partial Sill: 3.122. Right panel: Scatterplot of predicted values versus observed values for the model of Bottom Salinity Minimum.

Table 34. Results of cross-validation of the kriged model for the Bottom Salinity Minimum.

Prediction error	**Value**
Number of Observations	606
Overall Mean Error	0.013
Root Mean Square Prediction Error	0.435
Standardized Mean	0.013
Standardized Root Mean Square Prediction Error	1.251
Average Standard Error	0.346

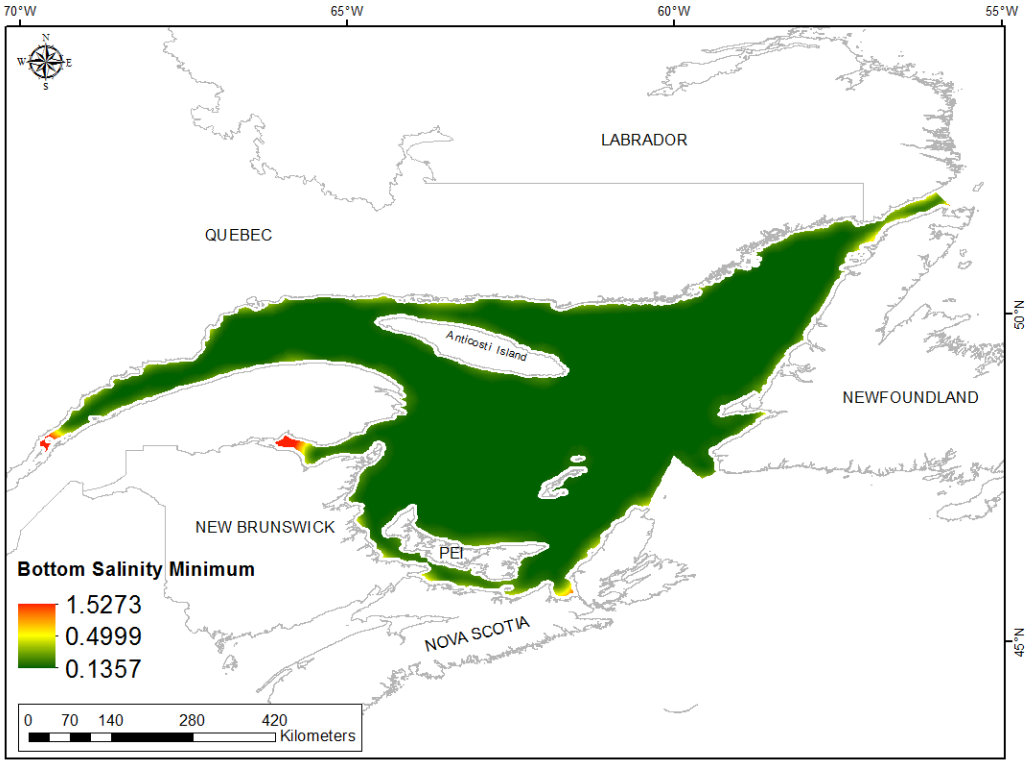

Fig. 84. Prediction standard error surface of Bottom Salinity Minimum.

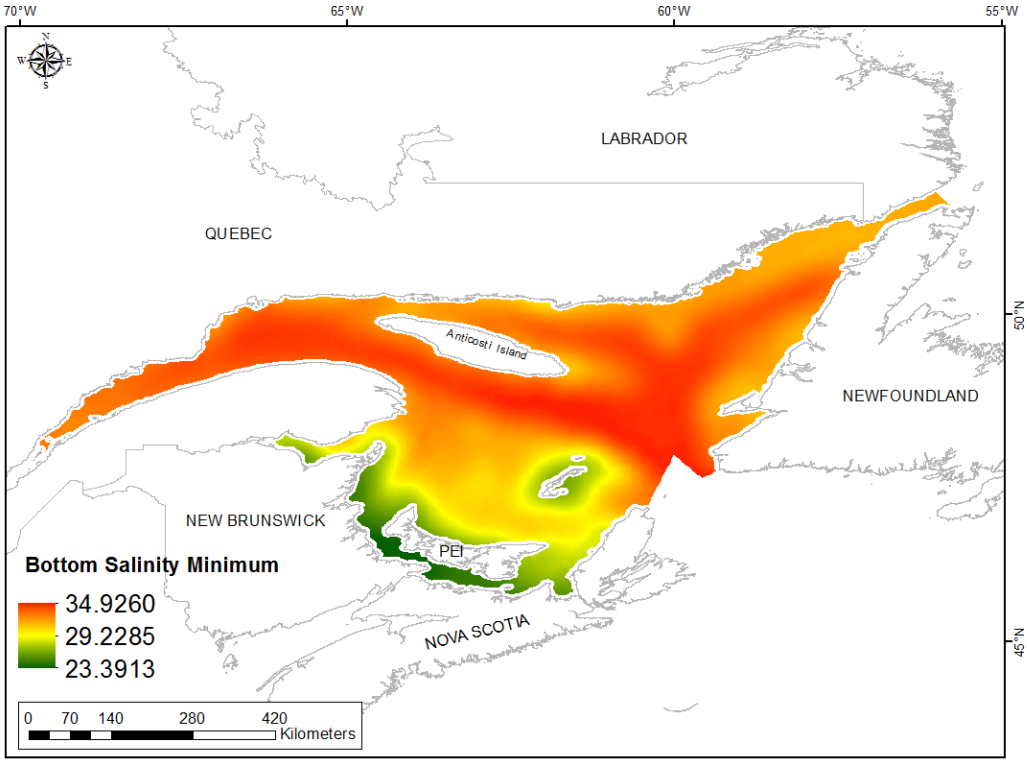

Fig. 85. Interpolated prediction surface of Bottom Salinity Minimum.

Bottom Salinity Maximum

This variable displayed a left-skewed distribution prior to modeling (Table 35, Fig. 86). The data were lower than predicted by a normal distribution at low and high values (Fig. 87). Mid-range values were slightly higher than the reference line. These data points were spatially cohesive with specific areas of under-prediction found in the Laurentian Channel and in the Northumberland Strait with large areas of over-prediction that were less cohesive (Fig. 87).

The semivariogram showed moderate autocorrelation present in the data and there was a good predictive fit (Fig. 88). The kriged model showed good cross-validation statistics (Table 36) indicating that it was good at prediction. The error map showed low error and no strong spatial pattern over the spatial extent but was higher along the coast (Fig. 89). The kriged surface is presented in Fig. 90.

Table 35. Distributional properties of Bottom Salinity Maximum.

Property	Value
Number of Observations	606
Minimum	28.376
Maximum	35.442
Mean	33.425
Median	33.524
Standard Deviation	1.388
Skewness	-0.962
Kurtosis	3.918

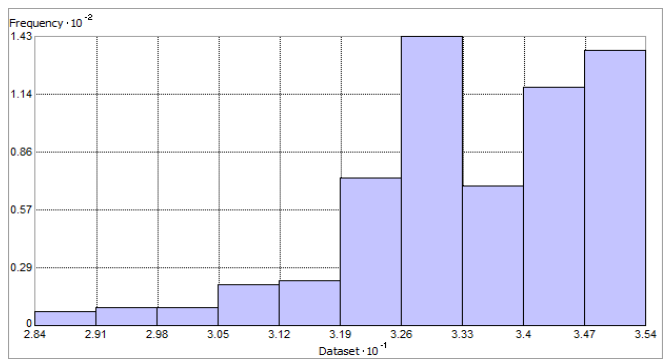

Fig. 86. Distribution of Bottom Salinity Maximum. Histogram was illustrated using 10 bins. X axis shown at 10^{-1}; Y axis is shown at 10^{-2}.

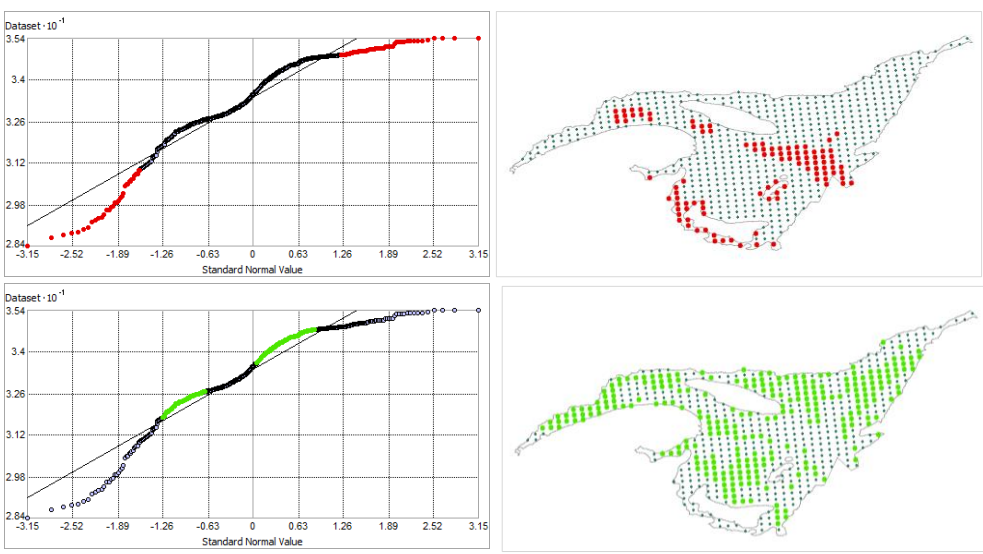

Fig. 87. Normal Q-Q plot for data values of Bottom Salinity Maximum. Points falling under (upper panel) and over (bottom panel) the reference line are mapped.

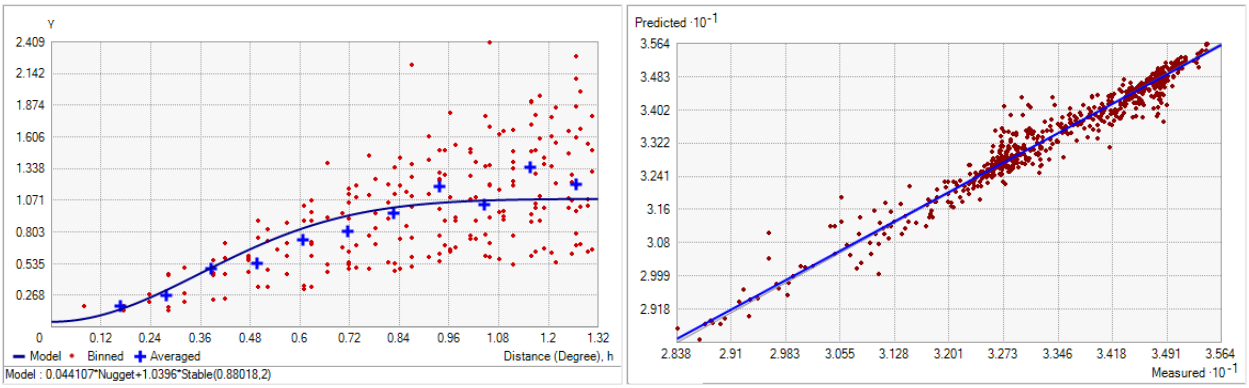

Fig. 88. Left panel: Semivariogram of Bottom Salinity Maximum. Binned values are shown as red dots; average points are shown as blue crosses; the model fit to the averaged values is shown as a blue line. Lag size: 0.100 degrees; number of lags: 12; Parameter: 2; Range: 0.800 degrees; Partial Sill: 6.547. Right panel: Scatterplot of predicted values versus observed values for the model of Bottom Salinity Maximum.

Table 36. Results of cross-validation of the kriged model for the Bottom Salinity Maximum.

Prediction error	**Value**
Number of Observations	606
Overall Mean Error	0.012
Root Mean Square Prediction Error	0.307
Standardized Mean	0.021
Standardized Root Mean Square Prediction Error	1.065
Average Standard Error	0.288

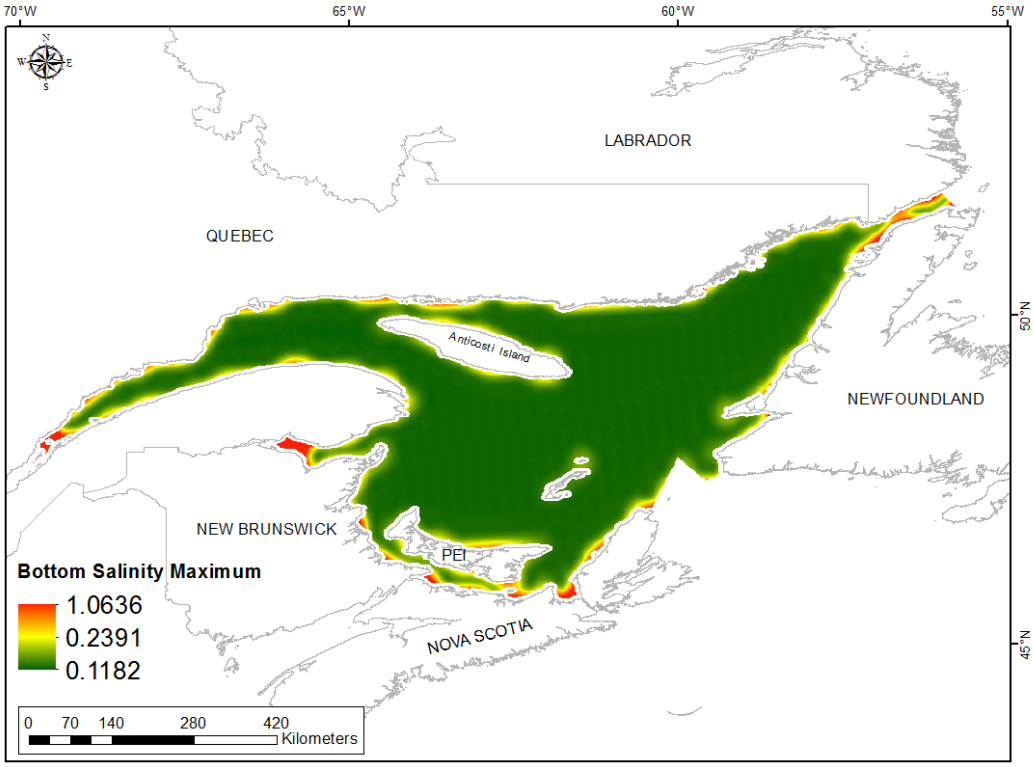

Fig. 89. Prediction standard error surface of Bottom Salinity Maximum.

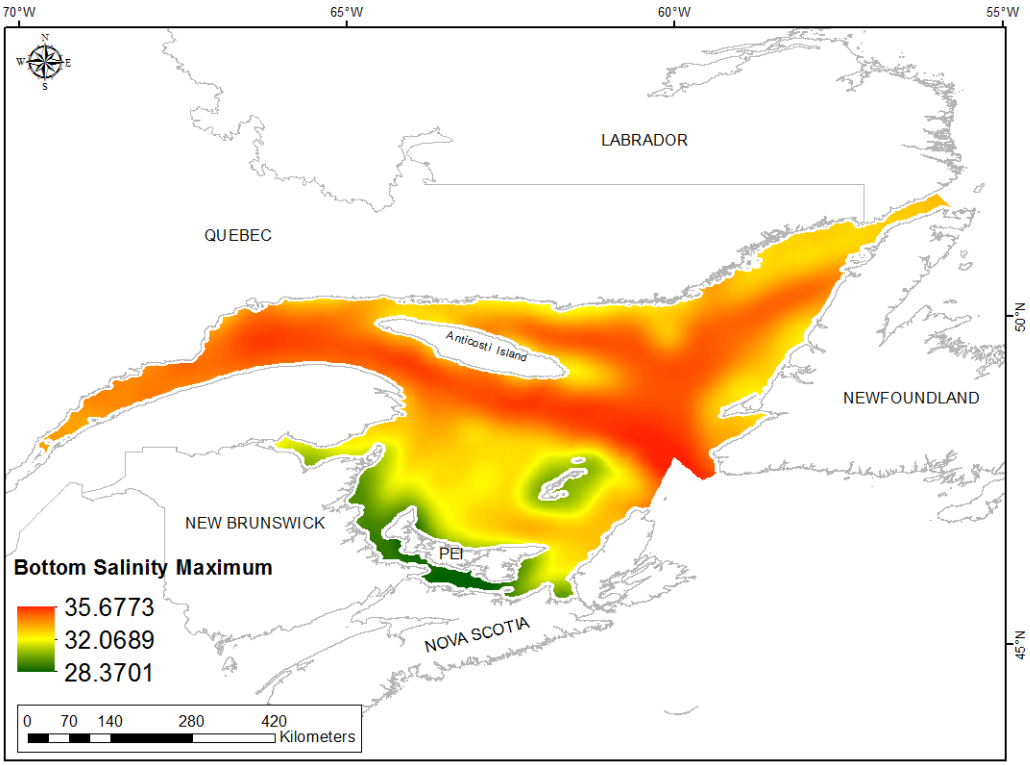

Fig. 90. Interpolated prediction surface of Bottom Salinity Maximum.

Bottom Salinity Range

This variable displayed a right-skewed distribution prior to modeling (Table 37, Fig. 91). The data deviated strongly from a normal distribution at both the tails and mid-values (Fig. 92). Values under and over the reference line showed a spatial pattern (Fig. 92).

The semivariogram showed moderate autocorrelation present in the data and there was a good predictive fit (Fig. 93). The kriged model showed fair cross-validation statistics (Table 38). The error map showed low error and no strong spatial pattern over the spatial extent but was higher along the coast (Fig. 94). The kriged surface is presented in Fig. 95.

Table 37. Distributional properties of Bottom Salinity Range.

Property	Value
Number of Observations	606
Minimum	0.310
Maximum	5.575
Mean	1.435
Median	1.050
Standard Deviation	1.060
Skewness	1.671
Kurtosis	5.272

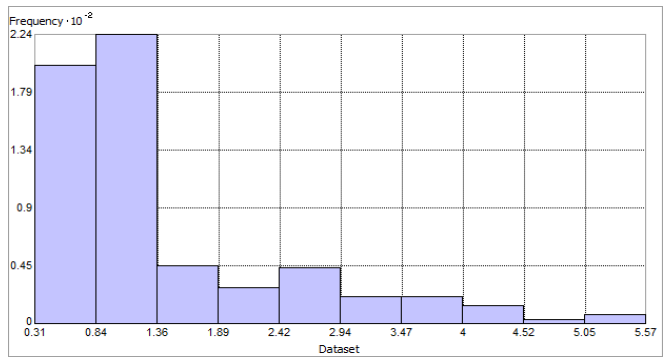

Fig. 91. Distribution of Bottom Salinity Range. Histogram was illustrated using 10 bins. Y axis is shown at 10^{-2}.

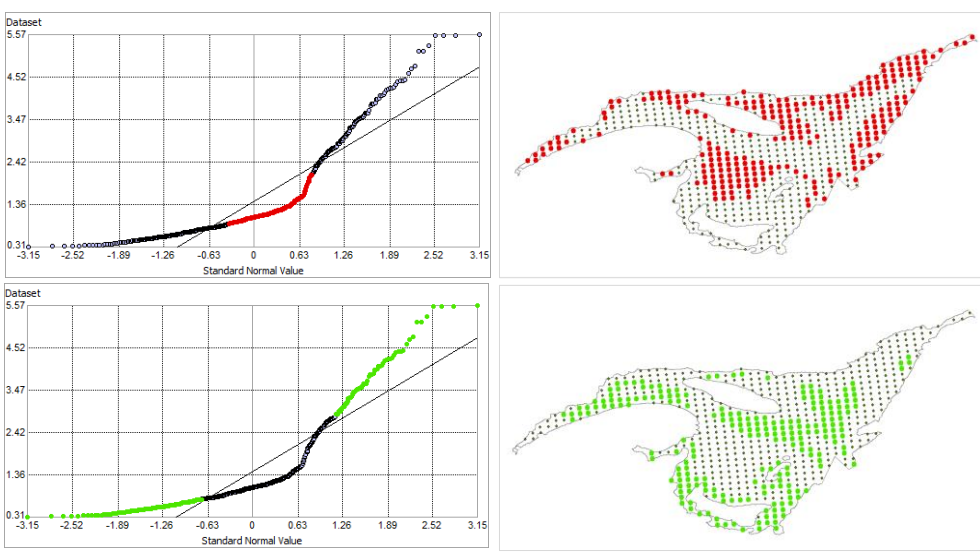

Fig. 92. Normal Q-Q plot for data values of Bottom Salinity Range. Points falling under (upper panel) and over (bottom panel) the reference line are mapped.

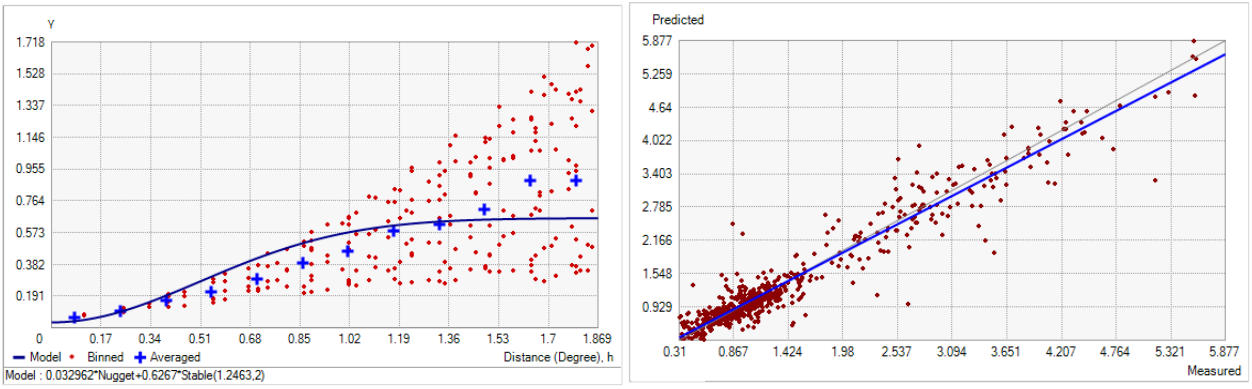

Fig. 93. Left panel: Semivariogram of Bottom Salinity Range. Binned values are shown as red dots; average points are shown as blue crosses; the model fit to the averaged values is shown as a blue line. Lag size: 0.156 degrees; number of lags: 12; Parameter: 2; Range: 1.246 degrees; Partial Sill: 0.627. Right panel: Scatterplot of predicted values versus observed values for the model of Bottom Salinity Range.

Table 38. Results of cross-validation of the kriged model for the Bottom Salinity Range.

Prediction error	**Value**
Number of Observations	606
Overall Mean Error	-0.003
Root Mean Square Prediction Error	0.299
Standardized Mean	-0.002
Standardized Root Mean Square Prediction Error	1.354
Average Standard Error	0.216

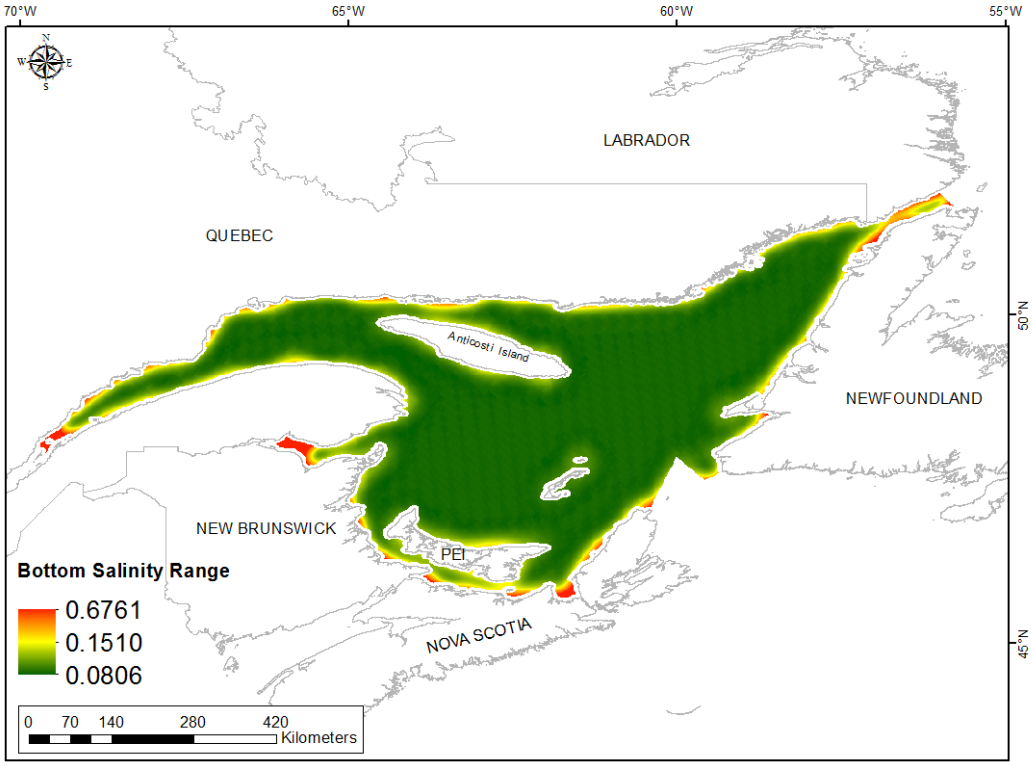

Fig. 94. Prediction standard error surface of Bottom Salinity Range.

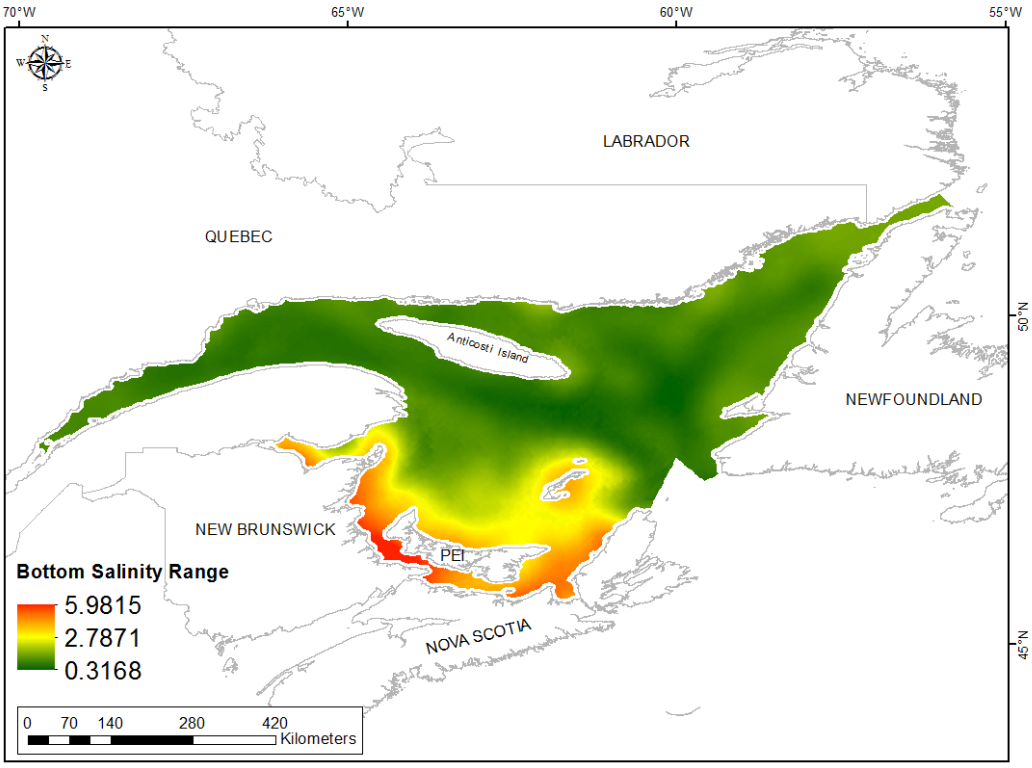

Fig. 95. Interpolated prediction surface of Bottom Salinity Range.

Bottom Salinity Average Minimum

This variable displayed a left-skewed distribution prior to modeling (Table 39, Fig. 96). The data were lower than predicted by a normal distribution at low and high values (Fig. 97). Mid-range values were slightly higher than the reference line. There was a strong spatial pattern to the under- and over-prediction (Fig. 97).

The semivariogram showed moderate autocorrelation present in the data and there was a good predictive fit (Fig. 98). The kriged model showed good cross-validation statistics (Table 40) indicating that it was good at prediction. The error map showed low error and no strong spatial pattern over the spatial extent but was higher along the coast (Fig. 99). The kriged surface is presented in Fig. 100.

Table 39. Distributional properties of Bottom Salinity Average Minimum.

Property	Value
Number of Observations	606
Minimum	24.599
Maximum	34.718
Mean	32.404
Median	32.758
Standard Deviation	2.094
Skewness	-1.343
Kurtosis	4.824

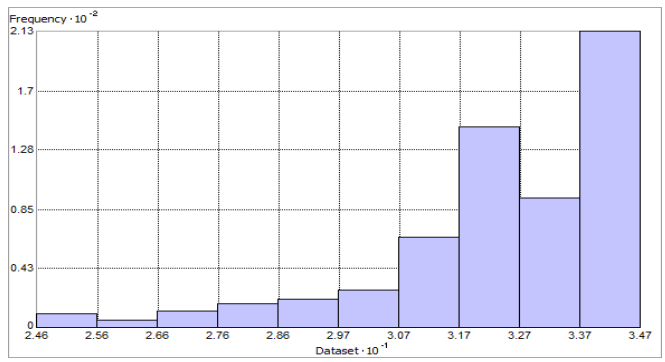

Fig. 96. Distribution of Bottom Salinity Average Minimum. Histogram was illustrated using 10 bins. X axis is shown at 10^{-1}; Y axis is shown at 10^{-2}.

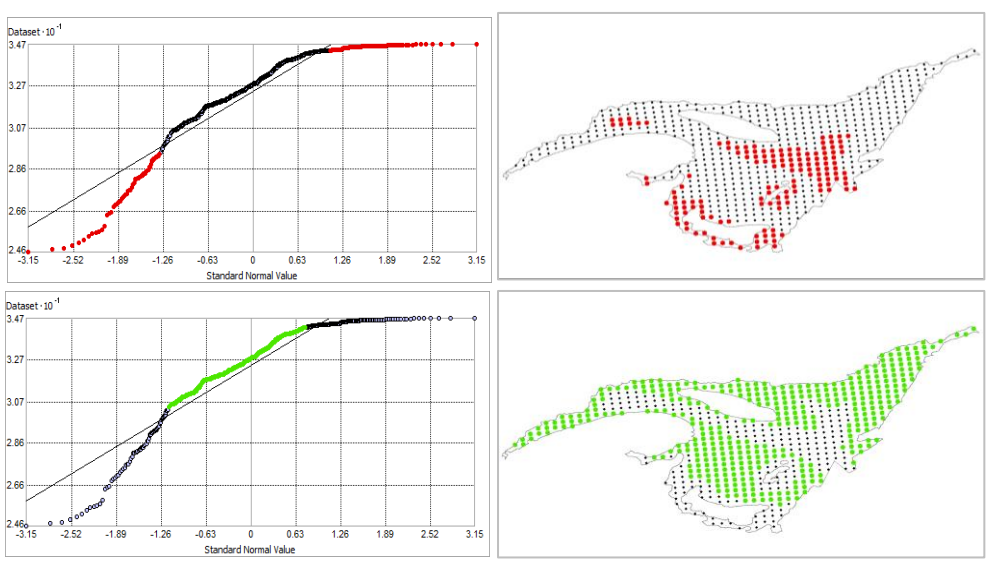

Fig. 97. Normal Q-Q plot for data values of Bottom Salinity Average Minimum (°C). Points falling under (upper panel) and over (bottom panel) the reference line are mapped.

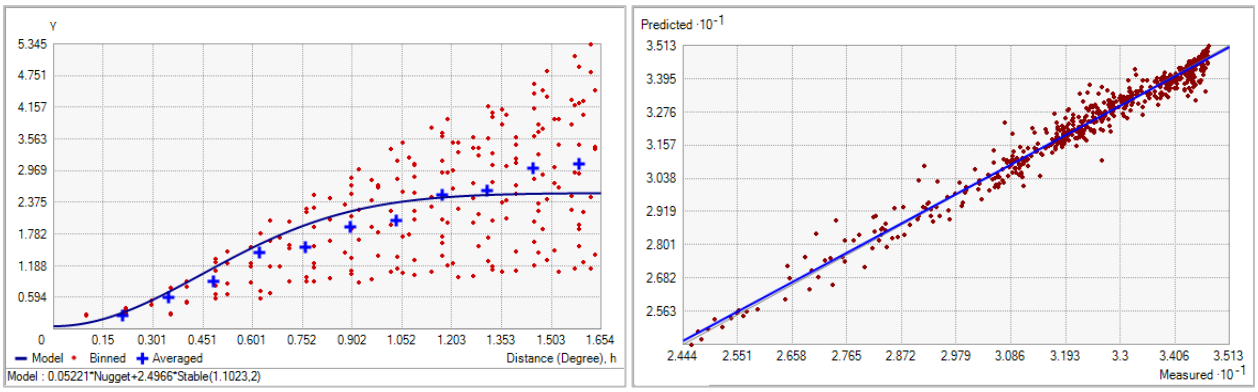

Fig. 98. Left panel: Semivariogram of Bottom Salinity Average Minimum. Binned values are shown as red dots; average points are shown as blue crosses; the model fit to the averaged values is shown as a blue line. Lag size: 0.138 degrees; number of lags: 12; Parameter: 2; Range: 1.102 degrees; Partial Sill: 2.497. Right panel: Scatterplot of predicted values versus observed values for the model of Bottom Salinity Average Minimum.

Table 40. Results of cross-validation of the kriged model for the Bottom Salinity Average Minimum.

Prediction error	**Value**
Number of Observations	606
Overall Mean Error	0.012
Root Mean Square Prediction Error	0.369
Standardized Mean	0.016
Standardized Root Mean Square Prediction Error	1.240
Average Standard Error	0.299

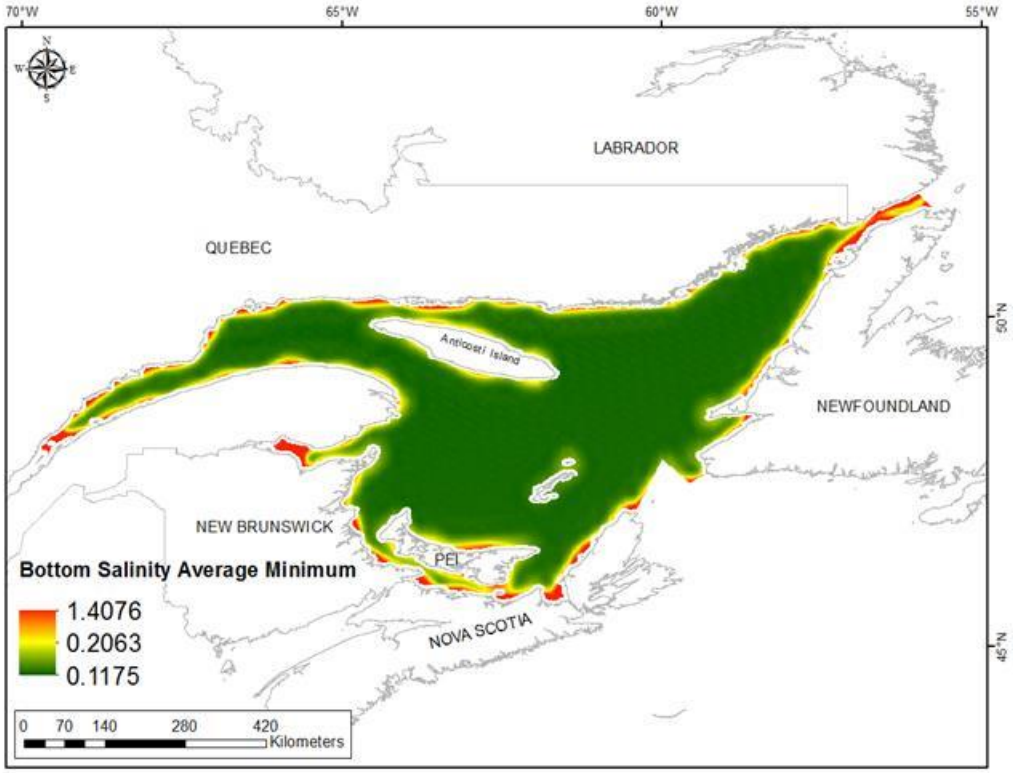

Fig. 99. Prediction standard error surface of Bottom Salinity Average Minimum.

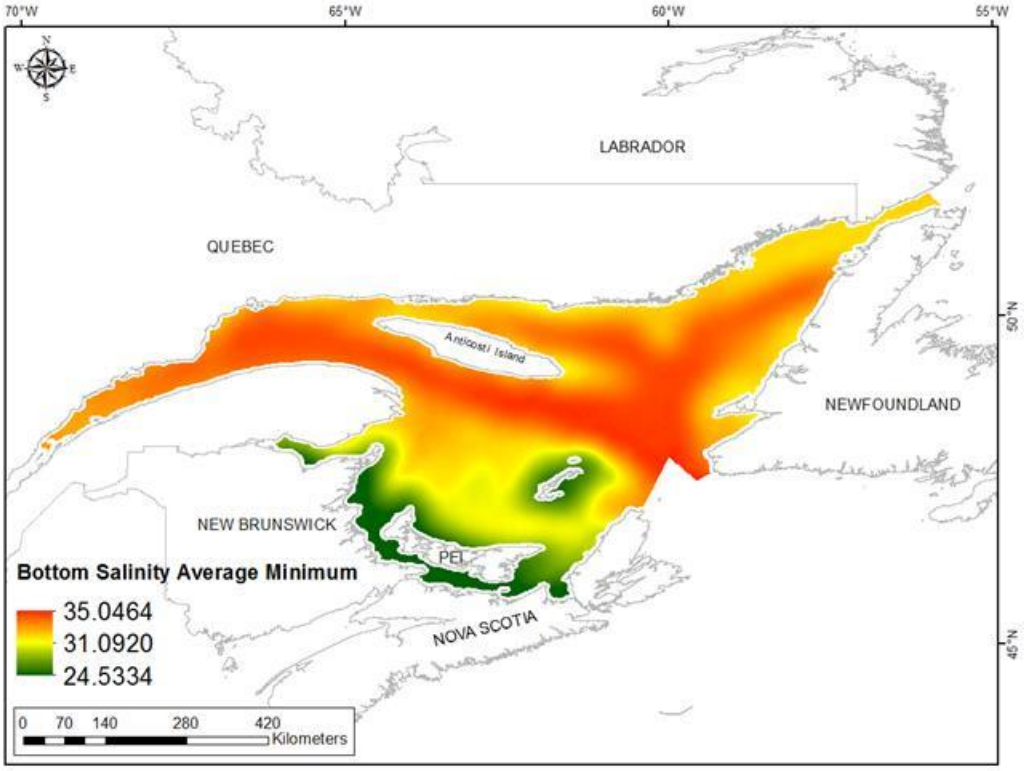

Fig. 100. Interpolated prediction surface of Bottom Salinity Average Minimum.

Bottom Salinity Average Maximum

This variable displayed a right-skewed distribution prior to modeling (Table 41, Fig. 101). The data were lower than predicted by a normal distribution at low and high values (Fig. 102). Mid-range values were slightly higher than the reference line. There was strong spatial cohesion to the under-prediction (Fig. 102).

The semivariogram showed moderate autocorrelation present in the data and there was a good predictive fit (Fig. 103). The kriged model showed good cross-validation statistics (Table 42) indicating that it was good at prediction. The error map showed low error and no strong spatial pattern over the spatial extent but was higher along the coast (Fig. 104). The kriged surface is presented in Fig. 105.

Table 41. Distributional properties of Bottom Salinity Average Maximum.

Property	Value
Number of Observations	606
Minimum	28.376
Maximum	35.442
Mean	33.425
Median	33.524
Standard Deviation	1.388
Skewness	-0.962
Kurtosis	3.918

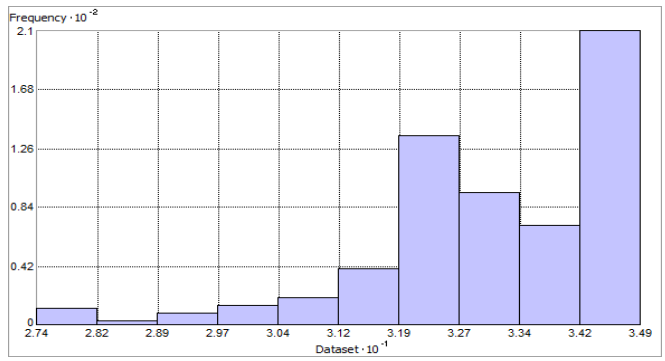

Fig. 101. Distribution of Bottom Salinity Average Maximum. Histogram was illustrated using 10 bins. X axis is shown at 10^{-1}; Y axis is shown at 10^{-2}.

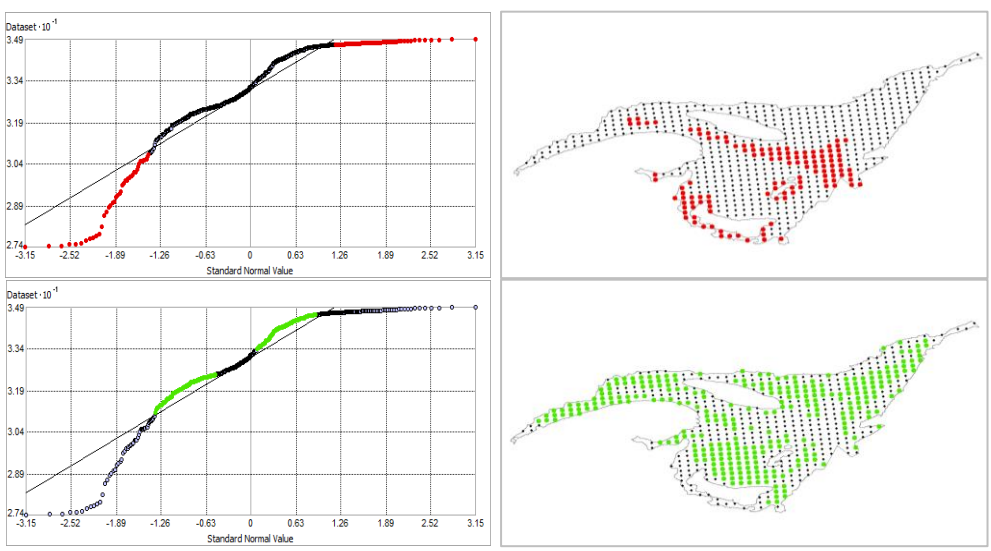

Fig. 102. Normal Q-Q plot for data values of Bottom Salinity Average Maximum. Points falling under (upper panel) and over (bottom panel) the reference line are mapped.

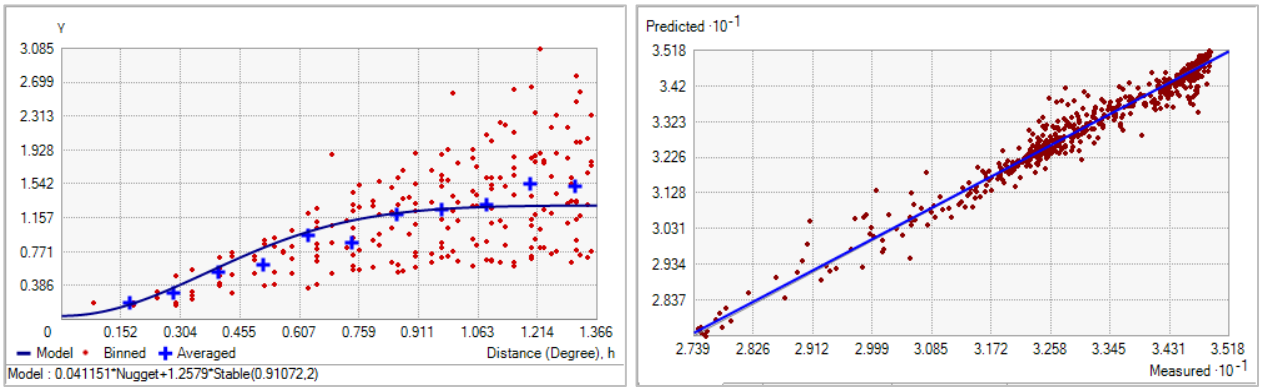

Fig. 103. Left panel: Semivariogram of Bottom Salinity Average Maximum. Binned values are shown as red dots; average points are shown as blue crosses; the model fit to the averaged values is shown as a blue line. Lag size: 0.114 degrees; number of lags: 12; Parameter: 2; Range: 0.911 degrees; Partial Sill: 1.258. Right panel: Scatterplot of predicted values versus observed values for the model of Bottom Salinity Average Maximum.

Table 42. Results of cross-validation of the kriged model for the Bottom Salinity Average Maximum.

Prediction error	**Value**
Number of Observations	606
Overall Mean Error	0.014
Root Mean Square Prediction Error	0.316
Standardized Mean	0.026
Standardized Root Mean Square Prediction Error	1.133
Average Standard Error	0.281

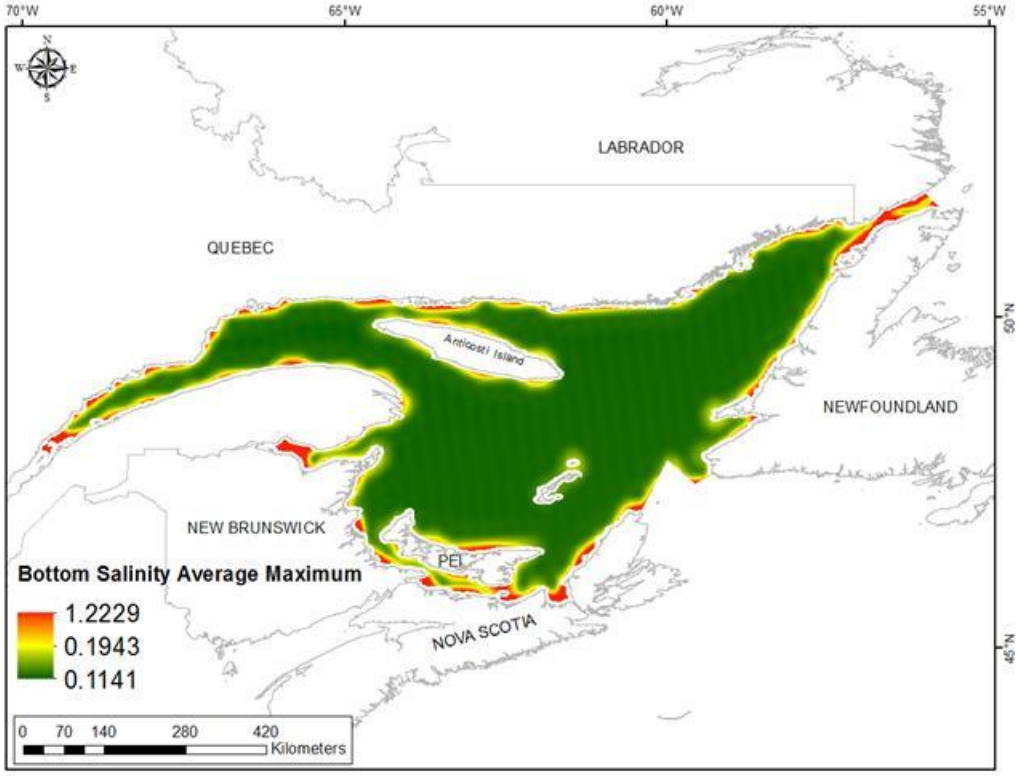

Fig. 104. Prediction standard error surface of Bottom Salinity Average Maximum.

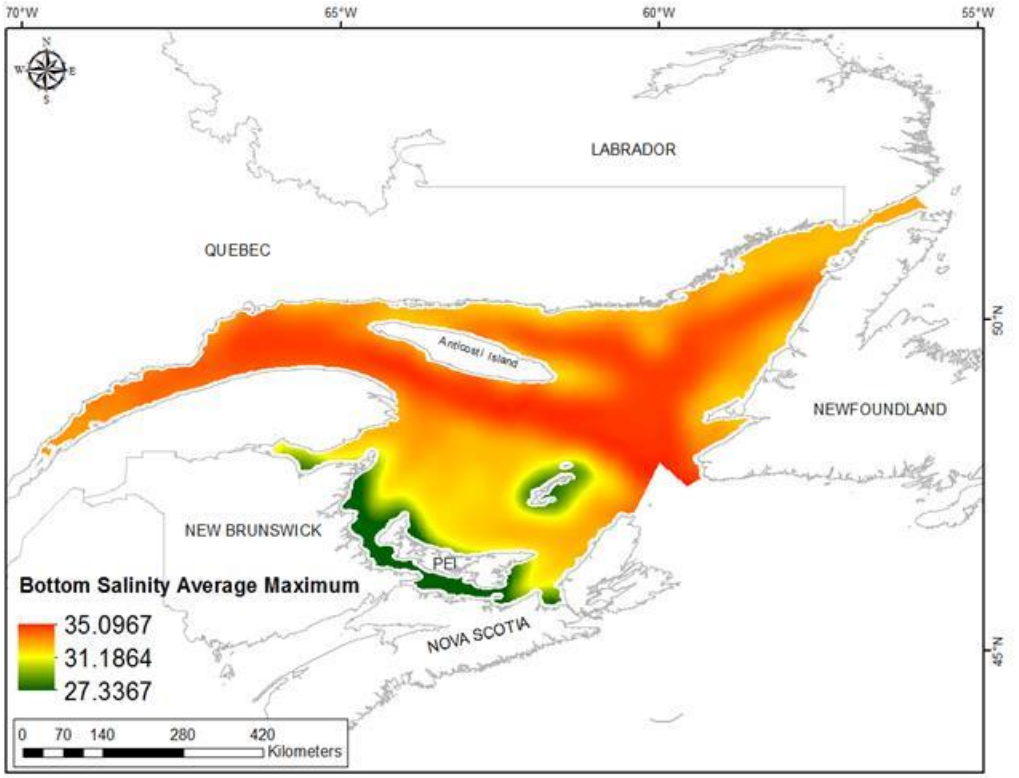

Fig. 105. Interpolated prediction surface of Bottom Salinity Average Maximum.

Bottom Salinity Average Range

This variable displayed a right-skewed distribution prior to modeling (Table 43, Fig. 106). The data were higher than predicted by a normal distribution at low and high values, and mid-range values were lower than the reference line (Fig. 107). There was a pattern to the under- and over-prediction (Fig. 107).

The semivariogram showed weak autocorrelation present in the data, however there was a good predictive fit (Fig. 108). The kriged model showed good cross-validation statistics (Table 44) indicating that it was good at prediction. The error map showed a 'bullseye' pattern with error increasing with distance from data points (Fig. 109). The kriged surface is presented in Fig. 110.

Table 43. Distributional properties of Bottom Salinity Average Range.

Property	Value
Number of Observations	606
Minimum	0.118
Maximum	3.037
Mean	0.686
Median	0.447
Standard Deviation	0.624
Skewness	1.874
Kurtosis	5.922

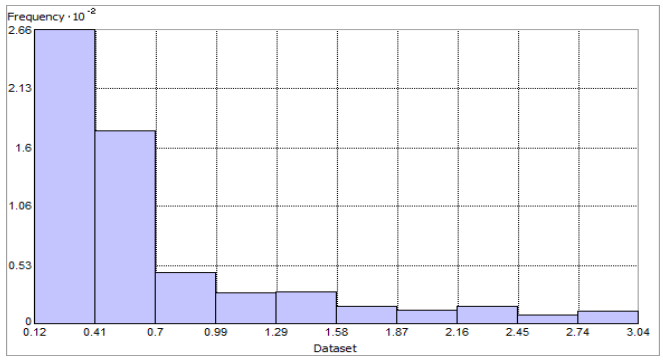

Fig. 106. Distribution of Bottom Salinity Average Range. Histogram was illustrated using 10 bins. Y axis is shown at 10^{-2}.

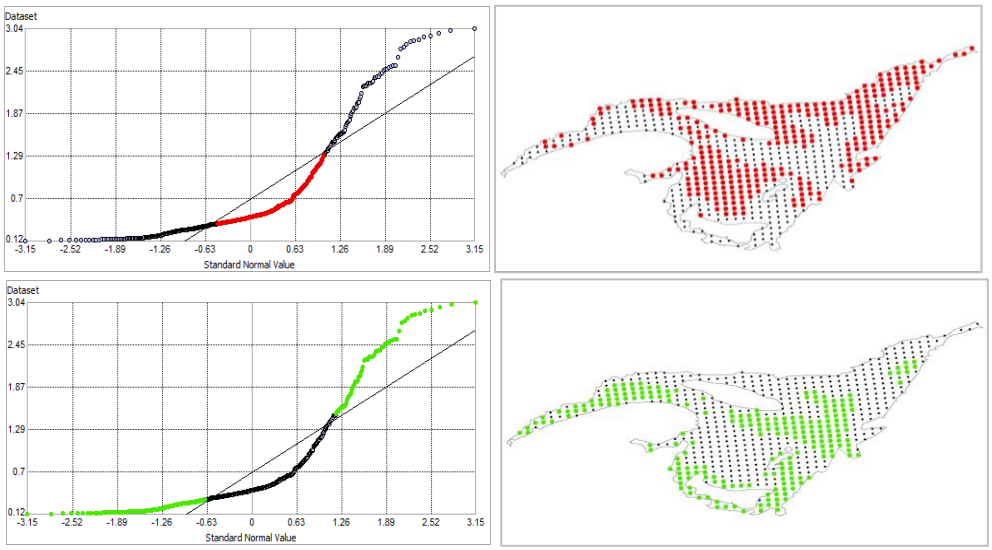

Fig. 107. Normal Q-Q plot for data values of Bottom Salinity Average Range. Points falling under (upper panel) and over (bottom panel) the reference line are mapped.

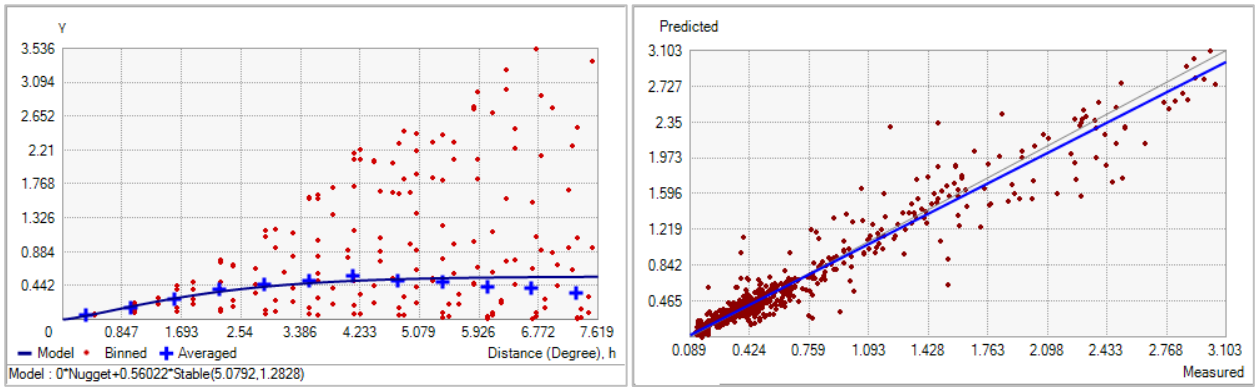

Fig. 108. Left panel: Semivariogram of Bottom Salinity Average Range. Binned values are shown as red dots; average points are shown as blue crosses; the model fit to the averaged values is shown as a blue line. Lag size: 0.635 degrees; number of lags: 12; Parameter: 2; Range: 5.079 degrees; Partial Sill: 0.560. Right panel: Scatterplot of predicted values versus observed values for the model of Bottom Salinity Average Range.

Table 44. Results of cross-validation of the kriged model for the Bottom Salinity Average Range.

Prediction error	**Value**
Number of Observations	606
Overall Mean Error	-0.002
Root Mean Square Prediction Error	0.168
Standardized Mean	-0.008
Standardized Root Mean Square Prediction Error	1.251
Average Standard Error	0.128

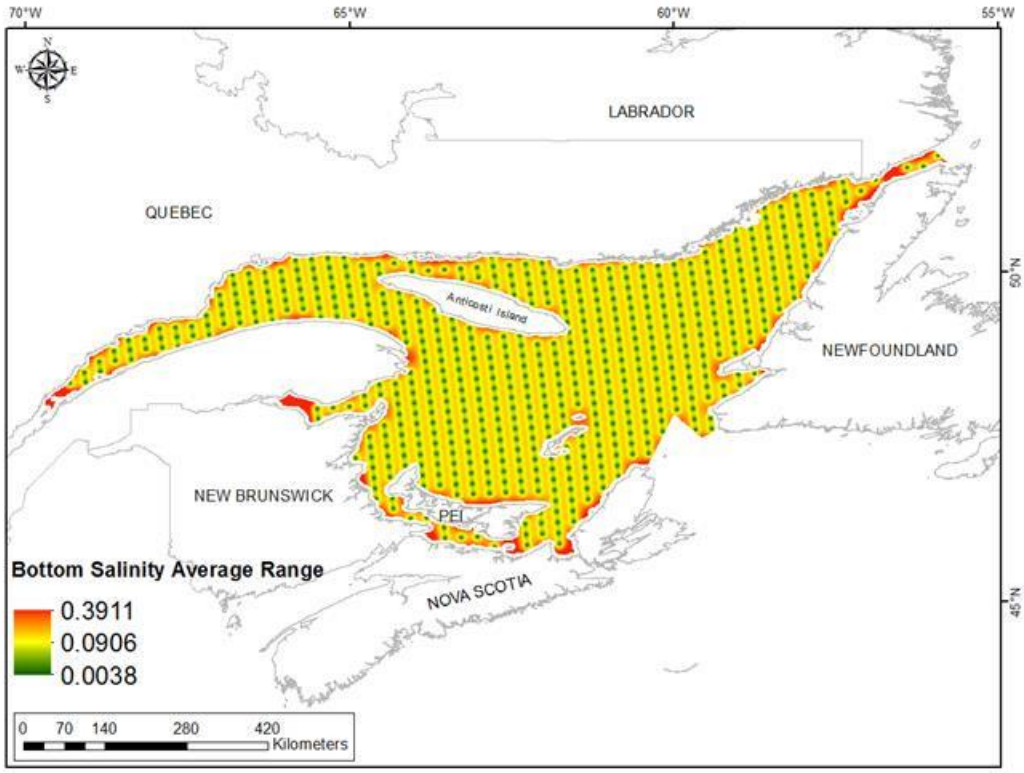

Fig. 109. Prediction standard error surface of Bottom Salinity Average Range.

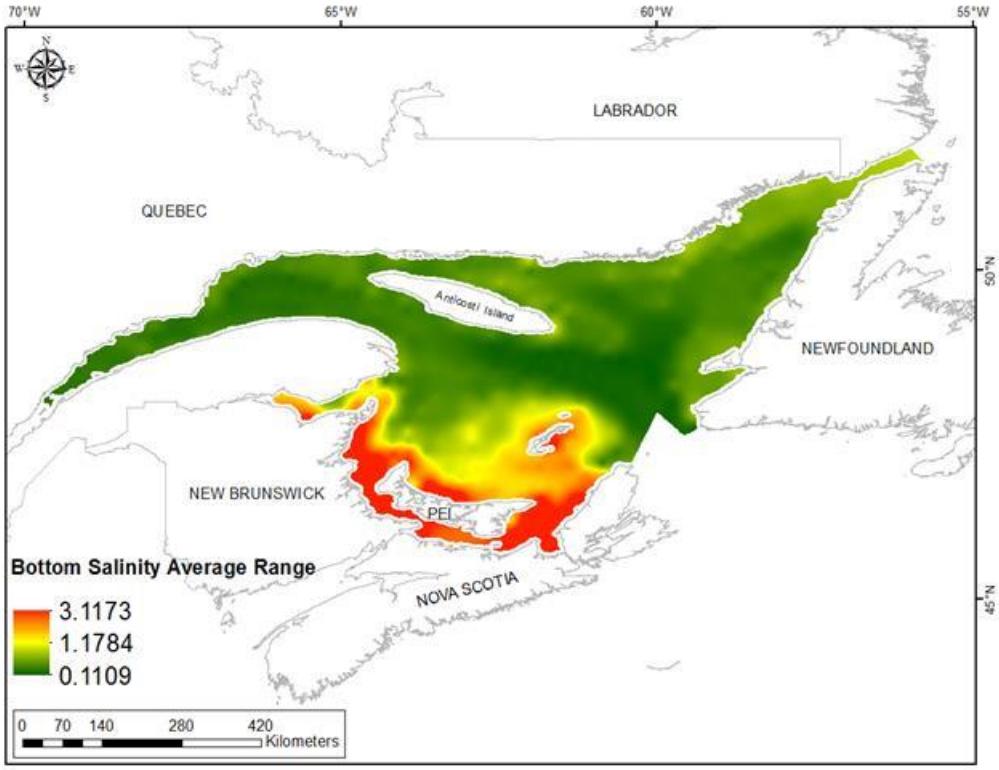

Fig. 110. Interpolated prediction surface of Bottom Salinity Average Range.

Surface Salinity Mean

This variable displayed a left-skewed distribution and slight bimodality (Table 45, Fig. 111). The data were lower than predicted by a normal distribution at low and high values (Fig. 112). Mid-range values were slightly higher than the reference line. There was a strong spatial pattern to the under- and over-prediction (Fig. 112).

The semivariogram showed weak autocorrelation present in the data (Fig. 113). There was good predictive fit (Table 46). The kriged model showed poor cross-validation statistics (Table 46). The standardized root mean square was greater than 1 indicating that variability in the predictions has been underestimated. The error map showed low error and no strong spatial pattern over the spatial extent but was slightly higher in the Gulf of St. Lawrence estuary and Chaleur Bay (Fig. 114). The kriged surface is presented in Fig. 115.

Table 45. Distributional properties of Surface Salinity Mean.

Property	Value
Number of Observations	606
Minimum	18.213
Maximum	31.431
Mean	27.886
Median	28.568
Standard Deviation	3.112
Skewness	-1.452
Kurtosis	4.316

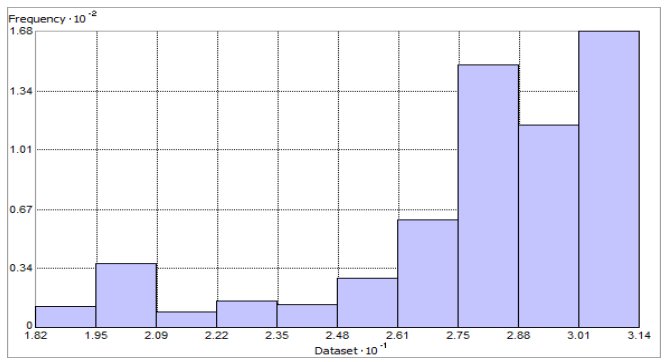

Fig. 111. Distribution of Surface Salinity Mean. Histogram was illustrated using 10 bins. Y axis is shown at 10^{-2}.

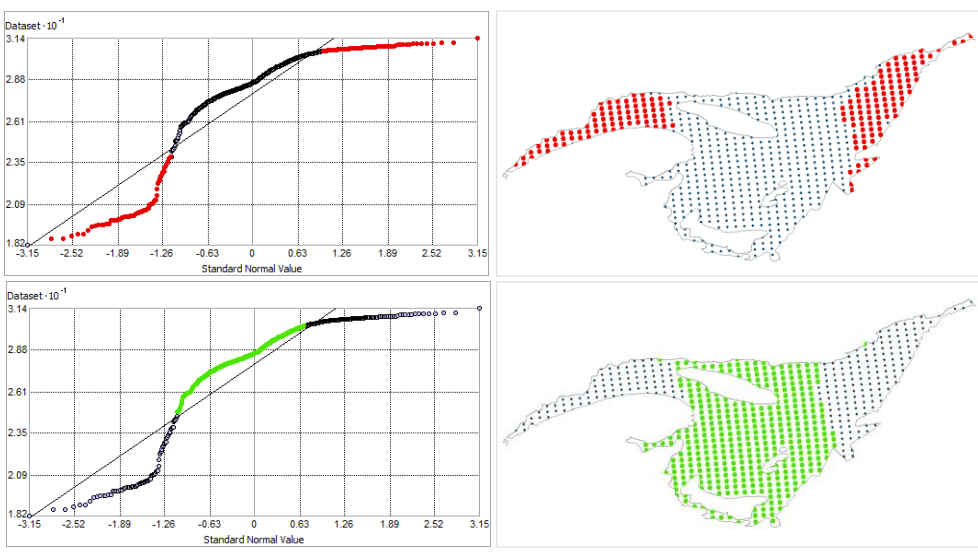

Fig. 112. Normal Q-Q plot for data values of Surface Salinity Mean. Points falling under (upper panel) and over (bottom panel) the reference line are mapped.

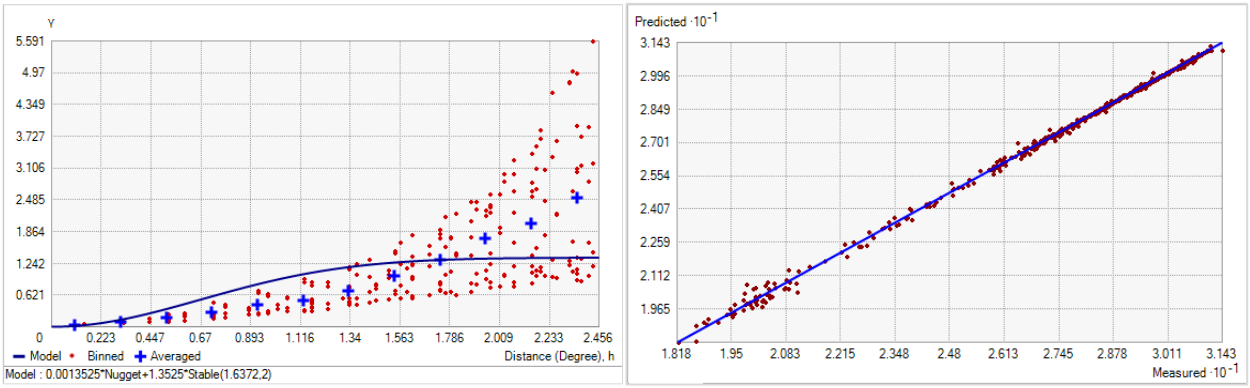

Fig. 113. Left panel: Semivariogram of Surface Salinity Mean. Binned values are shown as red dots; average points are shown as blue crosses; the model fit to the averaged values is shown as a blue line. Lag size: 0.205 degrees; number of lags: 12; Parameter: 2; Range: 1.637 degrees; Partial Sill: 1.353. Right panel: Scatterplot of predicted values versus observed values for the model of Surface Salinity Mean.

Table 46. Results of cross-validation of the kriged model for the Surface Salinity Mean.

Prediction error	**Value**
Number of Observations	606
Overall Mean Error	4.202×10^{-5}
Root Mean Square Prediction Error	0.118
Standardized Mean	0.012
Standardized Root Mean Square Prediction Error	2.138
Average Standard Error	0.053

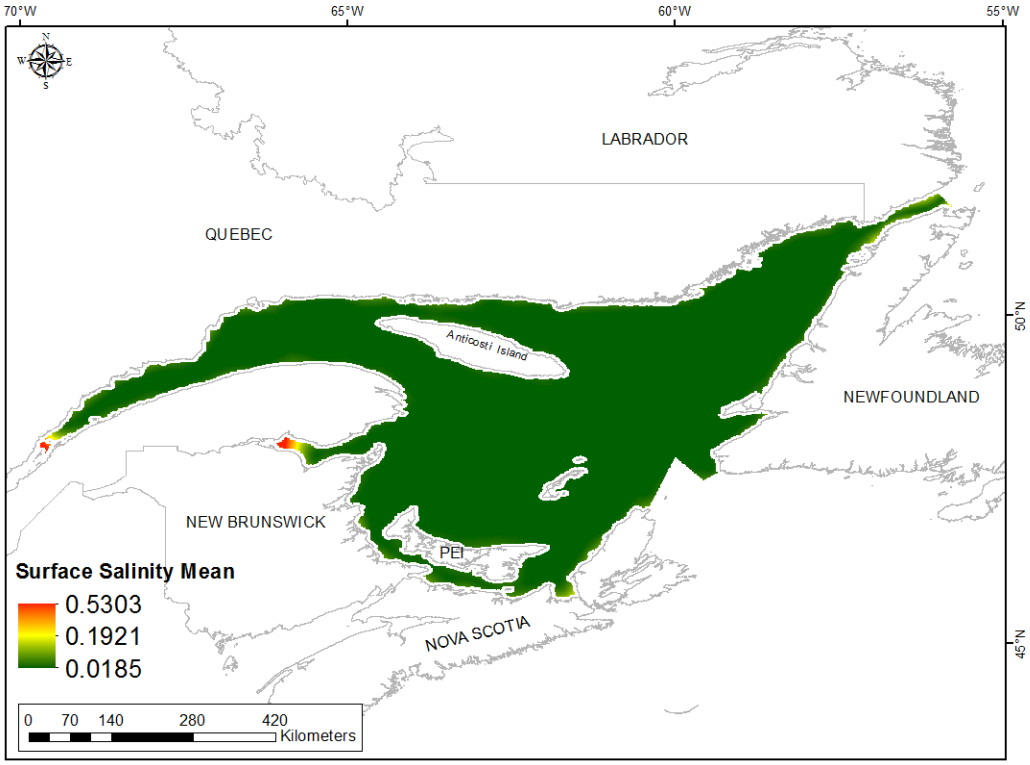

Fig. 114. Prediction standard error surface of Surface Salinity Mean.

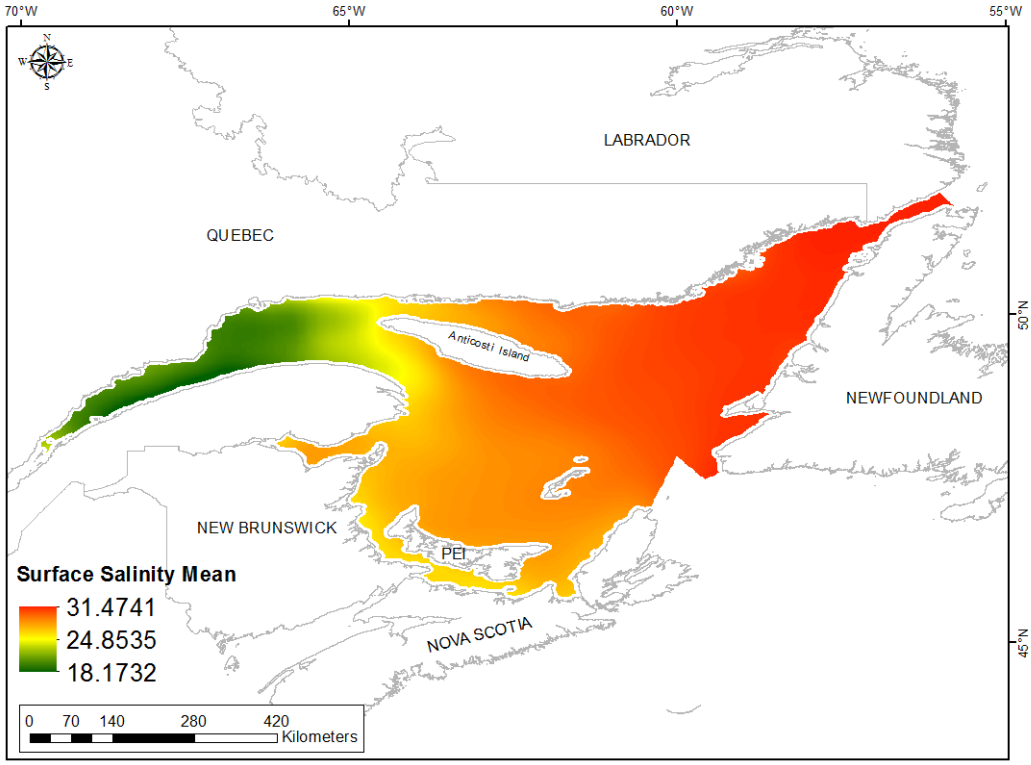

Fig. 115. Interpolated prediction surface of Surface Salinity Mean.

Surface Salinity Minimum

This variable displayed a left-skewed distribution and slight bimodality (Table 47, Fig. 116). The data were lower than predicted by a normal distribution at low and high values (Fig. 117). Mid-range values were slightly higher than the reference line. There was a strong spatial pattern to the under- and over-prediction (Fig. 117).

The semivariogram showed weak autocorrelation present in the data (Fig. 118) The kriged model showed good fit between predicted and measured values (Fig. 118) but poor cross-validation statistics (Table 46). The standardized root mean square was greater than 1 indicating that variability in the predictions has been underestimated. The error map showed low error and no strong spatial pattern over the spatial extent but was slightly higher in the Gulf of St. Lawrence estuary and Chaleur Bay (Fig. 119). The kriged surface is presented in Fig. 120.

Table 47. Distributional properties of Surface Salinity Minimum.

Property	Value
Number of Observations	606
Minimum	10.820
Maximum	29.633
Mean	23.456
Median	25.126
Standard Deviation	4.411
Skewness	-1.296
Kurtosis	3.623

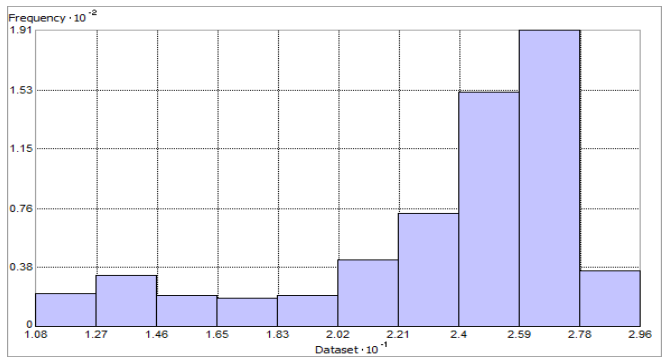

Fig. 116. Distribution of Surface Salinity Minimum. Histogram was illustrated using 10 bins. X axis is shown at 10^{-1}; Y axis is shown at 10^{-2}.

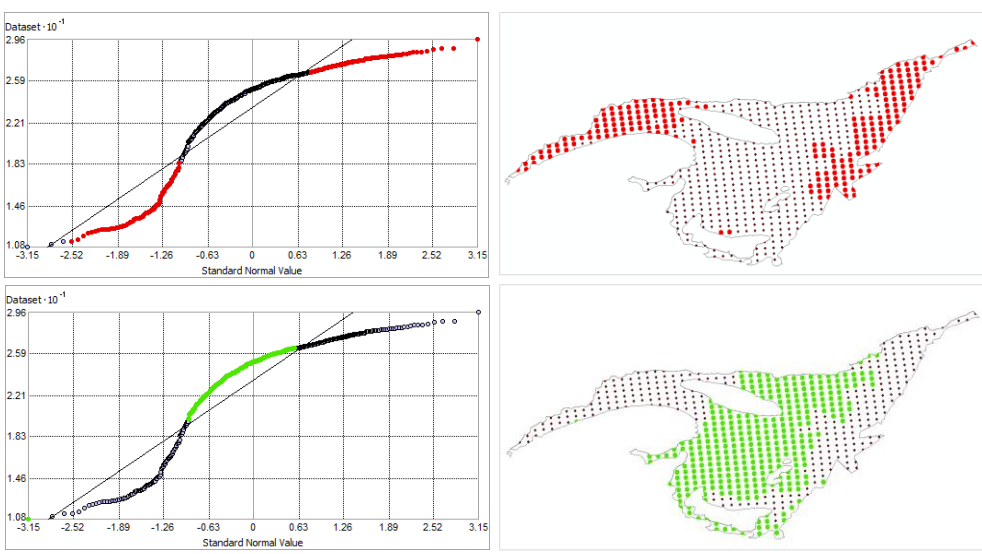

Fig. 117. Normal Q-Q plot for data values of Surface Salinity Minimum. Points falling under (upper panel) and over (bottom panel) the reference line are mapped.

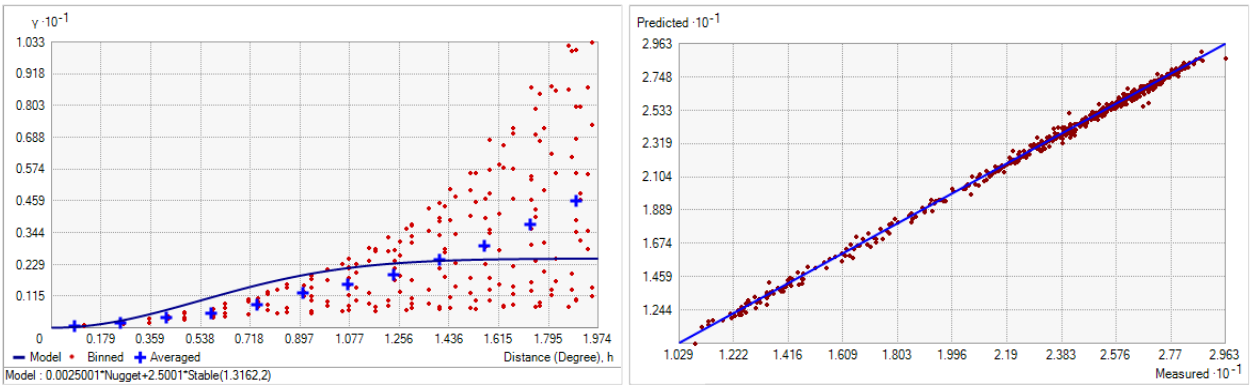

Fig. 118. Left panel: Semivariogram of Surface Salinity Minimum. Binned values are shown as red dots; average points are shown as blue crosses; the model fit to the averaged values is shown as a blue line. Lag size: 0.165 degrees; number of lags: 12; Parameter: 2; Range: 1.316 degrees; Partial Sill: 2.500. Right panel: Scatterplot of predicted values versus observed values for the model of Surface Salinity Minimum.

Table 48. Results of cross-validation of the kriged model for the Surface Salinity Minimum.

Prediction error	**Value**
Number of Observations	606
Overall Mean Error	-3.387×10^{-4}
Root Mean Square Prediction Error	0.212
Standardized Mean	0.009
Standardized Root Mean Square Prediction Error	2.718
Average Standard Error	0.086

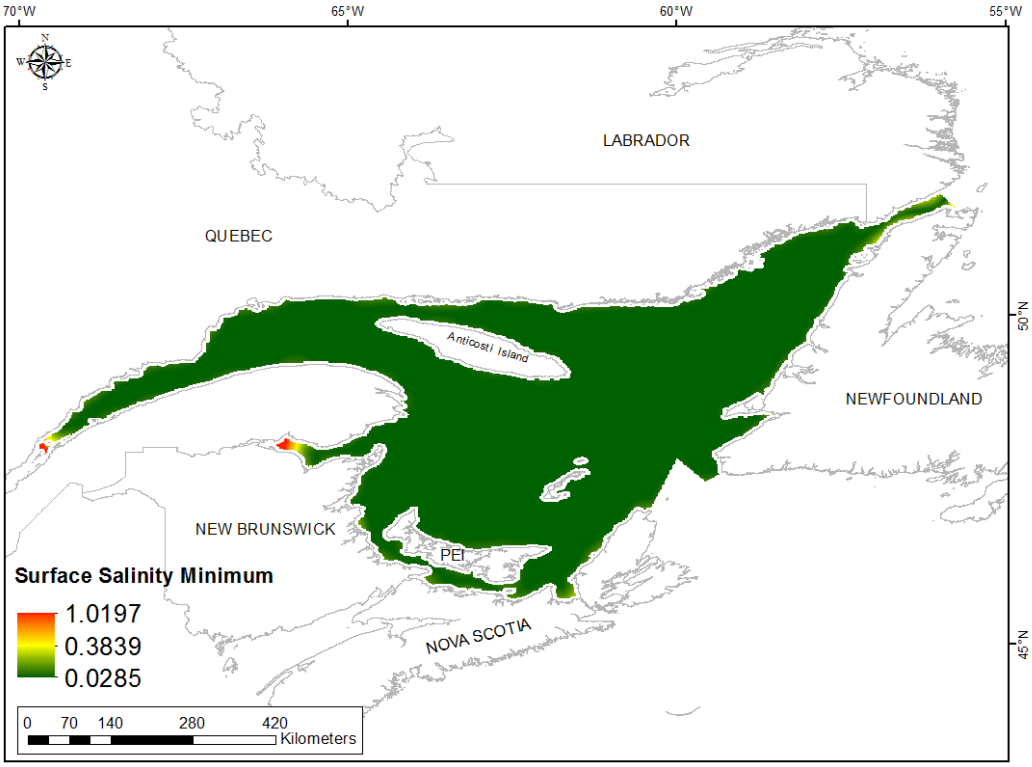

Fig. 119. Prediction standard error surface of Surface Salinity Minimum.

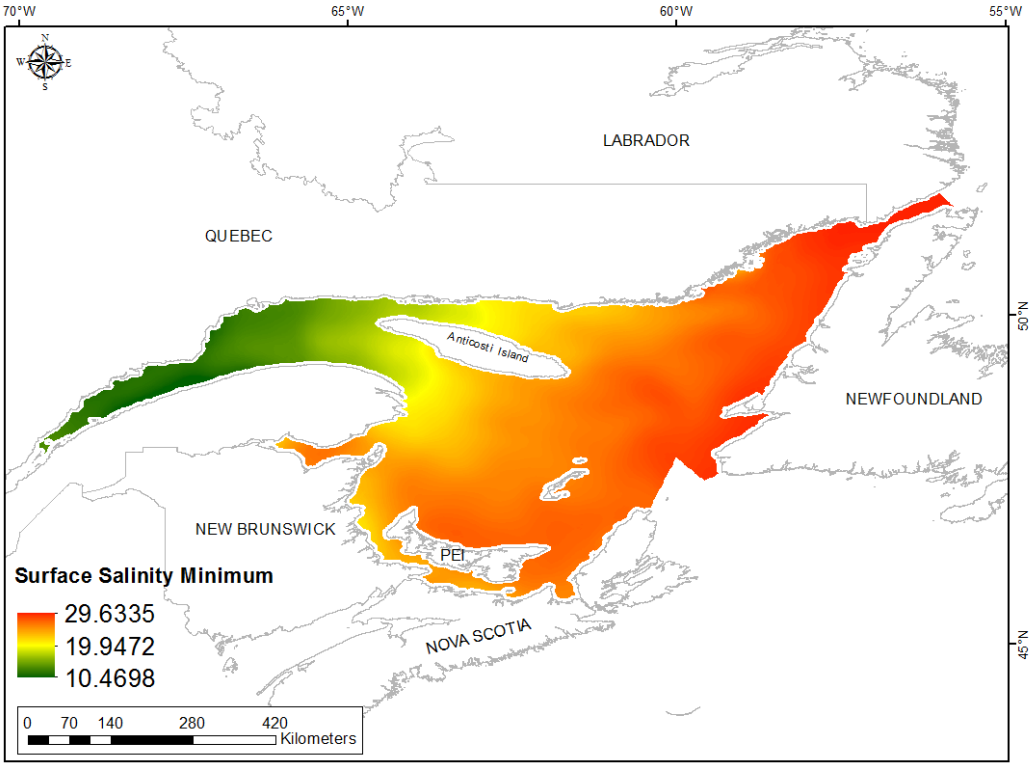

Fig. 120. Interpolated prediction surface of Surface Salinity Minimum.

Surface Salinity Maximum

This variable displayed a left-skewed distribution prior to modeling (Table 49, Fig. 121). The data were lower than predicted by a normal distribution at low and high values (Fig. 122). Mid-range values were slightly higher than the reference line. There was a strong spatial pattern to the under- and over-prediction (Fig. 122).

The semivariogram showed moderate autocorrelation present in the data and an excellent predictive fit (Fig. 123). The model showed good cross-validation statistics (Table 50) indicating that it was good at prediction, although the standardized root mean square was less than 1 indicating that variability in the predictions has been overestimated. The error map showed low error and no strong spatial pattern over the spatial extent but was slightly higher in the Gulf of St. Lawrence estuary and Chaleur Bay (Fig. 124). The kriged surface is presented in Fig. 125.

Table 49. Distributional properties of Surface Salinity Maximum.

Property	Value
Number of Observations	606
Minimum	25.477
Maximum	33.061
Mean	30.859
Median	31.492
Standard Deviation	1.537
Skewness	-1.217
Kurtosis	3.847

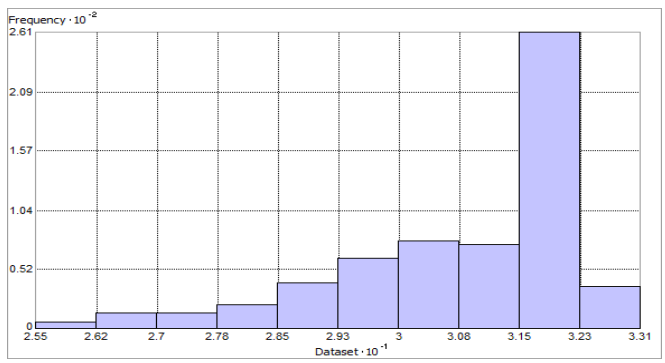

Fig. 121. Distribution of Surface Salinity Maximum. Histogram was illustrated using 10 bins. X axis is shown at 10^{-1}; Y axis is shown at 10^{-2}.

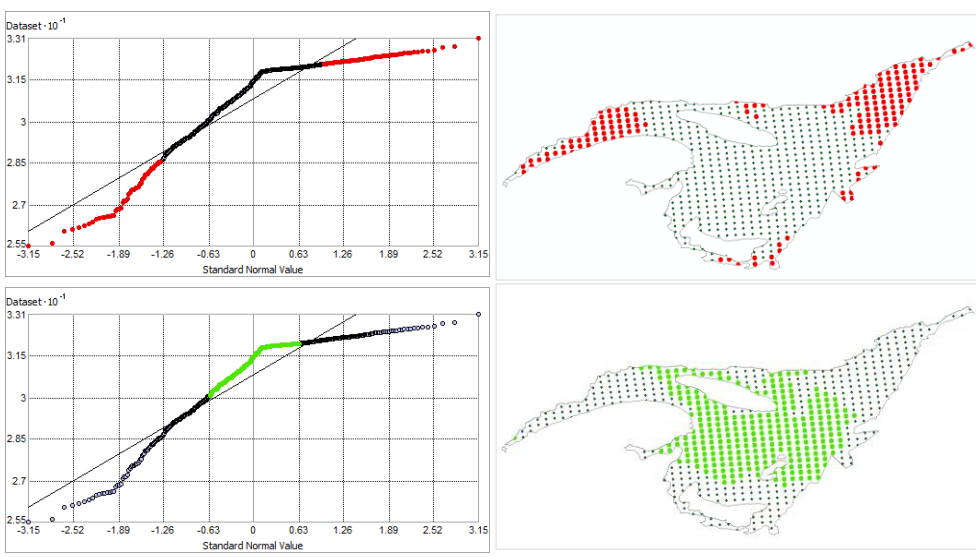

Fig. 122. Normal Q-Q plot for data values of Surface Salinity Maximum. Points falling under (upper panel) and over (bottom panel) the reference line are mapped.

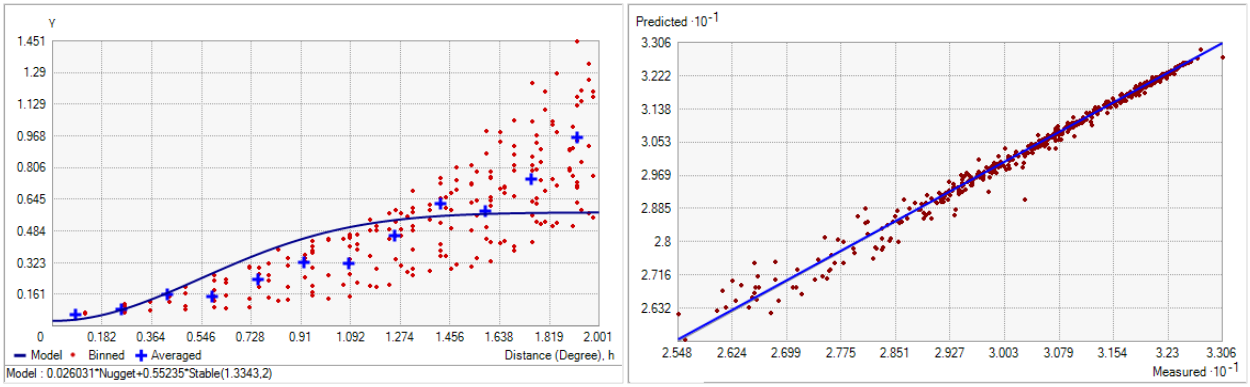

Fig. 123. Left panel: Semivariogram of Surface Salinity Maximum. Binned values are shown as red dots; average points are shown as blue crosses; the model fit to the averaged values is shown as a blue line. Lag size: 0.167 degrees; number of lags: 12; Parameter: 2; Range: 1.334 degrees; Partial Sill: 0.552. Right panel: Scatterplot of predicted values versus observed values for the model of Surface Salinity Maximum.

Table 50. Results of cross-validation of the kriged model for the Surface Salinity Maximum.

Prediction error	**Value**
Number of Observations	606
Overall Mean Error	-0.001
Root Mean Square Prediction Error	0.161
Standardized Mean	-0.002
Standardized Root Mean Square Prediction Error	0.803
Average Standard Error	0.190

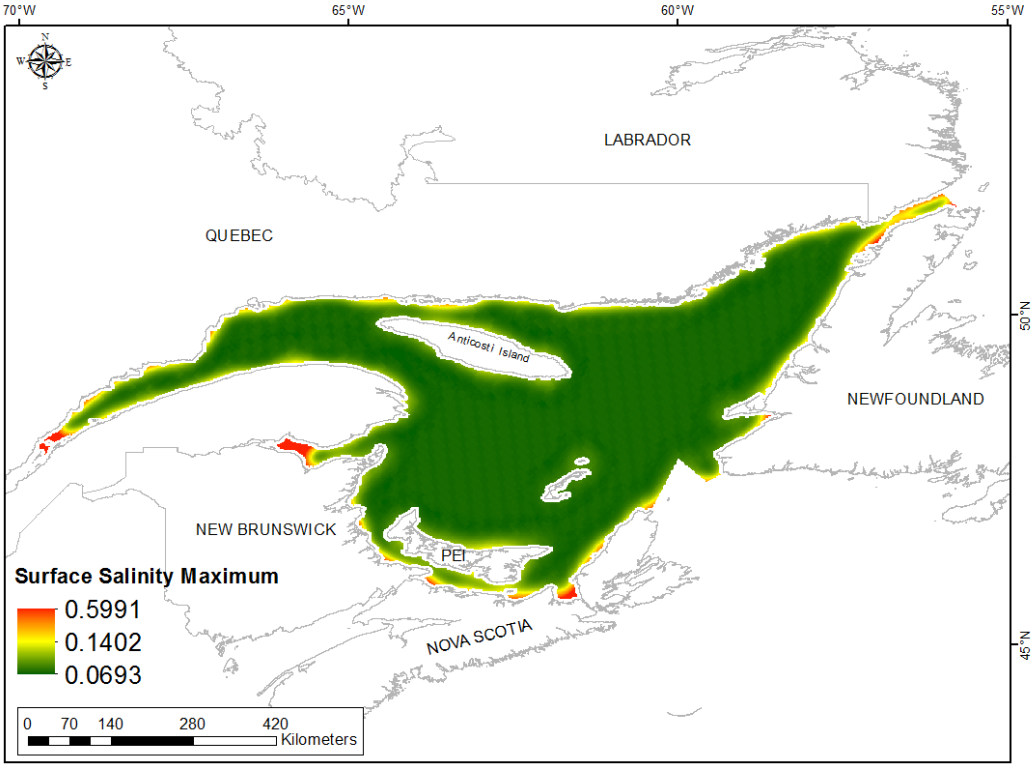

Fig. 124. Prediction standard error surface of Surface Salinity Maximum.

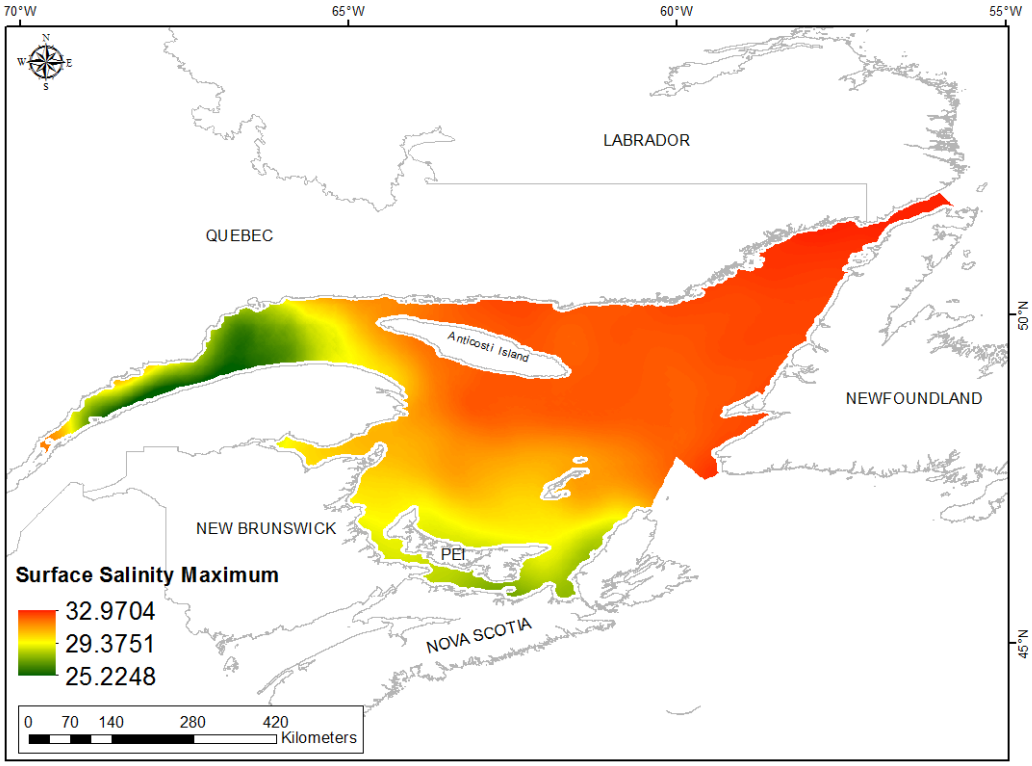

Fig. 125. Interpolated prediction surface of Surface Salinity Maximum.

Surface Salinity Range

This variable displayed a right-skewed distribution and slight bimodality (Table 51, Fig. 126). The data were higher than predicted by a normal distribution at low and high values (Fig. 127), with mid-range values falling lower than the reference line. There was a strong spatial pattern to the under- and over-prediction (Fig. 127).

The semivariogram showed weak autocorrelation present in the data (Fig. 128). The model showed a good fit between measured and predicted values (Fig. 128) but poor cross-validation statistics indicating that it was poor at prediction (Table 52). The standardized root mean square was greater than 1 indicating that variability in the predictions has been underestimated. The error map showed low error over the spatial extent but was slightly higher in the Gulf of St. Lawrence estuary and Chaleur Bay (Fig. 129). The kriged surface is presented in Fig. 130.

Table 51. Distributional properties of Surface Salinity Range.

Property	Value
Number of Observations	606
Minimum	2.256
Maximum	17.467
Mean	7.403
Median	6.055
Standard Deviation	3.585
Skewness	0.889
Kurtosis	2.705

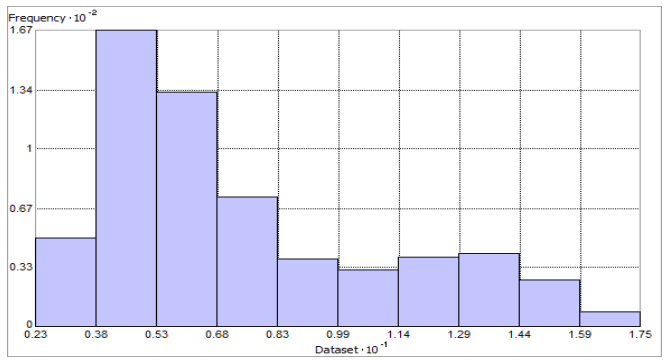

Fig. 126. Distribution of Surface Salinity Range. Histogram was illustrated using 10 bins. X axis is shown at $10^{-1;}$ Y axis at 10^{-2}.

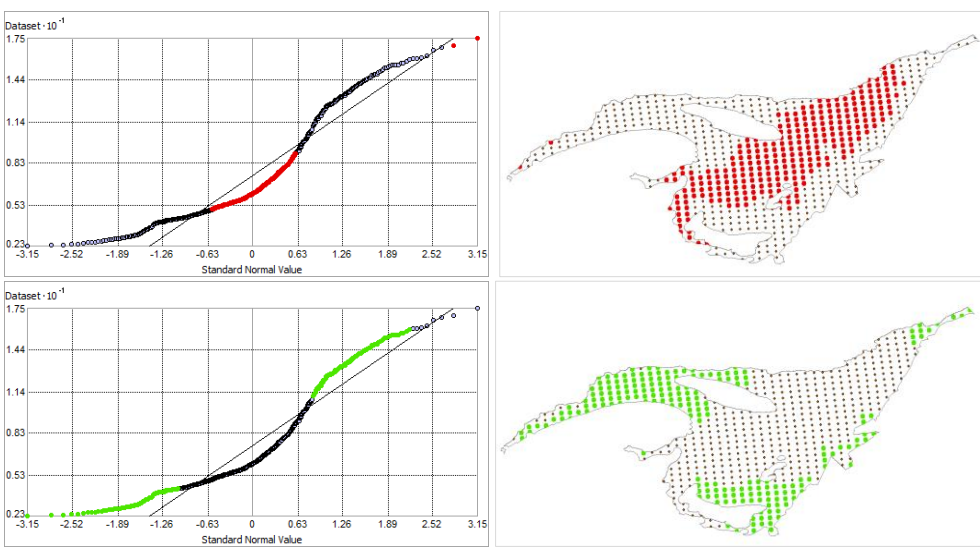

Fig. 127. Normal Q-Q plot for data values of Surface Salinity Range. Points falling under (upper panel) and over (bottom panel) the reference line are mapped.

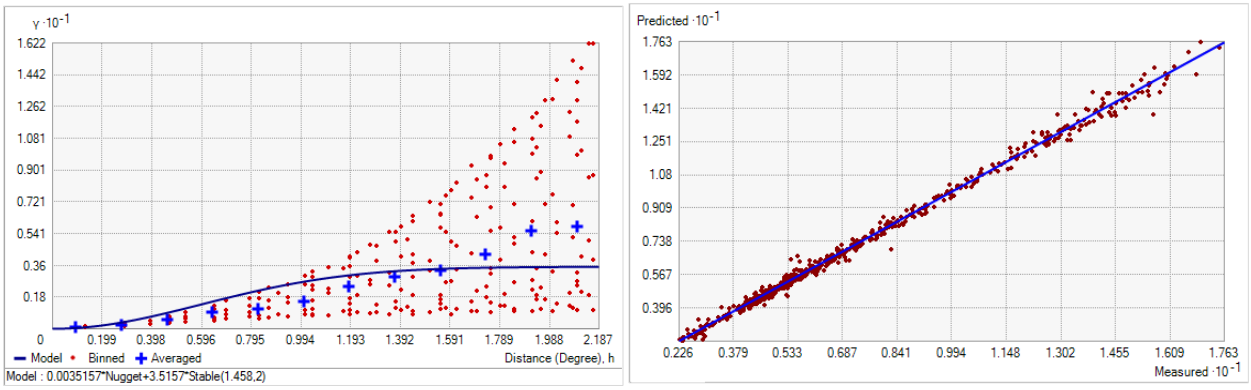

Fig. 128. Left panel: Semivariogram of Surface Salinity Range. Binned values are shown as red dots; average points are shown as blue crosses; the model fit to the averaged values is shown as a blue line. Lag size: 0.182 degrees; number of lags: 12; Parameter: 2; Range: 1.458 degrees; Partial Sill: 3.516. Right panel: Scatterplot of predicted values versus observed values for the model of Surface Salinity Range.

Table 52. Results of cross-validation of the kriged model for the Surface Salinity Range.

Prediction error	**Value**
Number of Observations	606
Overall Mean Error	0.002
Root Mean Square Prediction Error	0.251
Standardized Mean	0.008
Standardized Root Mean Square Prediction Error	2.860
Average Standard Error	0.093

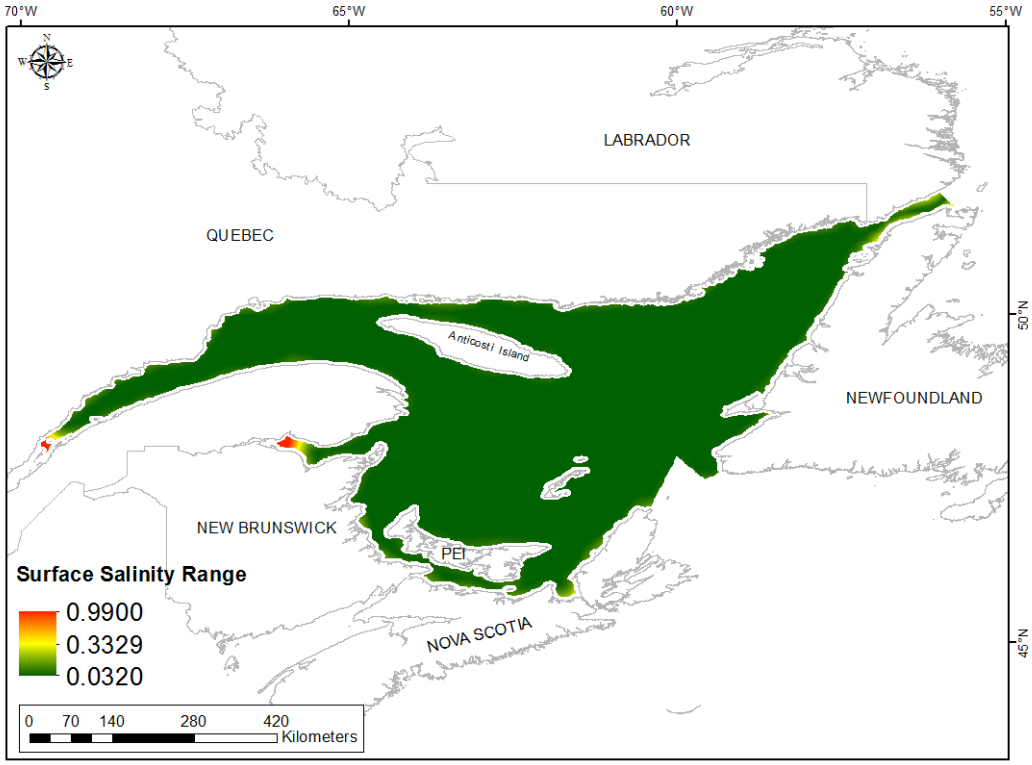

Fig. 129. Prediction standard error surface of Surface Salinity Range.

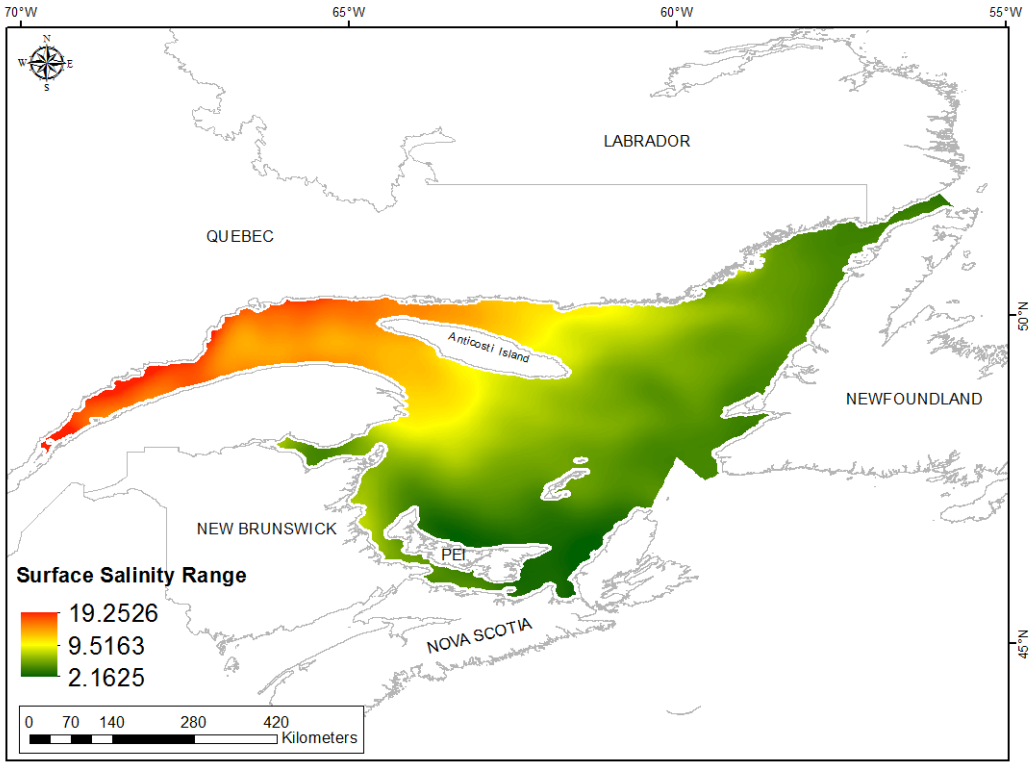

Fig. 130. Interpolated prediction surface of Surface Salinity Range.

Surface Salinity Average Minimum

This variable displayed a left-skewed distribution with slight bimodality (Table 53, Fig. 131). The data were lower than predicted by a normal distribution at low and high values (Fig. 132). Mid-range values were slightly higher than the reference line. There was a strong spatial pattern to the under- and over-prediction (Fig. 132).

The semivariogram showed weak autocorrelation present in the data, but excellent predictive fit (Fig. 133). The model showed poor cross-validation statistics (Table 54). The standardized root mean square was greater than 1 indicating that variability in the predictions has been underestimated. The error map showed low error and no strong spatial pattern over the spatial extent but was higher along the coast (Fig. 134). The kriged surface is presented in Fig. 135.

Table 53. Distributional properties of Surface Salinity Average Minimum.

Property	Value
Number of Observations	606
Minimum	12.853
Maximum	30.256
Mean	25.173
Median	26.611
Standard Deviation	4.244
Skewness	-1.368
Kurtosis	3.801

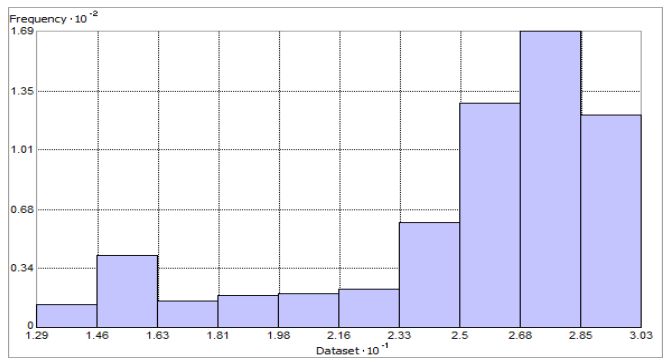

Fig. 131. Distribution of Surface Salinity Average Minimum. Histogram was illustrated using 10 bins. X axis is shown at $10^{-}1$; Y axis is shown at 10^{-2}.

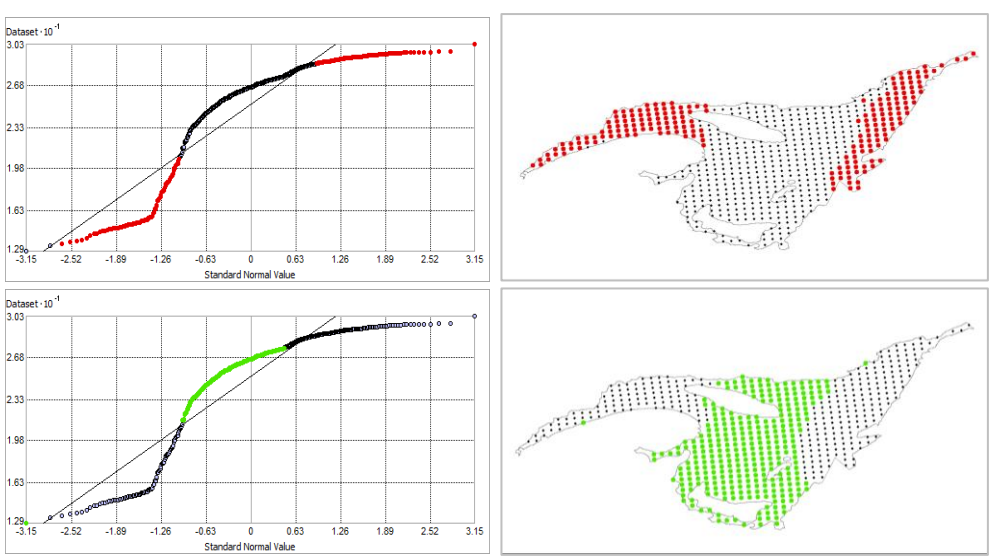

Fig. 132. Normal Q-Q plot for data values of Surface Salinity Average Minimum. Points falling under (upper panel) and over (bottom panel) the reference line are mapped.

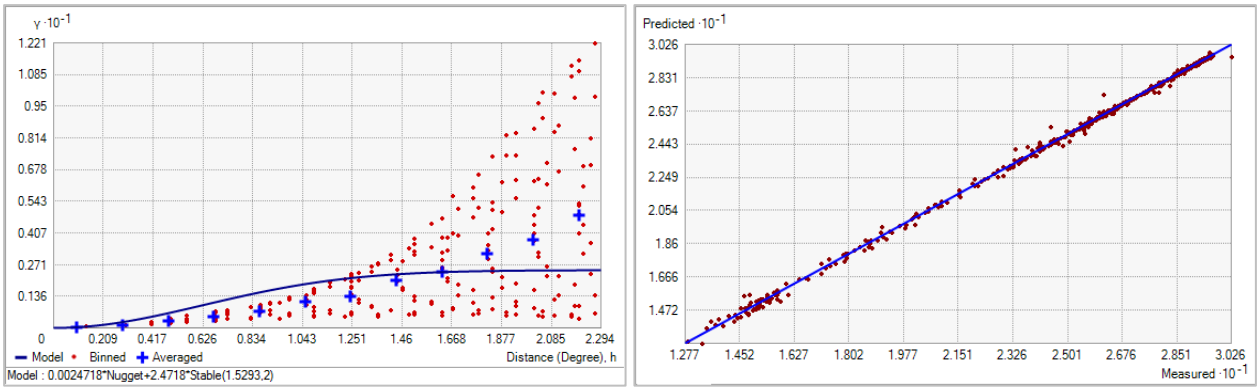

Fig. 133. Left panel: Semivariogram of Surface Salinity Average Minimum. Binned values are shown as red dots; average points are shown as blue crosses; the model fit to the averaged values is shown as a blue line. Lag size: 0.191 degrees; number of lags: 12; Parameter: 2; Range: 1.529 degrees; Partial Sill: 2.472. Right panel: Scatterplot of predicted values versus observed values for the model of Surface Salinity Average Minimum.

Table 54. Results of cross-validation of the kriged model for the Surface Salinity Average Minimum.

Prediction error	**Value**
Number of Observations	606
Overall Mean Error	2.904×10^{-3}
Root Mean Square Prediction Error	0.158
Standardized Mean	0.030
Standardized Root Mean Square Prediction Error	2.018
Average Standard Error	0.075

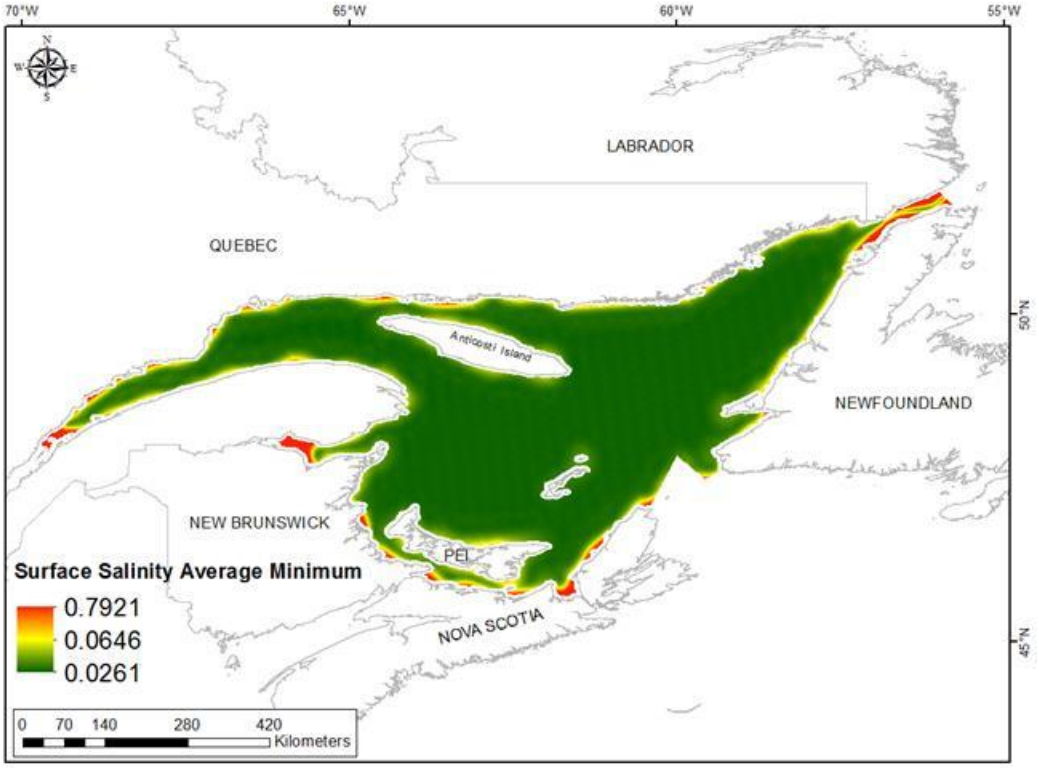

Fig. 134. Prediction standard error surface of Surface Salinity Average Minimum.

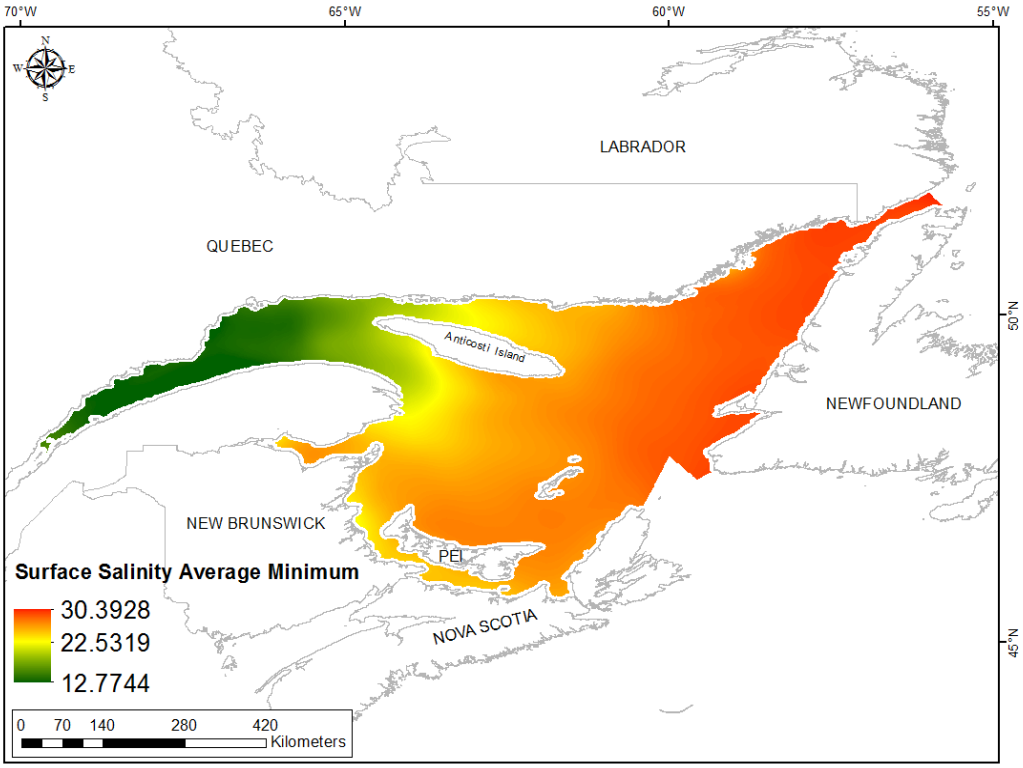

Fig. 135. Interpolated prediction surface of Surface Salinity Average Minimum.

Surface Salinity Average Maximum

This variable displayed a left-skewed distribution and slight bimodality (Table 55, Fig. 136). The data were either lower or higher than predicted by a normal distribution with the former occurring at the tails of the distribution and the latter through the mid-region (Fig. 137). There was a strong spatial pattern to the under- and over-prediction (Fig. 137).

The semivariogram showed weak to moderate autocorrelation present in the data but excellent predictive fit (Fig. 138). The model showed poor cross-validation statistics (Table 56). The standardized root mean square was greater than 1 indicating that variability in the predictions has been underestimated. The error map showed low error and no strong spatial pattern over the spatial extent but was higher along the coast (Fig. 139). The kriged surface is presented in Fig. 140.

Table 55. Distributional properties of Surface Salinity Average Maximum.

Property	Value
Number of Observations	606
Minimum	22.681
Maximum	32.383
Mean	29.931
Median	30.648
Standard Deviation	2.109
Skewness	-1.316
Kurtosis	4.165

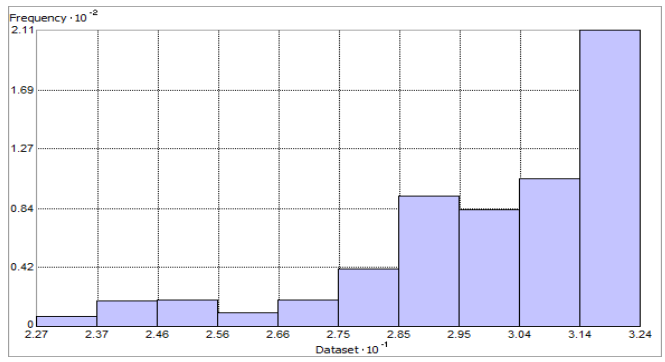

Fig. 136. Distribution of Surface Salinity Average Maximum. Histogram was illustrated using 10 bins. X axis is shown at 10^{-1}; Y axis is shown at 10^{-2}.

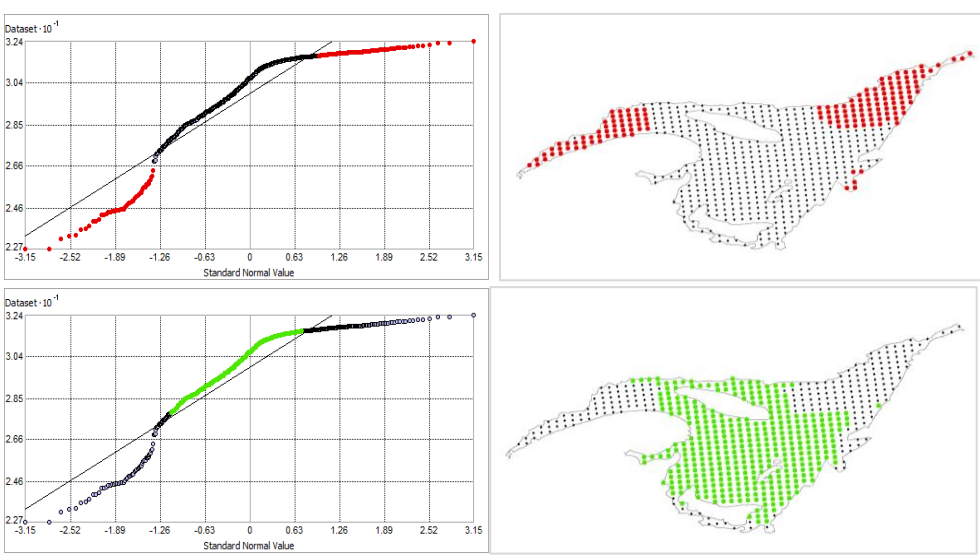

Fig. 137. Normal Q-Q plot for data values of Surface Salinity Average Maximum. Points falling under (upper panel) and over (bottom panel) the reference line are mapped.

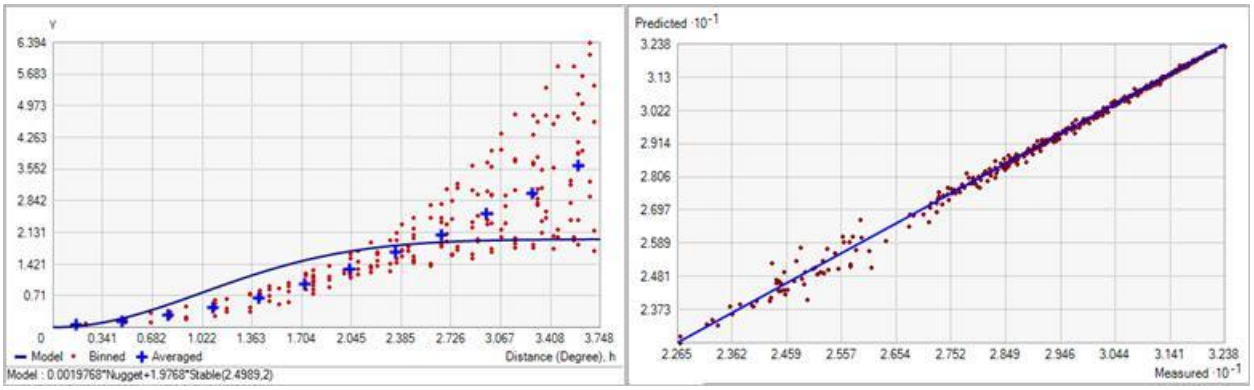

Fig. 138. Left panel: Semivariogram of Surface Salinity Average Maximum. Binned values are shown as red dots; average points are shown as blue crosses; the model fit to the averaged values is shown as a blue line. Lag size: 0.312 degrees; number of lags: 12; Parameter: 2; Range: 2.499 degrees; Partial Sill: 1.977. Right panel: Scatterplot of predicted values versus observed values for the model of Surface Salinity Average Maximum.

Table 56. Results of cross-validation of the kriged model for the Surface Salinity Average Maximum.

Prediction error	**Value**
Number of Observations	606
Overall Mean Error	-0.001
Root Mean Square Prediction Error	0.131
Standardized Mean	-0.002
Standardized Root Mean Square Prediction Error	2.266
Average Standard Error	0.053

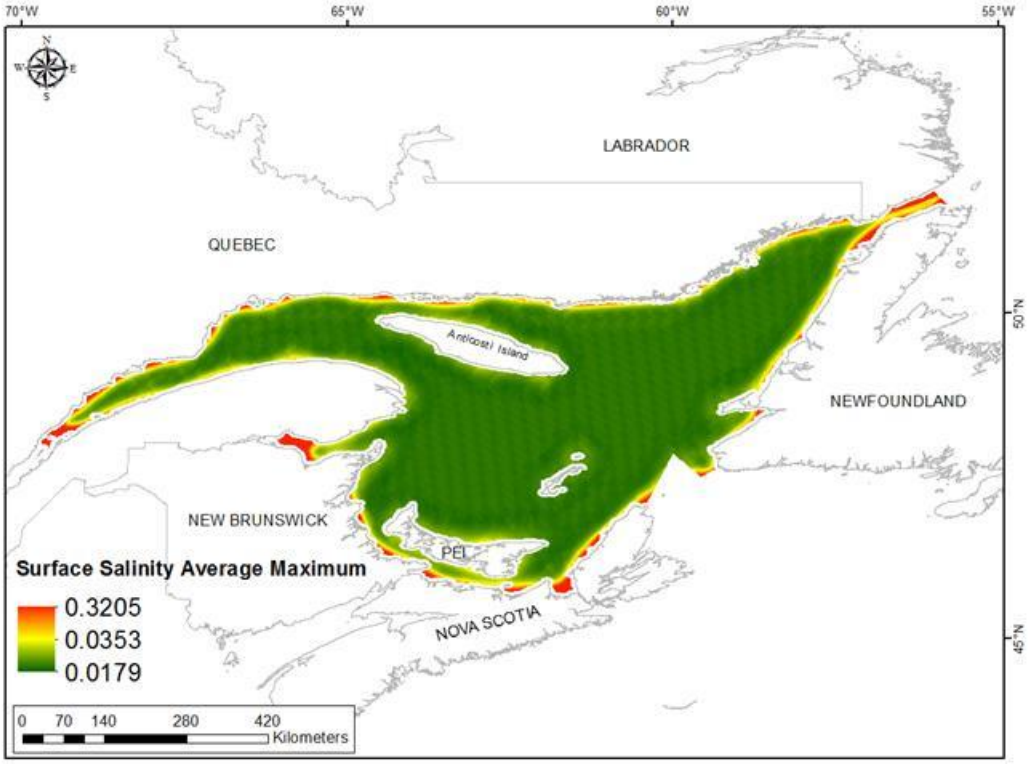

Fig. 139. Prediction standard error surface of Surface Salinity Average Maximum.

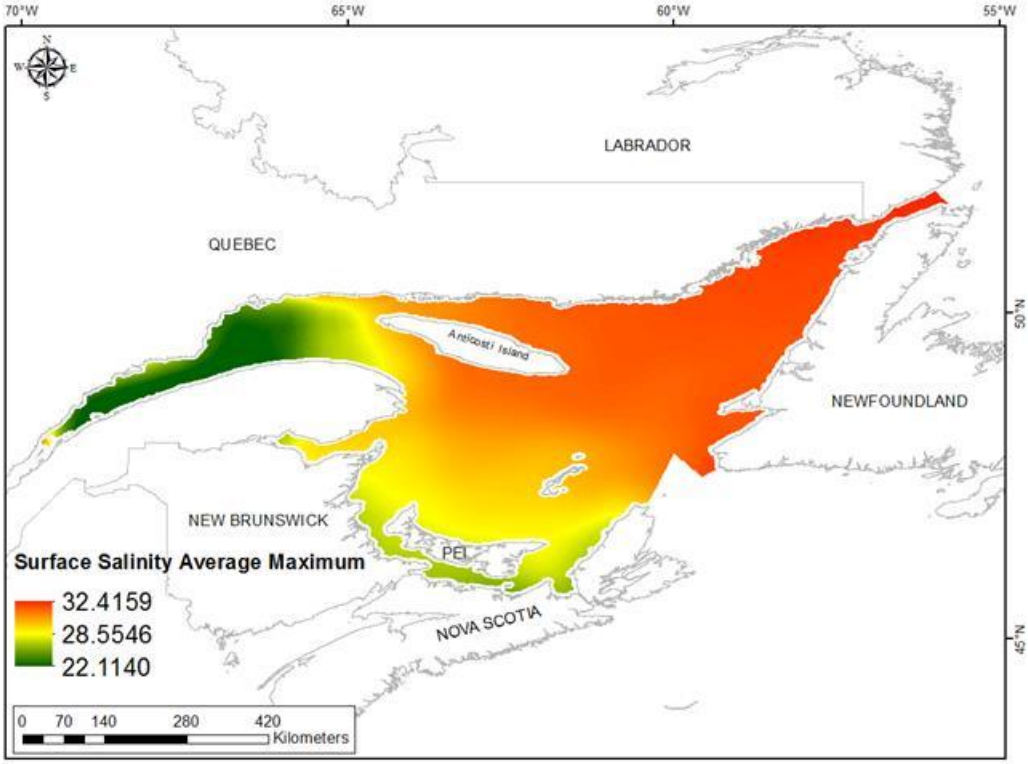

Fig. 140. Interpolated prediction surface of Surface Salinity Average Maximum.

Surface Salinity Average Range

This variable displayed a bimodal distribution prior to modelling (Table 57, Fig. 141). The data did not fit well to a normal distribution and oscillated about the reference line (Fig. 142). There was a strong spatial pattern to the under- and over-predicted values (Fig. 142).

The semivariogram showed autocorrelation present in the data and excellent predictive fit of the model (Fig. 143). The model showed fair cross-validation statistics (Table 58). The error map showed a 'bullseye' pattern with error increasing with distance from data points (Fig. 144). The kriged surface is presented in Fig. 145.

Table 57. Distributional properties of Surface Salinity Average Range.

Property	Value
Number of Observations	606
Minimum	0.943
Maximum	11.695
Mean	4.758
Median	3.640
Standard Deviation	2.786
Skewness	0.834
Kurtosis	2.395

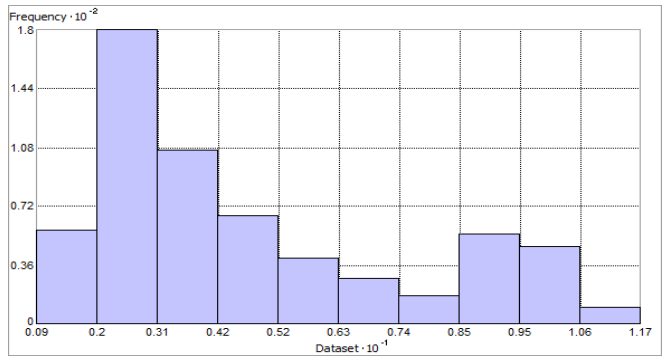

Fig. 141. Distribution of Surface Salinity Average Range. Histogram was illustrated using 10 bins. X axis is shown at 10^{-1}; Y axis is shown at 10^{-2}.

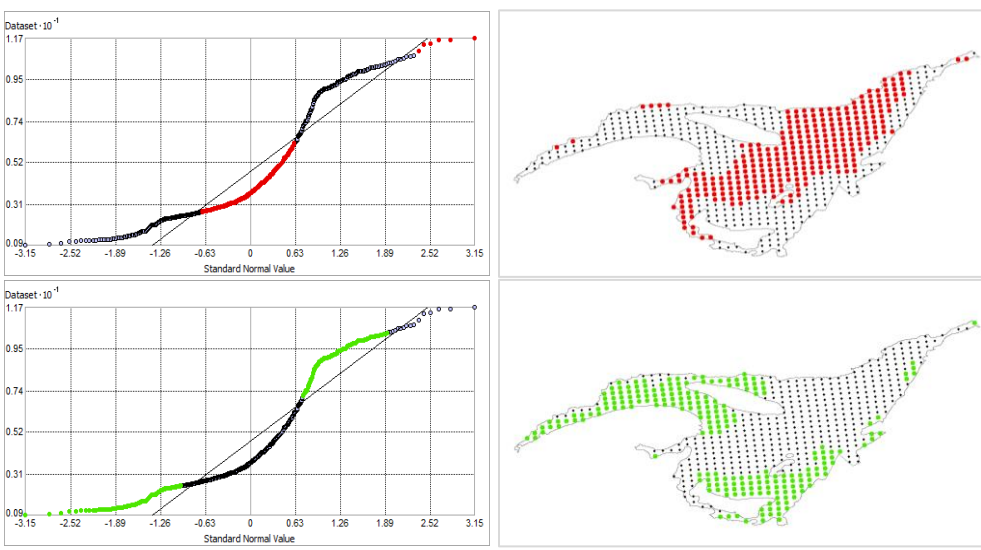

Fig. 142. Normal Q-Q plot for data values of Surface Salinity Average Range. Points falling under (upper panel) and over (bottom panel) the reference line are mapped.

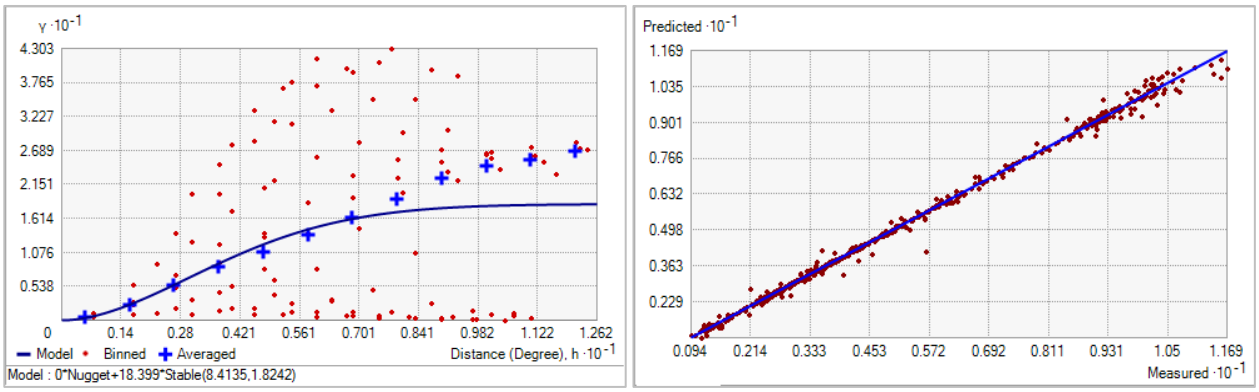

Fig. 143. Left panel: Semivariogram of Surface Salinity Average Range. Binned values are shown as red dots; average points are shown as blue crosses; the model fit to the averaged values is shown as a blue line. Lag size: 1.052 degrees; number of lags: 12; Parameter: 1.824; Range: 8.413 degrees; Partial Sill: 18.399. Right panel: Scatterplot of predicted values versus observed values for the model of Surface Salinity Average Range.

Table 58. Results of cross-validation of the kriged model for the Surface Salinity Average Range.

Prediction error	**Value**
Number of Observations	606
Overall Mean Error	-0.004
Root Mean Square Prediction Error	0.155
Standardized Mean	-0.019
Standardized Root Mean Square Prediction Error	1.393
Average Standard Error	0.097

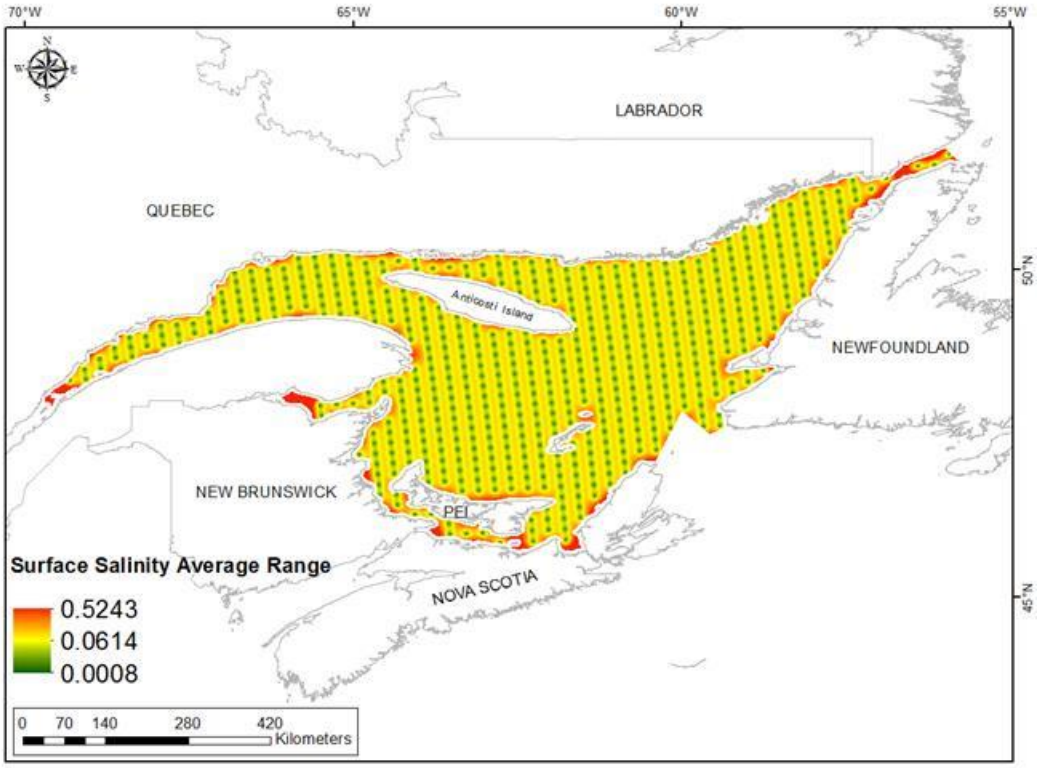

Fig. 144. Prediction standard error surface of Surface Salinity Average Range.

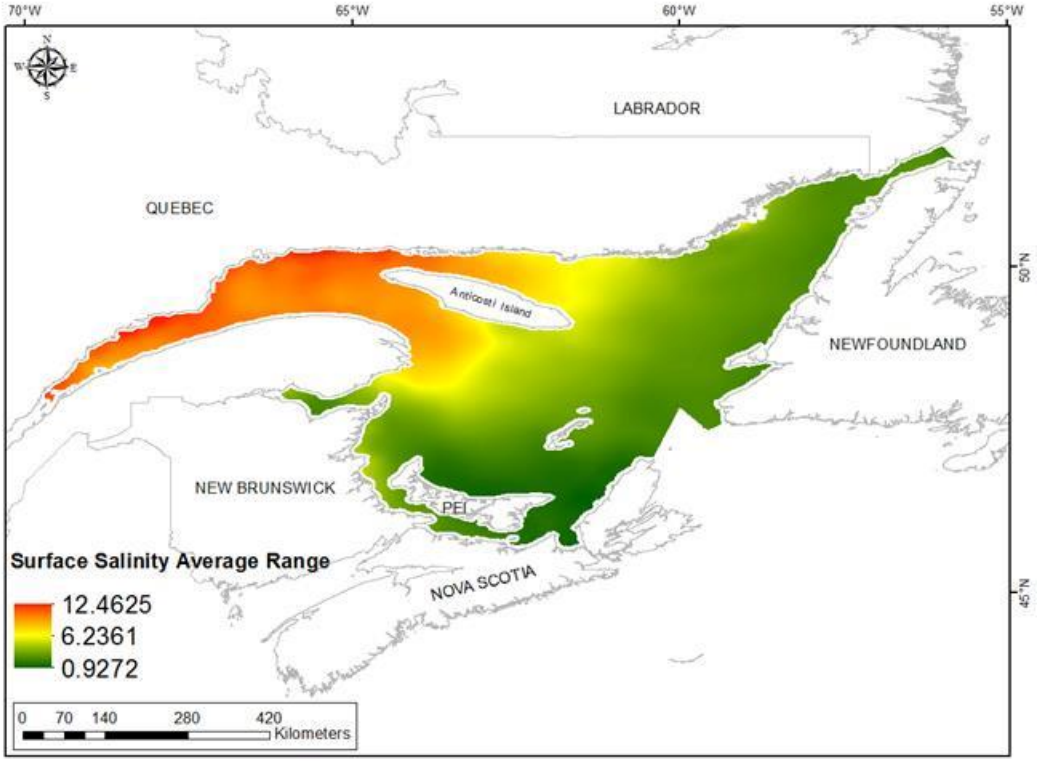

Fig. 145. Interpolated prediction surface of Surface Salinity Average Range.

Current Speed

Currents move water and heat around in the world's oceans and influence the chemical composition of the water column. Upwelling and downwelling currents strongly influence the distribution and abundance of marine life. Similarly, current speed determines the rate at which food particles reach benthic species through both vertical and horizontal transmission and consequently influences the distribution of filter-feeding species. Upwelling currents enhance productivity in the water column, while downwelling currents bring food and oxygen to the sea floor. Organisms also use currents for active and passive transport for migration and dispersal. Current speed can influence morphology, especially of marine macrophytes.

Bottom Current Mean

This variable displayed a right-skewed distribution with very high kurtosis prior to modeling (Table 59, Fig. 146). The data were higher than predicted by a normal distribution at the tails, particularly at high values (Fig. 147). Mid-range values were slightly lower than the reference line. The areas of over- and under-prediction did not show a strong spatial pattern with both error types distributed through the spatial extent (Fig. 147).

The semivariogram showed very weak autocorrelation present in the data and there was a very poor fit between measured and predicted values (Fig. 148). Nevertheless, the model showed good cross-validation statistics (Table 60) indicating that it was good at prediction. The error map showed low error over the study extent except for along the coast where it was higher (Fig. 149). The kriged surface is presented in Fig. 150.

Table 59. Distributional properties of Bottom Current Mean (m s^{-1}).

Property	Value
Number of Observations	589
Minimum	0.002
Maximum	0.123
Mean	0.010
Median	0.008
Standard Deviation	0.009
Skewness	5.120
Kurtosis	48.210

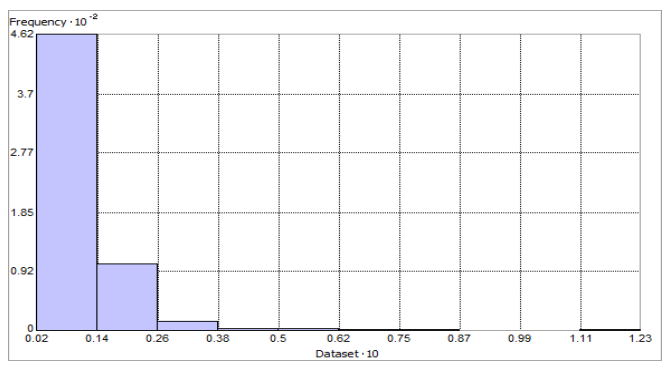

Fig. 146. Distribution of Bottom Current Mean (m s^{-1}). Histogram was illustrated using 10 bins. Y axis is shown at 10^{-2}.

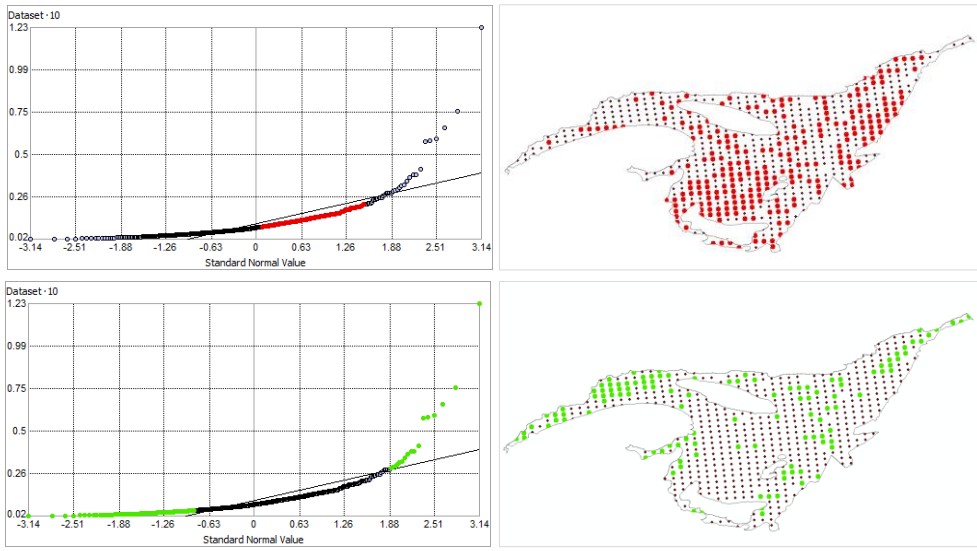

Fig. 147. Normal Q-Q plot for data values of Bottom Current Mean (m s^{-1}). Points falling under (upper panel) and over (bottom panel) the reference line are mapped.

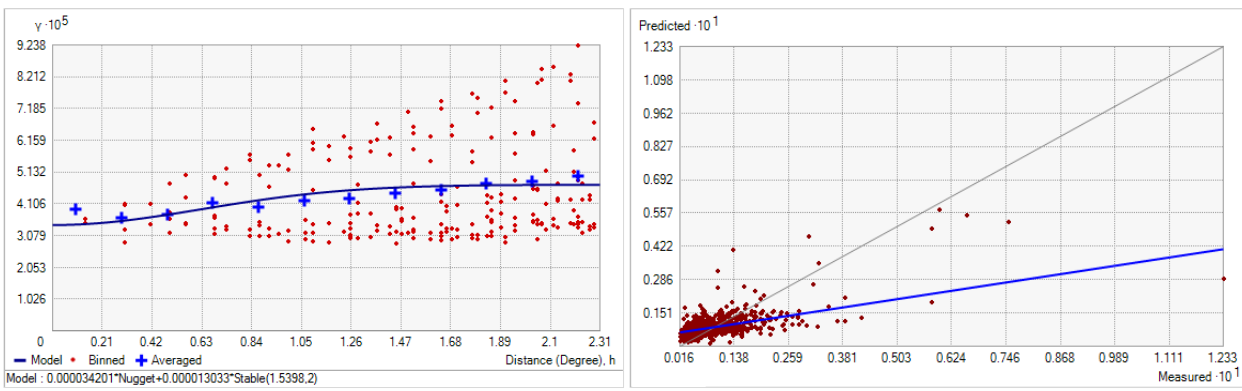

Fig. 148. Left panel: Semivariogram of Bottom Current Mean (m s^{-1}). Binned values are shown as red dots; average points are shown as blue crosses; the model fit to the averaged values is shown as a blue line. Lag size: 0.192 degrees; number of lags: 12; Parameter: 2; Range: 1.540 degrees; Partial Sill: 0.000. Right panel: Scatterplot of predicted values versus observed values for the model of Bottom Current Mean (m s^{-1}).

Table 60. Results of cross-validation of the kriged model for the Bottom Current Mean (m s^{-1}).

Prediction error	**Value**
Number of Observations	589
Overall Mean Error	-6.671×10^{-5}
Root Mean Square Prediction Error	0.007
Standardized Mean	-0.009
Standardized Root Mean Square Prediction Error	1.151
Average Standard Error	0.006

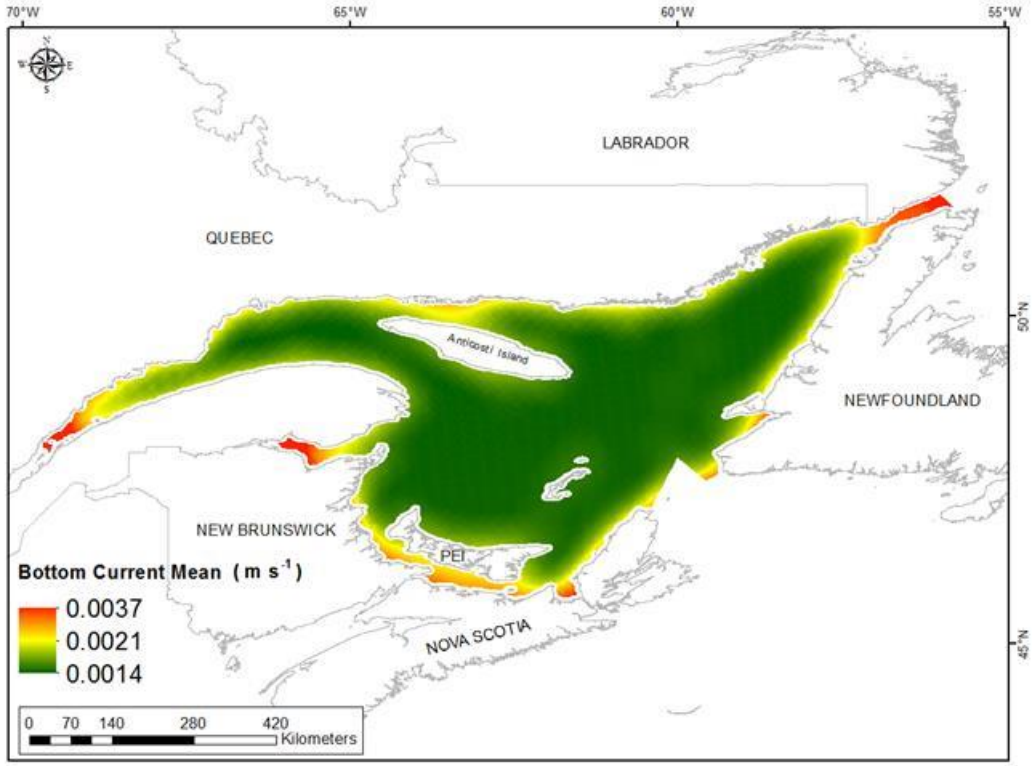

Fig. 149. Prediction standard error surface of Bottom Current Mean (m s^{-1}).

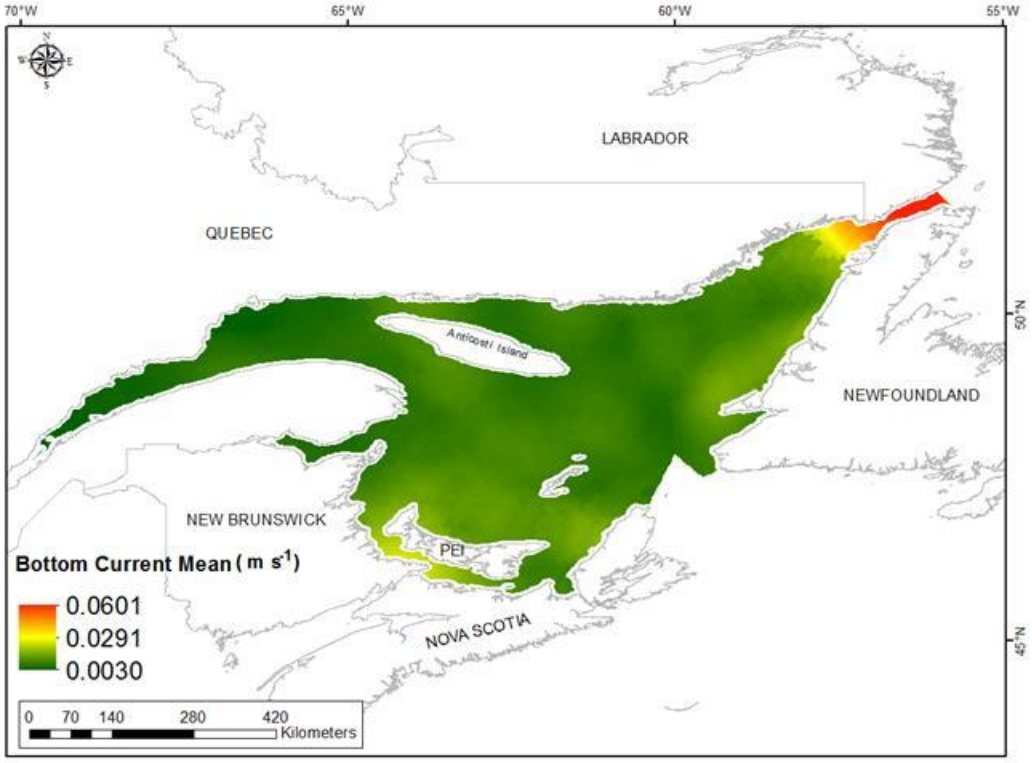

Fig. 150. Interpolated prediction surface of Bottom Current Mean (m s^{-1}).

Bottom Current Minimum

This variable displayed a right-skewed distribution with high kurtosis prior to modeling (Table 61, Fig. 151). The data were higher than predicted by a normal distribution at low and high values and lower than predicted at mid-range values (Fig. 152). The areas of over- and under-prediction did not show a strong spatial pattern with both error types distributed throughout the spatial extent (Fig. 152).

The semivariogram showed little autocorrelation present in the data and poor fit between measured and predicted values of the model (Fig. 153). Nevertheless, the model showed excellent cross-validation statistics (Table 62) indicating that it was very good at prediction. The error map showed a 'bullseye' pattern with error increasing with distance from data points (Fig. 154). The kriged surface is presented in Fig. 155.

Table 61. Distributional properties of Bottom Current Minimum (m s^{-1}).

Property	Value
Number of Observations	589
Minimum	1.000×10^{-6}
Maximum	0.004
Mean	4.028×10^{-4}
Median	2.412×10^{-4}
Standard Deviation	5.072×10^{-4}
Skewness	2.303
Kurtosis	10.851

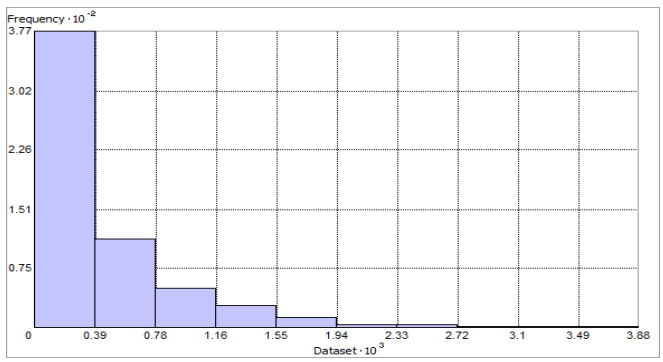

Fig. 151. Distribution of Bottom Current Minimum (m s^{-1}). Histogram was illustrated using 10 bins. X axis shown at 10^{-2}; Y axis is shown at 10^{-3}.

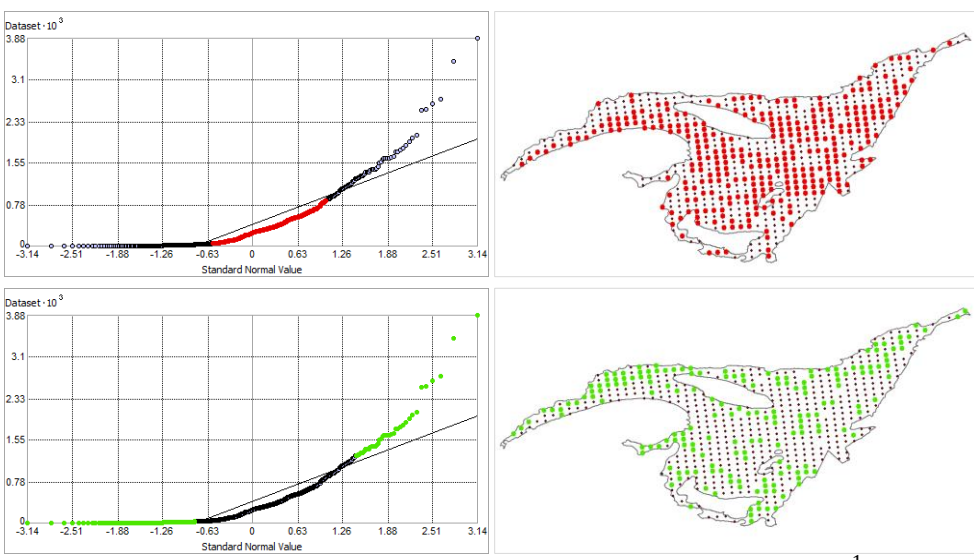

Fig. 152. Normal Q-Q plot for data values of Bottom Current Minimum (m s^{-1}). Points falling under (upper panel) and over (bottom panel) the reference line are mapped.

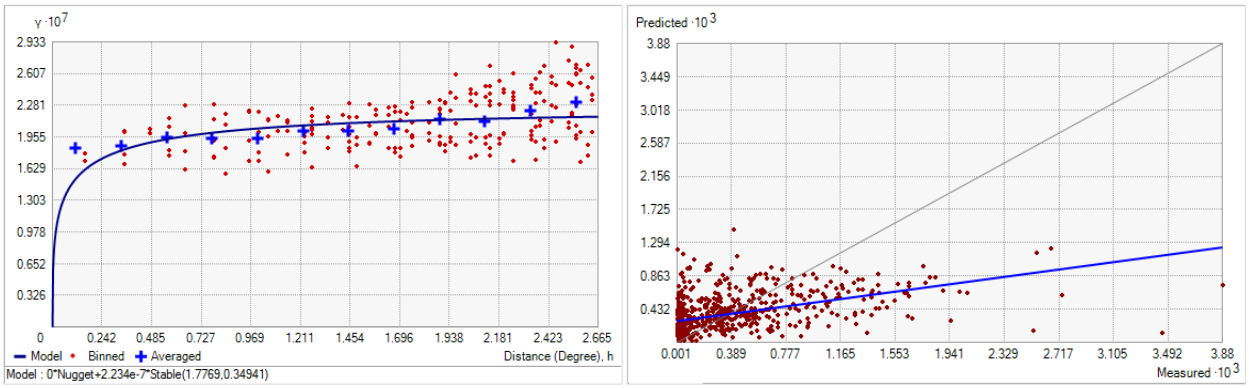

Fig. 153. Left panel: Semivariogram of Bottom Current Minimum (m s^{-1}). Binned values are shown as red dots; average points are shown as blue crosses; the model fit to the averaged values is shown as a blue line. Lag size: 0.222 degrees; number of lags: 12; Parameter: 0.349; Range: 1.777 degrees; Partial Sill: 2.230 x 10^{-7}. Right panel: Scatterplot of predicted values versus observed values for the model of Bottom Current Minimum (m s^{-1}).

Table 62. Results of cross-validation of the kriged model for Bottom Current Minimum (m s^{-1}).

Prediction error	**Value**
Number of Observations	589
Overall Mean Error	4.117 x 10^{-8}
Root Mean Square Prediction Error	4.644 x 10^{-4}
Standardized Mean	-5.412 x 10^{-7}
Standardized Root Mean Square Prediction Error	1.075
Average Standard Error	4.295 x 10^{-4}

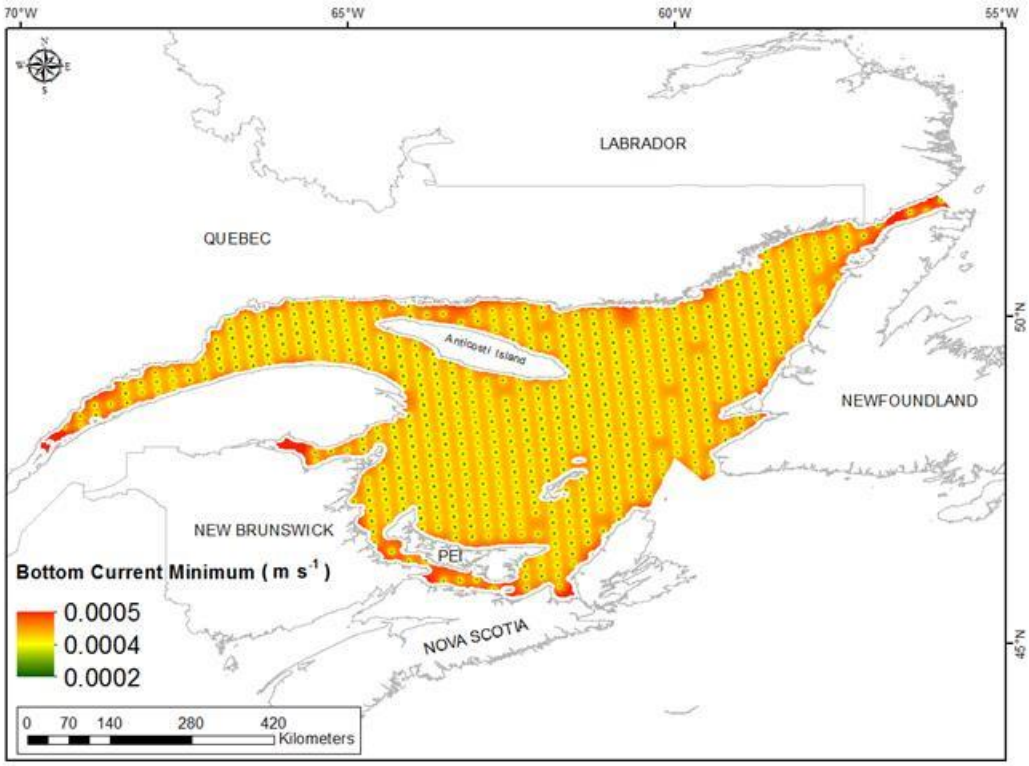

Fig. 154. Prediction standard error surface of Bottom Current Minimum (m s^{-1}).

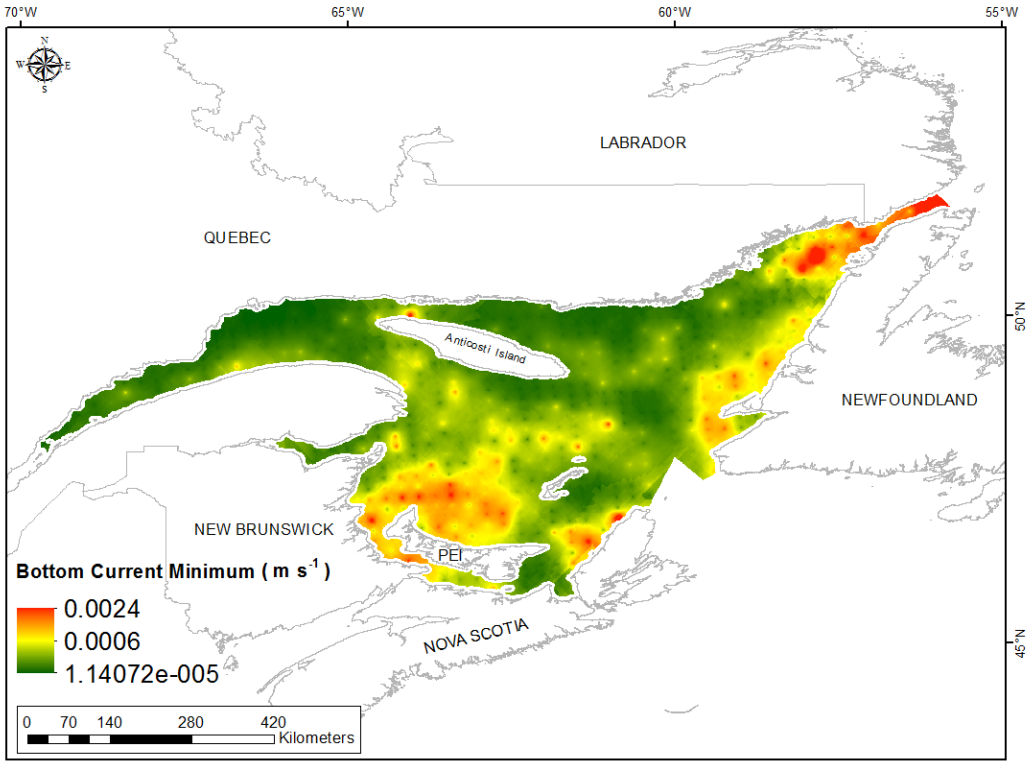

Fig. 155. Interpolated prediction surface of Bottom Current Minimum (m s^{-1}).

Bottom Current Maximum

This variable displayed a right-skewed distribution with very high kurtosis prior to modeling (Table 63, Fig. 156). The data were higher than predicted by a normal distribution at high values (Fig. 157). Mid-range values were slightly lower than the reference line. The areas of over- and under-prediction did not show a strong spatial pattern with both error types distributed through the spatial extent (Fig. 157).

The semivariogram showed weak autocorrelation present in the data and the kriged model show poor fit between measured and predicted values (Fig. 158). Nevertheless, the model showed excellent cross-validation statistics (Table 64) indicating that it was very good at prediction. The error map showed no spatial pattern over the study extent except for along the coast where the error was high (Fig. 159). The kriged surface is presented in Fig. 160.

Table 63. Distributional properties of Bottom Current Maximum (m s^{-1}).

Property	Value
Number of Observations	589
Minimum	0.006
Maximum	0.353
Mean	0.037
Median	0.030
Standard Deviation	0.031
Skewness	4.309
Kurtosis	32.870

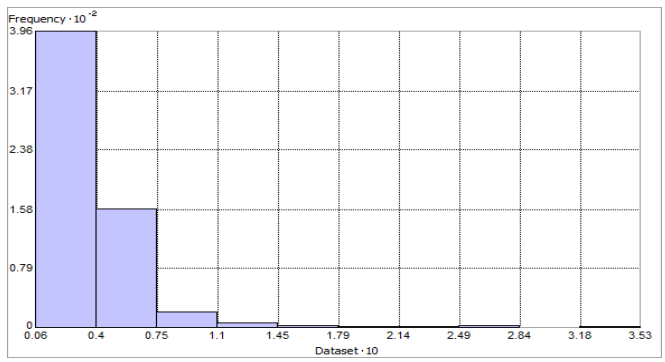

Fig. 156. Distribution of Bottom Current Maximum (m s^{-1}). Histogram was illustrated using 10 bins. Y axis is shown at 10^{-2}.

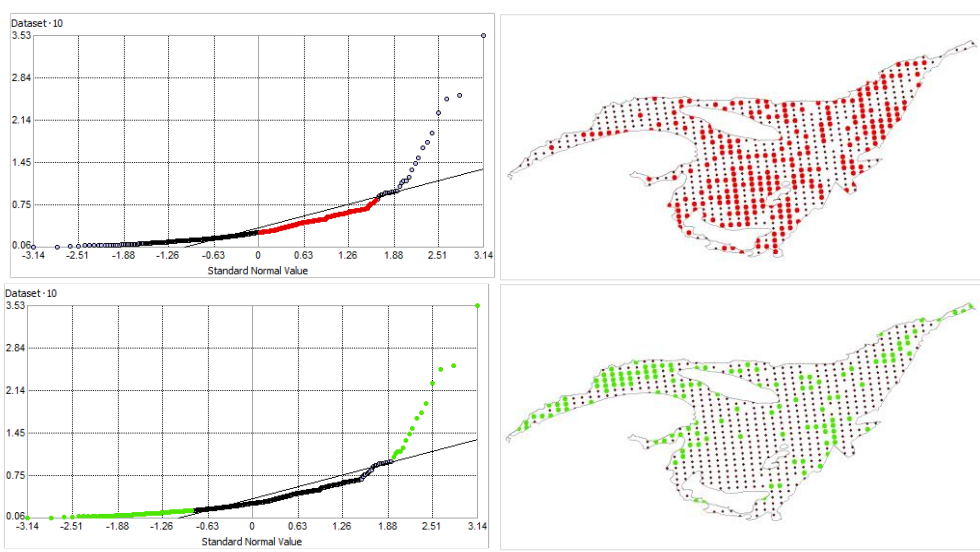

Fig. 157. Normal Q-Q plot for data values of Bottom Current Maximum (m s^{-1}). Points falling under (upper panel) and over (bottom panel) the reference line are mapped.

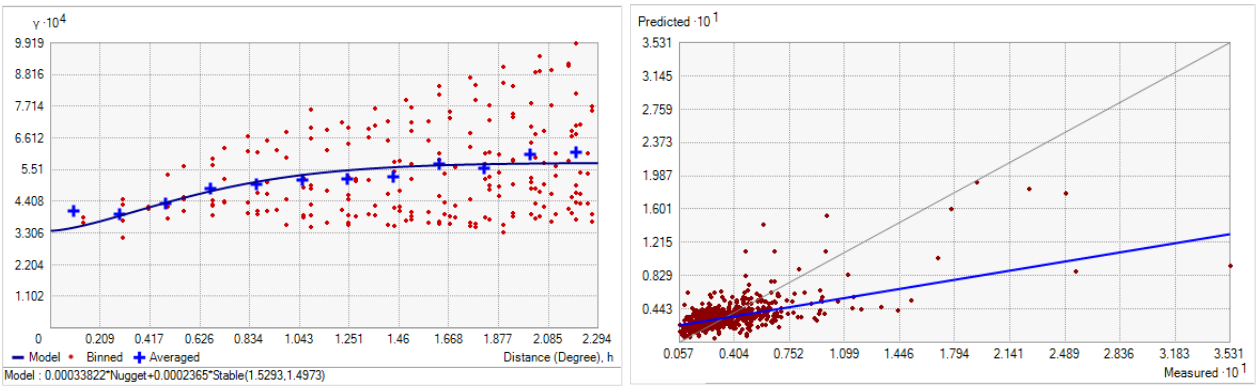

Fig. 158. Left panel: Semivariogram of Bottom Current Maximum (m s^{-1}). Binned values are shown as red dots; average points are shown as blue crosses; the model fit to the averaged values is shown as a blue line. Lag size: 0.191 degrees; number of lags: 12; Parameter: 1.497; Range: 1.529 degrees; Partial Sill: 0.0002. Right panel: Scatterplot of predicted values versus observed values for the model of Bottom Current Maximum (m s^{-1}).

Table 64. Results of cross-validation of the kriged model for Bottom Current Maximum (m s^{-1}).

Prediction error	**Value**
Number of Observations	589
Overall Mean Error	-2.142×10^{-4}
Root Mean Square Prediction Error	0.023
Standardized Mean	-0.009
Standardized Root Mean Square Prediction Error	1.128
Average Standard Error	0.020

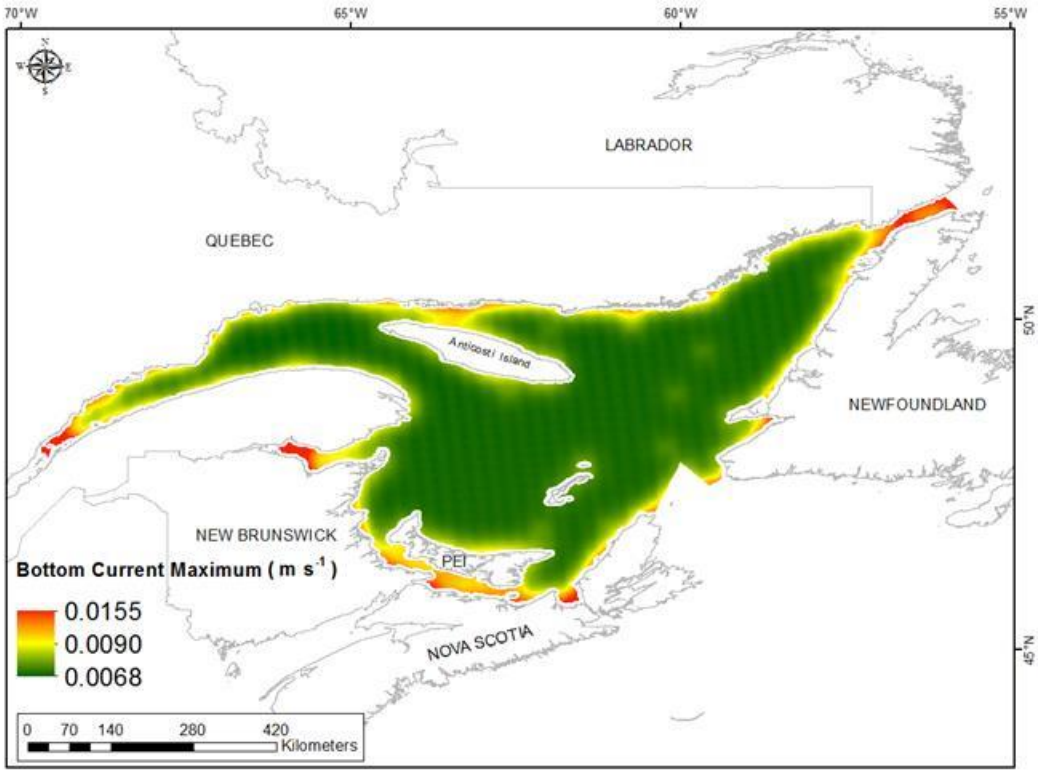

Fig. 159. Prediction standard error surface of Bottom Current Maximum (m s^{-1}).

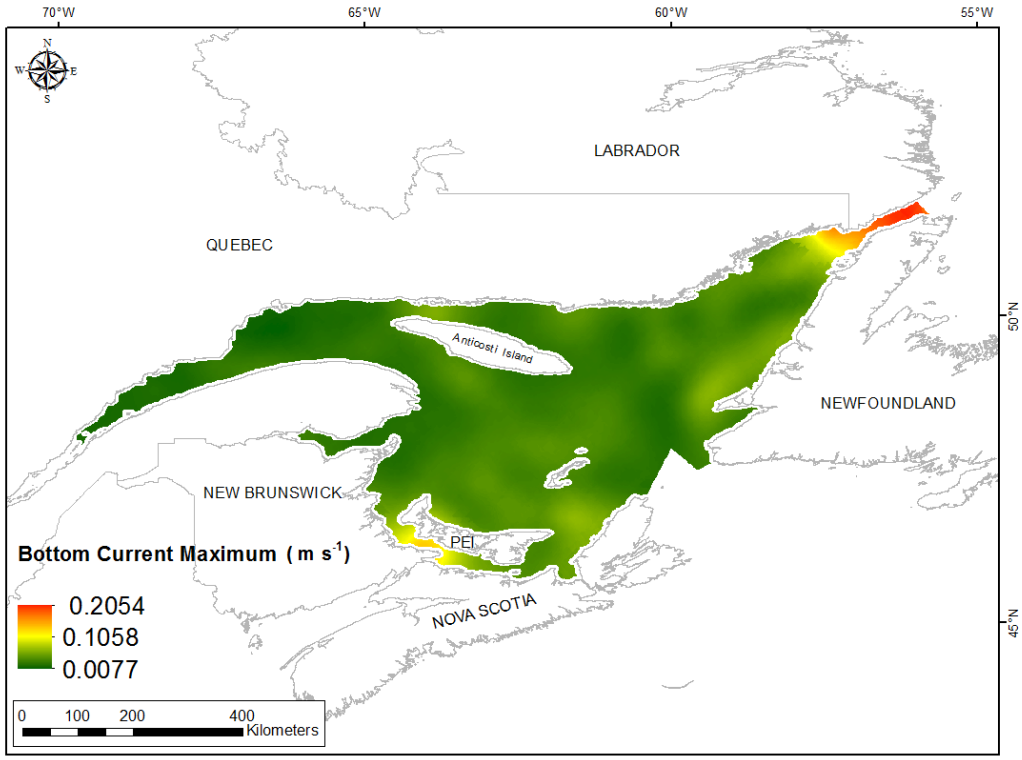

Fig. 160. Interpolated prediction surface of Bottom Current Maximum (m s^{-1}).

Bottom Current Range

This variable displayed a right-skewed distribution with a single large outlier to modeling (Table 65, Fig. 161). The data were higher than predicted by a normal distribution at high values (Fig. 162). Mid-range values were slightly lower than the reference line. The areas of over- and under-prediction did not show a strong spatial pattern with both error types distributed through the spatial extent (Fig. 162).

The semivariogram showed weak autocorrelation present in the data and the models showed poor fit between the measured and predicted values (Fig. 163). Nevertheless, the model showed good cross-validation statistics (Table 66) indicating that it was good at prediction. The error map showed no spatial pattern over the study extent except for along the coast where it was high (Fig. 164). The kriged surface is presented in Fig. 165.

Table 65. Distributional properties of Bottom Current Range (m s^{-1}).

Property	Value
Number of Observations	589
Minimum	0.006
Maximum	0.352
Mean	0.037
Median	0.029
Standard Deviation	0.031
Skewness	4.348
Kurtosis	33.370

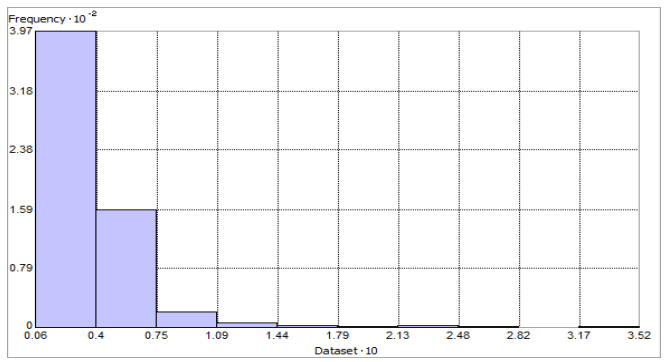

Fig. 161. Distribution of Bottom Current Range (m s^{-1}). Histogram was illustrated using 10 bins. Y axis is shown at 10^{-2}.

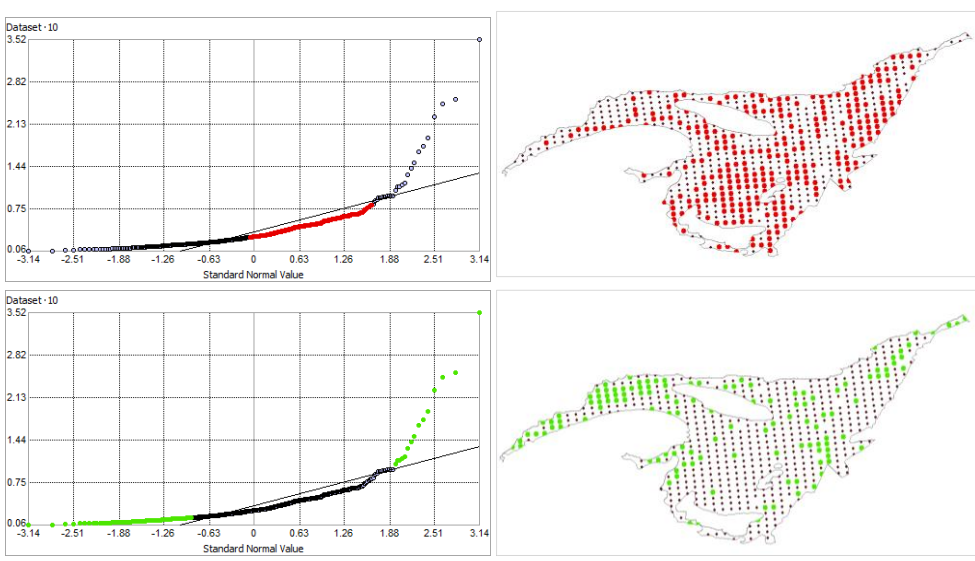

Fig. 162. Normal Q-Q plot for data values of Bottom Current Range (m s^{-1}). Points falling under (upper panel) and over (bottom panel) the reference line are mapped.

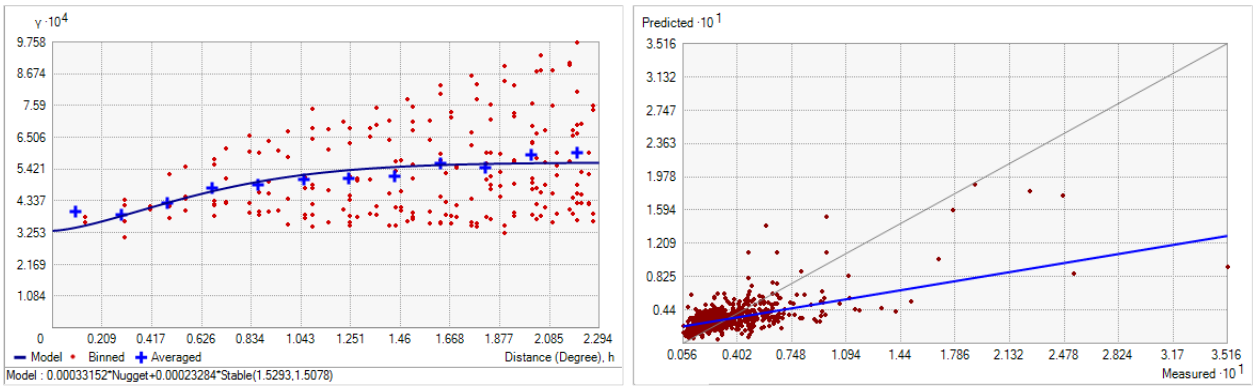

Fig. 163. Left panel: Semivariogram of Bottom Current Range (m s^{-1}). Binned values are shown as red dots; average points are shown as blue crosses; the model fit to the averaged values is shown as a blue line. Lag size: 0.191 degrees; number of lags: 12; Parameter: 1.508; Range: 1.529 degrees; Partial Sill: 2.328 x 10^{-4}. Right panel: Scatterplot of predicted values versus observed values for the model of Bottom Current Range (m s^{-1}).

Table 66. Results of cross-validation of the kriged model for Bottom Current Range (m s^{-1}).

Prediction error	**Value**
Number of Observations	589
Overall Mean Error	-2.124 x 10^{-4}
Root Mean Square Prediction Error	0.023
Standardized Mean	-0.009
Standardized Root Mean Square Prediction Error	1.130
Average Standard Error	0.020

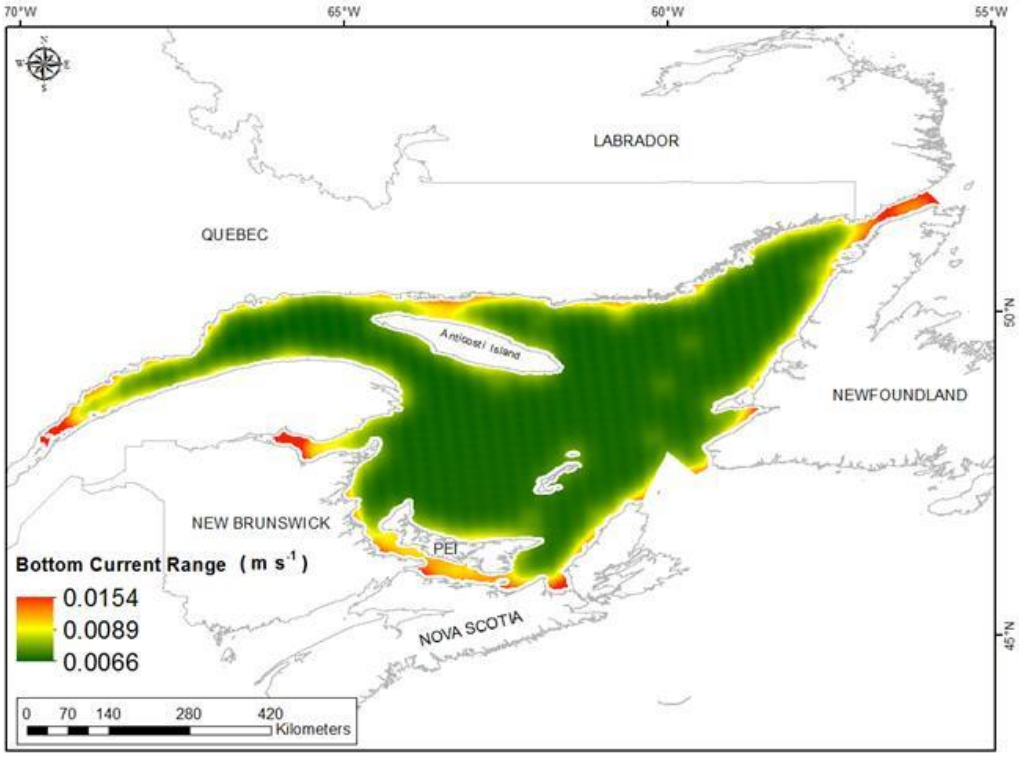

Fig. 164. Prediction standard error surface of Bottom Current Range (m s^{-1}).

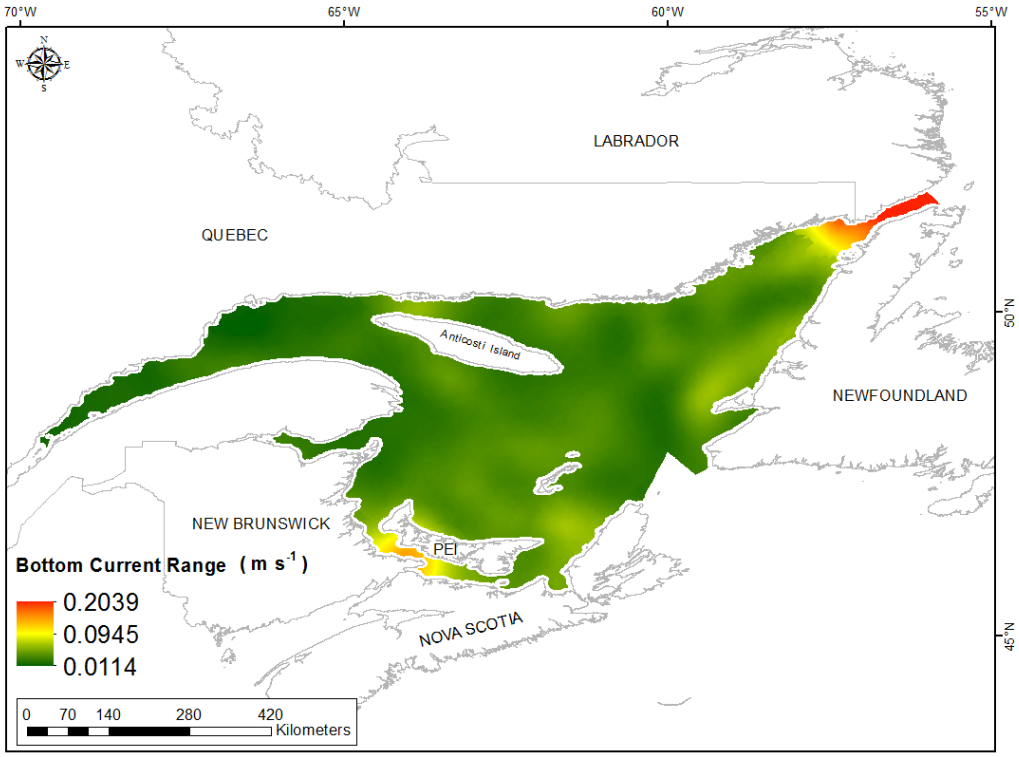

Fig. 165. Interpolated prediction surface of Bottom Current Range (m s^{-1}).

Bottom Current Average Minimum

This variable displayed a right-skewed distribution and an isolated outlier at the upper data range (Table 67, Fig. 166). The data were higher than predicted by a normal distribution at high values (Fig. 167). Mid-range values were slightly lower than the reference line. The areas of over- and under-prediction did not show a strong spatial pattern with both error types distributed across the spatial extent (Fig. 167).

The semivariogram showed little autocorrelation present in the data and the model showed poor fit between measured and predicted values (Fig. 168). Nevertheless, the model showed good cross-validation statistics (Table 68) indicating that it was good at prediction. The error map showed no spatial pattern over the study extent except for along the coast where it was high (Fig. 169). The kriged surface is presented in Fig. 170.

Table 67. Distributional properties of Bottom Current Average Minimum (m s^{-1}).

Property	Value
Number of Observations	589
Minimum	1.720×10^{-4}
Maximum	0.026
Mean	2.146×10^{-3}
Median	1.621×10^{-3}
Standard Deviation	2.078×10^{-3}
Skewness	3.958
Kurtosis	35.155

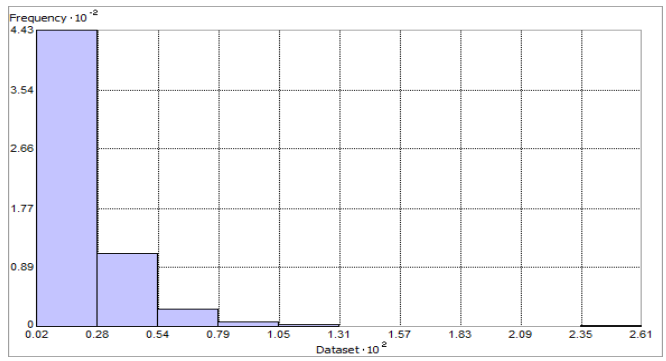

Fig. 166. Distribution of Bottom Current Average Minimum (m s^{-1}). Histogram was illustrated using 10 bins. X axis is shown at 10^2; Y axis is shown at 10^{-2}.

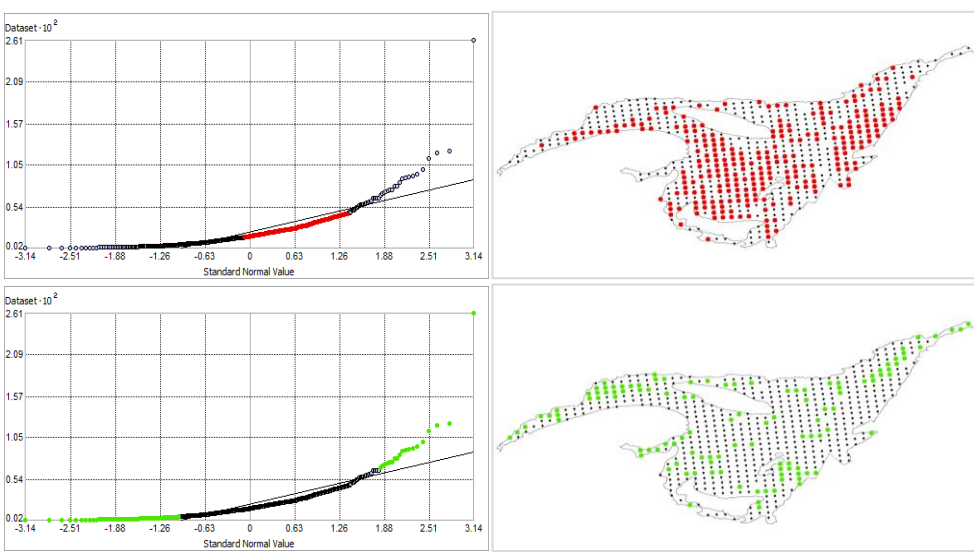

Fig. 167. Normal Q-Q plot for data values of Bottom Current Average Minimum (m s^{-1}). Points falling under (upper panel) and over (bottom panel) the reference line are mapped.

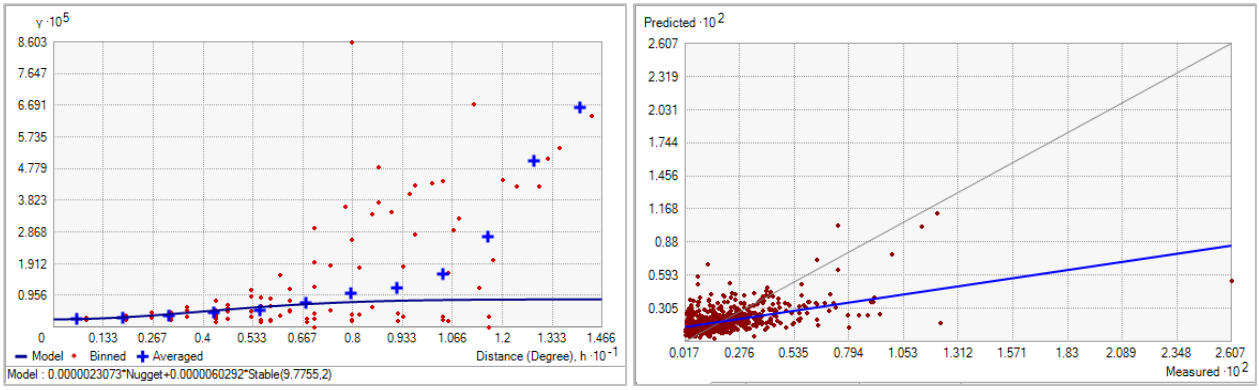

Fig. 168. Left panel: Semivariogram of Bottom Current Average Minimum (m s^{-1}). Binned values are shown as red dots; average points are shown as blue crosses; the model fit to the averaged values is shown as a blue line. Lag size: 1.222 degrees; number of lags: 12; Parameter: 2; Range: 9.775 degrees; Partial Sill: 6.029 x 10^{-6}. Right panel: Scatterplot of predicted values versus observed values for the model of Bottom Current Average Minimum (m s^{-1}).

Table 68. Results of cross-validation of the kriged model for Bottom Current Average Minimum (m s^{-1}).

Prediction error	**Value**
Number of Observations	589
Overall Mean Error	-1.922 x 10^{-6}
Root Mean Square Prediction Error	0.002
Standardized Mean	-0.001
Standardized Root Mean Square Prediction Error	1.118
Average Standard Error	0.002

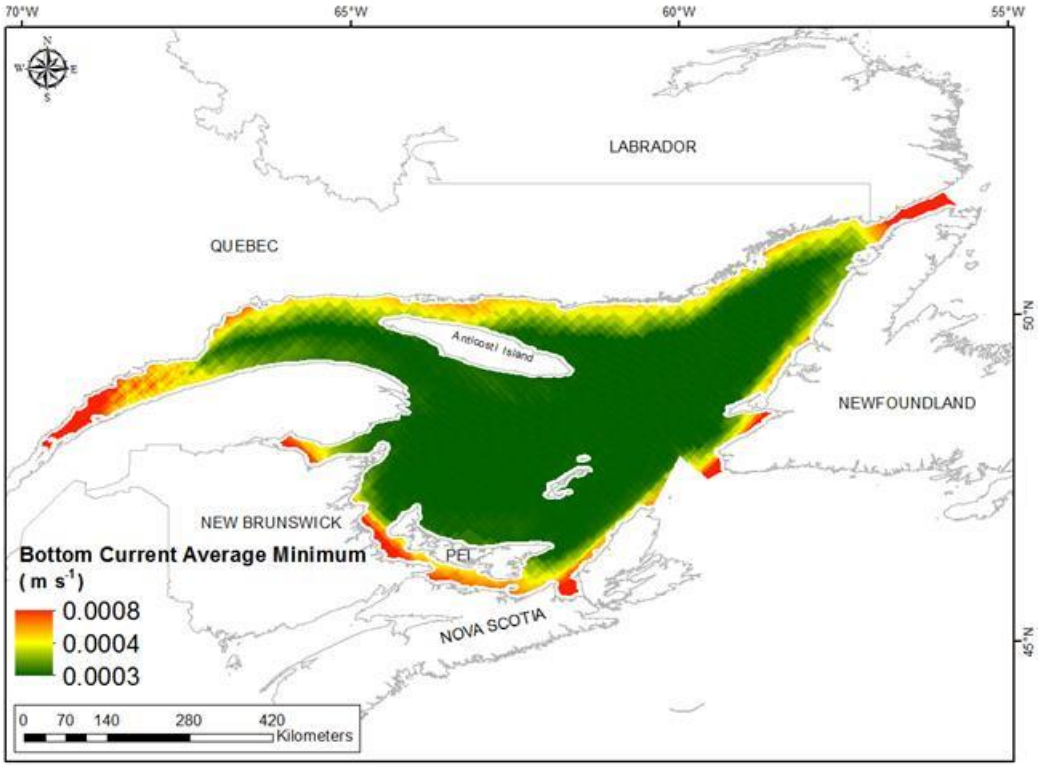

Fig. 169. Prediction standard error surface of Bottom Current Average Minimum (m s^{-1}).

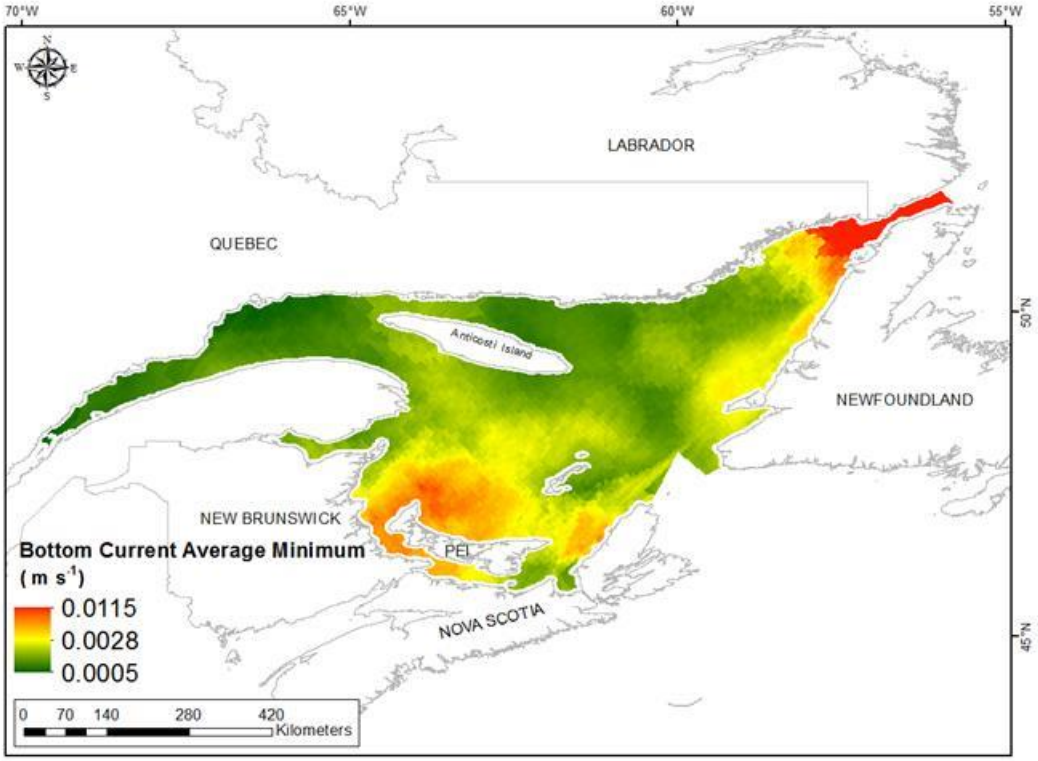

Fig. 170. Interpolated prediction surface of Bottom Current Average Minimum (m s^{-1}).

Bottom Current Average Maximum

This variable displayed a right-skewed distribution with a outlying data in the upper range (Table 69, Fig. 171). The data were higher than predicted by a normal distribution at high values and lower at mid-range values (Fig. 172). The areas of over- and under-prediction did not show a strong spatial pattern with both error types distributed across the spatial extent (Fig. 172).

The semivariogram showed weak autocorrelation present in the data and the model showed poor fit between measured and predicted values (Fig. 173). Nevertheless, the model showed good cross-validation statistics (Table 70) indicating that it was good at prediction. The error map showed no spatial pattern over the study extent except for along the coast where it was high (Fig. 174). The kriged surface is presented in Fig. 175.

Table 69. Distributional properties of Bottom Current Average Maximum (m s^{-1}).

Property	Value
Number of Observations	589
Minimum	0.003
Maximum	0.273
Mean	0.024
Median	0.019
Standard Deviation	0.022
Skewness	5.200
Kurtosis	44.578

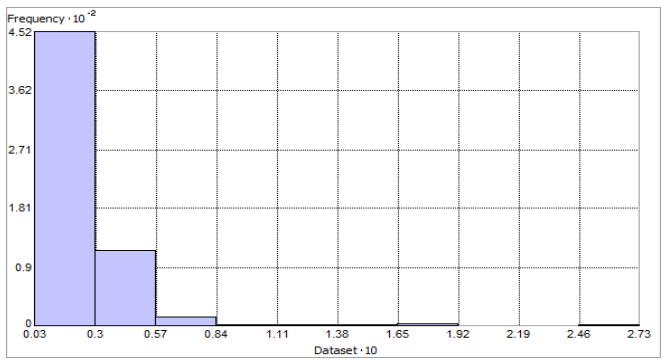

Fig. 171. Distribution of Bottom Current Average Maximum (m s^{-1}). Histogram was illustrated using 10 bins. X axis is shown at 10; Y axis is shown at 10^{-2}.

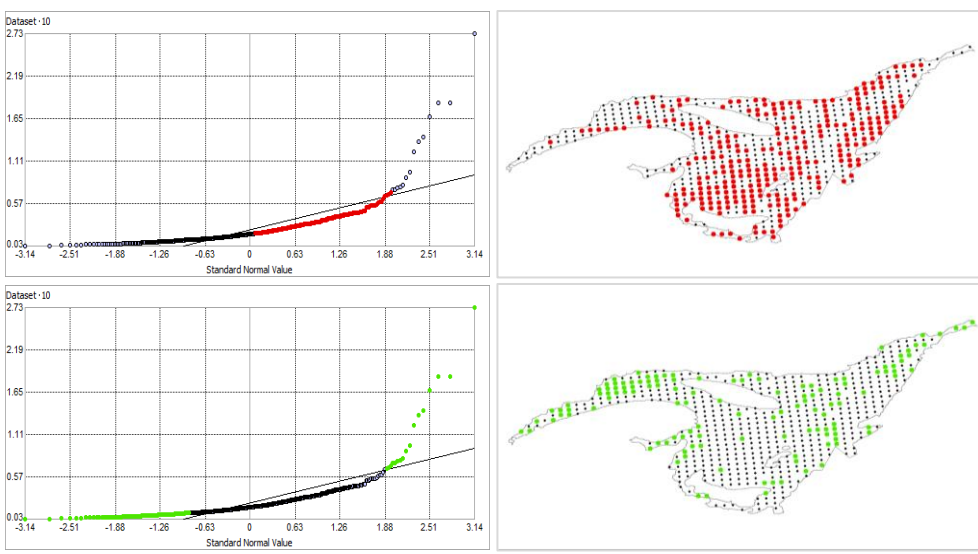

Fig. 172. Normal Q-Q plot for data values of Bottom Current Average Maximum (m s^{-1}). Points falling under (upper panel) and over (bottom panel) the reference line are mapped.

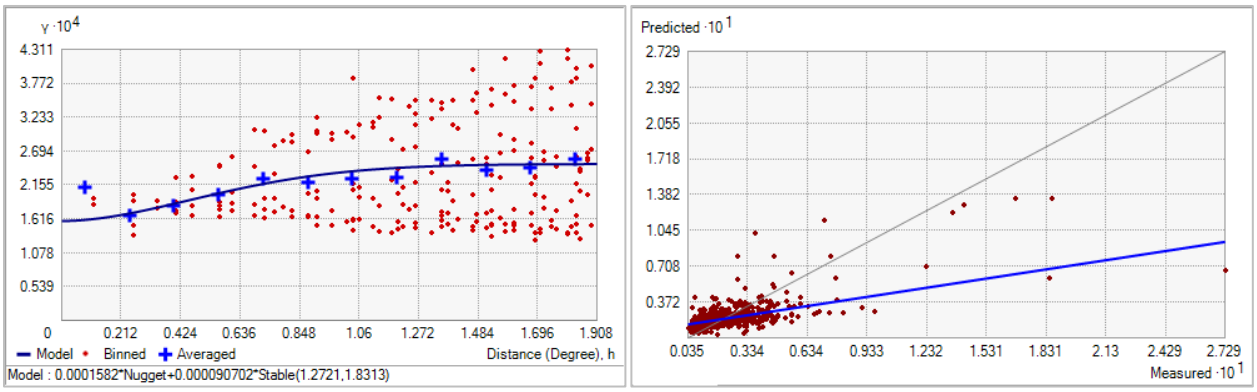

Fig. 173. Left panel: Semivariogram of Bottom Current Average Maximum (m s^{-1}). Binned values are shown as red dots; average points are shown as blue crosses; the model fit to the averaged values is shown as a blue line. Lag size: 0.159 degrees; number of lags: 12; Parameter: 1.831; Range: 1.272 degrees; Partial Sill: 9.070 x 10^{-5}. Right panel: Scatterplot of predicted values versus observed values for the model of Bottom Current Average Maximum (m s^{-1}).

Table 70. Results of cross-validation of the kriged model for Bottom Current Average Maximum (m s^{-1}).

Prediction error	**Value**
Number of Observations	589
Overall Mean Error	-1.791 x 10^{-4}
Root Mean Square Prediction Error	0.016
Standardized Mean	-0.011
Standardized Root Mean Square Prediction Error	1.173
Average Standard Error	0.013

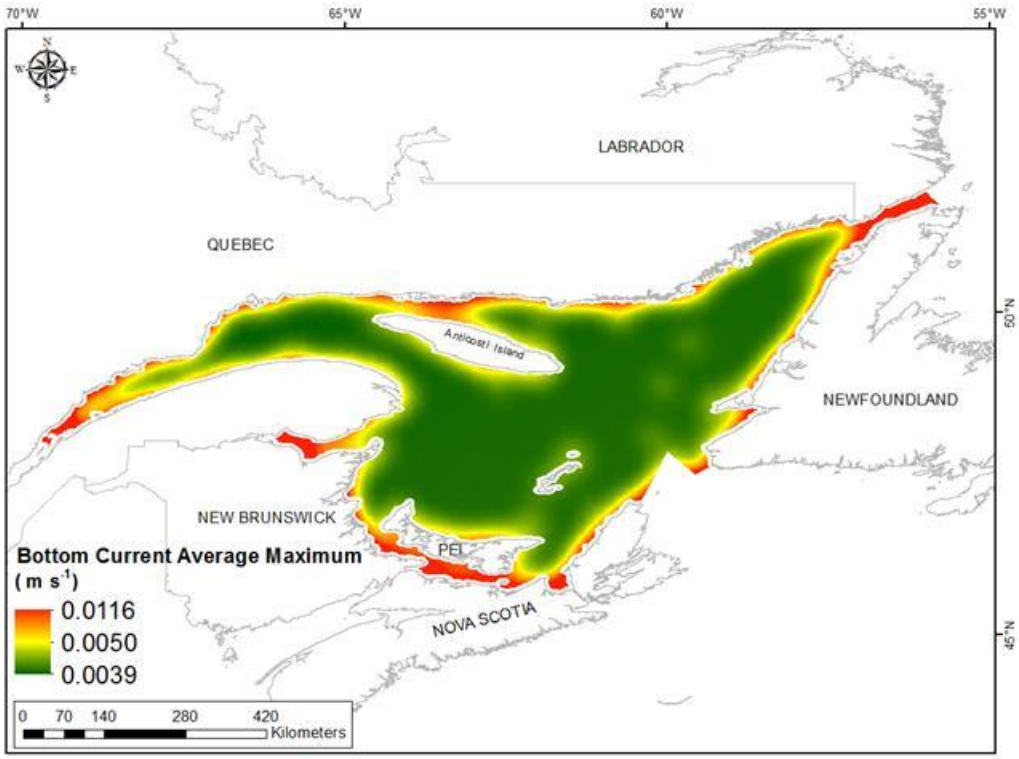

Fig. 174. Prediction standard error surface of Bottom Current Average Maximum (m s^{-1}).

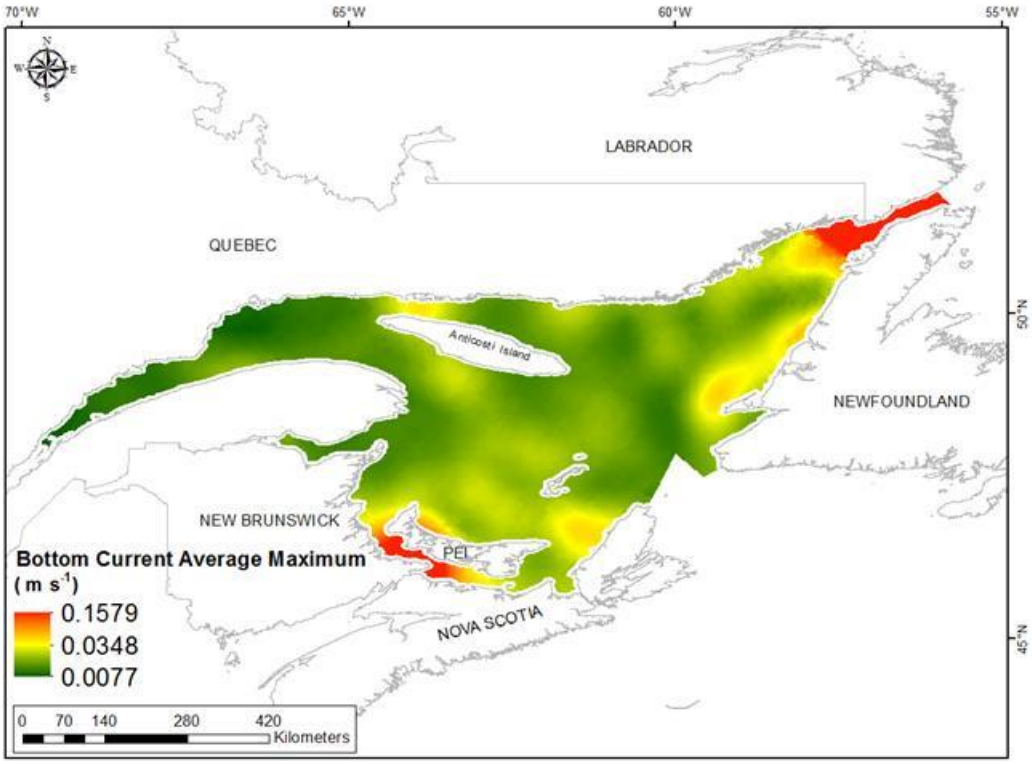

Fig. 175. Interpolated prediction surface of Bottom Current Average Maximum (m s^{-1}).

Bottom Current Average Range

This variable displayed a right-skewed distribution with outlying data in the upper range (Table 71, Fig. 176). The data were higher than predicted by a normal distribution at high values (Fig. 177). Mid-range values were slightly lower than the reference line. The areas of over- and under-prediction did not show a strong spatial pattern with both error types distributed across the spatial extent (Fig. 177).

The semivariogram showed weak autocorrelation present in the data and the model showed poor fit between measured and predicted values (Fig. 178). Nevertheless, the model showed good cross-validation statistics (Table 72) indicating that it was good at prediction. The error map showed no spatial pattern over the study extent except for along the coast where it was high (Fig. 179). The kriged surface is presented in Fig. 180.

Table 71. Distributional properties of Bottom Current Average Range (m s^{-1}).

Property	Value
Number of Observations	589
Minimum	0.003
Maximum	0.247
Mean	0.022
Median	0.017
Standard Deviation	0.022
Skewness	5.257
Kurtosis	44.263

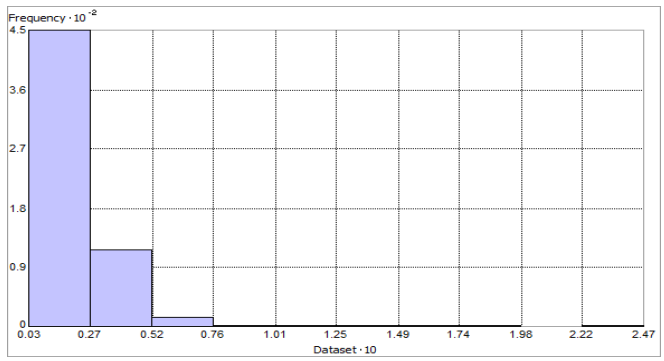

Fig. 176. Distribution of Bottom Current Average Range (m s^{-1}). Histogram was illustrated using 10 bins. X axis is shown at 10; Y axis is shown at 10^{-2}.

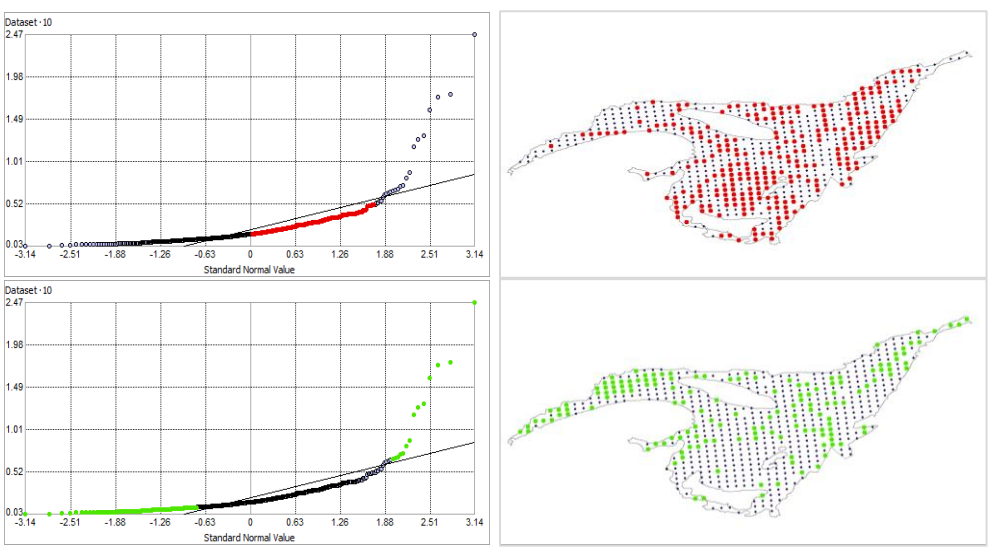

Fig. 177. Normal Q-Q plot for data values of Bottom Current Average Range (m s^{-1}). Points falling under (upper panel) and over (bottom panel) the reference line are mapped.

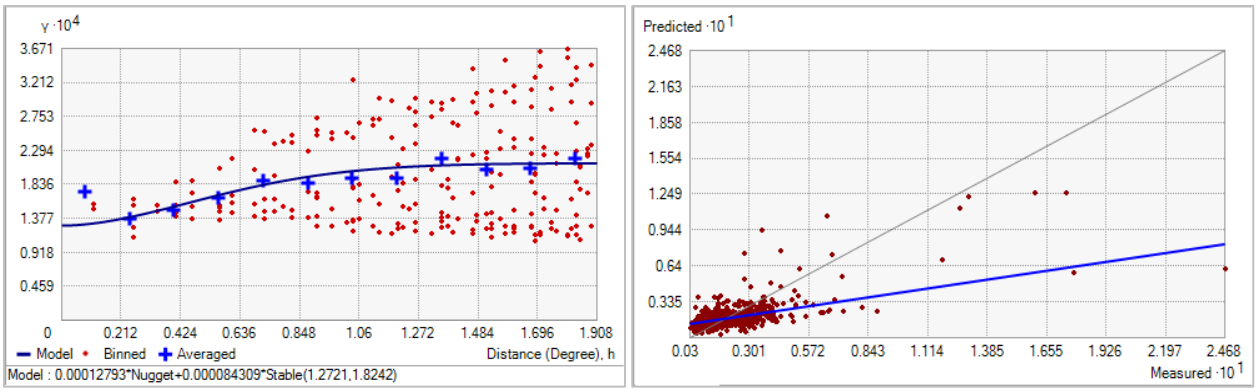

Fig. 178. Left panel: Semivariogram of Bottom Current Average Range (m s^{-1}). Binned values are shown as red dots; average points are shown as blue crosses; the model fit to the averaged values is shown as a blue line. Lag size: 0.59 degrees; number of lags: 12; Parameter: 1.824; Range: 1.272 degrees; Partial Sill: 8.430 x 10^{-5}. Right panel: Scatterplot of predicted values versus observed values for the model of Bottom Current Average Range (m s^{-1}).

Table 72. Results of cross-validation of the kriged model for the Bottom Current Average Range (m s^{-1}).

Prediction error	**Value**
Number of Observations	589
Overall Mean Error	-0.0002
Root Mean Square Prediction Error	0.015
Standardized Mean	-0.011
Standardized Root Mean Square Prediction Error	1.178
Average Standard Error	0.012

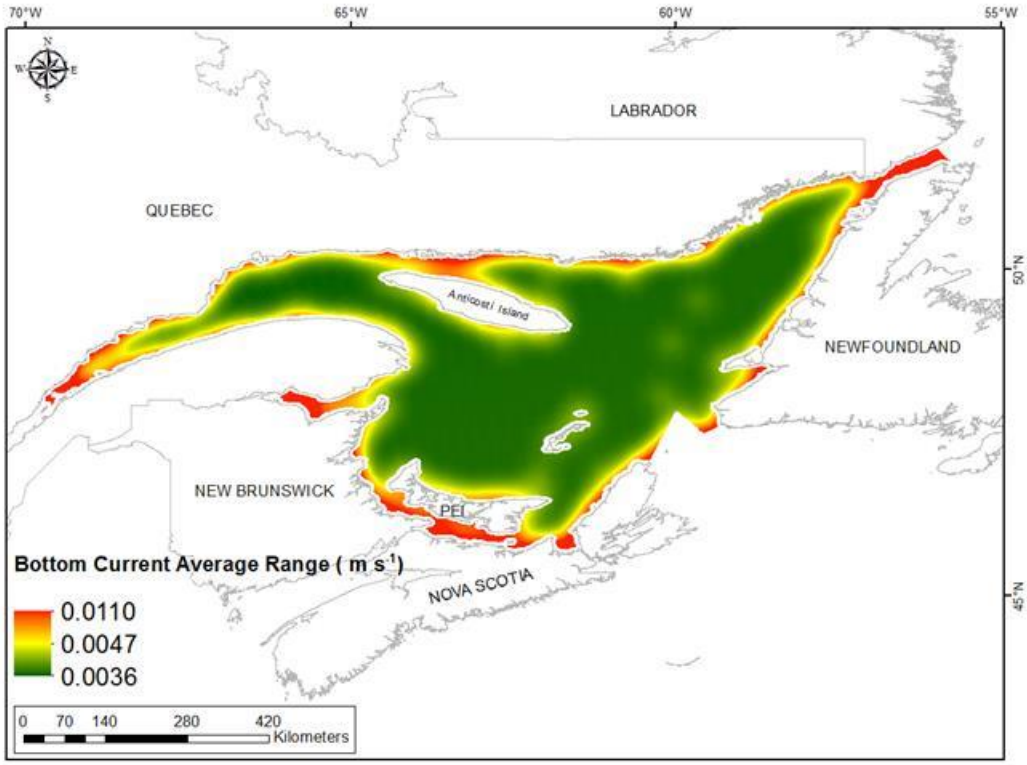

Fig. 179. Prediction standard error surface of Bottom Current Average Range (m s^{-1}).

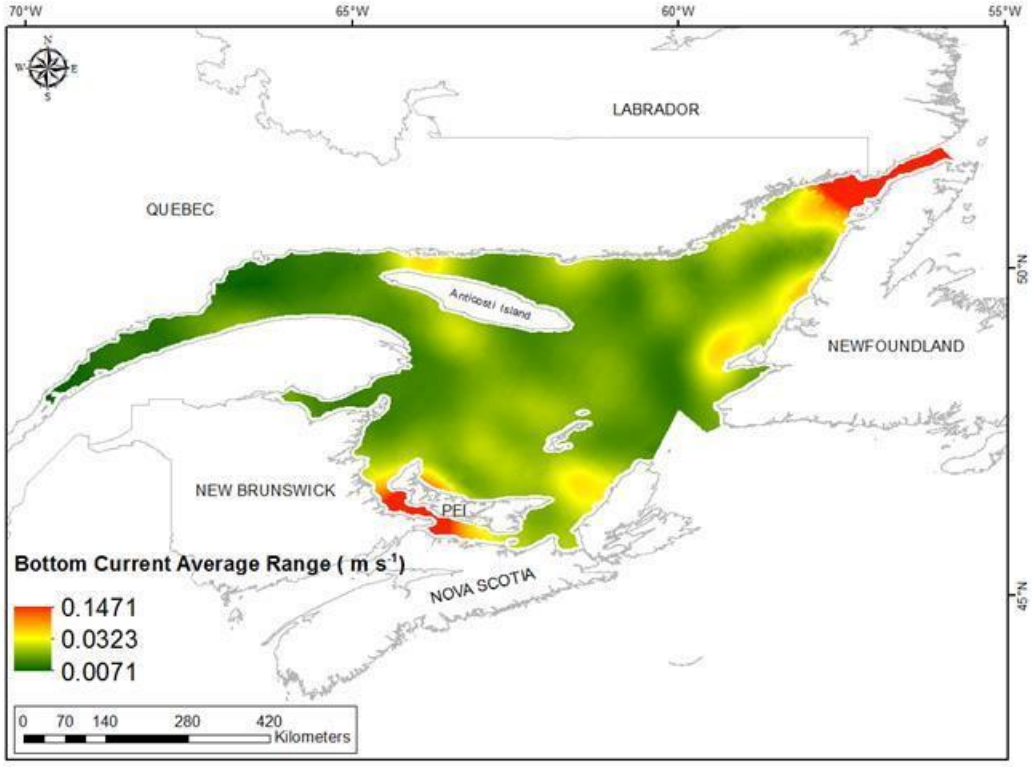

Fig. 180. Interpolated prediction surface of Bottom Current Average Range (m s^{-1}).

Surface Current Mean

This variable displayed a slightly right-skewed distribution with high kurtosis prior to modeling (Table 73, Fig. 181). The data were higher than predicted by a normal distribution at low and high values (Fig. 182). Mid-range values were slightly lower than the reference line. The areas of over- and under-prediction showed a spatial pattern (Fig. 182).

The semivariogram showed no autocorrelation present in the data and the model showed slightly poor fit between measured and observed values (Fig. 183). Nevertheless, the model showed good cross-validation statistics (Table 74) indicating that it was good at prediction. The error map showed no spatial pattern over the study extent except for along the coast where it was high (Fig. 141). The kriged surface is presented in Fig. 185.

Table 73. Distributional properties of Surface Current Mean (m s^{-1}).

Property	Value
Number of Observations	581
Minimum	0.020
Maximum	0.279
Mean	0.074
Median	0.064
Standard Deviation	0.036
Skewness	2.339
Kurtosis	10.019

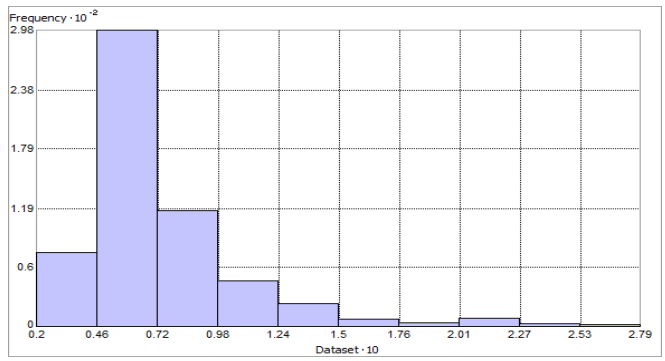

Fig. 181. Distribution of Surface Current Mean (m s^{-1}). Histogram was illustrated using 10 bins. Y axis is shown at 10^{-2}.

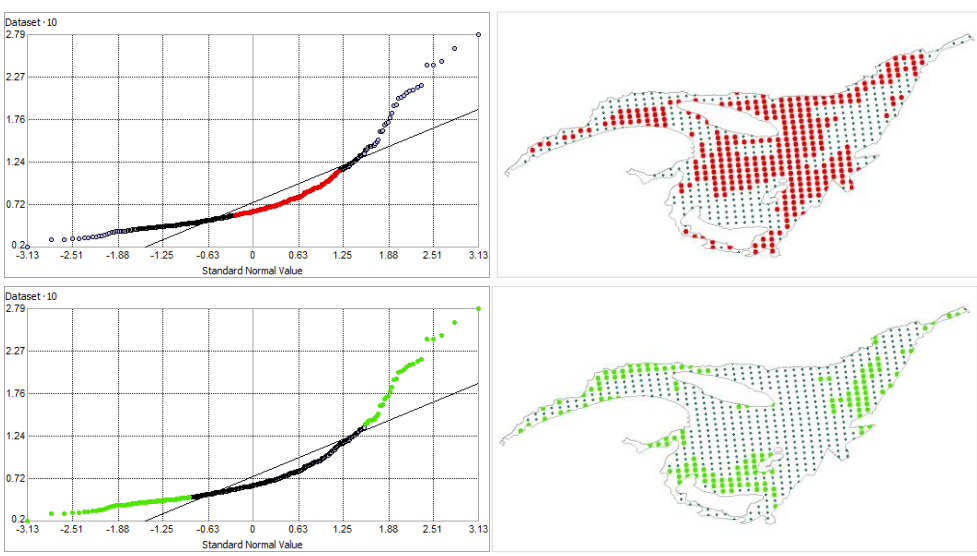

Fig. 182. Normal Q-Q plot for data values of Surface Current Mean (m s^{-1}). Points falling under (upper panel) and over (bottom panel) the reference line are mapped.

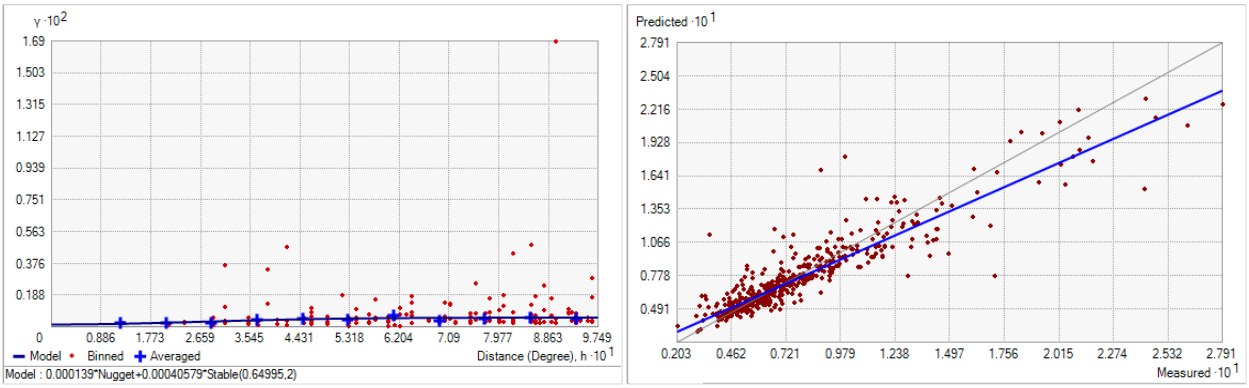

Fig. 183. Left panel: Semivariogram of Surface Current Mean (m s^{-1}). Binned values are shown as red dots; average points are shown as blue crosses; the model fit to the averaged values is shown as a blue line. Lag size: 0.081 degrees; number of lags: 12; Parameter: 2; Range: 0.650 degrees; Partial Sill: 4.058 x 10^{-4}. Right panel: Scatterplot of predicted values versus observed values for the model of Surface Current Mean (m s^{-1}).

Table 74. Results of cross-validation of the kriged model for Surface Current Mean (m s^{-1}).

Prediction error	**Value**
Number of Observations	581
Overall Mean Error	-1.9354 x 10^{-4}
Root Mean Square Prediction Error	0.014
Standardized Mean	-0.010
Standardized Root Mean Square Prediction Error	0.866
Average Standard Error	0.015

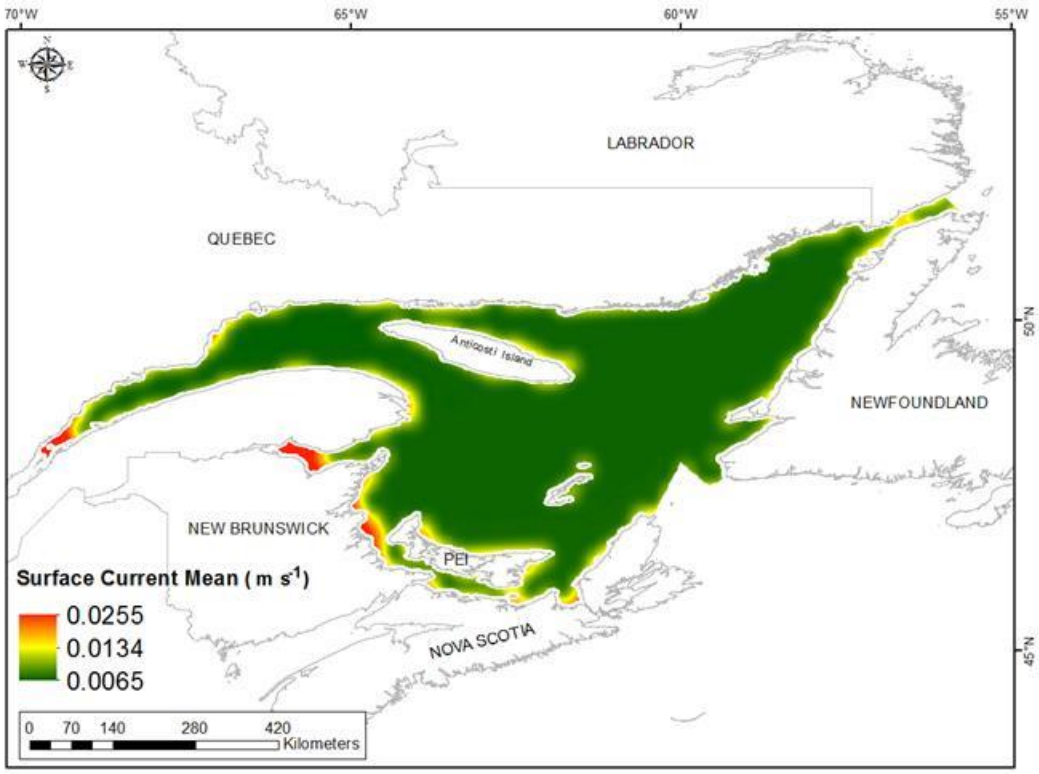

Fig. 184. Prediction standard error surface of Surface Current Mean (m s^{-1}).

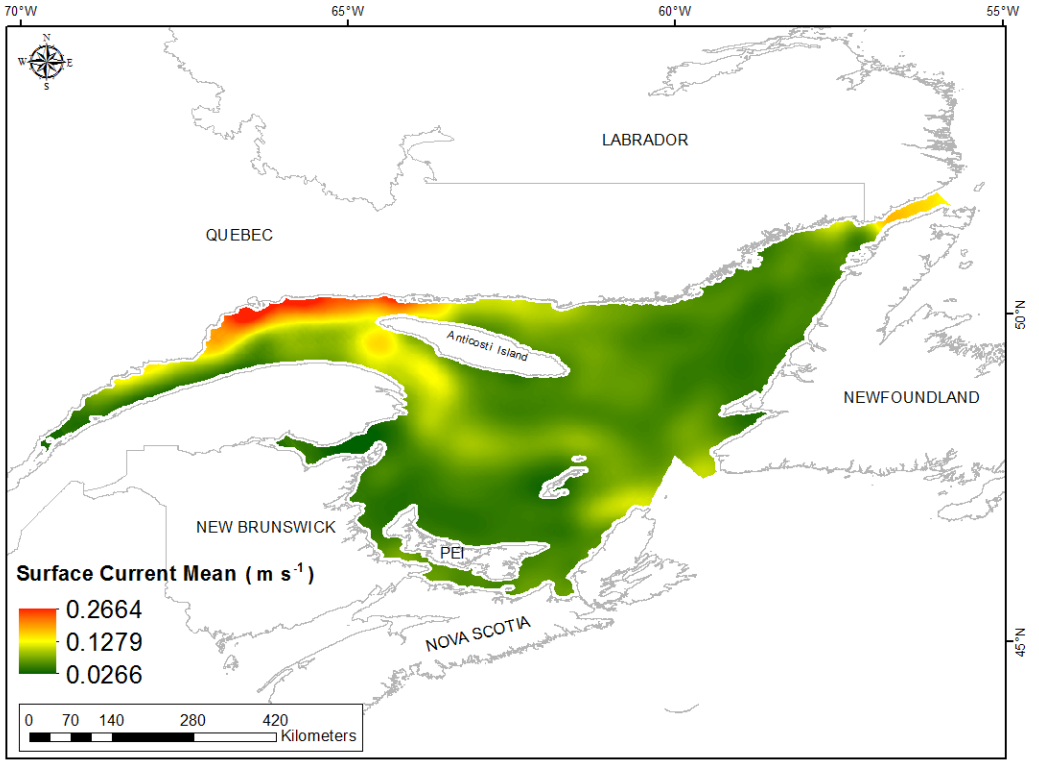

Fig. 185. Interpolated prediction surface of Surface Current Mean (m s^{-1}).

Surface Current Minimum

This variable displayed a right-skewed distribution with outlying data in the upper range (Table 75, Fig. 186). The data were higher than predicted by a normal distribution at high values (Fig. 187). Mid-range values were slightly lower than the reference line. The areas of over- and under-prediction did not show a strong spatial pattern with both error types distributed across the spatial extent (Fig. 187).

The semivariogram showed little autocorrelation present in the data and the model showed poor fit between measured and predicted values (Fig. 188). Nevertheless, the model showed excellent cross-validation statistics (Table 76) indicating that it was very good at prediction. The error map showed a 'bullseye' pattern with error increasing with distance from data points (Fig. 189). The kriged surface is presented in Fig. 190.

Table 75. Distributional properties of Surface Current Minimum (m s^{-1}).

Property	Value
Number of Observations	581
Minimum	4.000×10^{-6}
Maximum	0.042
Mean	0.005
Median	0.004
Standard Deviation	0.005
Skewness	3.068
Kurtosis	18.867

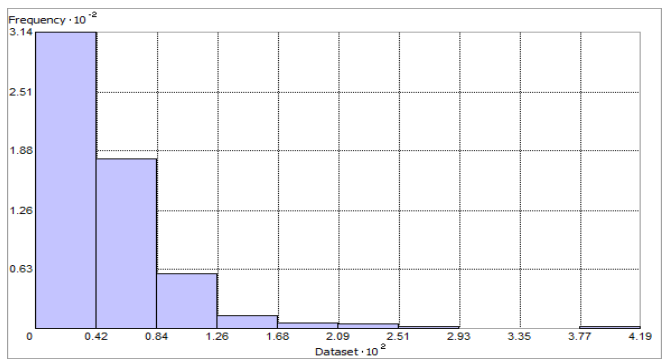

Fig. 186. Distribution of Surface Current Minimum (m s^{-1}). Histogram was illustrated using 10 bins. X axis shown at 10^2; Y axis shown at 10^{-2}.

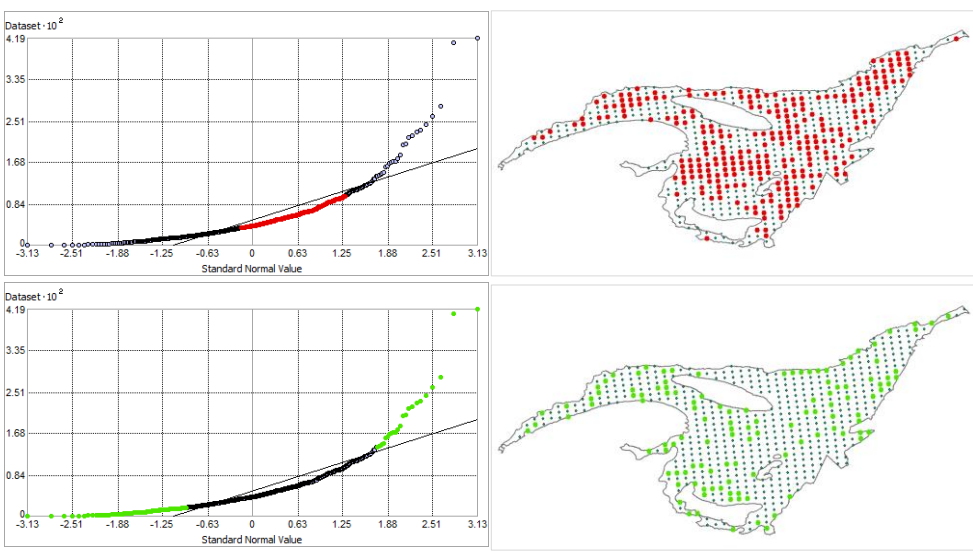

Fig. 187. Normal Q-Q plot for data values of Surface Current Minimum (m s^{-1}). Points falling under (upper panel) and over (bottom panel) the reference line are mapped.

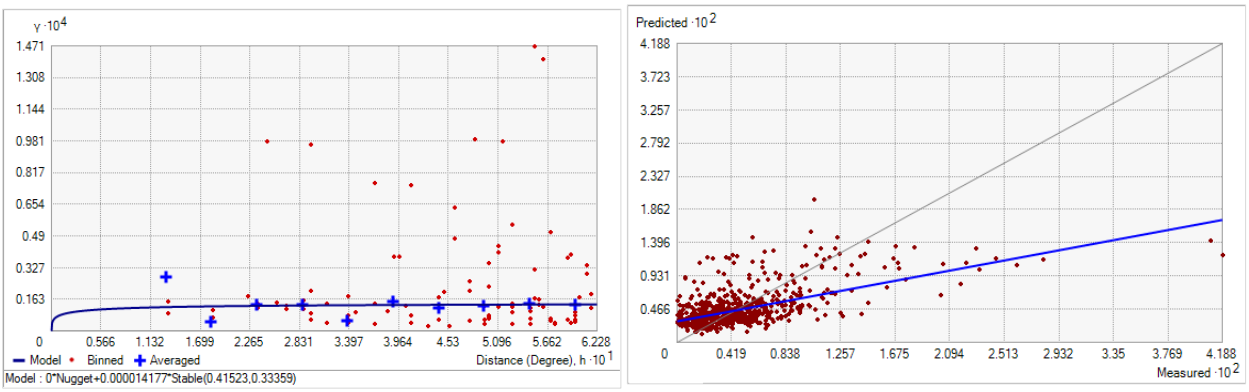

Fig. 188. Left panel: Semivariogram of Surface Current Minimum (m s^{-1}). Binned values are shown as red dots; average points are shown as blue crosses; the model fit to the averaged values is shown as a blue line. Lag size: 0.052 degrees; number of lags: 12; Parameter: 0.334; Range: 0.415 degrees; Partial Sill: 1.420 x 10^{-4}. Right panel: Scatterplot of predicted values versus observed values for the model of Surface Current Minimum (m s^{-1}).

Table 76. Results of cross-validation of the kriged model for Surface Current Minimum (m s^{-1}).

Prediction error	**Value**
Number of Observations	581
Overall Mean Error	8.678 x 10^{-8}
Root Mean Square Prediction Error	0.004
Standardized Mean	-7.366 x 10^{-4}
Standardized Root Mean Square Prediction Error	0.979
Average Standard Error	0.004

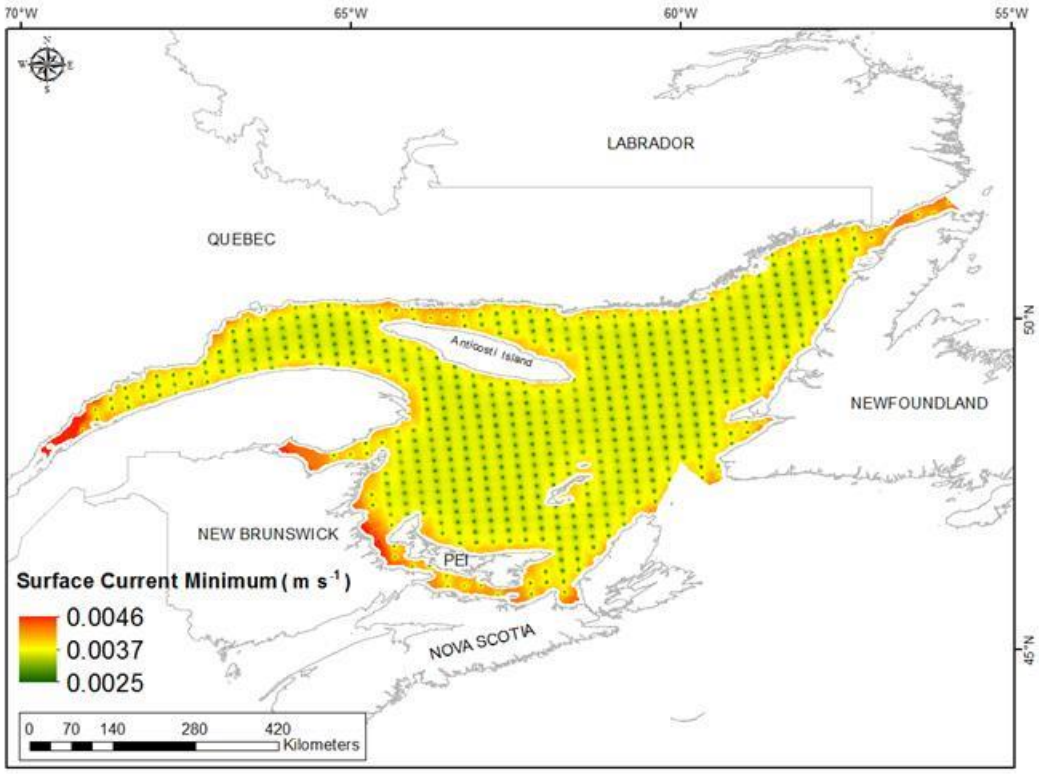

Fig. 189. Prediction standard error surface of Surface Current Minimum (m s^{-1}).

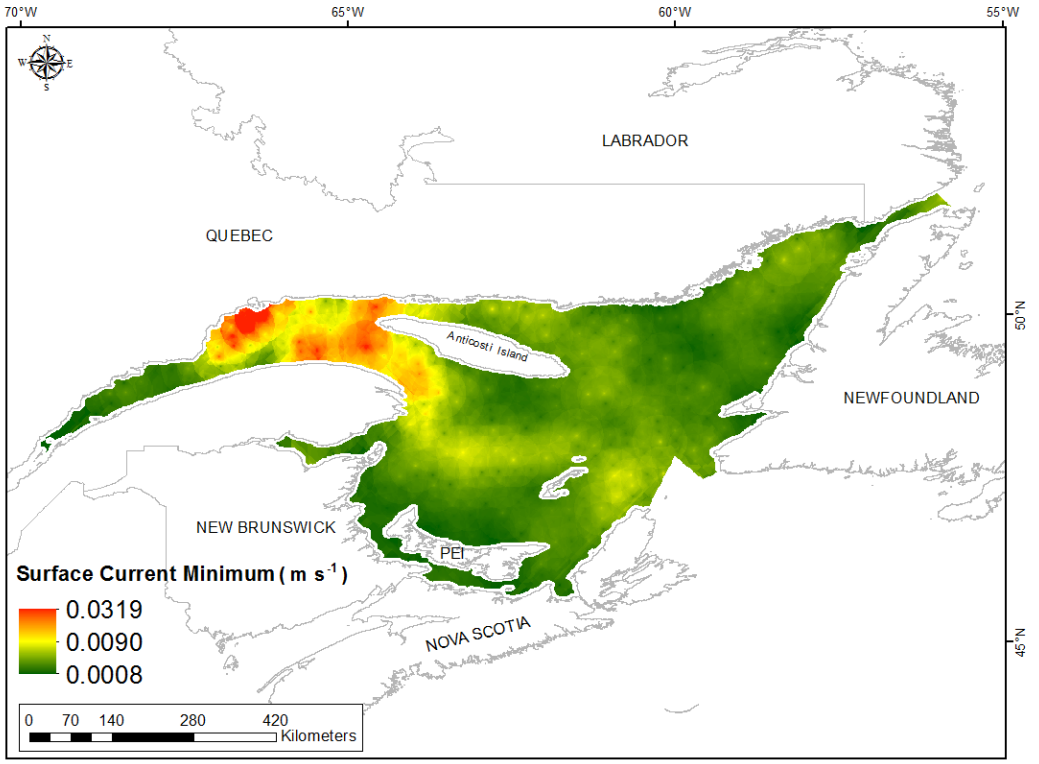

Fig. 190. Interpolated prediction surface of Surface Current Minimum (m s^{-1}).

Surface Current Maximum

This variable displayed a slightly right-skewed distribution with high kurtosis prior to modeling (Table 77, Fig. 191). The data were higher than predicted by a normal distribution at low and high values (Fig. 192). Mid-range values were slightly lower than the reference line. The areas of over- and under-prediction showed spatial pattern (Fig. 192).

The semivariogram showed little autocorrelation present in the data and the model showed poor fit between measured and predicted values (Fig. 193). Nevertheless, the model showed excellent cross-validation statistics (Table 78) indicating that it was very good at prediction. The error map showed no spatial pattern over the study extent except for along the coast where it was high (Fig. 194). The kriged surface is presented in Fig. 195.

Table 77. Distributional properties of Surface Current Maximum (m s^{-1}).

Property	Value
Number of Observations	581
Minimum	0.070
Maximum	0.609
Mean	0.208
Median	0.185
Standard Deviation	0.085
Skewness	1.760
Kurtosis	6.853

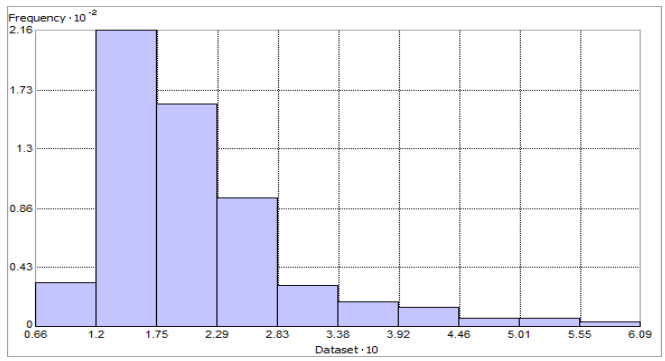

Fig. 191. Distribution of Surface Current Maximum (m s^{-1}). Histogram was illustrated using 10 bins. Y axis is shown at 10^{-2}.

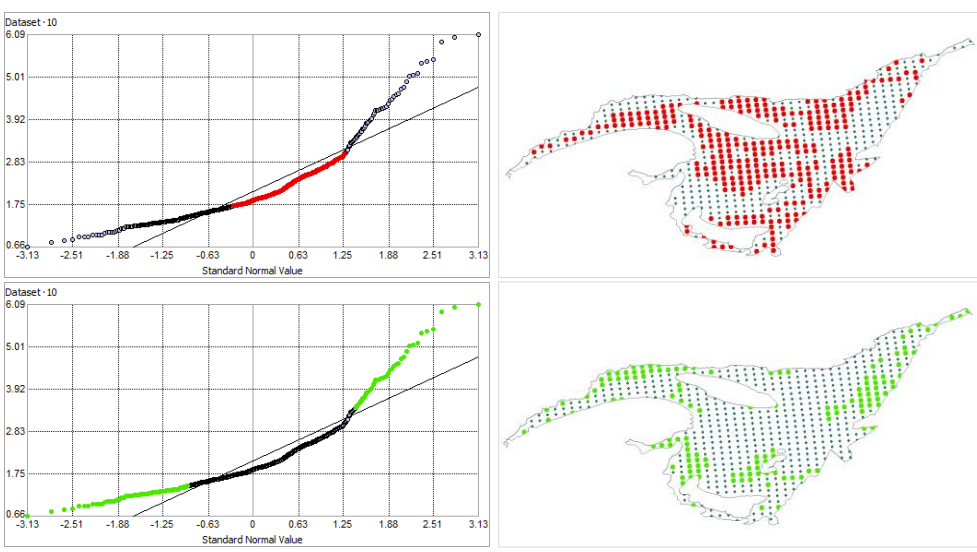

Fig. 192. Normal Q-Q plot for data values of Surface Current Maximum (m s^{-1}). Points falling under (upper panel) and over (bottom panel) the reference line are mapped.

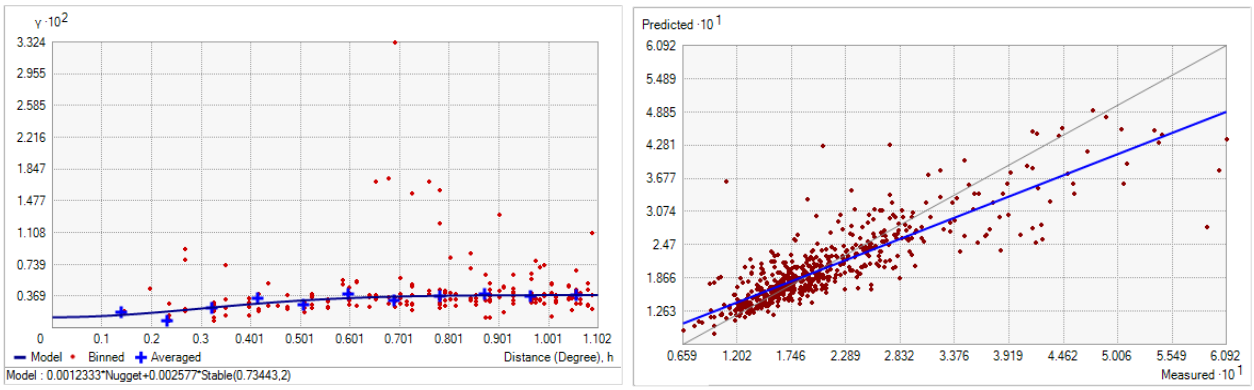

Fig. 193. Left panel: Semivariogram of Surface Current Maximum (m s^{-1}). Binned values are shown as red dots; average points are shown as blue crosses; the model fit to the averaged values is shown as a blue line. Lag size: 0.092 degrees; number of lags: 12; Parameter: 2; Range: 0.734 degrees; Partial Sill: 0.003. Right panel: Scatterplot of predicted values versus observed values for the model of Surface Current Maximum (m s^{-1}).

Table 78. Results of cross-validation of the kriged model for the Surface Current Maximum (m s^{-1}).

Prediction error	**Value**
Number of Observations	581
Overall Mean Error	-7.630×10^{-4}
Root Mean Square Prediction Error	0.044
Standardized Mean	-0.012
Standardized Root Mean Square Prediction Error	0.996
Average Standard Error	0.042

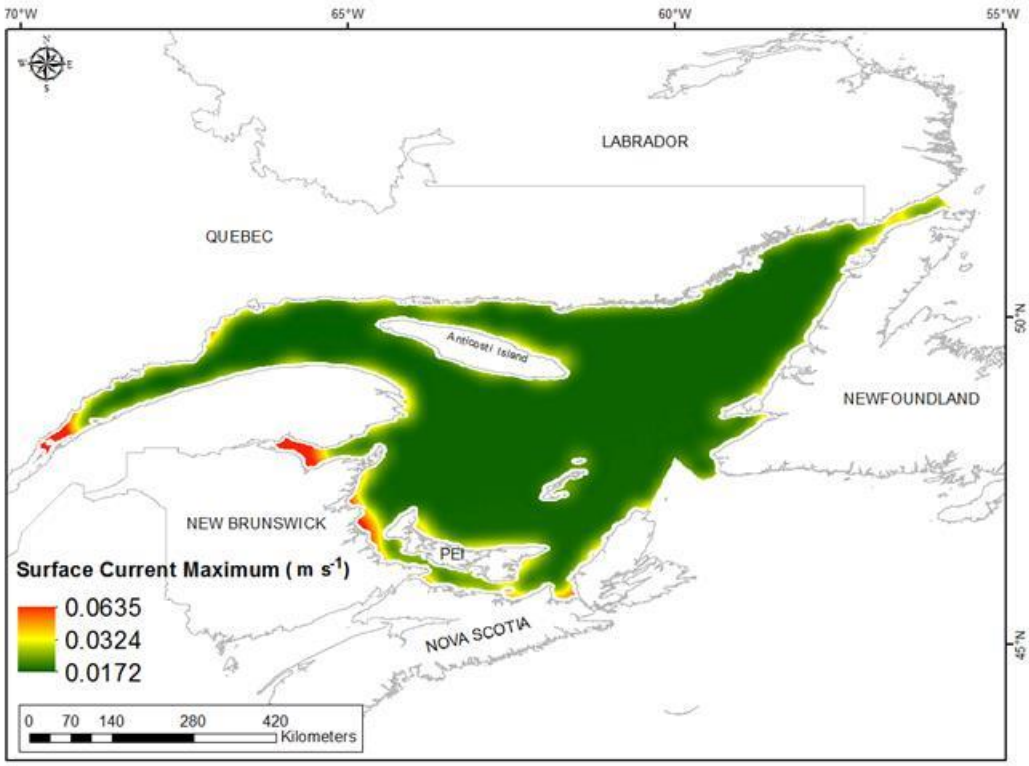

Fig. 194. Prediction standard error surface of Surface Current Maximum (m s^{-1}).

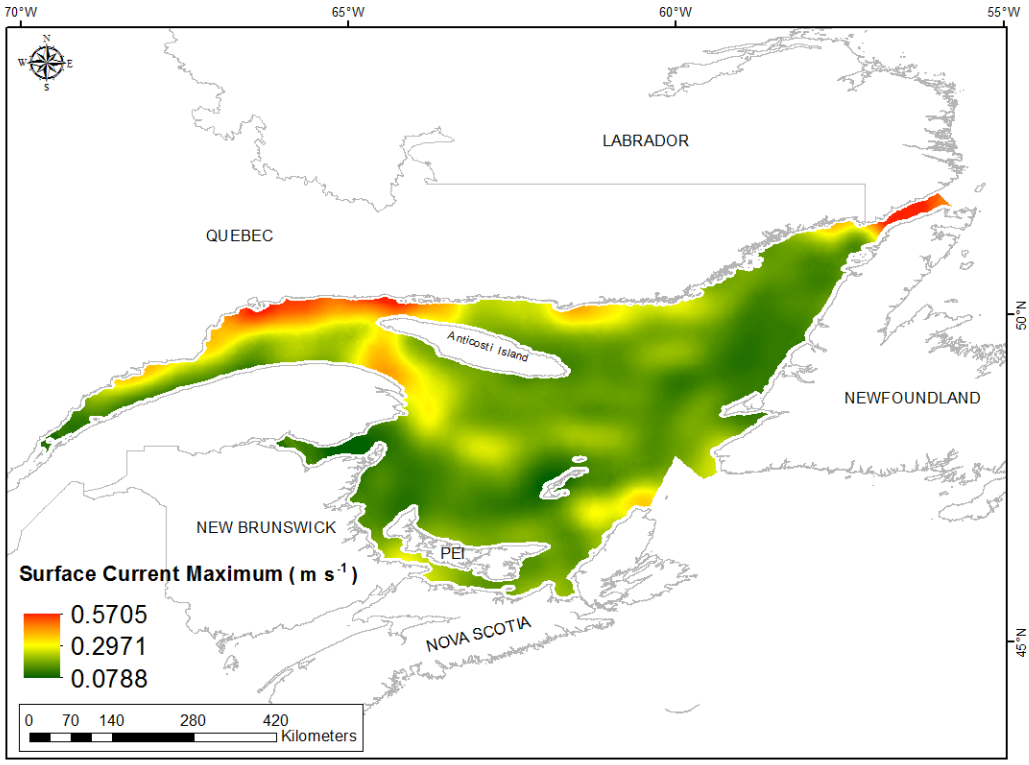

Fig. 195. Interpolated prediction surface of Surface Current Maximum (m s^{-1}).

Surface Current Range

This variable displayed a slightly right-skewed distribution with kurtosis prior to modeling (Table 79, Fig. 196). The data were higher than predicted by a normal distribution at low and high values (Fig. 197). Mid-range values were slightly lower than the reference line. The areas of over- and under-prediction showed a spatial pattern (Fig. 197).

The semivariogram showed little autocorrelation present in the data and the model showed poor fit between measured and predicted values (Fig. 198). Nevertheless, the model showed excellent cross-validation statistics (Table 80) indicating that it was very good at prediction. The error map showed no spatial pattern over the study extent except for some areas along the coast where it was high (Fig. 199). The kriged surface is presented in Fig. 200.

Table 79. Distributional properties of Surface Current Range (m s^{-1}).

Property	Value
Number of Observations	581
Minimum	0.062
Maximum	0.608
Mean	0.203
Median	0.181
Standard Deviation	0.084
Skewness	1.784
Kurtosis	7.021

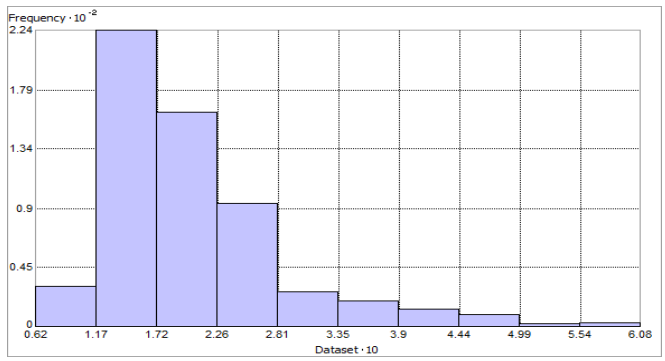

Fig. 196. Distribution of Surface Current Range (m s^{-1}). Histogram was illustrated using 10 bins. Y axis is shown at 10^{-2}.

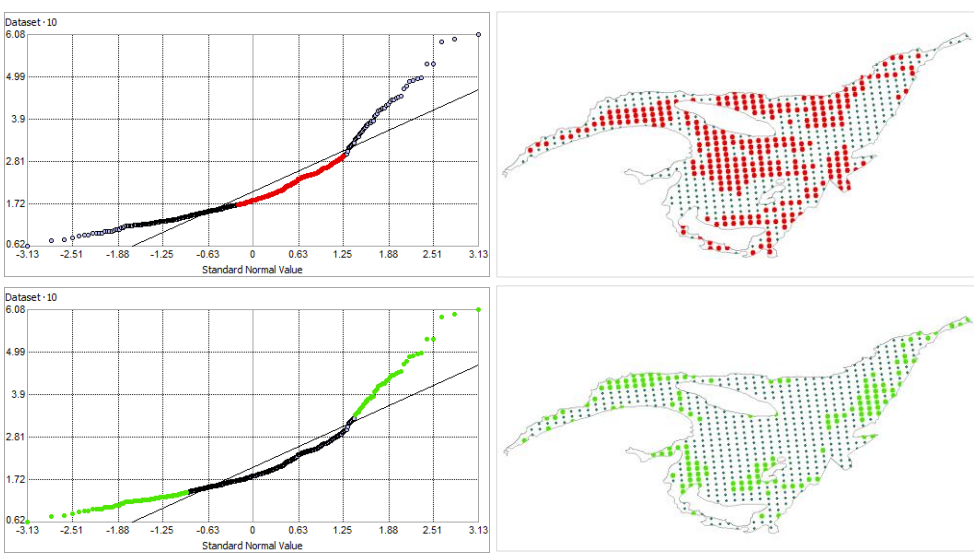

Fig. 197. Normal Q-Q plot for data values of Surface Current Range (m s^{-1}). Points falling under (upper panel) and over (bottom panel) the reference line are mapped.

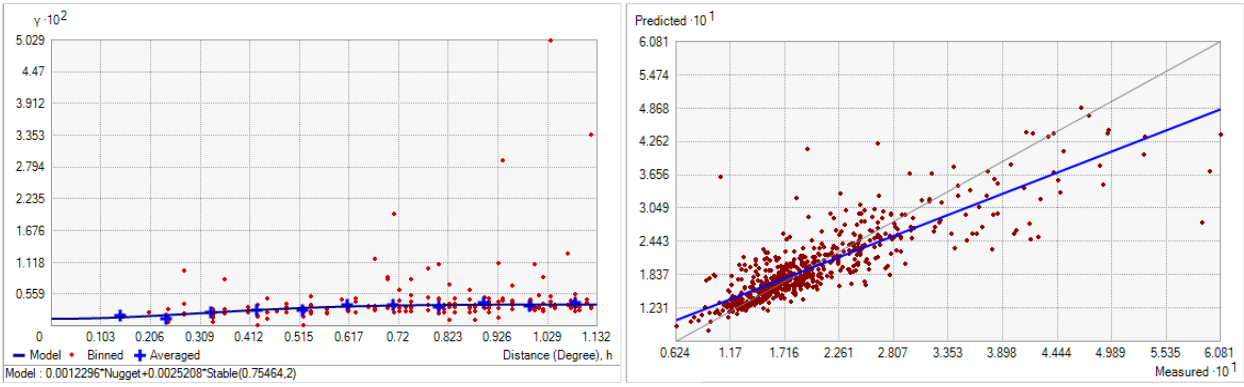

Fig. 198. Left panel: Semivariogram of Surface Current Range (m s^{-1}). Binned values are shown as red dots; average points are shown as blue crosses; the model fit to the averaged values is shown as a blue line. Lag size: 0.092 degrees; number of lags: 12; Parameter: 2; Range: 0.734 degrees; Partial Sill: 0.003. Right panel: Scatterplot of predicted values versus observed values for the model of Surface Current Range (m s^{-1}).

Table 80. Results of cross-validation of the kriged model for the Surface Current Range (m s^{-1}).

Prediction error	**Value**
Number of Observations	581
Overall Mean Error	-7.426×10^{-4}
Root Mean Square Prediction Error	0.044
Standardized Mean	-0.012
Standardized Root Mean Square Prediction Error	0.999
Average Standard Error	0.042

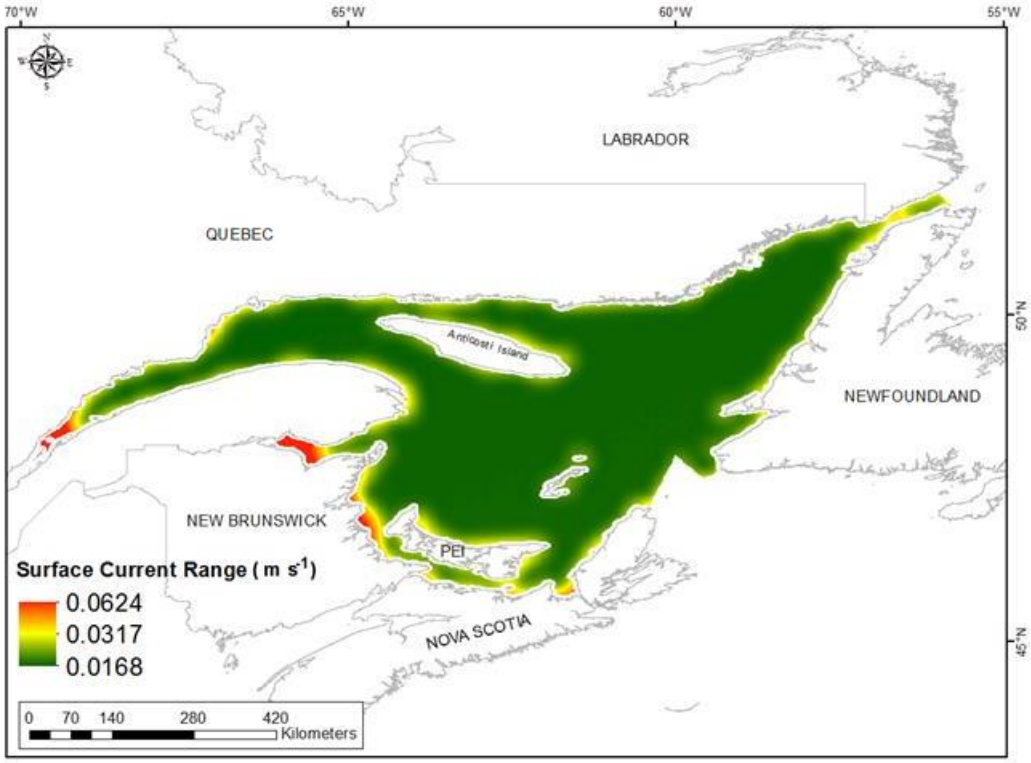

Fig. 199. Prediction standard error surface of Surface Current Range (m s^{-1}).

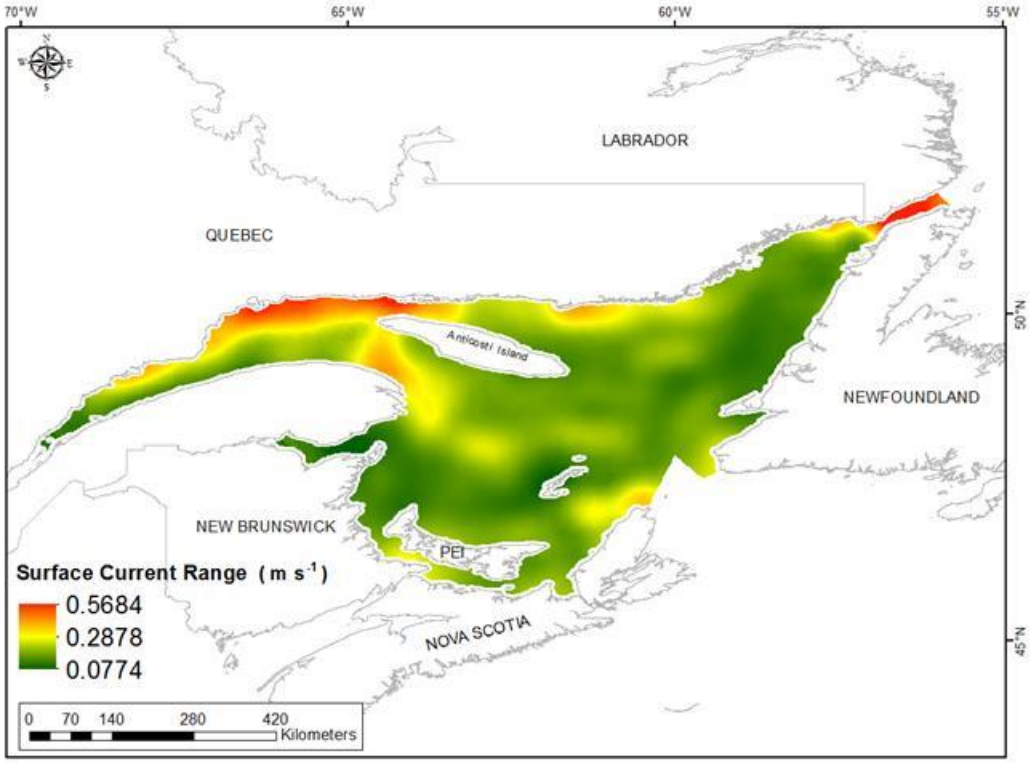

Fig. 200. Interpolated prediction surface of Surface Current Range (m s^{-1}).

Surface Current Average Minimum

This variable displayed a slightly right-skewed distribution with kurtosis prior to modeling (Table 81, Fig. 201). The data were higher than predicted by a normal distribution at low and high values (Fig. 202). Mid-range values were slightly lower than the reference line. The areas of over- and under-prediction showed a spatial pattern (Fig. 202).

The semivariogram showed no autocorrelation present in the data and the model showed poor fit between measured and predicted values (Fig. 203). Nevertheless, the model showed good cross-validation statistics (Table 82) indicating that it was good at prediction. The error map showed no spatial pattern over the study extent except for some areas along the coast where it was high (Fig. 204). The kriged surface is presented in Fig. 205.

Table 81. Distributional properties of Surface Current Average Minimum (m s^{-1}).

Property	Value
Number of Observations	581
Minimum	0.002
Maximum	0.094
Mean	0.022
Median	0.018
Standard Deviation	0.013
Skewness	2.113
Kurtosis	9.113

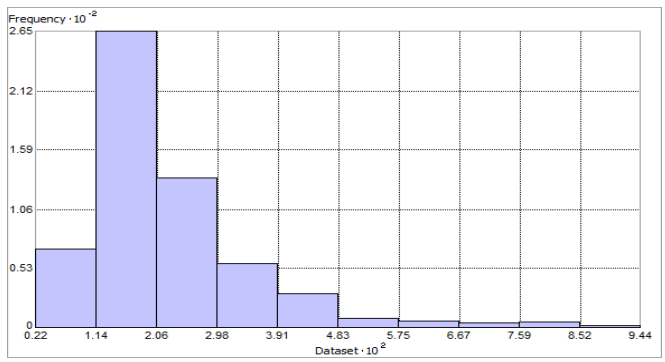

Fig. 201. Distribution of Surface Current Average Minimum (m s^{-1}). Histogram was illustrated using 10 bins. X axis shown at 10^2; Y axis shown at 10^{-2}.

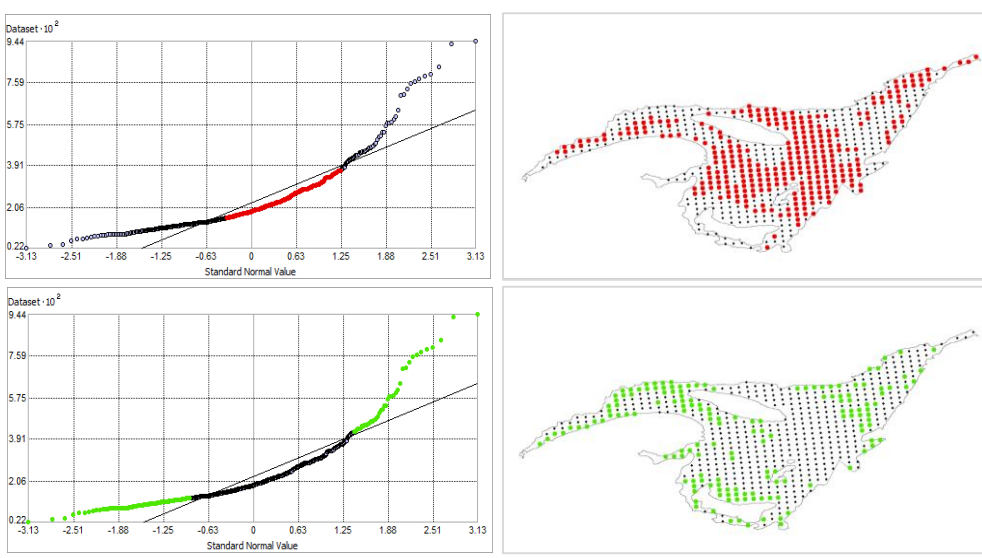

Fig. 202. Normal Q-Q plot for data values of Surface Current Average Minimum (m s^{-1}). Points falling under (upper panel) and over (bottom panel) the reference line are mapped.

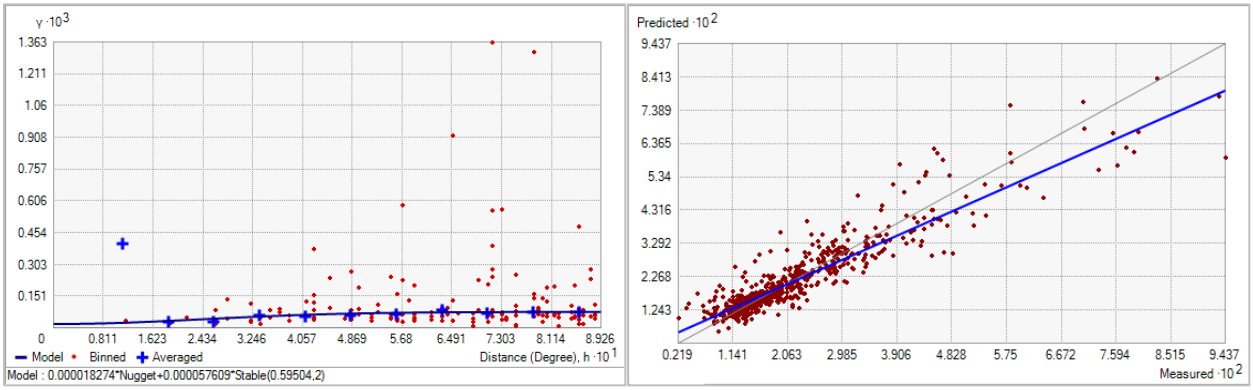

Fig. 203. Left panel: Semivariogram of Surface Current Average Minimum (m s^{-1}). Binned values are shown as red dots; average points are shown as blue crosses; the model fit to the averaged values is shown as a blue line. Lag size: 0.074 degrees; number of lags: 12; Parameter: 2; Range: 0.595 degrees; Partial Sill: 5.761 x 10^{-5}. Right panel: Scatterplot of predicted values versus observed values for the model of Surface Current Average Minimum (m s^{-1}).

Table 82. Results of cross-validation of the kriged model for the Surface Current Average Minimum (m s^{-1}).

Prediction error	**Value**
Number of Observations	581
Overall Mean Error	7.676 x 10^{-5}
Root Mean Square Prediction Error	0.005
Standardized Mean	0.005
Standardized Root Mean Square Prediction Error	0.880
Average Standard Error	0.006

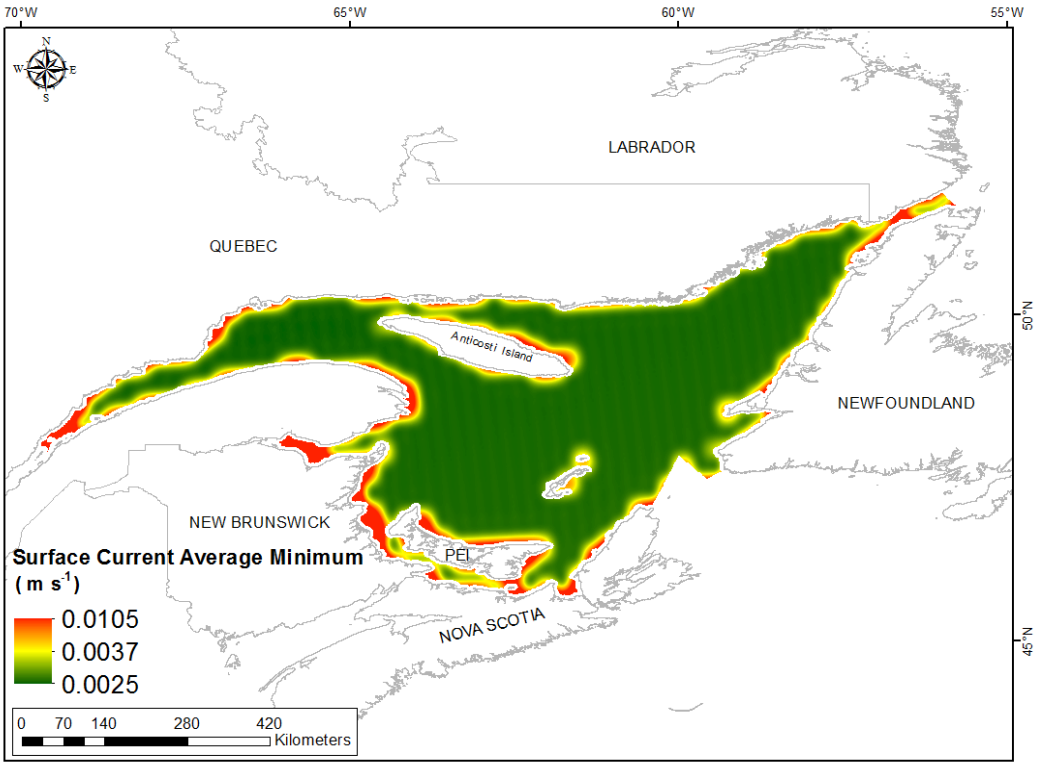

Fig. 204. Prediction standard error surface of Surface Current Average Minimum (m s^{-1}).

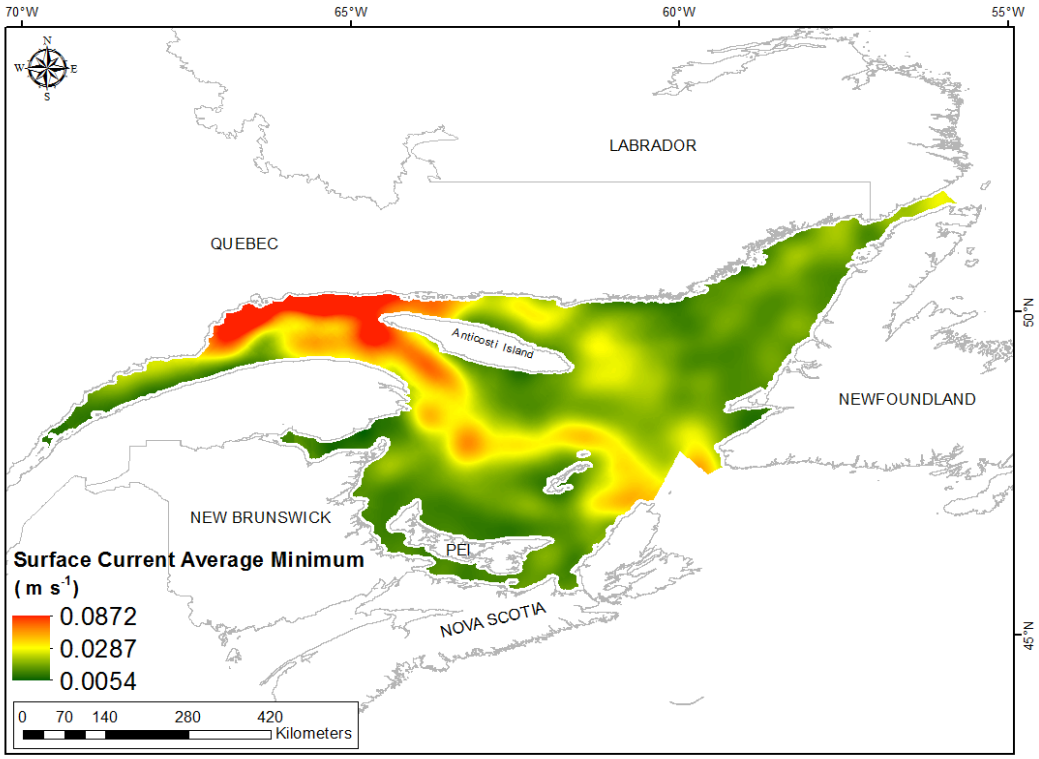

Fig. 205. Interpolated prediction surface of Surface Current Average Minimum (m s^{-1}).

Surface Current Average Maximum

This variable displayed a slightly right-skewed distribution with kurtosis prior to modeling (Table 83, Fig. 206). The data were higher than predicted by a normal distribution at low and high values (Fig. 207). Mid-range values were slightly lower than the reference line. The areas of over- and under-prediction showed a strong spatial pattern (Fig. 207).

The semivariogram showed no autocorrelation present in the data and the model showed poor fit between measured and predicted values (Fig. 208). Nevertheless, the model showed excellent cross-validation statistics (Table 84) indicating that it was very good at prediction. The error map showed no spatial pattern over the study extent except for some areas along the coast where it was high (Fig. 209). The kriged surface is presented in Fig. 210.

Table 83. Distributional properties of Surface Current Average Maximum (m s^{-1}).

Property	Value
Number of Observations	581
Minimum	0.055
Maximum	0.456
Mean	0.144
Median	0.126
Standard Deviation	0.063
Skewness	2.055
Kurtosis	8.202

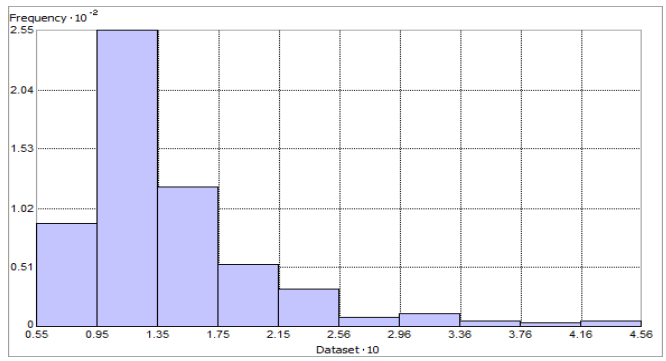

Fig. 206. Distribution of Surface Current Average Maximum (m s^{-1}). Histogram was illustrated using 10 bins. X axis shown at 10; Y axis shown at 10^{-2}.

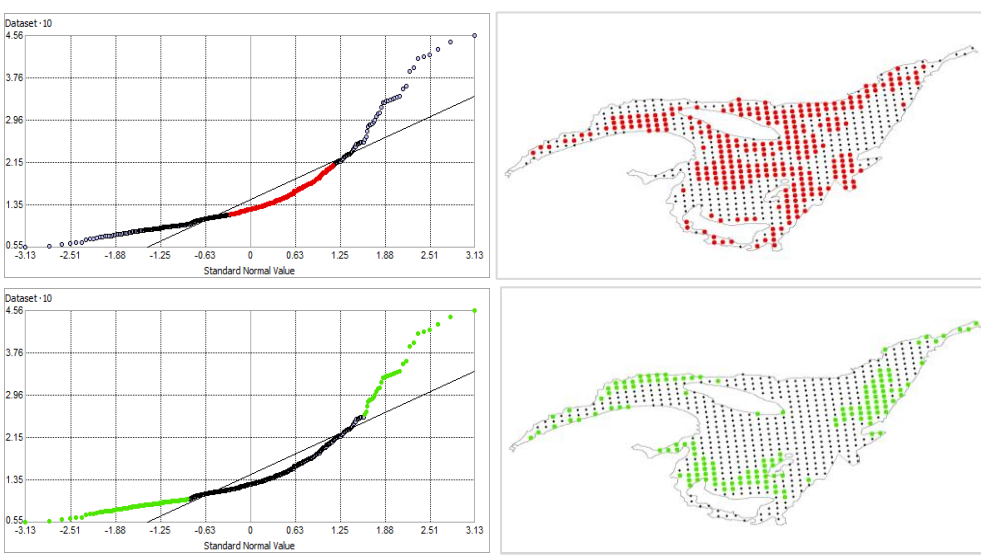

Fig. 207. Normal Q-Q plot for data values of Surface Current Average Maximum (m s^{-1}). Points falling under (upper panel) and over (bottom panel) the reference line are mapped.

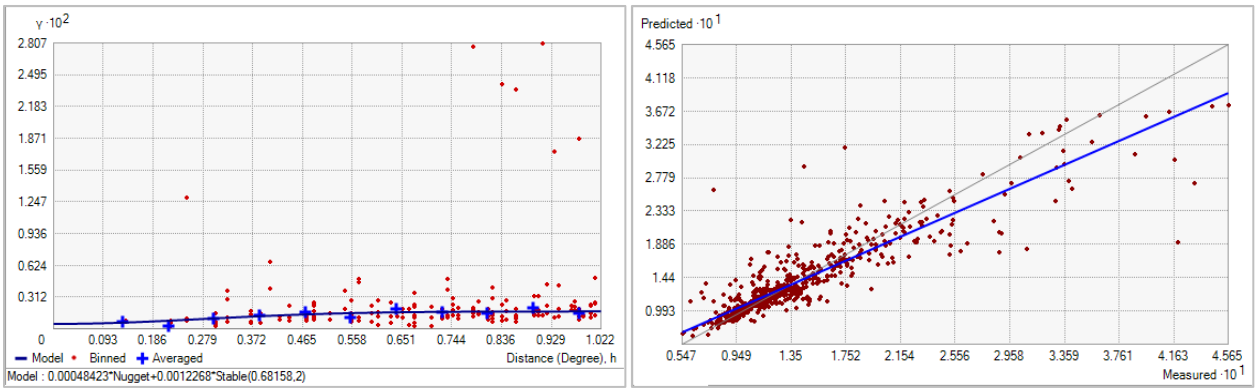

Fig. 208. Left panel: Semivariogram of Surface Current Average Maximum (m s^{-1}). Binned values are shown as red dots; average points are shown as blue crosses; the model fit to the averaged values is shown as a blue line. Lag size: 0.085 degrees; number of lags: 12; Parameter: 2; Range: 0.681 degrees; Partial Sill: 0.001. Right panel: Scatterplot of predicted values versus observed values for the model of Surface Current Average Maximum (m s^{-1}).

Table 84. Results of cross-validation of the kriged model for the Surface Current Average Maximum (m s^{-1}).

Prediction error	**Value**
Number of Observations	581
Overall Mean Error	-6.378×10^{-4}
Root Mean Square Prediction Error	0.028
Standardized Mean	-0.016
Standardized Root Mean Square Prediction Error	0.947
Average Standard Error	0.027

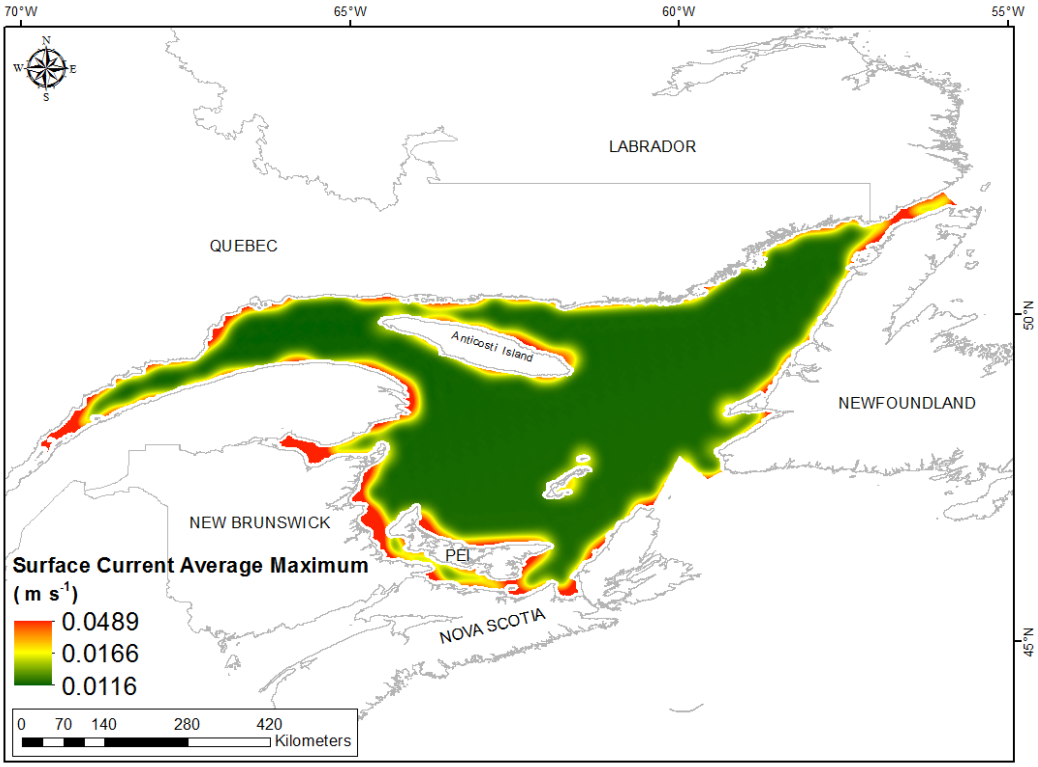

Fig. 209. Prediction standard error surface of Surface Current Average Maximum (m s^{-1}).

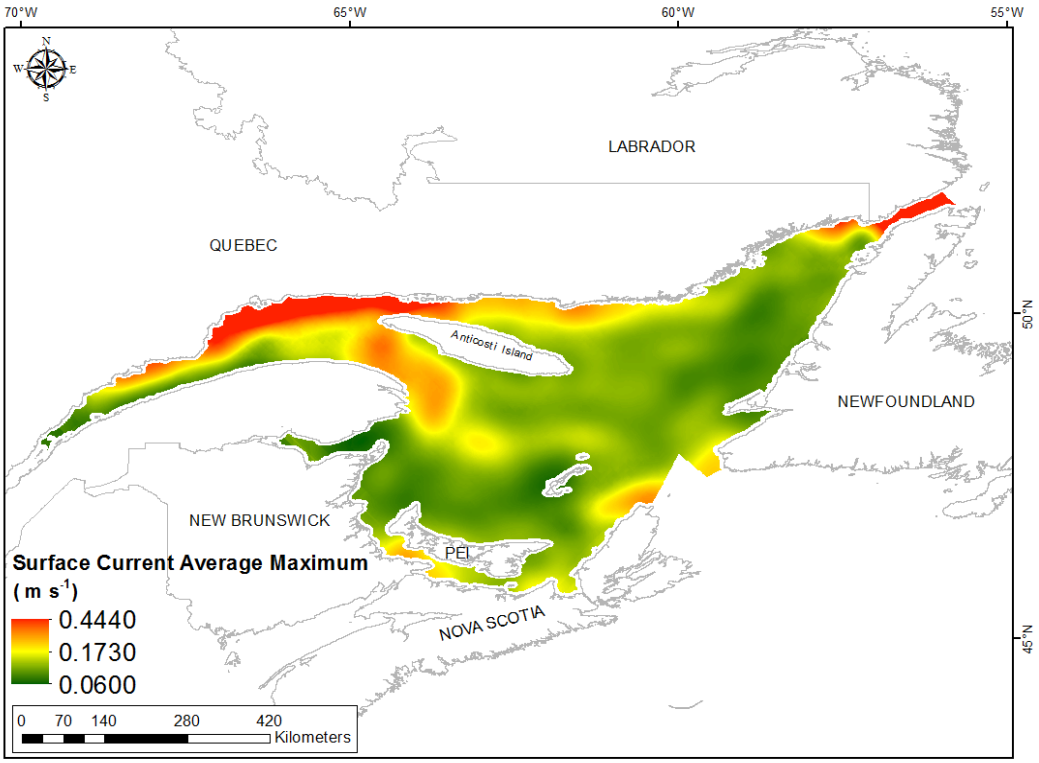

Fig. 210. Interpolated prediction surface of Surface Current Average Maximum (m s^{-1}).

Surface Current Average Range

This variable displayed a slightly right-skewed distribution with kurtosis prior to modeling (Table 85, Fig. 211). The data were higher than predicted by a normal distribution at low and high values (Fig. 212). Mid-range values were slightly lower than the reference line. The areas of over- and under-prediction showed a strong spatial pattern (Fig. 212).

The semivariogram showed moderate autocorrelation present in the data and the model showed poor fit between measured and predicted values (Fig. 213). Nevertheless, the model showed excellent cross-validation statistics (Table 86) indicating that it was very good at prediction. The error map showed a 'bullseye' pattern with error increasing with distance from data points (Fig. 214). The kriged surface is presented in Fig. 215.

Table 85. Distributional properties of Surface Current Average Range (m s^{-1}).

Property	Value
Number of Observations	581
Minimum	0.046
Maximum	0.398
Mean	0.122
Median	0.105
Standard Deviation	0.053
Skewness	2.114
Kurtosis	8.670

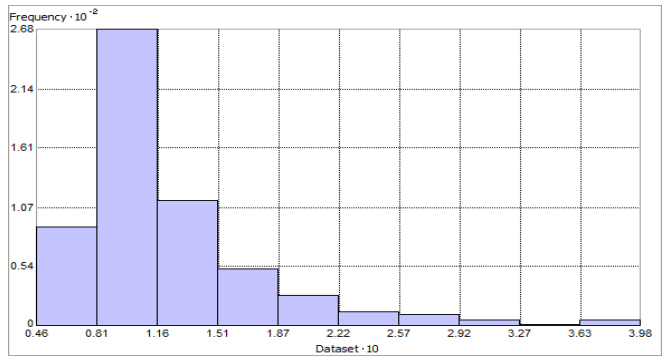

Fig. 211. Distribution of Surface Current Average Range (m s^{-1}). Histogram was illustrated using 10 bins. X axis shown at 10; Y axis shown at 10^{-2}.

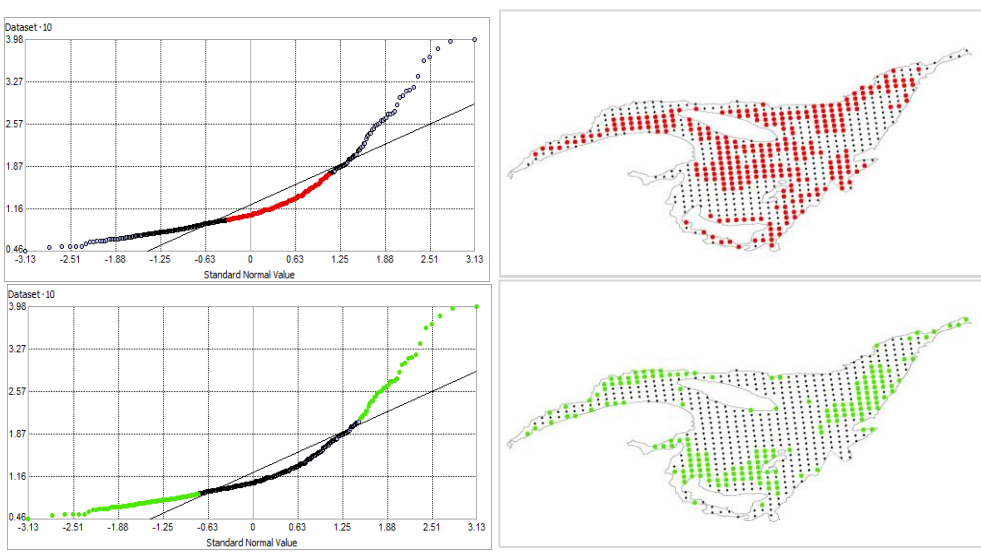

Fig. 212. Normal Q-Q plot for data values of Surface Current Average Range (m s^{-1}). Points falling under (upper panel) and over (bottom panel) the reference line are mapped.

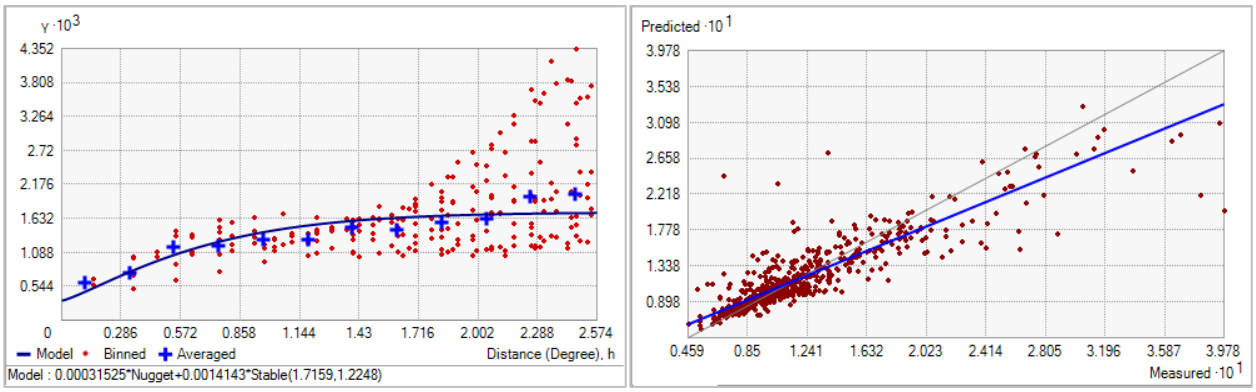

Fig. 213. Left panel: Semivariogram of Surface Current Average Range (m s^{-1}). Binned values are shown as red dots; average points are shown as blue crosses; the model fit to the averaged values is shown as a blue line. Lag size: 0.214 degrees; number of lags: 12; Parameter: 1.225; Range: 1.716 degrees; Partial Sill: 0.001. Right panel: Scatterplot of predicted values versus observed values for the model of Surface Current Average Range (m s^{-1}).

Table 86. Results of cross-validation of the kriged model for the Surface Current Average Range (m s^{-1}).

Prediction error	**Value**
Number of Observations	581
Overall Mean Error	-3.461×10^{-4}
Root Mean Square Prediction Error	0.026
Standardized Mean	-0.007
Standardized Root Mean Square Prediction Error	0.982
Average Standard Error	0.025

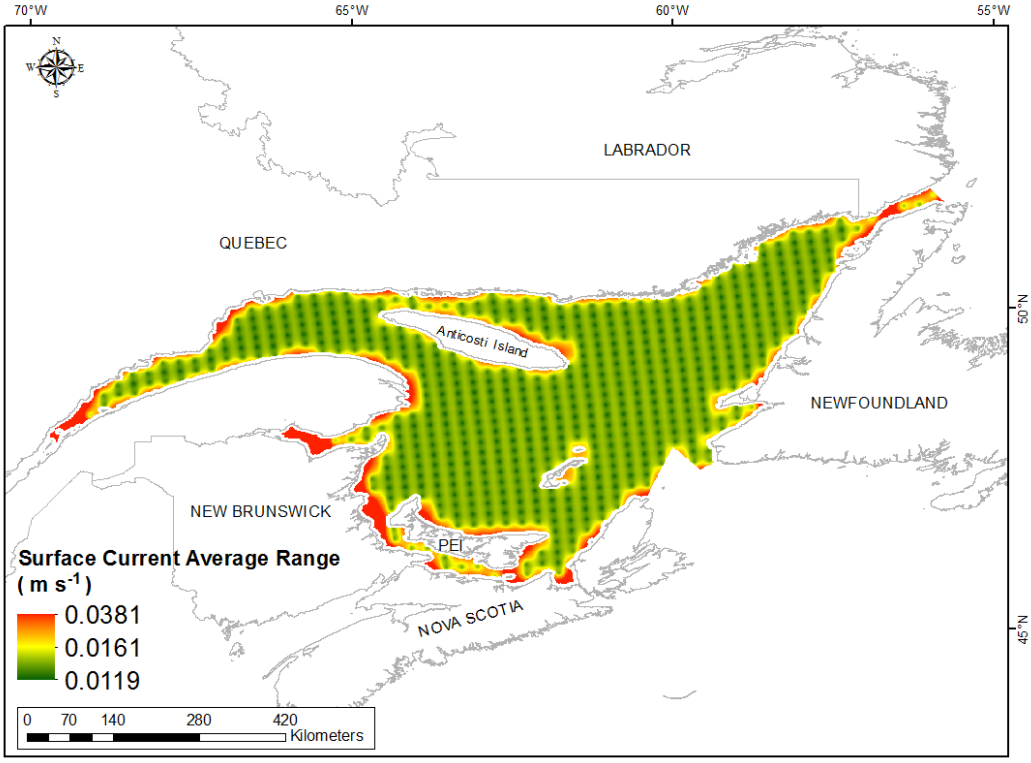

Fig. 214. Prediction standard error surface of Surface Current Average Range (m s^{-1}).

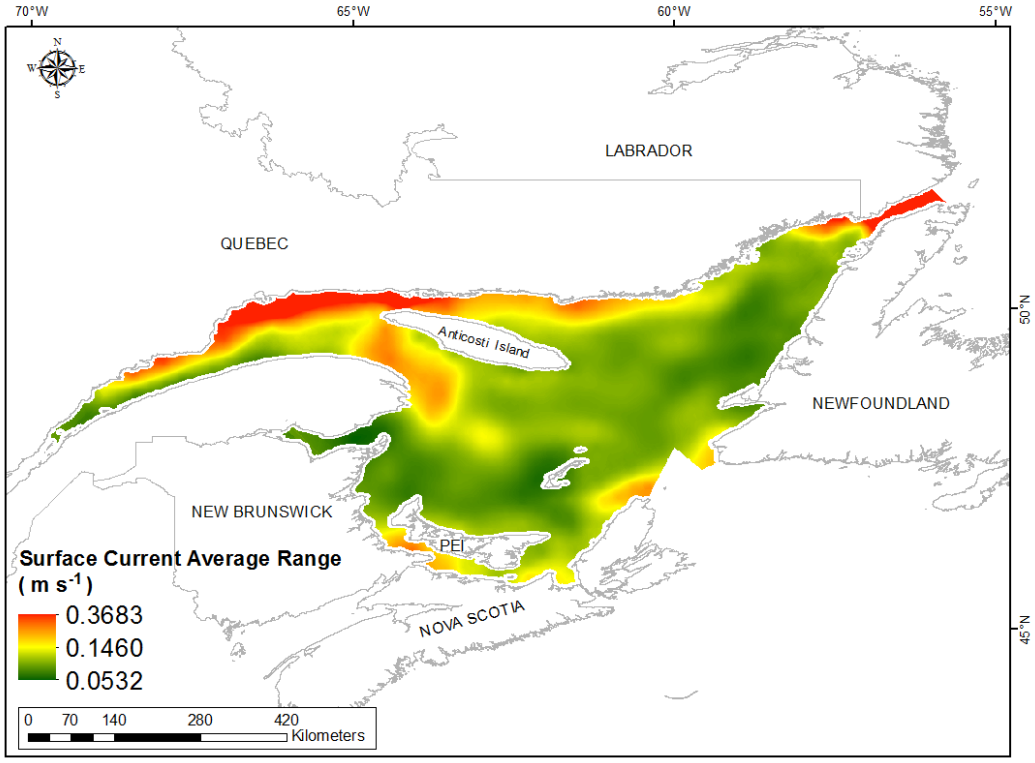

Fig. 215. Interpolated prediction surface of Surface Current Average Range (m s^{-1}).

Maximum Seasonal Mixed Layer Depth

Maximum mixed layer depth, or, the depth at which surface vertical mixing dissipates, is a near-universal feature of the open ocean (de Boyer Montégut et al., 2004). Within this mixed layer, salinity, temperature, or density are nearly uniform, a phenonmenon caused by surface forcing, lateral advection, and internal wave processes that vary on diurnal, intra-seasonal, seasonal, and inter-annual scales (de Boyer Montégut et al., 2004). The depth of this mixed zone can show large spatial variability, ranging from less than 20 m in the summer hemisphere, to more than 500 m in the winter hemisphere at subpolar latitudes (de Boyer Montégut et al., 2004). The mixed layer depth has a significant influence on primary production in the surface waters. As the mixed layer depth increases it entrains nutrients from deeper waters below, supplying additional nutrients for primary production (Polovina, 1995; Carstensen et al., 2002).

Maximum Spring Mixed Layer Depth

This variable displayed a severely right-skewed distribution with outlying data in the upper range (Table 87, Fig. 216). The data were higher than predicted by a normal distribution at low and high values (Fig. 217). Mid-range values deviated only slightly from the reference line. The areas of over- and under-prediction showed a strong spatial pattern (Fig. 217).

The semivariogram showed no autocorrelation present in the data and the model showed a good fit between measured and predicted values (Fig. 218). The model showed good cross-validation statistics (Table 88) indicating that it was very good at prediction. The error map showed no spatial pattern over the study extent except for some areas along the coast where it was high (Fig. 219). The kriged surface is presented in Fig. 220.

Table 87. Distributional properties of Maximum Spring Mixed Layer Depth (m).

Property	Value
Number of Observations	606
Minimum	10.768
Maximum	78.749
Mean	20.421
Median	20.509
Standard Deviation	6.404
Skewness	1.686
Kurtosis	15.216

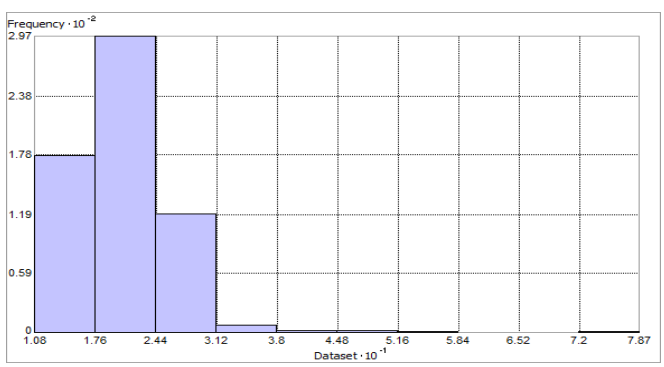

Fig. 216. Distribution of Maximum Spring Mixed Layer Depth (m). Histogram was illustrated using 10 bins. X axis shown at 10^{-1}; Y axis shown at 10^{-2}.

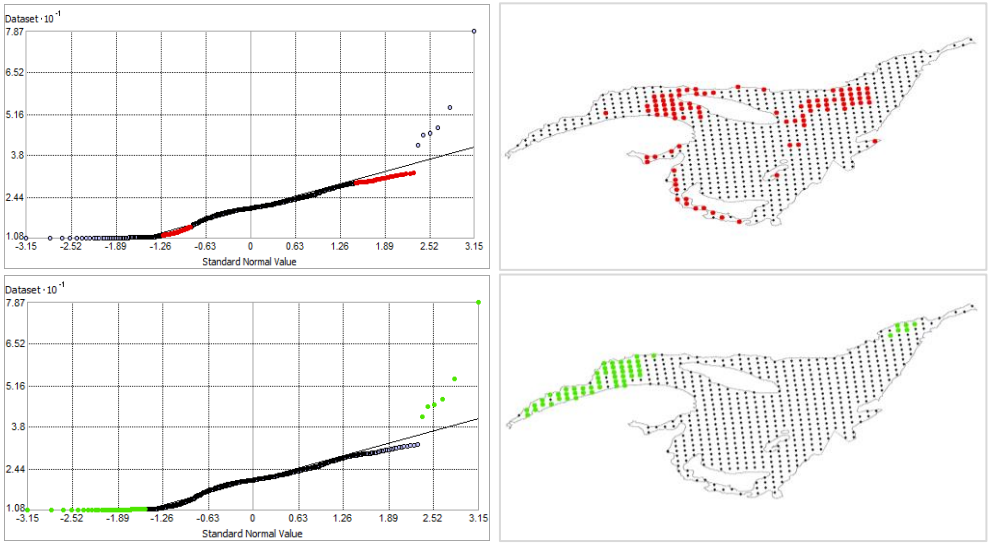

Fig. 217. Normal Q-Q plot for data values of Maximum Spring Mixed Layer Depth (m). Points falling under (upper panel) and over (bottom panel) the reference line are mapped.

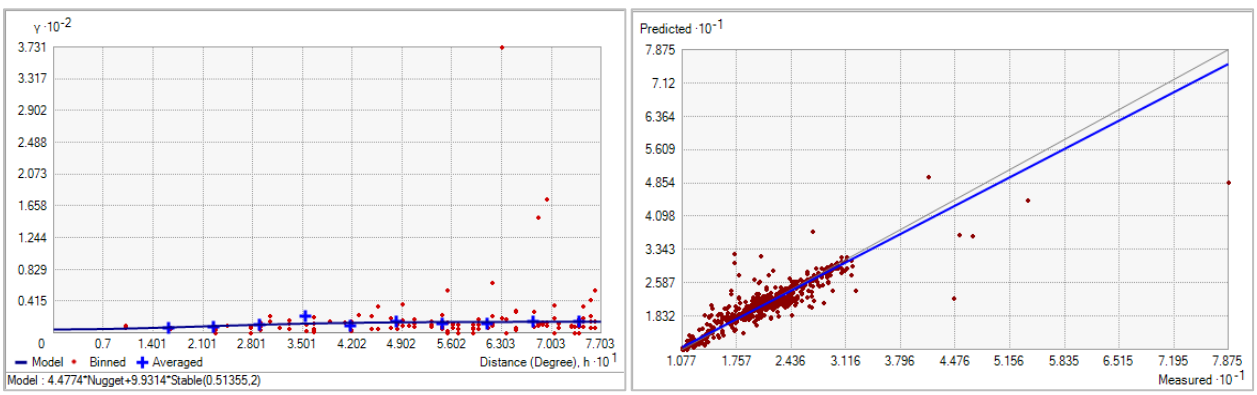

Fig. 218. Left panel: Semivariogram of Maximum Spring Mixed Layer Depth (m). Binned values are shown as red dots; average points are shown as blue crosses; the model fit to the averaged values is shown as a blue line. Lag size: 0.064 degrees; number of lags: 12; Parameter: 2; Range: 0.513 degrees; Partial Sill: 9.931. Right panel: Scatterplot of predicted values versus observed values for the model of Maximum Spring Mixed Layer Depth (m).

Table 88. Results of cross-validation of the kriged model for the Maximum Spring Mixed Layer Depth (m).

Prediction error	**Value**
Number of Observations	606
Overall Mean Error	0.050
Root Mean Square Prediction Error	2.684
Standardized Mean	0.011
Standardized Root Mean Square Prediction Error	0.935
Average Standard Error	2.845

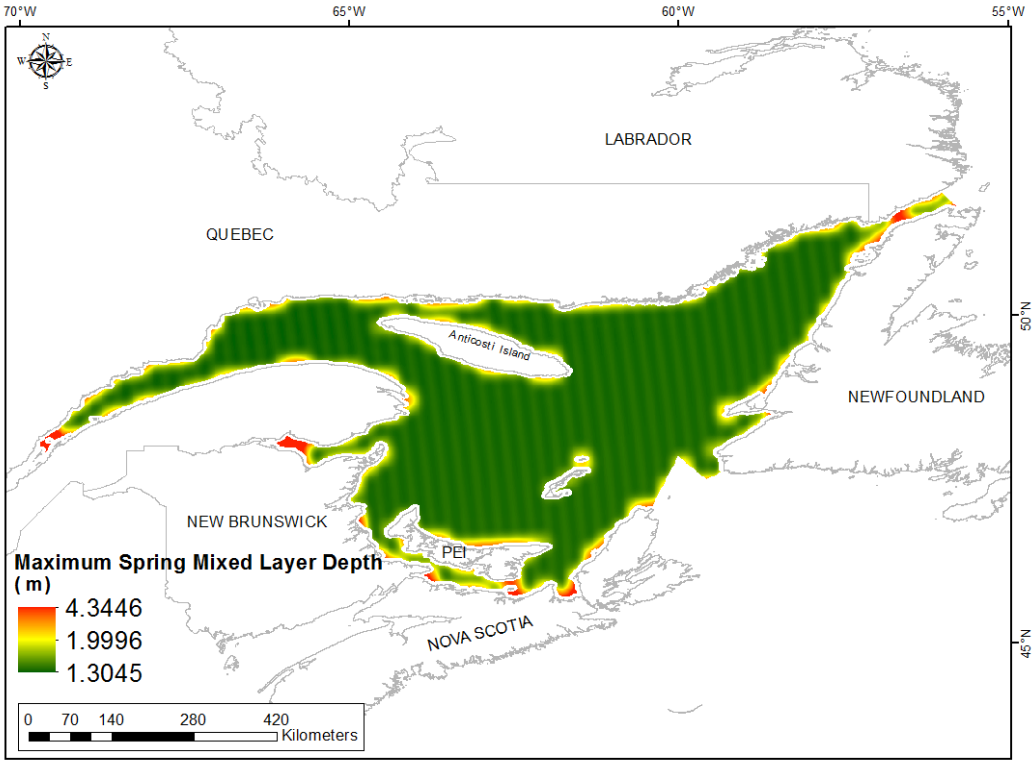

Fig. 219. Prediction standard error surface of Maximum Spring Mixed Layer Depth (m).

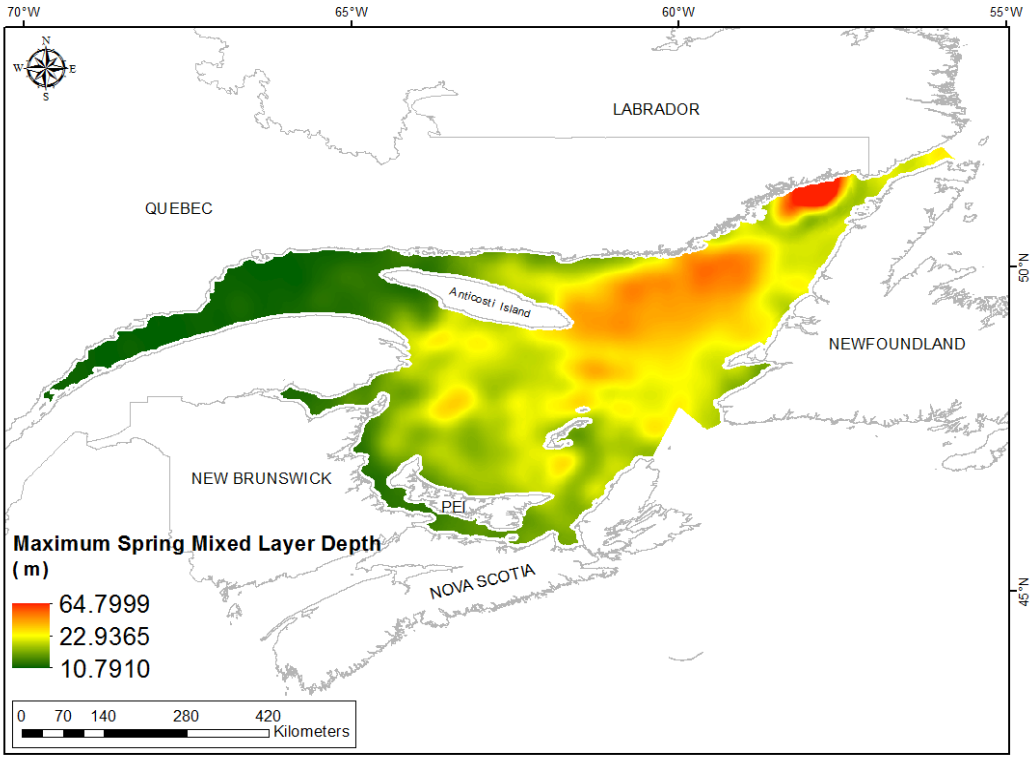

Fig. 220. Interpolated prediction surface of Maximum Spring Mixed Layer Depth (m).

Maximum Summer Mixed Layer Depth

This variable displayed a severely right-skewed distribution with outlying data in the upper range (Table 89, Fig. 221). The data were higher than predicted by a normal distribution at low and high values (Fig. 222). Mid-range values deviated only slightly from the reference line. The areas of over- and under-prediction showed a spatial pattern (Fig. 222).

The semivariogram showed moderate autocorrelation present in the data and the model showed a good fit between measured and predicted values (Fig. 223). The model showed good cross-validation statistics (Table 90) indicating that it was very good at prediction. The error map showed no spatial pattern over the study extent except for some areas along the coast where it was high (Fig. 224). The kriged surface is presented in Fig. 225.

Table 89. Distributional properties of Maximum Summer Mixed Layer Depth (m).

Property	Value
Number of Observations	606
Minimum	10.768
Maximum	22.430
Mean	12.974
Median	12.826
Standard Deviation	1.761
Skewness	0.928
Kurtosis	4.463

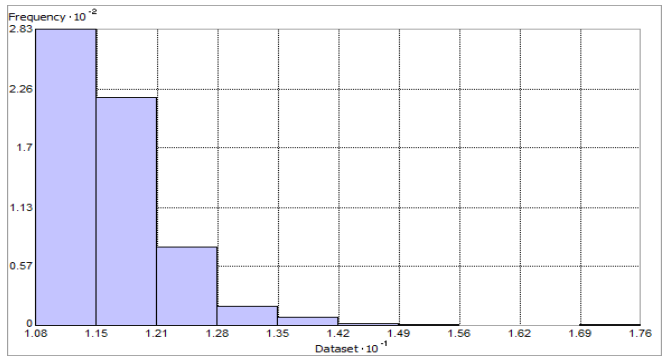

Figure 221. Distribution of Maximum Summer Mixed Layer Depth (m). Histogram was illustrated using 10 bins. X axis shown at 10^{-1}; Y axis shown at 10^{-2}.

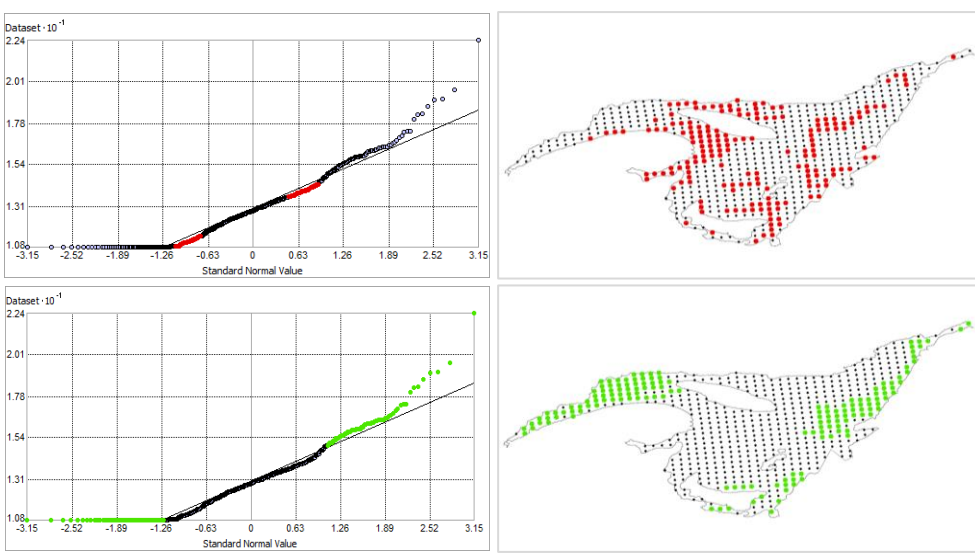

Fig. 222. Normal Q-Q plot for data values of Maximum Summer Mixed Layer Depth (m). Points falling under (upper panel) and over (bottom panel) the reference line are mapped.

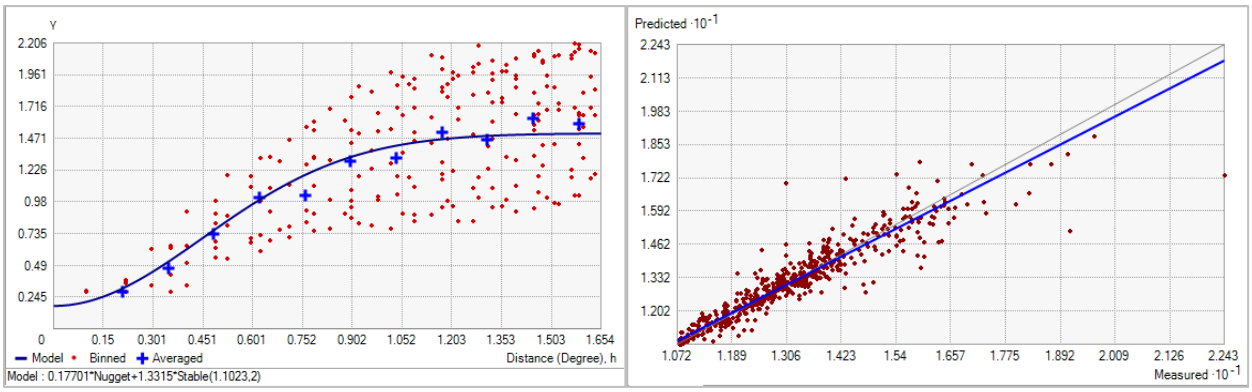

Fig. 223. Left panel: Semivariogram of Maximum Summer Mixed Layer Depth (m). Binned values are shown as red dots; average points are shown as blue crosses; the model fit to the averaged values is shown as a blue line. Lag size: 0.138 degrees; number of lags: 12; Parameter: 2; Range: 1.102 degrees; Partial Sill: 1.331. Right panel: Scatterplot of predicted values versus observed values for the model of Maximum Summer Mixed Layer Depth (m).

Table 90. Results of cross-validation of the kriged model for the Maximum Summer Mixed Layer Depth (m).

Prediction error	**Value**
Number of Observations	606
Overall Mean Error	-7.198×10^{-4}
Root Mean Square Prediction Error	0.573
Standardized Mean	0.001
Standardized Root Mean Square Prediction Error	1.080
Average Standard Error	0.493

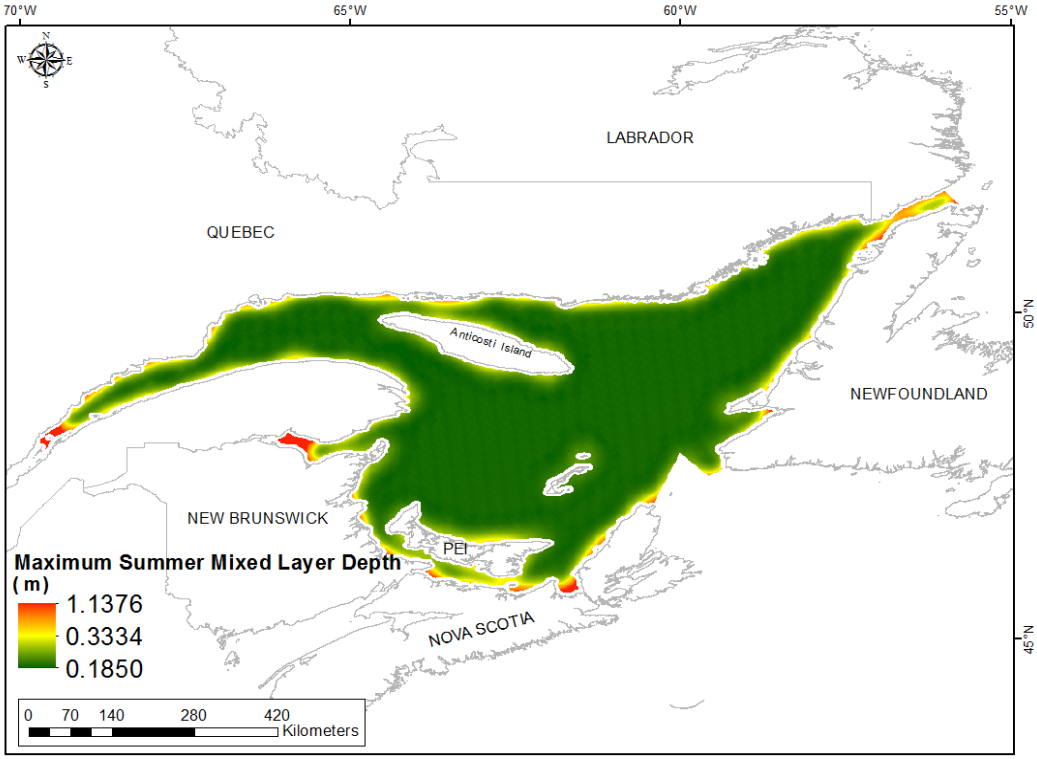

Fig. 224. Prediction standard error surface of Maximum Summer Mixed Layer Depth (m).

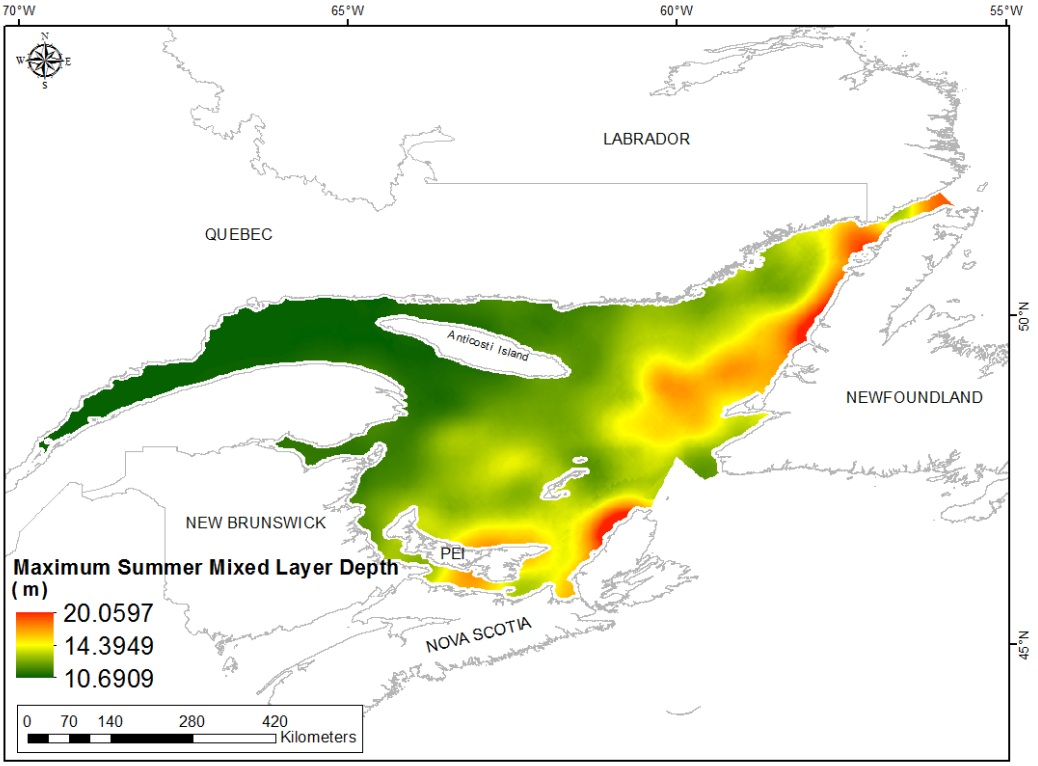

Fig. 225. Interpolated prediction surface of Maximum Summer Mixed Layer Depth (m).

Maximum Fall Mixed Layer Depth

This variable displayed a right-skewed distribution and an outlier at the upper range (Table 91, Fig. 226). The data were higher than predicted by a normal distribution at low and high values (Fig. 227). Mid-range values deviated only slightly from the reference line. The areas of over- and under-prediction showed a strong spatial pattern (Fig. 227).

The semivariogram showed weak autocorrelation present in the data and the model showed a good fit between measured and predicted values (Fig. 228). The model showed good cross-validation statistics (Table 92) indicating that it was very good at prediction. The error map showed low error in a linear pattern over the study extent except along the coast where it was higher (Fig. 229). The kriged surface is presented in Fig. 230.

Table 91. Distributional properties of Maximum Fall Mixed Layer Depth (m).

Property	Value
Number of Observations	606
Minimum	11.039
Maximum	148.070
Mean	29.385
Median	28.215
Standard Deviation	14.651
Skewness	2.918
Kurtosis	19.273

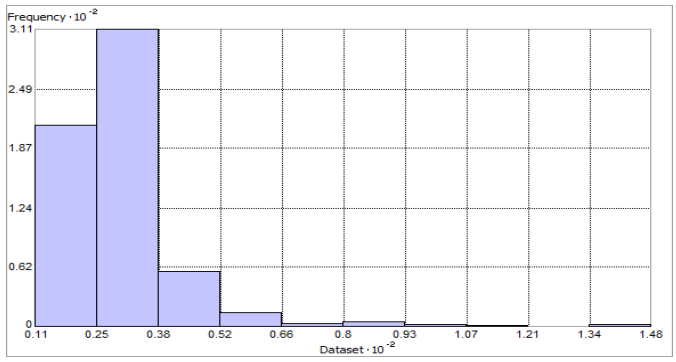

Fig. 226. Distribution of Maximum Fall Mixed Layer Depth (m). Histogram was illustrated using 10 bins. X and Y axes shown at 10^{-2}.

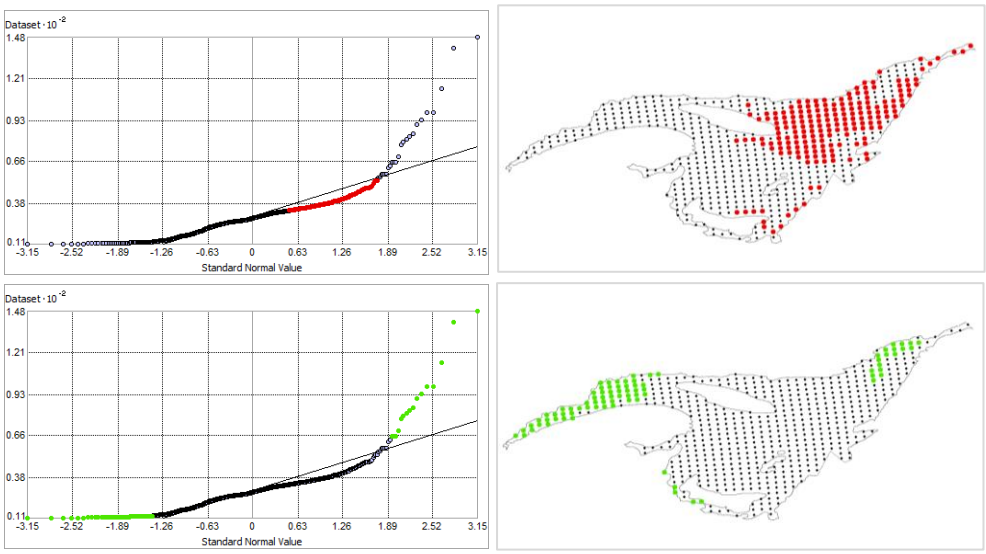

Fig. 227. Normal Q-Q plot for data values of Maximum Fall Mixed Layer Depth (m). Points falling under (upper panel) and over (bottom panel) the reference line are mapped.

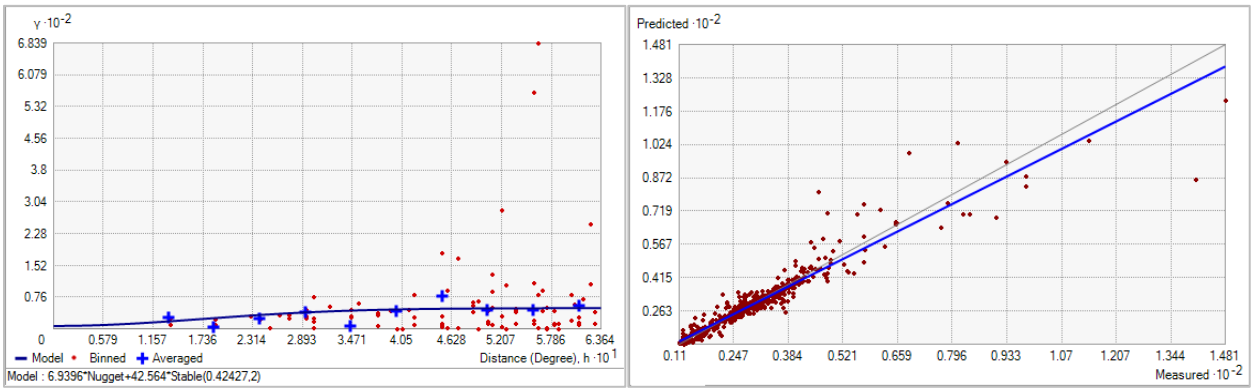

Fig. 228. Left panel: Semivariogram of Maximum Fall Mixed Layer Depth (m). Binned values are shown as red dots; average points are shown as blue crosses; the model fit to the averaged values is shown as a blue line. Lag size: 0.053 degrees; number of lags: 12; Parameter: 2; Range: 0.424 degrees; Partial Sill: 42.564. Right panel: Scatterplot of predicted values versus observed values for the model of Maximum Fall Mixed Layer Depth (m).

Table 92. Results of cross-validation of the kriged model for the Maximum Fall Mixed Layer Depth (m).

Prediction error	**Value**
Number of Observations	606
Overall Mean Error	0.064
Root Mean Square Prediction Error	4.607
Standardized Mean	0.007
Standardized Root Mean Square Prediction Error	0.927
Average Standard Error	4.742

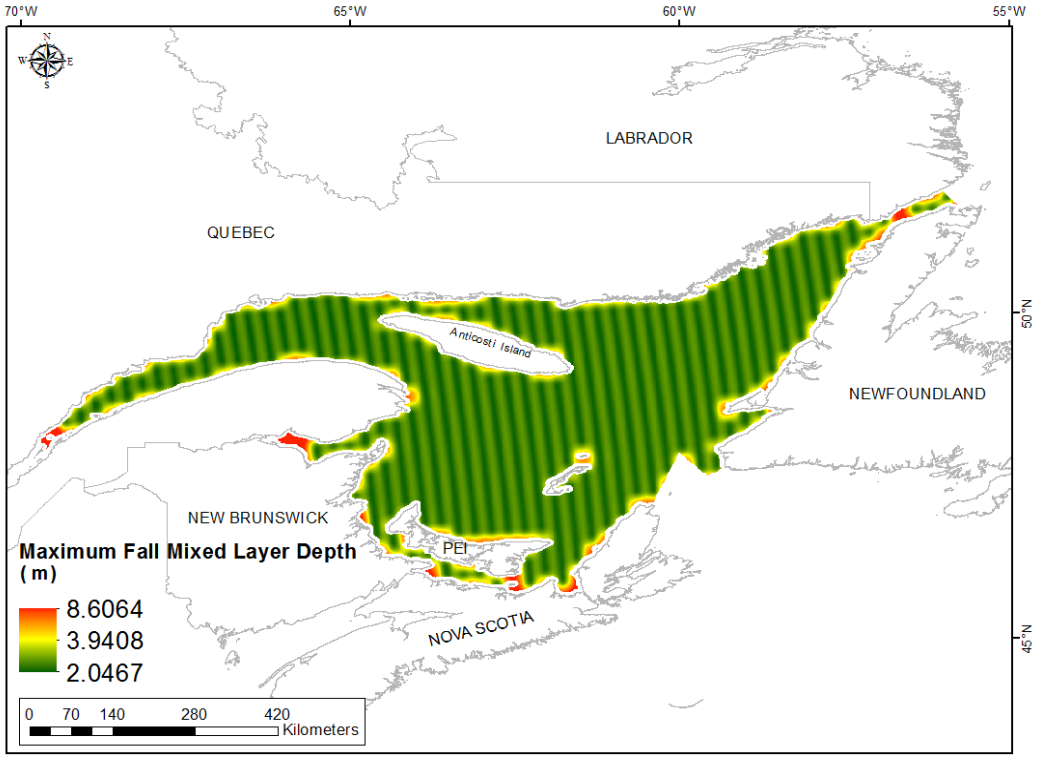

Fig. 229. Prediction standard error surface of Maximum Fall Mixed Layer Depth (m).

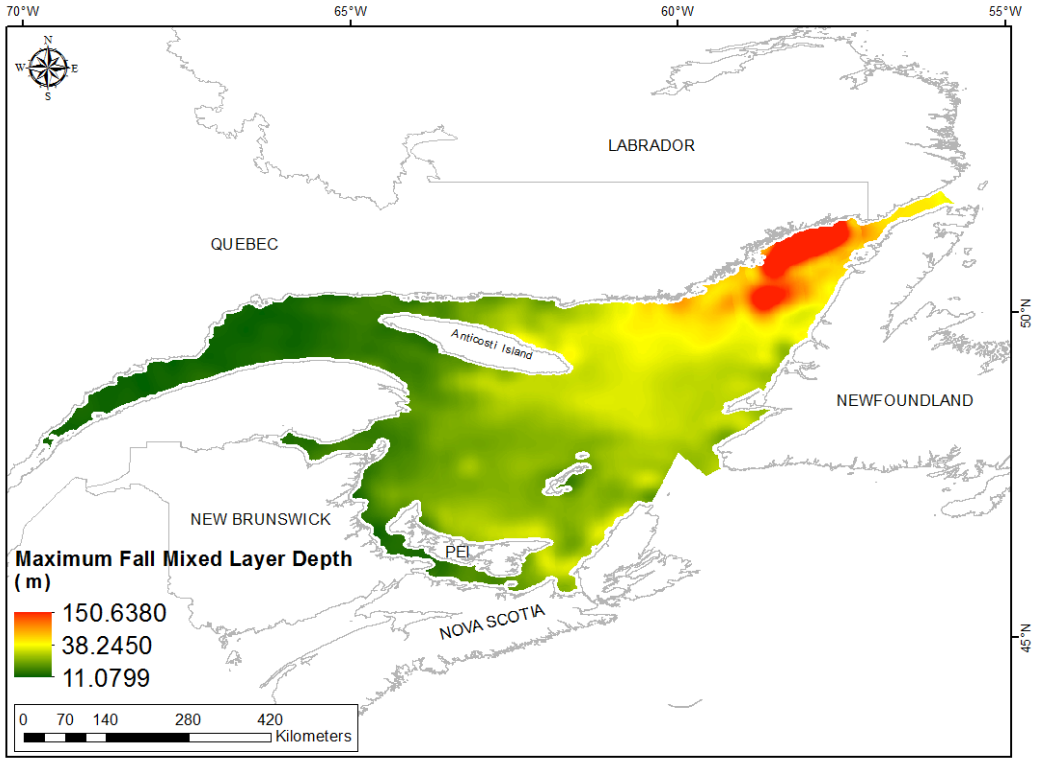

Fig. 230. Interpolated prediction surface of Maximum Fall Mixed Layer Depth (m).

Maximum Winter Mixed Layer Depth

This variable displayed a right-skewed distribution and high kurtosis (Table 93, Fig. 231). The data were higher than predicted by a normal distribution at low and high values (Fig. 232). Mid-range values deviated only slightly from the reference line. The areas of over- and under-prediction showed a strong spatial pattern (Fig. 232).

The semivariogram showed little to no autocorrelation present in the data and the model showed a good fit between measured and predicted values (Fig. 233). The model showed good cross-validation statistics (Table 94) indicating that it was very good at prediction. The error map showed low error in a linear pattern over the study extent except for some areas along the coast where it was high (Fig. 234). The kriged surface is presented in Fig. 235.

Table 93. Distributional properties of Maximum Winter Mixed Layer Depth (m).

Property	Value
Number of Observations	606
Minimum	10.822
Maximum	151.080
Mean	36.623
Median	35.620
Standard Deviation	17.165
Skewness	1.792
Kurtosis	11.175

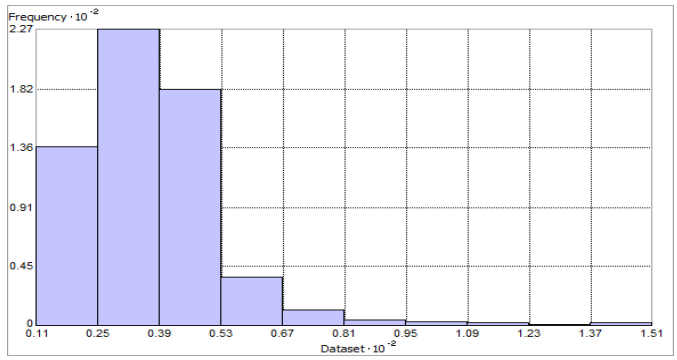

Fig. 231. Distribution of Maximum Winter Mixed Layer Depth (m). Histogram was illustrated using 10 bins. X and Y axes shown at 10^{-2}.

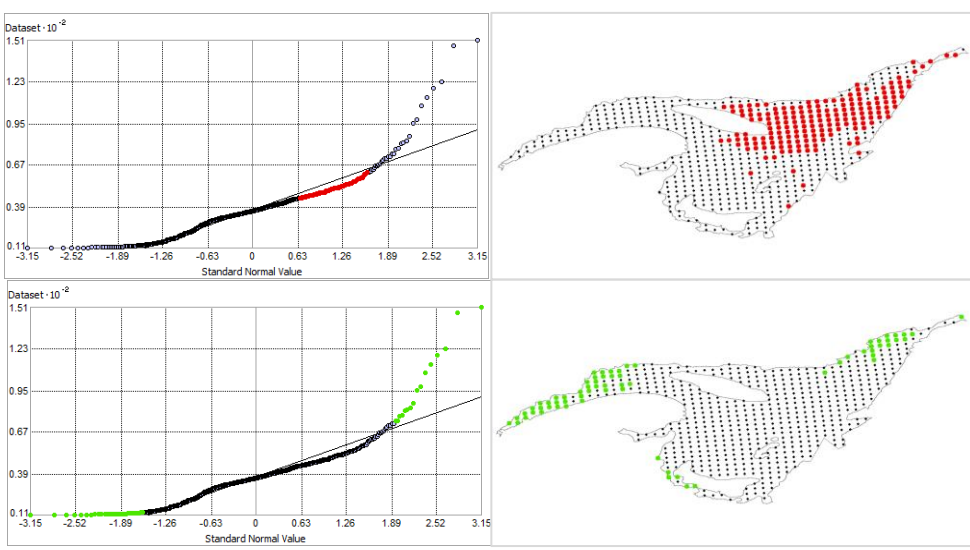

Fig. 232. Normal Q-Q plot for data values of Maximum Winter Mixed Layer Depth (m). Points falling under (upper panel) and over (bottom panel) the reference line are mapped.

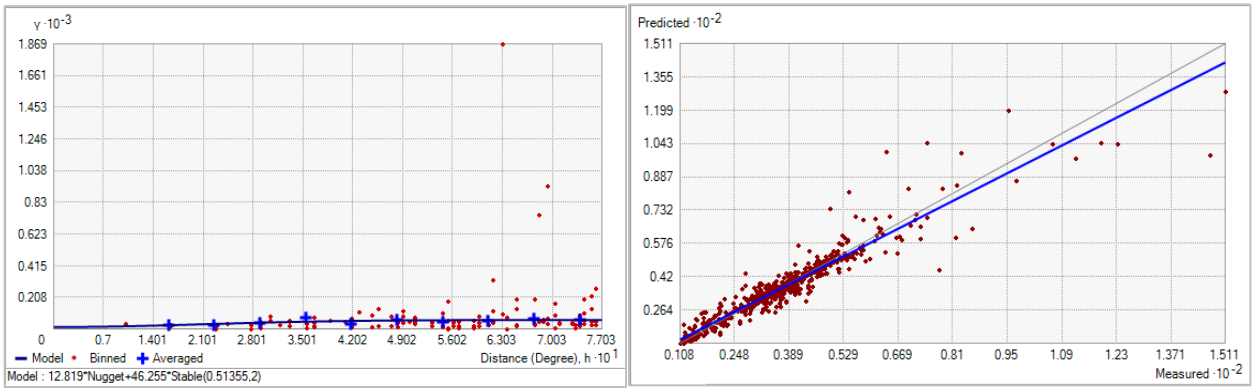

Fig. 233. Left panel: Semivariogram of Maximum Winter Mixed Layer Depth (m). Binned values are shown as red dots; average points are shown as blue crosses; the model fit to the averaged values is shown as a blue line. Lag size: 0.064 degrees; number of lags: 12; Parameter: 2; Range: 0.514 degrees; Partial Sill: 46.255. Right panel: Scatterplot of predicted values versus observed values for the model of Maximum Winter Mixed Layer Depth (m).

Table 94. Results of cross-validation of the kriged model for the Maximum Winter Mixed Layer Depth (m).

Prediction error	**Value**
Number of Observations	606
Overall Mean Error	0.054
Root Mean Square Prediction Error	5.394
Standardized Mean	0.005
Standardized Root Mean Square Prediction Error	0.991
Average Standard Error	5.168

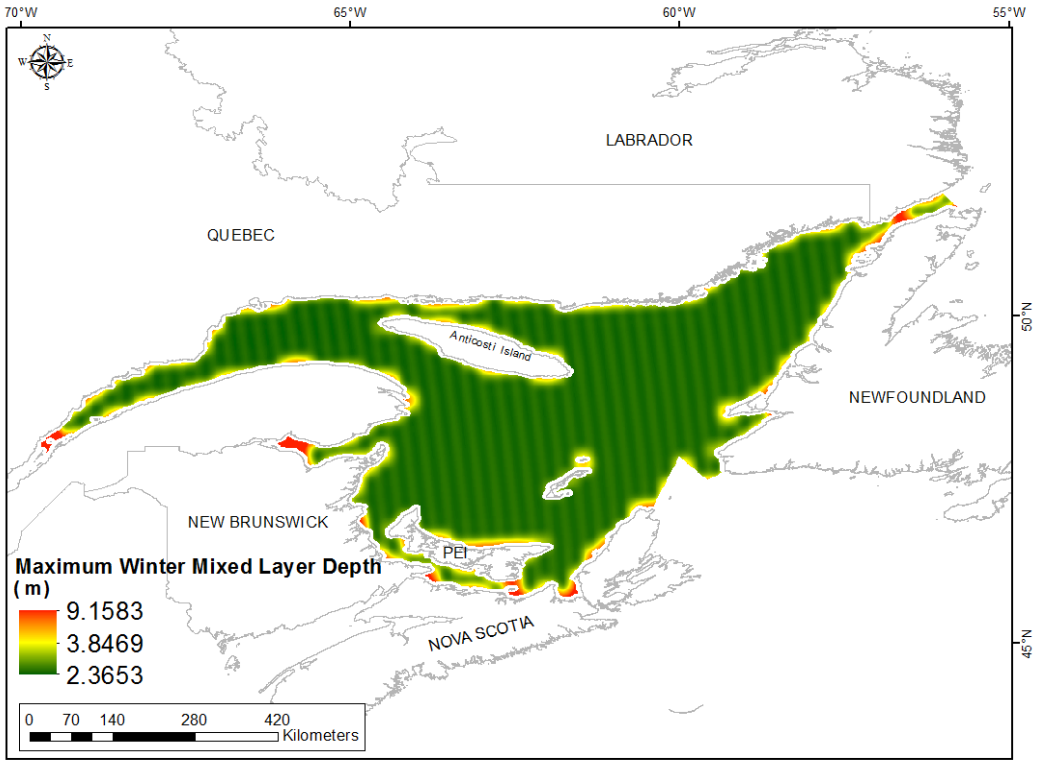

Fig. 234. Prediction standard error surface of Maximum Winter Mixed Layer Depth (m).

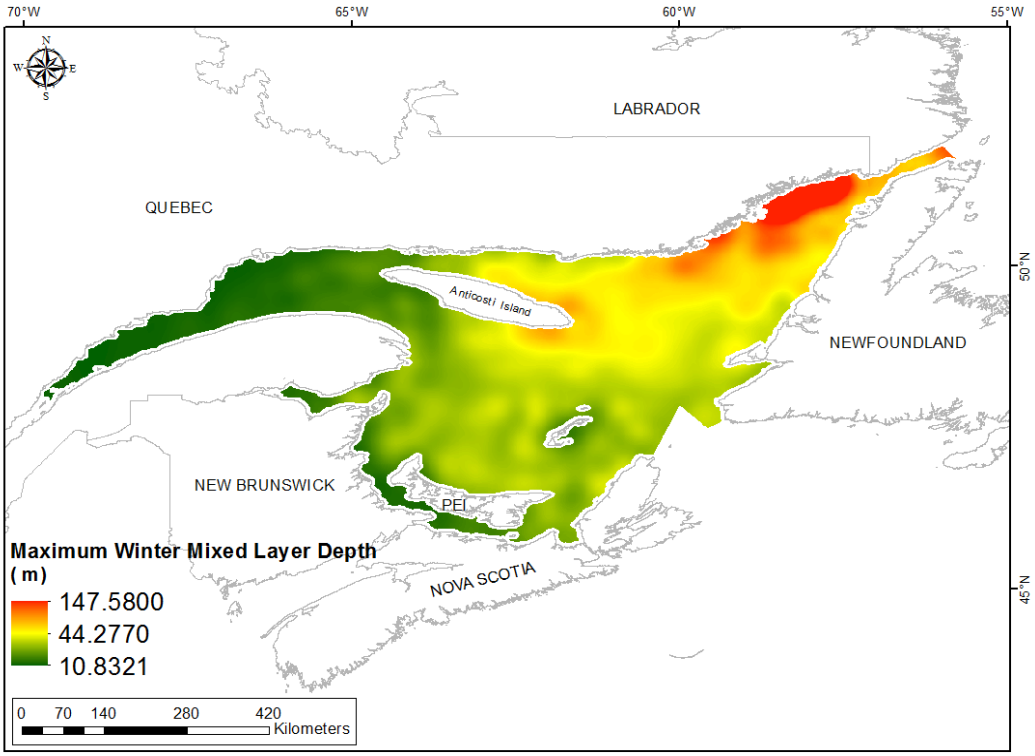

Fig. 235. Interpolated prediction surface of Maximum Winter Mixed Layer Depth (m).

Maximum Average Spring Mixed Layer Depth

This variable displayed a plateau-like, right-skewed distribution with outlying data in the upper range (Table 95, Fig. 236). The data closely followed a normal distribution except for at the highest data values where it oscillated about the reference line (Fig. 237). The areas of over- and under-prediction showed a strong spatial pattern (Fig. 237).

The semivariogram showed little to no autocorrelation present in the data and the model showed a good fit between measured and predicted values (Fig. 238). The model showed good cross-validation statistics (Table 96) indicating that it was very good at prediction. The error map showed low error in a linear pattern over the study extent except for some areas along the coast where it was high (Fig. 239). The kriged surface is presented in Fig. 240.

Table 95. Distributional properties of Maximum Average Spring Mixed Layer Depth (m).

Property	Value
Number of Observations	606
Minimum	10.768
Maximum	30.404
Mean	14.397
Median	14.081
Standard Deviation	2.722
Skewness	0.812
Kurtosis	4.359

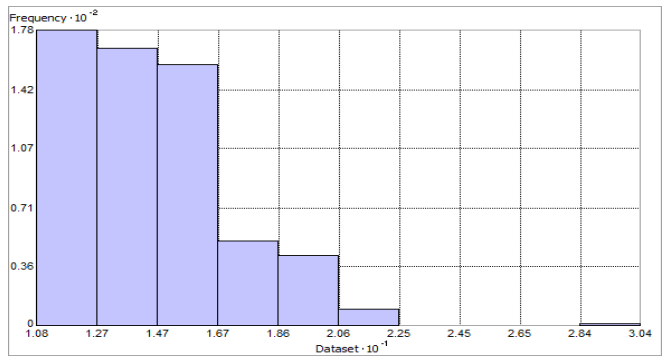

Fig. 236. Distribution of Maximum Average Spring Mixed Layer Depth (m). Histogram was illustrated using 10 bins. X axis shown at 10^{-1}; Y axis shown at 10^{-2}.

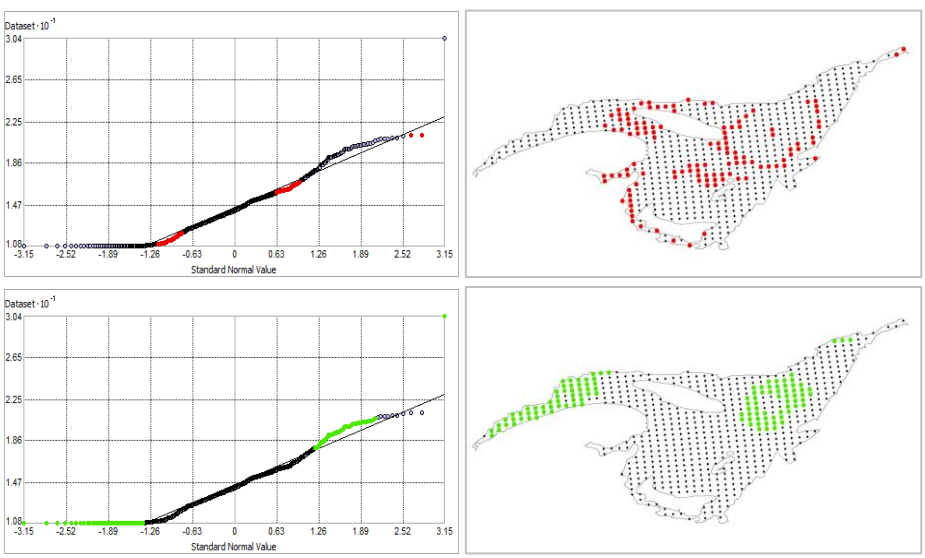

Fig. 237. Normal Q-Q plot for data values of Maximum Average Spring Mixed Layer Depth (m). Points falling under (upper panel) and over (bottom panel) the reference line are mapped.

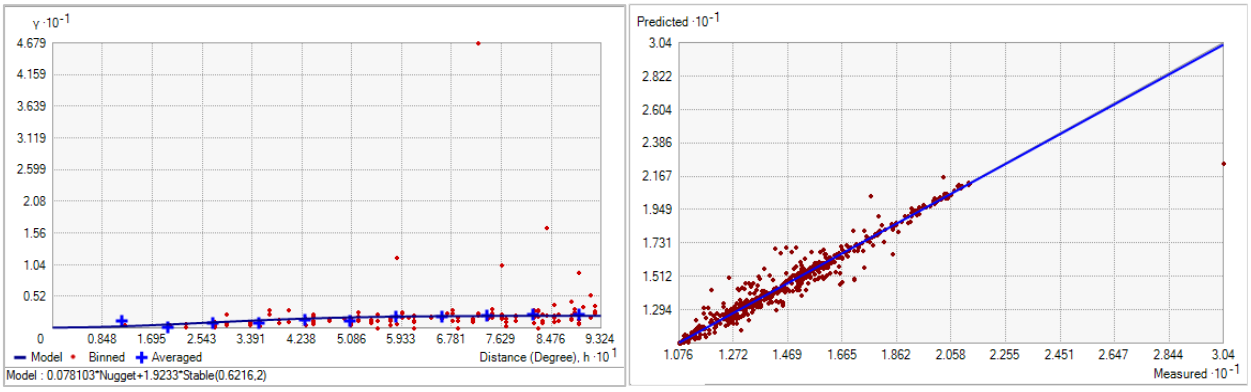

Fig. 238. Left panel: Semivariogram of Maximum Average Spring Mixed Layer Depth (m). Binned values are shown as red dots; average points are shown as blue crosses; the model fit to the averaged values is shown as a blue line. Lag size: 0.078 degrees; number of lags: 12; Parameter: 2; Range: 0.622 degrees; Partial Sill: 1.923. Right panel: Scatterplot of predicted values versus observed values for the model of Maximum Average Spring Mixed Layer Depth (m).

Table 96. Results of cross-validation of the kriged model for the Maximum Average Spring Mixed Layer Depth (m).

Prediction error	**Value**
Number of Observations	606
Overall Mean Error	0.031
Root Mean Square Prediction Error	0.620
Standardized Mean	0.037
Standardized Root Mean Square Prediction Error	1.164
Average Standard Error	0.500

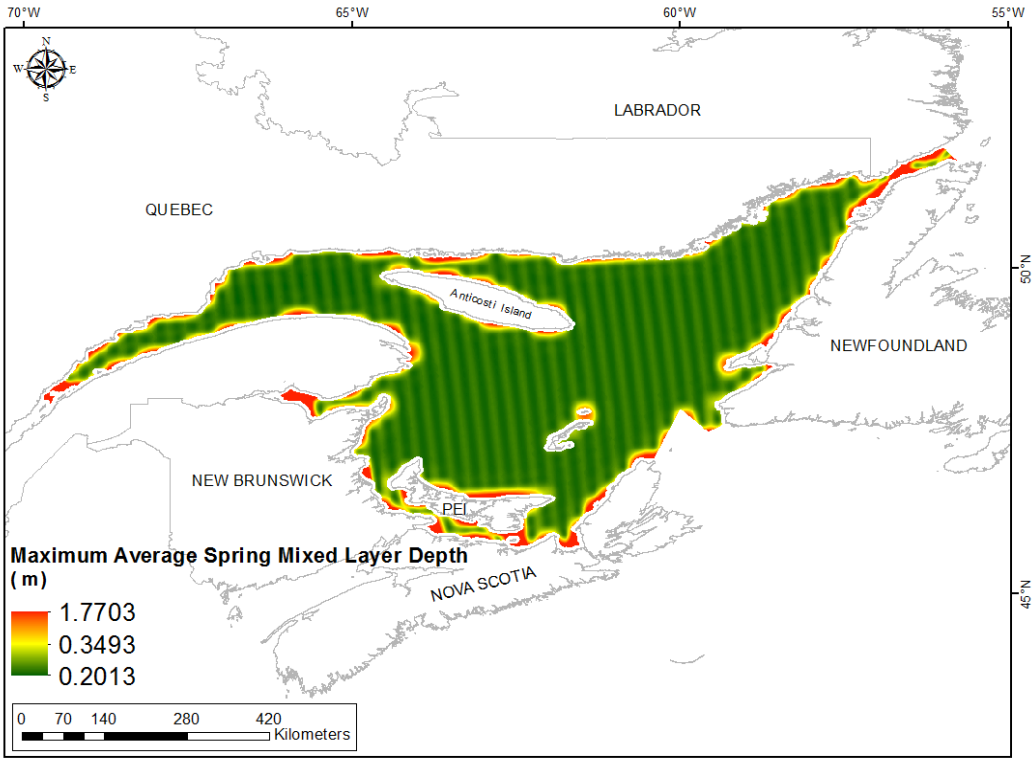

Fig. 239. Prediction standard error surface of Maximum Average Spring Mixed Layer Depth (m).

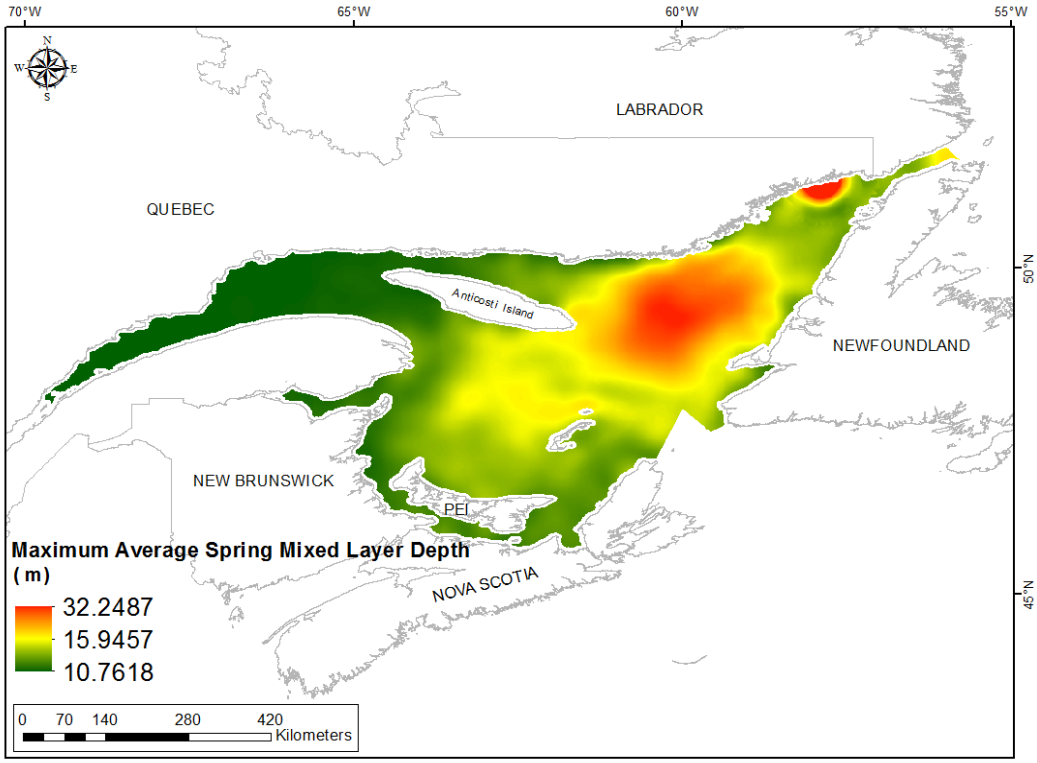

Fig. 240. Interpolated prediction surface of Maximum Average Spring Mixed Layer Depth (m).

Maximum Average Summer Mixed Layer Depth

This variable displayed a right-skewed distribution with outlying data in the upper range (Table 97, Fig. 241). The data were higher than predicted by a normal distribution at low and high values (Fig. 242). Mid-range values deviated only slightly from the reference line. The areas of over- and under-prediction showed a strong spatial pattern (Fig. 242).

The semivariogram showed moderate autocorrelation present in the data and the model showed a good fit between measured and predicted values (Fig. 243). The model showed good cross-validation statistics (Table 98) indicating that it was very good at prediction. The error map showed low error in a slight linear pattern over the study extent except for some areas along the coast where it was high (Fig. 244). The kriged surface is presented in Fig. 245.

Table 97. Distributional properties of Maximum Average Summer Mixed Layer Depth (m).

Property	Value
Number of Observations	606
Minimum	10.768
Maximum	30.404
Mean	14.397
Median	14.081
Standard Deviation	2.722
Skewness	0.812
Kurtosis	4.359

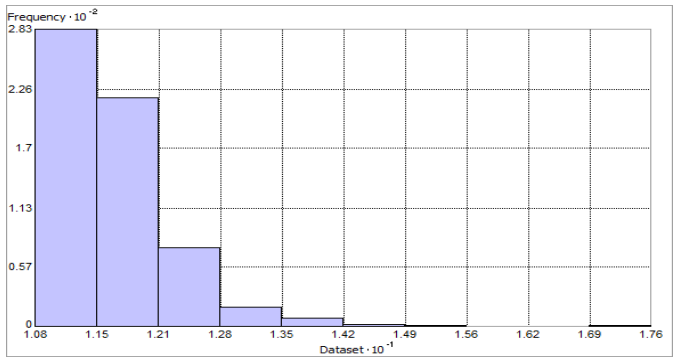

Fig. 241. Distribution of Maximum Average Summer Mixed Layer Depth (m). Histogram was illustrated using 10 bins. X axis shown at 10^{-1}; Y axis shown at 10^{-2}.

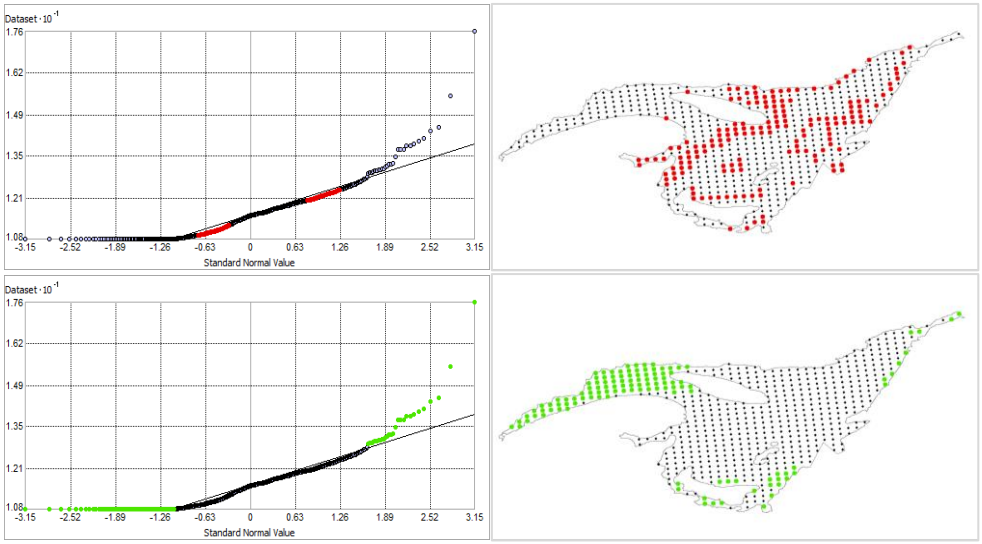

Fig. 242. Normal Q-Q plot for data values of Maximum Average Summer Mixed Layer Depth (m). Points falling under (upper panel) and over (bottom panel) the reference line are mapped.

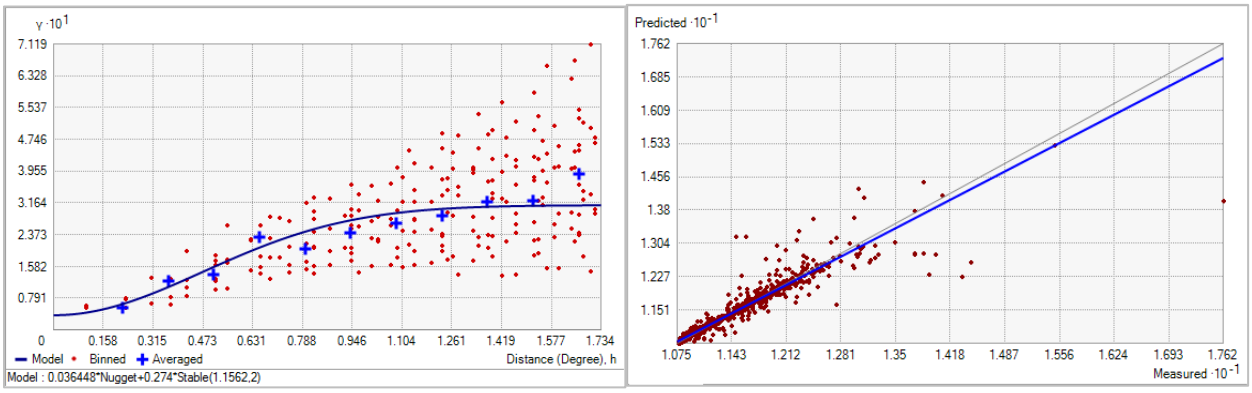

Fig. 243. Left panel: Semivariogram of Maximum Average Summer Mixed Layer Depth (m). Binned values are shown as red dots; average points are shown as blue crosses; the model fit to the averaged values is shown as a blue line. Lag size: 0.078 degrees; number of lags: 12; Parameter: 2; Range: 0.622 degrees; Partial Sill: 1.923. Right panel: Scatterplot of predicted values versus observed values for the model of Maximum Average Summer Mixed Layer Depth (m).

Table 98. Results of cross-validation of the kriged model for the Maximum Average Summer Mixed Layer Depth (m).

Prediction error	**Value**
Number of Observations	606
Overall Mean Error	3.527×10^{-4}
Root Mean Square Prediction Error	0.301
Standardized Mean	0.002
Standardized Root Mean Square Prediction Error	1.202
Average Standard Error	0.222

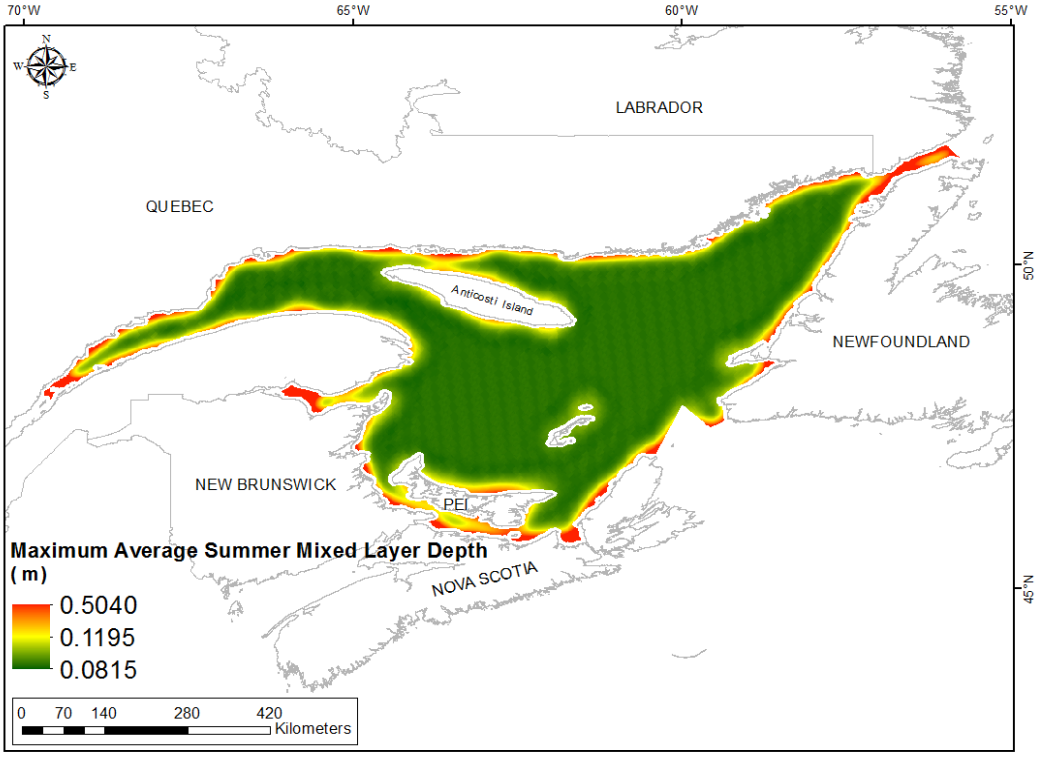

Fig. 244. Prediction standard error surface of Maximum Average Summer Mixed Layer Depth (m).

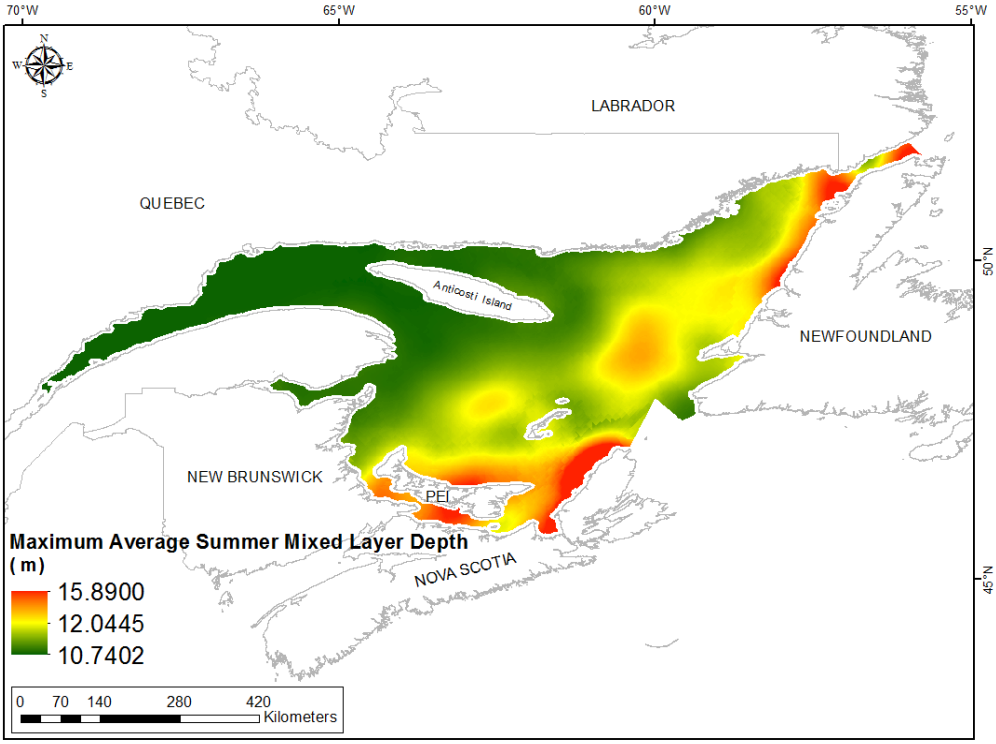

Fig. 245. Interpolated prediction surface of Maximum Average Summer Mixed Layer Depth (m).

Maximum Average Fall Mixed Layer Depth

This variable displayed a right-skewed distribution with several outlying points in the upper range (Table 99, Fig. 246). The data were higher than predicted by a normal distribution at low and high values (Fig. 247). Mid-range values deviated only slightly from the reference line. The areas of over- and under-prediction showed a strong spatial pattern (Fig. 247).

The semivariogram showed weak autocorrelation present in the data and the model showed a good fit between measured and predicted values (Fig. 248). The model showed good cross-validation statistics (Table 100) indicating that it was very good at prediction. The error map showed low error in a linear pattern over the study extent except along the coast where it was high (Fig. 249). The kriged surface is presented in Fig. 250.

Table 99. Distributional properties of Maximum Average Fall Mixed Layer Depth (m).

Property	Value
Number of Observations	606
Minimum	10.790
Maximum	91.591
Mean	22.262
Median	22.363
Standard Deviation	7.984
Skewness	1.766
Kurtosis	14.453

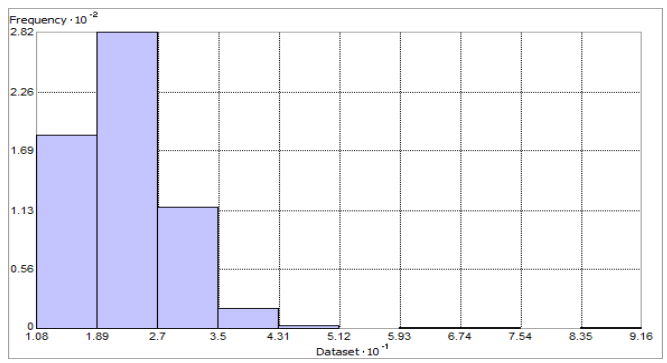

Fig. 246. Distribution of Maximum Average Fall Mixed Layer Depth (m). Histogram was illustrated using 10 bins. X axis shown at 10^{-1}; Y axis shown at 10^{-2}.

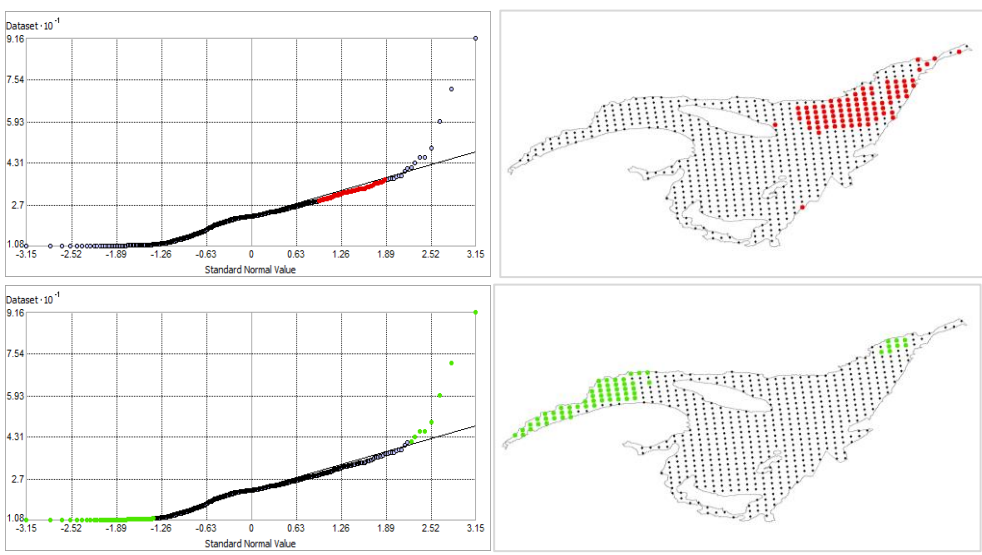

Fig. 247. Normal Q-Q plot for data values of Maximum Average Fall Mixed Layer Depth (m). Points falling under (upper panel) and over (bottom panel) the reference line are mapped.

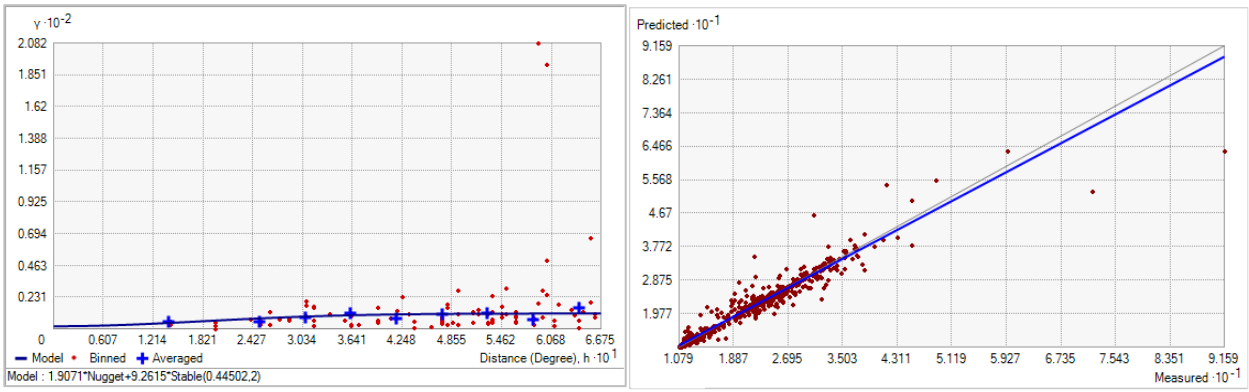

Fig. 248. Left panel: Semivariogram of Maximum Average Fall Mixed Layer Depth (m). Binned values are shown as red dots; average points are shown as blue crosses; the model fit to the averaged values is shown as a blue line. Lag size: 0.056 degrees; number of lags: 12; Parameter: 2; Range: 0.445 degrees; Partial Sill: 9.261. Right panel: Scatterplot of predicted values versus observed values for the model of Maximum Average Fall Mixed Layer Depth (m).

Table 100. Results of cross-validation of the kriged model for the Maximum Average Fall Mixed Layer Depth (m).

Prediction error	**Value**
Number of Observations	606
Overall Mean Error	0.066
Root Mean Square Prediction Error	2.373
Standardized Mean	0.017
Standardized Root Mean Square Prediction Error	0.967
Average Standard Error	2.280

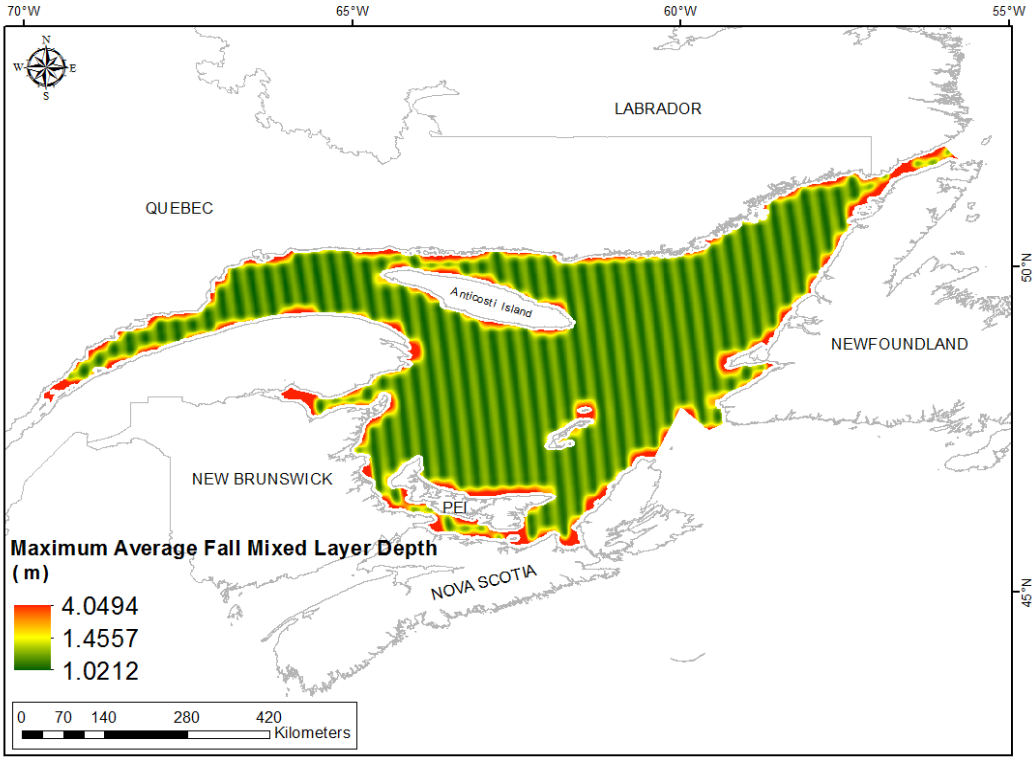

Fig. 249. Prediction standard error surface of Maximum Average Fall Mixed Layer Depth (m).

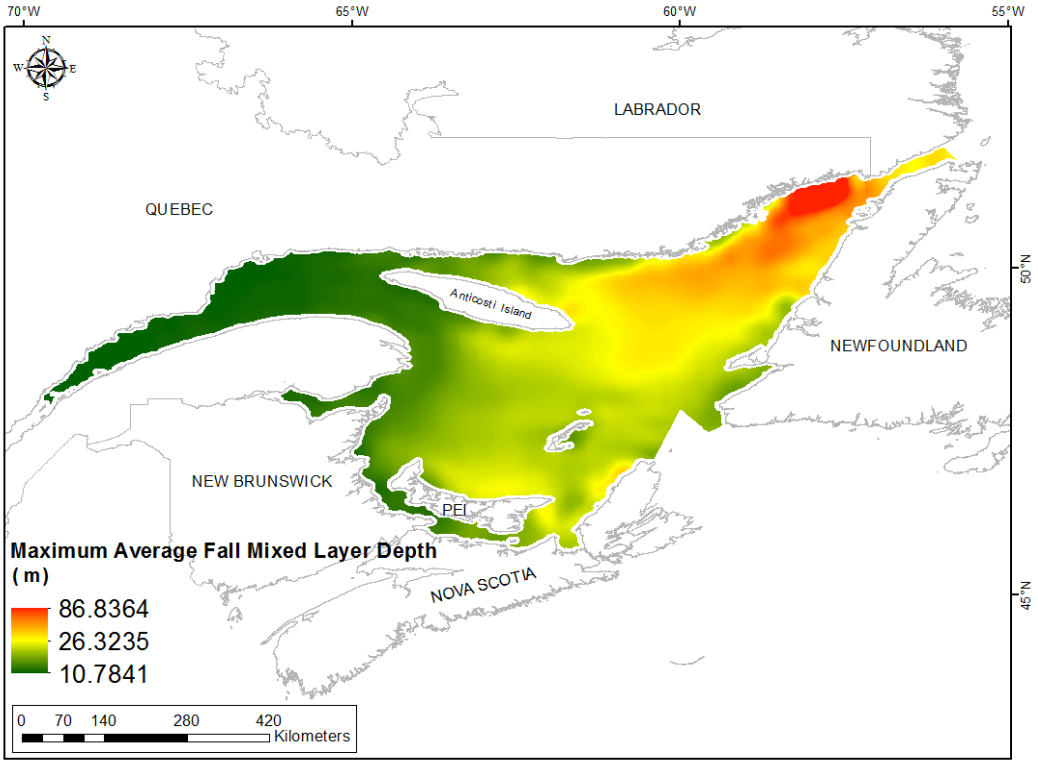

Fig. 250. Interpolated prediction surface of Maximum Average Fall Mixed Layer Depth (m).

Maximum Average Winter Mixed Layer Depth

This variable displayed a right-skewed distribution and several outlying points in the upper range (Table 101, Fig. 251). The data were higher than predicted by a normal distribution at low and high values (Fig. 252). Mid-range values deviated only slightly from the reference line. The areas of over- and under-prediction showed a strong spatial pattern (Fig. 252).

The semivariogram showed little to no autocorrelation present in the data and the model showed a good fit between measured and predicted values (Fig. 253). The model showed good cross-validation statistics (Table 102) indicating that it was very good at prediction. The error map showed low error in a slight linear pattern over the study extent except for some areas along the coast where it was high (Fig. 254). The kriged surface is presented in Fig. 255.

Table 101. Distributional properties of Maximum Average Winter Mixed Layer Depth (m).

Property	Value
Number of Observations	606
Minimum	10.775
Maximum	123.320
Mean	28.100
Median	27.415
Standard Deviation	11.925
Skewness	1.596
Kurtosis	11.788

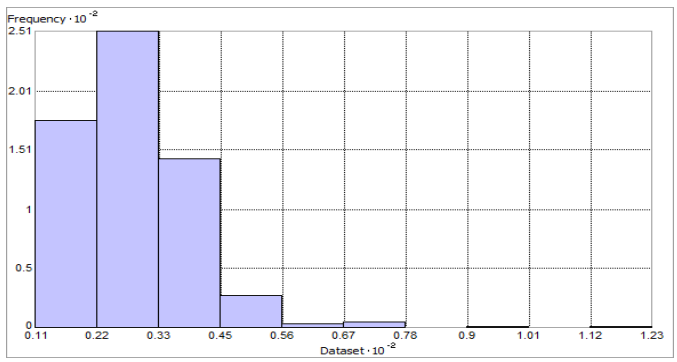

Fig. 251. Distribution of Maximum Average Fall Mixed Layer Depth (m). Histogram was illustrated using 10 bins. X and Y axes shown at 10^{-2}.

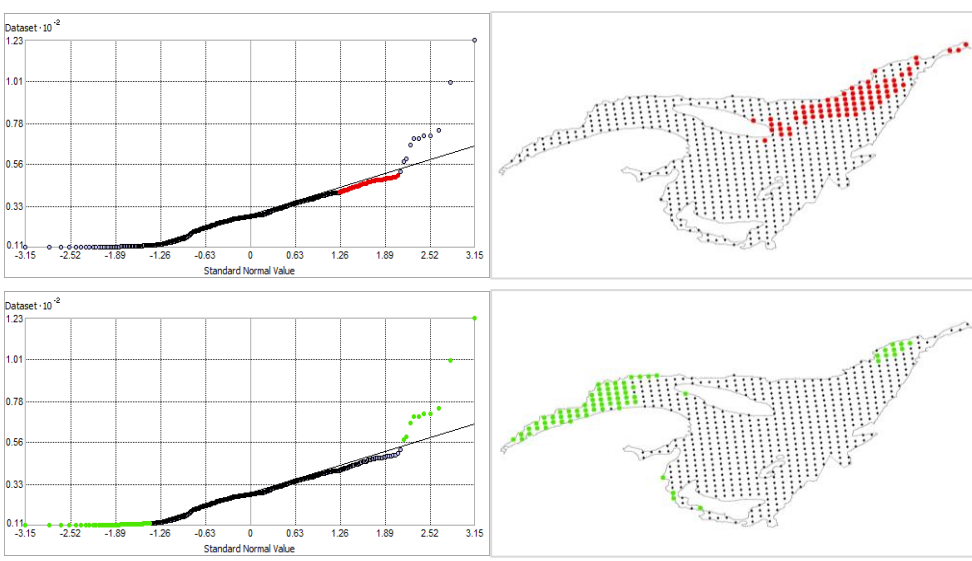

Fig. 252. Normal Q-Q plot for data values of Maximum Average Winter Mixed Layer Depth (m). Points falling under (upper panel) and over (bottom panel) the reference line are mapped.

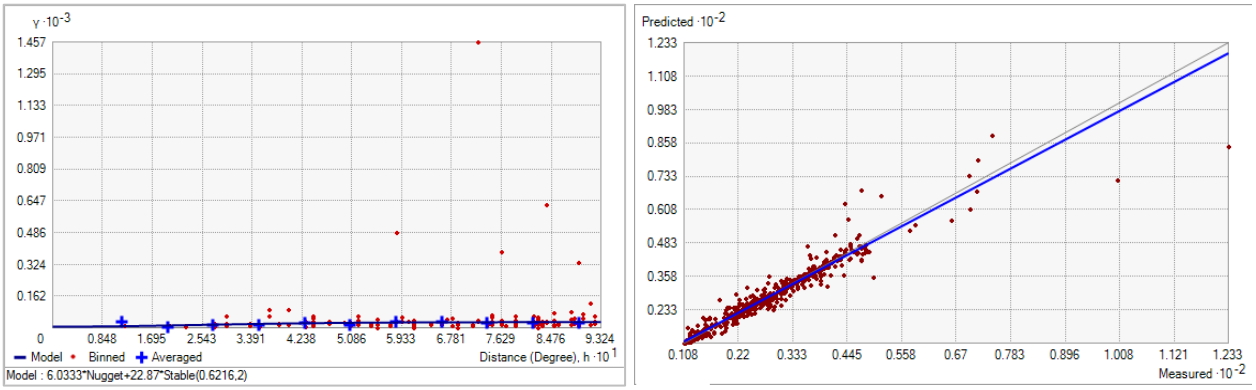

Fig. 253. Left panel: Semivariogram of Maximum Average Winter Mixed Layer Depth (m). Binned values are shown as red dots; average points are shown as blue crosses; the model fit to the averaged values is shown as a blue line. Lag size: 0.078 degrees; number of lags: 12; Parameter: 2; Range: 0.622 degrees; Partial Sill: 22.870. Right panel: Scatterplot of predicted values versus observed values for the model of Maximum Average Winter Mixed Layer Depth (m).

Table 102. Results of cross-validation of the kriged model for the Maximum Average Winter Mixed Layer Depth (m).

Prediction error	**Value**
Number of Observations	606
Overall Mean Error	0.053
Root Mean Square Prediction Error	3.270
Standardized Mean	0.009
Standardized Root Mean Square Prediction Error	0.942
Average Standard Error	3.272

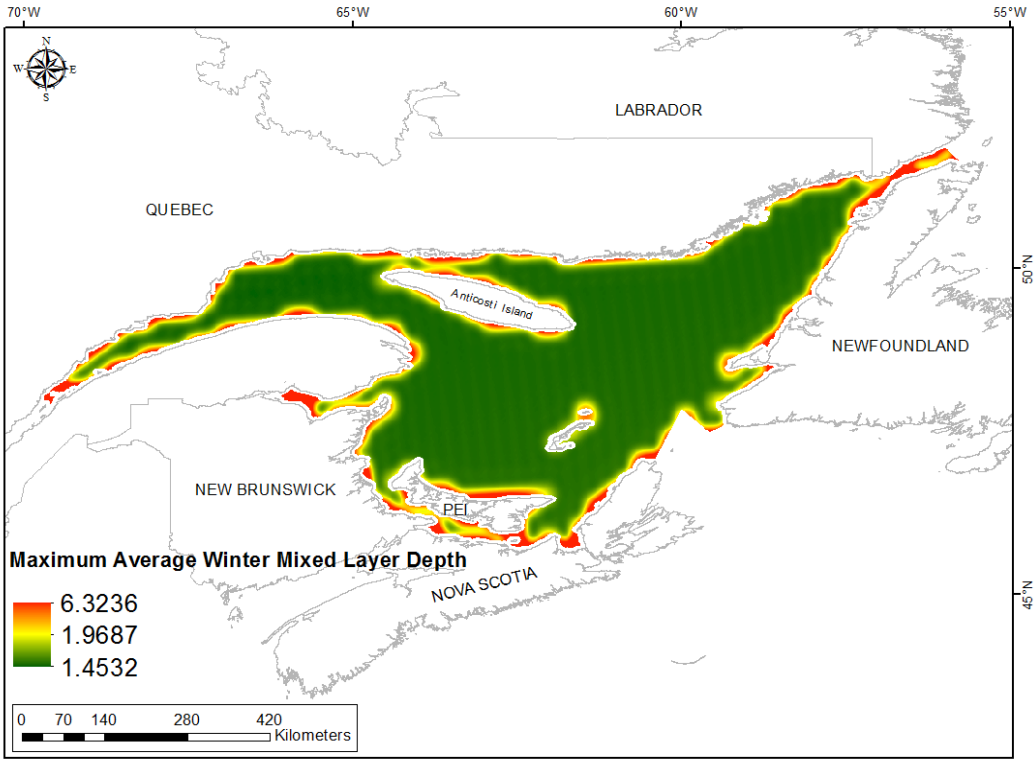

Fig. 254. Prediction standard error surface of Maximum Average Winter Mixed Layer Depth (m).

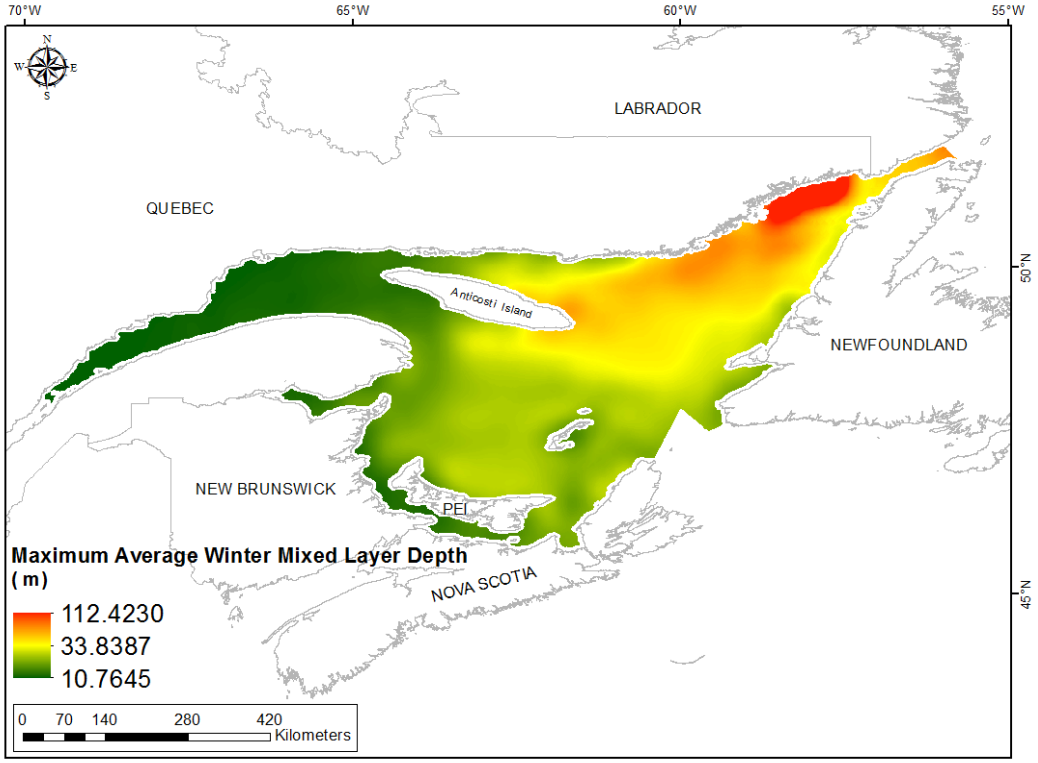

Fig. 255. Interpolated prediction surface of Maximum Average Winter Mixed Layer Depth (m).

Bottom Shear

Bottom shear stress is a function of the maximum predicted tidal current and reflects friction pressure on the seabed. Its unit is Pa or pascal, which is equivalent to one newton (1 N) of force over one meter squared. Shear stress near the seabed causes sediment erosion and affects vertical mixing and conditions conducive to sediment deposition (Cheng et al., 1999).

Bottom Shear Mean

This variable displayed a severely right-skewed, discontinuous distribution (Table 103, Fig. 256). The data were higher than predicted by a normal distribution at high values (Fig. 257). Mid-range values were slightly lower than the reference line. The areas of over- and under-prediction showed no spatial pattern (Fig. 257).

The semivariogram showed no autocorrelation present in the data and the model showed very poor fit between measured and predicted values (Fig. 258). Nevertheless, the model showed fair cross-validation statistics (Table 104) indicating that it was good at prediction. The error map showed no spatial pattern over the study extent except for some areas along the coast where it was high (Fig. 259). The kriged surface is presented in Fig. 260.

Table 103. Distributional properties of Bottom Shear Mean (Pa).

Property	Value
Number of Observations	589
Minimum	5.694×10^{-4}
Maximum	0.091
Mean	0.004
Median	0.003
Standard Deviation	0.005
Skewness	9.909
Kurtosis	145.48

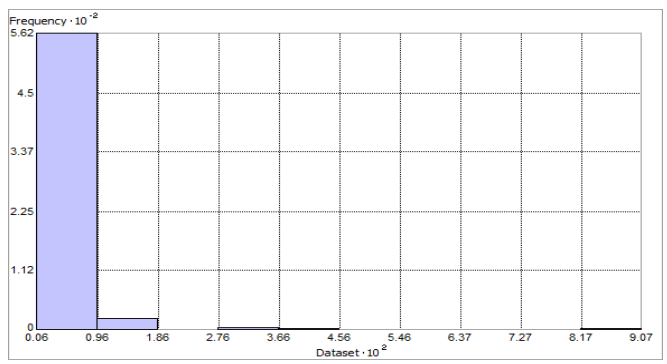

Fig. 256. Distribution of Bottom Shear Mean (Pa). Histogram was illustrated using 10 bins. X and Y axes shown at 10^2 and 10^{-2}, respectively.

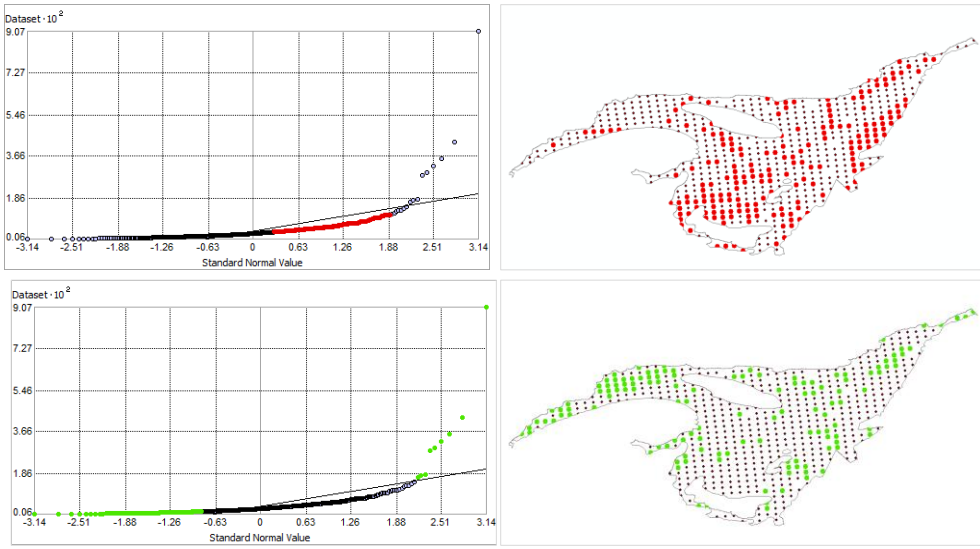

Fig. 257. Normal Q-Q plot for data values of Bottom Shear Mean (Pa). Points falling under (upper panel) and over (bottom panel) the reference line are mapped.

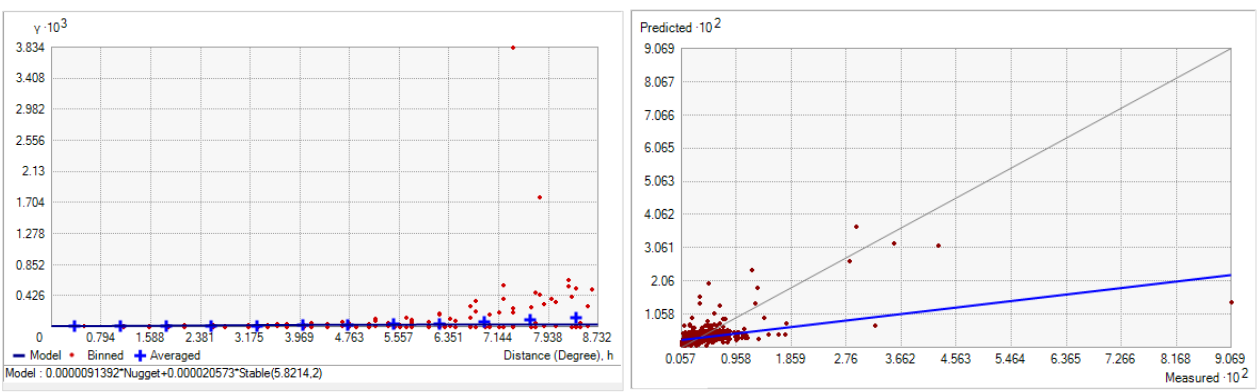

Fig. 258. Left panel: Semivariogram of Bottom Shear Mean (Pa). Binned values are shown as red dots; average points are shown as blue crosses; the model fit to the averaged values is shown as a blue line. Lag size: 0.728 degrees; number of lags: 12; Parameter: 2; Range: 5.821 degrees; Partial Sill: 2.057 x 10^{-5}. Right panel: Scatterplot of predicted values versus observed values for the model of Bottom Shear Mean (Pa).

Table 104. Results of cross-validation of the kriged model for the Bottom Shear Mean (Pa).

Prediction error	**Value**
Number of Observations	589
Overall Mean Error	1.408 x 10^{-6}
Root Mean Square Prediction Error	0.004
Standardized Mean	7.921 x 10^{-4}
Standardized Root Mean Square Prediction Error	1.322
Average Standard Error	0.003

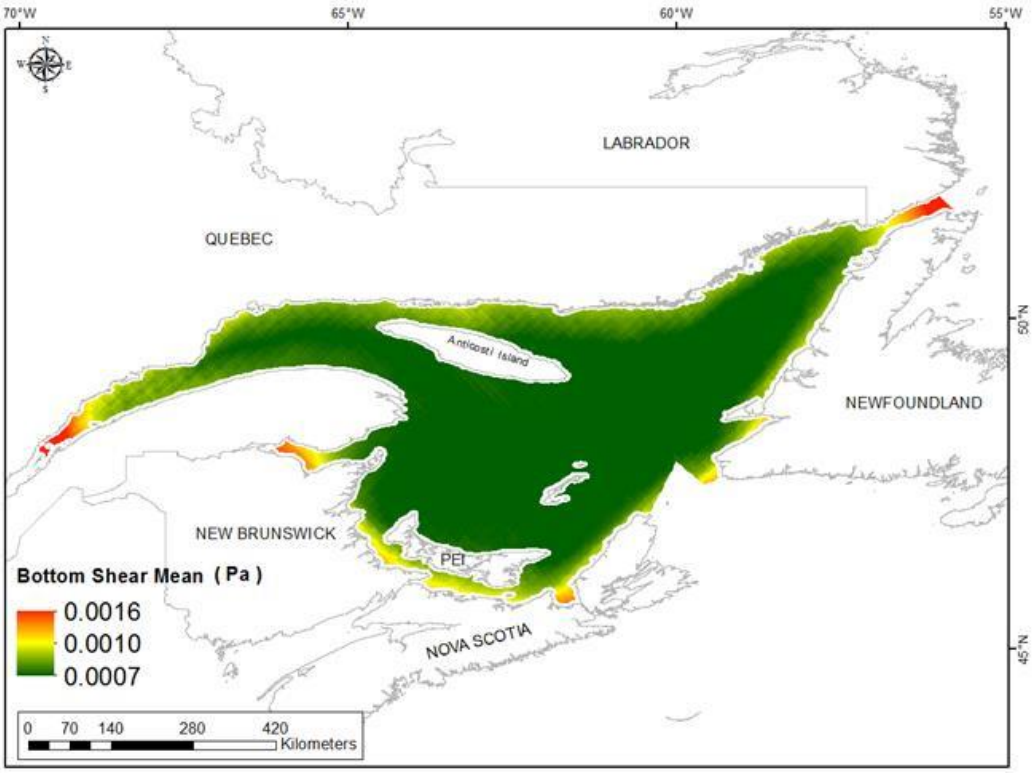

Fig. 259. Prediction standard error surface of Bottom Shear Mean (Pa).

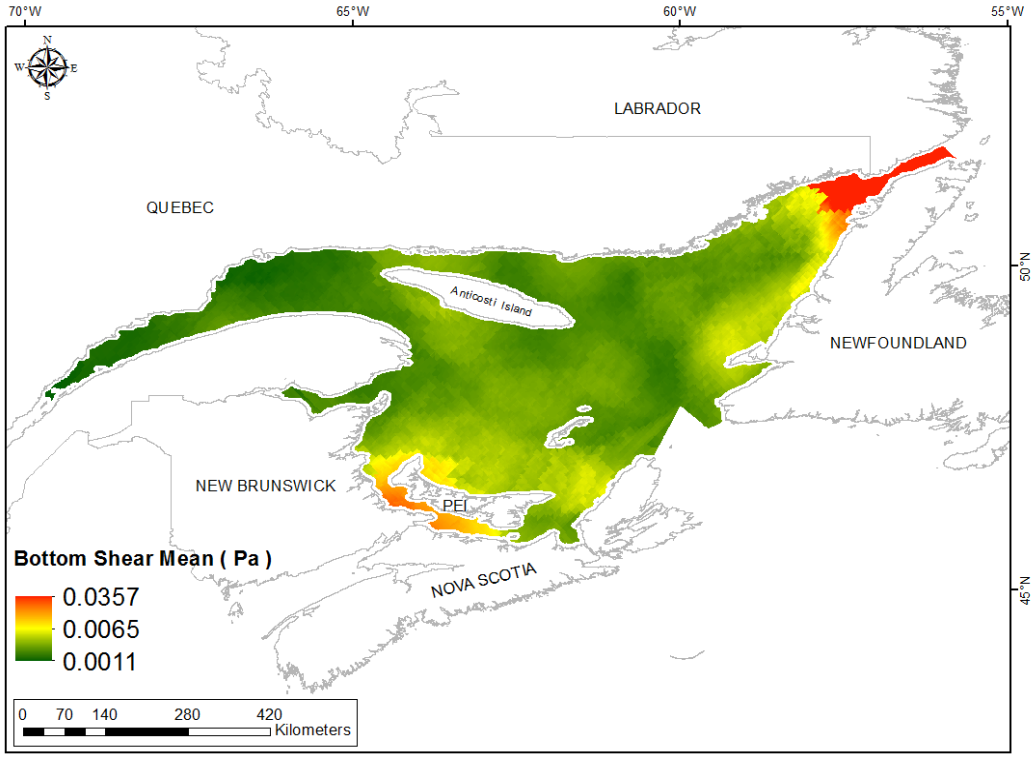

Fig, 260. Interpolated prediction surface of Bottom Shear Mean (Pa).

Bottom Shear Minimum

This variable displayed a highly right-skewed distribution with kurtosis prior to modeling (Table 105, Fig. 261). The data were higher than predicted by a normal distribution at high values (Fig. 262). Mid-range values were slightly lower than the reference line. The areas of over- and under-prediction showed no spatial pattern (Fig. 262).

The semivariogram showed autocorrelation present in the data and the model showed very poor fit between measured and predicted values (Fig. 263). Nevertheless, the model showed good cross-validation statistics (Table 106) indicating that it was good at prediction. The error map showed a 'bullseye' pattern with error increasing with distance from data points (Fig. 264). The kriged surface is presented in Fig. 265.

Table 105. Distributional properties of Bottom Shear Minimum (Pa).

Property	Value
Number of Observations	589
Minimum	1.000×10^{-6}
Maximum	0.001
Mean	1.430×10^{-4}
Median	9.000×10^{-5}
Standard Deviation	1.800×10^{-1}
Skewness	2.307
Kurtosis	10.876

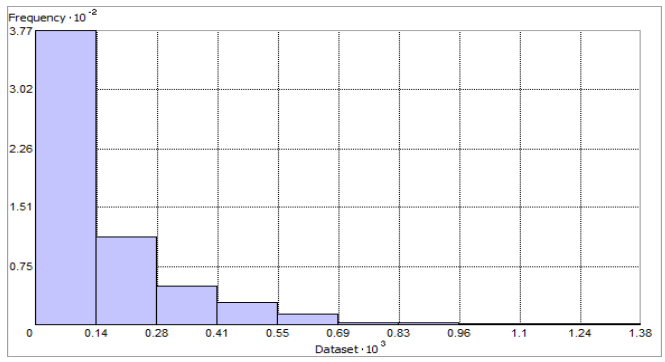

Fig. 261. Distribution of Bottom Shear Minimum (Pa). Histogram was illustrated using 10 bins. X axis shown at 10^2; Y axis shown at 10^{-2}.

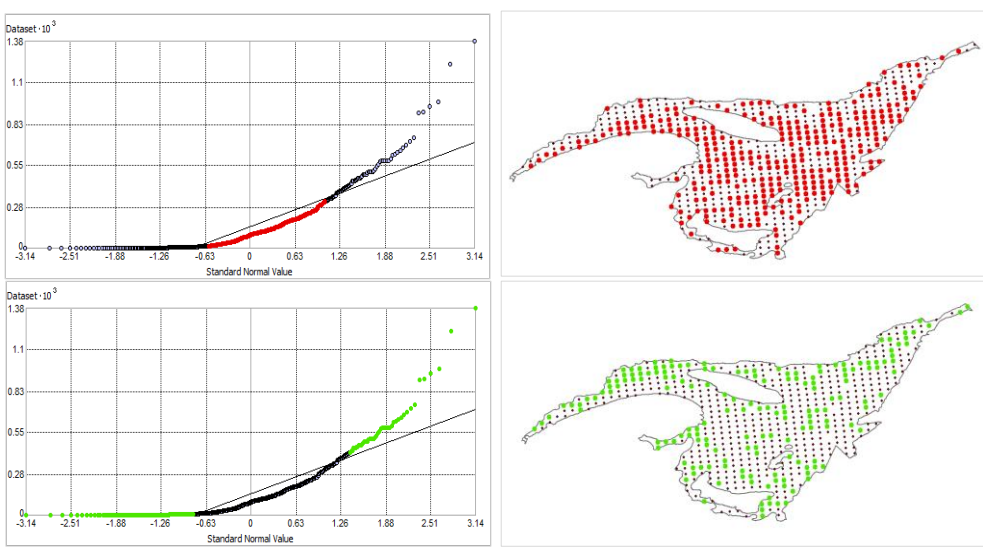

Fig. 262. Normal Q-Q plot for data values of Bottom Shear Minimum (Pa). Points falling under (upper panel) and over (bottom panel) the reference line are mapped.

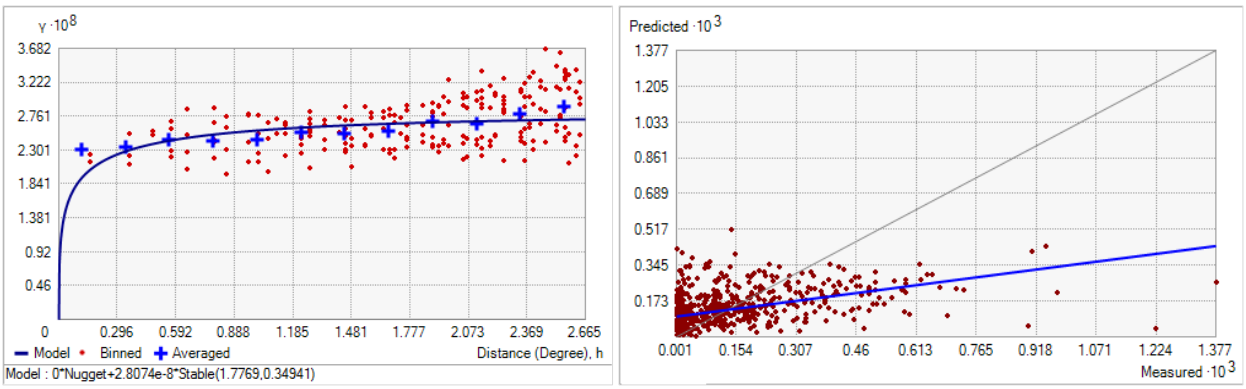

Fig. 263. Left panel: Semivariogram of Bottom Shear Minimum (Pa). Binned values are shown as red dots; average points are shown as blue crosses; the model fit to the averaged values is shown as a blue line. Lag size: 0.222 degrees; number of lags: 12; Parameter: 0.349; Range: 1.777 degrees; Partial Sill: 2.807 x 10^{-8}. Right panel: Scatterplot of predicted values versus observed values for the model of Bottom Shear Minimum (Pa).

Table 106. Results of cross-validation of the kriged model for the Bottom Shear Minimum.

Prediction error	**Value**
Number of Observations	589
Overall Mean Error	8.850 x 10^{-9}
Root Mean Square Prediction Error	1.650 x 10^{-4}
Standardized Mean	-3.160 x 10^{-5}
Standardized Root Mean Square Prediction Error	1.075
Average Standard Error	1.522 x 10^{-4}

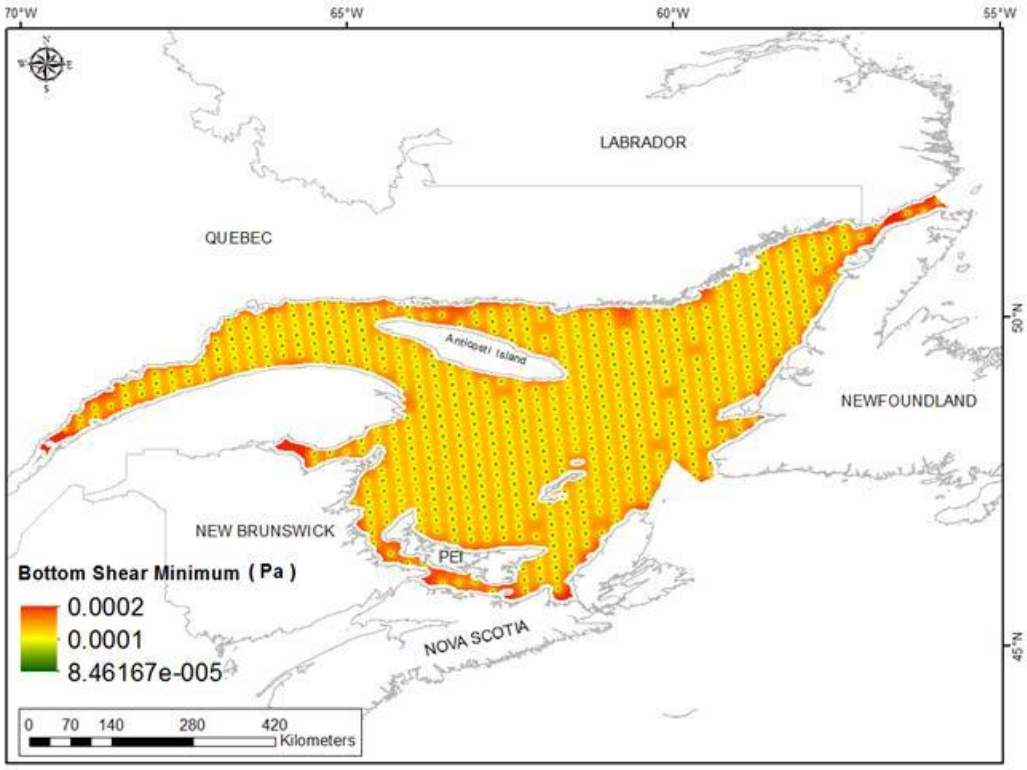

Fig. 264. Prediction standard error surface of Bottom Shear Minimum (Pa).

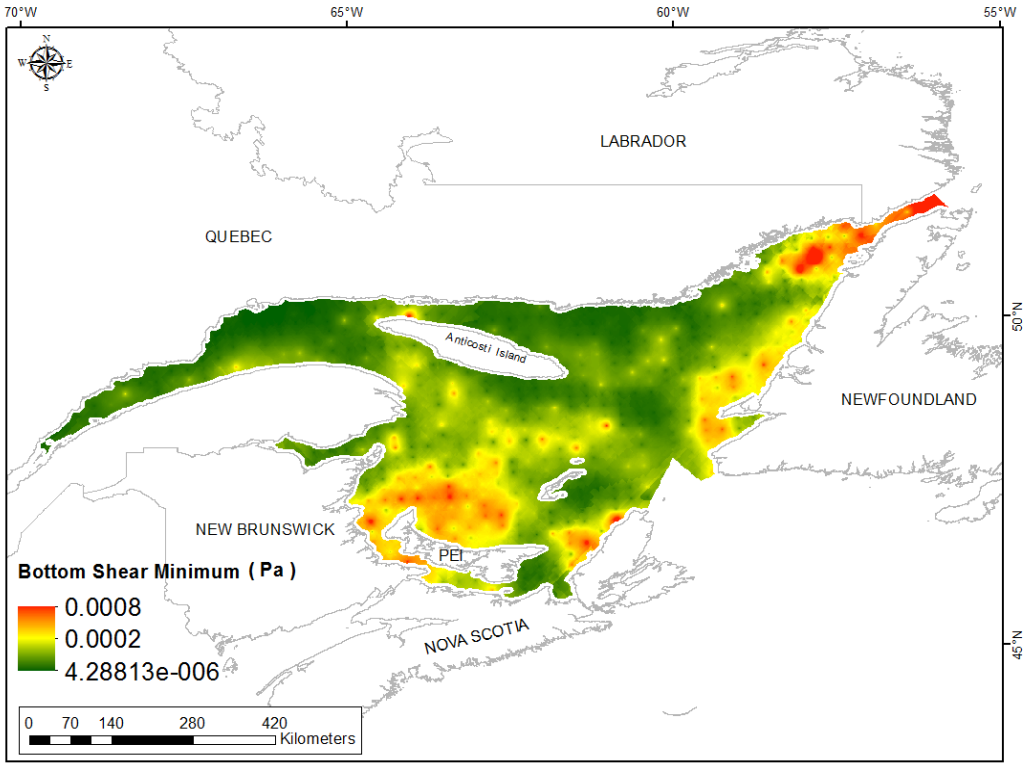

Fig. 265. Interpolated prediction surface of Bottom Shear Minimum (Pa).

Bottom Shear Maximum

This variable displayed a severely right-skewed distribution with outlying data in the upper range (Table 107, Fig. 266). The data were higher than predicted by a normal distribution at high values (Fig. 267). Mid-range values were slightly lower than the reference line. The areas of over- and under-prediction showed no strong spatial pattern (Fig. 267).

The semivariogram showed no autocorrelation present in the data and the model showed a poor fit between measured and observed values (Fig. 268). The model showed fair cross-validation statistics (Table 108). The error map showed no spatial pattern over the study extent except for some areas along the coast where it was high (Fig. 269). The kriged surface is presented in Fig. 270.

Table 107. Distributional properties of Bottom Shear Maximum (Pa).

Property	Value
Number of Observations	589
Minimum	0.002
Maximum	0.459
Mean	0.016
Median	0.011
Standard Deviation	0.028
Skewness	9.959
Kurtosis	134.290

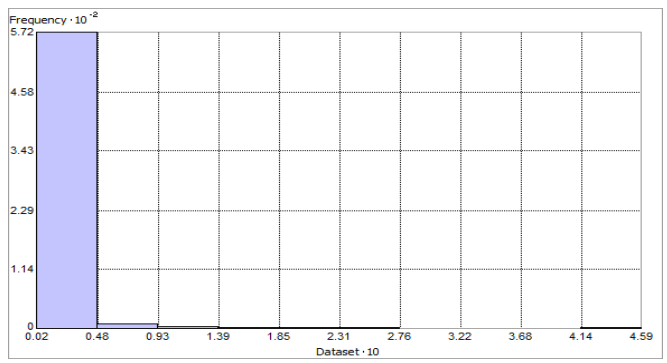

Fig. 266. Distribution of Bottom Shear Maximum (Pa). Histogram was illustrated using 10 bins. Y axis is shown at 10^{-2}.

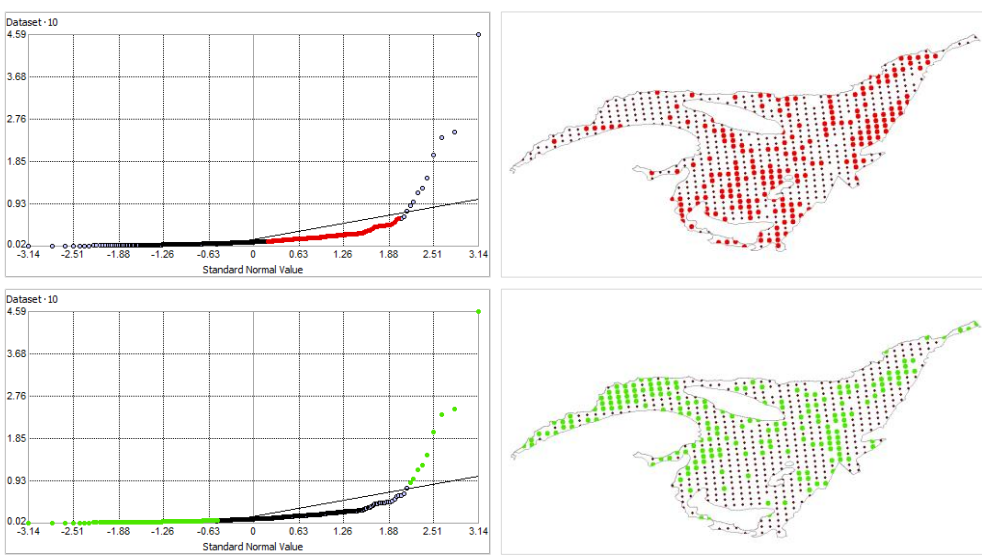

Fig. 267. Normal Q-Q plot for data values of Bottom Shear Maximum (Pa). Points falling under (upper panel) and over (bottom panel) the reference line are mapped.

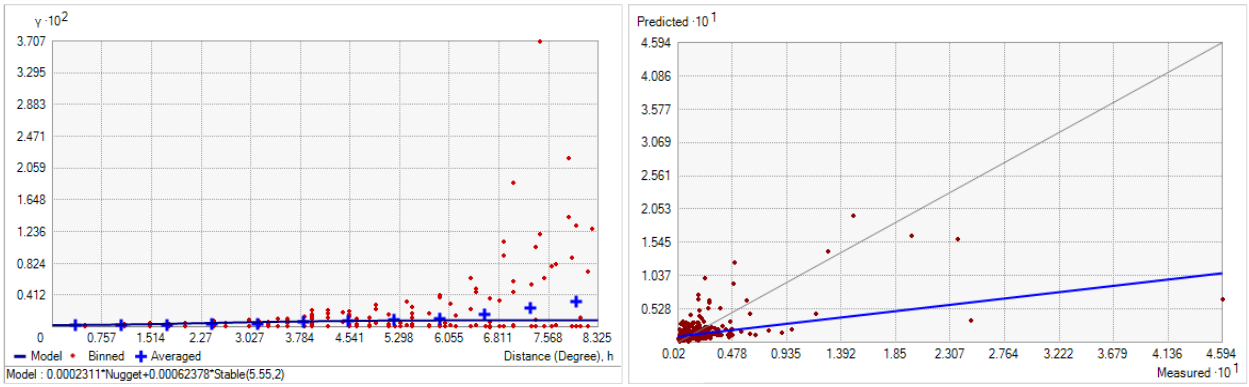

Fig. 268. Left panel: Semivariogram of Bottom Shear Maximum (Pa). Binned values are shown as red dots; average points are shown as blue crosses; the model fit to the averaged values is shown as a blue line. Lag size: 0.694 degrees; number of lags: 12; Parameter: 2; Range: 5.550 degrees; Partial Sill: 6.240 x 10^{-4}. Right panel: Scatterplot of predicted values versus observed values for the model of Bottom Shear Maximum (Pa).

Table 108. Results of cross-validation of the kriged model for the Bottom Shear Maximum.

Prediction error	**Value**
Number of Observations	589
Overall Mean Error	8.824 x 10^{-5}
Root Mean Square Prediction Error	0.022
Standardized Mean	0.006
Standardized Root Mean Square Prediction Error	1.408
Average Standard Error	0.016

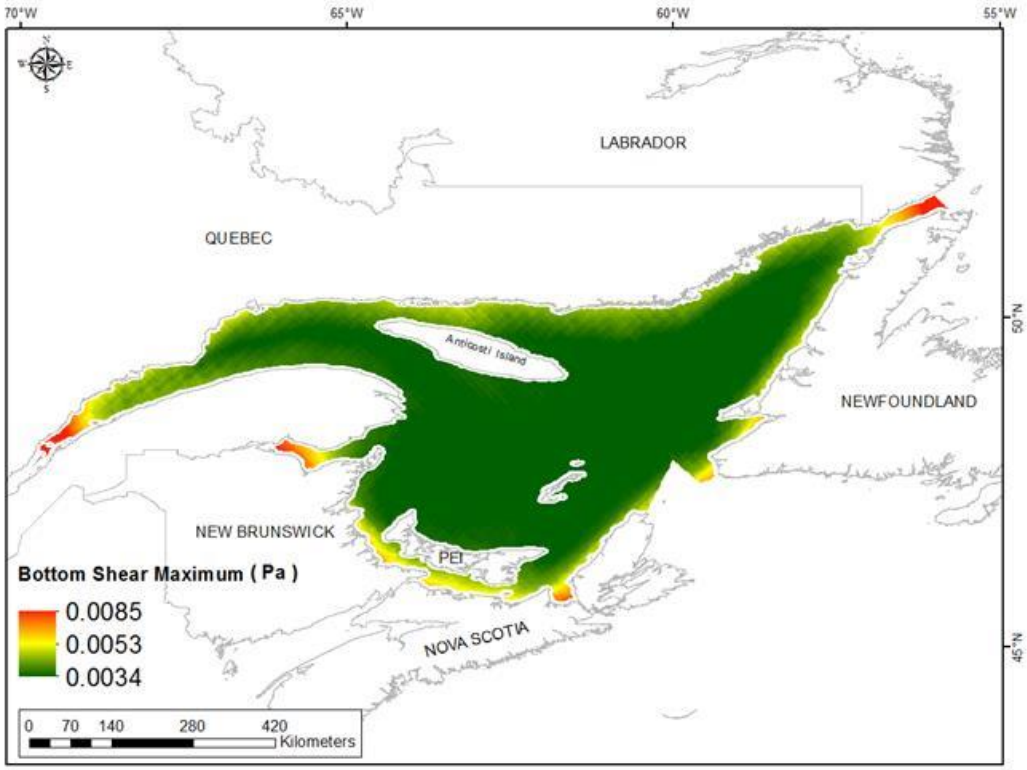

Fig. 269. Prediction standard error surface of Bottom Shear Maximum (Pa).

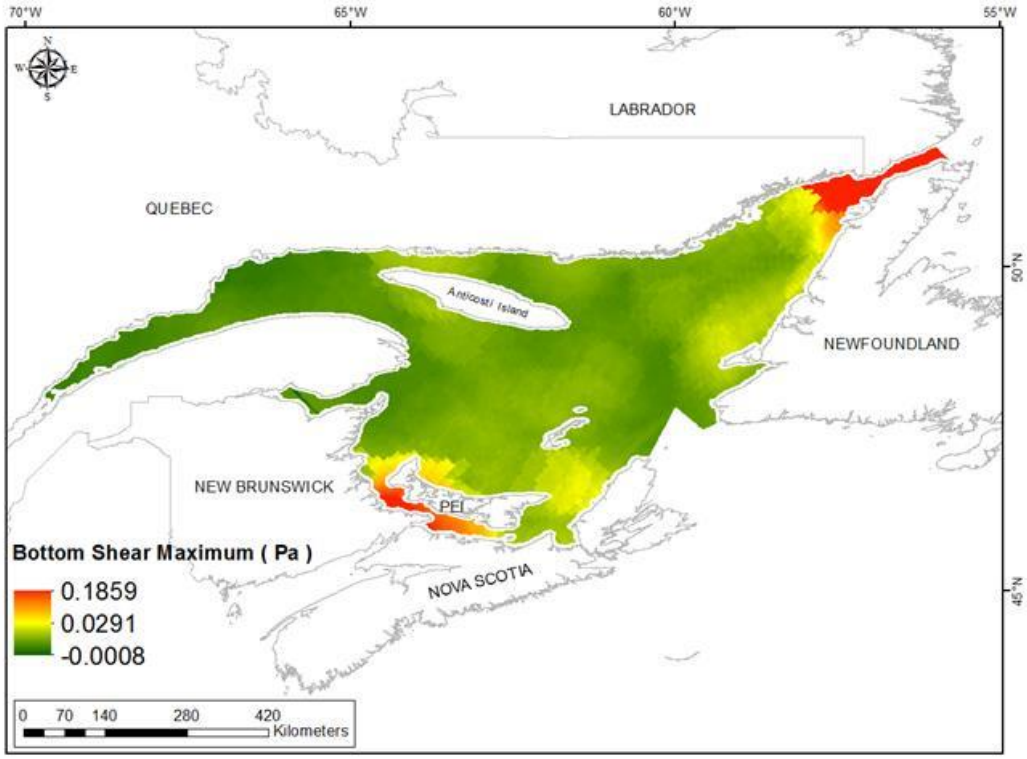

Fig. 270. Interpolated prediction surface of Bottom Shear Maximum (Pa).

Bottom Shear Range

This variable displayed a severely right-skewed distribution with outlying data in the upper range (Table 109, Fig. 271). The data were higher than predicted by a normal distribution at high values (Fig. 272). Mid-range values were slightly lower than the reference line. The areas of over- and under-prediction showed no strong spatial pattern (Fig. 272).

The semivariogram showed no autocorrelation present in the data and the model showed a poor fit between measured and observed values (Fig. 273). The model showed fair cross-validation statistics (Table 110). The error map showed no spatial pattern over the study extent except for some areas along the coast where it was high (Fig. 274). The kriged surface is presented in Fig. 275.

Table 109. Distributional properties of Bottom Shear Range (Pa).

Property	Value
Number of Observations	589
Minimum	0.002
Maximum	0.459
Mean	0.016
Median	0.011
Standard Deviation	0.027
Skewness	10.000
Kurtosis	135.140

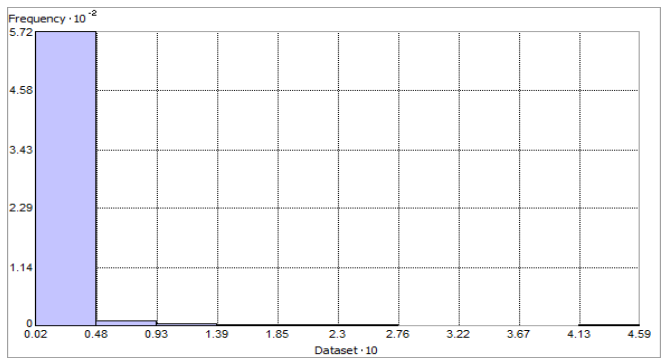

Fig. 271. Distribution of Bottom Shear Range (Pa). Histogram was illustrated using 10 bins. Y axis is shown at 10^{-2}.

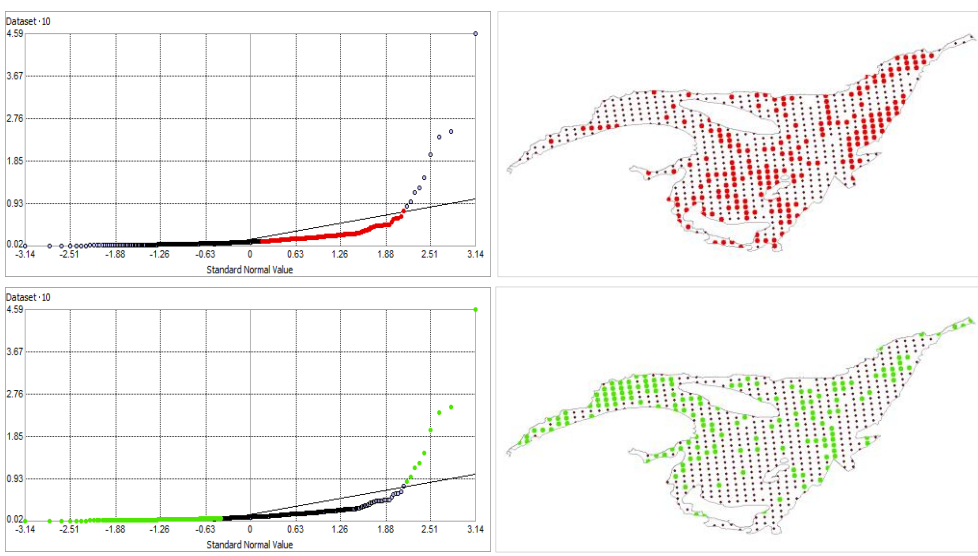

Fig. 272. Normal Q-Q plot for data values of Bottom Shear Range (Pa). Points falling under (upper panel) and over (bottom panel) the reference line are mapped.

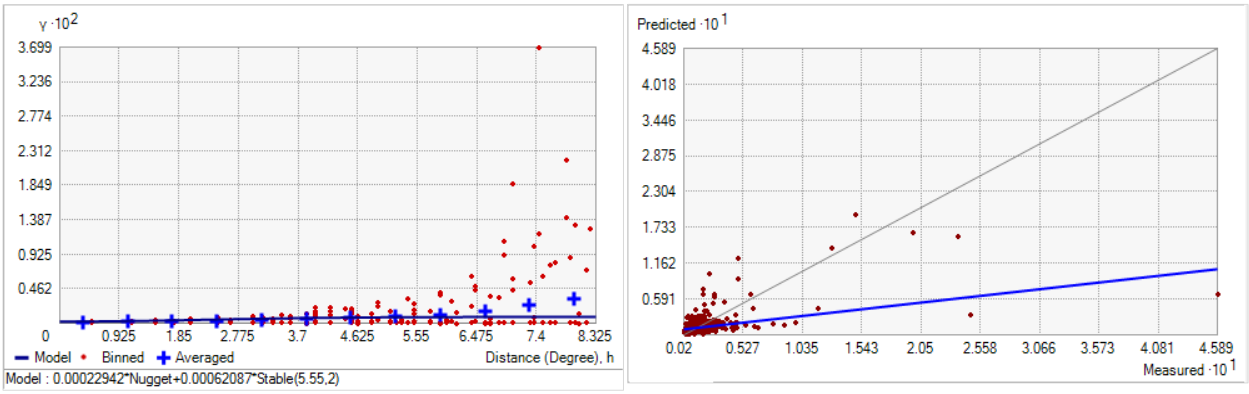

Fig. 273. Left panel: Semivariogram of Bottom Shear Range (Pa). Binned values are shown as red dots; average points are shown as blue crosses; the model fit to the averaged values is shown as a blue line. Lag size: 0.694 degrees; number of lags: 12; Parameter: 2; Range: 5.550 degrees; Partial Sill: 6.241 x 10^{-4}. Right panel: Scatterplot of predicted values versus observed values for the model of Bottom Shear Range (Pa).

Table 110. Results of cross-validation of the kriged model for the Bottom Shear Range.

Prediction error	**Value**
Number of Observations	589
Overall Mean Error	8.862 x 10^{-5}
Root Mean Square Prediction Error	0.022
Standardized Mean	0.006
Standardized Root Mean Square Prediction Error	1.410
Average Standard Error	0.016

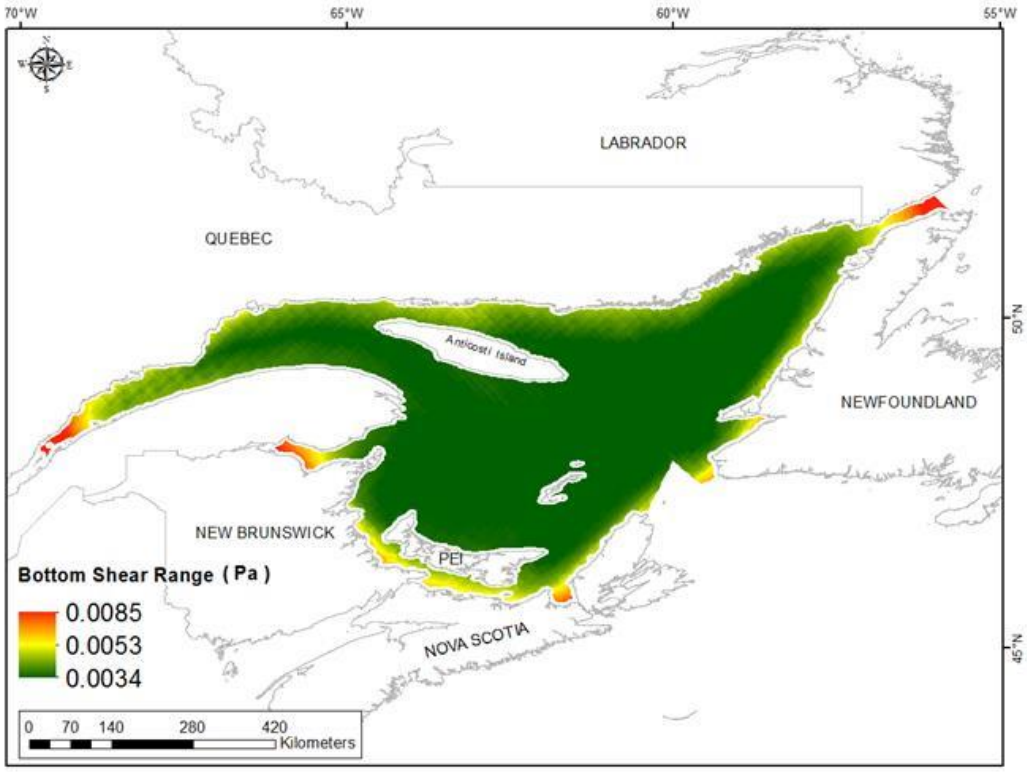

Fig. 274. Prediction standard error surface of Bottom Shear Range (Pa).

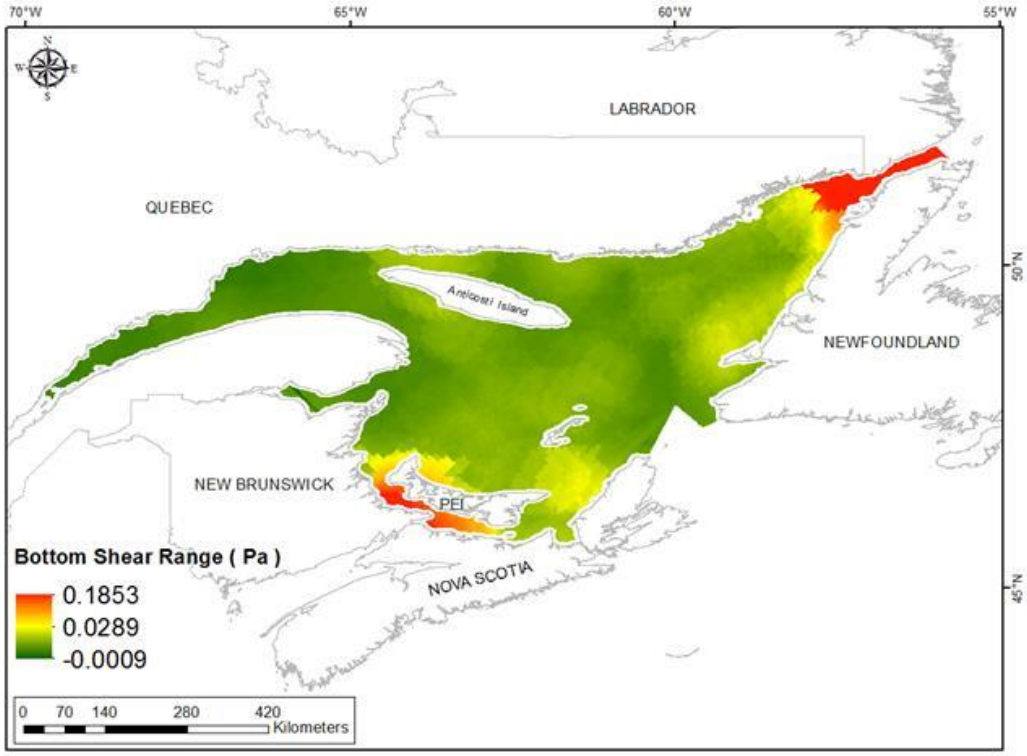

Fig. 275. Interpolated prediction surface of Bottom Shear Range (Pa).

Bottom Shear Average Minimum

This variable displayed a severely right-skewed distribution with outlying data in the upper range (Table 111, Fig. 276). The data were higher than predicted by a normal distribution at high values (Fig. 277). Mid-range values were slightly lower than the reference line. The areas of over- and under-prediction showed no strong spatial pattern (Fig. 277).

The semivariogram showed no autocorrelation present in the data and the model showed a poor fit between measured and observed values (Fig. 278). Nevertheless, the model showed good cross-validation statistics (Table 112) indicating that it was good at prediction. The error map showed no spatial pattern over the study extent except for some areas along the coast where it was high (Fig. 279). The kriged surface is presented in Fig. 280.

Table 111. Distributional properties of Bottom Shear Average Minimum (Pa).

Property	Value
Number of Observations	589
Minimum	6.100×10^{-5}
Maximum	0.011
Mean	7.650×10^{-4}
Median	5.750×10^{-4}
Standard Deviation	7.730×10^{-4}
Skewness	4.935
Kurtosis	52.826

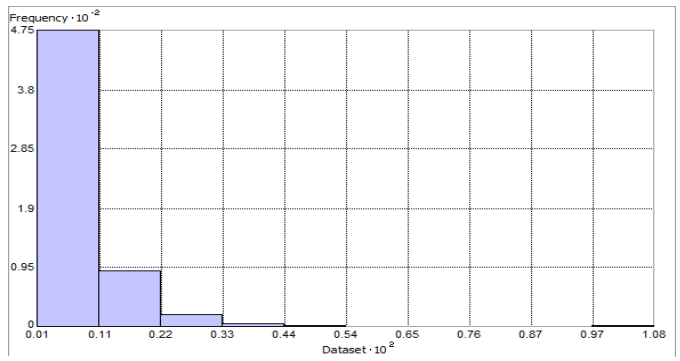

Fig. 276. Distribution of Bottom Shear Average Minimum (m s^{-1}). Histogram was illustrated using 10 bins. X axis is shown at 10^2; Y axis is shown at 10^{-2}.

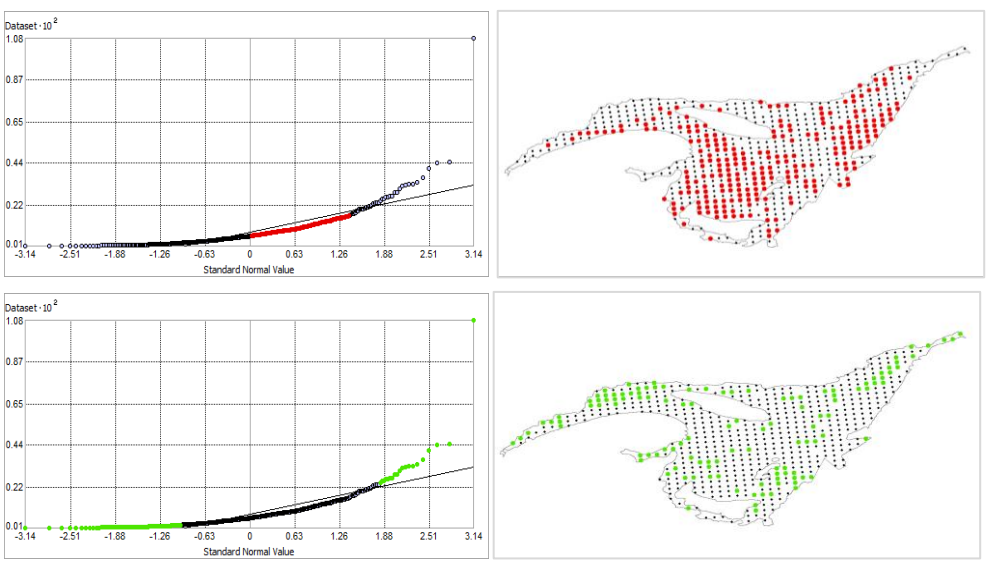

Fig. 277. Normal Q-Q plot for data values of Bottom Shear Average Minimum (Pa). Points falling under (upper panel) and over (bottom panel) the reference line are mapped.

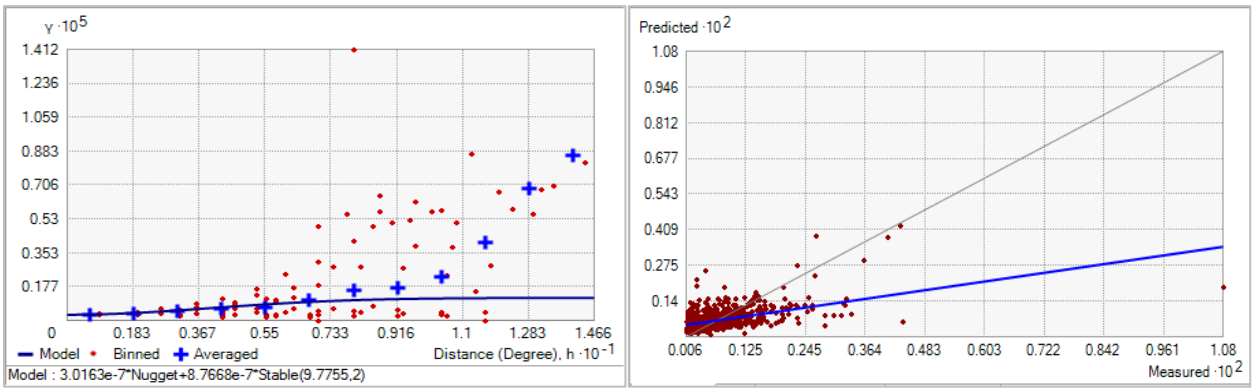

Fig. 278. Left panel: Semivariogram of Bottom Shear Average Minimum (Pa). Binned values are shown as red dots; average points are shown as blue crosses; the model fit to the averaged values is shown as a blue line. Lag size: 1.222 degrees; number of lags: 12; Parameter: 2; Range: 9.775 degrees; Partial Sill: 8.767 x 10^{-7}. Right panel: Scatterplot of predicted values versus observed values for the model of Bottom Shear Average Minimum (Pa).

Table 112. Results of cross-validation of the kriged model for Bottom Shear Average Minimum.

Prediction error	**Value**
Number of Observations	589
Overall Mean Error	-6.462 x 10^{-7}
Root Mean Square Prediction Error	6.580 x 10^{-4}
Standardized Mean	-0.001
Standardized Root Mean Square Prediction Error	1.162
Average Standard Error	5.650 x 10^{-4}

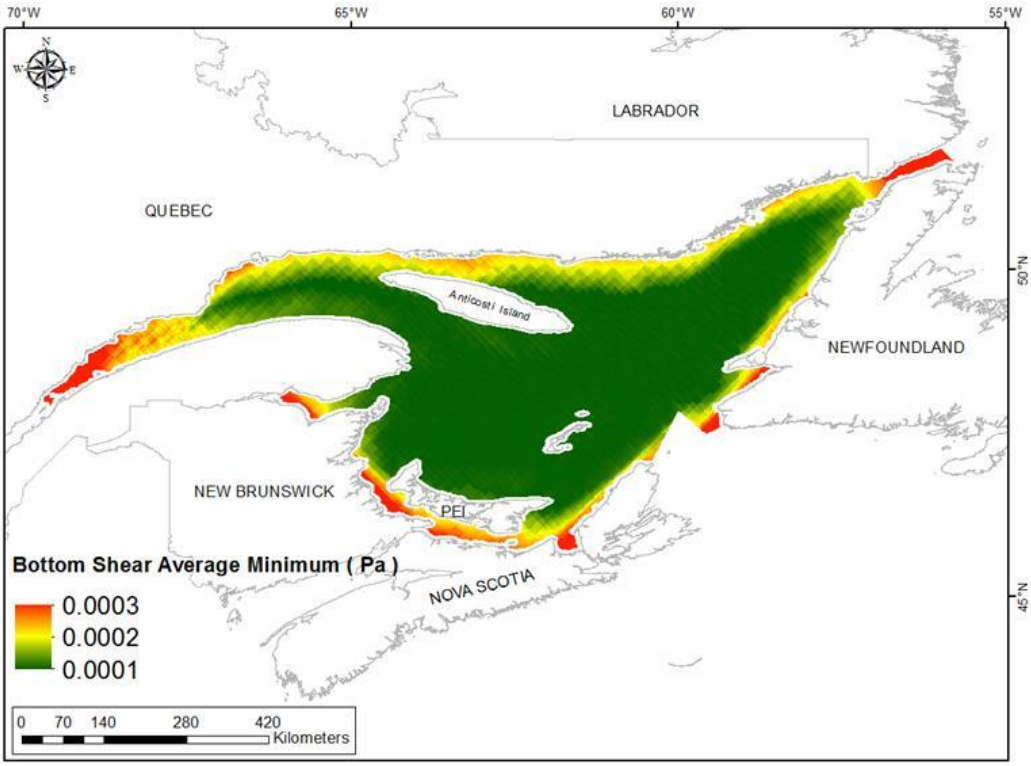

Fig. 279. Prediction standard error surface of Bottom Shear Average Minimum (Pa).

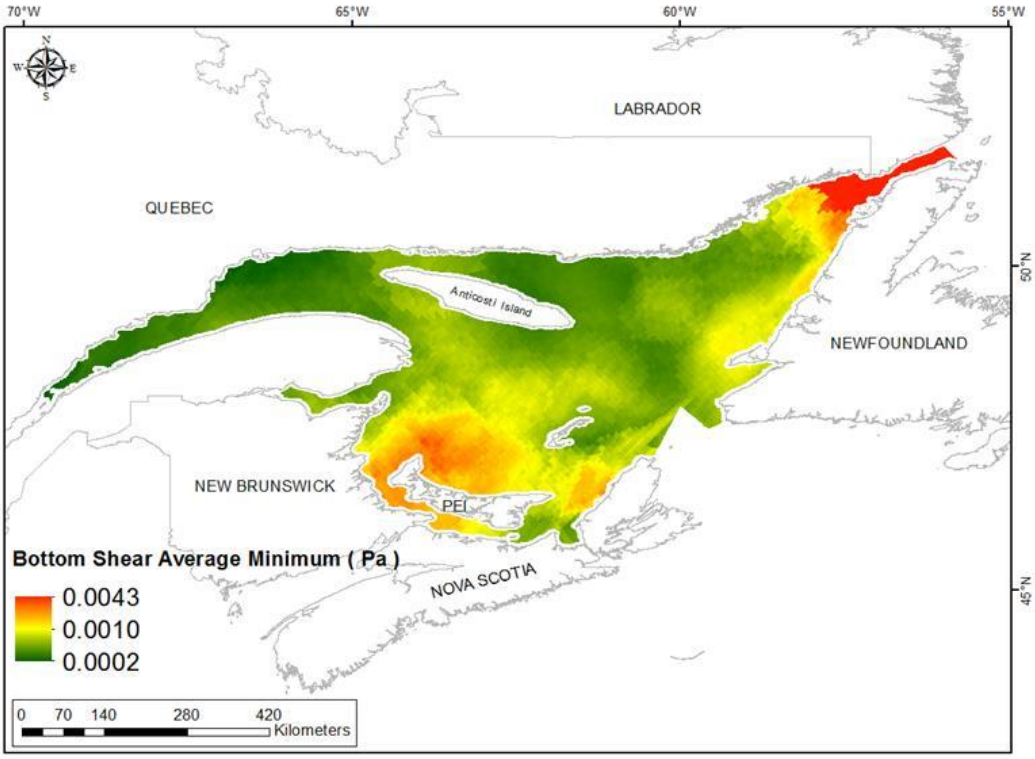

Fig. 280. Interpolated prediction surface of Bottom Shear Average Minimum (Pa).

Bottom Shear Average Maximum

This variable displayed a severely right-skewed distribution with outlying data in the upper range (Table 113, Fig. 281). The data were higher than predicted by a normal distribution at high values (Fig. 282). Mid-range values were slightly lower than the reference line. The areas of over- and under-prediction showed no strong spatial pattern (Fig. 282).

The semivariogram showed no autocorrelation present in the data and the model showed a poor fit between measured and observed values (Fig. 283). The model showed fair cross-validation statistics (Table 114). The error map showed no spatial pattern over the study extent except for some areas along the coast where it was high (Fig. 284). The kriged surface is presented in Fig. 285.

Table 113. Distributional properties of Bottom Shear Average Maximum (Pa).

Property	Value
Number of Observations	589
Minimum	0.001
Maximum	0.292
Mean	0.010
Median	0.007
Standard Deviation	0.017
Skewness	10.673
Kurtosis	152.060

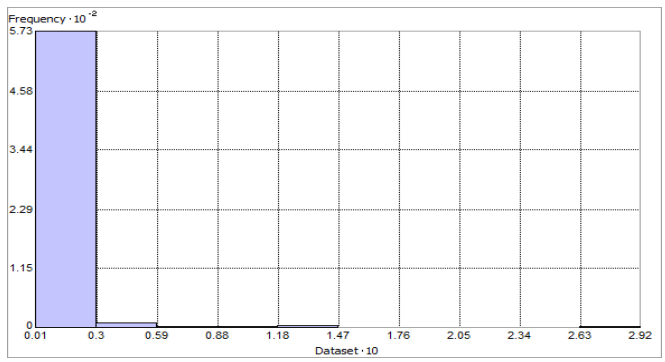

Fig. 281. Distribution of Bottom Shear Average Maximum (m s^{-1}). Histogram was illustrated using 10 bins. X axis is shown at 10; Y axis is shown at 10^{-2}.

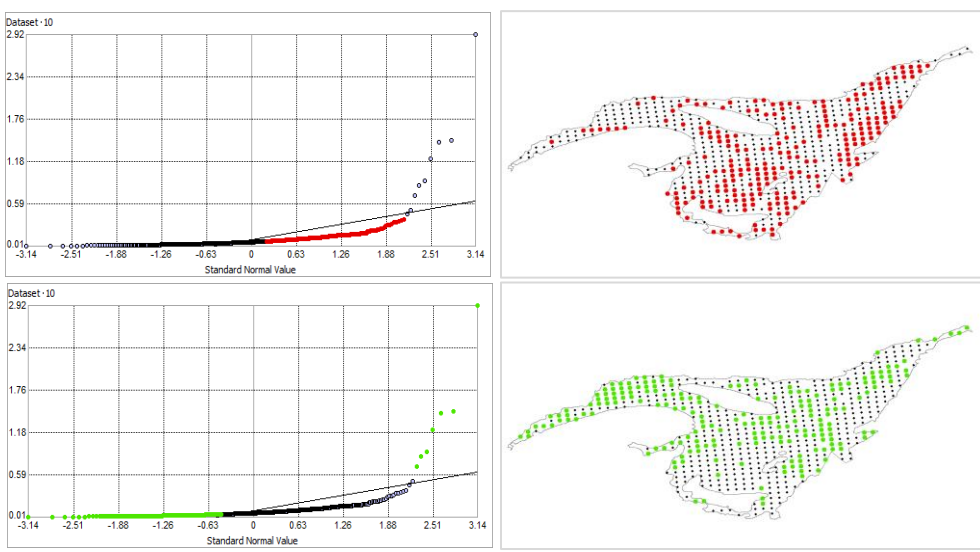

Fig. 282. Normal Q-Q plot for data values of Bottom Shear Average Maximum (Pa). Points falling under (upper panel) and over (bottom panel) the reference line are mapped.

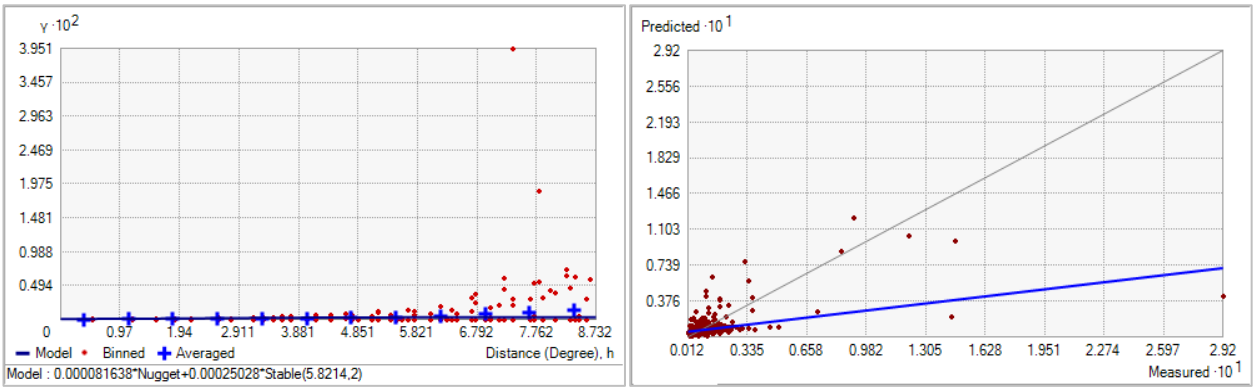

Fig. 283. Left panel: Semivariogram of Bottom Shear Average Maximum (Pa). Binned values are shown as red dots; average points are shown as blue crosses; the model fit to the averaged values is shown as a blue line. Lag size: 0.728 degrees; number of lags: 12; Parameter: 2; Range: 5.821 degrees; Partial Sill: 2.503 x 10^{-4}. Right panel: Scatterplot of predicted values versus observed values for the model of Bottom Shear Average Maximum (Pa).

Table 114. Results of cross-validation of the kriged model for the Bottom Shear Average Maximum (Pa).

Prediction error	**Value**
Number of Observations	589
Overall Mean Error	5.823 x 10^{-5}
Root Mean Square Prediction Error	0.014
Standardized Mean	0.007
Standardized Root Mean Square Prediction Error	1.440
Average Standard Error	0.009

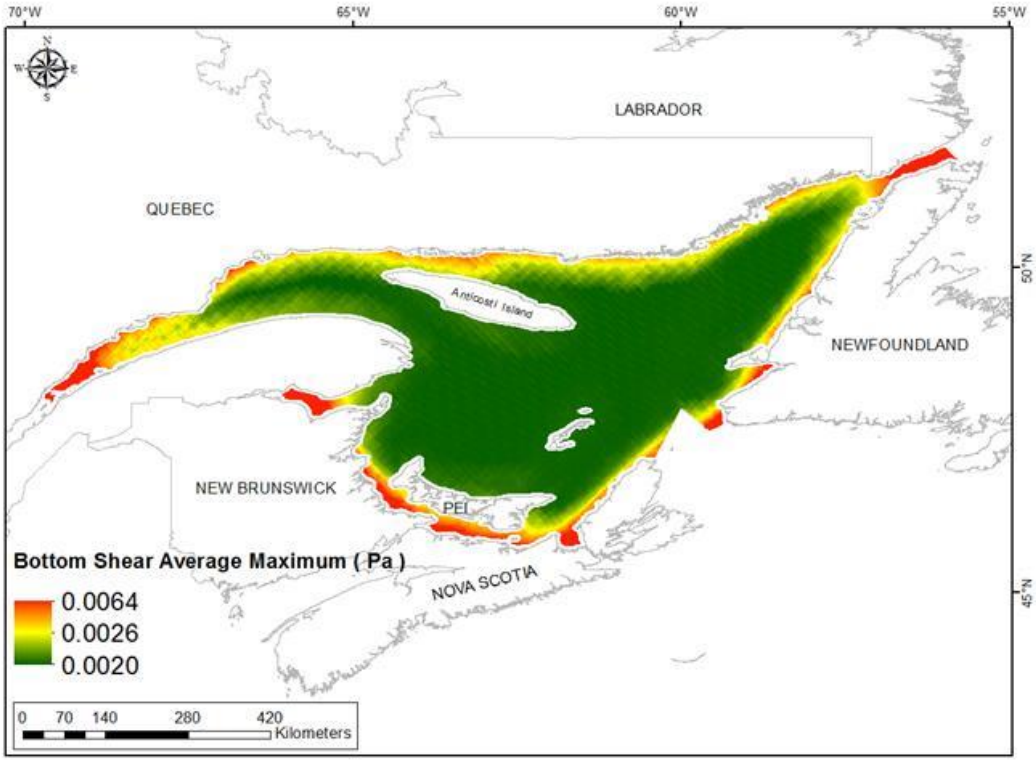

Fig. 284. Prediction standard error surface of Bottom Shear Average Maximum (Pa).

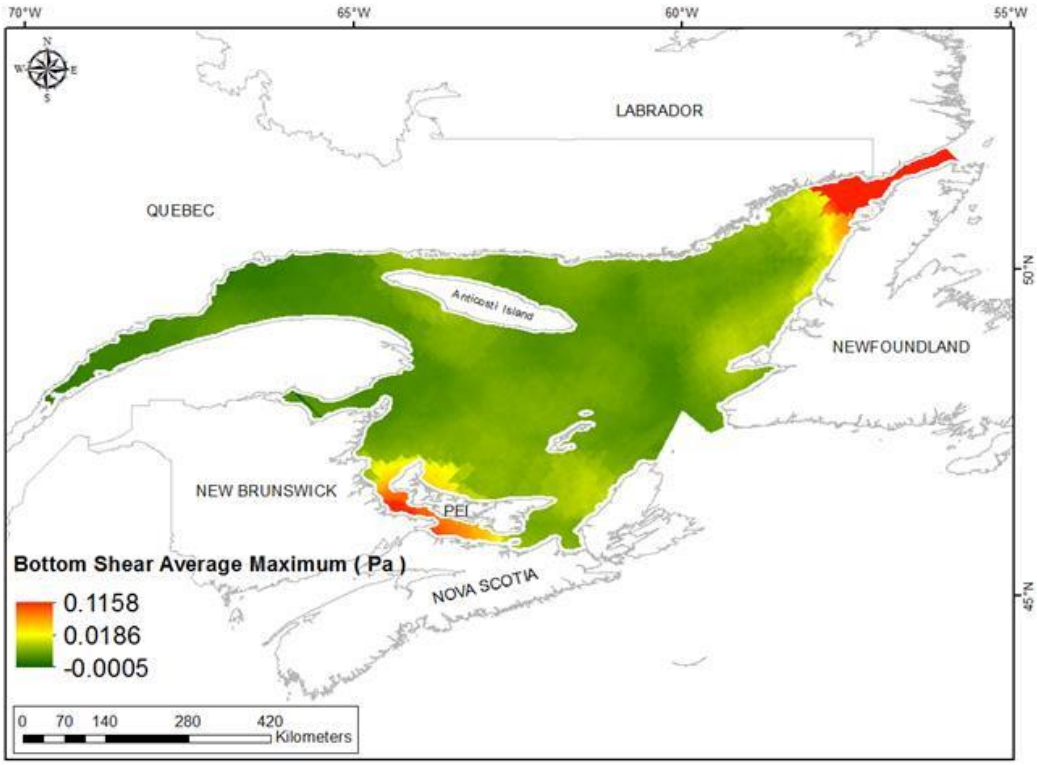

Fig. 285. Interpolated prediction surface of Bottom Shear Average Maximum (Pa).

Bottom Shear Average Range

This variable displayed a severely right-skewed distribution with outlying data in the upper range (Table 115, Fig. 286). The data were higher than predicted by a normal distribution at high values (Fig. 287). Mid-range values were slightly lower than the reference line. The areas of over- and under-prediction showed no strong spatial pattern (Fig. 287).

The semivariogram showed no autocorrelation present in the data and the model showed a poor fit between measured and observed values (Fig. 288). The model showed fair cross-validation statistics (Table 116). The error map showed no spatial pattern over the study extent except for some areas along the coast where it was high (Fig. 289). The kriged surface is presented in Fig. 290.

Table 115. Distributional properties of Bottom Shear Average Range (Pa).

Property	Value
Number of Observations	589
Minimum	0.002
Maximum	0.459
Mean	0.016
Median	0.011
Standard Deviation	0.027
Skewness	10.000
Kurtosis	135.140

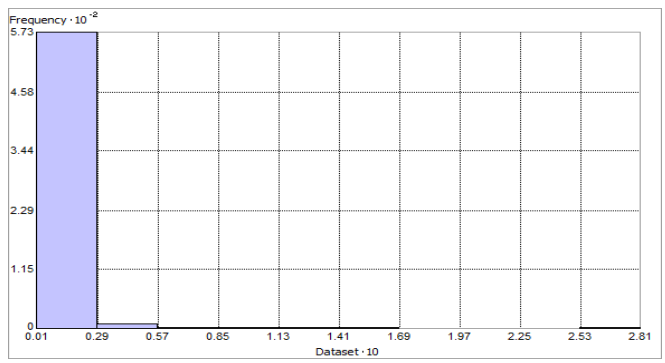

Fig. 286. Distribution of Bottom Shear Average Range (m s^{-1}). Histogram was illustrated using 10 bins. X axis is shown at 10; Y axis is shown at 10^{-2}.

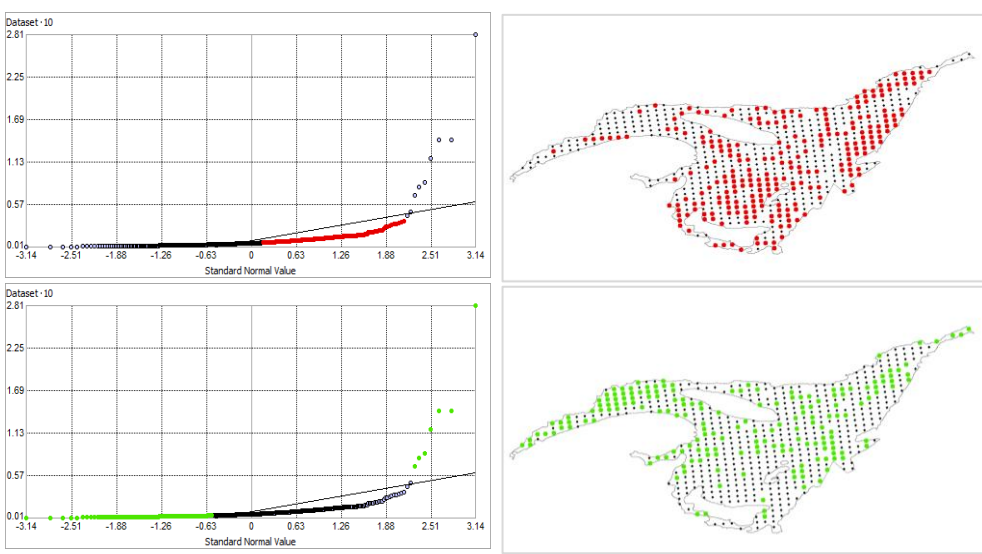

Fig. 287. Normal Q-Q plot for data values of Bottom Shear Average Range (Pa). Points falling under (upper panel) and over (bottom panel) the reference line are mapped.

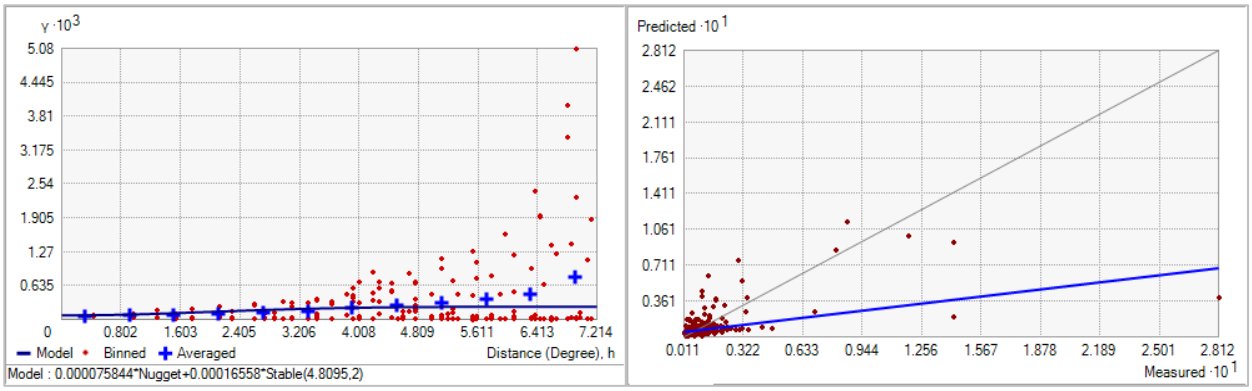

Fig. 288. Left panel: Semivariogram of Bottom Shear Average Range (Pa). Binned values are shown as red dots; average points are shown as blue crosses; the model fit to the averaged values is shown as a blue line. Lag size: 0.601 degrees; number of lags: 12; Parameter: 2; Range: 4.809 degrees; Partial Sill: 1.656 x 10^{-4}. Right panel: Scatterplot of predicted values versus observed values for the model of Bottom Shear Average Range (Pa).

Table 116. Results of cross-validation of the kriged model for Bottom Shear Average Range.

Prediction error	**Value**
Number of Observations	589
Overall Mean Error	3.459 x 10^{-5}
Root Mean Square Prediction Error	0.013
Standardized Mean	0.005
Standardized Root Mean Square Prediction Error	1.437
Average Standard Error	0.009

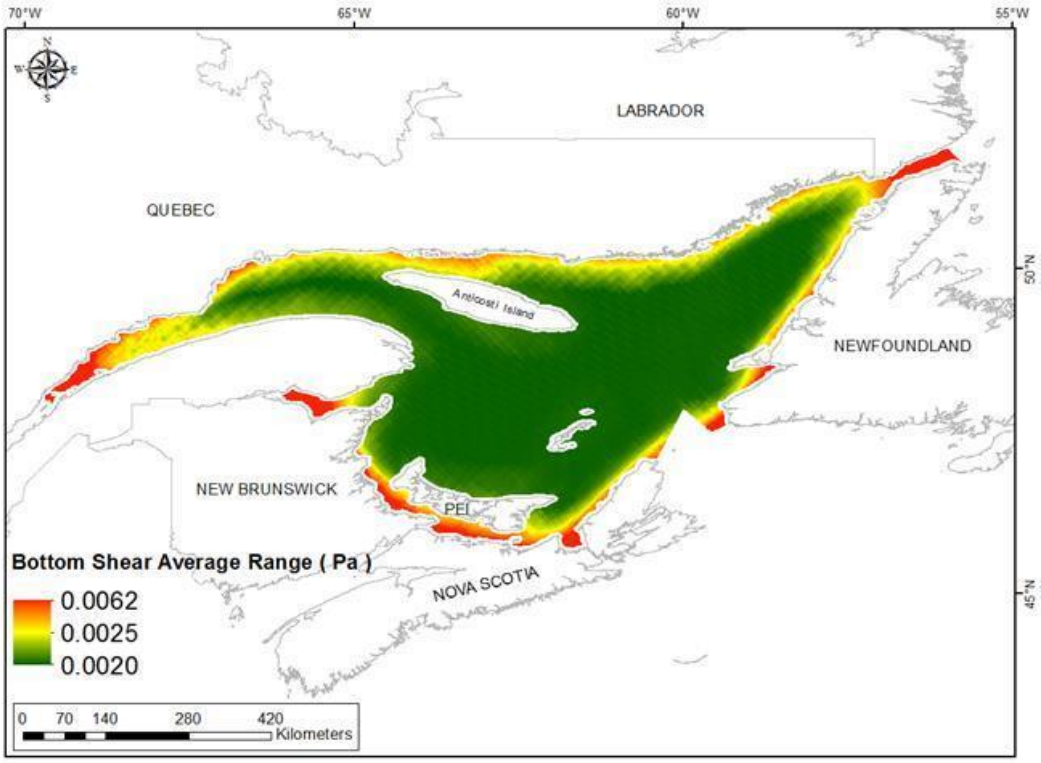

Fig. 289. Prediction standard error surface of Bottom Shear Average Range (Pa).

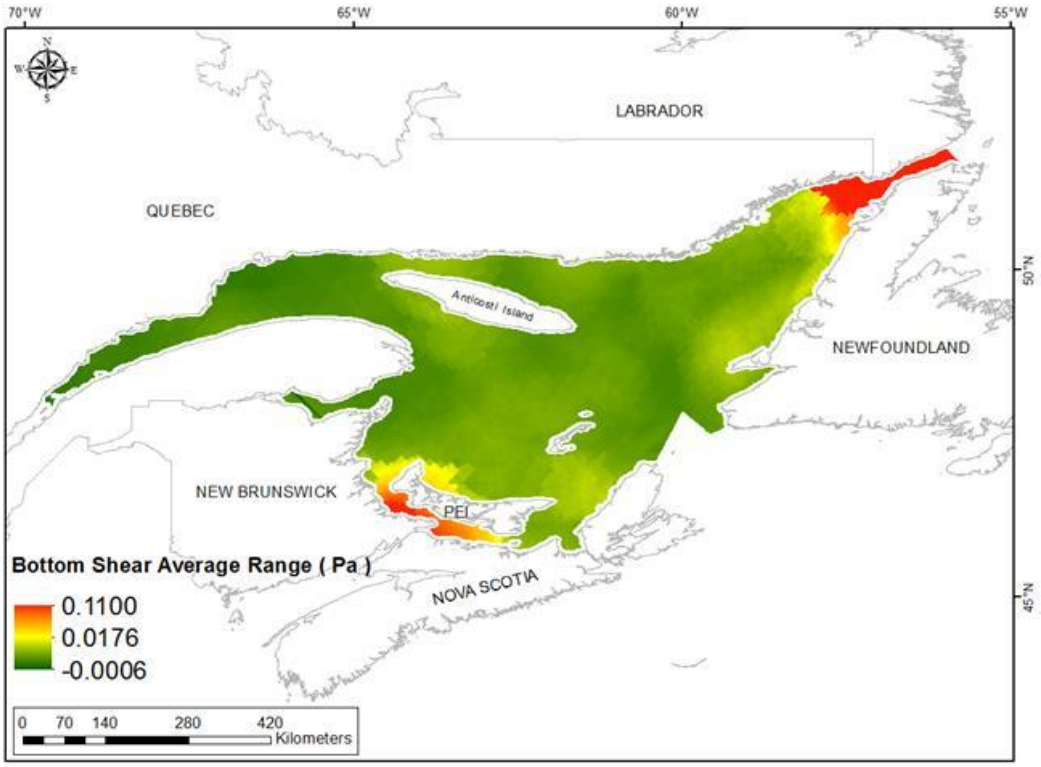

Fig. 290. Interpolated prediction surface of Bottom Shear Average Range (Pa).

Sea Surface Chlorophyll *a*

Sea surface chlorophyll *a* concentration is a proxy for phytoplankton biomass and is therefore related to the vertical flux of particulate organic carbon and food supply to the seafloor (Lutz et al., 2007). Gradients in food supply have often been identified as the main factor in controlling changes in benthic biomass, diversity, distribution, and zonation in the deep sea (Levin et al., 2001; Carney, 2005; Soltwedel et al., 2009; MacDonald et al., 2010; Papiol et al., 2012). In the northwest Atlantic, surface chlorophyll *a* has shown to be an important determinant in generalized linear models of megafaunal abundance and richness (Beazley et al. 2013) and was an important variable in random forest models predicting the presence of *Geodia* sponge and sponge grounds (Knudby et al., 2013). The spring phytoplankton bloom is thought to be a controlling factor in the reproductive cycles of several deep-sea corals (Sun et al., 2010a; 2010b; 2011; Mercier and Hamel, 2011) and sponges (Spetland et al., 2007) in the north Atlantic. Therefore, we expect that seasonal over annual measures of chlorophyll *a* will be more important in species distribution models.

MODIS Case I Spring Chlorophyll *a* Mean

This variable displayed a right-skewed distribution with kurtosis prior to modeling (Table 117, Fig. 291). The data were higher than predicted by a normal distribution at the upper range and lower than predicted at mid values (Fig. 292). The areas of under- and over-prediction showed a strong spatial pattern over the spatial extent (Fig. 292).

The semivariogram showed moderate autocorrelation present in the data and the model showed a very good fit between measured and predicted values (Fig. 293). The model showed good cross-validation statistics (Table 118) indicating that it was good at prediction. The error map showed low error over most of the study extent except for along the coast where it was high (Fig. 294). The kriged surface is presented in Fig. 295.

Table 117. Distributional properties of MODIS Case I Spring Chlorophyll *a* Mean (mg m^{-3}).

Property	Value
Number of Observations	74353
Minimum	0.679
Maximum	13.268
Mean	2.605
Median	1.853
Standard Deviation	2.006
Skewness	1.804
Kurtosis	6.038

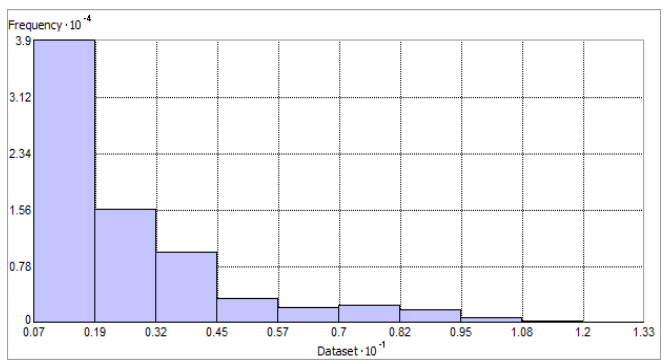

Fig. 291. Distribution of MODIS Case I Spring Chlorophyll *a* Mean (mg m^{-3}). Histogram was illustrated using 10 bins. X and Y axes are shown at 10^{-1} and 10^{-4} respectively.

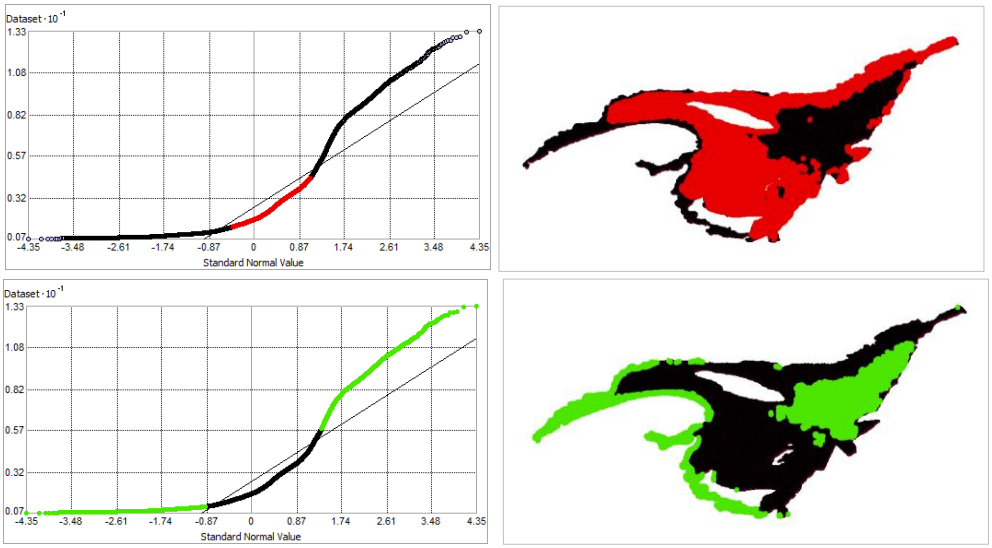

Fig. 292. Normal Q-Q plot for data values of MODIS Case I Spring Chlorophyll *a* Mean (mg m^{-3}). Points falling under (upper panel) and over (bottom panel) the reference line are mapped.

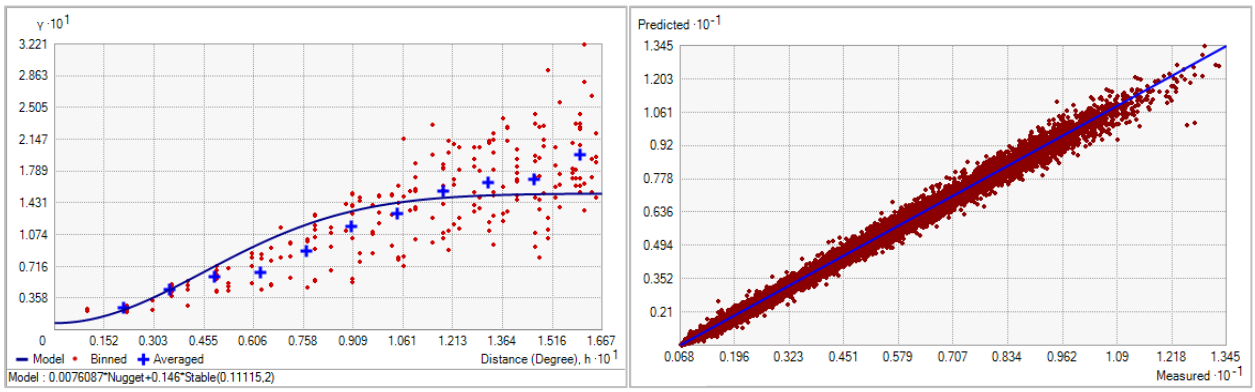

Fig. 293. Left panel: Semivariogram of MODIS Case I Spring Chlorophyll *a* Mean (mg m^{-3}). Binned values are shown as red dots; average points are shown as blue crosses; the model fit to the averaged values is shown as a blue line. Lag size: 0.014 degrees; number of lags: 12; Parameter: 2; Range: 0.111 degrees; Partial Sill: 0.146. Right panel: Scatterplot of predicted values versus observed values for the model of MODIS Case I Spring Chlorophyll *a* Mean (mg m^{-3}).

Table 118. Results of cross-validation of the kriged model for the MODIS Case I Spring Chlorophyll *a* Mean (mg m^{-3}).

Prediction error	**Value**
Number of Observations	74353
Overall Mean Error	4.033×10^{-4}
Root Mean Square Prediction Error	0.114
Standardized Mean	0.005
Standardized Root Mean Square Prediction Error	1.120
Average Standard Error	0.100

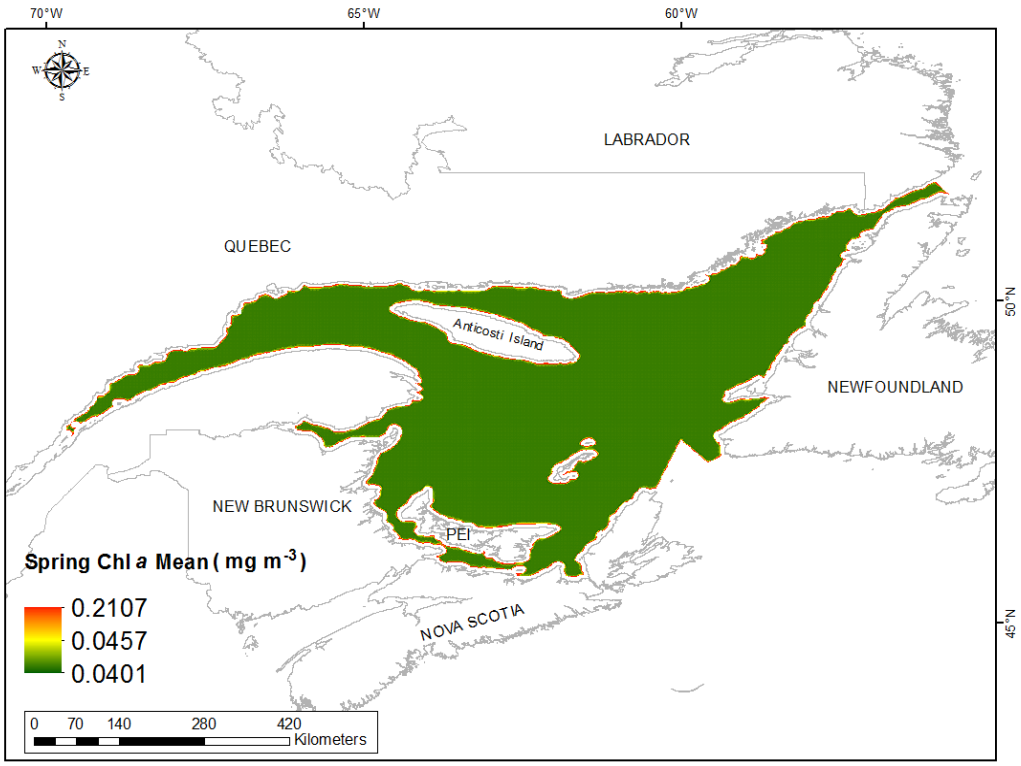

Fig. 294. Prediction standard error surface of MODIS Case I Spring Chlorophyll *a* Mean (mg m^{-3}).

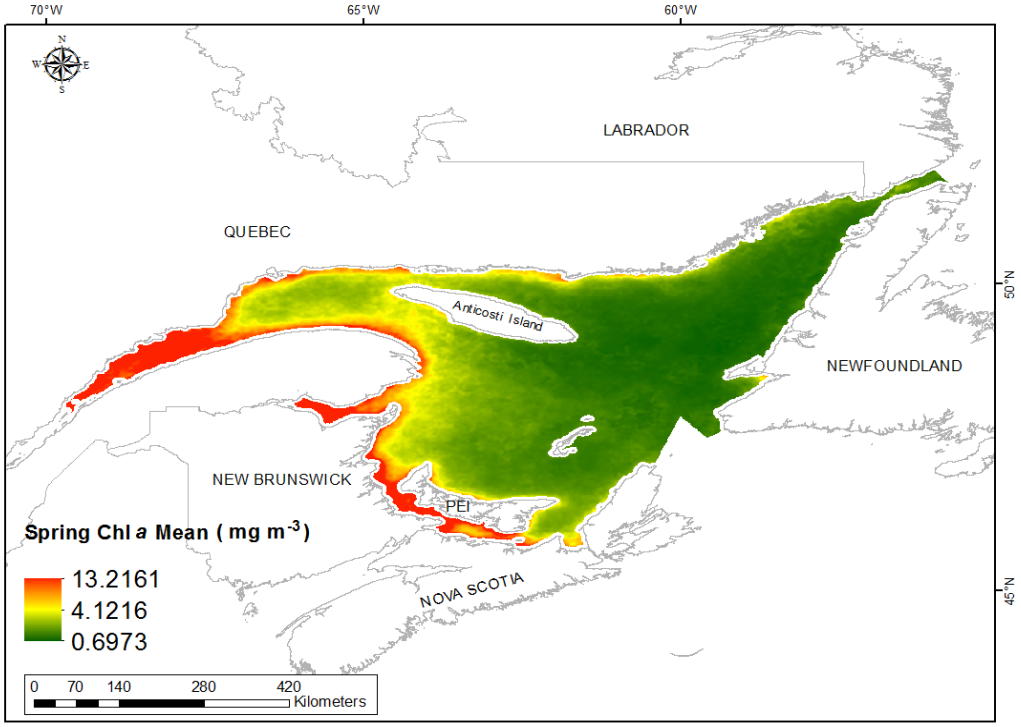

Fig. 295. Interpolated prediction surface of Spring Chlorophyll *a* Mean (mg m^{-3}).

MODIS Case I Spring Chlorophyll *a* Minimum

This variable displayed a right-skewed distribution with kurtosis prior to modeling (Table 119, Fig. 296). The data were higher than predicted by a normal distribution at the upper range and lower than predicted at mid values (Fig. 297). The areas of under- and over-prediction showed a strong spatial pattern over the spatial extent (Fig. 297).

The semivariogram showed moderate autocorrelation present in the data and the model showed a very good fit between measured and predicted values (Fig. 298). The model showed fair cross-validation statistics (Table 120). The error map showed low error over most of the study extent except for along the coast where it was high (Fig. 299). The kriged surface is presented in Fig. 300.

Table 119. Distributional properties of MODIS Case I Spring Chlorophyll *a* Minimum (mg m^{-3}).

Property	Value
Number of Observations	74353
Minimum	0.178
Maximum	10.273
Mean	1.589
Median	0.974
Standard Deviation	1.430
Skewness	2.248
Kurtosis	7.935

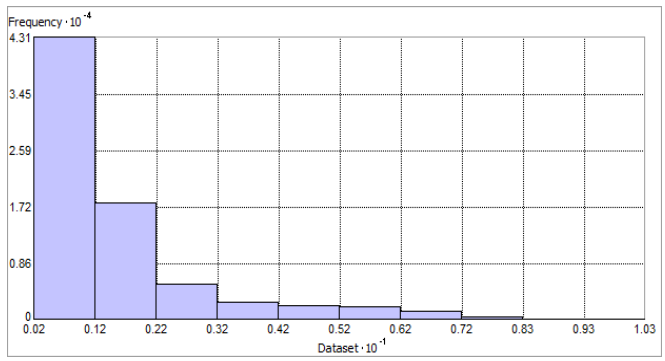

Fig. 296. Distribution of MODIS Case I Spring Chlorophyll *a* Minimum (mg m^{-3}). Histogram was illustrated using 10 bins. X and Y axes are shown at 10^{-1} and 10^{-4} respectively.

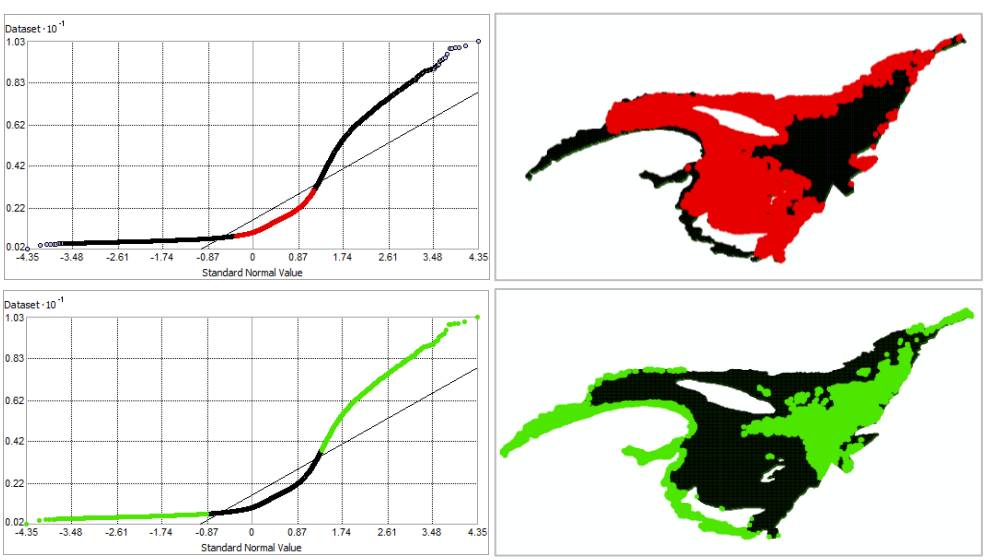

Fig. 297. Normal Q-Q plot for data values of MODIS Case I Spring Chlorophyll *a* Minimum (mg m^{-3}). Points falling under (upper panel) and over (bottom panel) the reference line are mapped.

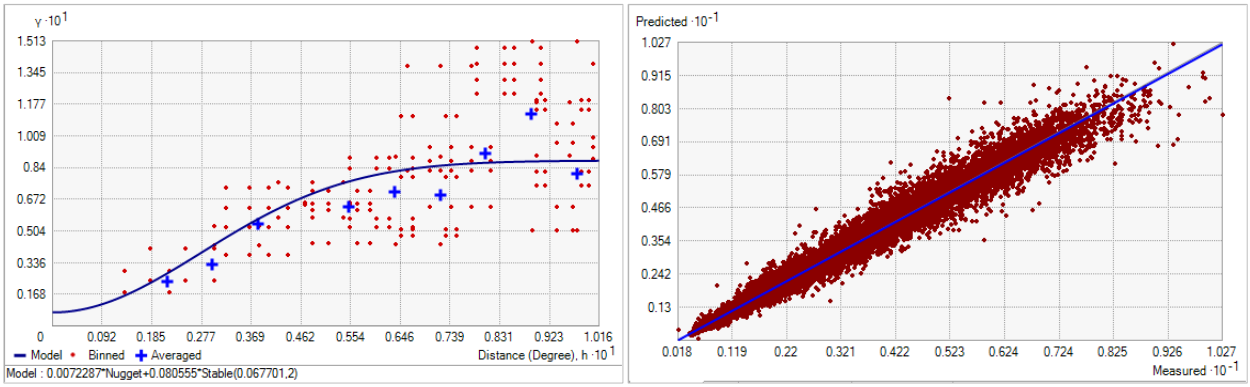

Fig. 298. Left panel: Semivariogram of MODIS Case I Spring Chlorophyll *a* Minimum (mg m^{-3}). Binned values are shown as red dots; average points are shown as blue crosses; the model fit to the averaged values is shown as a blue line. Lag size: 0.008 degrees; number of lags: 12; Parameter: 2; Range: 0.068 degrees; Partial Sill: 0.081. Right panel: Scatterplot of predicted values versus observed values for the variable Spring Chlorophyll *a* Minimum.

Table 120. Results of cross-validation of the kriged model for the MODIS Case I Spring Chlorophyll *a* Minimum (mg m^{-3}).

Prediction error	**Value**
Number of Observations	74353
Overall Mean Error	3.211×10^{-4}
Root Mean Square Prediction Error	0.157
Standardized Mean	-0.002
Standardized Root Mean Square Prediction Error	1.424
Average Standard Error	0.107

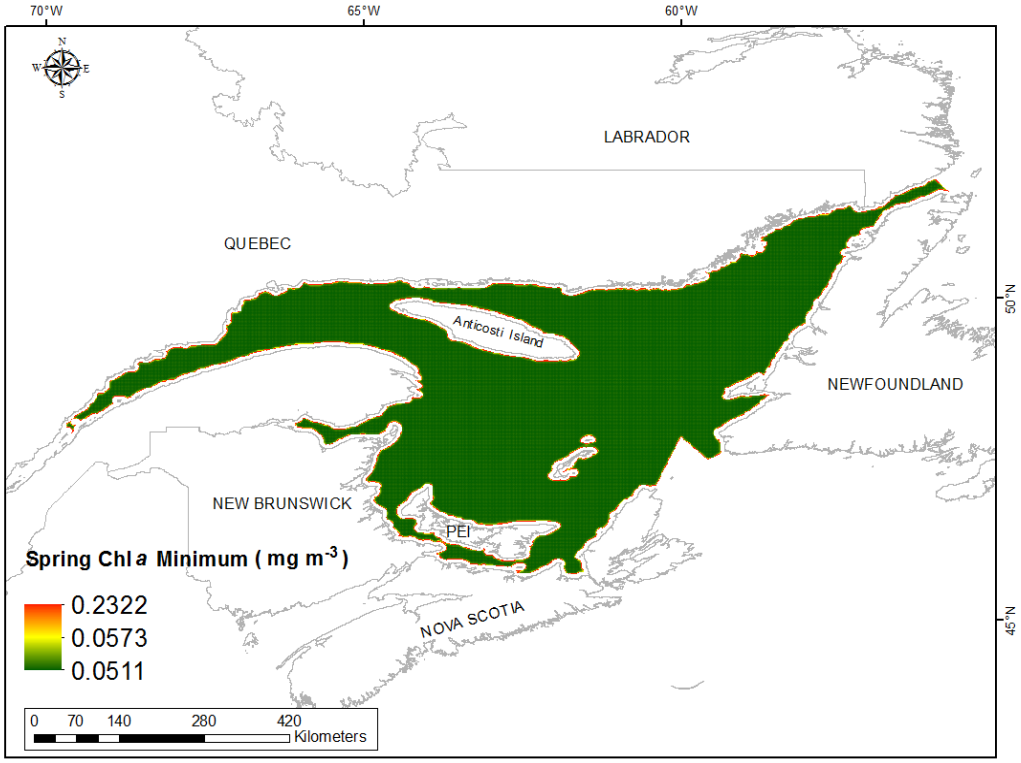

Fig. 299. Prediction standard error surface of MODIS Case I Spring Chlorophyll *a* Minimum (mg m^{-3}).

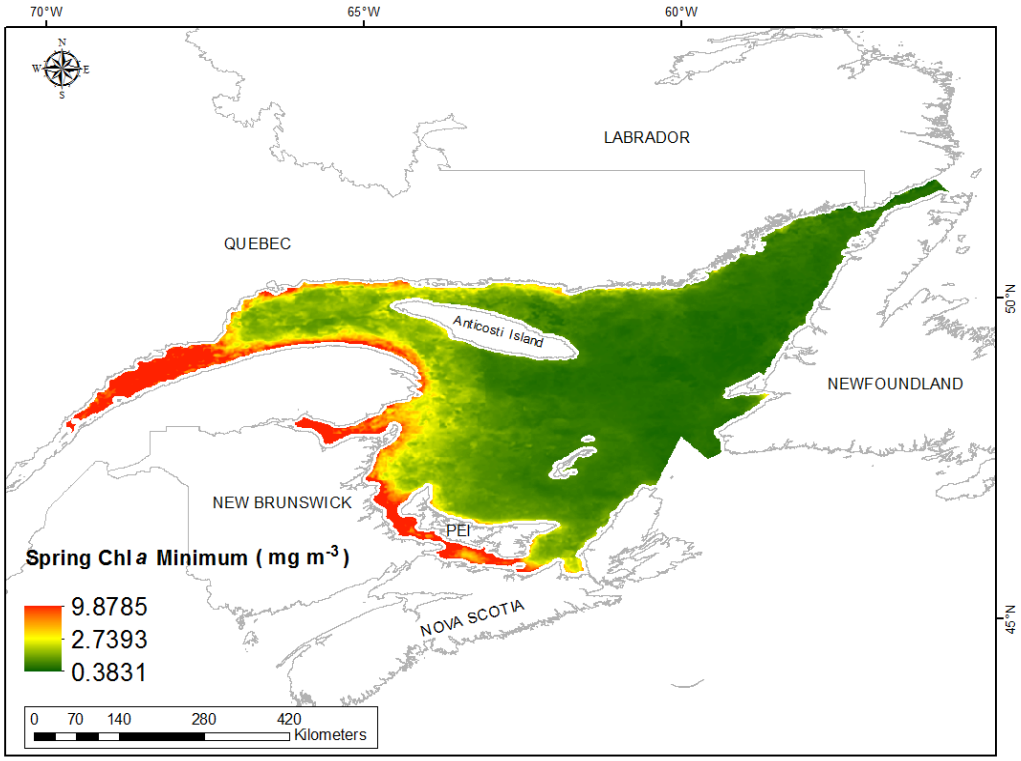

Fig. 300. Interpolated prediction surface of MODIS Case I Spring Chlorophyll *a* Minimum (mg m^{-3}).

MODIS Case I Spring Chlorophyll *a* Maximum

This variable displayed a right-skewed distribution with kurtosis prior to modeling (Table 121, Fig. 301). The data were higher than predicted by a normal distribution at the upper range and lower than predicted at mid values (Fig. 302). The areas of under- and over-prediction showed a strong spatial pattern over the spatial extent (Fig. 302).

The semivariogram showed moderate autocorrelation present in the data and the model showed a very good fit between measured and predicted values (Fig. 303). The model showed fair cross-validation statistics (Table 122). The error map showed medium to high error in a grid-like pattern over the study extent (Fig. 304). The kriged surface is presented in Fig. 305.

Table 121. Distributional properties of MODIS Case I Spring Chlorophyll *a* Maximum (mg m^{-3}).

Property	Value
Number of Observations	74353
Minimum	0.858
Maximum	22.000
Mean	4.149
Median	3.317
Standard Deviation	2.710
Skewness	1.597
Kurtosis	5.640

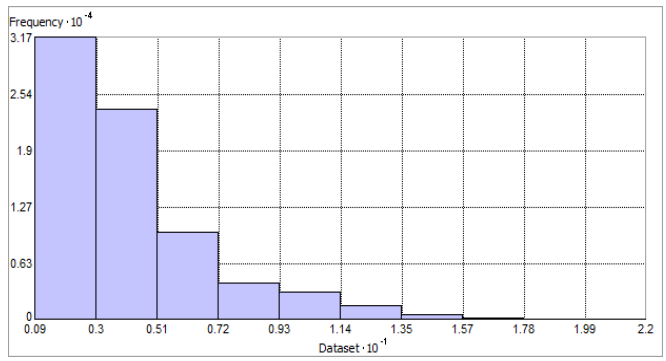

Fig. 301. Distribution of MODIS Case I Spring Chlorophyll *a* Maximum (mg m^{-3}). Histogram was illustrated using 10 bins. X and Y axes are shown at 10^{-1} and 10^{-4} respectively.

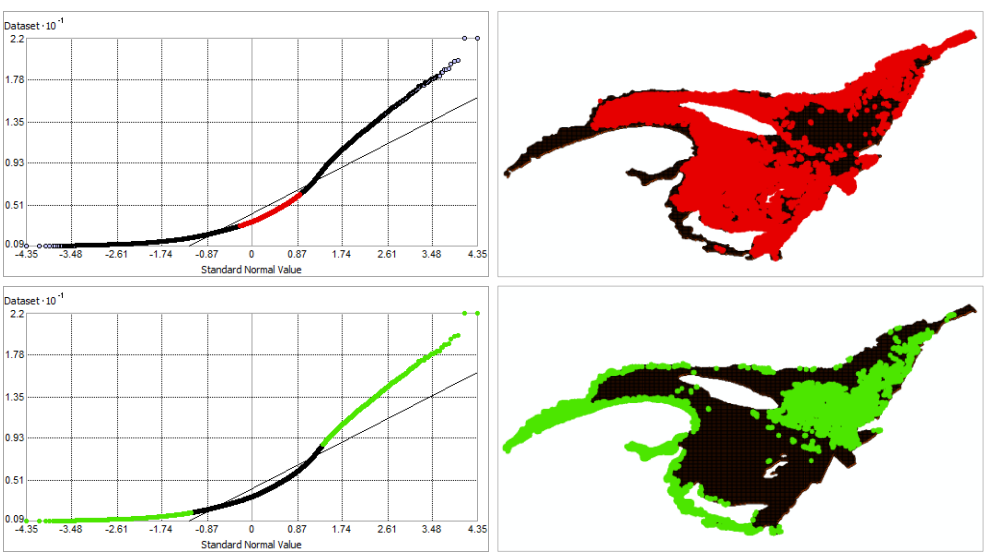

Fig. 302. Normal Q-Q plot for data values of MODIS Case I Spring Chlorophyll *a* Maximum (mg m^{-3}). Points falling under (upper panel) and over (lower panel) the reference line are mapped.

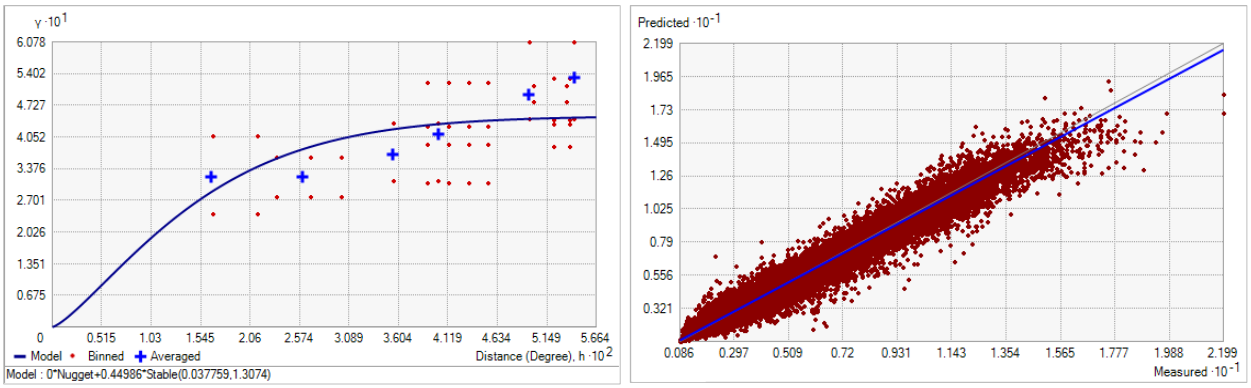

Fig. 303. Left panel: Semivariogram of MODIS Case I Spring Chlorophyll *a* Maximum (mg m^{-3}). Binned values are shown as red dots; average points are shown as blue crosses; the model fit to the averaged values is shown as a blue line. Lag size: 0.005 degrees; number of lags: 12; Parameter: 1.307; Range: 0.038 degrees; Partial Sill: 0.450. Right panel: Scatterplot of predicted values versus observed values for the variable MODIS Case I Spring Chlorophyll *a* Maximum (mg m^{-3}).

Table 122. Results of cross-validation of the kriged model for MODIS Case I Spring Chlorophyll *a* Maximum (mg m^{-3}).

Prediction error	**Value**
Number of Observations	74353
Overall Mean Error	-0.002
Root Mean Square Prediction Error	0.460
Standardized Mean	-0.003
Standardized Root Mean Square Prediction Error	0.810
Average Standard Error	0.564

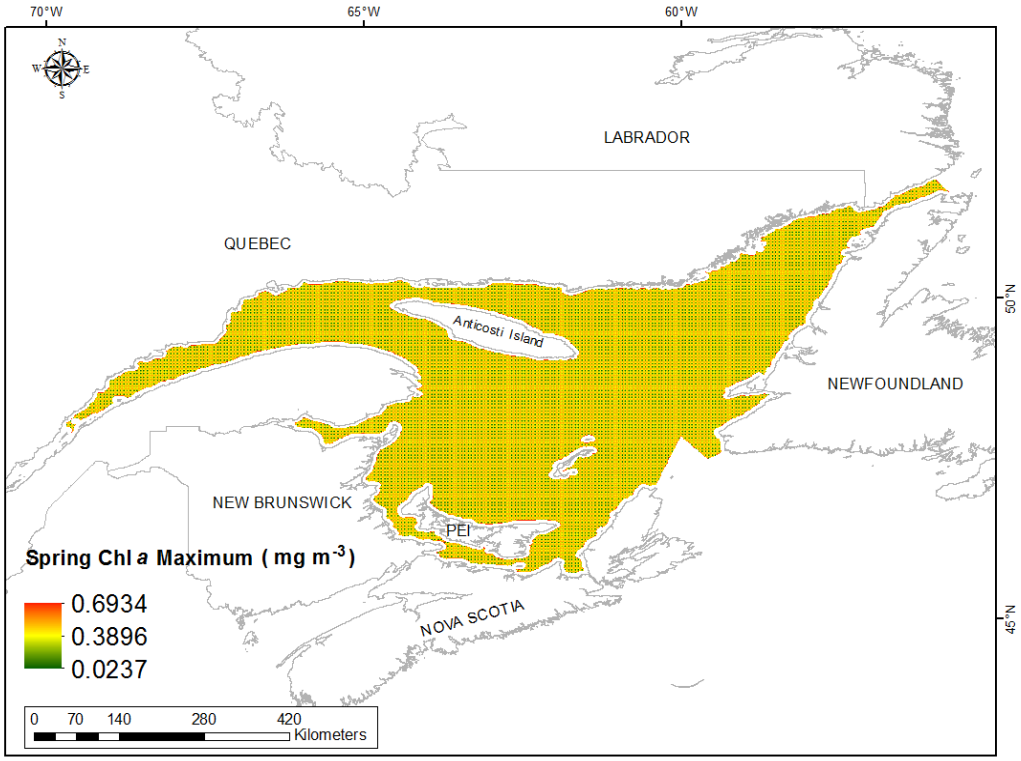

Fig. 304. Prediction standard error surface of MODIS Case I Spring Chlorophyll *a* Maximum (mg m^{-3}).

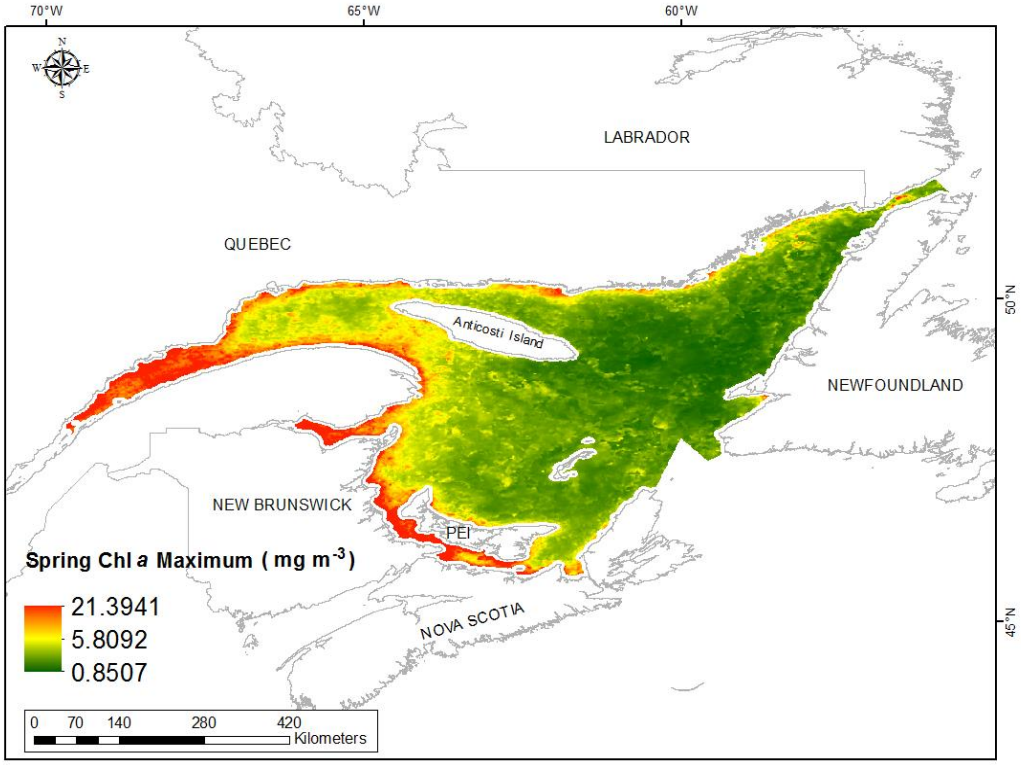

Fig. 305. Interpolated prediction surface of MODIS Case I Spring Chlorophyll *a* Maximum (mg m^{-3}).

MODIS Case I Spring Chlorophyll *a* Range

This variable displayed a right-skewed distribution with kurtosis prior to modeling (Table 123, Fig. 306). The data were higher than predicted by a normal distribution at the upper range and lower than predicted at mid values (Fig. 307). The areas of under- and over-prediction showed a strong spatial pattern over the spatial extent (Fig. 307).

The semivariogram showed moderate autocorrelation present in the data and the model showed a very good fit between measured and predicted values (Fig. 308). The model showed good cross-validation statistics (Table 124) indicating that it was good at prediction. The error map showed medium to high error in a grid-like pattern over the study extent (Fig. 309). The kriged surface is presented in Fig. 310.

Table 123. Distributional properties of MODIS Case I Spring Chlorophyll *a* Range (mg m^{-3}).

Property	Value
Number of Observations	74353
Minimum	0.2001
Maximum	14.945
Mean	2.560
Median	2.209
Standard Deviation	1.543
Skewness	1.357
Kurtosis	5.607

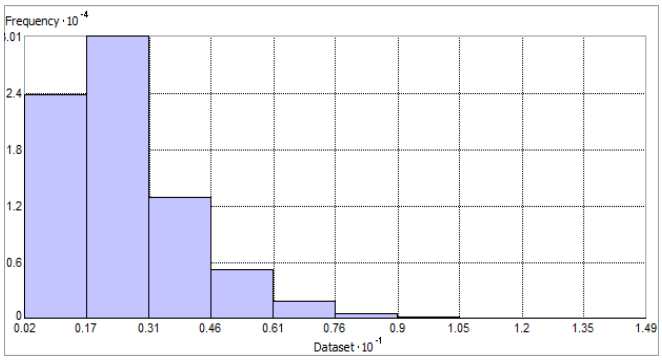

Fig. 306. Distribution of MODIS Case I Spring Chlorophyll *a* Range (mg m^{-3}). Histogram was illustrated using 10 bins. X and Y axes are shown at 10^{-1} and 10^{-4} respectively.

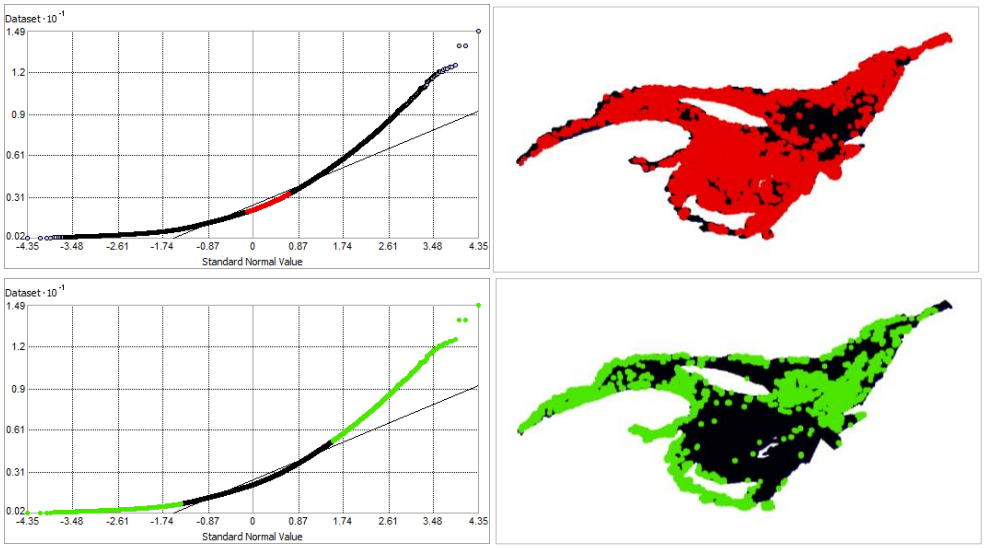

Fig. 307. Normal Q-Q plot for data values of MODIS Case I Spring Chlorophyll *a* Range (mg m^{-3}). Points falling under (upper panel) and over (bottom panel) the reference line are mapped.

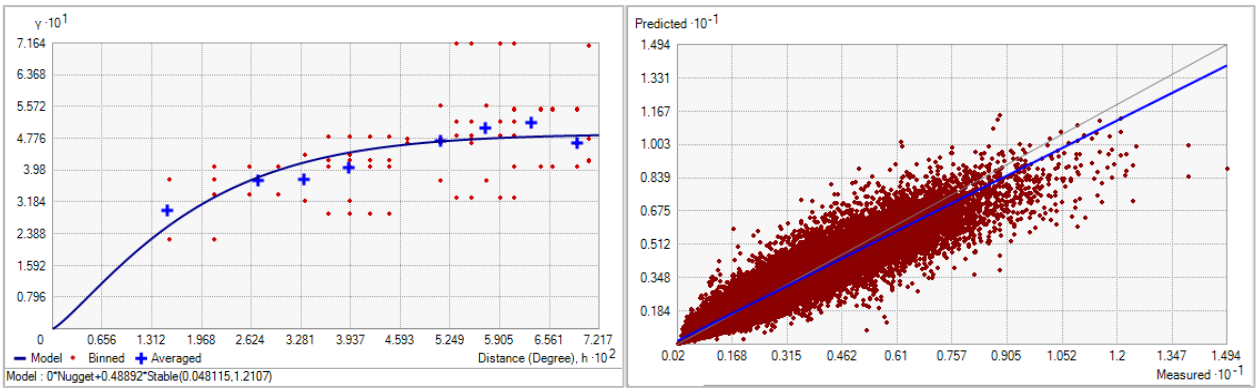

Fig. 308. Left panel: Semivariogram of MODIS Case I Spring Chlorophyll *a* Range (mg m^{-3}). Binned values are shown as red dots; average points are shown as blue crosses; the model fit to the averaged values is shown as a blue line. Lag size: 0.006 degrees; number of lags: 12; Parameter: 1.211; Range: 0.048 degrees; Partial Sill: 0.489. Right panel: Scatterplot of predicted values versus observed values for the variable MODIS Case I Spring Chlorophyll *a* Range (mg m^{-3}).

Table 124. Results of cross-validation of the kriged model for MODIS Case I Spring Chlorophyll *a* Range (mg m^{-3}).

Prediction error	**Value**
Number of Observations	74353
Overall Mean Error	-0.001
Root Mean Square Prediction Error	0.476
Standardized Mean	-0.001
Standardized Root Mean Square Prediction Error	0.873
Average Standard Error	0.542

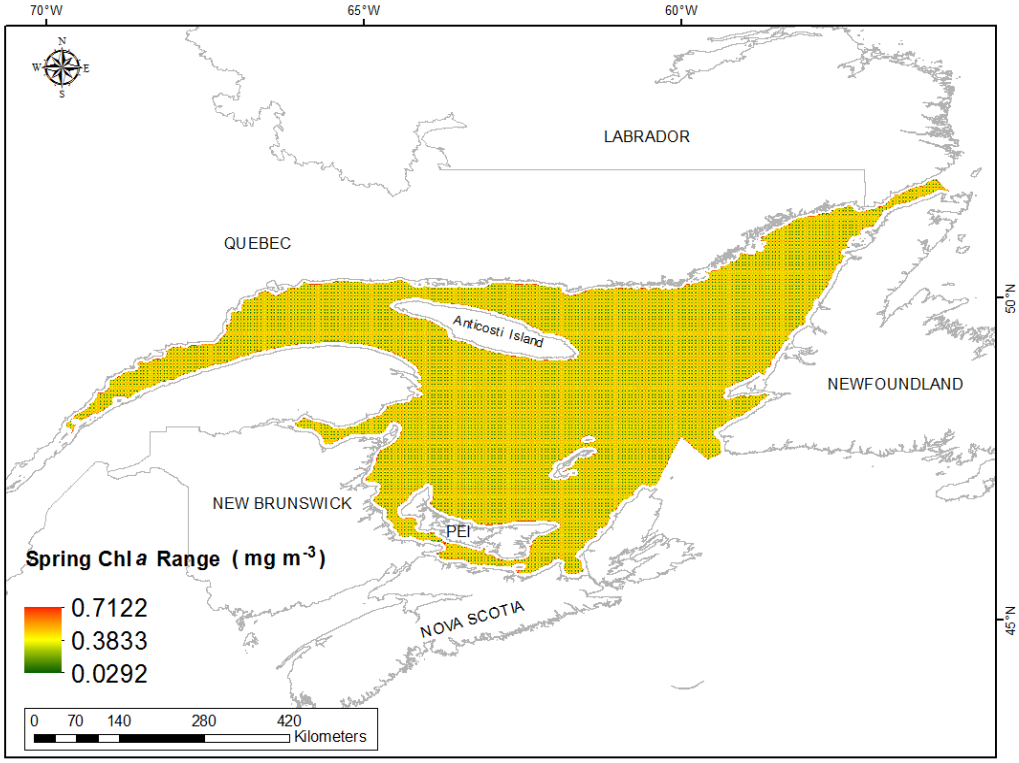

Fig. 309. Prediction standard error surface of MODIS Case I Spring Chlorophyll *a* Range (mg m^{-3}).

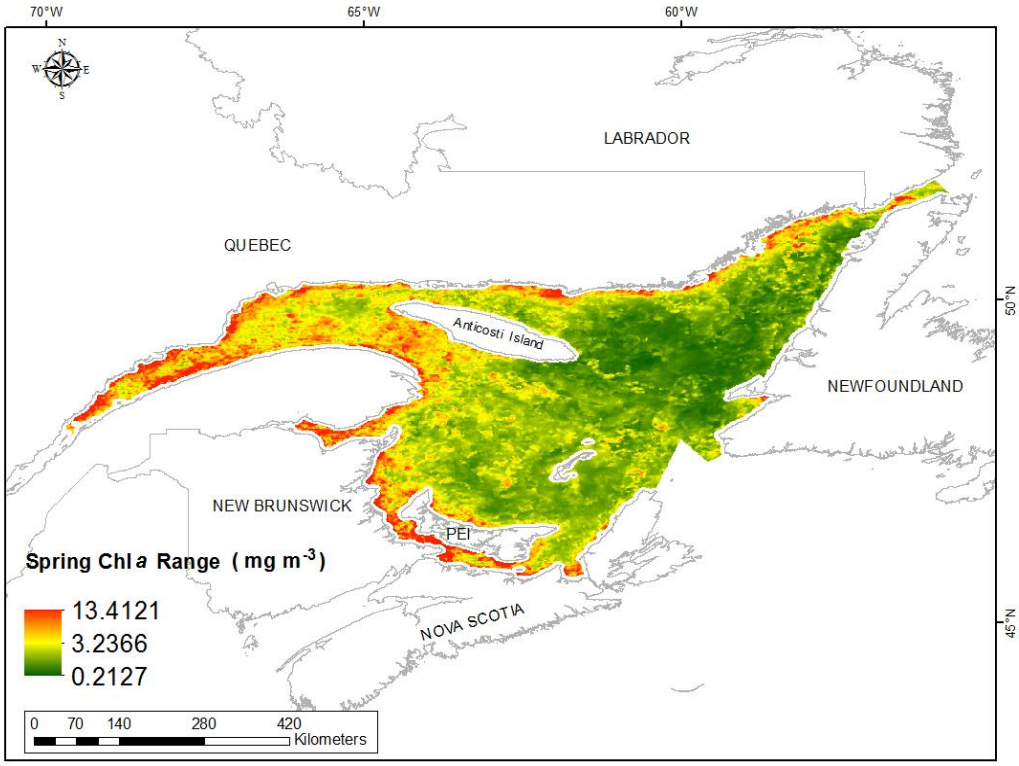

Fig. 310. Interpolated prediction surface of MODIS Case I Spring Chlorophyll *a* Range (mg m^{-3}).

MODIS Case I Summer Chlorophyll *a* Mean

This variable displayed a right-skewed distribution with kurtosis prior to modeling (Table 125, Fig. 311). The data were higher than predicted by a normal distribution at the upper range and lower than predicted at mid values (Fig. 312). The areas of under- and over-prediction showed a strong spatial pattern over the spatial extent (Fig. 312).

The semivariogram showed moderate autocorrelation present in the data and the model showed a very good fit between measured and predicted values (Fig. 313). The model showed good cross-validation statistics (Table 126) indicating that it was good at prediction. The error map showed low error over the study extent with higher error around the coast (Fig. 314). The kriged surface is presented in Fig. 315.

Table 125. Distributional properties of MODIS Case I Summer Chlorophyll *a* Mean (mg m^{-3}).

Property	Value
Number of Observations	74353
Minimum	0.652
Maximum	15.754
Mean	2.174
Median	1.534
Standard Deviation	2.031
Skewness	2.529
Kurtosis	10.008

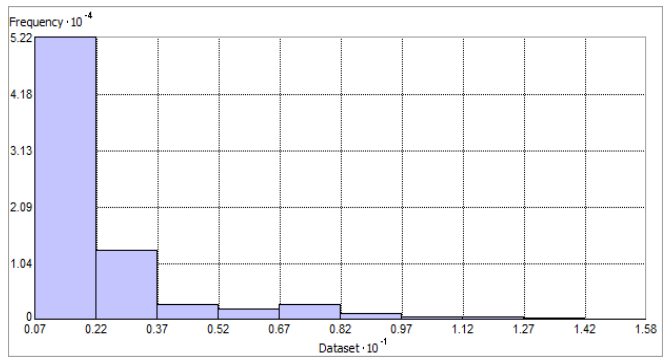

Fig. 311. Distribution of MODIS Case I Summer Chlorophyll *a* Mean (mg m^{-3}). Histogram was illustrated using 10 bins. X and Y axes are shown at 10^{-1} and 10^{-4} respectively.

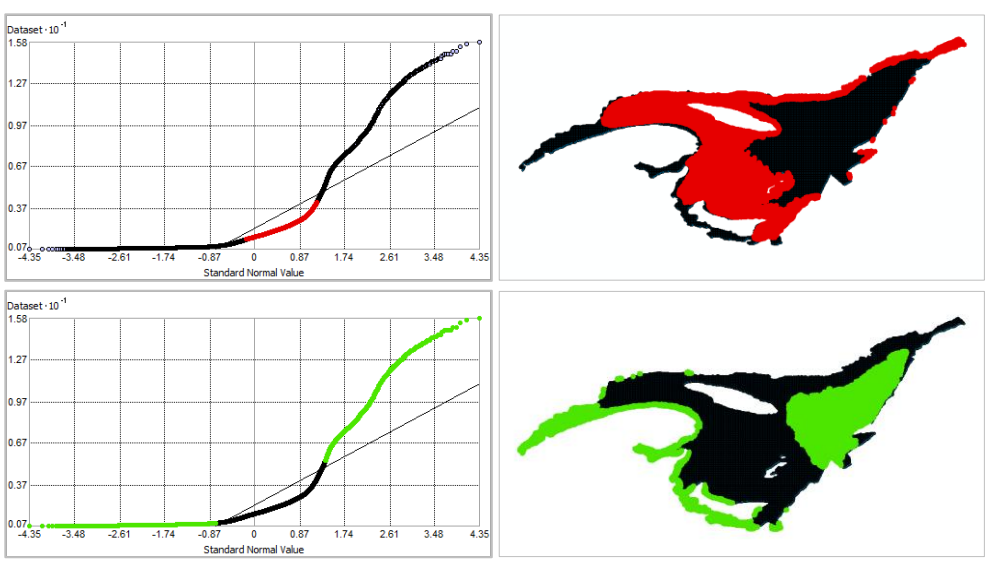

Fig. 312. Normal Q-Q plot for data values of MODIS Case I Summer Chlorophyll *a* Mean (mg m^{-3}). Points falling under (upper panel) and over (bottom panel) the reference line are mapped.

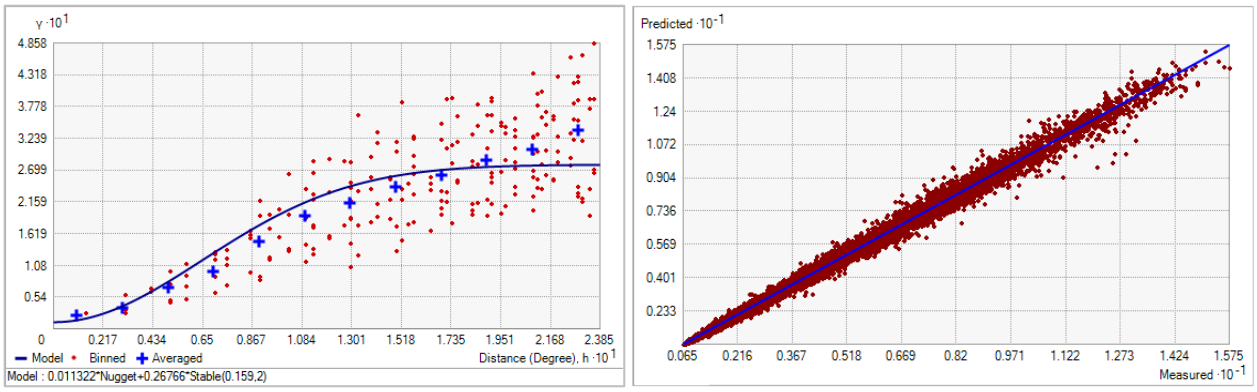

Fig. 313. Left panel: Semivariogram of MODIS Case I Summer Chlorophyll *a* Mean (mg m^{-3}). Binned values are shown as red dots; average points are shown as blue crosses; the model fit to the averaged values is shown as a blue line. Lag size: 0.020 degrees; number of lags: 12; Parameter: 2; Range: 0.159 degrees; Partial Sill: 0.268. Right panel: Scatterplot of predicted values versus observed values for the variable MODIS Case I Summer Chlorophyll *a* Mean (mg m^{-3}).

Table 126. Results of cross-validation of the kriged model for the MODIS Case I Summer Chlorophyll *a* Mean (mg m^{-3}).

Prediction error	**Value**
Number of Observations	74353
Overall Mean Error	0.001
Root Mean Square Prediction Error	0.112
Standardized Mean	0.012
Standardized Root Mean Square Prediction Error	0.932
Average Standard Error	0.118

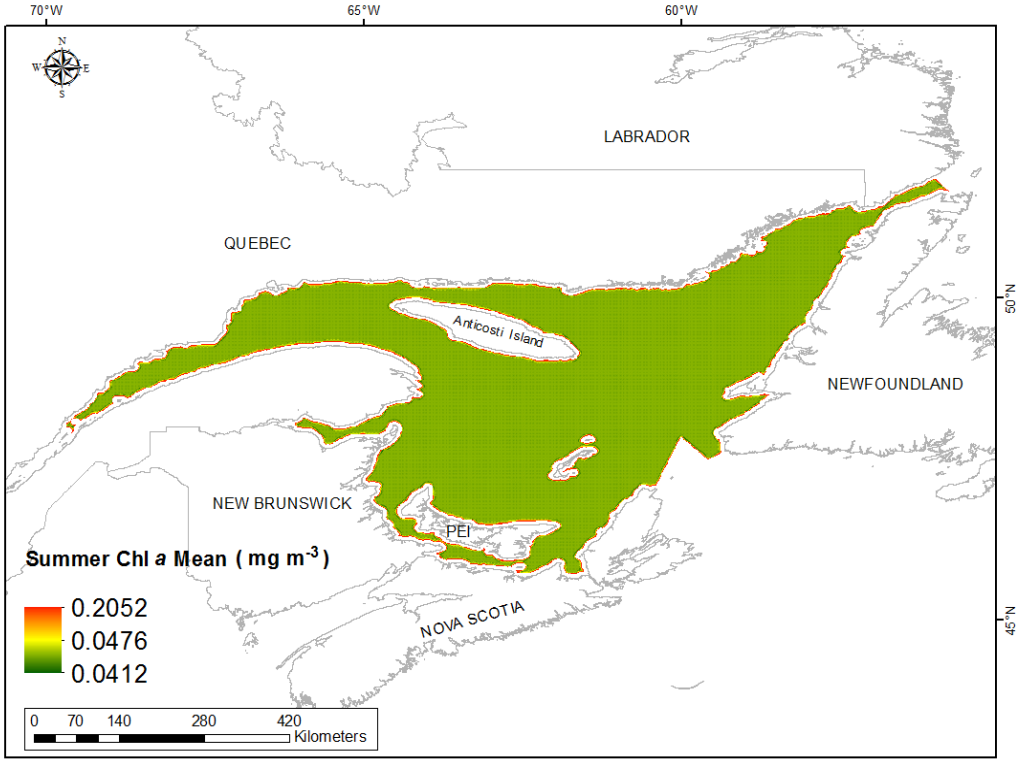

Fig. 314. Prediction standard error surface of MODIS Case I Summer Chlorophyll *a* Mean (mg m^{-3}).

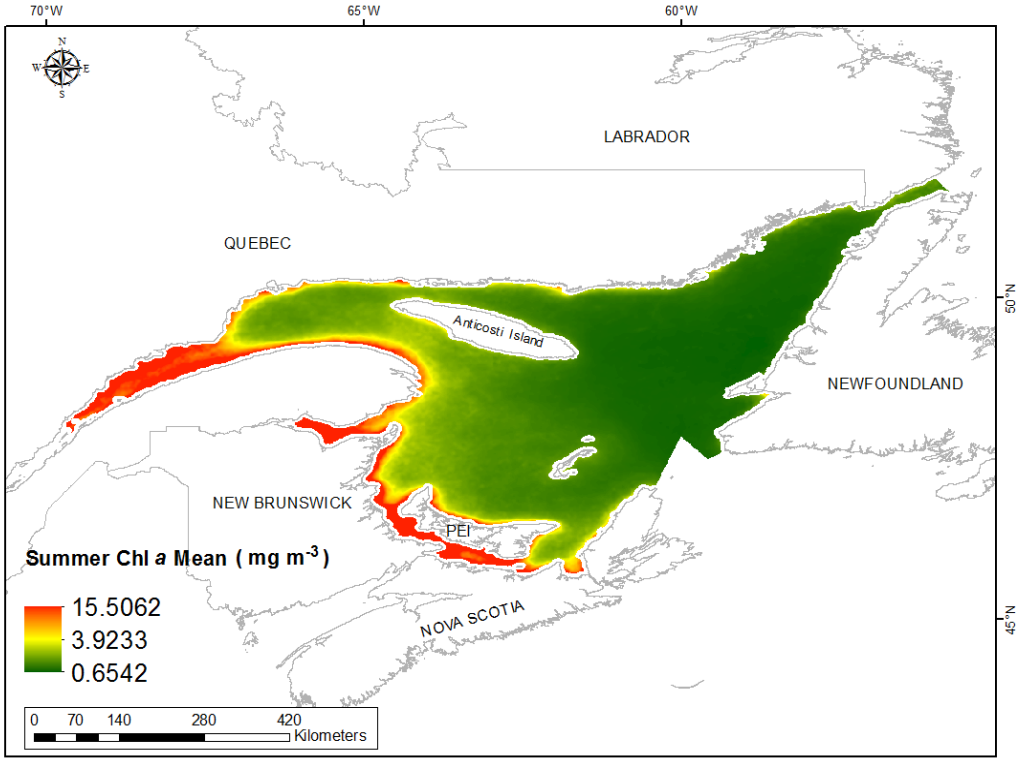

Fig. 315. Interpolated prediction surface of MODIS Case I Summer Chlorophyll *a* Mean (mg m^{-3}).

MODIS Case I Summer Chlorophyll *a* Minimum

This variable displayed a right-skewed distribution with kurtosis prior to modeling (Table 127, Fig. 316). The data were higher than predicted by a normal distribution at the upper range and lower than predicted at mid values (Fig. 317). The areas of under- and over-prediction showed a strong spatial pattern over the spatial extent (Fig. 317).

The semivariogram showed moderate autocorrelation present in the data and the model showed a very good fit between measured and predicted values (Fig. 318). The model showed good cross-validation statistics (Table 128) indicating that it was good at prediction. The error map showed low error over the study extent (Fig. 319). The kriged surface is presented in Fig. 320.

Table 127. Distributional properties of MODIS Case I Summer Chlorophyll *a* Minimum (mg m^{-3}).

Property	Value
Number of Observations	74353
Minimum	0.439
Maximum	13.284
Mean	1.464
Median	1.044
Standard Deviation	1.344
Skewness	3.026
Kurtosis	14.283

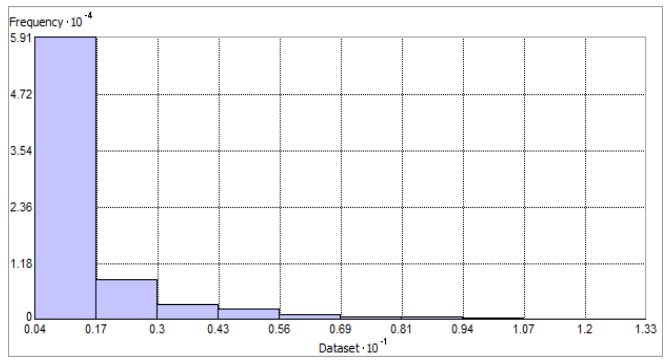

Fig. 316. Distribution of MODIS Case I Summer Chlorophyll *a* Minimum (mg m^{-3}). Histogram was illustrated using 10 bins. X and Y axes are shown at 10^{-1} and 10^{-4} respectively.

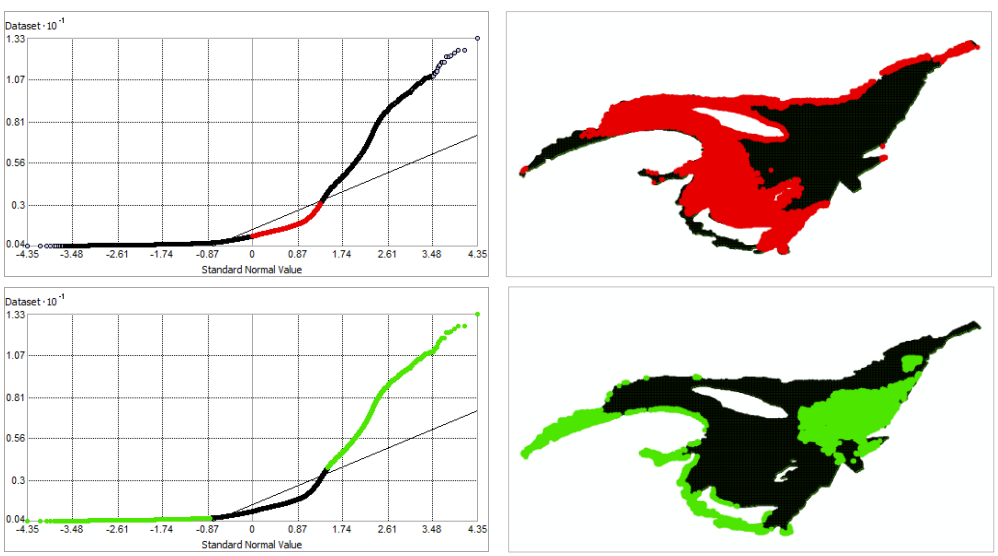

Fig. 317. Normal Q-Q plot for data values of MODIS Case I Summer Chlorophyll *a* Minimum (mg m^{-3}). Points falling under (upper panel) and over (bottom panel) the reference line are mapped.

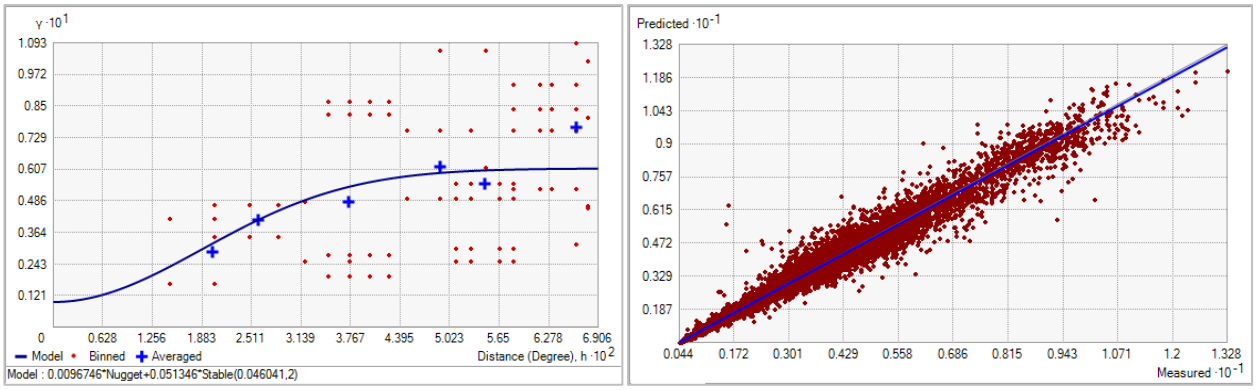

Fig. 318. Left panel: Semivariogram of MODIS Case I Summer Chlorophyll *a* Minimum (mg m^{-3}). Binned values are shown as red dots; average points are shown as blue crosses; the model fit to the averaged values is shown as a blue line. Lag size: 0.006 degrees; number of lags: 12; Parameter: 2; Range: 0.046 degrees; Partial Sill: 0.051. Right panel: Scatterplot of predicted values versus observed values for the variable MODIS Case I Summer Chlorophyll *a* Minimum (mg m^{-3}).

Table 128. Results of cross-validation of the kriged model for MODIS Case I Summer Chlorophyll *a* Minimum (mg m^{-3}).

Prediction error	**Value**
Number of Observations	74353
Overall Mean Error	-0.001
Root Mean Square Prediction Error	0.155
Standardized Mean	-0.005
Standardized Root Mean Square Prediction Error	1.016
Average Standard Error	0.145

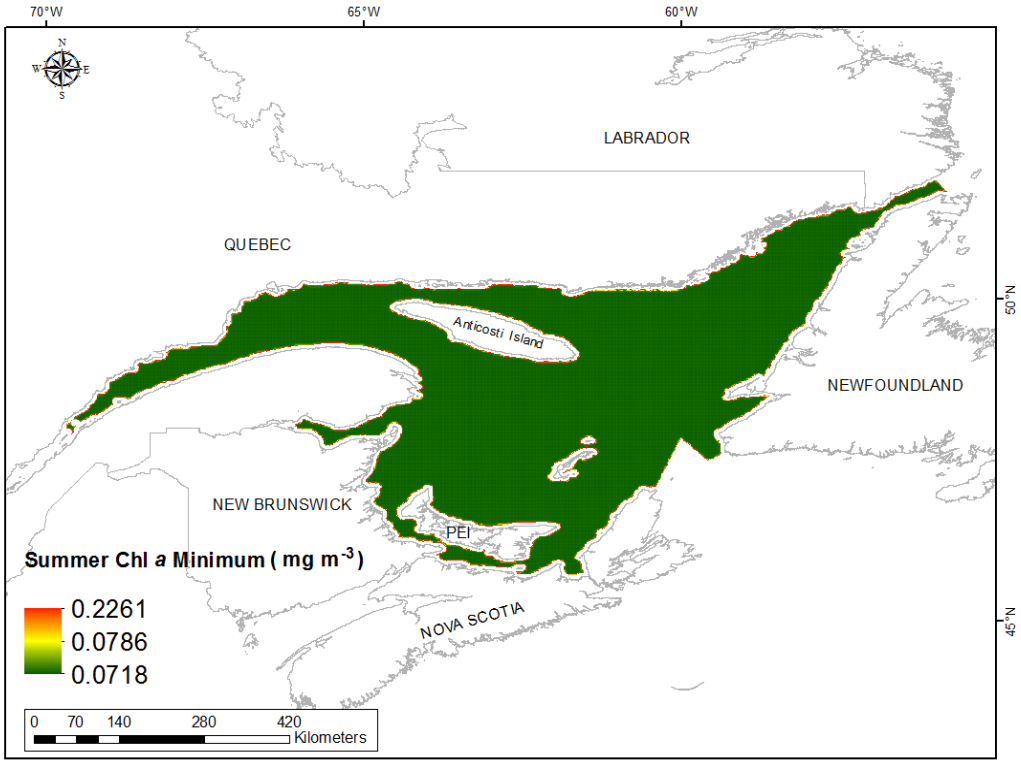

Fig. 319. Prediction standard error surface of MODIS Case I Summer Chlorophyll *a* Minimum (mg m^{-3}).

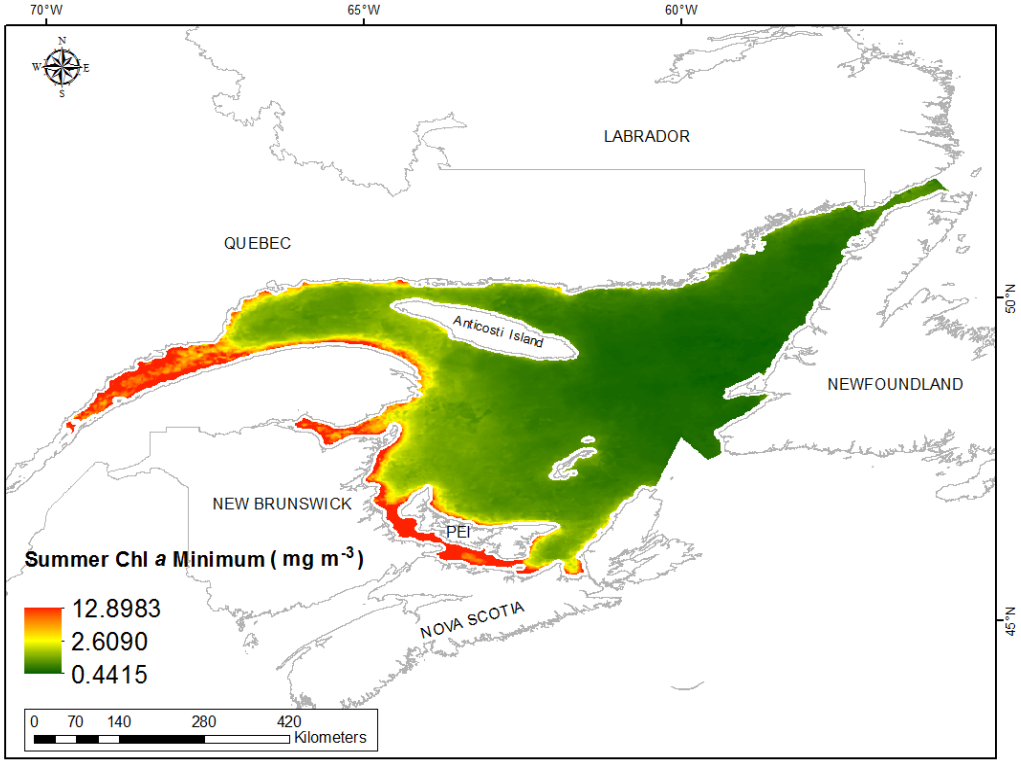

Fig. 320. Interpolated prediction surface of MODIS Case I Summer Chlorophyll *a* Minimum (mg m^{-3}).

MODIS Case I Summer Chlorophyll *a* Maximum

This variable displayed a right-skewed distribution with kurtosis prior to modeling (Table 129, Fig. 321). The data were higher than predicted by a normal distribution at the upper range and lower than predicted at mid values (Fig. 322). The areas of under- and over-prediction showed a strong spatial pattern over the spatial extent (Fig. 322).

The semivariogram showed moderate autocorrelation present in the data and the model showed a very good fit between measured and predicted values (Fig. 323). The model showed good cross-validation statistics (Table 130) indicating that it was good at prediction. The error map showed low error over the study extent (Fig. 324). The kriged surface is presented in Fig. 325.

Table 129. Distributional properties of MODIS Case I Summer Chlorophyll *a* Maximum (mg m^{-3}).

Property	Value
Number of Observations	74353
Minimum	0.779
Maximum	30.053
Mean	3.276
Median	2.345
Standard Deviation	3.015
Skewness	2.286
Kurtosis	8.903

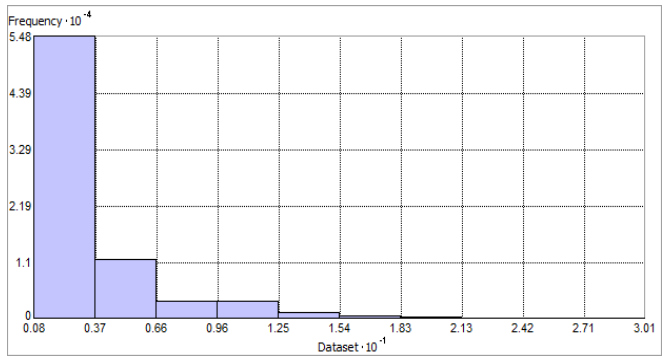

Fig. 321. Distribution of MODIS Case I Summer Chlorophyll *a* Maximum (mg m^{-3}). Histogram was illustrated using 10 bins. X and Y axes are shown at 10^{-1} and 10^{-4} respectively.

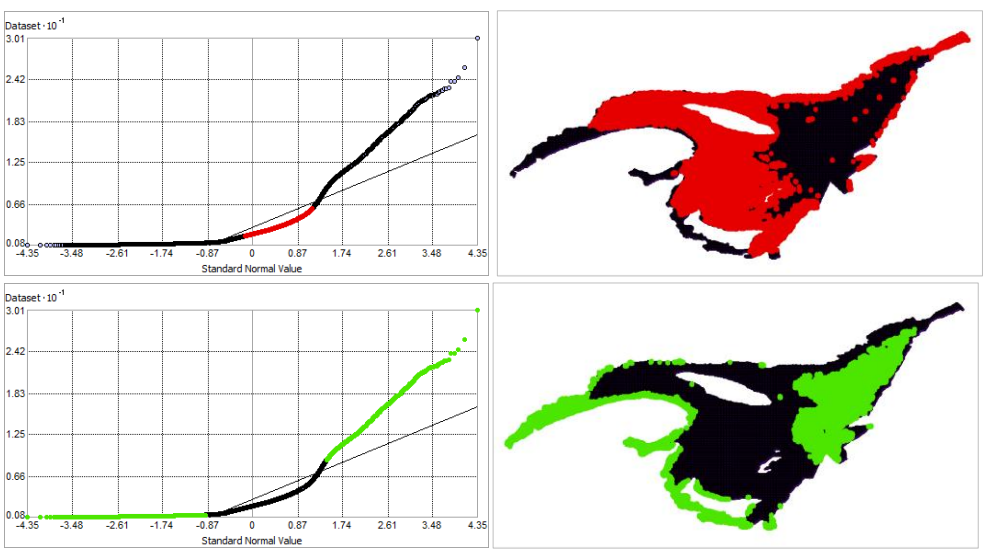

Fig. 322. Normal Q-Q plot for data values of MODIS Case I Summer Chlorophyll *a* Maximum (mg m^{-3}). Points falling under (upper panel) and over (bottom panel) the reference line are mapped.

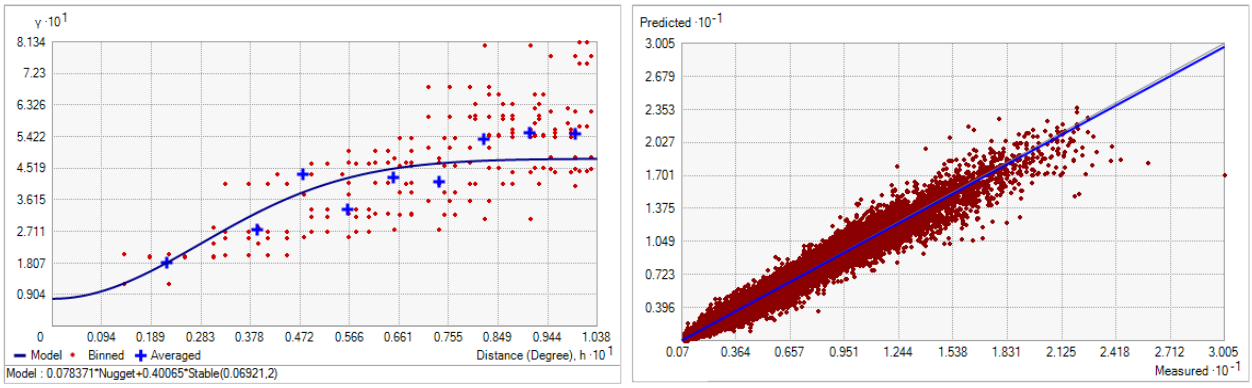

Fig. 323. Left panel: Semivariogram of MODIS Case I Summer Chlorophyll *a* Maximum (mg m^{-3}). Binned values are shown as red dots; average points are shown as blue crosses; the model fit to the averaged values is shown as a blue line. Lag size: 0.009 degrees; number of lags: 12; Parameter: 2; Range: 0.069 degrees; Partial Sill: 0.401. Right panel: Scatterplot of predicted values versus observed values for the variable MODIS Case I Summer Chlorophyll *a* Maximum (mg m^{-3}).

Table 130. Results of cross-validation of the kriged model for MODIS Case I Summer Chlorophyll *a* Maximum (mg m^{-3}).

Prediction error	**Value**
Number of Observations	74353
Overall Mean Error	-0.001
Root Mean Square Prediction Error	0.423
Standardized Mean	-0.002
Standardized Root Mean Square Prediction Error	1.236
Average Standard Error	0.335

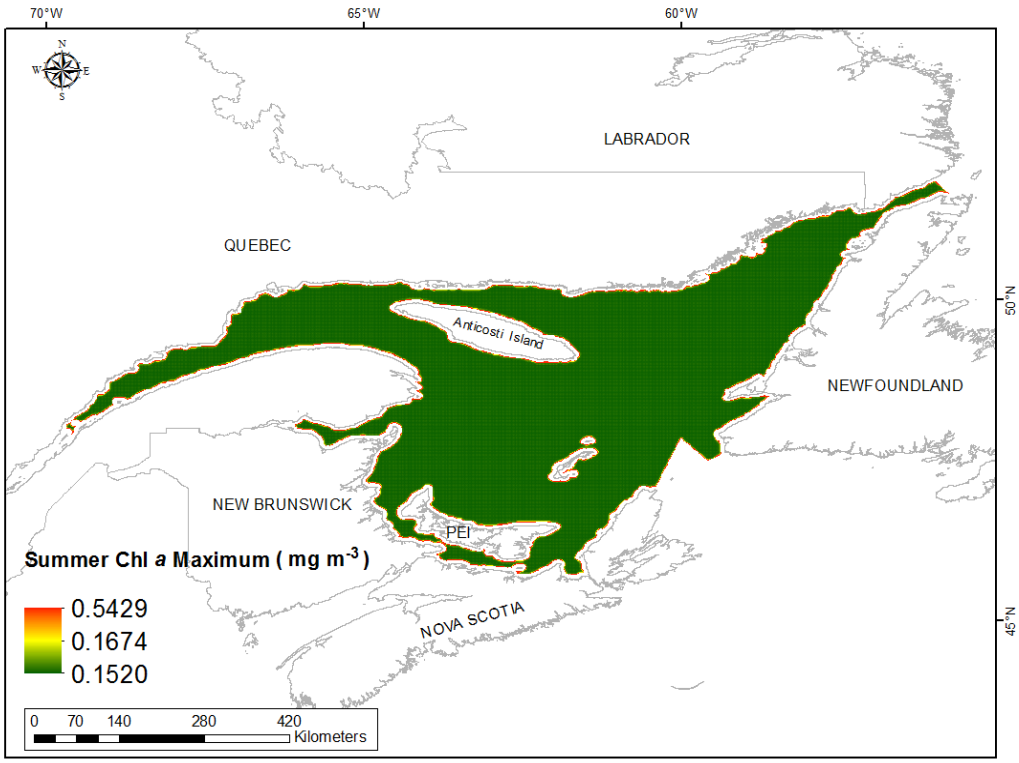

Fig. 324. Prediction standard error surface of MODIS Case I Summer Chlorophyll *a* Maximum (mg m^{-3}).

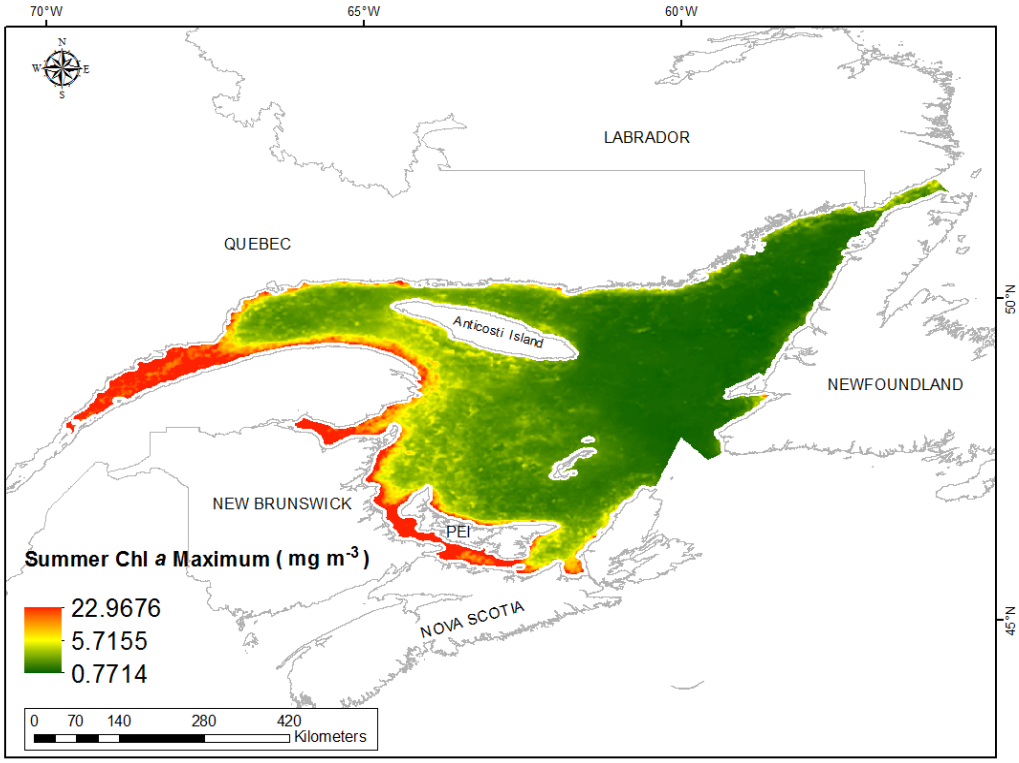

Fig. 325. Interpolated prediction surface of MODIS Case I Summer Chlorophyll *a* Maximum (mg m^{-3}).

MODIS Case I Summer Chlorophyll *a* Range

This variable displayed a right-skewed distribution with kurtosis prior to modeling (Table 131, Fig. 326). The data were higher than predicted by a normal distribution at the upper range and lower than predicted at mid values (Fig. 327). The areas of under- and over-prediction showed a strong spatial pattern over the spatial extent (Fig. 327).

The semivariogram showed moderate autocorrelation present in the data and the model showed a very good fit between measured and predicted values (Fig. 328). The model showed good cross-validation statistics (Table 132) indicating that it was good at prediction. The error map showed low error over the study extent (Fig. 329). The kriged surface is presented in Fig. 330.

Table 131. Distributional properties of MODIS Case I Summer Chlorophyll *a* Range (mg m^{-3}).

Property	Value
Number of Observations	74353
Minimum	0.180
Maximum	23.488
Mean	1.812
Median	1.219
Standard Deviation	1.806
Skewness	2.259
Kurtosis	9.797

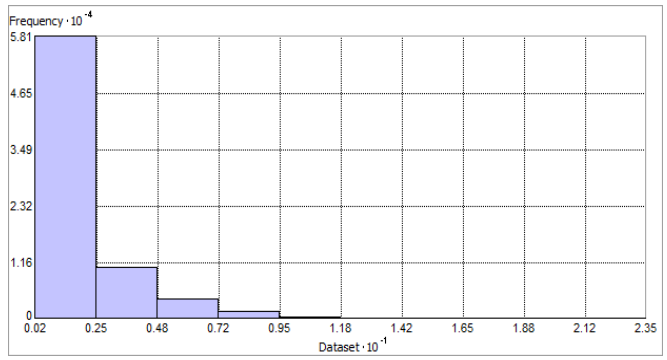

Fig. 326. Distribution of MODIS Case I Summer Chlorophyll *a* Range (mg m^{-3}). Histogram was illustrated using 10 bins. X and Y axes are shown at 10^{-1} and 10^{-4} respectively.

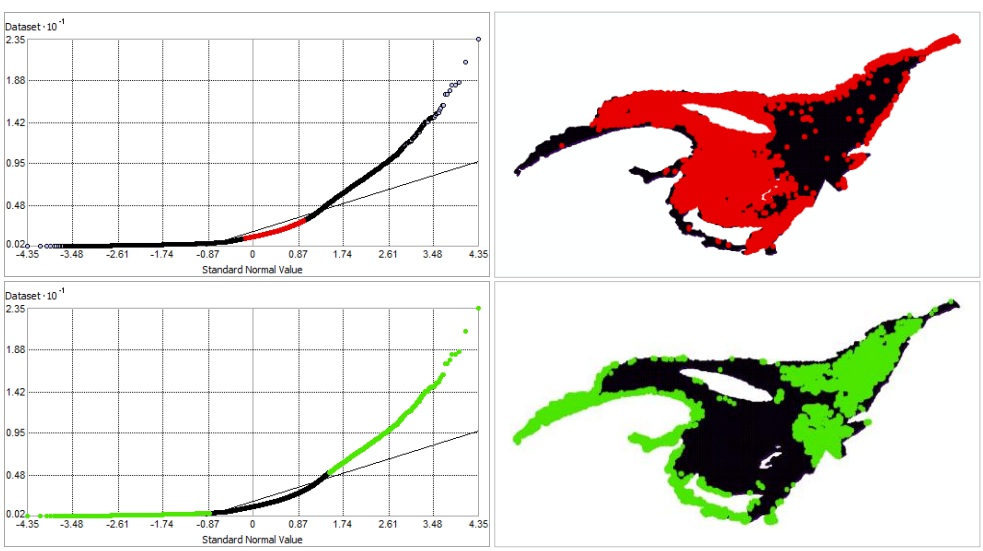

Fig. 327. Normal Q-Q plot for data values of MODIS Case I Summer Chlorophyll *a* Range (mg m^{-3}). Points falling under (upper panel) and over (bottom panel) the reference line are mapped.

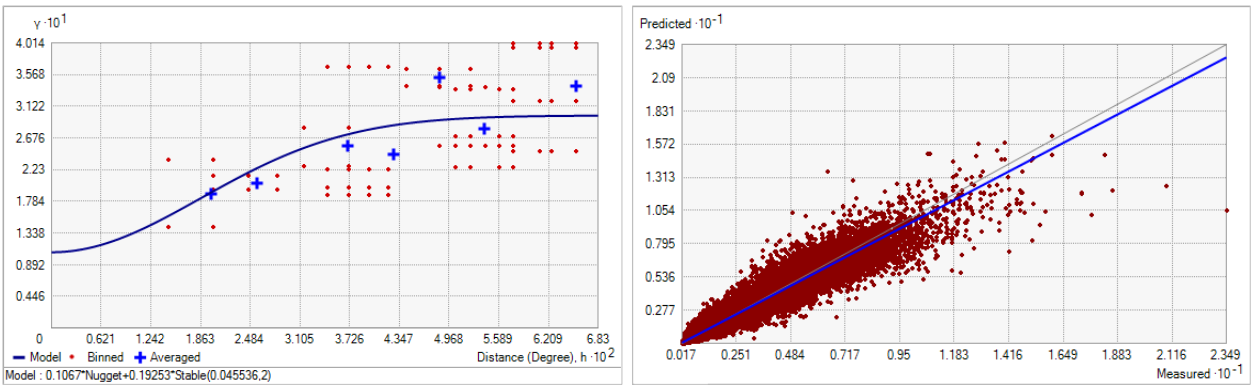

Fig. 328. Left panel: Semivariogram of MODIS Case I Summer Chlorophyll *a* Range (mg m^{-3}). Binned values are shown as red dots; average points are shown as blue crosses; the model fit to the averaged values is shown as a blue line. Lag size: 0.006 degrees; number of lags: 12; Parameter: 2; Range: 0.046 degrees; Partial Sill: 0.193. Right panel: Scatterplot of predicted values versus observed values for the variable MODIS Case I Summer Chlorophyll *a* Range (mg m^{-3}).

Table 132. Results of cross-validation of the kriged model for MODIS Case I Summer Chlorophyll *a* Range (mg m^{-3}).

Prediction error	**Value**
Number of Observations	74353
Overall Mean Error	-0.001
Root Mean Square Prediction Error	0.435
Standardized Mean	-0.003
Standardized Root Mean Square Prediction Error	1.023
Average Standard Error	0.419

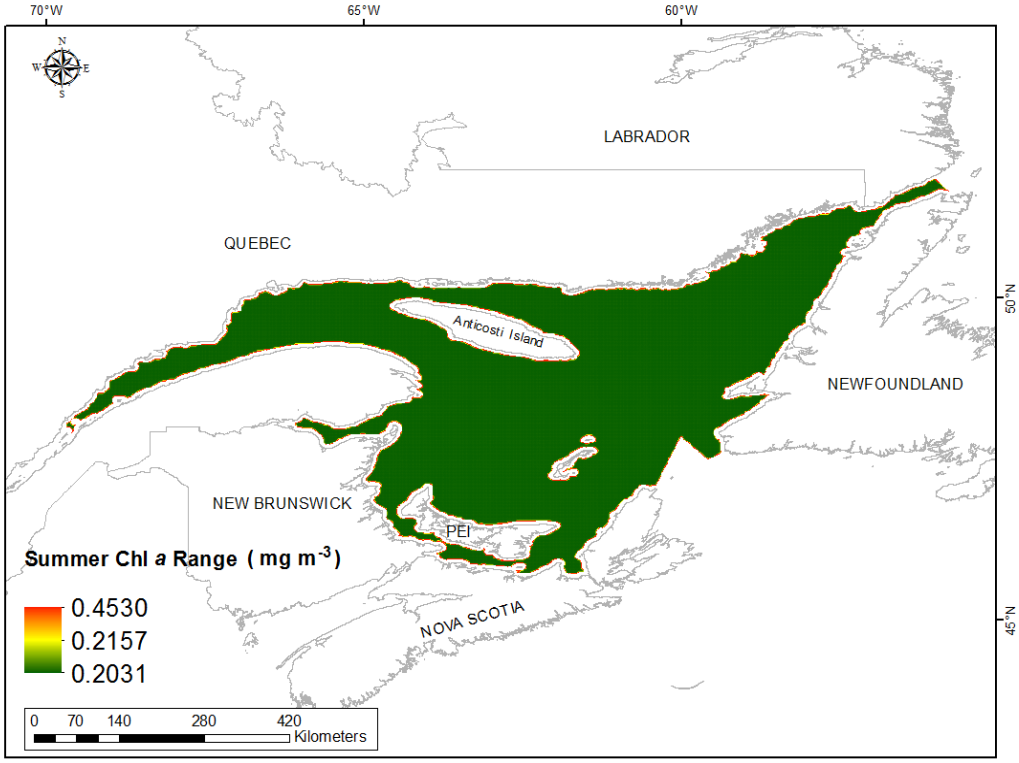

Fig. 329. Prediction standard error surface of MODIS Case I Summer Chlorophyll *a* Range (mg m^{-3}).

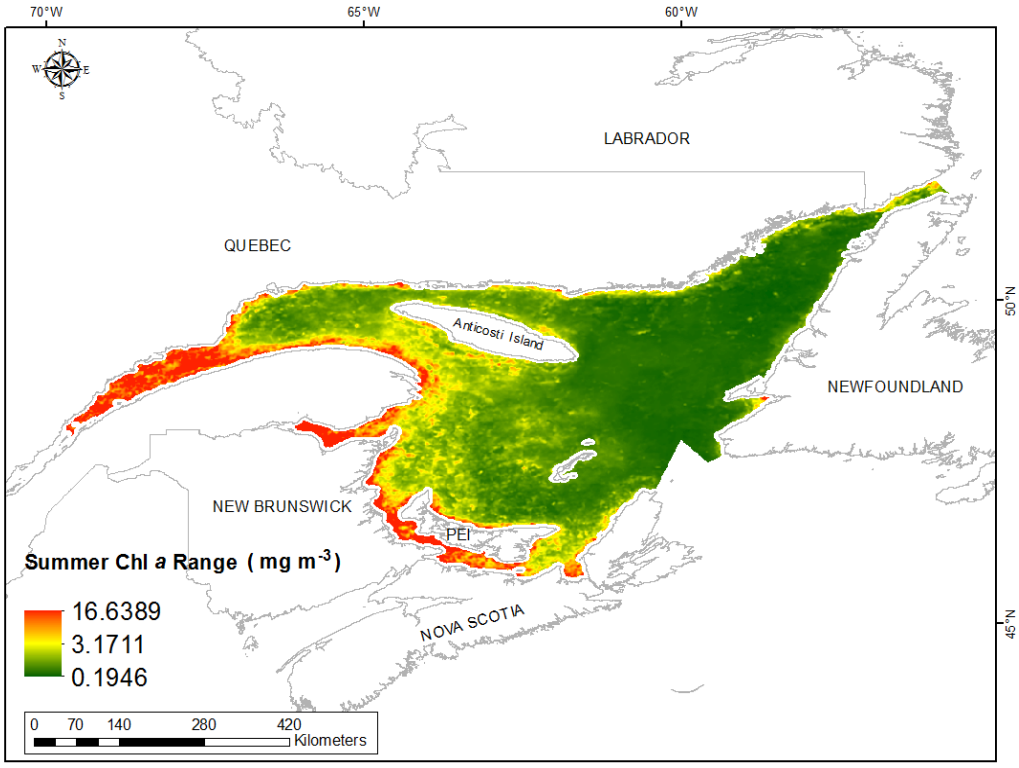

Fig. 330. Interpolated prediction surface of MODIS Case I Summer Chlorophyll *a* Range (mg m^{-3}).

MODIS Case I Fall Chlorophyll *a* Mean

This variable displayed a right-skewed distribution with kurtosis prior to modeling (Table 133, Fig. 331). The data were higher than predicted by a normal distribution at the upper range and lower than predicted at mid values (Fig. 332). The areas of under- and over-prediction showed a strong spatial pattern over the spatial extent (Fig. 332).

The semivariogram showed moderate autocorrelation present in the data and the model showed a very good fit between measured and predicted values (Fig. 333). The model showed good cross-validation statistics (Table 134) indicating that it was good at prediction. The error map showed low error over the study extent (Fig. 334). The kriged surface is presented in Fig. 335.

Table 133. Distributional properties of MODIS Case I Fall Chlorophyll *a* Mean (mg m^{-3}).

Property	Value
Number of Observations	74353
Minimum	0.728
Maximum	14.912
Mean	2.113
Median	1.590
Standard Deviation	1.703
Skewness	2.726
Kurtosis	11.608

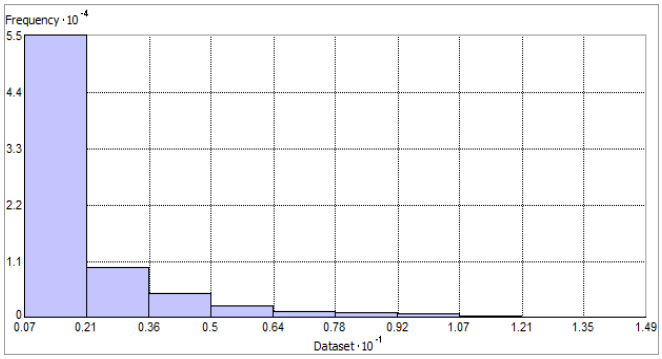

Fig. 331. Distribution of MODIS Case I Fall Chlorophyll *a* Mean (mg m^{-3}). Histogram was illustrated using 10 bins. X and Y axes are shown at 10^{-1} and 10^{-4} respectively.

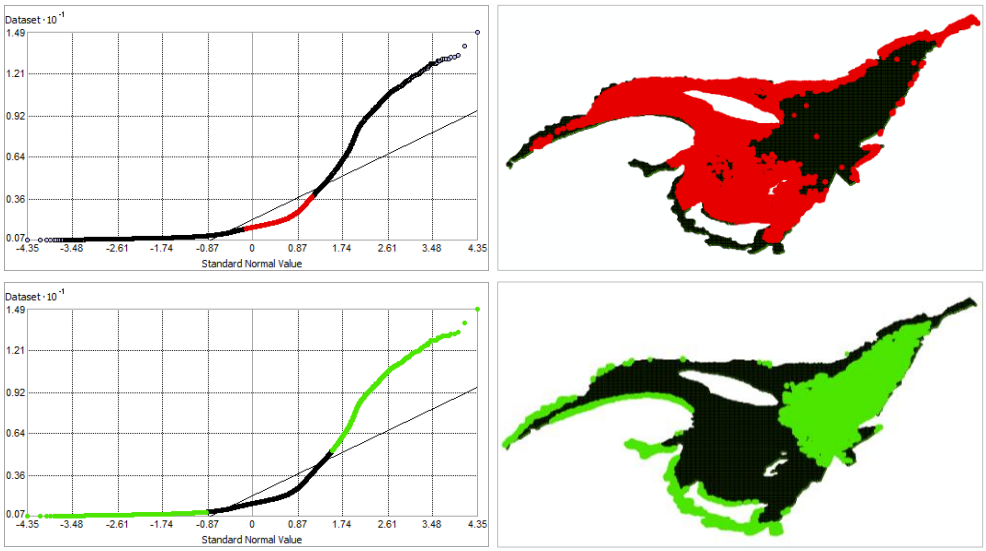

Fig. 332. Normal Q-Q plot for data values of MODIS Case I Fall Chlorophyll *a* Mean (mg m^{-3}). Points falling under (upper panel) and over (bottom panel) the reference line are mapped.

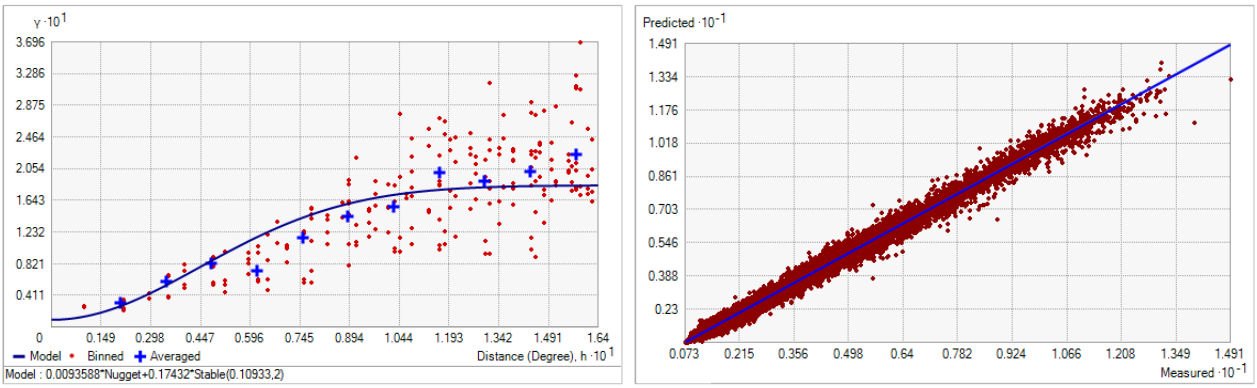

Fig. 333. Left panel: Semivariogram of MODIS Case I Fall Chlorophyll *a* Mean (mg m^{-3}). Binned values are shown as red dots; average points are shown as blue crosses; the model fit to the averaged values is shown as a blue line. Lag size: 0.014 degrees; number of lags: 12; Parameter: 2; Range: 0.109 degrees; Partial Sill: 0.174. Right panel: Scatterplot of predicted values versus observed values for the variable MODIS Case I Fall Chlorophyll *a* Mean (mg m^{-3}).

Table 134. Results of cross-validation of the kriged model for the MODIS Case I Fall Chlorophyll *a* Mean (mg m^{-3}).

Prediction error	**Value**
Number of Observations	74353
Overall Mean Error	4.077×10^{-4}
Root Mean Square Prediction Error	0.132
Standardized Mean	0.005
Standardized Root Mean Square Prediction Error	1.170
Average Standard Error	0.111

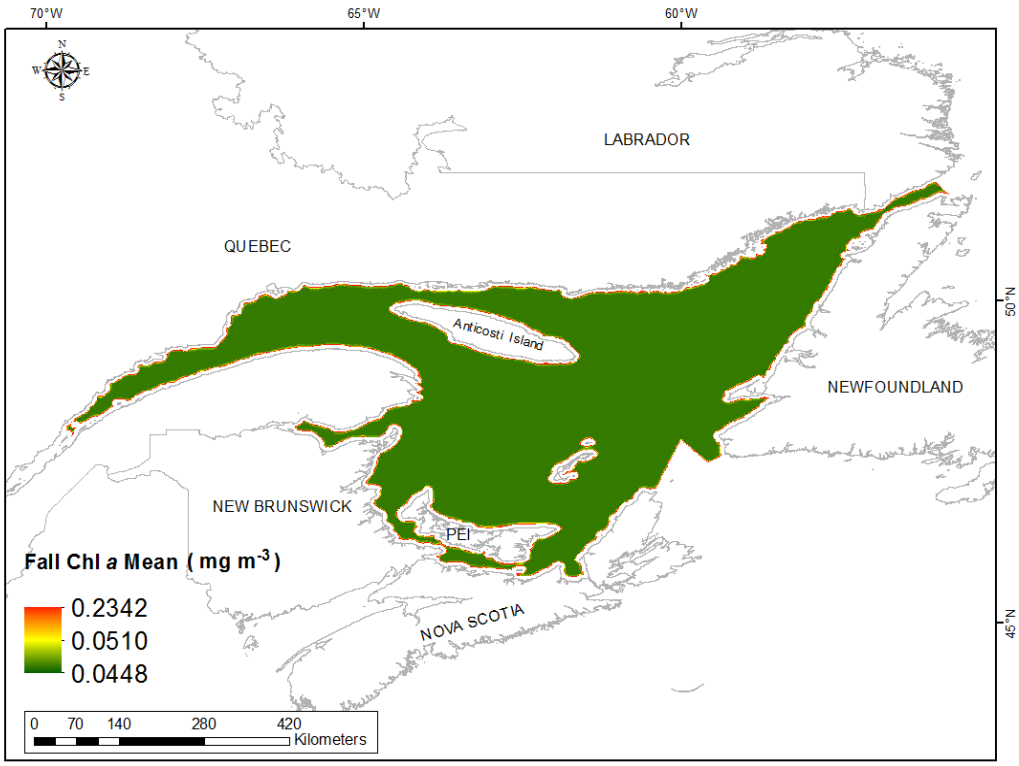

Fig. 334. Prediction standard error surface of MODIS Case I Fall Chlorophyll *a* Mean (mg m^{-3}).

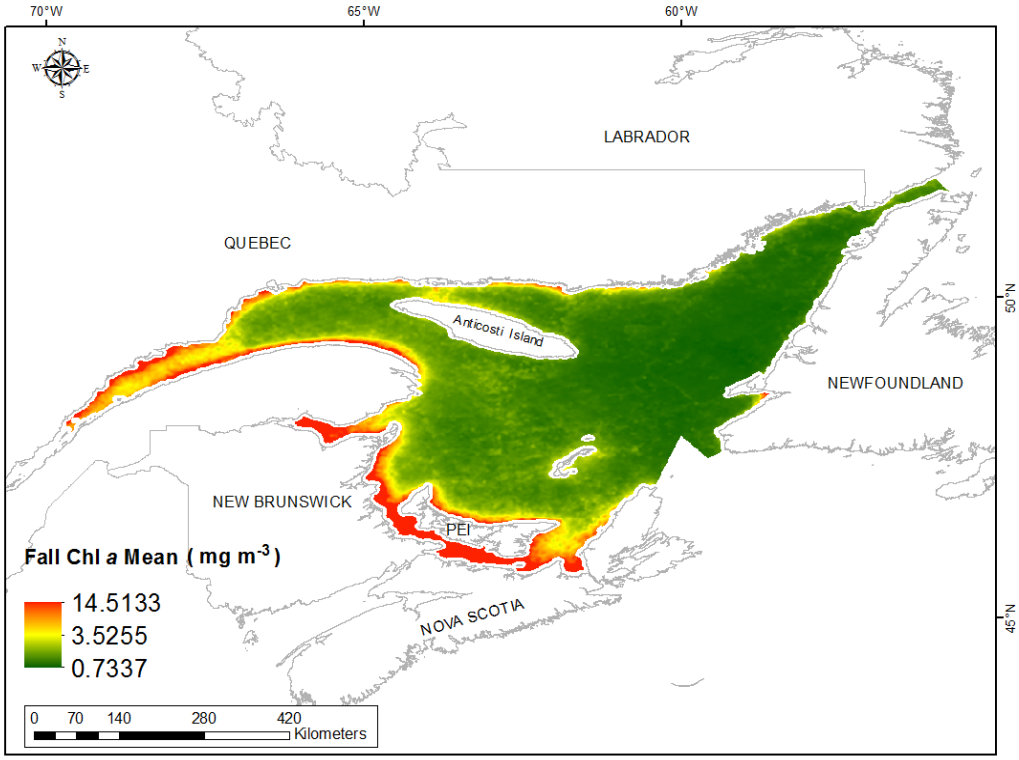

Fig. 335. Interpolated prediction surface of MODIS Case I Fall Chlorophyll *a* Mean (mg m^{-3}).

MODIS Case I Fall Chlorophyll *a* Minimum

This variable displayed a right-skewed distribution with kurtosis prior to modeling (Table 135, Fig. 336). The data were higher than predicted by a normal distribution at the upper range and lower than predicted at mid values (Fig. 337). The areas of under- and over-prediction showed a strong spatial pattern over the spatial extent (Fig. 337).

The semivariogram showed moderate autocorrelation present in the data and the model showed a very good fit between measured and predicted values (Fig. 338). The model showed good cross-validation statistics (Table 136) indicating that it was good at prediction. The error map showed medium to high error in a grid-like pattern over the study extent (Fig. 339). The kriged surface is presented in Fig. 340.

Table 135. Distributional properties of MODIS Case I Fall Chlorophyll *a* Minimum (mg m^{-3}).

Property	Value
Number of Observations	74353
Minimum	0.183
Maximum	10.664
Mean	1.185
Median	0.852
Standard Deviation	1.059
Skewness	3.727
Kurtosis	19.181

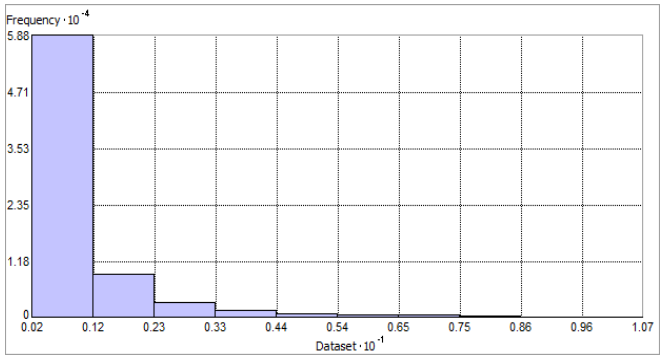

Fig. 336. Distribution of MODIS Case I Fall Chlorophyll *a* Minimum (mg m^{-3}). Histogram was illustrated using 10 bins. X and Y axes are shown at 10^{-1} and 10^{-4} respectively.

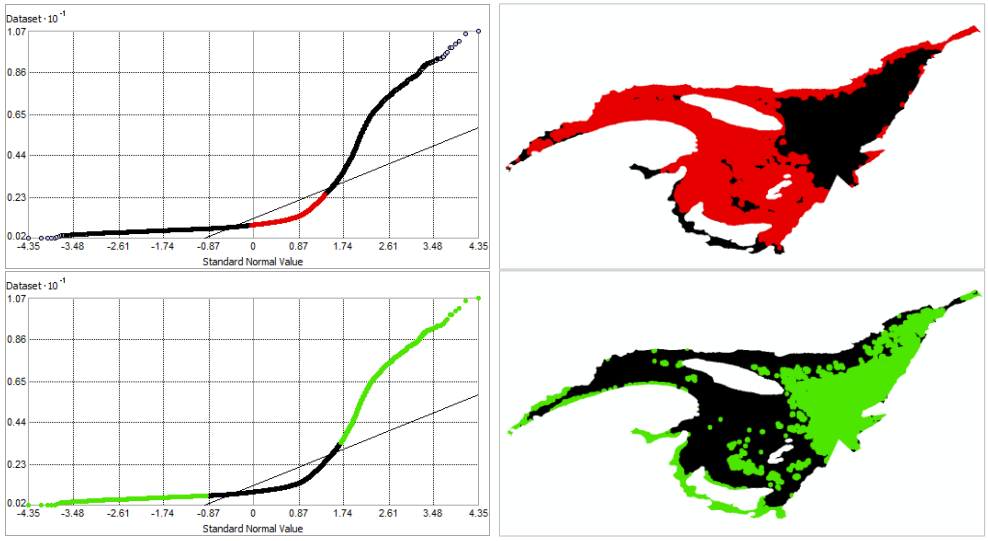

Fig. 337. Normal Q-Q plot for data values of MODIS Case I Fall Chlorophyll *a* Minimum (mg m^{-3}). Points falling under (upper panel) and over (bottom panel) the reference line are mapped.

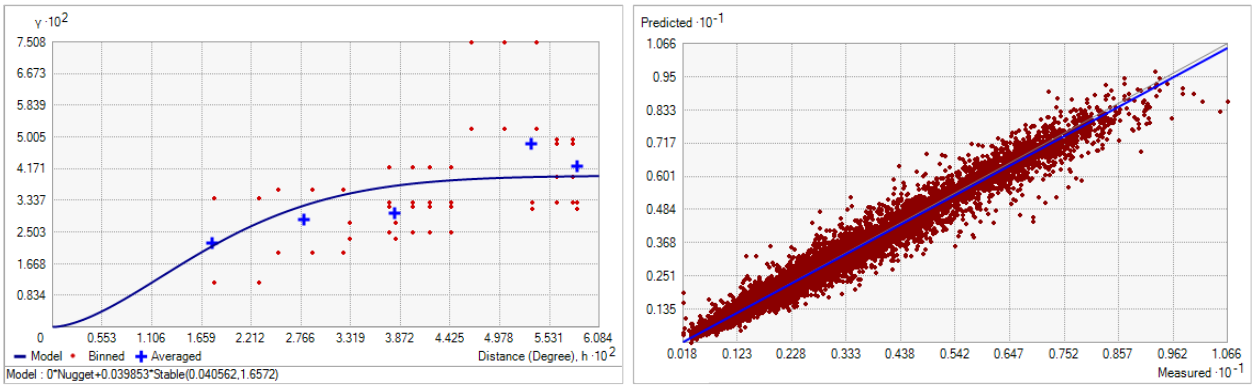

Fig. 338. Left panel: Semivariogram of MODIS Case I Fall Chlorophyll *a* Minimum (mg m^{-3}). Binned values are shown as red dots; average points are shown as blue crosses; the model fit to the averaged values is shown as a blue line. Lag size: 0.006 degrees; number of lags: 12; Parameter: 1.657; Range: 0.041 degrees; Partial Sill: 0.040. Right panel: Scatterplot of predicted values versus observed values for the variable MODIS Case I Fall Chlorophyll *a* Minimum (mg m^{-3}).

Table 136. Results of cross-validation of the kriged model for MODIS Case I Fall Chlorophyll *a* Minimum (mg m^{-3}).

Prediction error	**Value**
Number of Observations	74353
Overall Mean Error	-0.001
Root Mean Square Prediction Error	0.133
Standardized Mean	-0.005
Standardized Root Mean Square Prediction Error	0.975
Average Standard Error	0.132

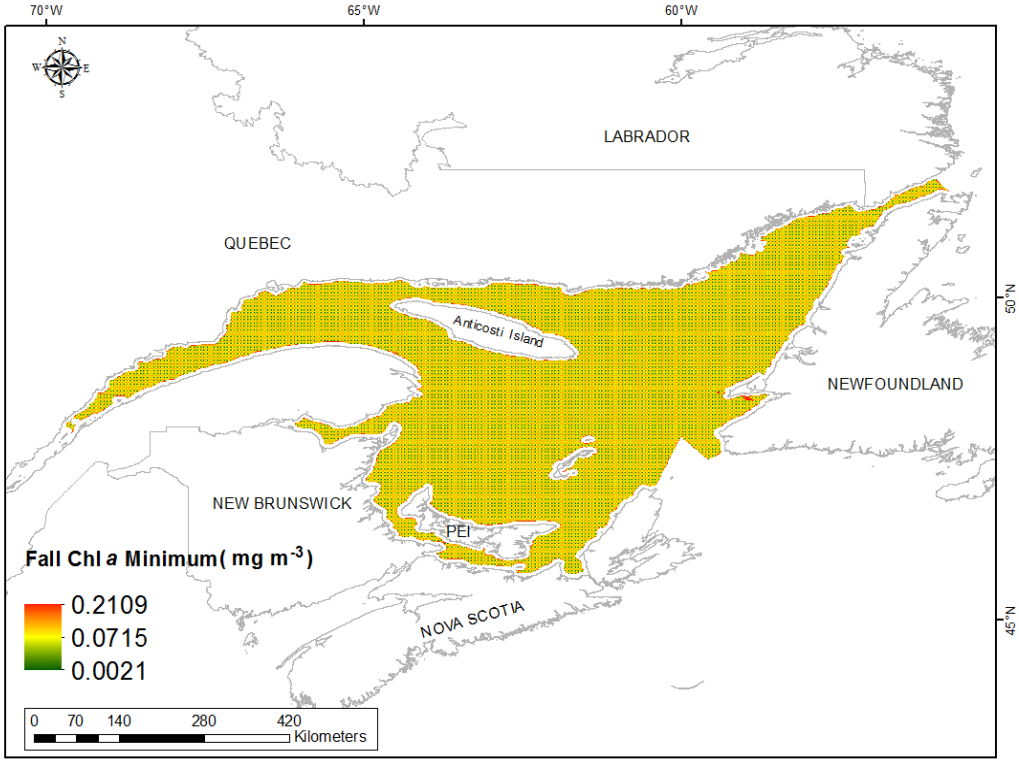

Fig. 339. Prediction standard error surface of MODIS Case I Fall Chlorophyll *a* Minimum (mg m^{-3}).

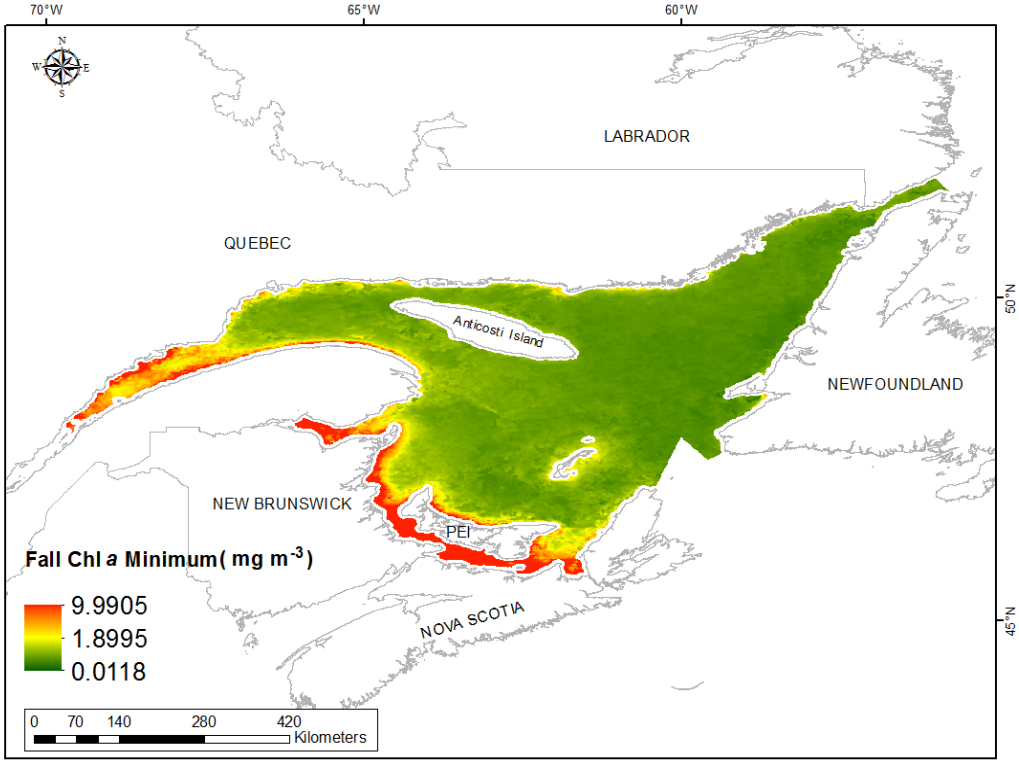

Fig. 340. Interpolated prediction surface of MODIS Case I Fall Chlorophyll *a* Minimum (mg m^{-3}).

MODIS Case I Fall Chlorophyll *a* Maximum

This variable displayed a right-skewed distribution with kurtosis prior to modeling (Table 137, Fig. 341). The data were higher than predicted by a normal distribution at the upper range and lower than predicted at mid values (Fig. 342). The areas of under- and over-prediction showed a strong spatial pattern over the spatial extent (Fig. 342).

The semivariogram showed moderate autocorrelation present in the data and the model showed a very good fit between measured and predicted values (Fig. 343). The model showed good cross-validation statistics (Table 138) indicating that it was good at prediction. The error map showed medium to high error in a grid-like pattern over the study extent (Fig. 344). The kriged surface is presented in Fig. 345.

Table 137. Distributional properties of MODIS Case I Fall Chlorophyll *a* Maximum (mg m^{-3}).

Property	Value
Number of Observations	74353
Minimum	0.911
Maximum	30.755
Mean	3.999
Median	3.170
Standard Deviation	2.872
Skewness	1.834
Kurtosis	7.316

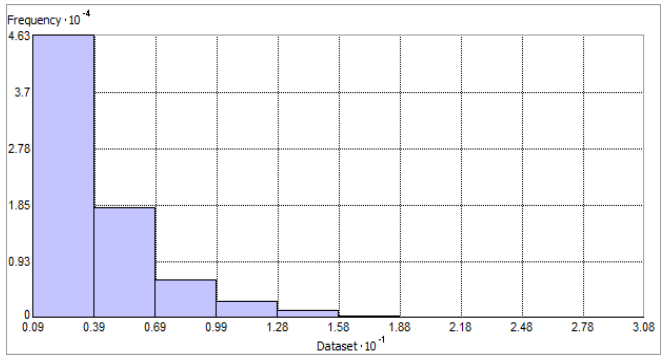

Fig. 341. Distribution of MODIS Case I Fall Chlorophyll *a* Maximum (mg m^{-3}). Histogram was illustrated using 10 bins. X and Y axes are shown at 10^{-1} and 10^{-4} respectively.

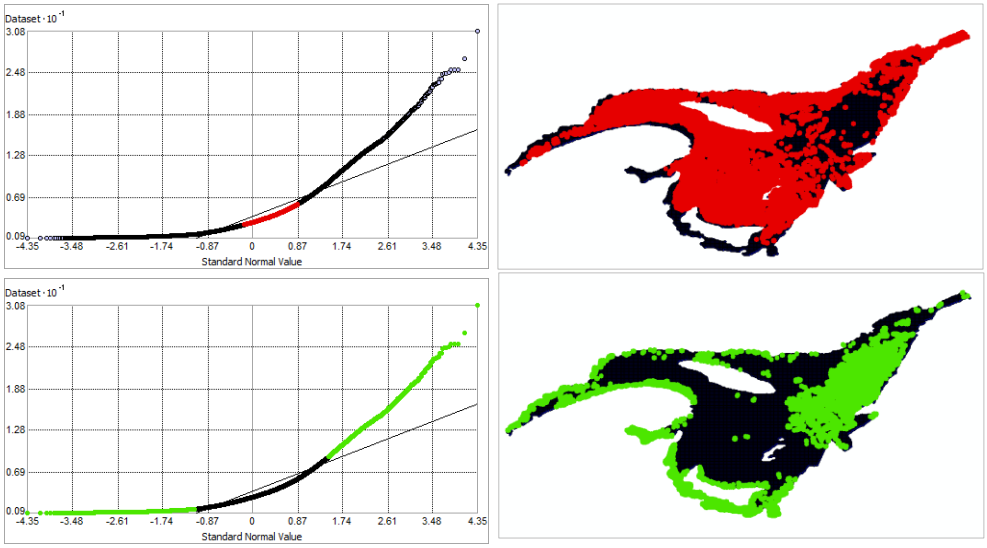

Fig. 342. Normal Q-Q plot for data values of MODIS Case I Fall Chlorophyll *a* Maximum (mg m^{-3}). Points falling under (upper panel) and over (bottom panel) the reference line are mapped.

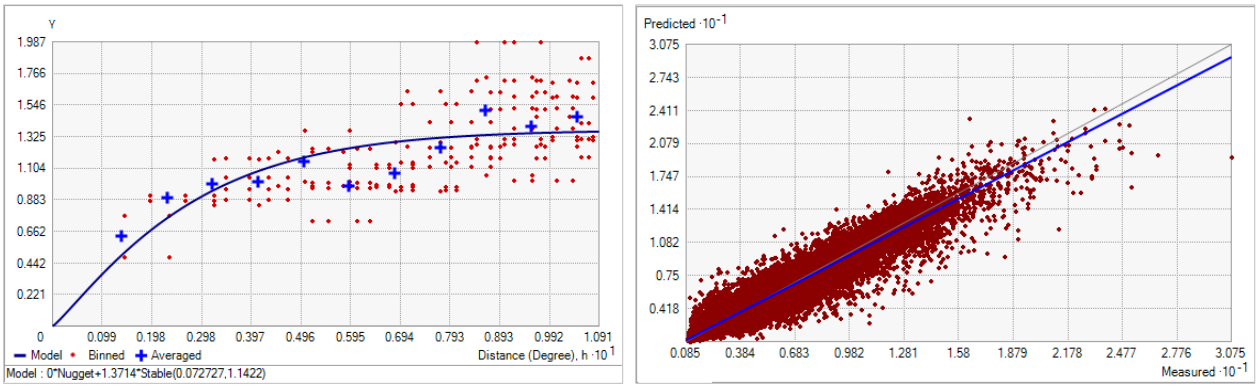

Fig. 343. Left panel: Semivariogram of MODIS Case I Fall Chlorophyll *a* Maximum (mg m^{-3}). Binned values are shown as red dots; average points are shown as blue crosses; the model fit to the averaged values is shown as a blue line. Lag size: 0.009 degrees; number of lags: 12; Parameter: 1.142; Range: 0.073 degrees; Partial Sill: 1.371. Right panel: Scatterplot of predicted values versus observed values for the variable MODIS Case I Fall Chlorophyll *a* Maximum (mg m^{-3}).

Table 138. Results of cross-validation of the kriged model for MODIS Case I Fall Chlorophyll *a* Maximum (mg m^{-3}).

Prediction error	**Value**
Number of Observations	74353
Overall Mean Error	-0.003
Root Mean Square Prediction Error	0.715
Standardized Mean	-0.002
Standardized Root Mean Square Prediction Error	0.930
Average Standard Error	0.763

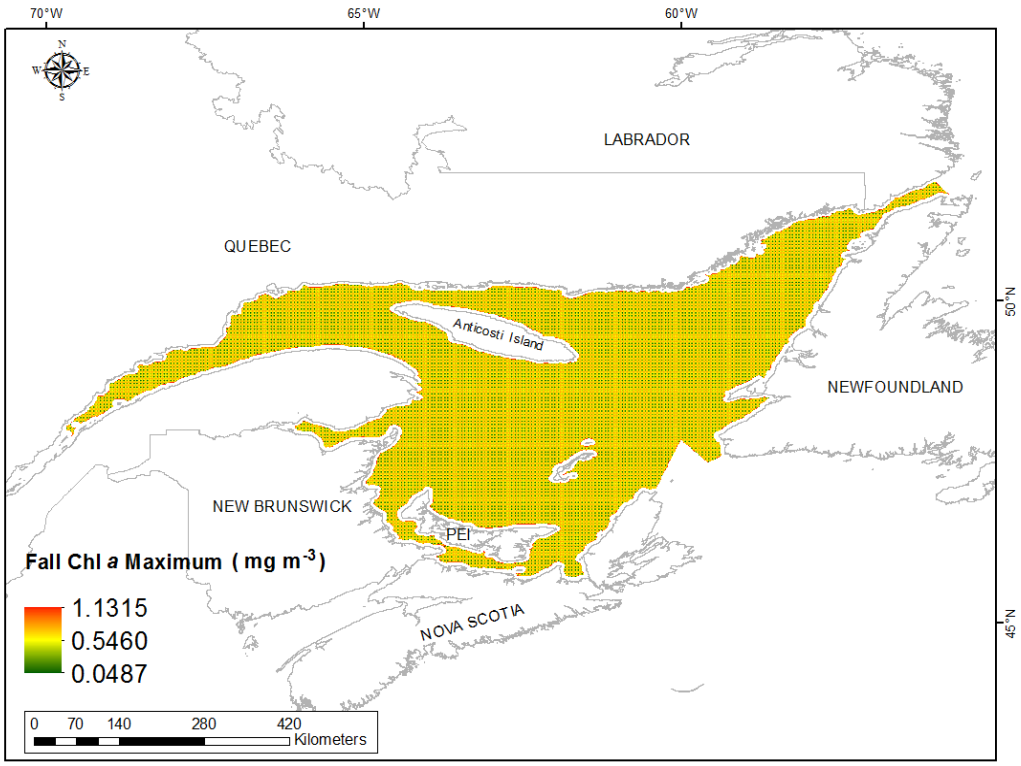

Fig. 344. Prediction standard error surface of MODIS Case I Fall Chlorophyll *a* Maximum (mg m^{3}).

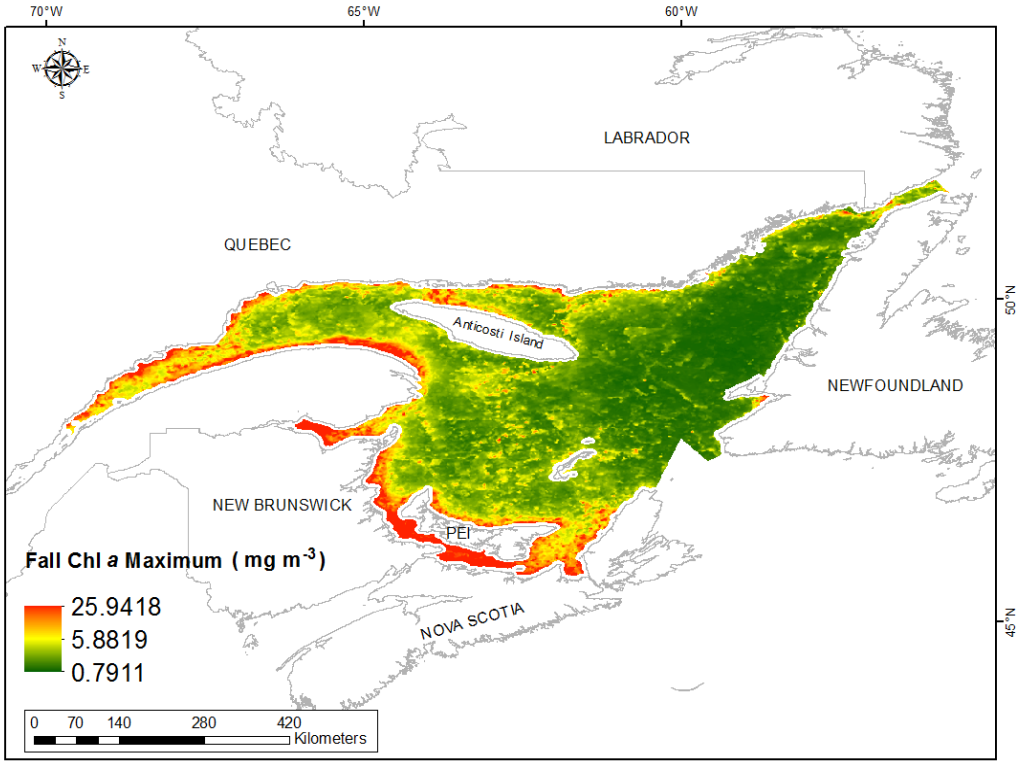

Fig. 345. Interpolated prediction surface of MODIS Case I Fall Chlorophyll *a* Maximum (mg m^{-3}).

MODIS Case I Fall Chlorophyll *a* Range

This variable displayed a right-skewed distribution with kurtosis prior to modeling (Table 139, Fig. 346). The data were higher than predicted by a normal distribution at the upper range and lower than predicted at mid values (Fig. 347). The areas of under- and over-prediction showed a strong spatial pattern over the spatial extent (Fig. 347).

The semivariogram showed moderate autocorrelation present in the data and the model showed a very good fit between measured and predicted values (Fig. 348). The model showed good cross-validation statistics (Table 140) indicating that it was good at prediction. The error map showed medium to high error in a grid-like pattern over the study extent (Fig. 349). The kriged surface is presented in Fig. 350.

Table 139. Distributional properties of MODIS Case I Fall Chlorophyll *a* Range (mg m^{-3}).

Property	Value
Number of Observations	74353
Minimum	0.230
Maximum	22.918
Mean	2.815
Median	2.245
Standard Deviation	2.146
Skewness	1.639
Kurtosis	6.980

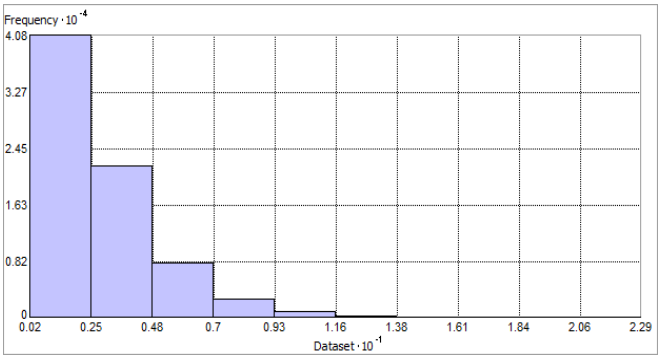

Fig. 346. Distribution of MODIS Case I Fall Chlorophyll *a* Range (mg m^{-3}). Histogram was illustrated using 10 bins. X and Y axes are shown at 10^{-1} and 10^{-4} respectively.

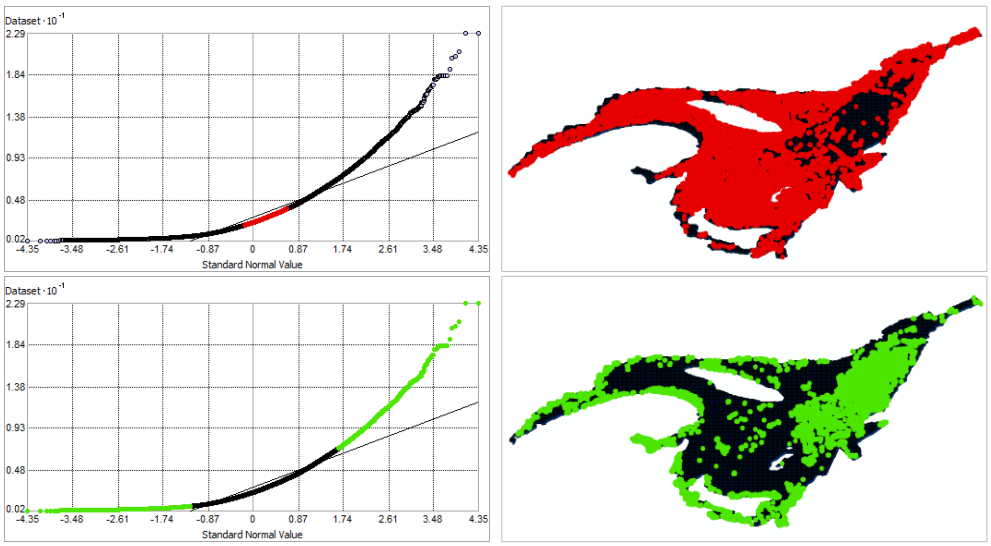

Fig. 347. Normal Q-Q plot for data values of MODIS Case I Fall Chlorophyll *a* Range (mg m^{-3}). Points falling under (upper panel) and over (bottom panel) the reference line are mapped.

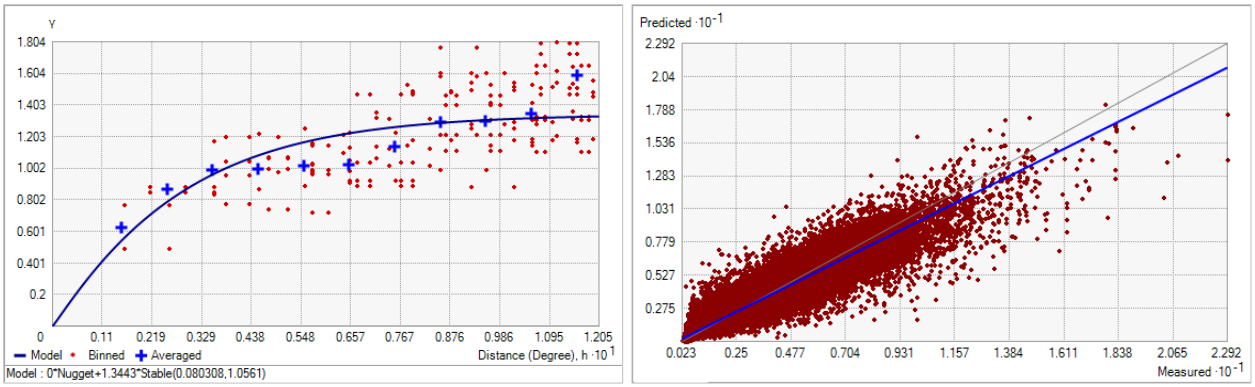

Fig. 348. Left panel: Semivariogram of MODIS Case I Fall Chlorophyll *a* Range (mg m^{-3}). Binned values are shown as red dots; average points are shown as blue crosses; the model fit to the averaged values is shown as a blue line. Lag size: 0.010 degrees; number of lags: 12; Parameter: 1.056; Range: 0.080 degrees; Partial Sill: 1.344. Right panel: Scatterplot of predicted values versus observed values for the variable MODIS Case I Fall Chlorophyll *a* Range (mg m^{-3}).

Table 140. Results of cross-validation of the kriged model for MODIS Case I Fall Chlorophyll *a* Range.

Prediction error	**Value**
Number of Observations	74353
Overall Mean Error	-0.002
Root Mean Square Prediction Error	0.722
Standardized Mean	-0.001
Standardized Root Mean Square Prediction Error	0.929
Average Standard Error	0.772

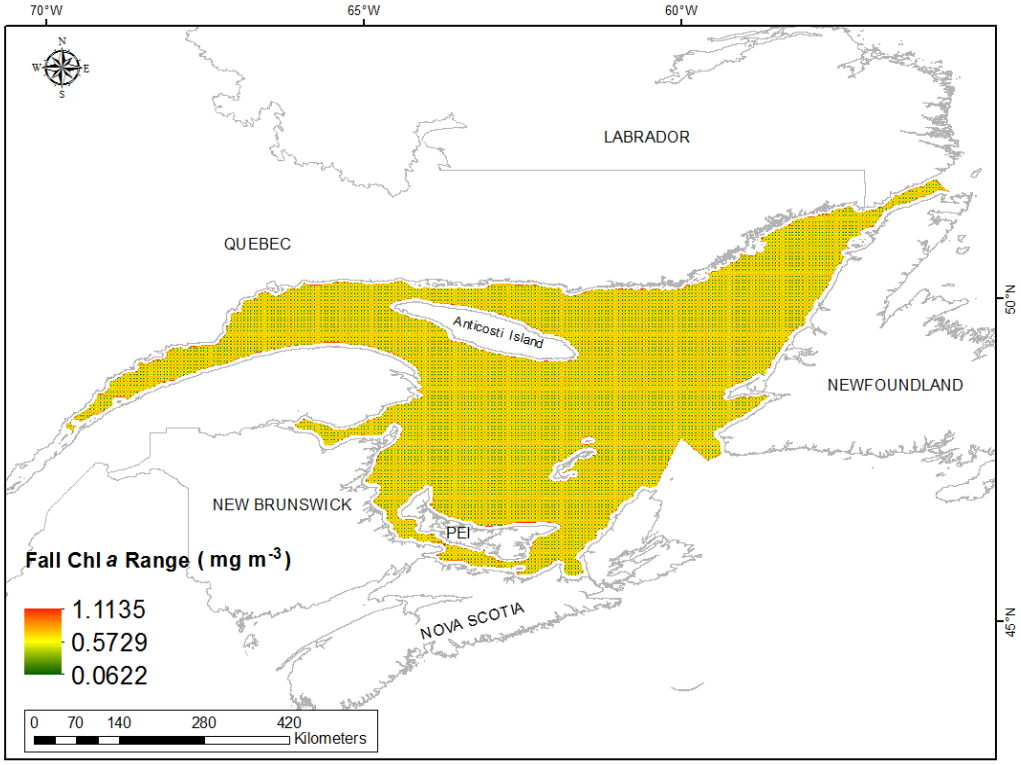

Fig. 349. Prediction standard error surface of MODIS Case I Fall Chlorophyll *a* Range (mg m^{-3}).

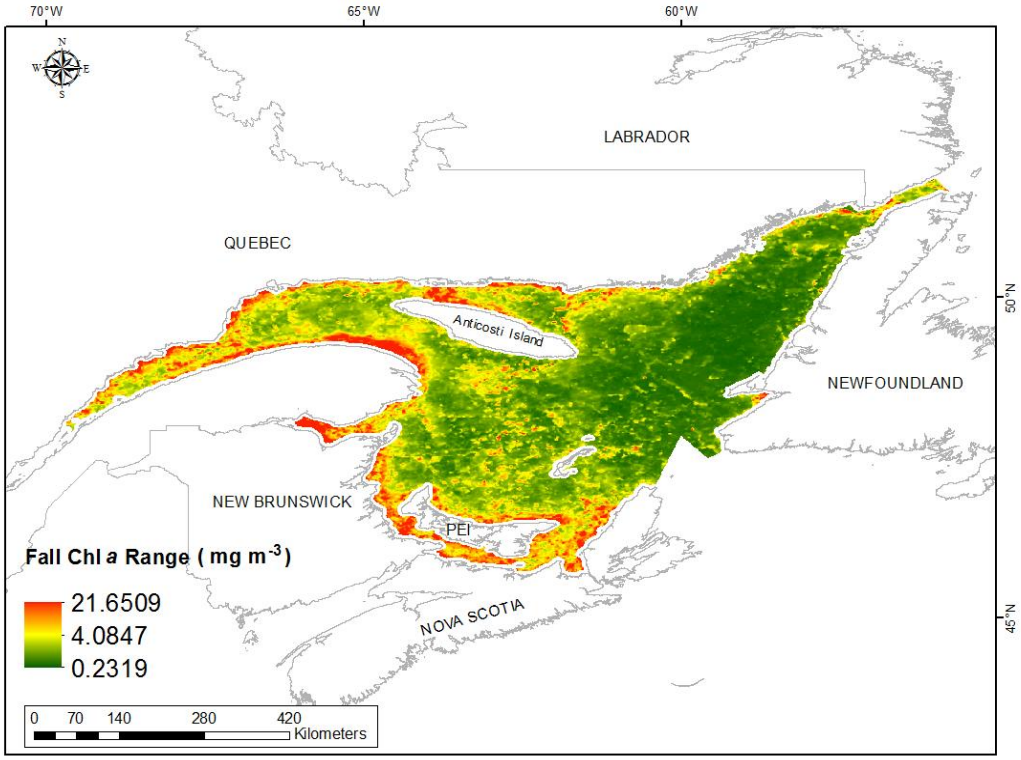

Fig. 350. Interpolated prediction surface of MODIS Case I Fall Chlorophyll *a* Range (mg m^{-3}).

MODIS Case I Annual Chlorophyll *a* Mean

This variable displayed a right-skewed distribution with kurtosis prior to modeling (Table 141, Fig. 351). The data were higher than predicted by a normal distribution at the upper range and lower than predicted at mid values (Fig. 352). The areas of under- and over-prediction showed a strong spatial pattern over the spatial extent (Fig. 352).

The semivariogram showed moderate autocorrelation present in the data and the model showed a very good fit between measured and predicted values (Fig. 353). The model showed good cross-validation statistics (Table 142) indicating that it was good at prediction. The error map showed relatively moderate error over the study extent (Fig. 354). The kriged surface is presented in Fig. 355.

Table 141. Distributional properties of MODIS Case I Annual Chlorophyll *a* Mean (mg m^{-3}).

Property	Value
Number of Observations	74353
Minimum	0.714
Maximum	12.798
Mean	2.206
Median	1.668
Standard Deviation	1.768
Skewness	2.244
Kurtosis	8.449

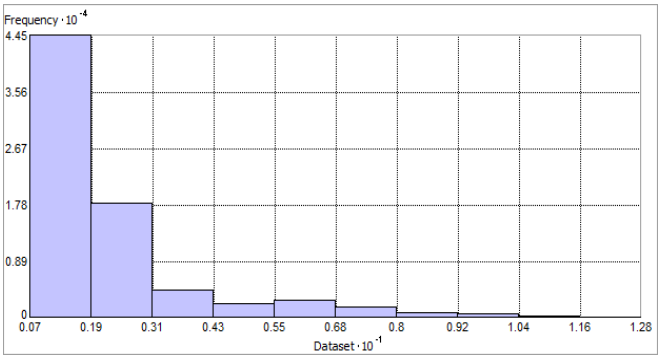

Fig. 351. Distribution of MODIS Case I Annual Chlorophyll *a* Mean (mg m^{-3}). Histogram was illustrated using 10 bins. X and Y axes are shown at 10^{-1} and 10^{-4} respectively.

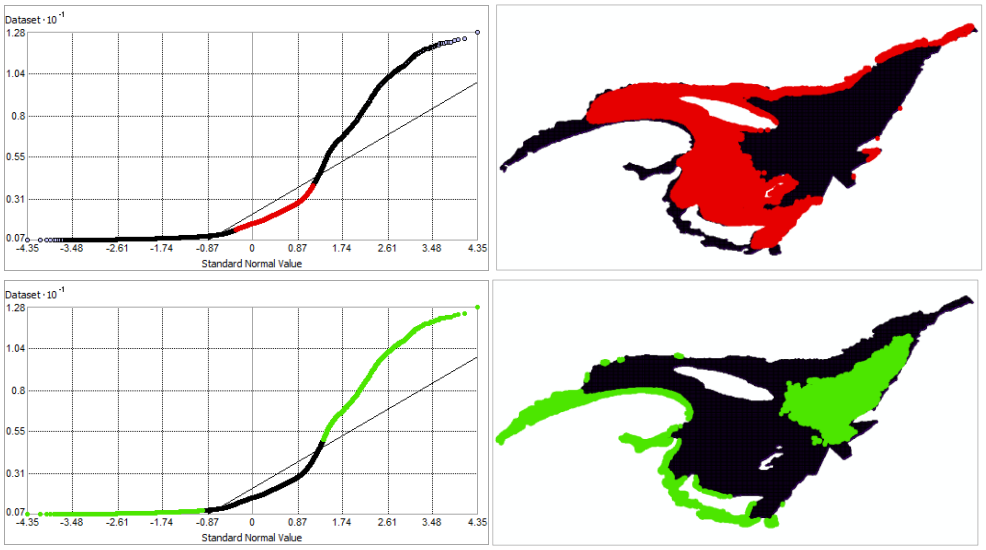

Fig. 352. Normal Q-Q plot for data values of MODIS Case I Annual Chlorophyll *a* Mean (mg m^{-3}). Points falling under (upper panel) and over (bottom panel) the reference line are mapped.

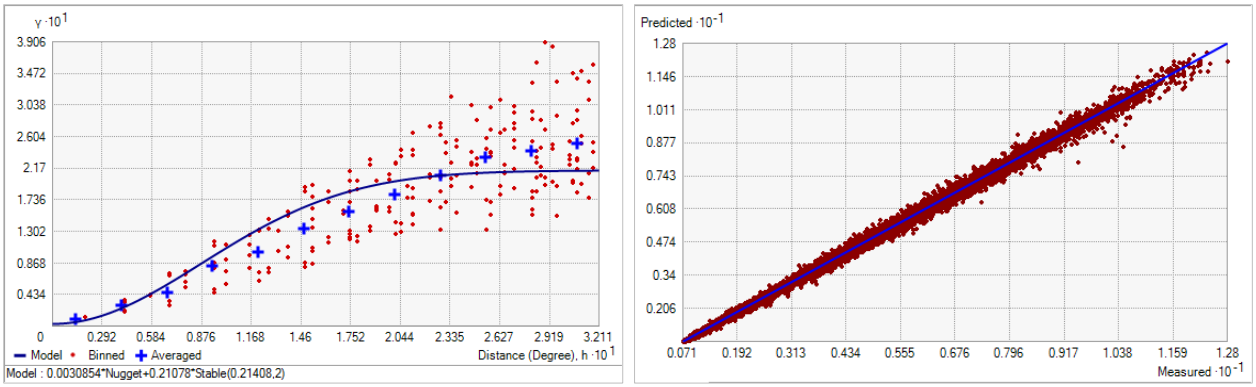

Fig. 353. Left panel: Semivariogram of MODIS Case I Annual Chlorophyll *a* Mean (mg m^{-3}). Binned values are shown as red dots; average points are shown as blue crosses; the model fit to the averaged values is shown as a blue line. Lag size: 0.027 degrees; number of lags: 12; Parameter: 2; Range: 0.214 degrees; Partial Sill: 0.211. Right panel: Scatterplot of predicted values versus observed values for the variable MODIS Case I Annual Chlorophyll *a* Mean (mg m^{-3}).

Table 142. Results of cross-validation of the kriged model for the MODIS Case I Annual Chlorophyll *a* Mean (mg m^{-3}).

Prediction error	**Value**
Number of Observations	74353
Overall Mean Error	0.001
Root Mean Square Prediction Error	0.070
Standardized Mean	0.022
Standardized Root Mean Square Prediction Error	1.131
Average Standard Error	0.061

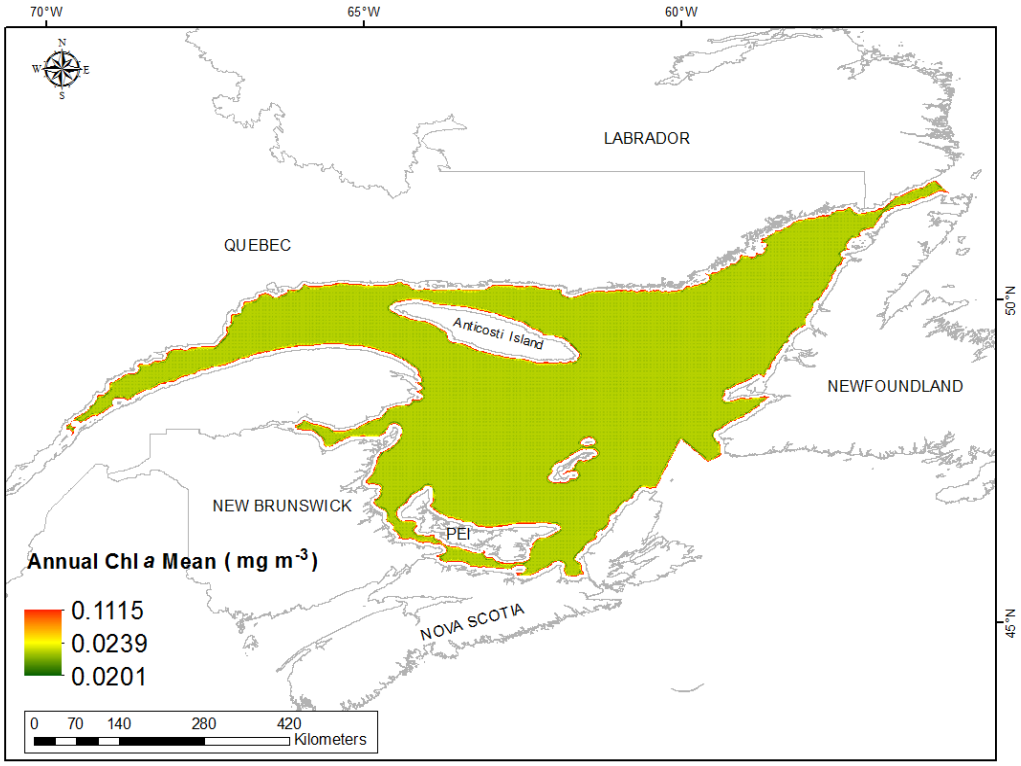

Fig. 354. Prediction standard error surface of MODIS Case I Annual Chlorophyll *a* Mean (mg m^{-3}).

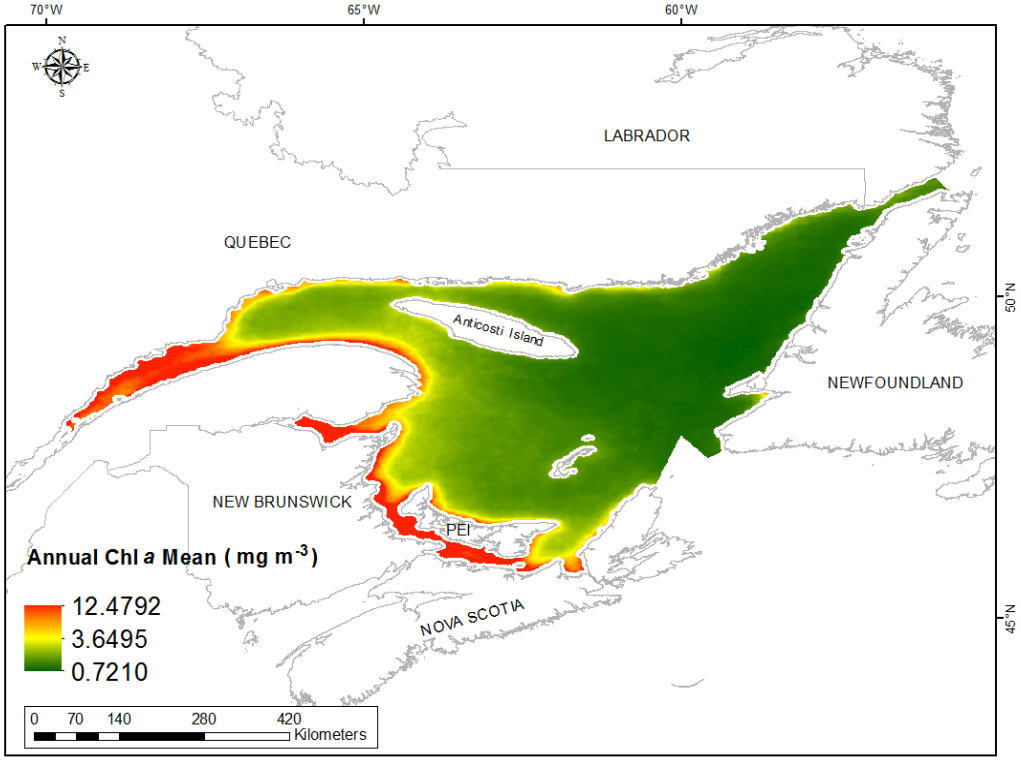

Fig. 355. Interpolated prediction surface of MODIS Case I Annual Chlorophyll *a* Mean (mg m^{-3}).

MODIS Case I Annual Chlorophyll *a* Minimum

This variable displayed a right-skewed distribution with kurtosis prior to modeling (Table 143, Fig. 356). The data were higher than predicted by a normal distribution at the upper range and lower than predicted at mid values (Fig. 357). The areas of under- and over-prediction showed a strong spatial pattern over the spatial extent (Fig. 357).

The semivariogram showed moderate autocorrelation present in the data and the model showed a very good fit between measured and predicted values (Fig. 358). The model showed good cross-validation statistics (Table 144) indicating that it was good at prediction. The error map showed relatively moderate error over the study extent (Fig. 359). The kriged surface is presented in Fig. 360.

Table 143. Distributional properties of MODIS Case I Annual Chlorophyll *a* Minimum (mg m^{-3}).

Property	Value
Number of Observations	74353
Minimum	0.527
Maximum	10.816
Mean	1.600
Median	1.137
Standard Deviation	1.389
Skewness	2.622
Kurtosis	10.635

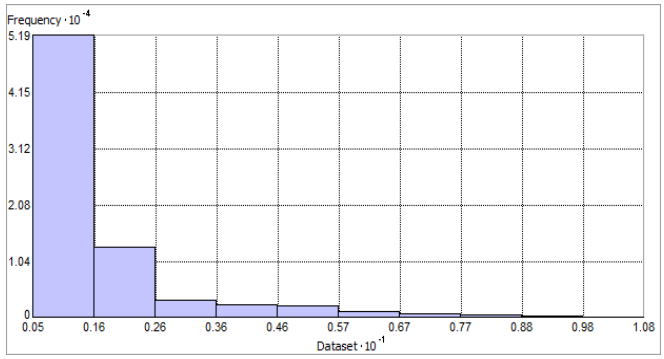

Fig. 356. Distribution of MODIS Case I Annual Chlorophyll *a* Minimum (mg m^{-3}). Histogram was illustrated using 10 bins. X and Y axes are shown at 10^{-1} and 10^{-4} respectively.

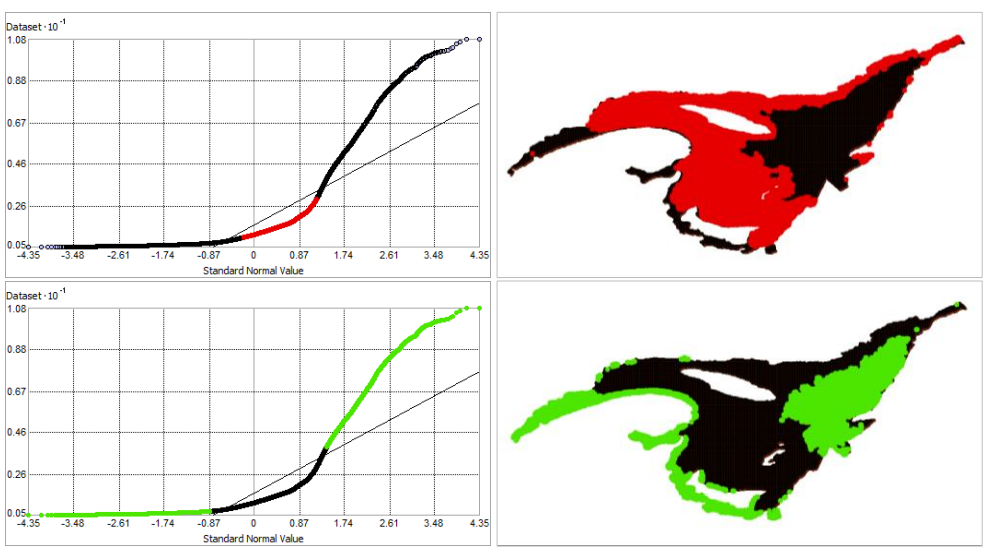

Fig. 357. Normal Q-Q plot for data values of MODIS Case I Annual Chlorophyll *a* Minimum (mg m^{-3}). Points falling under (upper panel) and over (bottom panel) the reference line are mapped.

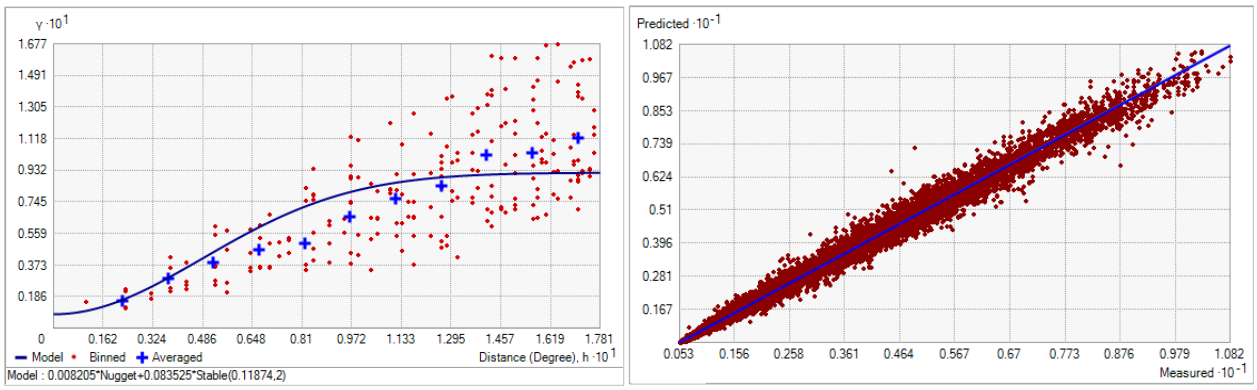

Fig. 358. Left panel: Semivariogram of MODIS Case I Annual Chlorophyll *a* Minimum (mg m^{-3}). Binned values are shown as red dots; average points are shown as blue crosses; the model fit to the averaged values is shown as a blue line. Lag size: 0.015 degrees; number of lags: 12; Parameter: 2; Range: 0.119 degrees; Partial Sill: 0.084. Right panel: Scatterplot of predicted values versus observed values for the variable MODIS Case I Annual Chlorophyll *a* Minimum (mg m^{-3}).

Table 144. Results of cross-validation of the kriged model for MODIS Case I Annual Chlorophyll *a* Minimum (mg m^{-3}).

Prediction error	**Value**
Number of Observations	74353
Overall Mean Error	8.993×10^{-4}
Root Mean Square Prediction Error	0.110
Standardized Mean	0.010
Standardized Root Mean Square Prediction Error	1.064
Average Standard Error	0.102

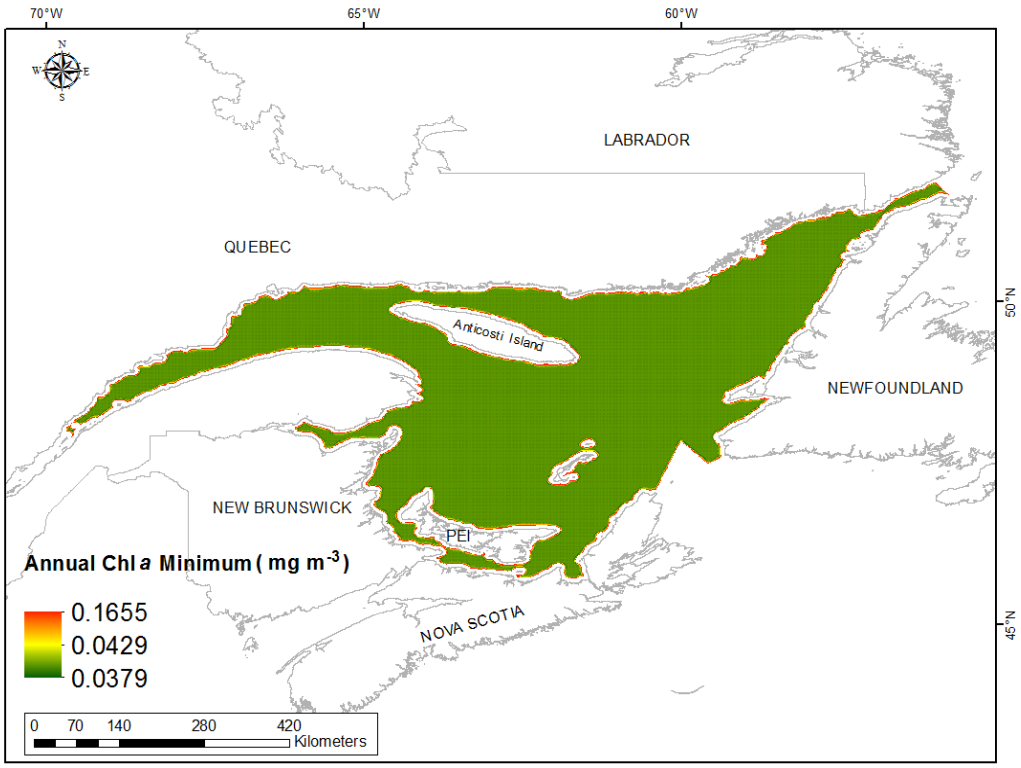

Fig. 359. Prediction standard error surface of MODIS Case I Annual Chlorophyll *a* Minimum (mg m^{-3}).

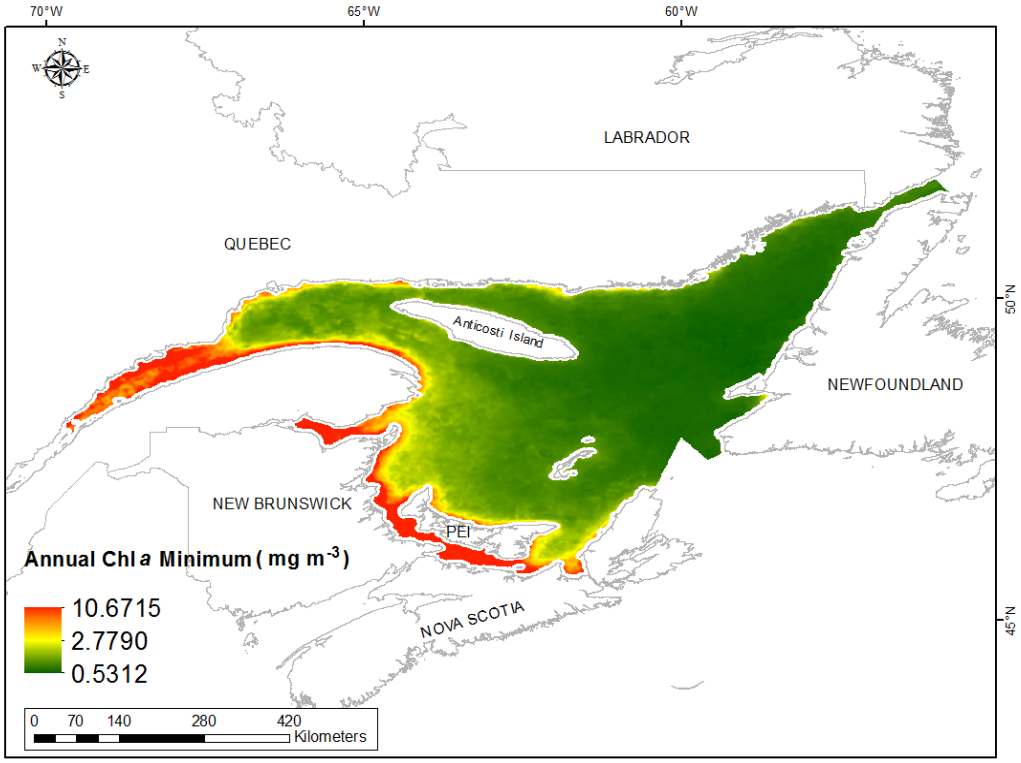

Fig. 360. Interpolated prediction surface of MODIS Case I Annual Chlorophyll *a* Minimum (mg m^{-3}).

MODIS Case I Annual Chlorophyll *a* Maximum

This variable displayed a right-skewed distribution with kurtosis prior to modeling (Table 145, Fig. 361). The data were higher than predicted by a normal distribution at the upper range and lower than predicted at mid values (Fig. 362). The areas of under- and over-prediction showed a strong spatial pattern over the spatial extent (Fig. 362).

The semivariogram showed moderate autocorrelation present in the data and the model showed a very good fit between measured and predicted values (Fig. 363). The model showed good cross-validation statistics (Table 146) indicating that it was good at prediction. The error map showed low error over the study extent (Fig. 364). The kriged surface is presented in Fig. 365.

Table 145. Distributional properties of MODIS Case I Annual Chlorophyll *a* Maximum (mg m^{-3}).

Property	Value
Number of Observations	74353
Minimum	0.823
Maximum	18.666
Mean	3.023
Median	2.371
Standard Deviation	2.253
Skewness	2.087
Kurtosis	7.937

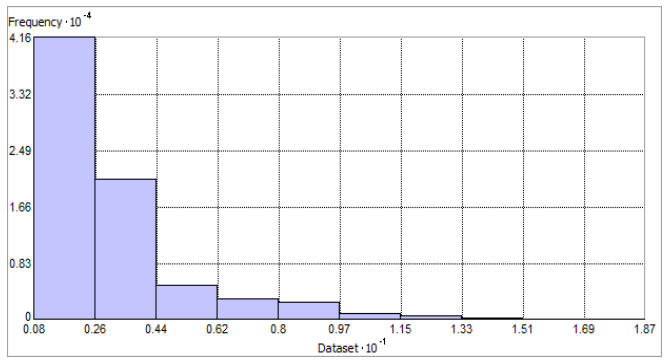

Fig. 361. Distribution of MODIS Case I Annual Chlorophyll *a* Maximum (mg m^{-3}). Histogram was illustrated using 10 bins. X and Y axes are shown at 10^{-1} and 10^{-4} respectively.

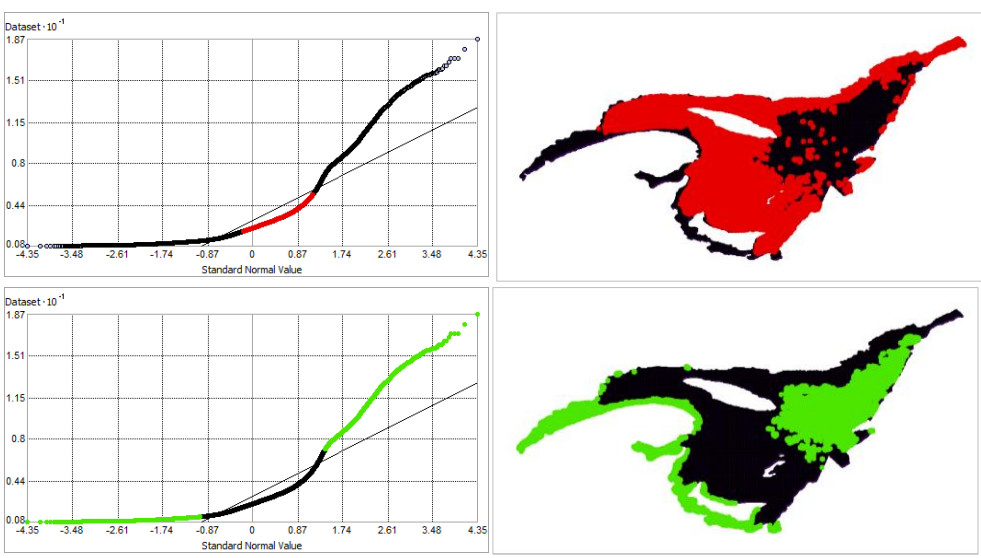

Fig. 362. Normal Q-Q plot for data values of MODIS Case I Annual Chlorophyll *a* Maximum (mg m^{-3}). Points falling under (upper panel) and over (bottom panel) the reference line are mapped.

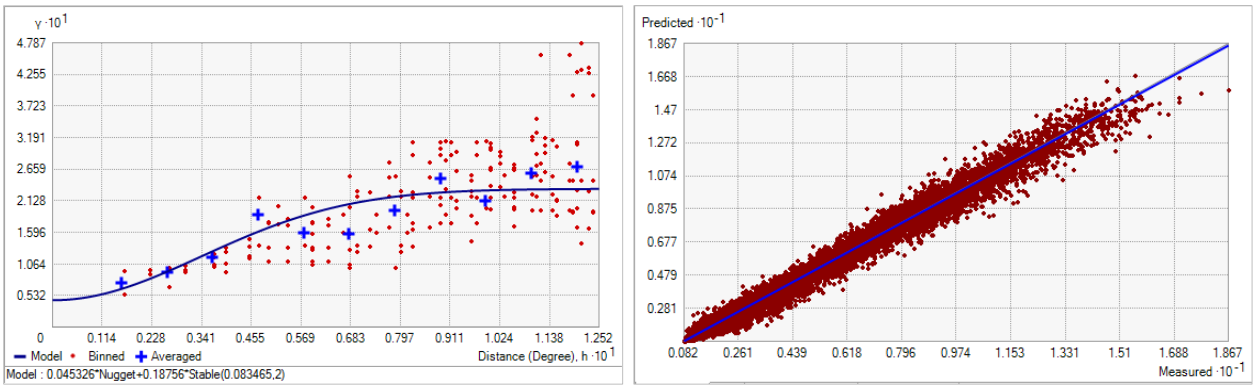

Fig. 363. Left panel: Semivariogram of MODIS Case I Annual Chlorophyll *a* Maximum (mg m^{-3}). Binned values are shown as red dots; average points are shown as blue crosses; the model fit to the averaged values is shown as a blue line. Lag size: 0.010 degrees; number of lags: 12; Parameter: 2; Range: 0.083 degrees; Partial Sill: 0.188. Right panel: Scatterplot of predicted values versus observed values for the variable MODIS Case I Annual Chlorophyll *a* Maximum (mg m^{-3}).

Table 146. Results of cross-validation of the kriged model for MODIS Case I Annual Chlorophyll *a* Maximum (mg m^{-3}).

Prediction error	**Value**
Number of Observations	74353
Overall Mean Error	-1.286×10^{-4}
Root Mean Square Prediction Error	0.236
Standardized Mean	6.611×10^{-4}
Standardized Root Mean Square Prediction Error	0.957
Average Standard Error	0.243

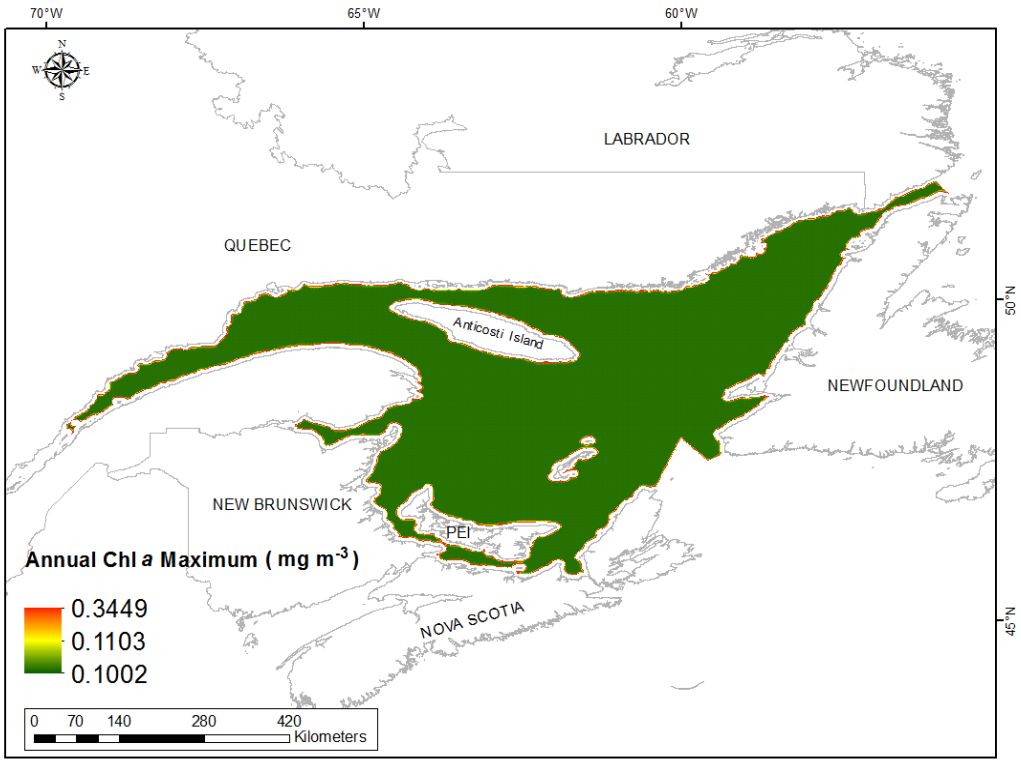

Fig. 364. Prediction standard error surface of MODIS Case I Annual Chlorophyll *a* Maximum (mg m^{-3}).

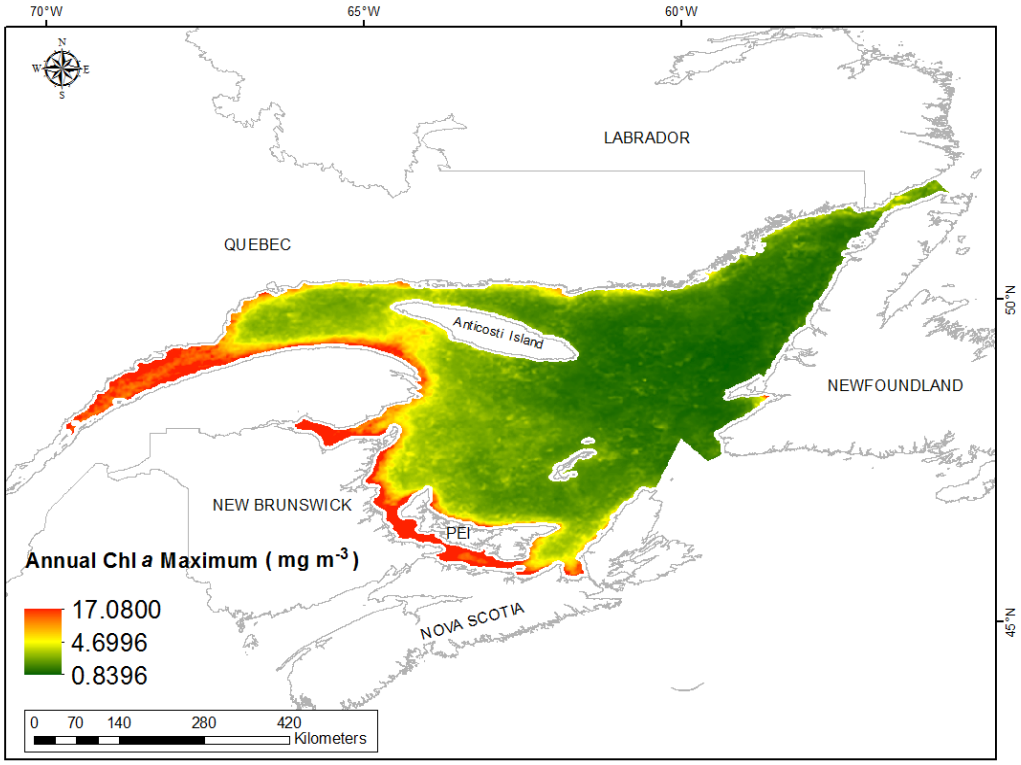

Fig. 365. Interpolated prediction surface of MODIS Case I Annual Chlorophyll *a* Maximum (mg m^{-3}).

MODIS Case I Annual Chlorophyll *a* Range

This variable displayed a right-skewed distribution with kurtosis prior to modeling (Table 147, Fig. 366). The data were higher than predicted by a normal distribution at the upper range and lower than predicted at mid values (Fig. 367). The areas of under- and over-prediction showed a strong spatial pattern over the spatial extent (Fig. 367).

The semivariogram showed moderate autocorrelation present in the data and the model showed a very good fit between measured and predicted values (Fig. 368). The model showed good cross-validation statistics (Table 148) indicating that it was good at prediction. The error map showed medium to high error in a grid-like pattern over the study extent (Fig. 369). The kriged surface is presented in Fig. 370.

Table 147. Distributional properties of MODIS Case I Annual Chlorophyll *a* Range (mg m^{-3}).

Property	Value
Number of Observations	74353
Minimum	0.170
Maximum	9.361
Mean	1.423
Median	1.156
Standard Deviation	1.000
Skewness	1.674
Kurtosis	6.664

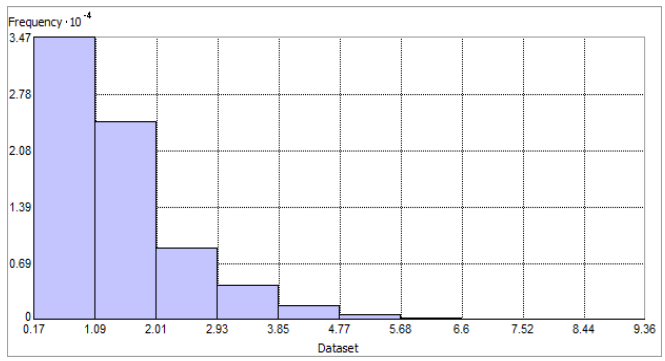

Fig. 366. Distribution of MODIS Case I Annual Chlorophyll *a* Range (mg m^{-3}). Histogram was illustrated using 10 bins. Y axis is shown at 10^{-4}.

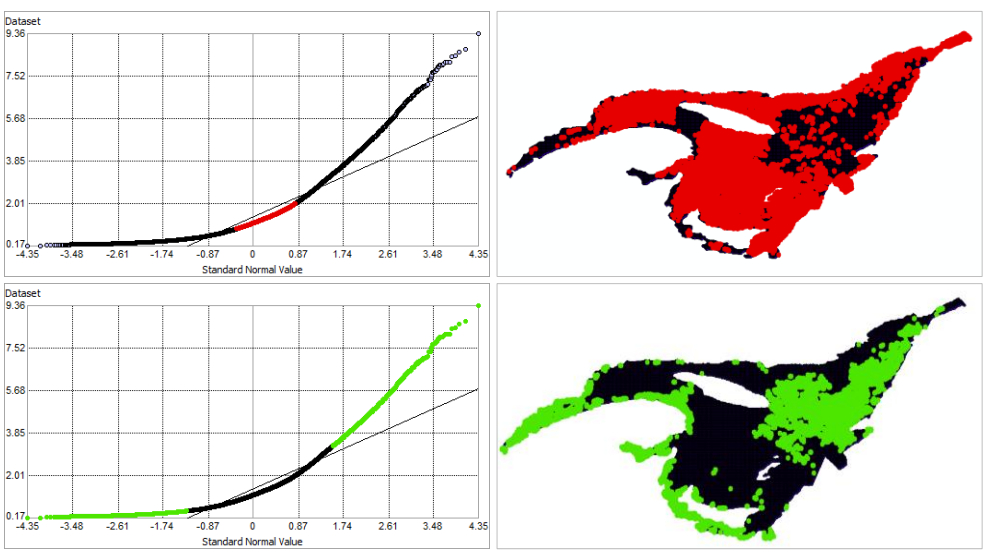

Fig. 367. Normal Q-Q plot for data values of MODIS Case I Annual Chlorophyll *a* Range (mg m^{-3}). Points falling under (upper panel) and over (bottom panel) the reference line are mapped.

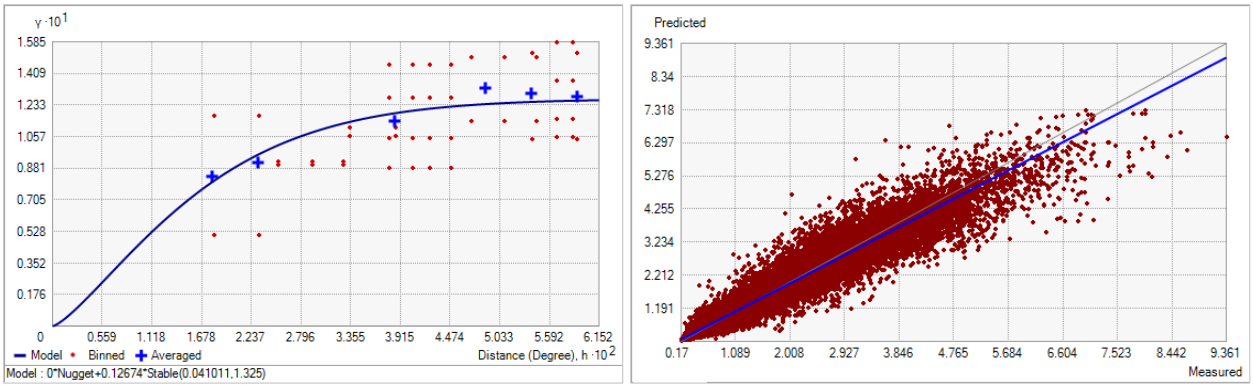

Fig. 368. Left panel: Semivariogram of MODIS Case I Annual Chlorophyll *a* Range (mg m^{-3}). Binned values are shown as red dots; average points are shown as blue crosses; the model fit to the averaged values is shown as a blue line. Lag size: 0.005 degrees; number of lags: 12; Parameter: 1.325; Range: 0.041 degrees; Partial Sill: 0.126. Right panel: Scatterplot of predicted values versus observed values for the variable MODIS Case I Annual Chlorophyll *a* Range (mg m^{-3}).

Table 148. Results of cross-validation of the kriged model for MODIS Case I Annual Chlorophyll *a* Range (mg m^{-3}).

Prediction error	**Value**
Number of Observations	74353
Overall Mean Error	-6.600×10^{-4}
Root Mean Square Prediction Error	0.248
Standardized Mean	-0.002
Standardized Root Mean Square Prediction Error	0.862
Average Standard Error	0.285

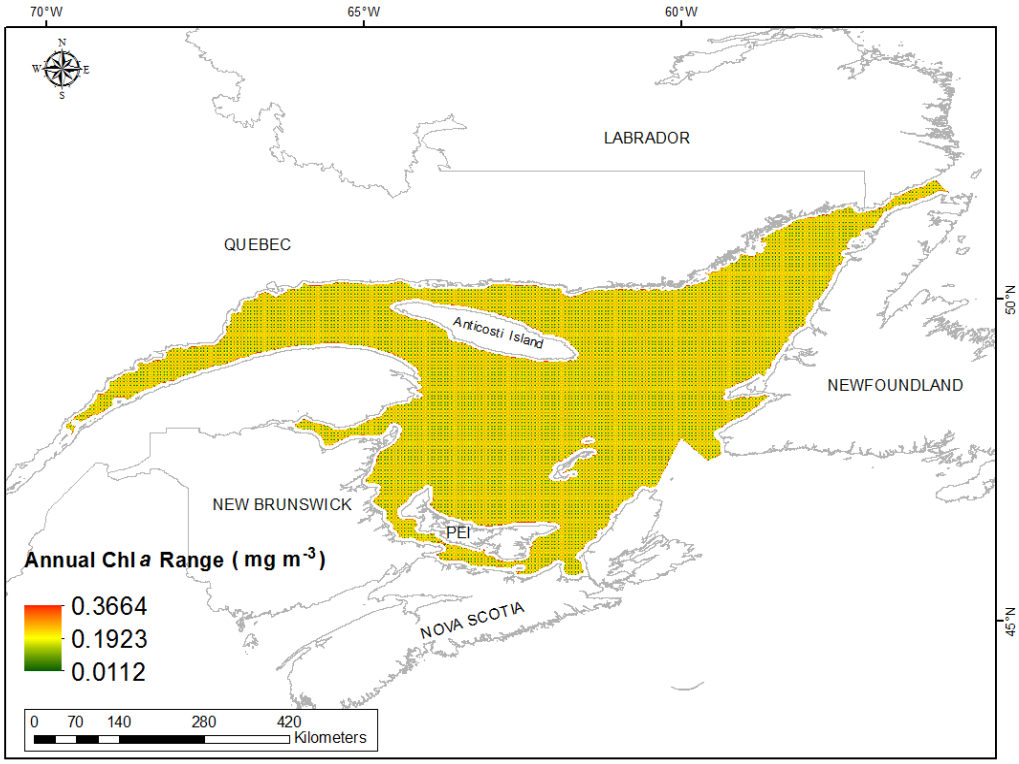

Fig. 369. Prediction standard error surface of MODIS Case I Annual Chlorophyll *a* Range (mg m^{-3}).

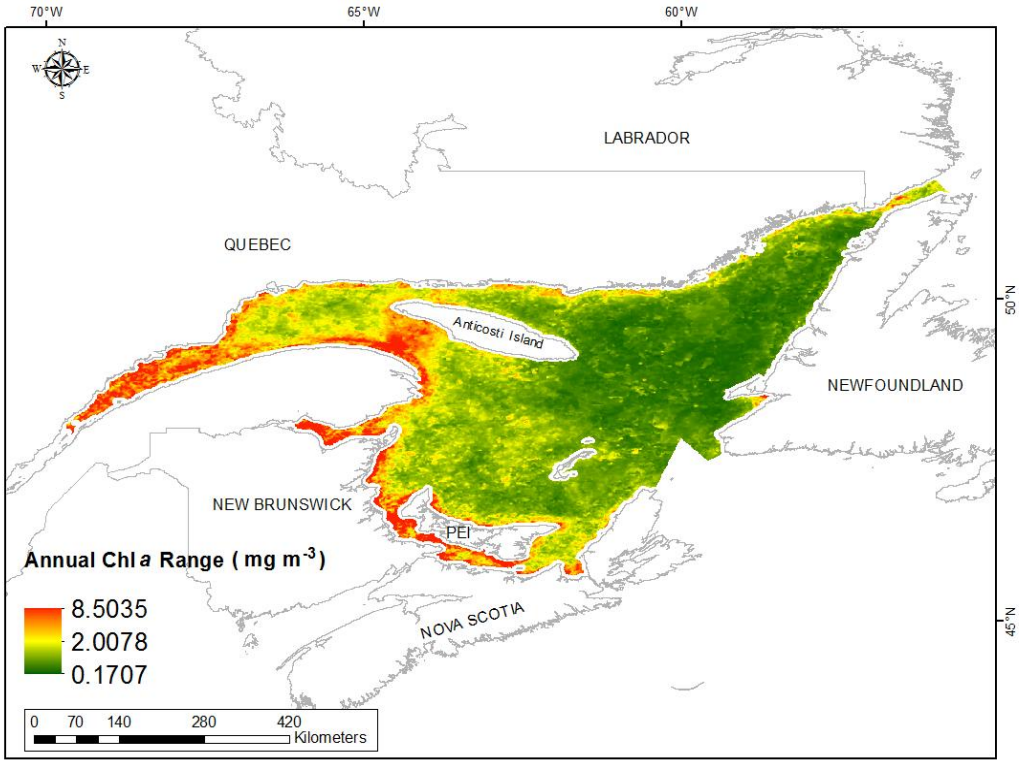

Fig. 370. Interpolated prediction surface of MODIS Case I Annual Chlorophyll *a* Range (mg m^{-3}).

MERIS Case II Spring Chlorophyll *a* Mean

This variable displayed a right-skewed distribution with kurtosis prior to modeling (Table 150, Fig. 371). The data were higher than predicted by a normal distribution at the upper range and lower than predicted at mid values (Fig. 372). The areas of under- and over-prediction showed a strong spatial pattern over the spatial extent (Fig. 372).

The semivariogram showed moderate autocorrelation present in the data and the model showed a very good fit between measured and predicted values (Fig. 373). However, the model showed poor cross-validation statistics (Table 150). The standardized root mean square was greater than 1 indicating that variability in the predictions has been underestimated. The error map showed low error over the study extent (Fig. 374). The kriged surface is presented in Fig. 375.

Table 149. Distributional properties of MERIS Case II Spring Chlorophyll *a* Mean (mg m^{-3}).

Property	Value
Number of Observations	74353
Minimum	0.4755
Maximum	6.0419
Mean	1.0630
Median	0.8928
Standard Deviation	0.6357
Skewness	2.8374
Kurtosis	12.7730

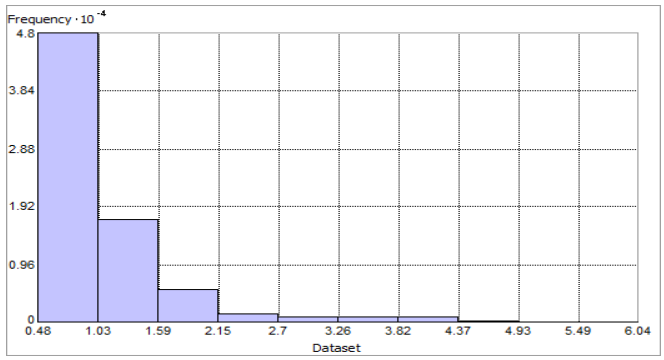

Fig. 371. Distribution of MERIS Case II Spring Chlorophyll *a* Mean (mg m^{-3}). Histogram was illustrated using 10 bins. Y axis is shown at 10^{-4}.

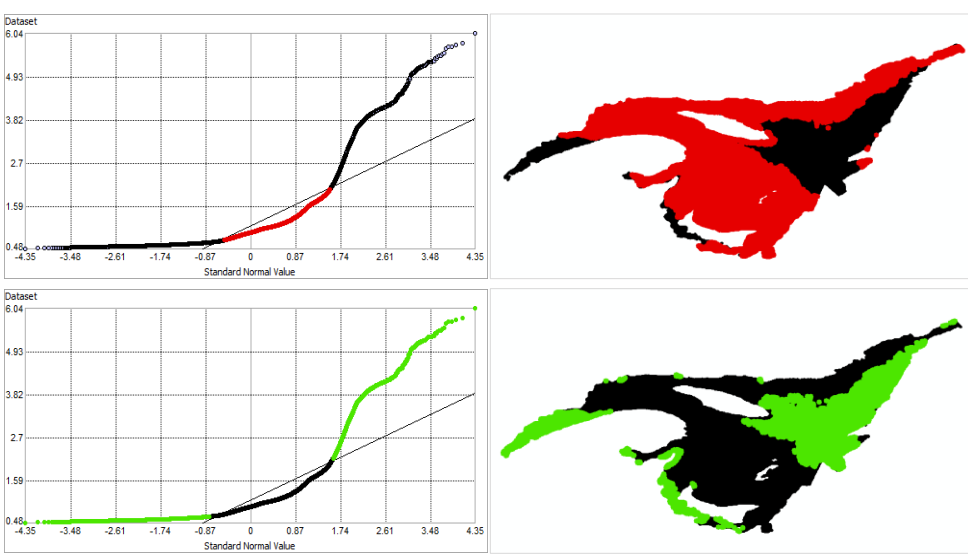

Fig. 372. Normal Q-Q plot for data values of MERIS Case II Spring Chlorophyll *a* Mean (mg m^{-3}). Points falling under (upper panel) and over (bottom panel) the reference line are mapped.

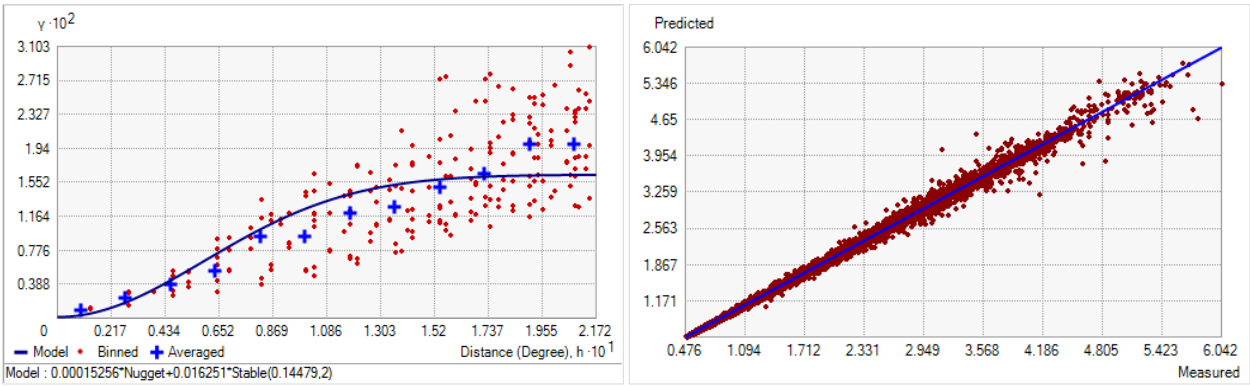

Fig. 373. Left panel: Semivariogram of MERIS Case II Spring Chlorophyll *a* Mean (mg m^{-3}). Binned values are shown as red dots; average points are shown as blue crosses; the model fit to the averaged values is shown as a blue line. Lag size: 0.018 degrees; number of lags: 12; Parameter: 2; Range: 0.145 degrees; Partial Sill: 0.016. Right panel: Scatterplot of predicted values versus observed values for the variable MERIS Case II Spring Chlorophyll *a* Mean (mg m^{-3}).

Table 150. Results of cross-validation of the kriged model for the MERIS Case II Spring Chlorophyll *a* Mean (mg m^{-3}).

Prediction error	**Value**
Number of Observations	74353
Overall Mean Error	5.132×10^{-5}
Root Mean Square Prediction Error	0.027
Standardized Mean	0.004
Standardized Root Mean Square Prediction Error	1.805
Average Standard Error	0.014

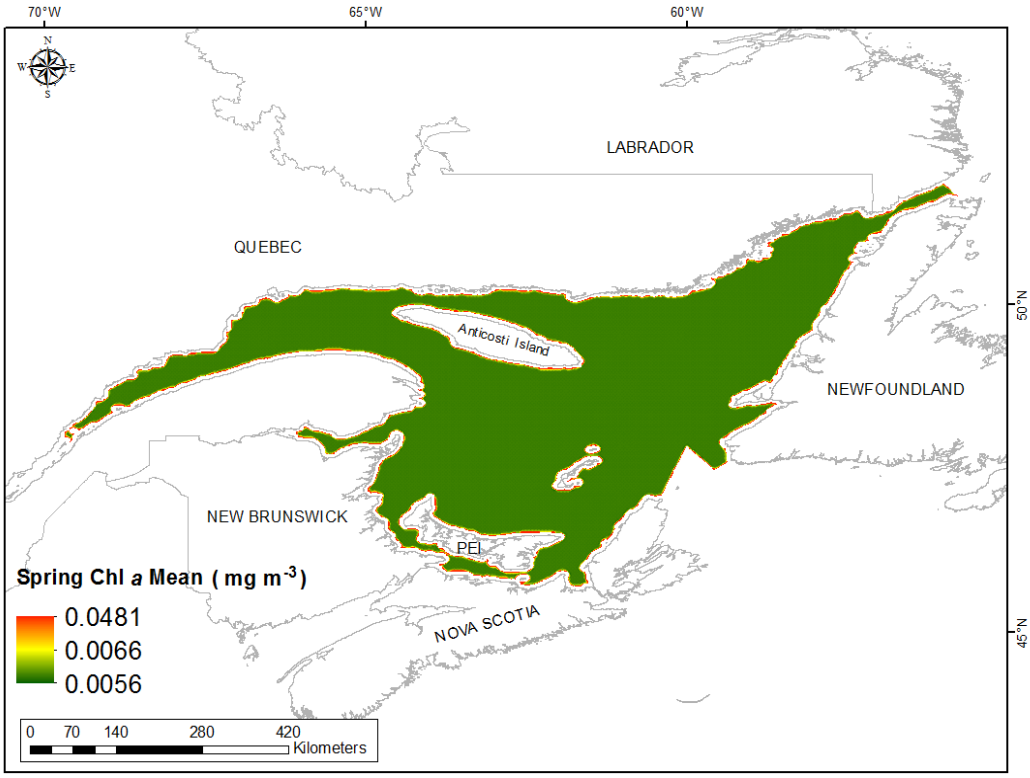

Fig. 374. Prediction standard error surface of MERIS Case II Spring Chlorophyll *a* Mean (mg m^{-3}).

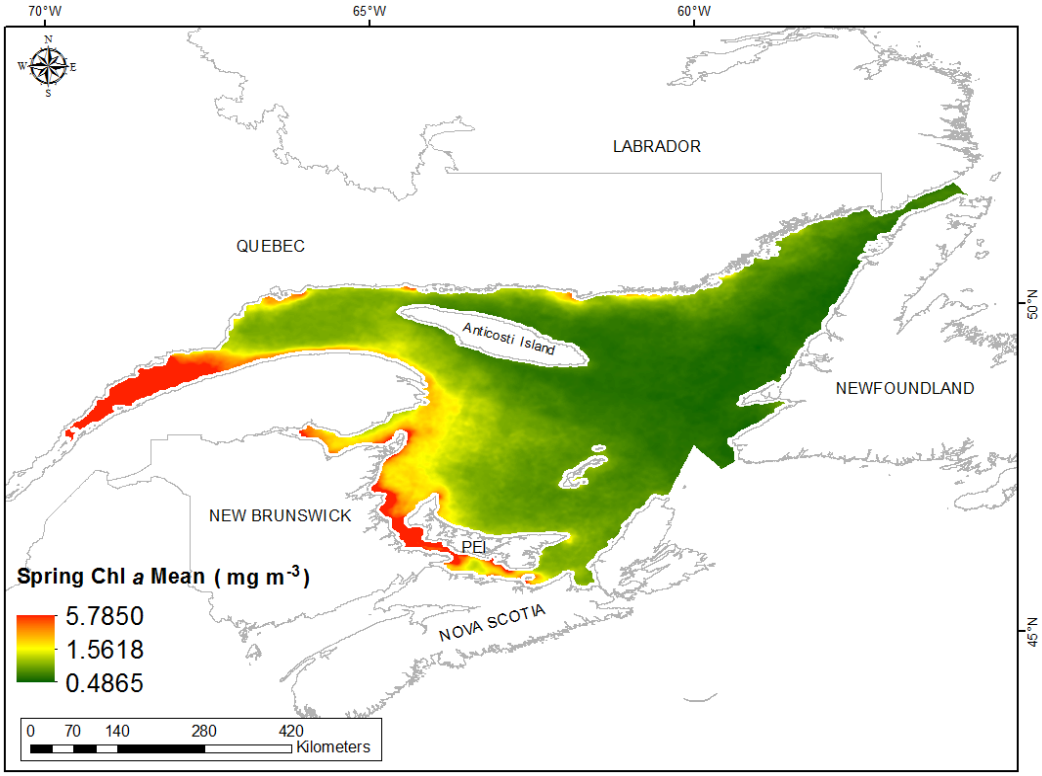

Fig. 375. Interpolated prediction surface of MERIS Case II Spring Chlorophyll *a* Mean (mg m^{-3}).

MERIS Case II Spring Chlorophyll *a* Minimum

This variable displayed a right-skewed distribution with kurtosis prior to modeling (Table 151, Fig. 376). The data were higher than predicted by a normal distribution at the upper range and lower than predicted at mid values (Fig. 377). The areas of under- and over-prediction showed a strong spatial pattern over the spatial extent (Fig. 377).

The semivariogram showed moderate autocorrelation present in the data and the model showed a very good fit between measured and predicted values (Fig. 378). However, the model showed poor cross-validation statistics (Table 152). The standardized root mean square was greater than 1 indicating that variability in the predictions has been underestimated. The error map showed low error over the study extent (Fig. 379). The kriged surface is presented in Fig. 380.

Table 151. Distributional properties of MERISCase II Spring Chlorophyll *a* Minimum (mg m^{-3}).

Property	Value
Number of Observations	74353
Minimum	0.343
Maximum	4.177
Mean	0.732
Median	0.610
Standard Deviation	0.378
Skewness	2.647
Kurtosis	11.772

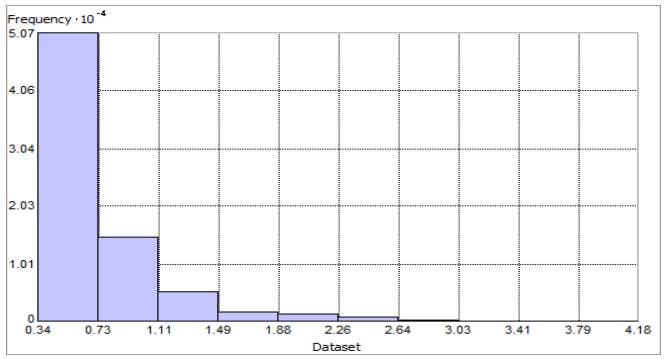

Fig. 376. Distribution of MERIS Case II Spring Chlorophyll *a* Minimum (mg m^{-3}). Histogram was illustrated using 10 bins. Y axis is shown at 10^{-4}.

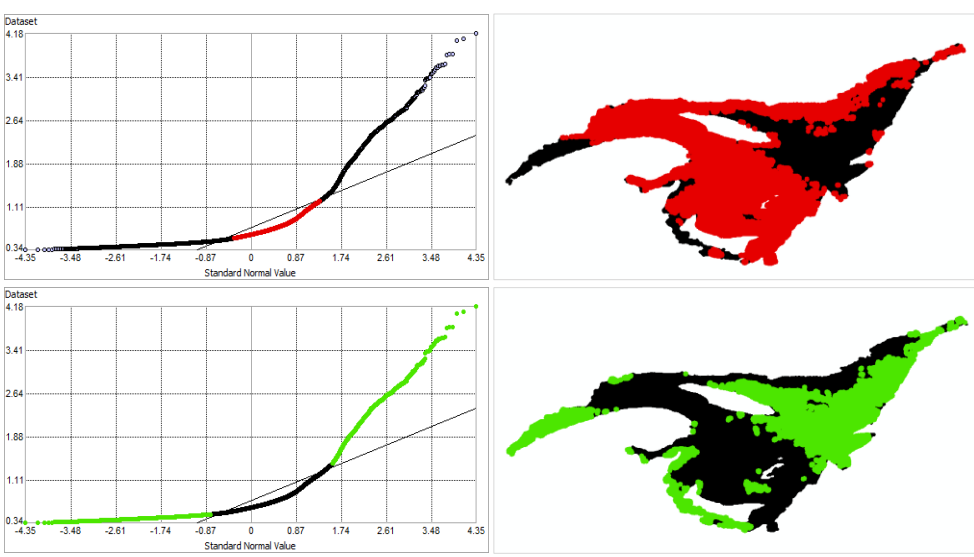

Fig. 377. Normal Q-Q plot for data values of MERIS Case II Spring Chlorophyll *a* Minimum (mg m^{-3}). Points falling under (upper panel) and over (bottom panel) the reference line are mapped.

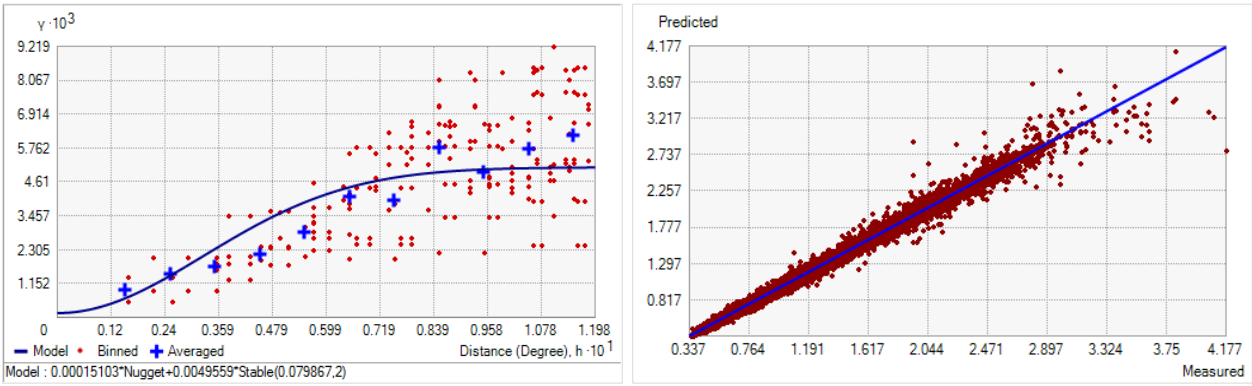

Fig. 378. Left panel: Semivariogram of MERIS Case II Spring Chlorophyll *a* Minimum (mg m^{-3}). Binned values are shown as red dots; average points are shown as blue crosses; the model fit to the averaged values is shown as a blue line. Lag size: 0.010 degrees; number of lags: 12; Parameter: 2; Range: 0.080 degrees; Partial Sill: 0.005. Right panel: Scatterplot of predicted values versus observed values for the variable MERIS Case II Spring Chlorophyll *a* Minimum (mg m^{-3}).

Table 152. Results of cross-validation of the kriged model for the MERIS Case II Spring Chlorophyll *a* Minimum (mg m^{-3}).

Prediction error	**Value**
Number of Observations	74353
Overall Mean Error	-6.416×10^{-5}
Root Mean Square Prediction Error	0.028
Standardized Mean	-0.003
Standardized Root Mean Square Prediction Error	1.768
Average Standard Error	0.015

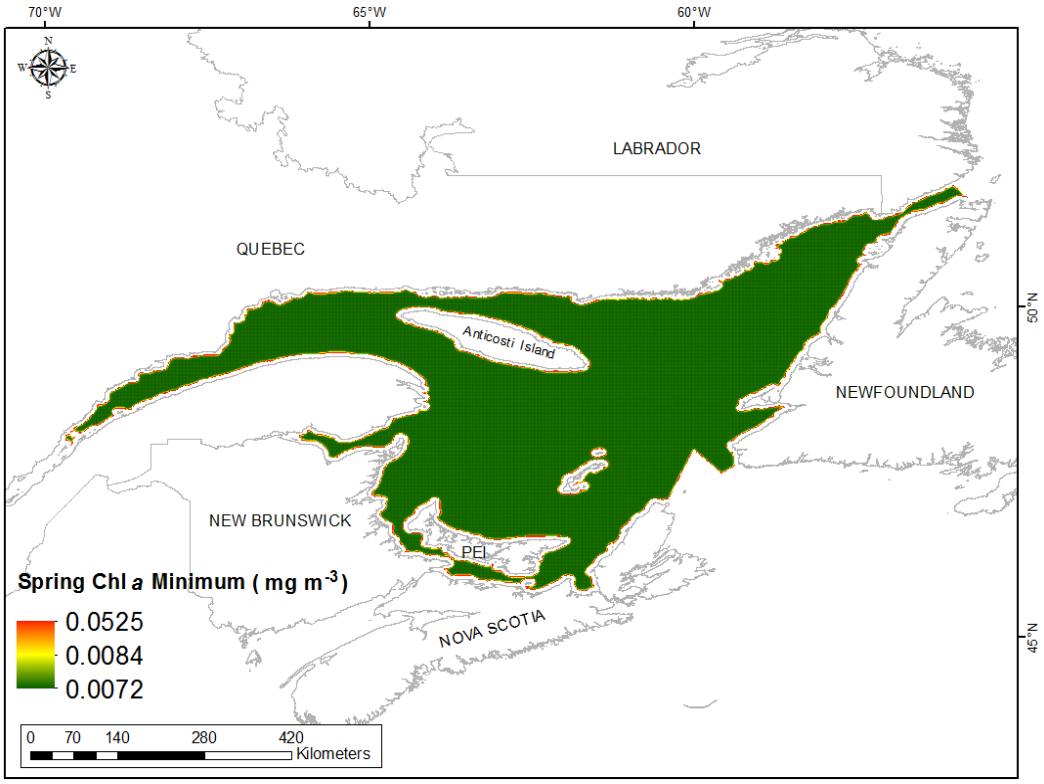

Fig. 379. Prediction standard error surface of MERIS Case II Spring Chlorophyll *a* Minimum (mg m^{-3}).

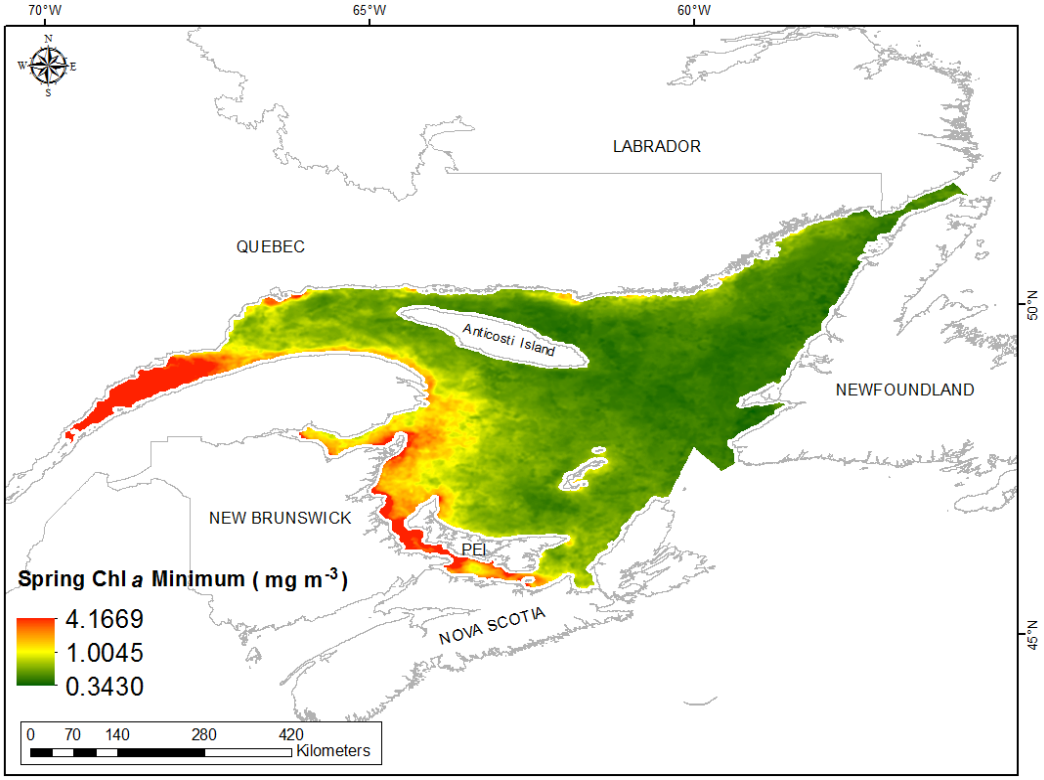

Fig. 380. Interpolated prediction surface of MERIS Case II Spring Chlorophyll *a* Minimum (mg m^{-3}).

MERIS Case II Spring Chlorophyll *a* Maximum

This variable displayed a right-skewed distribution with kurtosis prior to modeling (Table 153, Fig. 381). The data were higher than predicted by a normal distribution at the upper range and slightly lower than predicted at mid values (Fig. 382). The areas of under- and over-prediction showed a strong spatial pattern over the spatial extent (Fig. 382).

The semivariogram showed moderate autocorrelation present in the data and the model showed a very good fit between measured and predicted values (Fig. 383). The model showed good cross-validation statistics (Table 154) indicating that it was good at prediction. The error map showed relatively moderate error over the study extent (Fig. 384). The kriged surface is presented in Fig. 385.

Table 153. Distributional properties of MERIS Case II Spring Chlorophyll *a* Maximum (mg m^{-3}).

Property	Value
Number of Observations	74353
Minimum	0.574
Maximum	14.580
Mean	1.572
Median	1.337
Standard Deviation	0.973
Skewness	2.669
Kurtosis	13.761

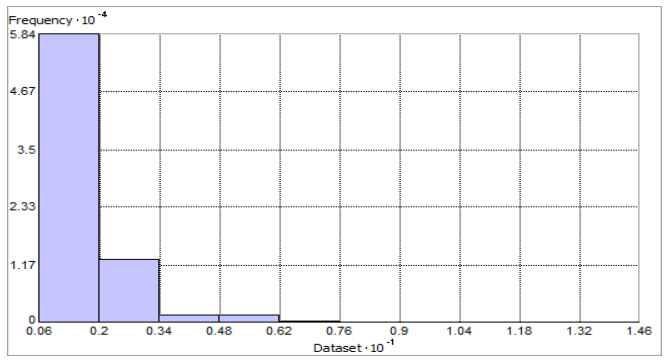

Fig. 381. Distribution of MERIS Case II Spring Chlorophyll *a* Maximum (mg m^{-3}). Histogram was illustrated using 10 bins. Y axis is shown at 10^{-4}.

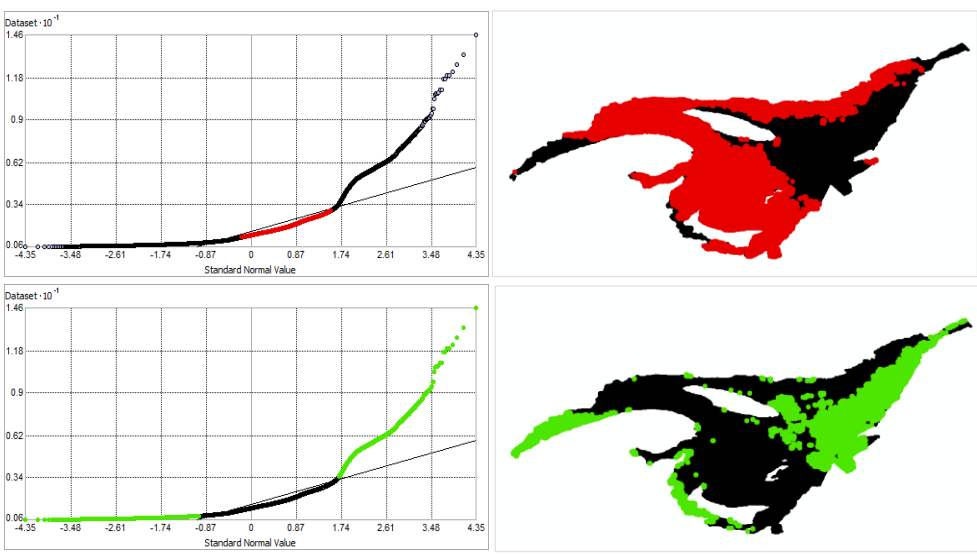

Fig. 382. Normal Q-Q plot for data values of MERIS Case II Spring Chlorophyll *a* Maximum (mg m^{-3}). Points falling under (upper panel) and over (bottom panel) the reference line are mapped.

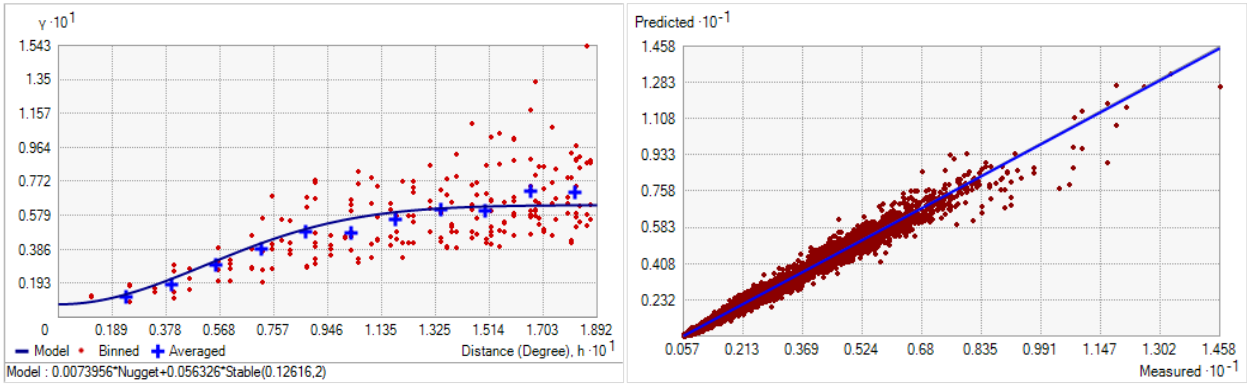

Fig. 383. Left panel: Semivariogram of MERIS Case II Spring Chlorophyll *a* Maximum (mg m^{-3}). Binned values are shown as red dots; average points are shown as blue crosses; the model fit to the averaged values is shown as a blue line. Lag size: 0.016 degrees; number of lags: 12; Parameter: 2; Range: 0.126 degrees; Partial Sill: 0.056. Right panel: Scatterplot of predicted values versus observed values for the variable MERIS Case II Spring Chlorophyll *a* Maximum (mg m^{-3}).

Table 154. Results of cross-validation of the kriged model for the MERIS Case II Spring Chlorophyll *a* Maximum (mg m^{-3}).

Prediction error	**Value**
Number of Observations	74353
Overall Mean Error	2.879×10^{-4}
Root Mean Square Prediction Error	0.090
Standardized Mean	0.003
Standardized Root Mean Square Prediction Error	0.941
Average Standard Error	0.095

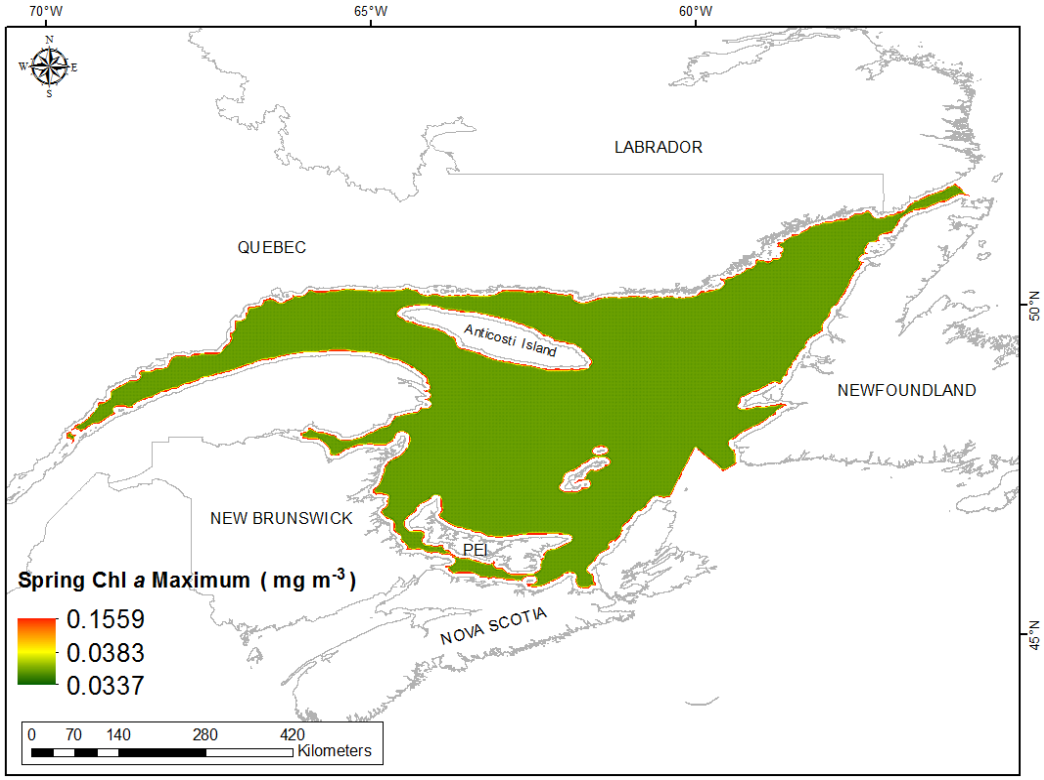

Fig. 384. Prediction standard error surface of MERIS Case II Spring Chlorophyll *a* Maximum (mg m^{-3}).

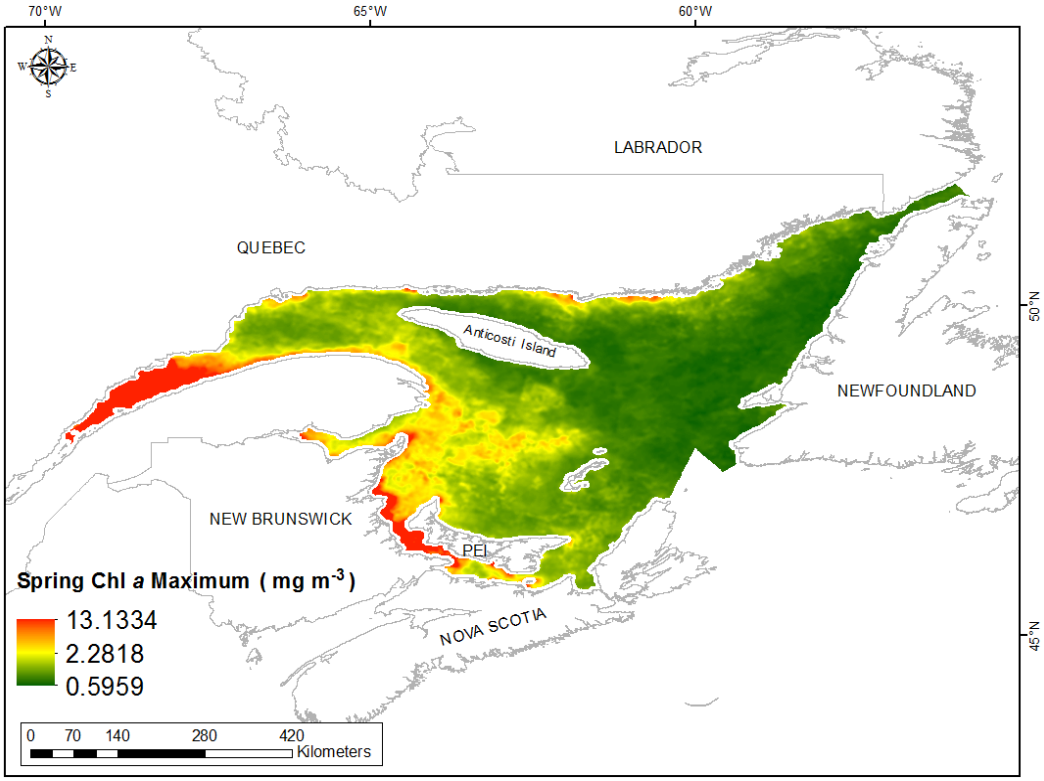

Fig. 385. Interpolated prediction surface of MERIS Case II Spring Chlorophyll *a* Maximum (mg m^{-3}).

MERIS Case II Spring Chlorophyll *a* Range

This variable displayed a strongly right-skewed distribution with kurtosis prior to modeling (Table 155, Fig. 386). The data were higher than predicted by a normal distribution at the upper range and lower than predicted at mid values (Fig. 387). The areas of under- and over-prediction showed a strong spatial pattern over the spatial extent (Fig. 387).

The semivariogram showed moderate autocorrelation present in the data and the model showed a very good fit between measured and predicted values (Fig. 388). The model showed good cross-validation statistics (Table 156) indicating that it was good at prediction. The error map showed low to moderate error over the study extent (Fig. 389). The kriged surface is presented in Fig. 390.

Table 155. Distributional properties of MERIS Case II Spring Chlorophyll *a* Range (mg m^{-3}).

Property	Value
Number of Observations	74353
Minimum	0.083
Maximum	11.240
Mean	0.840
Median	0.680
Standard Deviation	0.641
Skewness	2.750
Kurtosis	16.980

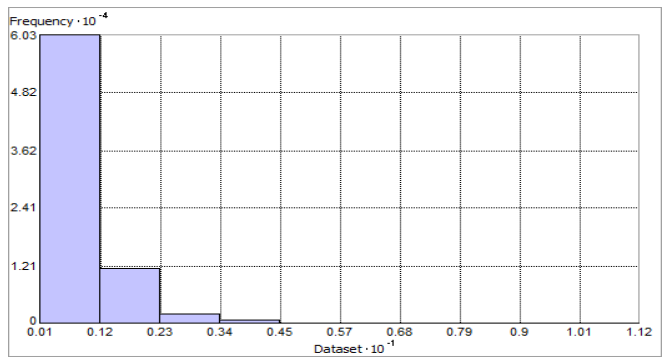

Fig. 386. Distribution of MERIS Case II Spring Chlorophyll *a* Range (mg m^{-3}). Histogram was illustrated using 10 bins. X and Y axes shown at 10^{-1} and 10^{-4} respectively.

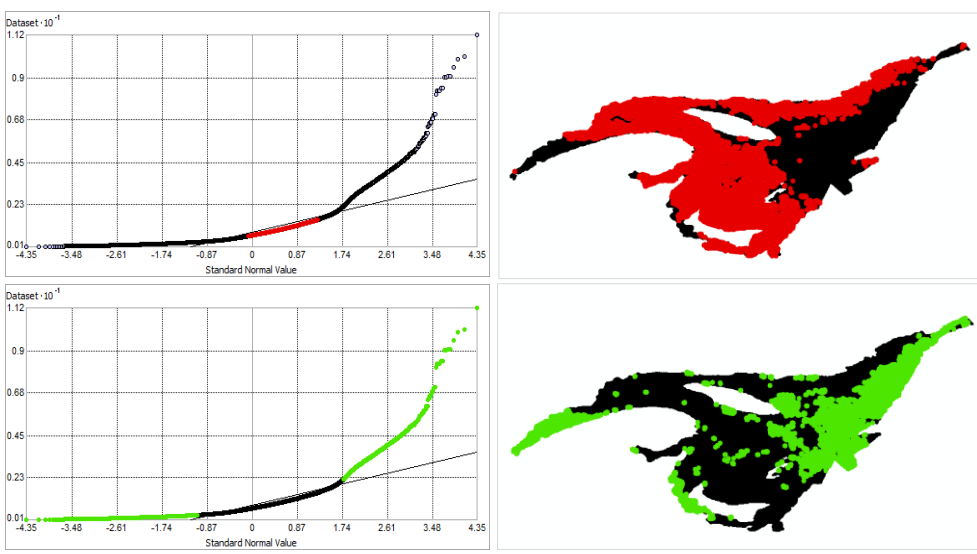

Fig. 387. Normal Q-Q plot for data values of MERIS Case II Spring Chlorophyll *a* Range (mg m^{-3}). Points falling under (upper panel) and over (bottom panel) the reference line are mapped.

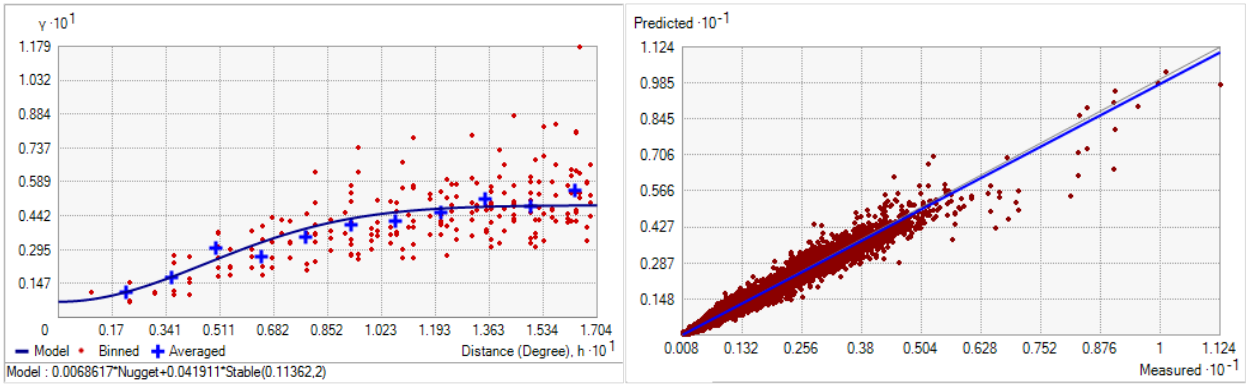

Fig. 388. Left panel: Semivariogram of MERIS Case II Spring Chlorophyll *a* Range (mg m^{-3}). Binned values are shown as red dots; average points are shown as blue crosses; the model fit to the averaged values is shown as a blue line. Lag size: 0.014 degrees; number of lags: 12; Parameter: 2; Range: 0.114 degrees; Partial Sill: 0.042. Right panel: Scatterplot of predicted values versus observed values for the variable MERIS Case II Spring Chlorophyll *a* Range (mg m^{-3}).

Table 156. Results of cross-validation of the kriged model for the MERIS Case II Spring Chlorophyll *a* Range (mg m^{-3}).

Prediction error	**Value**
Number of Observations	74353
Overall Mean Error	1.440×10^{-4}
Root Mean Square Prediction Error	0.090
Standardized Mean	0.002
Standardized Root Mean Square Prediction Error	0.970
Average Standard Error	0.092

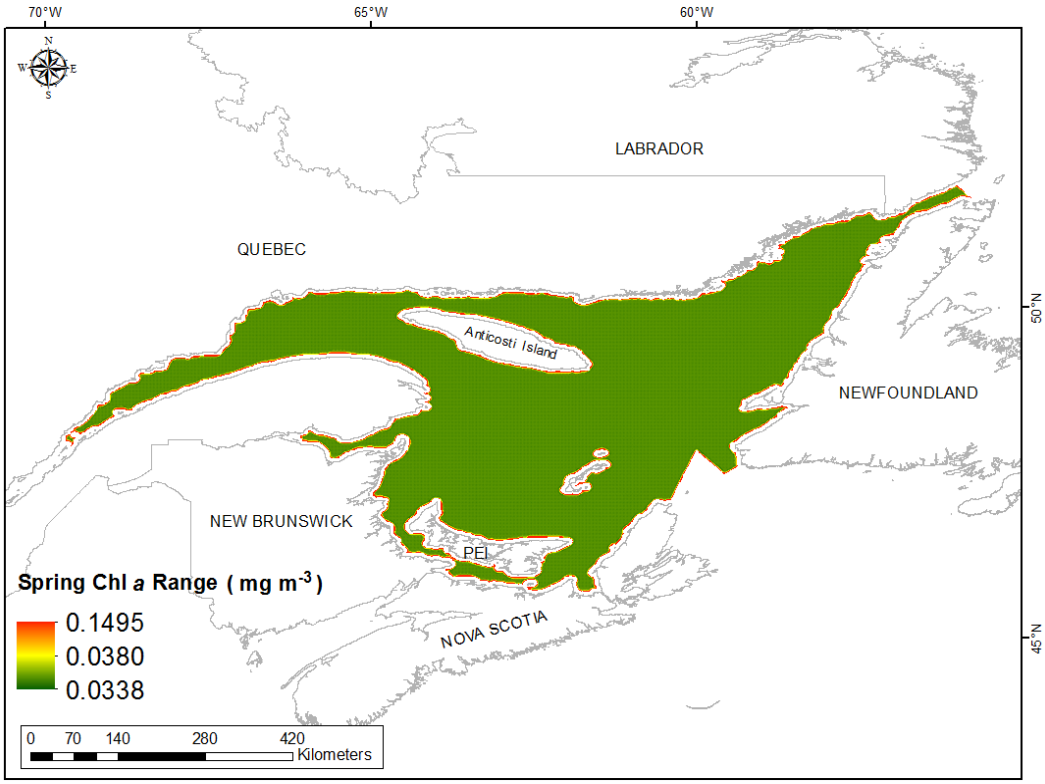

Fig. 389. Prediction standard error surface of MERIS Case II Spring Chlorophyll *a* Range (mg m^{-3}).

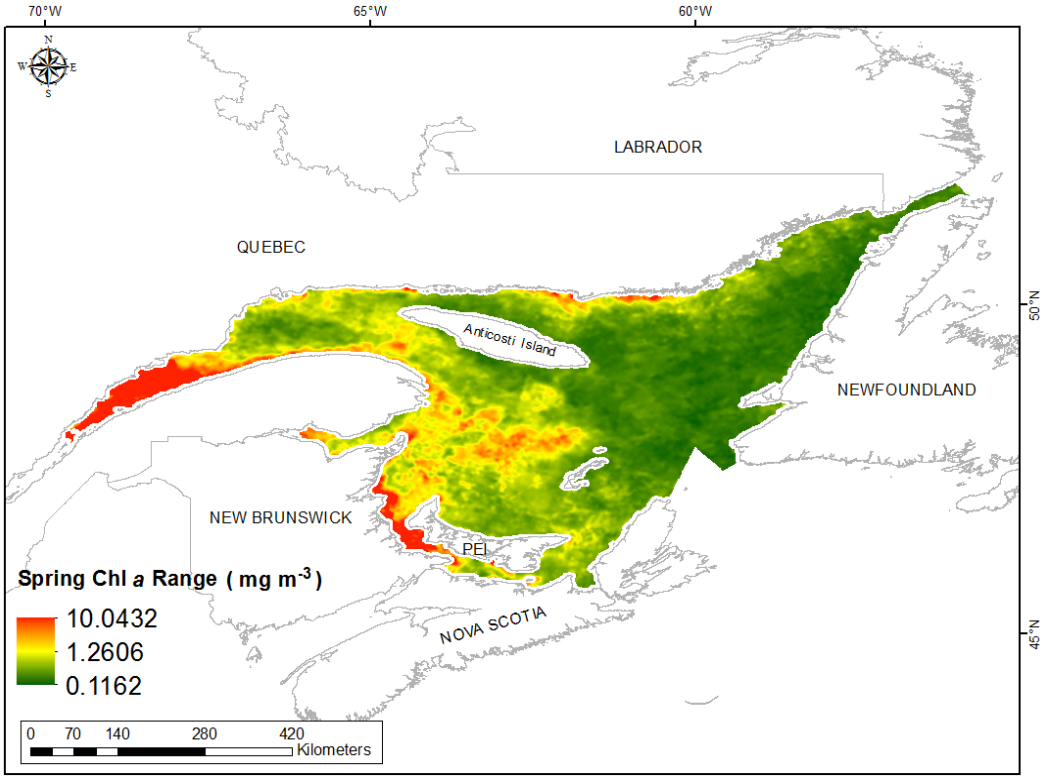

Fig. 390. Interpolated prediction surface of MERIS Case II Spring Chlorophyll *a* Range (mg m^{-3}).

MERIS Case II Summer Chlorophyll *a* Mean

This variable displayed a strongly right-skewed distribution with kurtosis prior to modeling (Table 157, Fig. 391). The data were higher than predicted by a normal distribution at the upper range and slightly lower than predicted at mid values (Fig. 392). The areas of under- and over-prediction showed a strong spatial pattern over the spatial extent (Fig. 392).

The semivariogram showed moderate autocorrelation present in the data and the model showed a very good fit between measured and predicted values (Fig. 393). The model showed fair cross-validation statistics (Table 158). The error map showed low error over the study extent (Fig. 394). The kriged surface is presented in Fig. 395.

Table 157. Distributional properties of MERIS Case II Summer Chlorophyll *a* Mean (mg m^{-3}).

Property	Value
Number of Observations	74353
Minimum	0.518
Maximum	5.118
Mean	0.936
Median	0.815
Standard Deviation	0.405
Skewness	2.650
Kurtosis	12.782

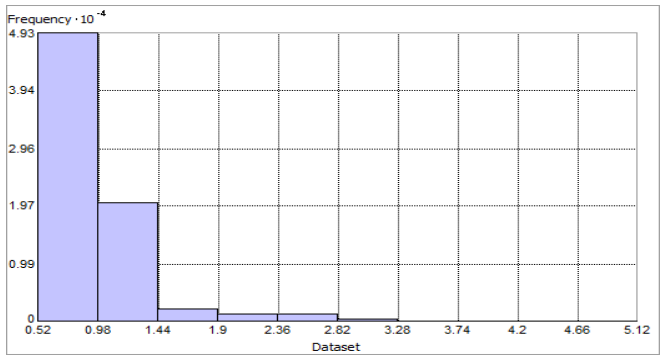

Fig. 391. Distribution of MERIS Case II Summer Chlorophyll *a* Mean (mg m^{-3}). Histogram was illustrated using 10 bins. Y axis is shown at 10^{-4}.

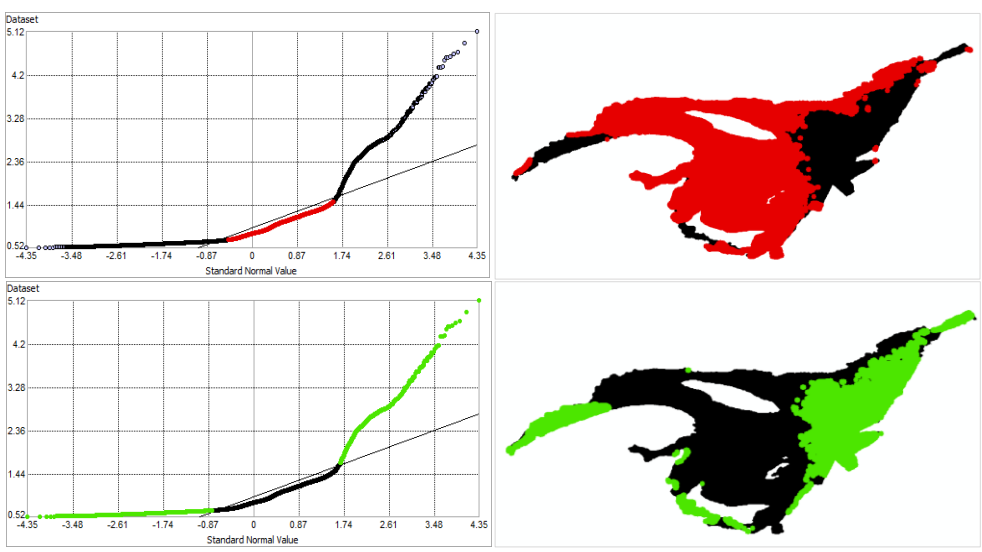

Fig. 392. Normal Q-Q plot for data values of MERIS Case II Summer Chlorophyll *a* Mean (mg m^{-3}). Points falling under (upper panel) and over (bottom panel) the reference line are mapped.

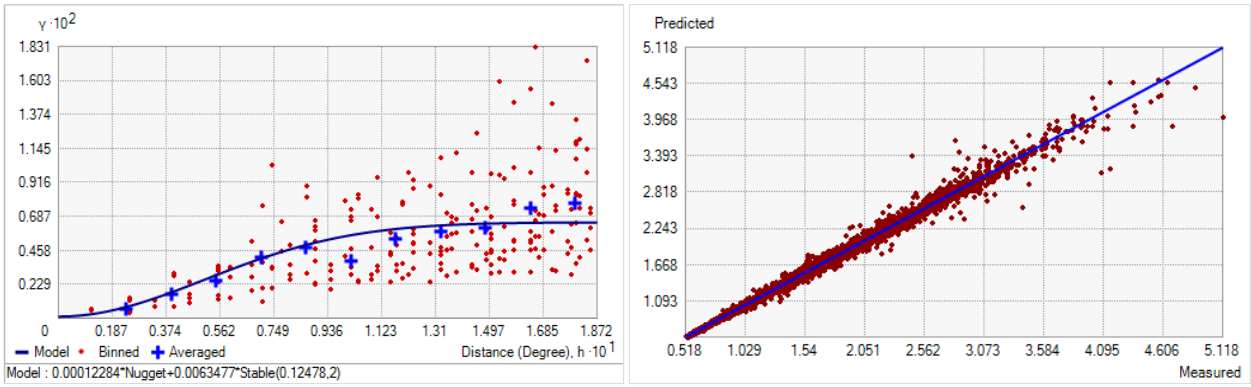

Fig. 393. Left panel: Semivariogram of MERIS Case II Summer Chlorophyll *a* Mean (mg m^{-3}). Binned values are shown as red dots; average points are shown as blue crosses; the model fit to the averaged values is shown as a blue line. Lag size: 0.016 degrees; number of lags: 12; Parameter: 2; Range: 0.125 degrees; Partial Sill: 0.006. Right panel: Scatterplot of predicted values versus observed values for the variable MERIS Case II Summer Chlorophyll *a* Mean (mg m^{-3}).

Table 158. Results of cross-validation of the kriged model for the MERIS Case II Summer Chlorophyll *a* Mean (mg m^{-3}).

Prediction error	**Value**
Number of Observations	74353
Overall Mean Error	-3.800×10^{-6}
Root Mean Square Prediction Error	0.020
Standardized Mean	4.760×10^{-4}
Standardized Root Mean Square Prediction Error	1.494
Average Standard Error	0.013

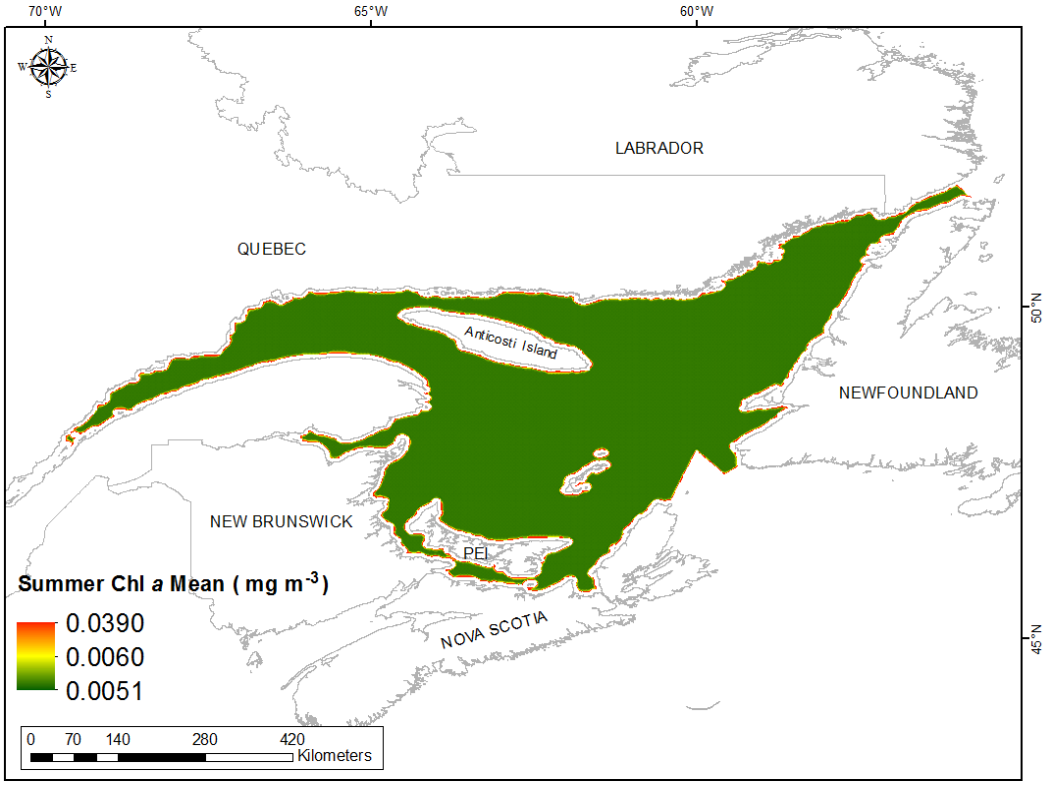

Fig. 394. Prediction standard error surface of MERIS Case II Summer Chlorophyll *a* Mean (mg m^{-3}).

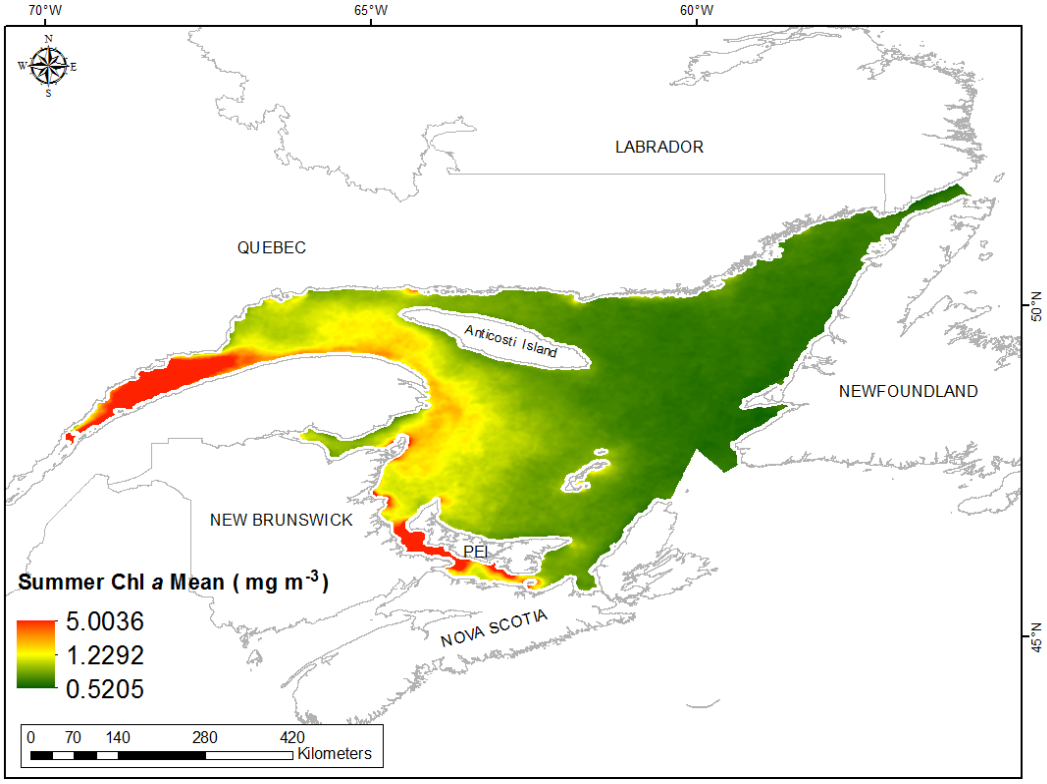

Fig. 395. Interpolated prediction surface of MERIS Case II Summer Chlorophyll *a* Mean (mg m^{-3}).

MERIS Case II Summer Chlorophyll *a* Minimum

This variable displayed a right-skewed distribution with kurtosis prior to modeling (Table 159, Fig. 396). The data were higher than predicted by a normal distribution at the lower and upper ranges and slightly lower than predicted at mid values (Fig. 397). The areas of under- and over-prediction showed a strong spatial pattern over the spatial extent (Fig. 397).

The semivariogram showed moderate autocorrelation present in the data and the model showed a very good fit between measured and predicted values (Fig. 389). The model showed good cross-validation statistics (Table 160) indicating that it was good at prediction. The error map showed relatively moderate error over the study extent (Fig. 399). The kriged surface is presented in Fig. 400.

Table 159. Distributional properties of MERIS Case II Summer Chlorophyll *a* Minimum (mg m^{-3}).

Property	Value
Number of Observations	74353
Minimum	0.352
Maximum	3.278
Mean	0.700
Median	0.640
Standard Deviation	0.236
Skewness	2.575
Kurtosis	14.678

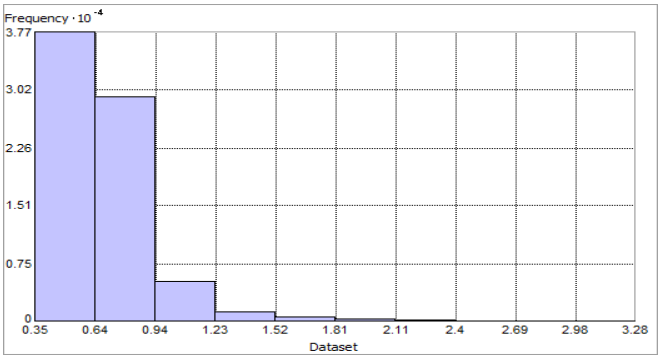

Fig. 396. Distribution of MERIS Case II Summer Chlorophyll *a* Minimum (mg m^{-3}). Histogram was illustrated using 10 bins. Y axis is shown at 10^{-4}.

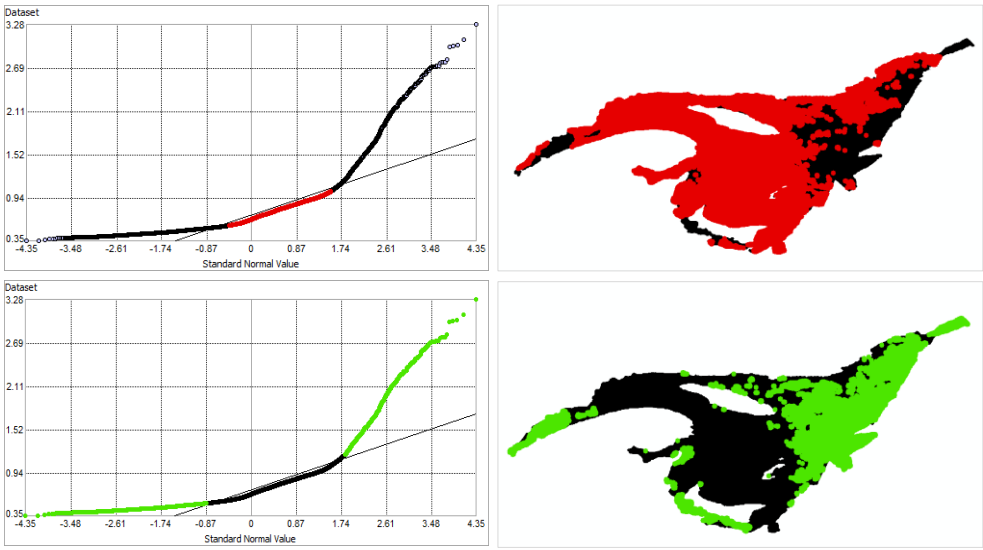

Fig. 397. Normal Q-Q plot for data values of MERIS Case II Summer Chlorophyll *a* Minimum (mg m^{-3}). Points falling under (upper panel) and over (bottom panel) the reference line are mapped.

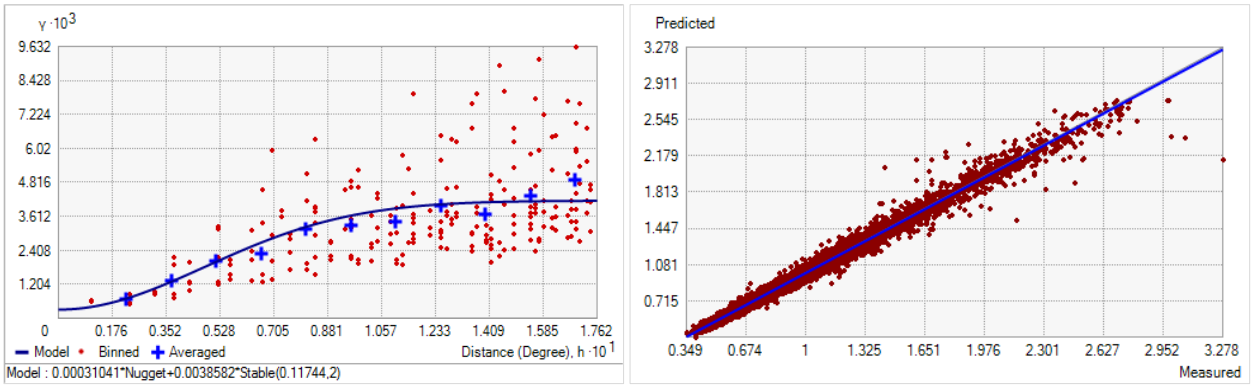

Fig. 398. Left panel: Semivariogram of MERIS Case II Summer Chlorophyll *a* Minimum (mg m^{-3}). Binned values are shown as red dots; average points are shown as blue crosses; the model fit to the averaged values is shown as a blue line. Lag size: 0.015 degrees; number of lags: 12; Parameter: 2; Range: 0.117 degrees; Partial Sill: 0.004. Right panel: Scatterplot of predicted values versus observed values for the variable MERIS Case II Summer Chlorophyll *a* Minimum (mg m^{-3}).

Table 160. Results of cross-validation of the kriged model for the MERIS Case II Summer Chlorophyll *a* Minimum (mg m^{-3}).

Prediction error	**Value**
Number of Observations	74353
Overall Mean Error	-5.933×10^{-6}
Root Mean Square Prediction Error	0.022
Standardized Mean	1.861×10^{-4}
Standardized Root Mean Square Prediction Error	1.079
Average Standard Error	0.020

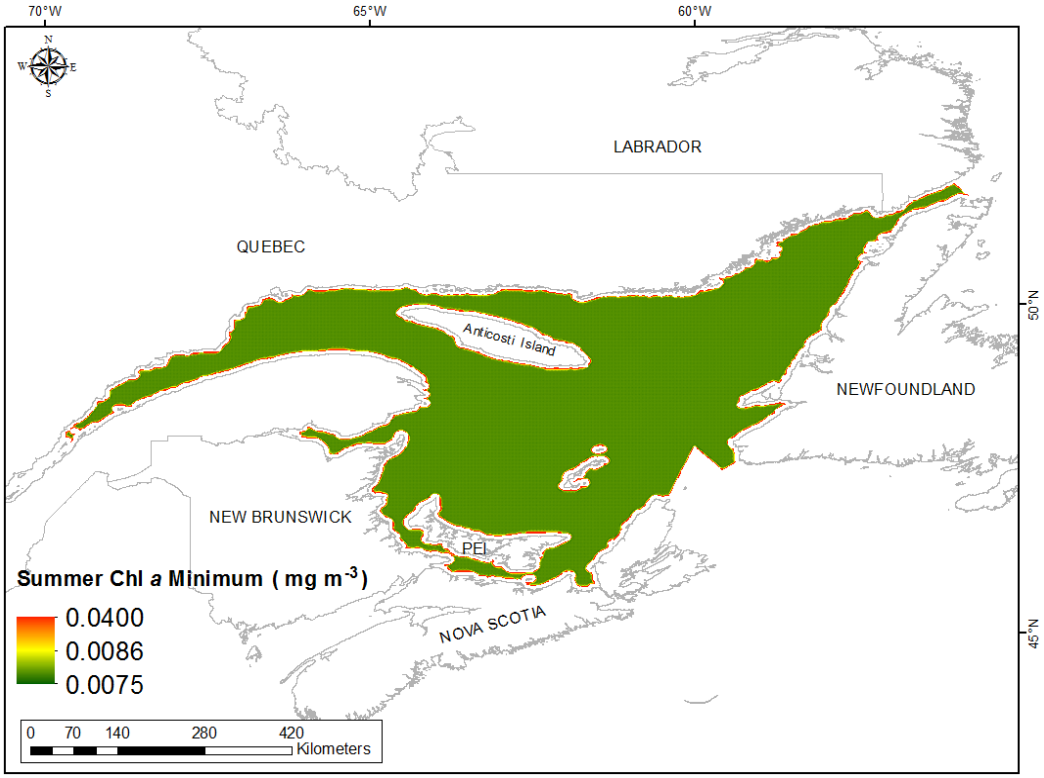

Fig. 399. Prediction standard error surface of MERIS Case II Summer Chlorophyll *a* Minimum (mg m^{-3}).

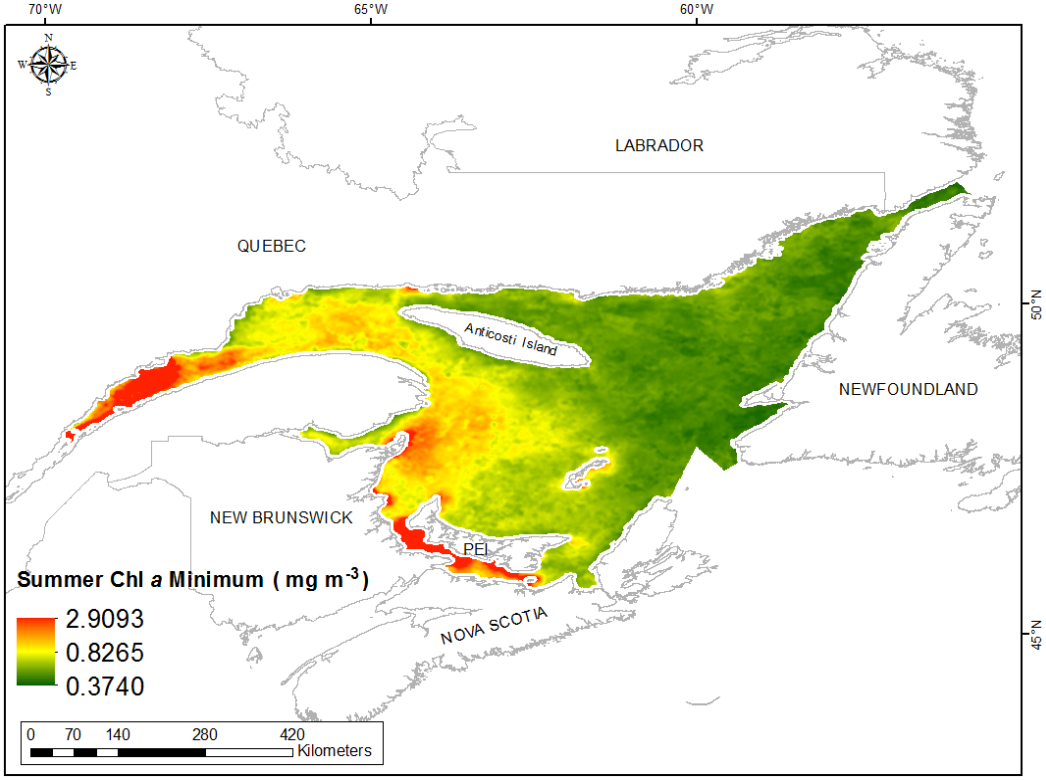

Fig. 400. Interpolated prediction surface of MERIS Case II Summer Chlorophyll *a* Minimum (mg m^{-3}).

MERIS Case II Summer Chlorophyll *a* Maximum

This variable displayed a right-skewed distribution with kurtosis prior to modeling (Table 161, Fig. 401). The data were higher than predicted by a normal distribution at the lower and upper ranges and slightly lower than predicted at mid values (Fig. 402). The areas of under- and over-prediction showed a strong spatial pattern over the spatial extent (Fig. 402).

The semivariogram showed moderate autocorrelation present in the data and the model showed a very good fit between measured and predicted values (Fig. 403). The model showed good cross-validation statistics (Table 162) indicating that it was good at prediction. The error map showed low error over the study extent (Fig. 404). The kriged surface is presented in Fig. 405.

Table 161. Distributional properties of MERIS Case II Summer Chlorophyll *a* Maximum (mg m^{-3}).

Property	Value
Number of Observations	74353
Minimum	0.595
Maximum	7.555
Mean	1.253
Median	1.015
Standard Deviation	0.657
Skewness	2.414
Kurtosis	10.755

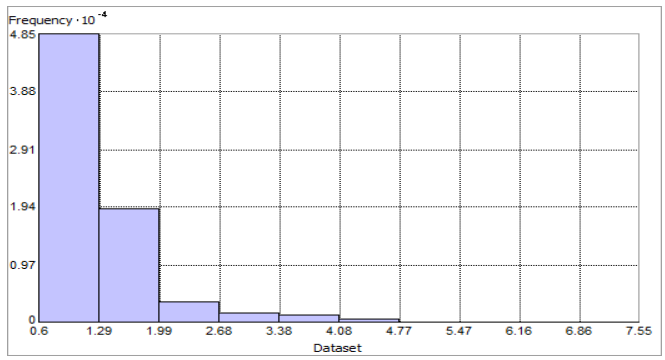

Fig. 401. Distribution of MERIS Case II Summer Chlorophyll *a* Maximum (mg m^{-3}). Histogram was illustrated using 10 bins. Y axis is shown at 10^{-4}.

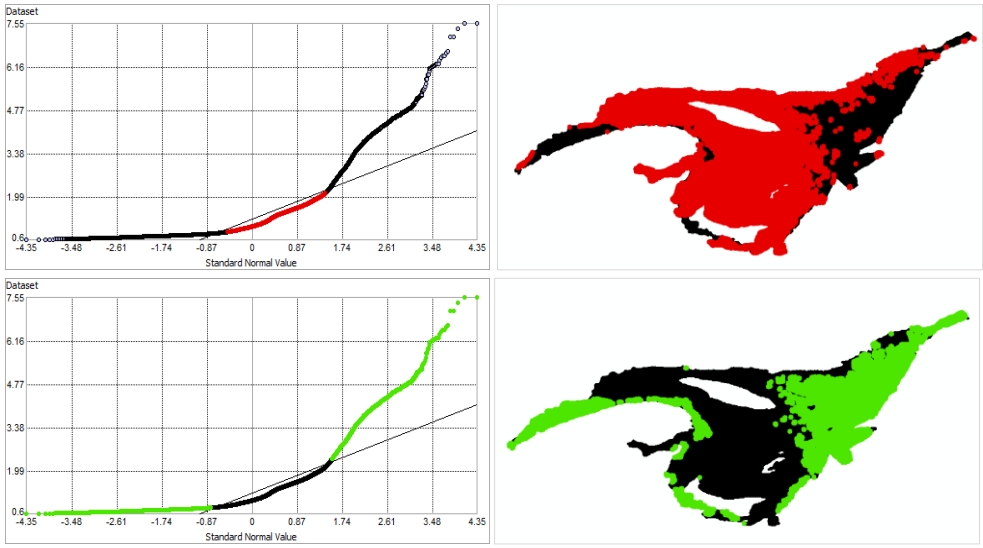

Fig. 402. Normal Q-Q plot for data values of MERIS Case II Summer Chlorophyll *a* Maximum (mg m^{-3}). Points falling under (upper panel) and over (bottom panel) the reference line are mapped.

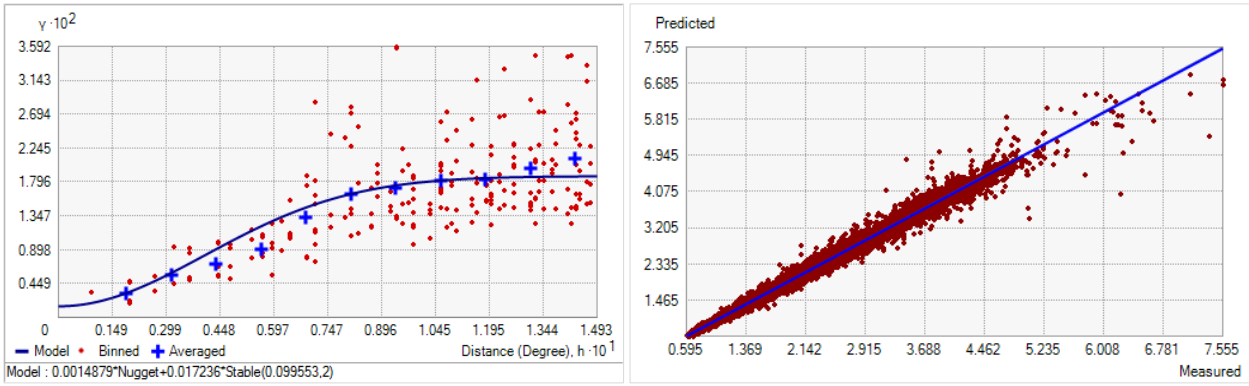

Fig. 403. Left panel: Semivariogram of MERIS Case II Summer Chlorophyll *a* Maximum (mg m^{-3}). Binned values are shown as red dots; average points are shown as blue crosses; the model fit to the averaged values is shown as a blue line. Lag size: 0.012 degrees; number of lags: 12; Parameter: 2; Range: 0.100 degrees; Partial Sill: 0.017. Right panel: Scatterplot of predicted values versus observed values for the variable MERIS Case II Summer Chlorophyll *a* Maximum (mg m^{-3}).

Table 162. Results of cross-validation of the kriged model for the MERIS Case II Summer Chlorophyll *a* Maximum (mg m^{-3}).

Prediction error	**Value**
Number of Observations	74353
Overall Mean Error	2.775×10^{-6}
Root Mean Square Prediction Error	0.051
Standardized Mean	2.035×10^{-4}
Standardized Root Mean Square Prediction Error	1.119
Average Standard Error	0.044

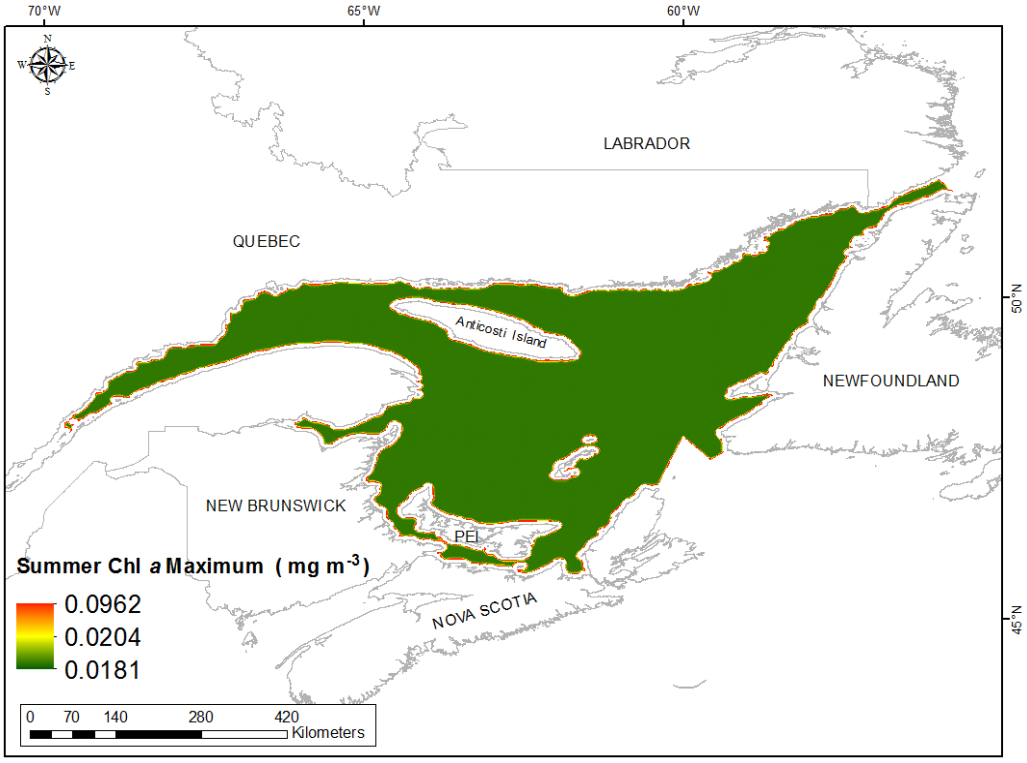

Fig. 404. Prediction standard error surface of MERIS Case II Summer Chlorophyll *a* Maximum (mg m^{-3}).

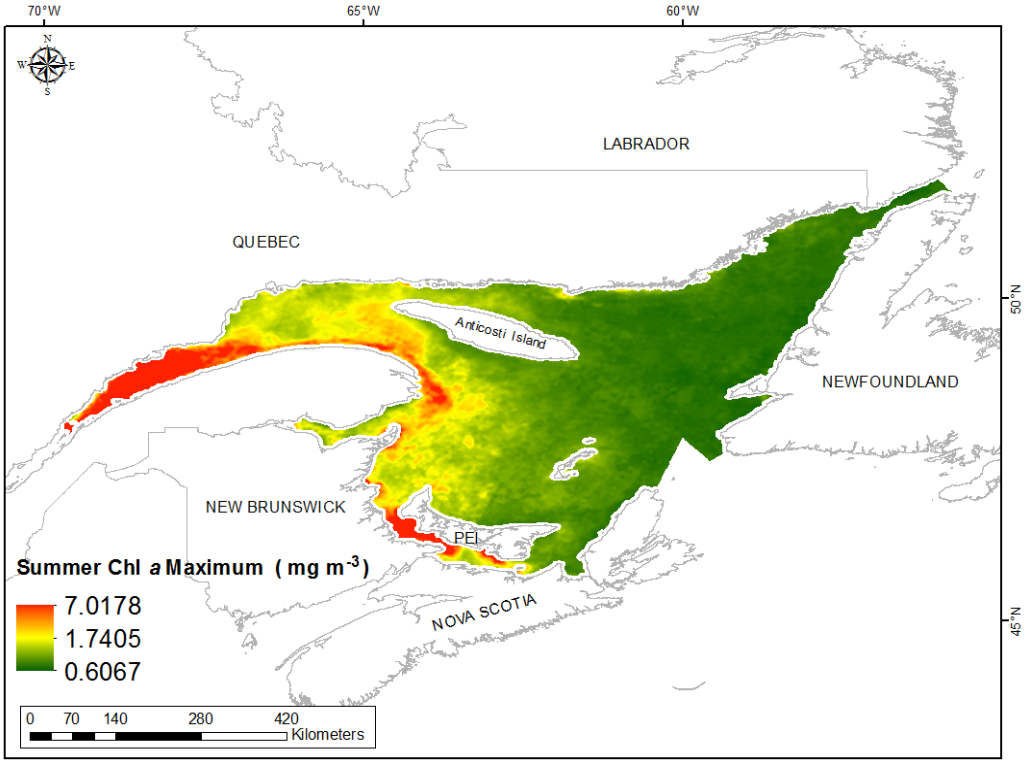

Fig. 405. Interpolated prediction surface of MERIS Case II Summer Chlorophyll *a* Maximum (mg m^{-3}).

MERIS Case II Summer Chlorophyll *a* Range

This variable displayed a right-skewed distribution with kurtosis prior to modeling (Table 163, Fig. 406). The data were higher than predicted by a normal distribution at the lower and upper ranges and slightly lower than predicted at mid values (Fig. 407). The areas of under- and over-prediction showed a strong spatial pattern over the spatial extent (Fig. 407).

The semivariogram showed moderate autocorrelation present in the data and the model showed a very good fit between measured and predicted values (Fig. 408). The model showed good cross-validation statistics (Table 164) indicating that it was good at prediction. The error map showed low error over the study extent (Fig. 409). The kriged surface is presented in Fig. 410.

Table 163. Distributional properties of MERIS Case II Summer Chlorophyll *a* Range (mg m^{-3}).

Property	Value
Number of Observations	74353
Minimum	0.075
Maximum	5.548
Mean	0.554
Median	0.377
Standard Deviation	0.463
Skewness	2.668
Kurtosis	12.378

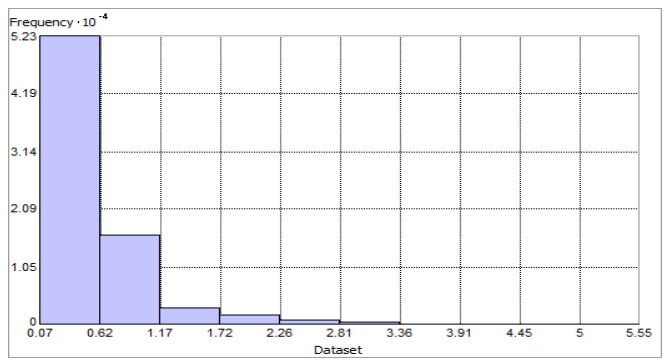

Fig. 406. Distribution of MERIS Case II Summer Chlorophyll *a* Range (mg m^{-3}). Histogram was illustrated using 10 bins. Y axis is shown at 10^{-4}.

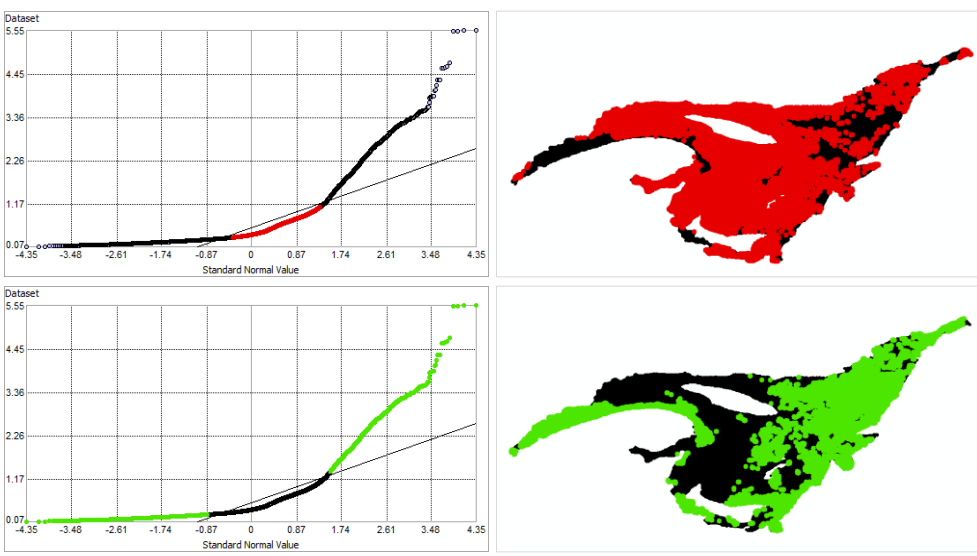

Fig. 407. Normal Q-Q plot for data values of MERIS Case II Summer Chlorophyll *a* Range (mg m^{-3}). Points falling under (upper panel) and over (bottom panel) the reference line are mapped.

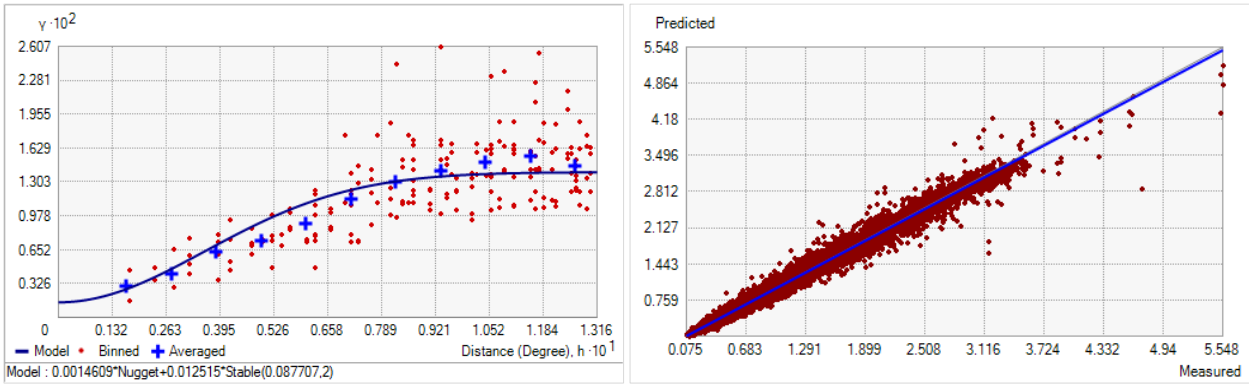

Fig. 408. Left panel: Semivariogram of MERIS Case II Summer Chlorophyll *a* Range (mg m^{-3}). Binned values are shown as red dots; average points are shown as blue crosses; the model fit to the averaged values is shown as a blue line. Lag size: 0.011 degrees; number of lags: 12; Parameter: 2; Range: 0.088 degrees; Partial Sill: 0.013. Right panel: Scatterplot of predicted values versus observed values for the variable MERIS Case II Summer Chlorophyll *a* Range (mg m^{-3}).

Table 164. Results of cross-validation of the kriged model for the MERIS Case II Summer Chlorophyll *a* Range (mg m^{-3}).

Prediction error	**Value**
Number of Observations	74353
Overall Mean Error	1.894×10^{-5}
Root Mean Square Prediction Error	0.050
Standardized Mean	3.035×10^{-4}
Standardized Root Mean Square Prediction Error	1.104
Average Standard Error	0.044

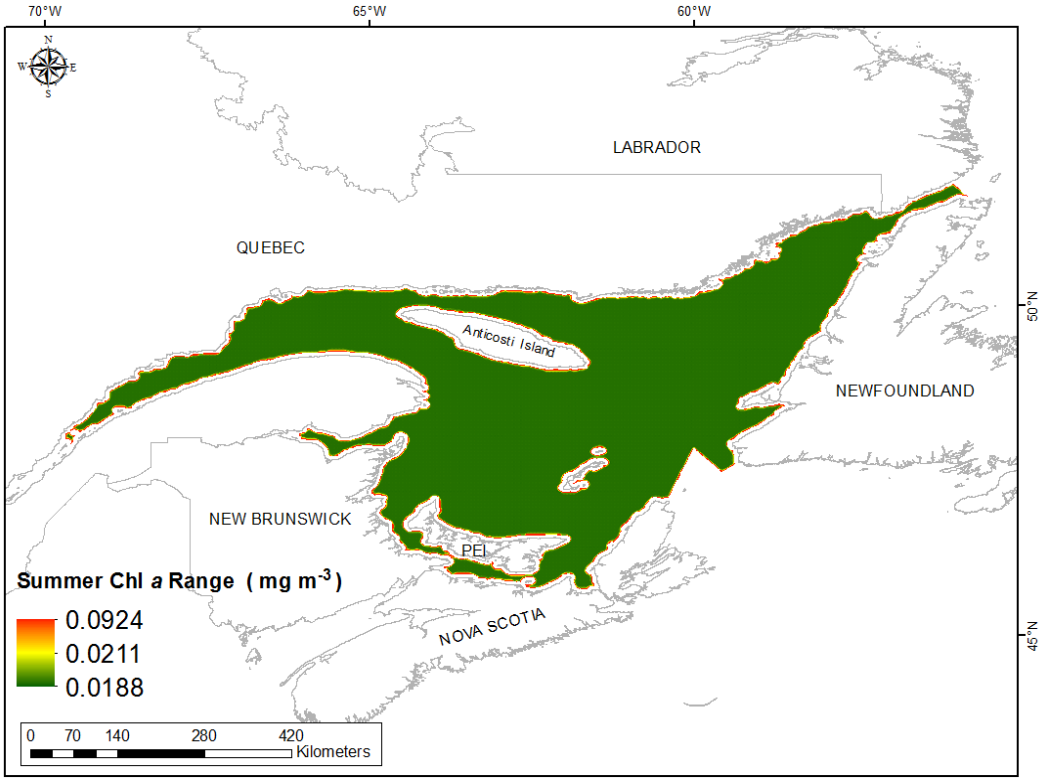

Fig. 409. Prediction standard error surface of MERIS Case II Summer Chlorophyll *a* Range (mg m^{-3}).

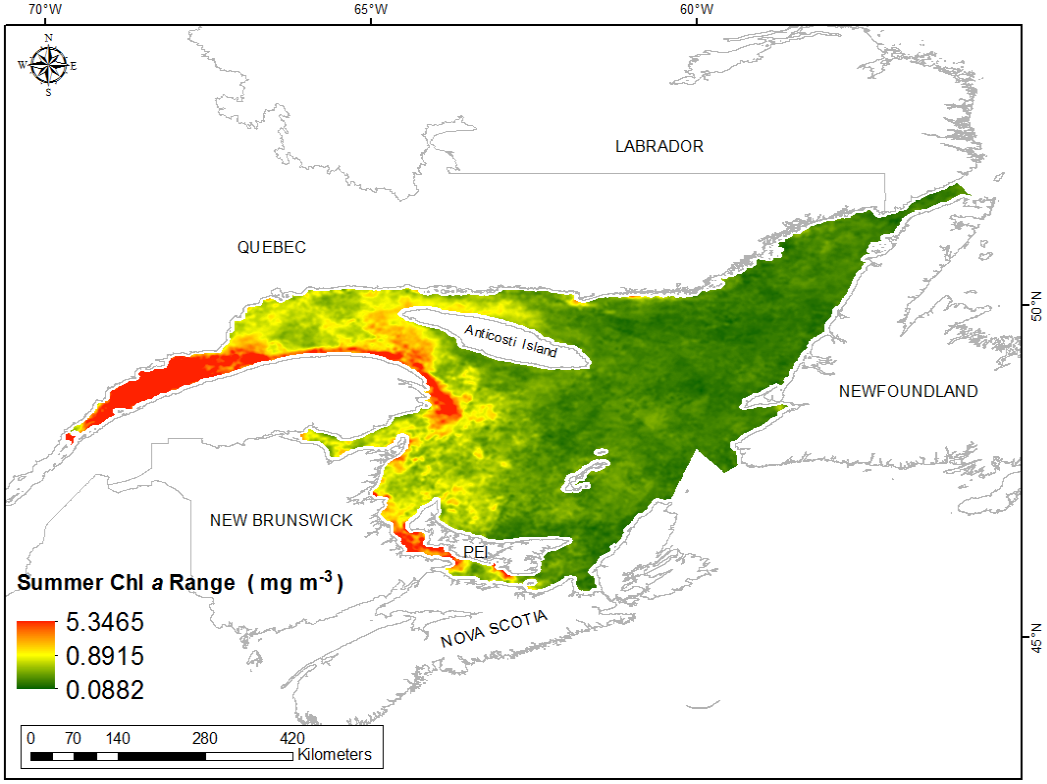

Fig. 410. Interpolated prediction surface of MERIS Case II Summer Chlorophyll *a* Range (mg m^{-3}).

MERIS Case II Fall Chlorophyll *a* Mean

This variable displayed a strongly right-skewed distribution with kurtosis prior to modeling (Table 165, Fig. 411). The data were higher than predicted by a normal distribution at the lower and upper ranges and slightly lower than predicted at mid values (Fig. 412). The areas of under- and over-prediction showed a strong spatial pattern over the spatial extent (Fig. 412).

The semivariogram showed moderate autocorrelation present in the data and the model showed a very good fit between measured and predicted values (Fig. 413). The model showed good cross-validation statistics (Table 166) indicating that it was good at prediction. The error map showed low error over the study extent (Fig. 414). The kriged surface is presented in Fig. 415.

Table 165. Distributional properties of MERIS Case II Fall Chlorophyll *a* Mean (mg m^{-3}).

Property	Value
Number of Observations	74353
Minimum	0.747
Maximum	7.765
Mean	1.068
Median	0.943
Standard Deviation	0.501
Skewness	5.433
Kurtosis	40.129

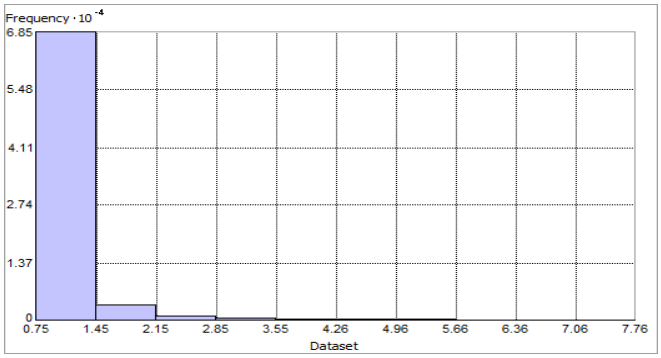

Fig. 411. Distribution of MERIS Case II Fall Chlorophyll *a* Mean (mg m^{-3}). Histogram was illustrated using 10 bins. Y axis is shown at 10^{-4}.

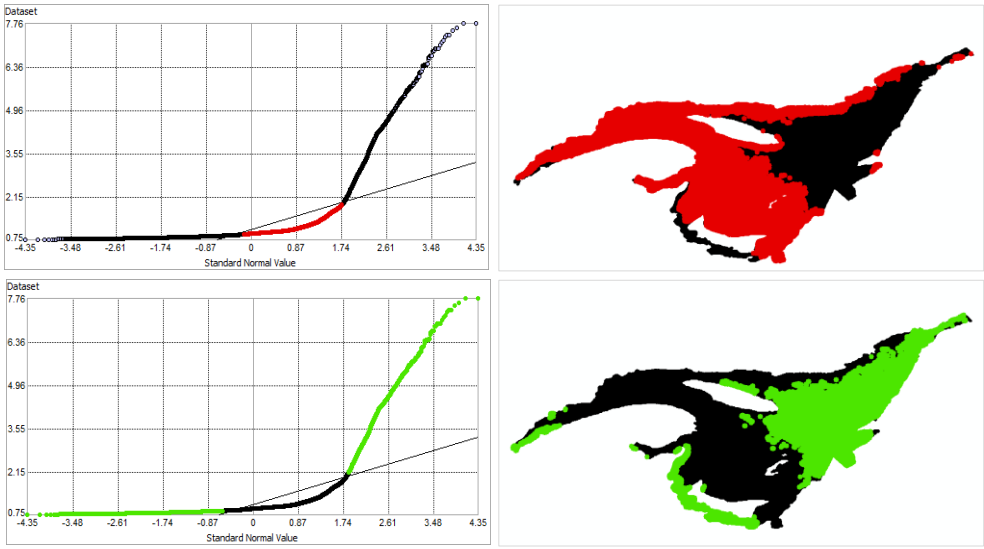

Fig. 412. Normal Q-Q plot for data values of MERIS Case II Fall Chlorophyll *a* Mean (mg m^{-3}). Points falling under (upper panel) and over (bottom panel) the reference line are mapped.

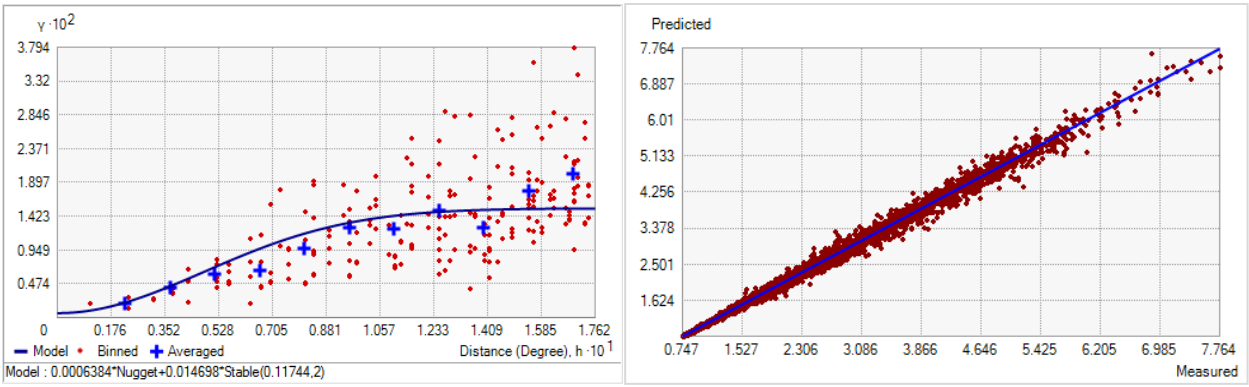

Fig. 413. Left panel: Semivariogram of MERIS Case II Fall Chlorophyll *a* Mean (mg m^{-3}). Binned values are shown as red dots; average points are shown as blue crosses; the model fit to the averaged values is shown as a blue line. Lag size: 0.015 degrees; number of lags: 12; Parameter: 2; Range: 0.117 degrees; Partial Sill: 0.015. Right panel: Scatterplot of predicted values versus observed values for the variable MERIS Case II Fall Chlorophyll *a* Mean (mg m^{-3}).

Table 166. Results of cross-validation of the kriged model for the MERIS Case II Fall Chlorophyll *a* Mean (mg m^{-3}).

Prediction error	**Value**
Number of Observations	74353
Overall Mean Error	8.335×10^{-5}
Root Mean Square Prediction Error	0.027
Standardized Mean	0.004
Standardized Root Mean Square Prediction Error	0.911
Average Standard Error	0.029

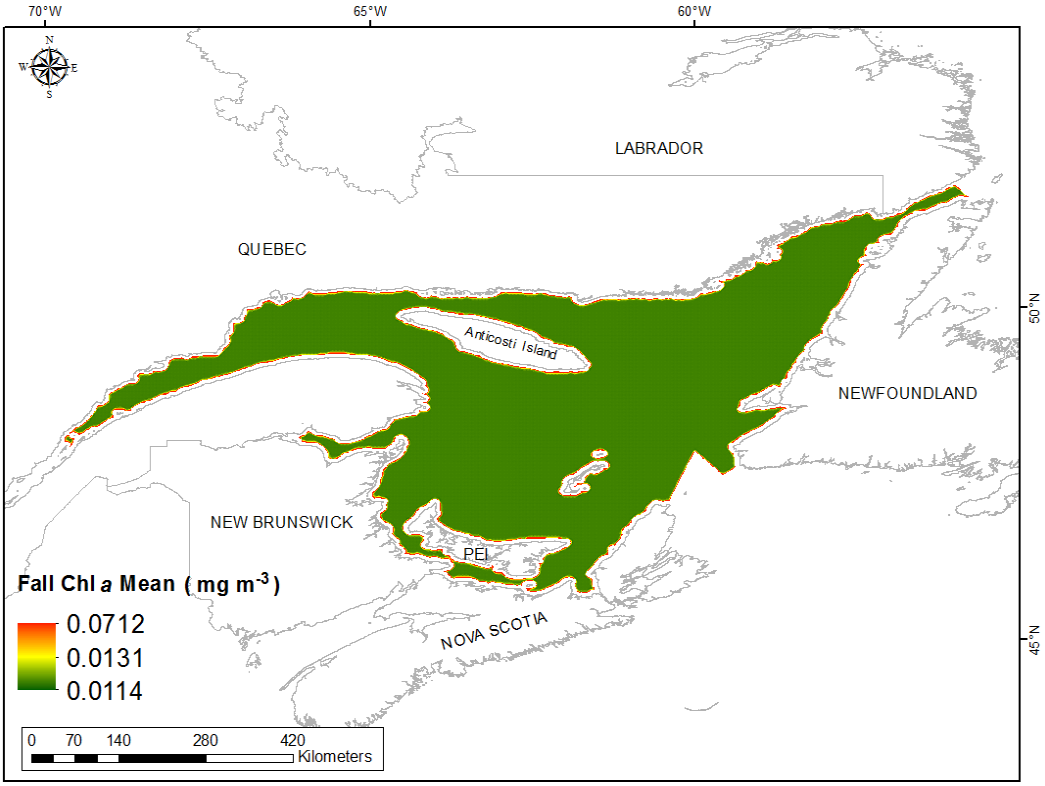

Fig. 414. Prediction standard error surface of MERIS Case II Fall Chlorophyll *a* Mean (mg m^{-3}).

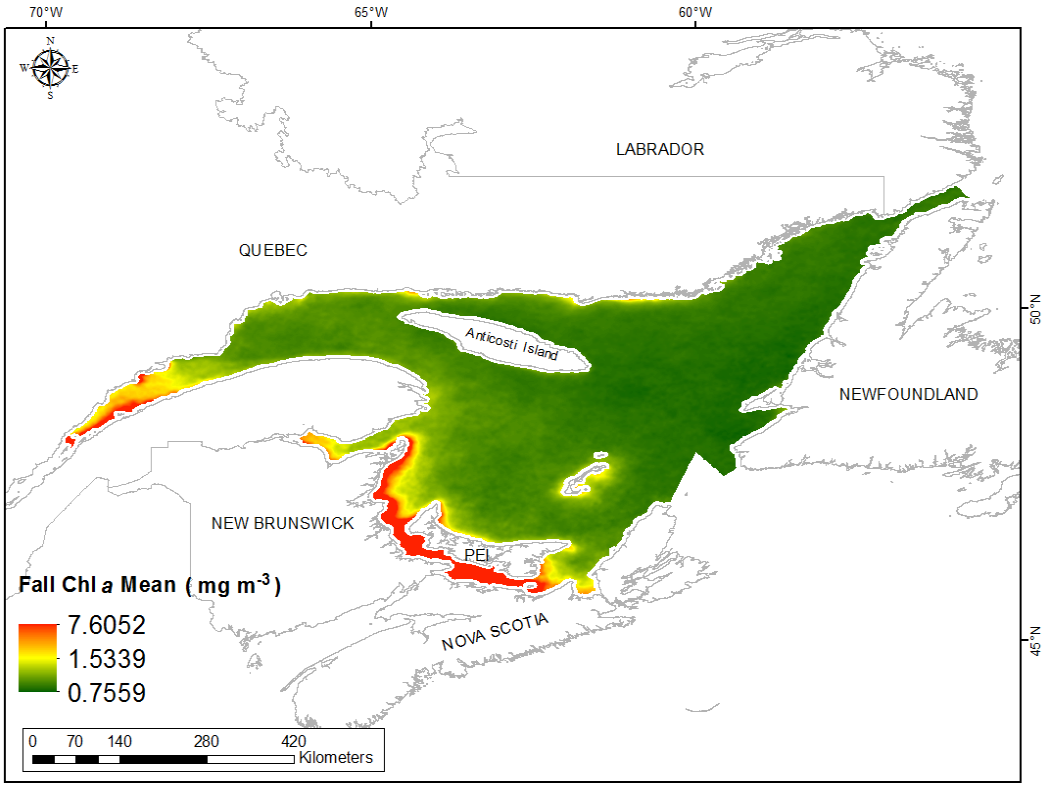

Fig. 415. Interpolated prediction surface of MERIS Case II Fall Chlorophyll *a* Mean (mg m^{-3}).

MERIS Case II Fall Chlorophyll *a* Minimum

This variable displayed a strongly right-skewed distribution with kurtosis prior to modeling (Table 167, Fig. 416). The data were higher than predicted by a normal distribution at the lower and upper ranges and lower than predicted at mid values (Fig. 417). The areas of under- and over-prediction showed a strong spatial pattern over the spatial extent (Fig. 417).

The semivariogram showed weak to moderate autocorrelation present in the data and the model showed a very good fit between measured and predicted values (Fig. 418). The model showed fair cross-validation statistics (Table 168). The error map showed low error over the study extent (Fig. 419). The kriged surface is presented in Fig. 420.

Table 167. Distributional properties of MERIS Case II Fall Chlorophyll *a* Minimum (mg m^{-3}).

Property	Value
Number of Observations	74353
Minimum	0.581
Maximum	5.028
Mean	0.873
Median	0.802
Standard Deviation	0.304
Skewness	5.778
Kurtosis	45.826

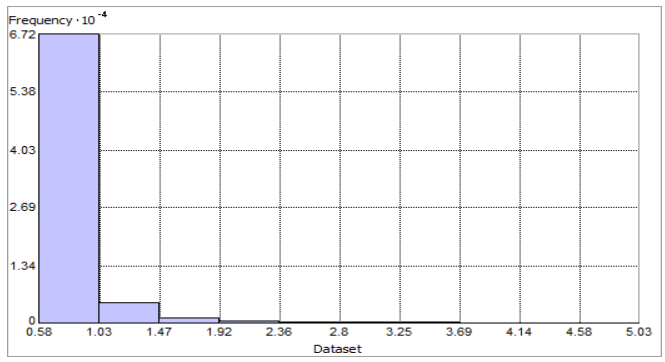

Fig. 416. Distribution of MERIS Case II Fall Chlorophyll *a* Minimum (mg m^{-3}). Histogram was illustrated using 10 bins. Y axis is shown at 10^{-4}.

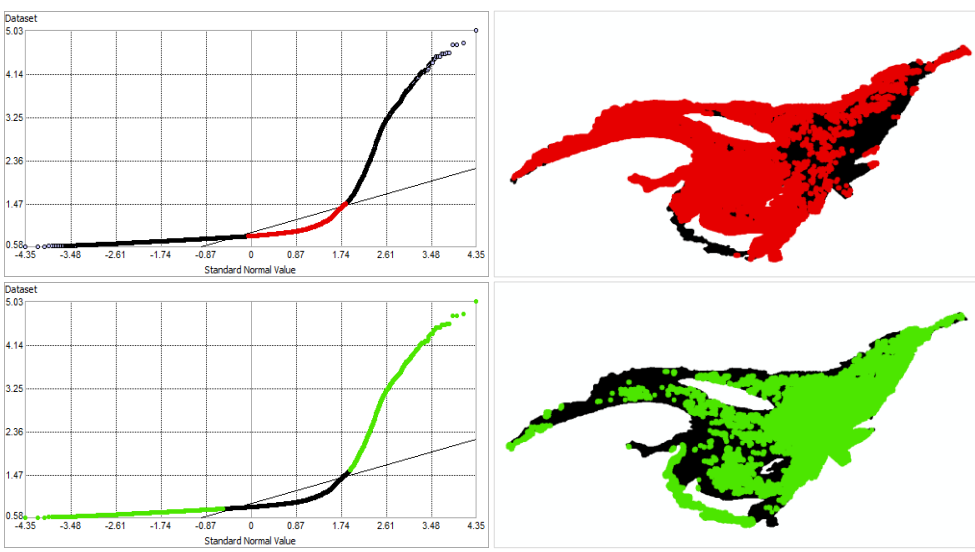

Fig. 417. Normal Q-Q plot for data values of MERIS Case II Fall Chlorophyll *a* Minimum (mg m^{-3}). Points falling under (upper panel) and over (bottom panel) the reference line are mapped.

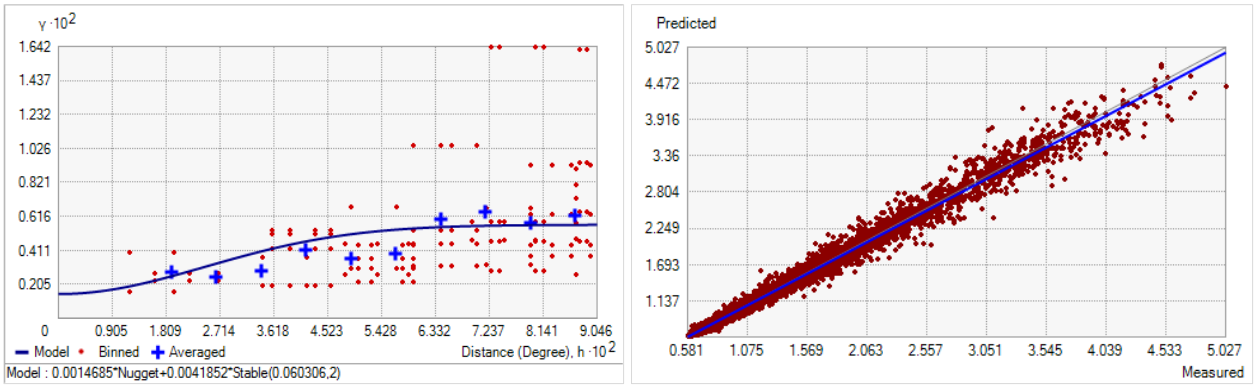

Fig. 418. Left panel: Semivariogram of MERIS Case II Fall Chlorophyll *a* Minimum (mg m^{-3}). Binned values are shown as red dots; average points are shown as blue crosses; the model fit to the averaged values is shown as a blue line. Lag size: 0.008 degrees; number of lags: 12; Parameter: 2; Range: 0.060 degrees; Partial Sill: 0.004. Right panel: Scatterplot of predicted values versus observed values for the variable MERIS Case II Fall Chlorophyll *a* Minimum (mg m^{-3}).

Table 168. Results of cross-validation of the kriged model for the MERIS Case II Fall Chlorophyll *a* Minimum (mg m^{-3}).

Prediction error	**Value**
Number of Observations	74353
Overall Mean Error	-9.158×10^{-5}
Root Mean Square Prediction Error	0.034
Standardized Mean	-0.001
Standardized Root Mean Square Prediction Error	0.720
Average Standard Error	0.046

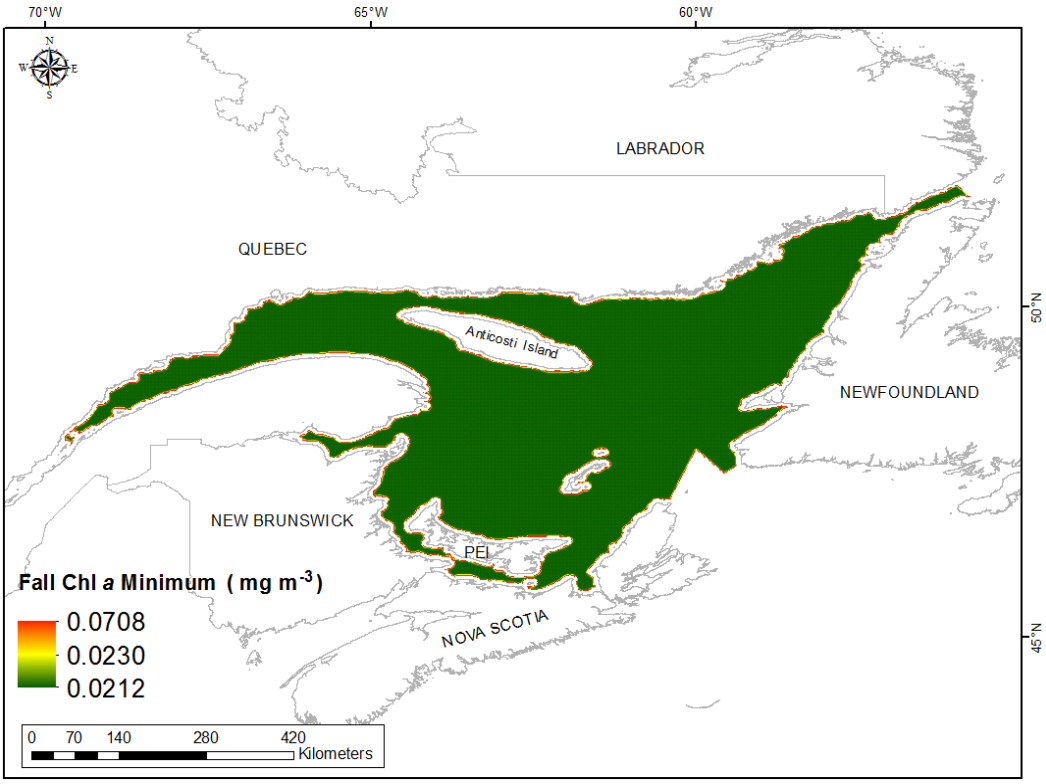

Fig. 419. Prediction standard error surface of MERIS Case II Fall Chlorophyll *a* Minimum (mg m^{-3}).

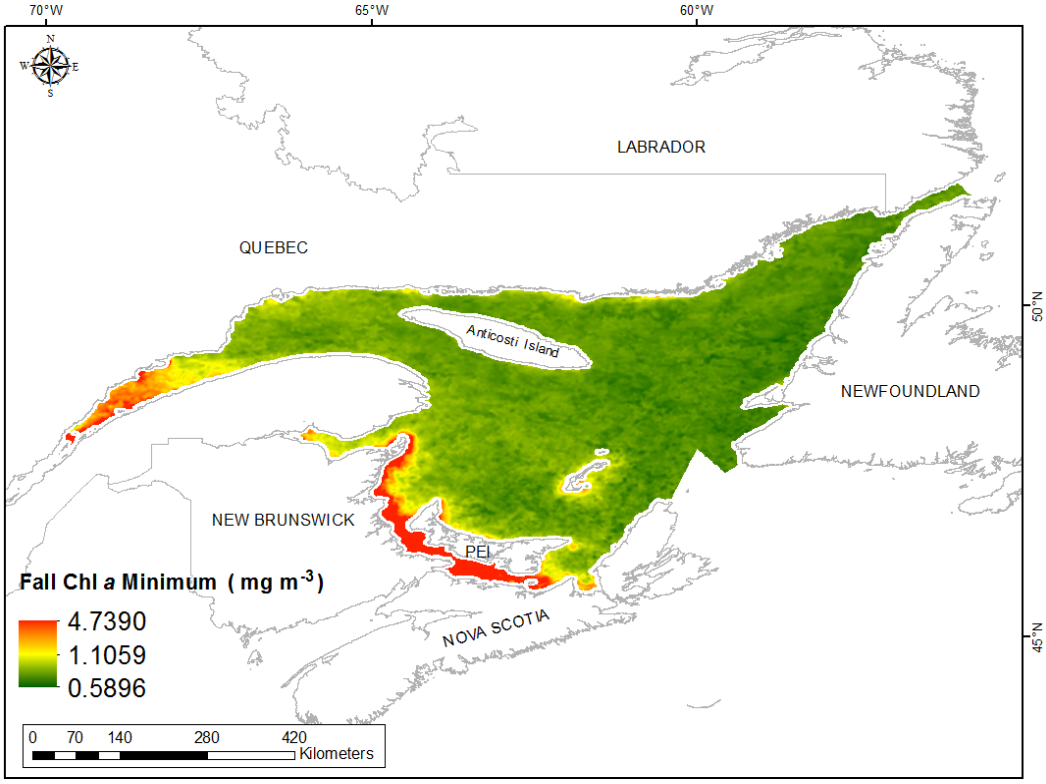

Fig. 420. Interpolated prediction surface of MERIS Case II Fall Chlorophyll *a* Minimum (mg m^{-3}).

MERIS Case II Fall Chlorophyll *a* Maximum

This variable displayed a strongly right-skewed distribution with kurtosis prior to modeling (Table 169, Fig. 421). The data were higher than predicted by a normal distribution at the lower and upper ranges and lower than predicted at mid values (Fig. 422). The areas of under- and over-prediction showed a strong spatial pattern over the spatial extent (Fig. 422).

The semivariogram showed moderate autocorrelation present in the data and the model showed a very good fit between measured and predicted values (Fig. 423). The model showed fair cross-validation statistics (Table 170). The error map showed low error over the study extent (Fig. 424). The kriged surface is presented in Fig. 425.

Table 169. Distributional properties of MERIS Case II Fall Chlorophyll *a* Maximum (mg m^{-3}).

Property	Value
Number of Observations	74353
Minimum	0.812
Maximum	12.041
Mean	1.314
Median	1.103
Standard Deviation	0.795
Skewness	5.225
Kurtosis	38.329

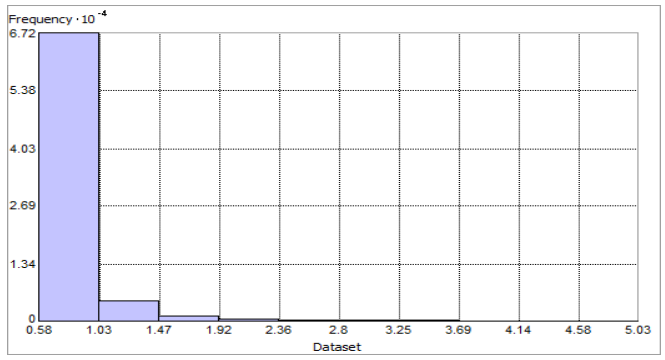

Fig. 421. Distribution of MERIS Case II Fall Chlorophyll *a* Maximum (mg m^{-3}). Histogram was illustrated using 10 bins. X and Y axes are shown at 10^{-1} and 10^{-4}, respectively.

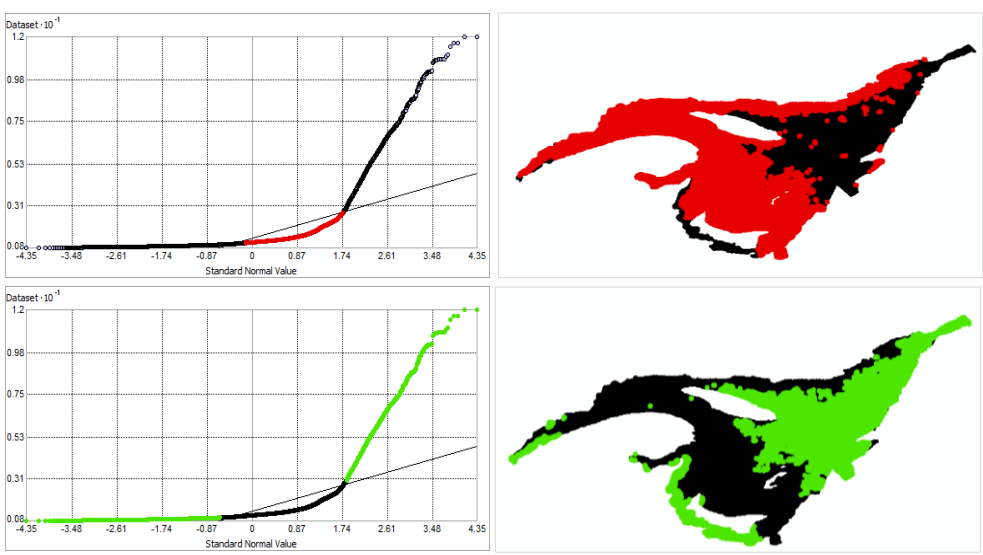

Fig. 422. Normal Q-Q plot for data values of MERIS Case II Fall Chlorophyll *a* Maximum (mg m^{-3}). Points falling under (upper panel) and over (bottom panel) the reference line are mapped.

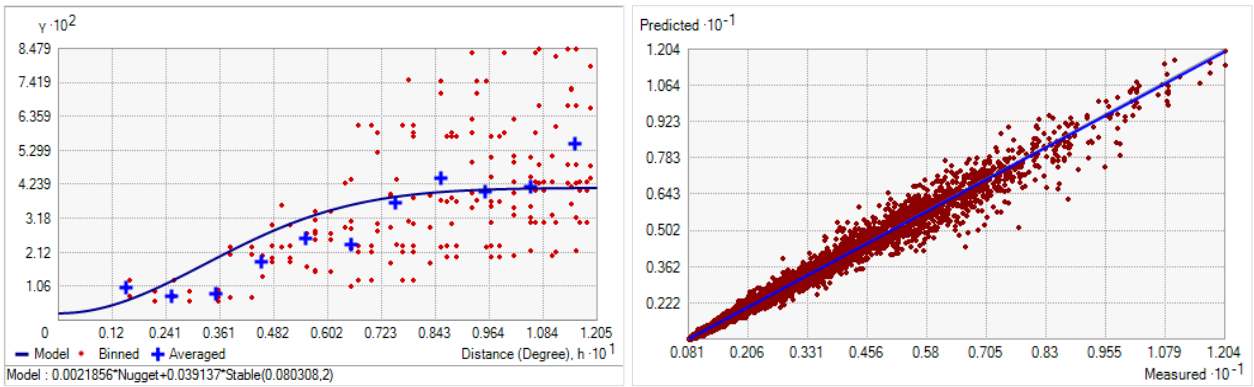

Fig. 423. Left panel: Semivariogram of MERIS Case II Fall Chlorophyll *a* Maximum (mg m^{-3}). Binned values are shown as red dots; average points are shown as blue crosses; the model fit to the averaged values is shown as a blue line. Lag size: 0.010 degrees; number of lags: 12; Parameter: 2; Range: 0.080 degrees; Partial Sill: 0.039. Right panel: Scatterplot of predicted values versus observed values for the variable MERIS Case II Fall Chlorophyll *a* Maximum (mg m^{-3}).

Table 170. Results of cross-validation of the kriged model for the MERIS Case II Fall Chlorophyll *a* Maximum (mg m^{-3}).

Prediction error	**Value**
Number of Observations	74353
Overall Mean Error	-2.071×10^{-4}
Root Mean Square Prediction Error	0.082
Standardized Mean	-0.002
Standardized Root Mean Square Prediction Error	1.389
Average Standard Error	0.057

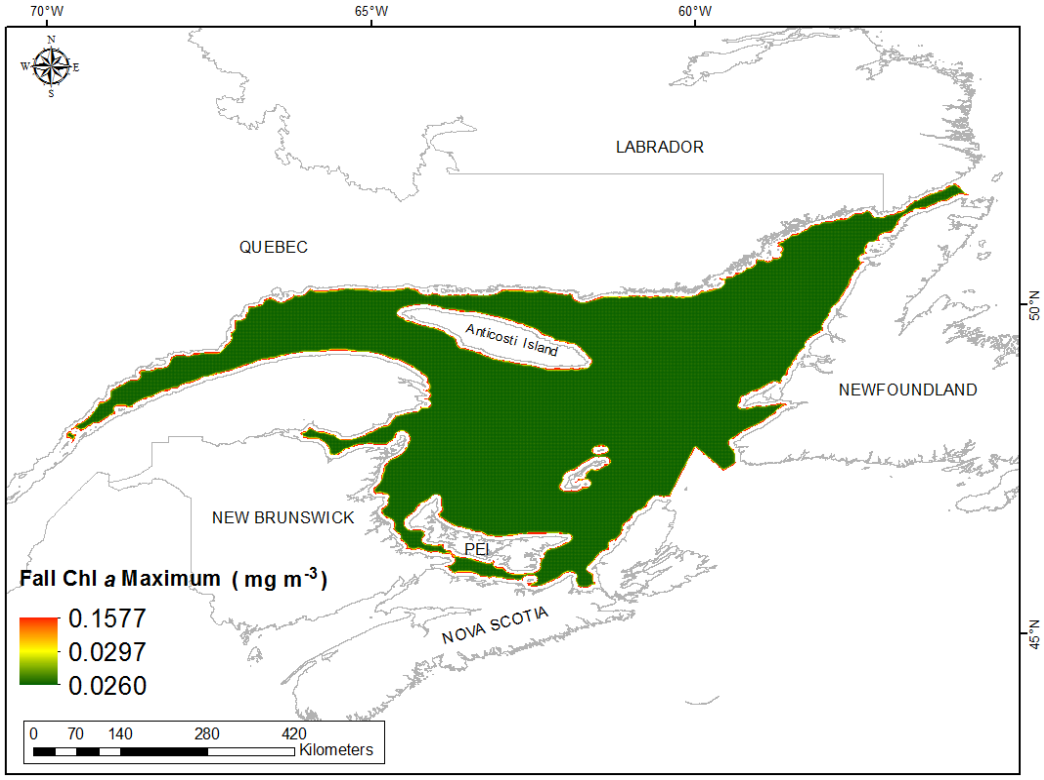

Fig. 424. Prediction standard error surface of MERIS Case II Fall Chlorophyll *a* Maximum (mg m^{-3}).

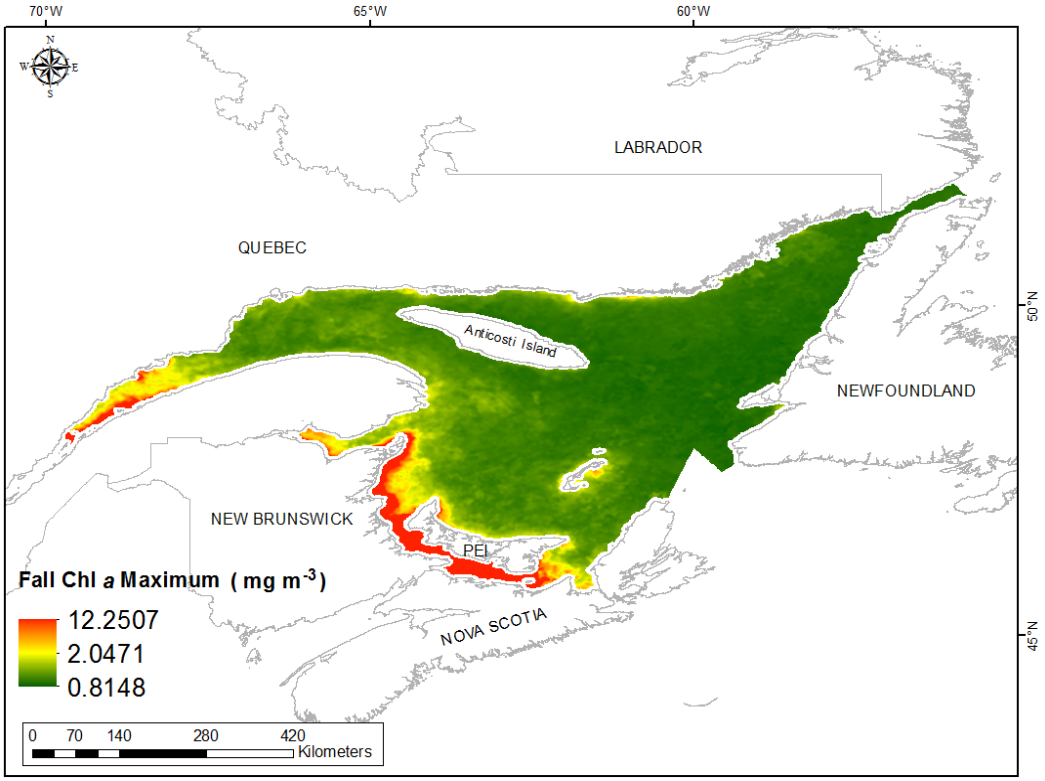

Fig. 425. Interpolated prediction surface of MERIS Case II Fall Chlorophyll *a* Maximum (mg m^{-3}).

MERIS Case II Fall Chlorophyll *a* Range

This variable displayed a strongly right-skewed distribution with extreme kurtosis prior to modeling (Table 172, Fig. 426). The data were higher than predicted by a normal distribution at the lower and upper ranges and lower than predicted at mid values (Fig. 427). The areas of under- and over-prediction showed a spatial pattern over the spatial extent (Fig. 427).

The semivariogram showed weak to moderate autocorrelation present in the data and the model showed a very good fit between measured and predicted values (Fig. 428). The model showed fair cross-validation statistics (Table 173). The error map showed low error over the study extent (Fig. 429). The kriged surface is presented in Fig. 430.

Table 171. Distributional properties of MERIS Case II Fall Chlorophyll *a* Range (mg m^{-3}).

Property	Value
Number of Observations	74353
Minimum	0.040
Maximum	8.687
Mean	0.441
Median	0.300
Standard Deviation	0.520
Skewness	5.222
Kurtosis	40.947

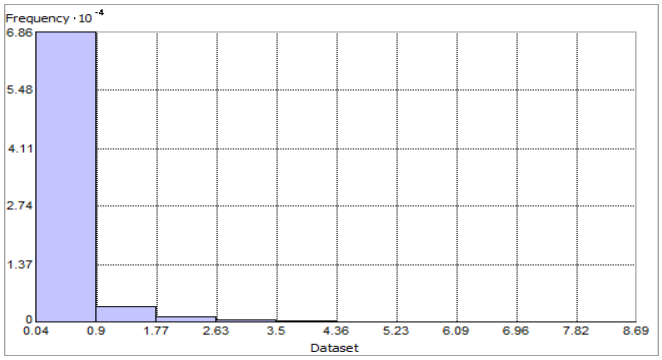

Fig. 426. Distribution of MERIS Case II Fall Chlorophyll *a* Range (mg m^{-3}). Histogram was illustrated using 10 bins. Y axis is shown at 10^{-4}.

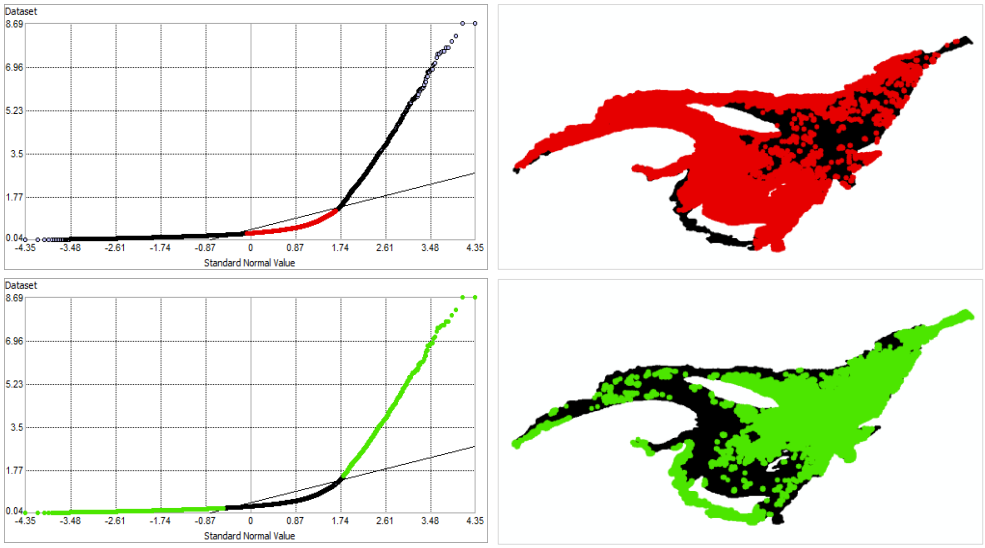

Fig. 427. Normal Q-Q plot for data values of MERIS Case II Fall Chlorophyll *a* Range (mg m^{-3}). Points falling under (upper panel) and over (bottom panel) the reference line are mapped.

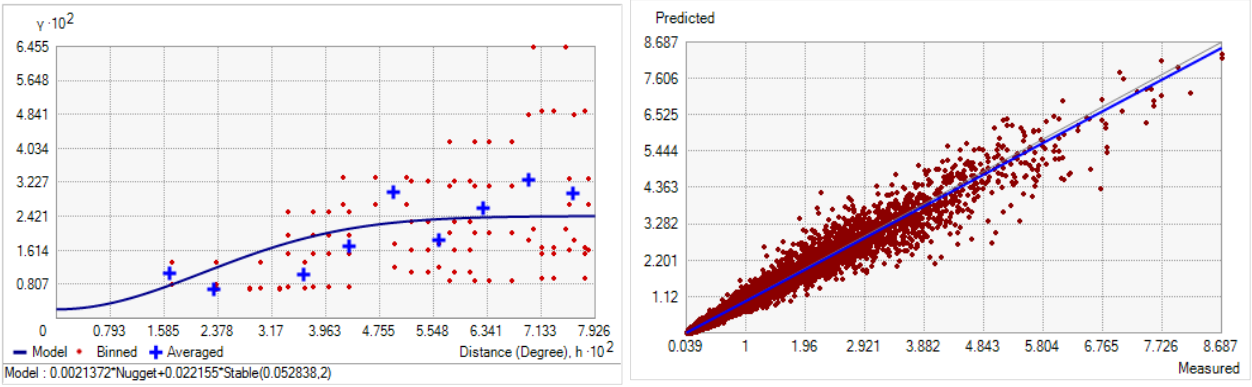

Fig. 428. Left panel: Semivariogram of MERIS Case II Fall Chlorophyll *a* Range (mg m^{-3}). Binned values are shown as red dots; average points are shown as blue crosses; the model fit to the averaged values is shown as a blue line. Lag size: 0.007 degrees; number of lags: 12; Parameter: 2; Range: 0.053 degrees; Partial Sill: 0.022. Right panel: Scatterplot of predicted values versus observed values for the variable MERIS Case II Fall Chlorophyll *a* Range (mg m^{-3}).

Table 172. Results of cross-validation of the kriged model for the MERIS Case II Fall Chlorophyll *a* Range (mg m^{-3}).

Prediction error	**Value**
Number of Observations	74353
Overall Mean Error	-3.249×10^{-4}
Root Mean Square Prediction Error	0.087
Standardized Mean	-0.003
Standardized Root Mean Square Prediction Error	1.229
Average Standard Error	0.068

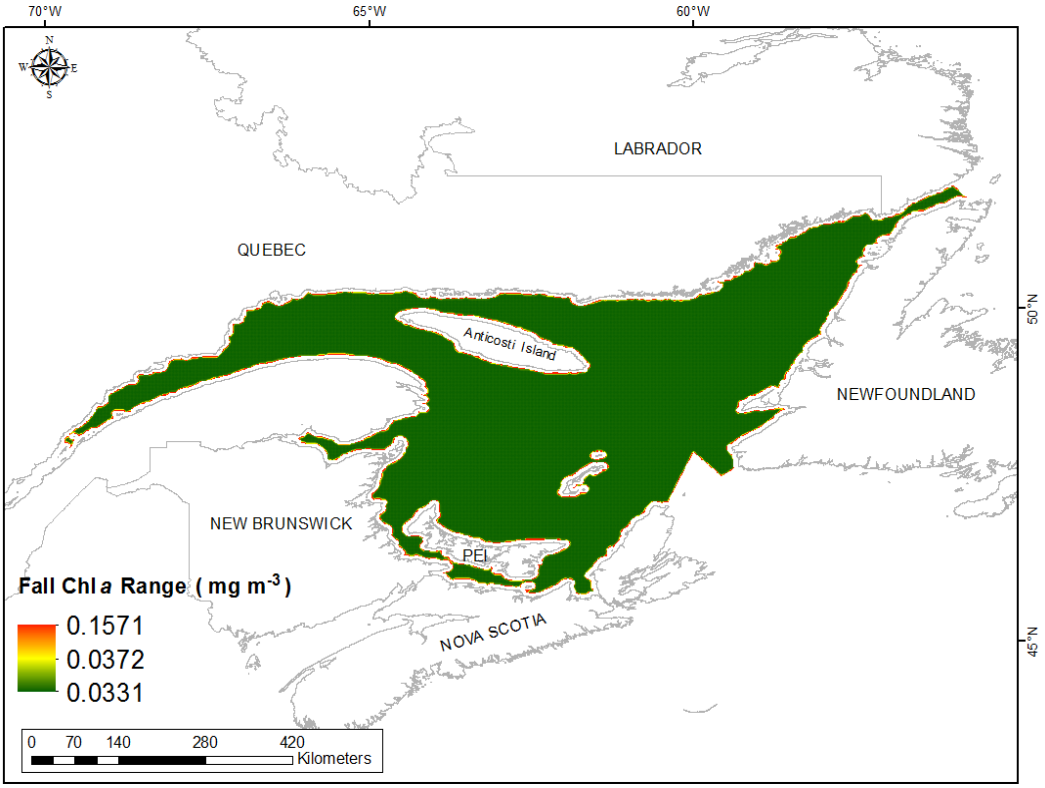

Fig. 429. Prediction standard error surface of MERIS Case II Fall Chlorophyll *a* Range (mg m^{-3}).

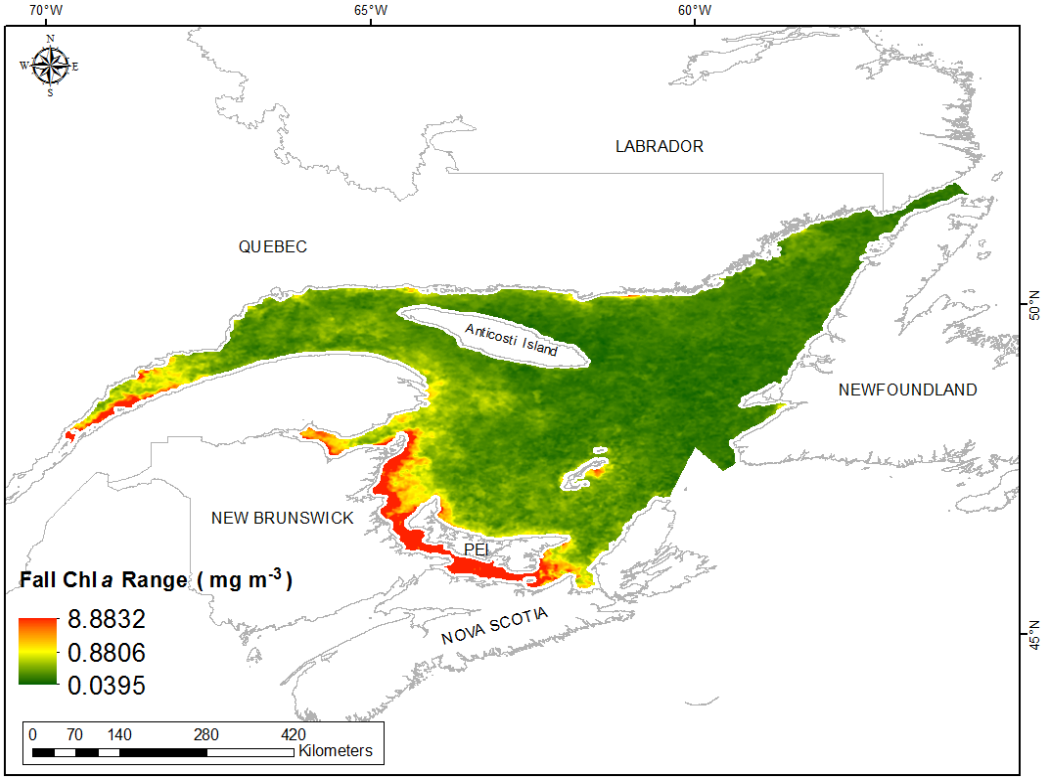

Fig. 430. Interpolated prediction surface of MERIS Case II Fall Chlorophyll *a* Range (mg m^{-3}).

MERIS Case II Annual Chlorophyll *a* Mean

This variable displayed a right-skewed distribution with kurtosis prior to modeling (Table 173, Fig. 431). The data were higher than predicted by a normal distribution at the lower and upper ranges and lower than predicted at mid values (Fig. 432). The areas of under- and over-prediction showed a strong spatial pattern over the spatial extent (Fig. 432).

The semivariogram showed moderate autocorrelation present in the data and the model showed a very good fit between measured and predicted values (Fig. 433). The model showed fair to poor cross-validation statistics (Table 174) indicating poor model performance. The error map showed low error over the study extent (Fig. 434). The kriged surface is presented in Fig. 435.

Table 173. Distributional properties of MERIS Case II Annual Chlorophyll *a* Mean (mg m^{-3}).

Property	Value
Number of Observations	74353
Minimum	0.627
Maximum	4.262
Mean	1.004
Median	0.916
Standard Deviation	0.365
Skewness	2.805
Kurtosis	13.406

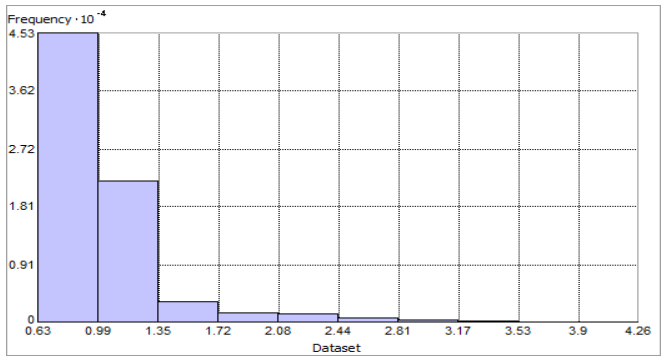

Fig. 431. Distribution of MERIS Case II Annual Chlorophyll *a* Mean (mg m^{-3}). Histogram was illustrated using 10 bins. Y axis is shown at 10^{-4}.

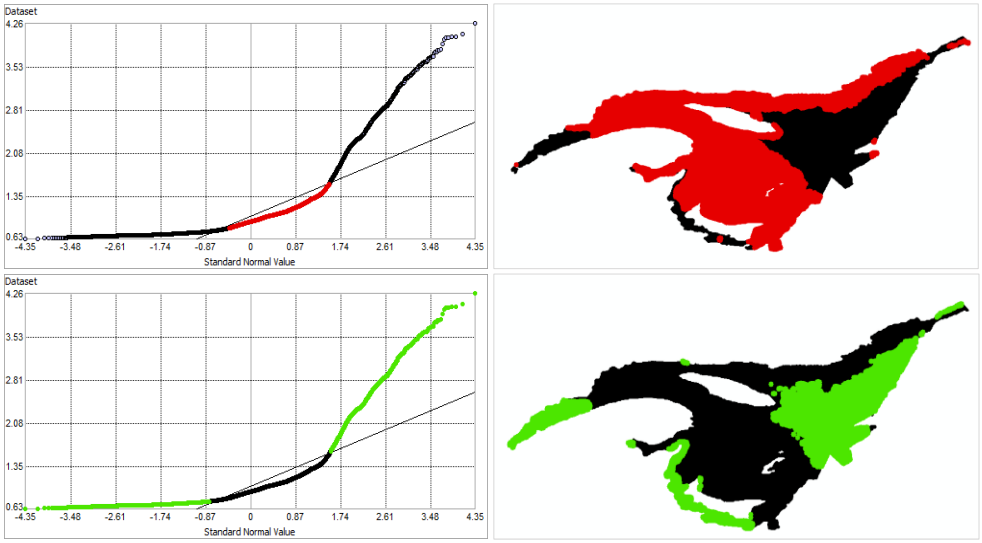

Fig. 432. Normal Q-Q plot for data values of MERIS Case II Annual Chlorophyll *a* Mean (mg m^{-3}). Points falling under (upper panel) and over (bottom panel) the reference line are mapped.

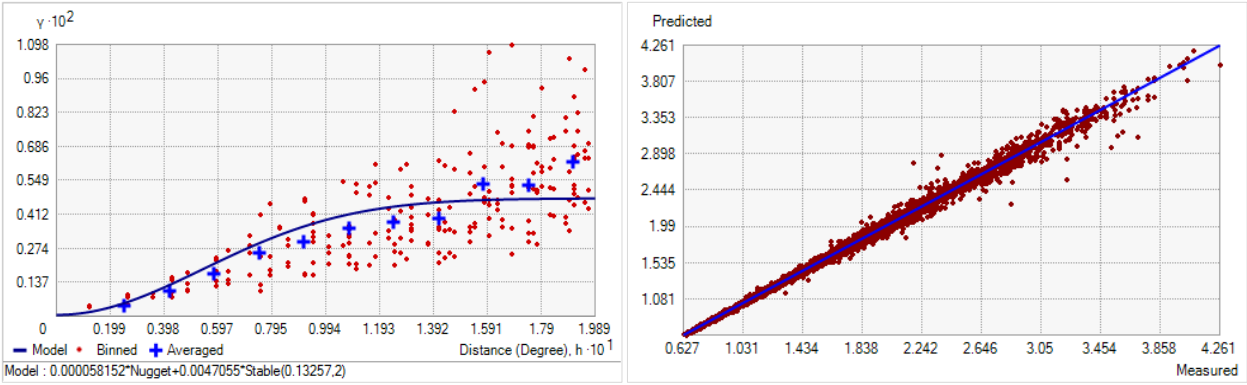

Fig. 433. Left panel: Semivariogram of MERIS Case II Annual Chlorophyll *a* Mean (mg m^{-3}). Binned values are shown as red dots; average points are shown as blue crosses; the model fit to the averaged values is shown as a blue line. Lag size: 0.017 degrees; number of lags: 12; Parameter: 2; Range: 0.133 degrees; Partial Sill: 0.005. Right panel: Scatterplot of predicted values versus observed values for the variable MERIS Case II Annual Chlorophyll *a* Mean (mg m^{-3}).

Table 174. Results of cross-validation of the kriged model for the MERIS Case II Annual Chlorophyll *a* Mean (mg m^{-3}).

Prediction error	**Value**
Number of Observations	74353
Overall Mean Error	2.071×10^{-5}
Root Mean Square Prediction Error	0.015
Standardized Mean	0.003
Standardized Root Mean Square Prediction Error	1.590
Average Standard Error	0.009

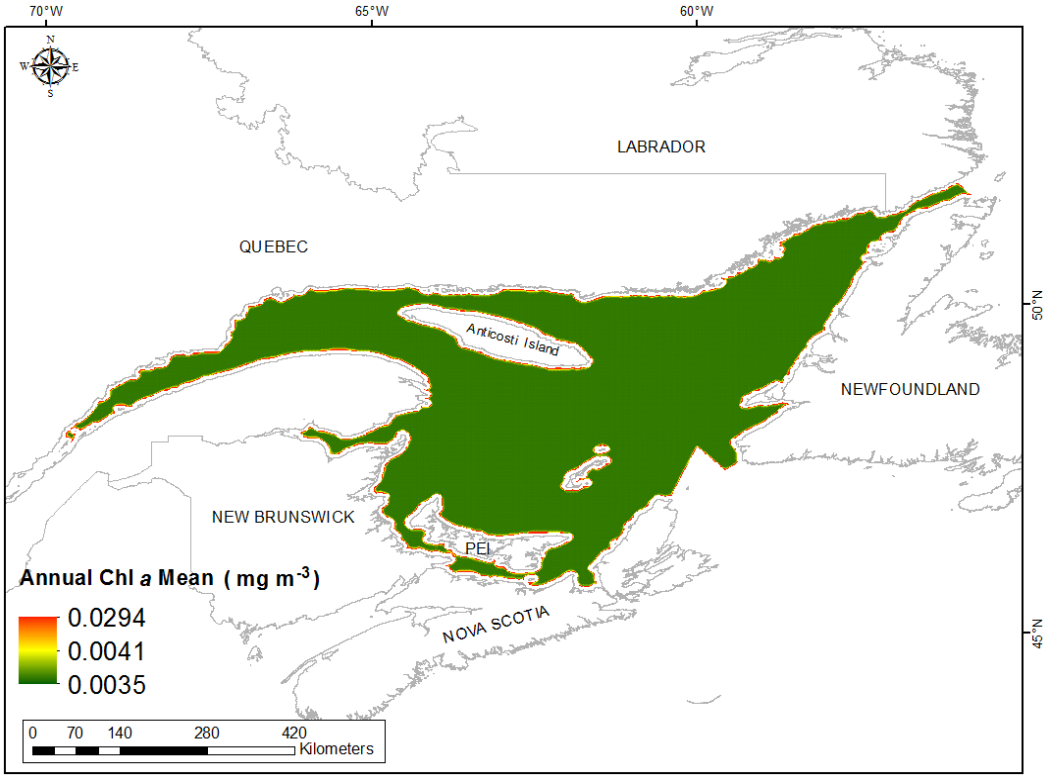

Fig. 434. Prediction standard error surface of MERIS Case II Annual Chlorophyll *a* Mean (mg m^{-3}).

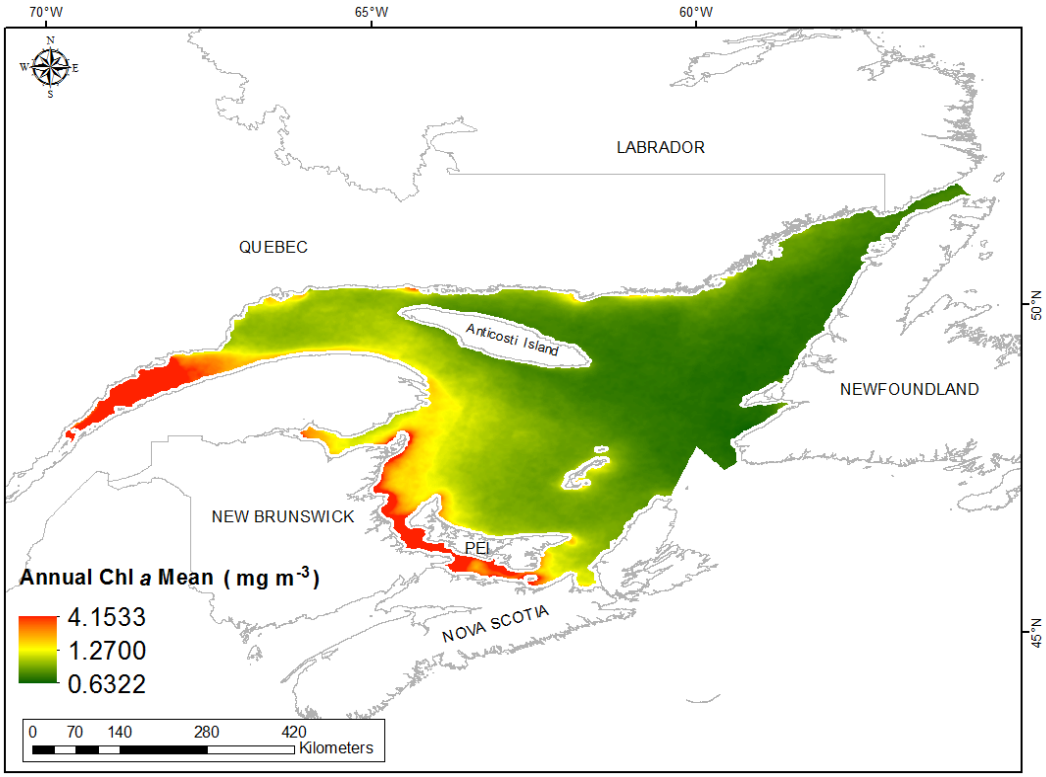

Fig. 435. Interpolated prediction surface of MERIS Case II Annual Chlorophyll *a* Mean (mg m^{-3}).

MERIS Case II Annual Chlorophyll *a* Minimum

This variable displayed a right-skewed distribution with kurtosis prior to modeling (Table 175, Fig. 436). The data were higher than predicted by a normal distribution at the lower and upper ranges and lower than predicted at mid values (Fig. 437). The areas of under- and over-prediction showed a strong spatial pattern over the spatial extent (Fig. 437).

The semivariogram showed moderate autocorrelation present in the data and the model showed a very good fit between measured and predicted values (Fig. 438). The model showed good cross-validation statistics (Table 176) indicating that it was good at prediction. The error map showed relatively moderate error over the study extent (Fig. 439). The kriged surface is presented in Fig. 440.

Table 175. Distributional properties of MERIS Case II Annual Chlorophyll *a* Minimum (mg m^{-3}).

Property	Value
Number of Observations	74353
Minimum	0.567
Maximum	3.338
Mean	0.876
Median	0.809
Standard Deviation	0.290
Skewness	2.680
Kurtosis	12.234

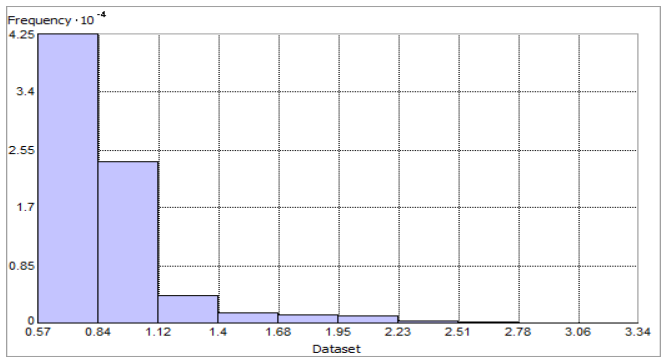

Fig. 436. Distribution of MERIS Case II Annual Chlorophyll *a* Minimum (mg m^{-3}). Histogram was illustrated using 10 bins. Y axis is shown at 10^{-4}.

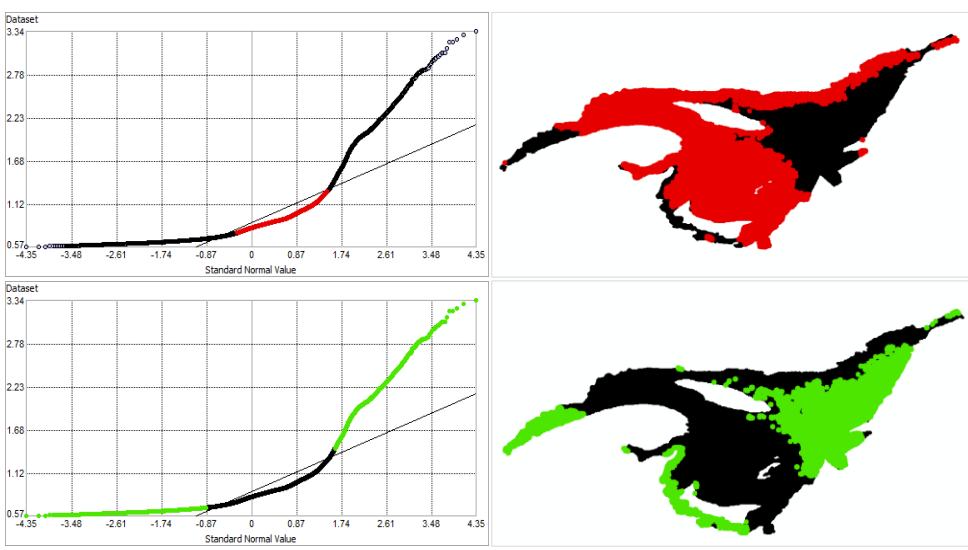

Fig. 437. Normal Q-Q plot for data values of MERIS Case II Annual Chlorophyll *a* Minimum (mg m^{-3}). Points falling under (upper panel) and over (bottom panel) the reference line are mapped.

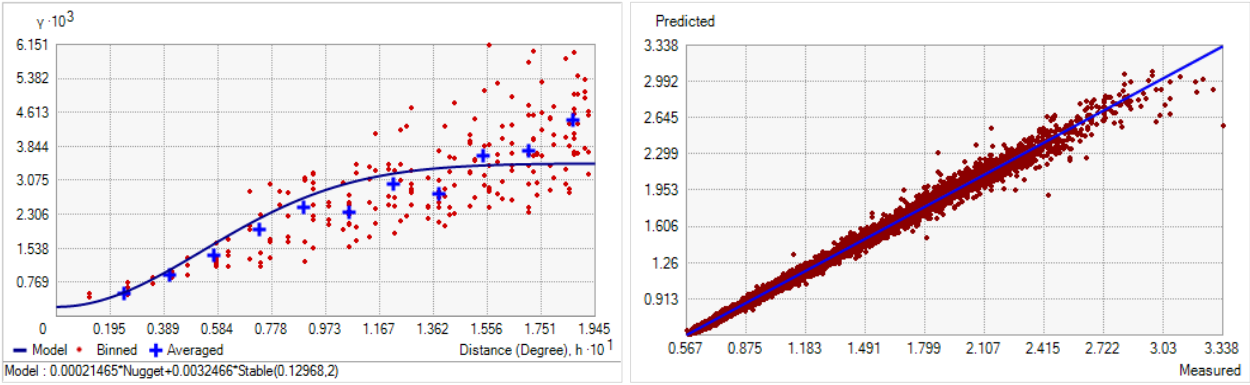

Fig. 438. Left panel: Semivariogram of MERIS Case II Annual Chlorophyll *a* Minimum (mg m^{-3}). Binned values are shown as red dots; average points are shown as blue crosses; the model fit to the averaged values is shown as a blue line. Lag size: 0.016 degrees; number of lags: 12; Parameter: 2; Range: 0.130 degrees; Partial Sill: 0.003. Right panel: Scatterplot of predicted values versus observed values for the variable MERIS Case II Annual Chlorophyll *a* Minimum (mg m^{-3}).

Table 176. Results of cross-validation of the kriged model for the MERIS Case II Annual Chlorophyll *a* Minimum (mg m^{-3}).

Prediction error	**Value**
Number of Observations	74353
Overall Mean Error	7.995×10^{-5}
Root Mean Square Prediction Error	0.018
Standardized Mean	0.005
Standardized Root Mean Square Prediction Error	1.095
Average Standard Error	0.016

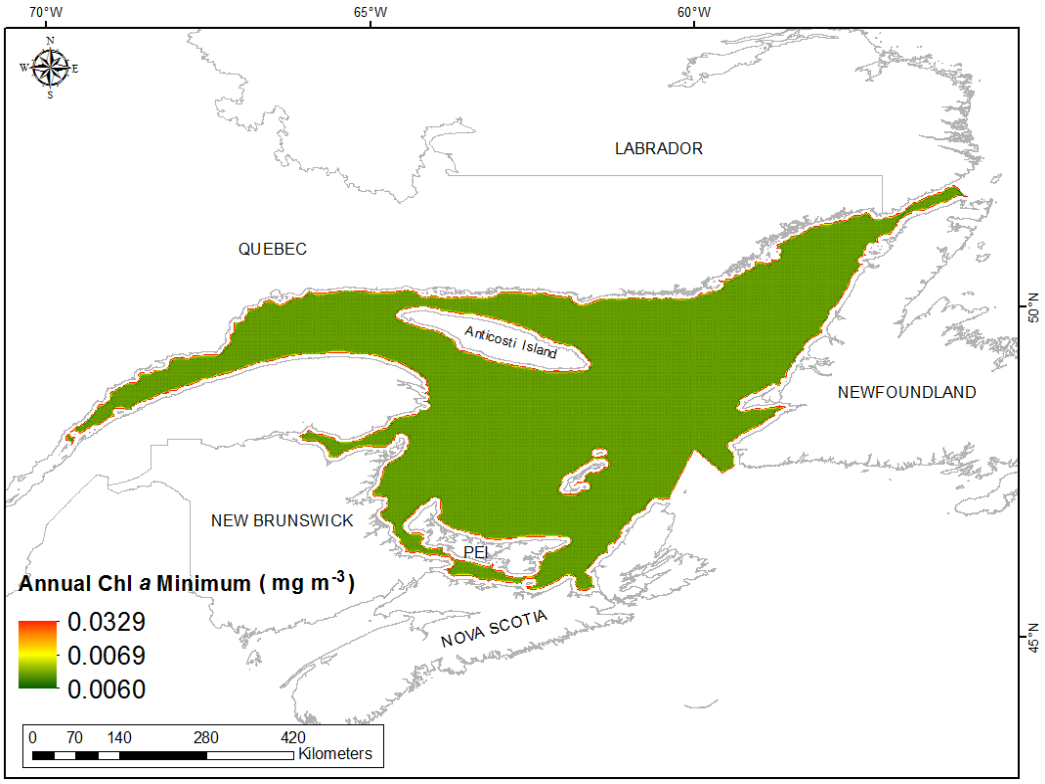

Fig. 439. Prediction standard error surface of MERIS Case II Annual Chlorophyll *a* Minimum (mg m^{-3}).

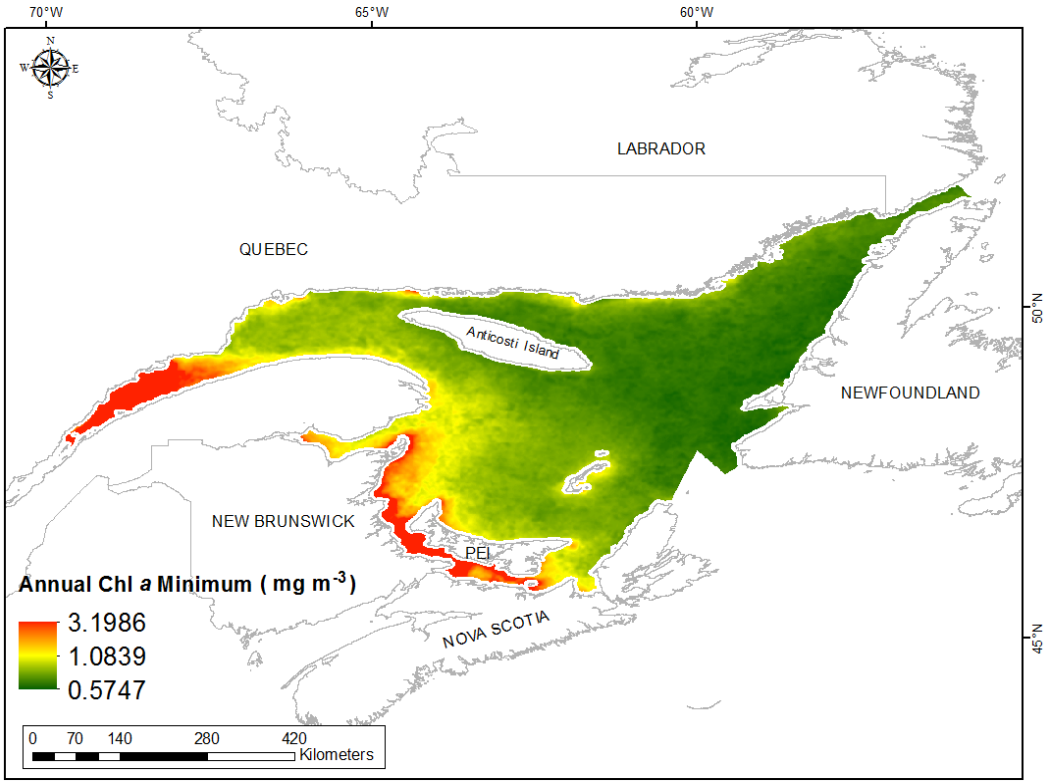

Fig. 440. Interpolated prediction surface of MERIS Case II Annual Chlorophyll *a* Minimum (mg m^{-3}).

MERIS Case II Annual Chlorophyll *a* Maximum

This variable displayed a right-skewed distribution with kurtosis prior to modeling (Table 177, Fig. 441). The data were higher than predicted by a normal distribution at the lower and upper ranges and lower than predicted at mid values (Fig. 442). The areas of under- and over-prediction showed a strong spatial pattern over the spatial extent (Fig. 442).

The semivariogram showed weak to moderate autocorrelation present in the data and the model showed a very good fit between measured and predicted values (Fig. 443). The model showed good cross-validation statistics (Table 178) indicating that it was good at prediction. The error map showed low error over the study extent (Fig. 444). The kriged surface is presented in Fig. 445.

Table 177. Distributional properties of MERIS Case II Annual Chlorophyll *a* Maximum (mg m^{-3}).

Property	Value
Number of Observations	74353
Minimum	0.707
Maximum	5.208
Mean	1.172
Median	1.061
Standard Deviation	0.460
Skewness	2.740
Kurtosis	13.181

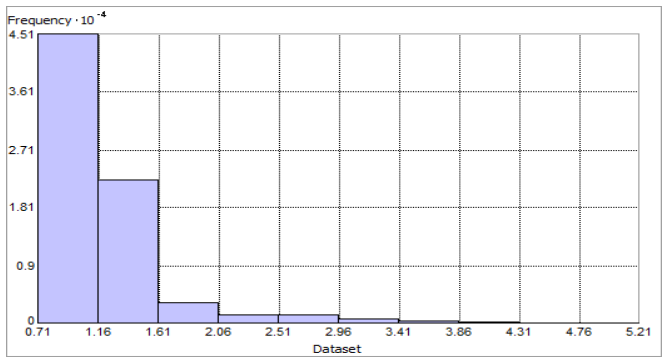

Fig. 441. Distribution of MERIS Case II Annual Chlorophyll *a* Maximum (mg m^{-3}). Histogram was illustrated using 10 bins. Y axis is shown at 10^{-4}.

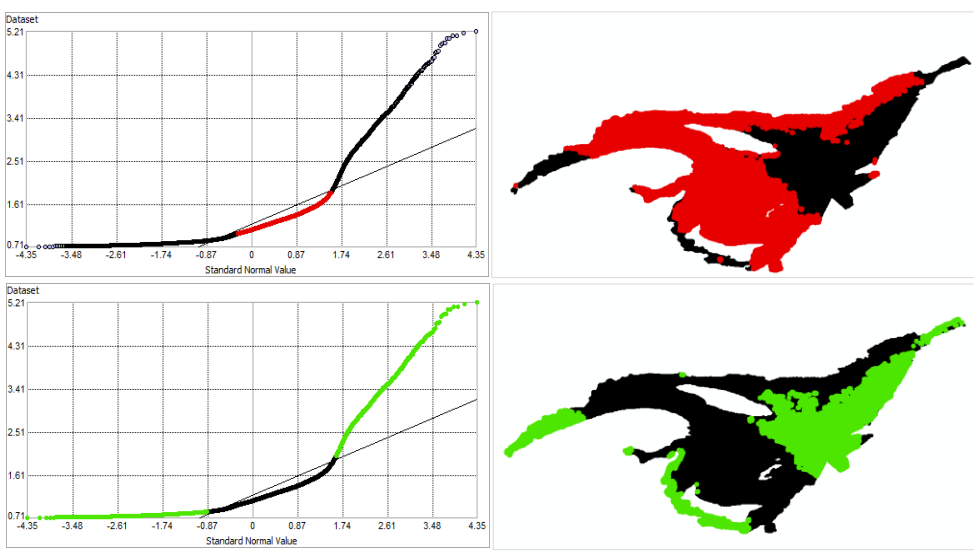

Fig. 442. Normal Q-Q plot for data values of MERIS Case II Annual Chlorophyll *a* Maximum (mg m^{-3}). Points falling under (upper panel) and over (bottom panel) the reference line are mapped.

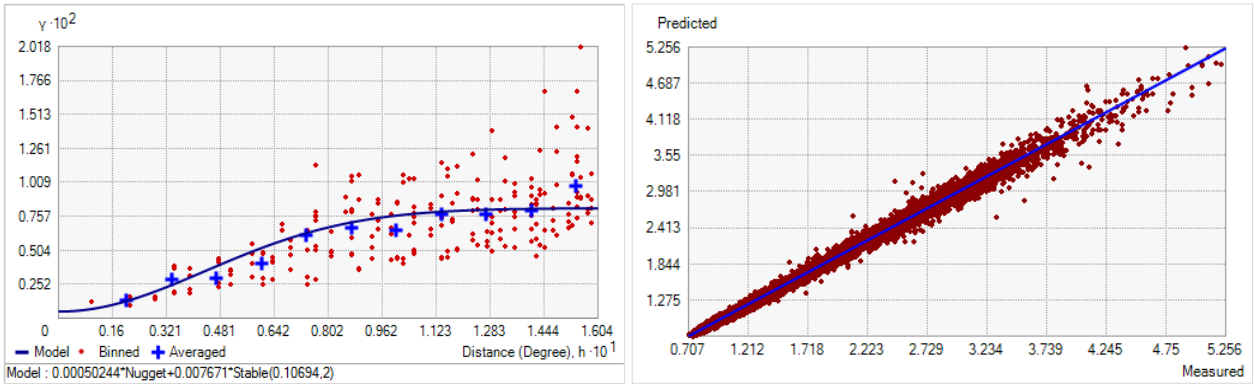

Fig. 443. Left panel: Semivariogram of MERIS Case II Annual Chlorophyll *a* Maximum (mg m^{-3}). Binned values are shown as red dots; average points are shown as blue crosses; the model fit to the averaged values is shown as a blue line. Lag size: 0.013 degrees; number of lags: 12; Parameter: 2; Range: 0.107 degrees; Partial Sill: 0.008. Right panel: Scatterplot of predicted values versus observed values for the variable MERIS Case II Annual Chlorophyll *a* Maximum (mg m^{-3}).

Table 178. Results of cross-validation of the kriged model for the MERIS Case II Annual Chlorophyll *a* Maximum (mg m^{-3}).

Prediction error	**Value**
Number of Observations	74353
Overall Mean Error	4.200×10^{-5}
Root Mean Square Prediction Error	0.031
Standardized Mean	0.002
Standardized Root Mean Square Prediction Error	1.194
Average Standard Error	0.026

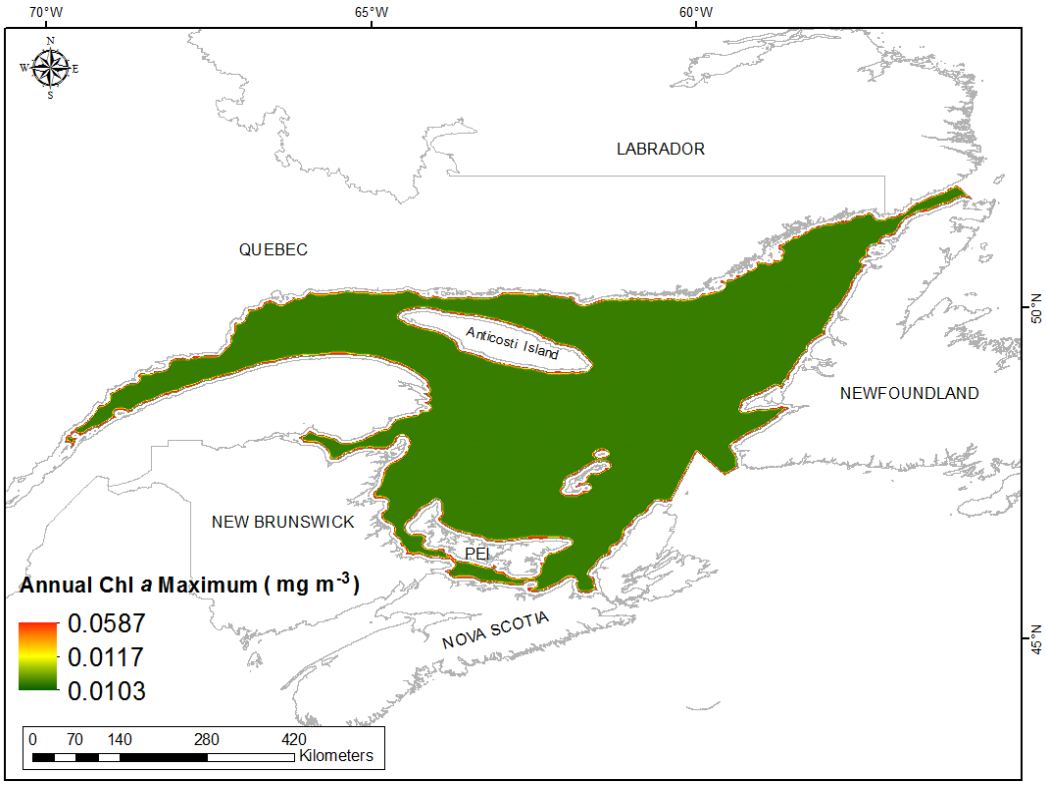

Fig. 444. Prediction standard error surface of MERIS Case II Annual Chlorophyll *a* Maximum (mg m^{-3}).

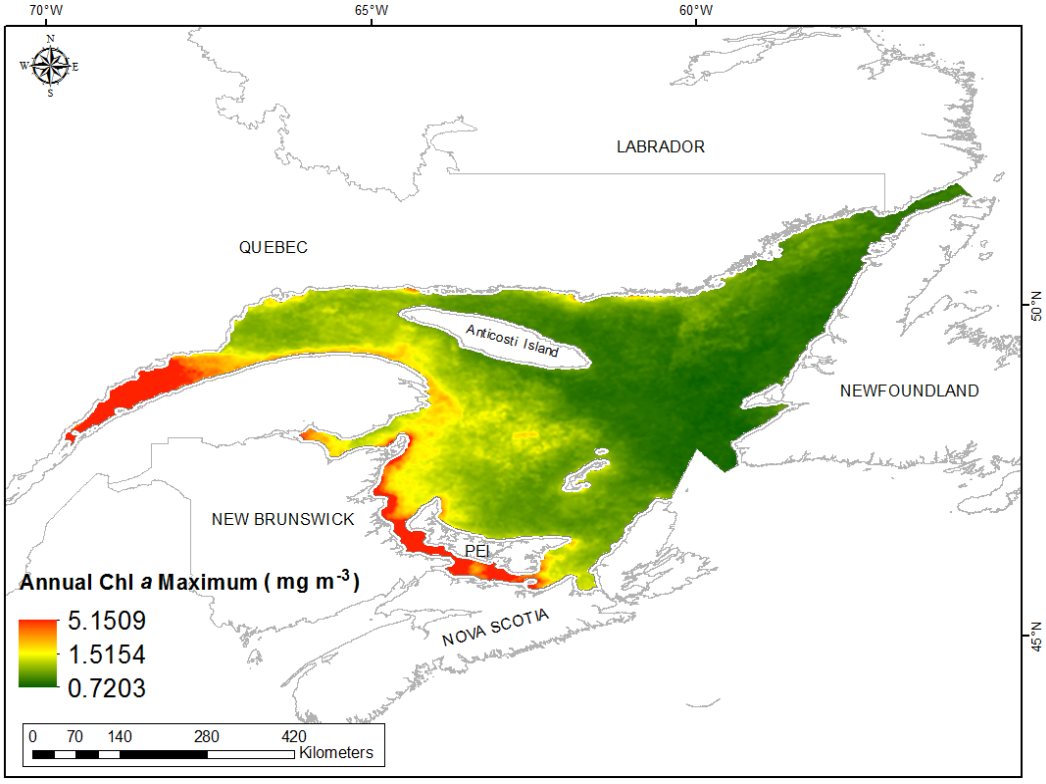

Fig. 445. Interpolated prediction surface of MERIS Case II Annual Chlorophyll *a* Maximum (mg m^{-3}).

MERIS Case II Annual Chlorophyll *a* Range

This variable displayed a right-skewed distribution with kurtosis prior to modeling (Table 179, Fig. 446). The data were higher than predicted by a normal distribution at the lower and upper ranges and slightly lower than predicted at mid values (Fig. 447). The areas of under- and over-prediction showed a spatial pattern over the spatial extent (Fig. 447).

The semivariogram showed moderate autocorrelation present in the data and the model showed a very good fit between measured and predicted values (Fig. 448). The model showed good cross-validation statistics (Table 180) indicating that it was good at prediction. The error map showed low error over the study extent except along the coast where it was higher (Fig. 449). The kriged surface is presented in Fig. 450.

Table 179. Distributional properties of MERIS Case II Annual Chlorophyll *a* Range (mg m^{-3}).

Property	Value
Number of Observations	74353
Minimum	0.037
Maximum	2.486
Mean	0.295
Median	0.245
Standard Deviation	0.196
Skewness	2.827
Kurtosis	15.839

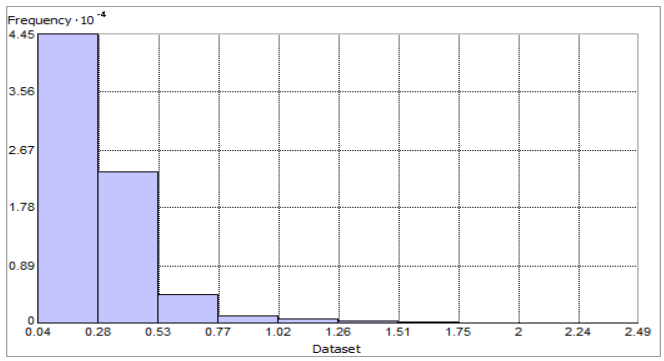

Fig. 446. Distribution of MERIS Case II Annual Chlorophyll *a* Range (mg m^{-3}). Histogram was illustrated using 10 bins. Y axis is shown at 10^{-4}.

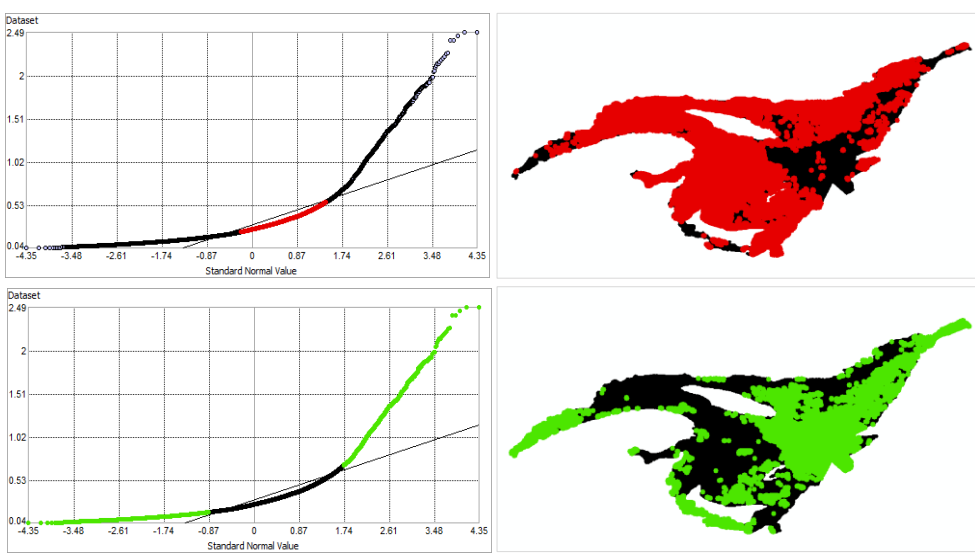

Fig. 447. Normal Q-Q plot for data values of MERIS Case II Annual Chlorophyll *a* Range (mg m^{-3}). Points falling under (upper panel) and over (bottom panel) the reference line are mapped.

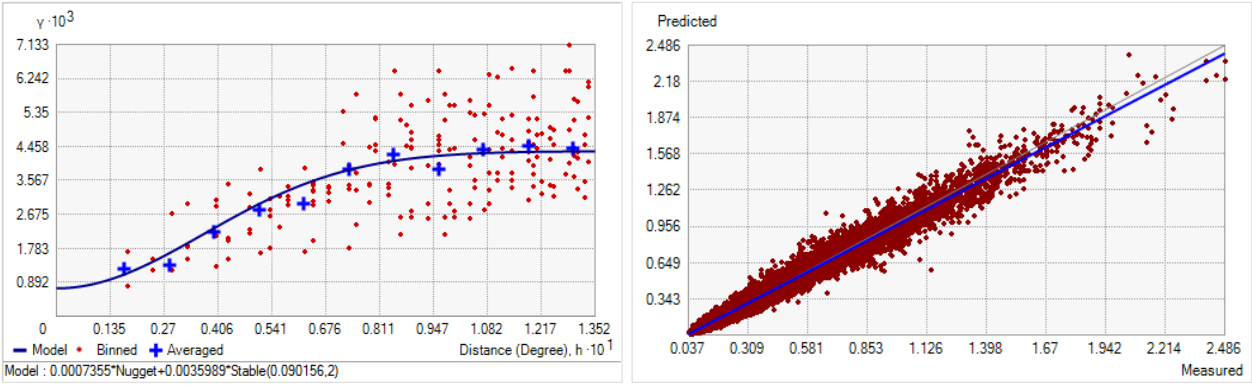

Fig. 448. Left panel: Semivariogram of MERIS Case II Annual Chlorophyll *a* Range (mg m^{-3}). Binned values are shown as red dots; average points are shown as blue crosses; the model fit to the averaged values is shown as a blue line. Lag size: 0.011 degrees; number of lags: 12; Parameter: 2; Range: 0.090 degrees; Partial Sill: 0.004. Right panel: Scatterplot of predicted values versus observed values for the variable MERIS Case II Annual Chlorophyll *a* Range (mg m^{-3}).

Table 180. Results of cross-validation of the kriged model for the MERIS Case II Annual Chlorophyll *a* Range (mg m^{-3}).

Prediction error	**Value**
Number of Observations	74353
Overall Mean Error	4.531×10^{-6}
Root Mean Square Prediction Error	0.032
Standardized Mean	2.913×10^{-4}
Standardized Root Mean Square Prediction Error	1.026
Average Standard Error	0.031

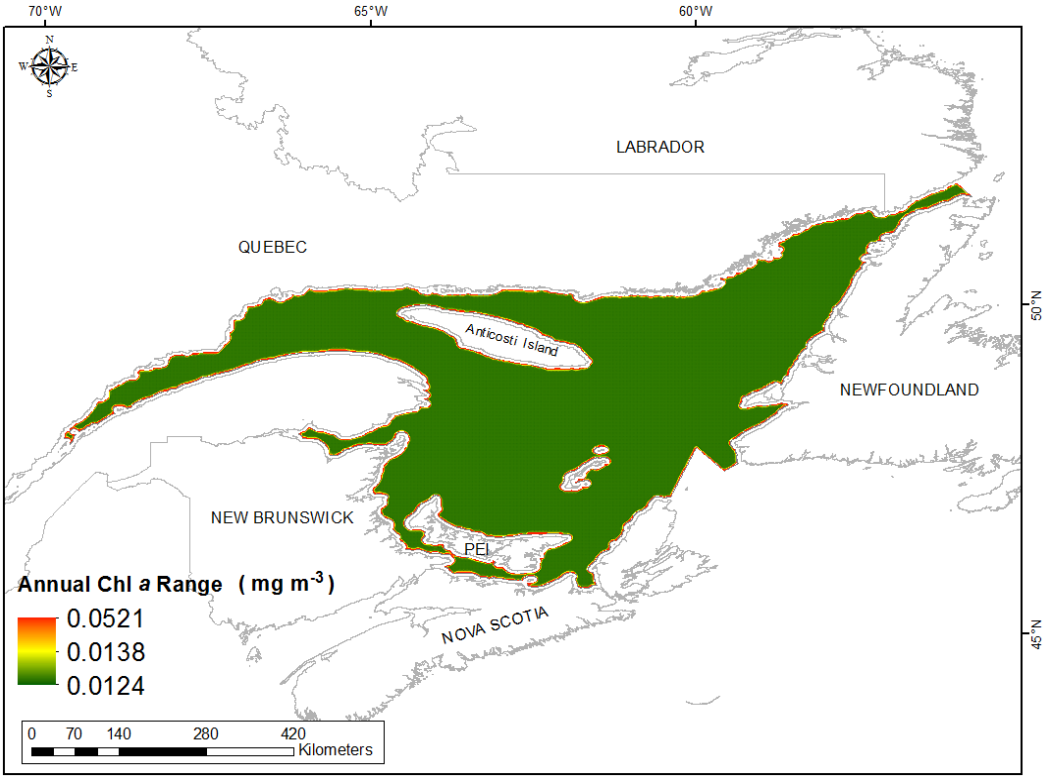

Fig. 449. Prediction standard error surface of MERIS Case II Annual Chlorophyll *a* Range (mg m^{-3}).

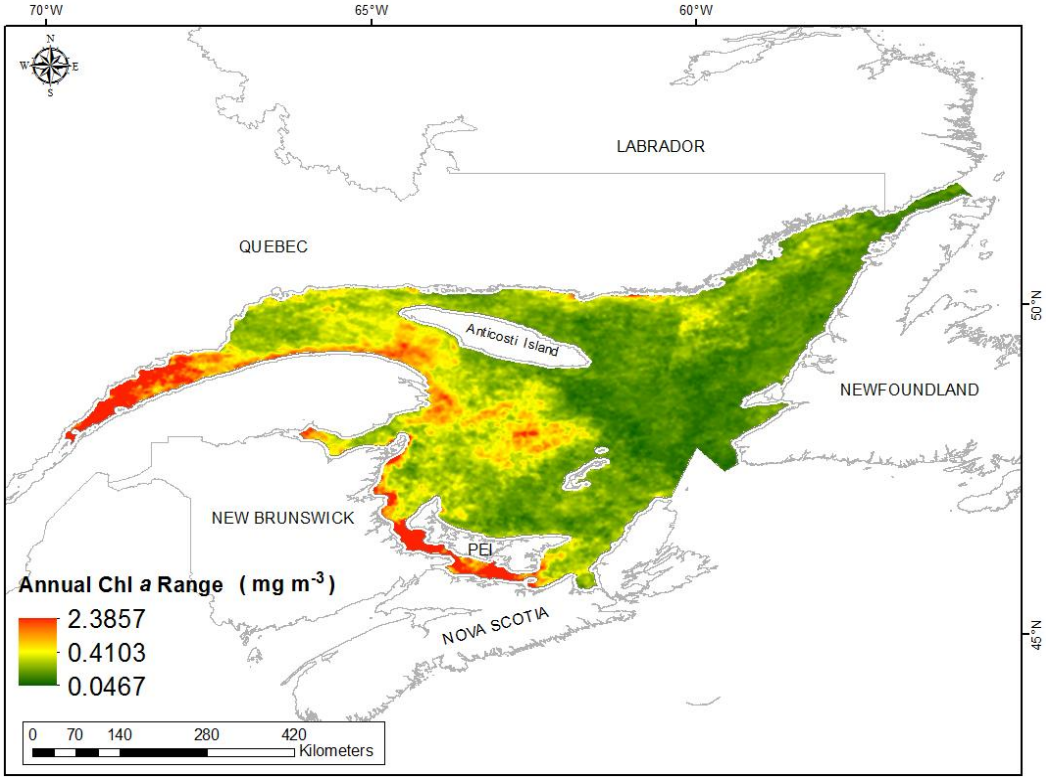

Fig. 450. Interpolated prediction surface of MERIS Case II Annual Chlorophyll *a* Range (mg m^{-3}).

Primary Production

Primary production measures the rate at which atmospheric or aqueous carbon dioxide is converted to organic carbon by autotrophs (Bender et al., 1987) and relates more directly to the flux of particulate organic carbon and food supply to the seafloor than sea surface chlorophyll *a* concentration. However, as satellite-derived chlorophyll *a* is a main source of data used in the calculation of the primary production variables in this report, we expect these variables to be highly correlated.

Spring Primary Production Mean

This variable displayed a bell-shaped distribution with extreme kurtosis prior to modeling (Table 181, Fig. 451). The data were higher than predicted by a normal distribution at low and high values however the mid-region was well-predicted (Fig. 452). The areas of over- and under-prediction showed no strong spatial pattern over the spatial extent (Fig. 452).

The semivariogram showed moderate autocorrelation present in the data and the model showed good fit between measured and predicted values (Fig. 453). Although the RMSPE and ASE were high, all other errors showed that the model was good at prediction (Table 182). The error map showed low error over the spatial extent but was slightly higher in the Gulf of St. Lawrence estuary, Chaleur Bay, and in the Strait of Belle Isle (Fig. 454). The kriged surface is presented in Fig. 455.

Table 181. Distributional properties of Spring Primary Production Mean (mg C m^{-2} day^{-1}).

Property	Value
Number of Observations	2204
Minimum	340.460
Maximum	1588.600
Mean	866.500
Median	857.850
Standard Deviation	153.140
Skewness	0.635
Kurtosis	0.635

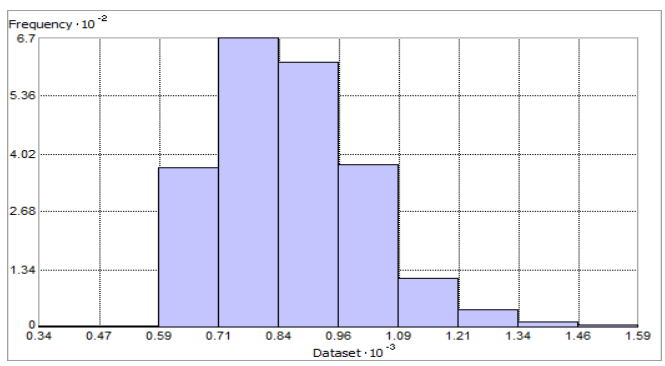

Fig. 451. Distribution of Spring Primary Production Mean (mg C m^{-2} day^{-1}). Histogram was illustrated using 10 bins. X axis is shown at 10^{-3}; Y axis shown at 10^{-2}.

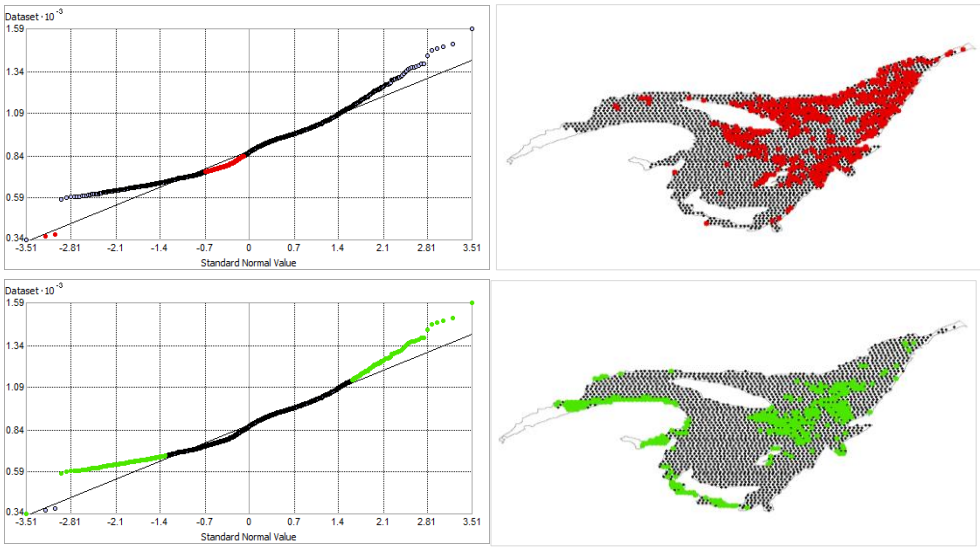

Fig. 452. Normal Q-Q plot for data values of Spring Primary Production Mean (mg C m^{-2} day^{-1}). Points falling under (upper panel) and over (bottom panel) the reference line are mapped.

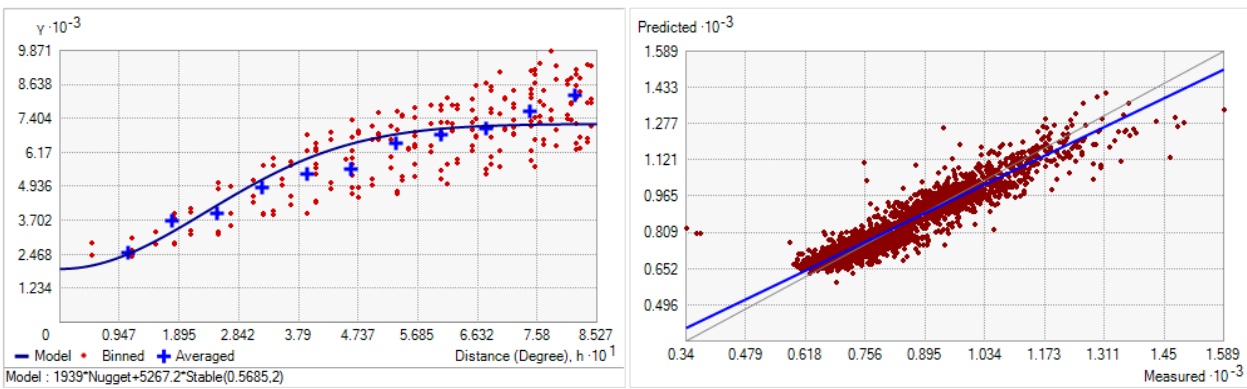

Fig. 453. Left panel: Semivariogram of Spring Primary Production Mean (mg C m^{-2} day^{-1}). Binned values are shown as red dots; average points are shown as blue crosses; the model fit to the averaged values is shown as a blue line. Lag size: 0.071 degrees; number of lags: 12; Parameter: 2; Range: 0.568 degrees; Partial Sill: 5267.222. Right panel: Scatterplot of predicted values versus observed values for the model of Spring Primary Production Mean (mg C m^{-2} day^{-1}).

Table 182. Results of cross-validation of the kriged model for Spring Primary Production Mean (mg C m^{-2} day^{-1}).

Prediction error	**Value**
Number of Observations	2204
Overall Mean Error	0.178
Root Mean Square Prediction Error	55.686
Standardized Mean	0.005
Standardized Root Mean Square Prediction Error	1.104
Average Standard Error	48.945

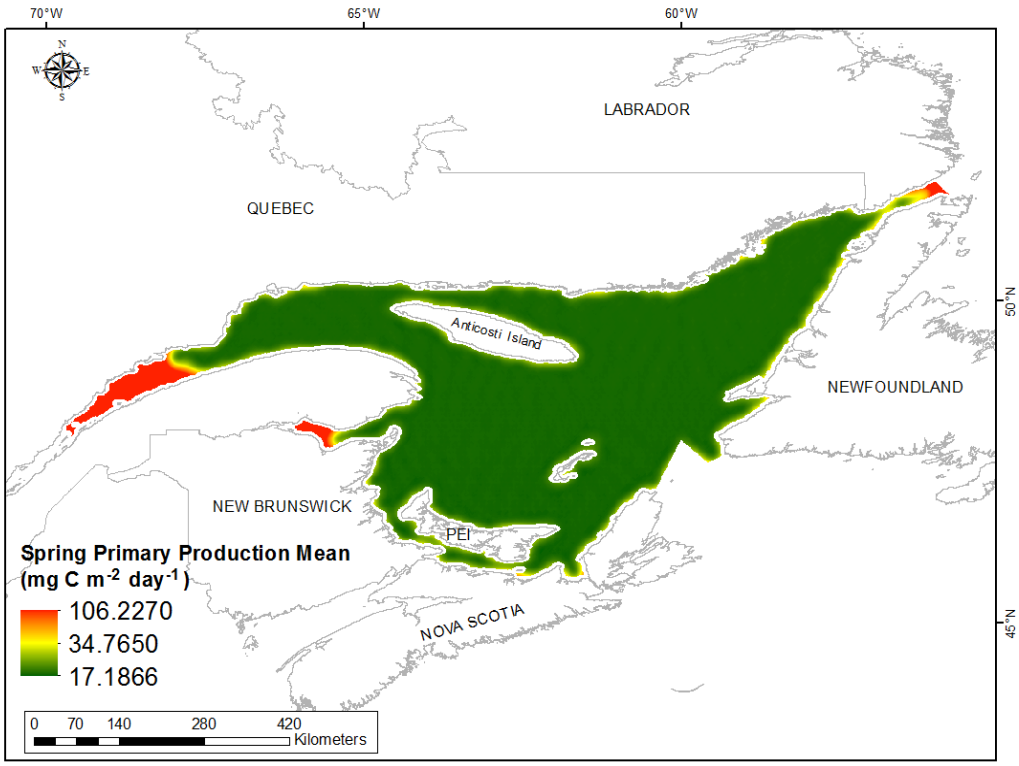

Fig. 454. Prediction standard error surface of Spring Primary Production Mean (mg C m^{-2} day^{-1}).

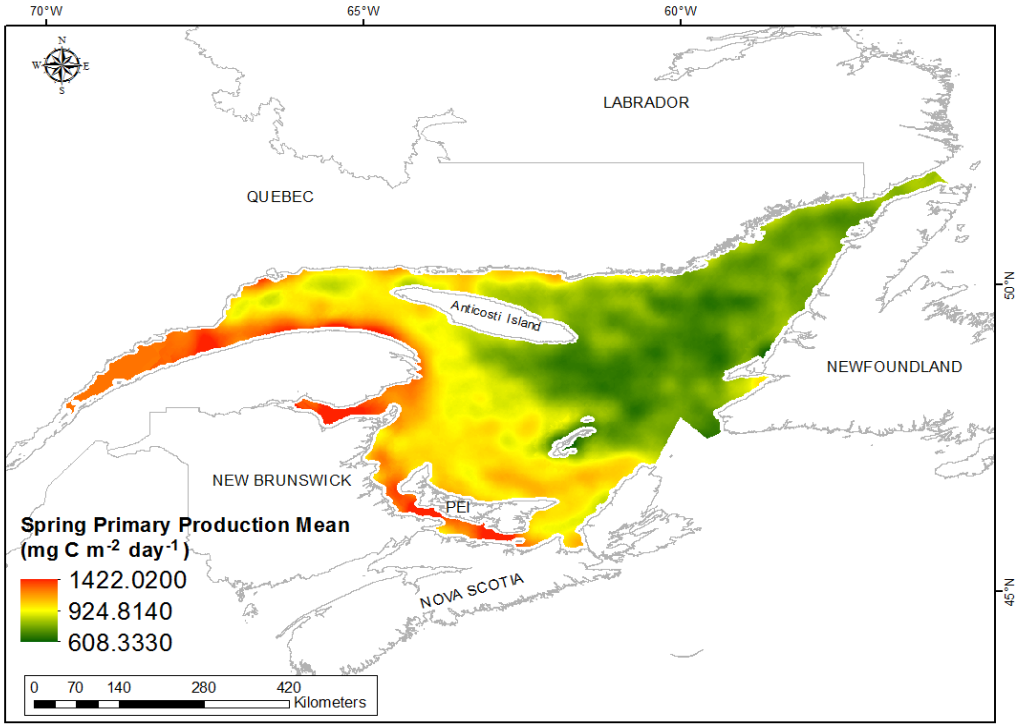

Fig. 455. Interpolated prediction surface of Spring Primary Production Mean (mg C m^{-2} day^{-1}).

Spring Primary Production Minimum

This variable displayed a bell-shaped distribution with right-skewness (Table 183, Fig. 456). The data were higher than predicted by a normal distribution at low and high values however the mid-region only slightly deviated from the reference line (Fig. 457). The areas of over- and under-prediction showed no strong spatial pattern over the spatial extent (Fig. 457).

The semivariogram showed moderate autocorrelation present in the data and the model showed a fair to poor fit between measured and predicted values (Fig. 458). Although the RMSPE and ASE were high, all other errors showed that the model was good at prediction (Table 184). The error map showed low error over the spatial extent but was slightly higher in the Gulf of St. Lawrence estuary, Chaleur Bay, and in the Strait of Belle Isle (Fig. 459). The kriged surface is presented in Fig. 460.

Table 183. Distributional properties of Spring Primary Production Minimum (mg C m^{-2} day^{-1}).

Property	Value
Number of Observations	2204
Minimum	162.930
Maximum	1241.800
Mean	512.030
Median	477.320
Standard Deviation	120.82
Skewness	1.396
Kurtosis	5.745

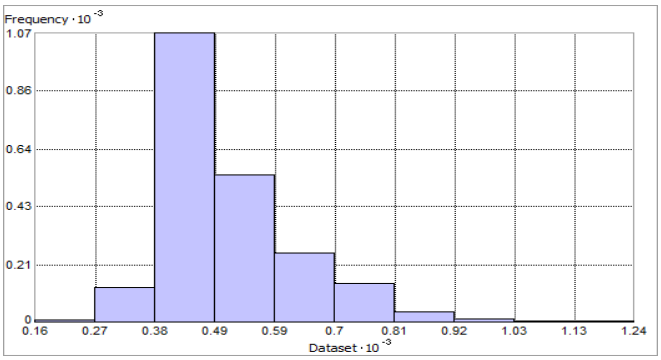

Fig. 456. Distribution of Spring Primary Production Minimum (mg C m^{-2} day^{-1}). Histogram was illustrated using 10 bins. X and Y axes shown at 10^{-3}.

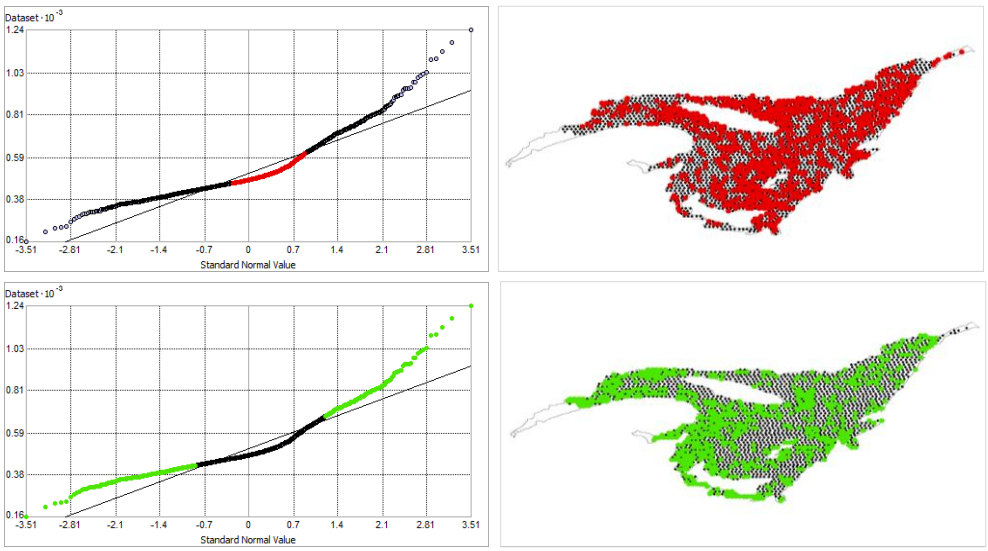

Fig. 457. Normal Q-Q plot for data values of Spring Primary Production Minimum (mg C m^{-2} day^{-1}). Points falling under (upper panel) and over (bottom panel) the reference line are mapped.

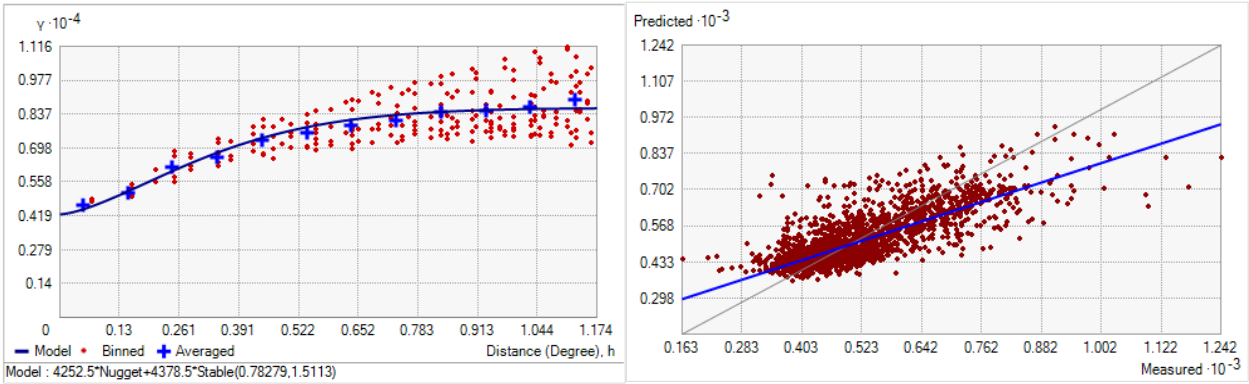

Fig. 458. Left panel: Semivariogram of Spring Primary Production Minimum (mg C m^{-2} day^{-1}). Binned values are shown as red dots; average points are shown as blue crosses; the model fit to the averaged values is shown as a blue line. Lag size: 0.098 degrees; number of lags: 12; Parameter: 1.511; Range: 0.783 degrees; Partial Sill: 4378.468. Right panel: Scatterplot of predicted values versus observed values for the model of Spring Primary Production Minimum (mg C m^{-2} day^{-1}).

Table 184. Results of cross-validation of the kriged model for the Spring Primary Production Minimum (mg C m^{-2} day^{-1}).

Prediction error	**Value**
Number of Observations	2204
Overall Mean Error	-0.349
Root Mean Square Prediction Error	76.054
Standardized Mean	-0.004
Standardized Root Mean Square Prediction Error	1.051
Average Standard Error	71.953

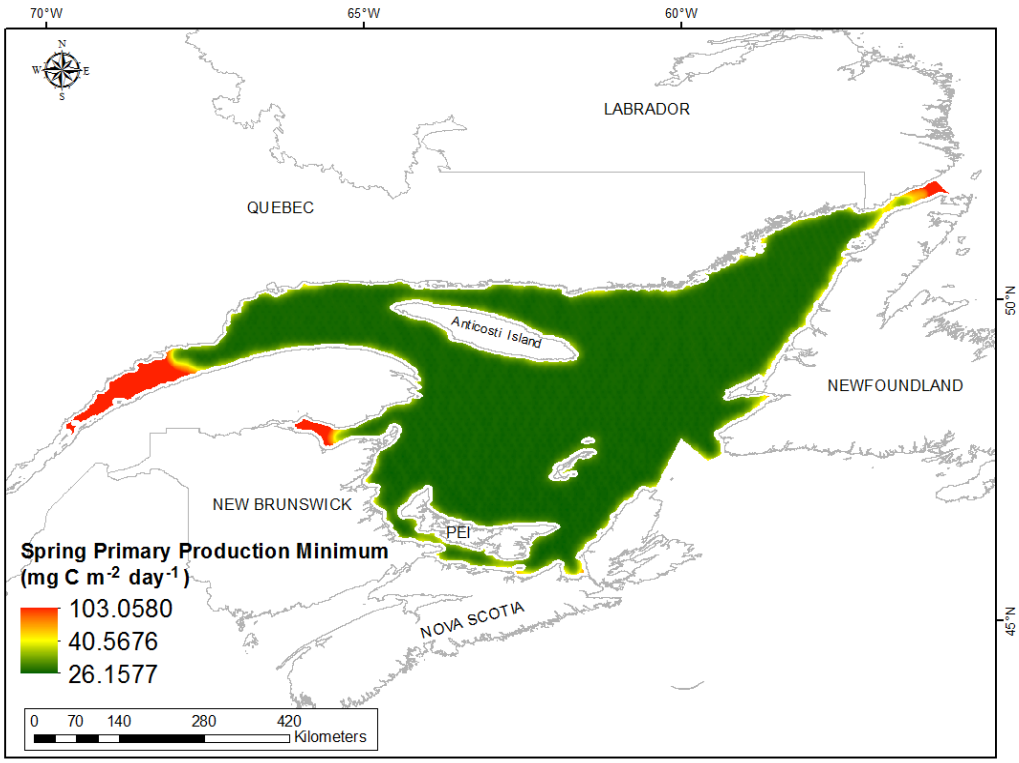

Fig. 459. Prediction standard error surface of Spring Primary Production Minimum (mg C m^{-2} day^{-1}).

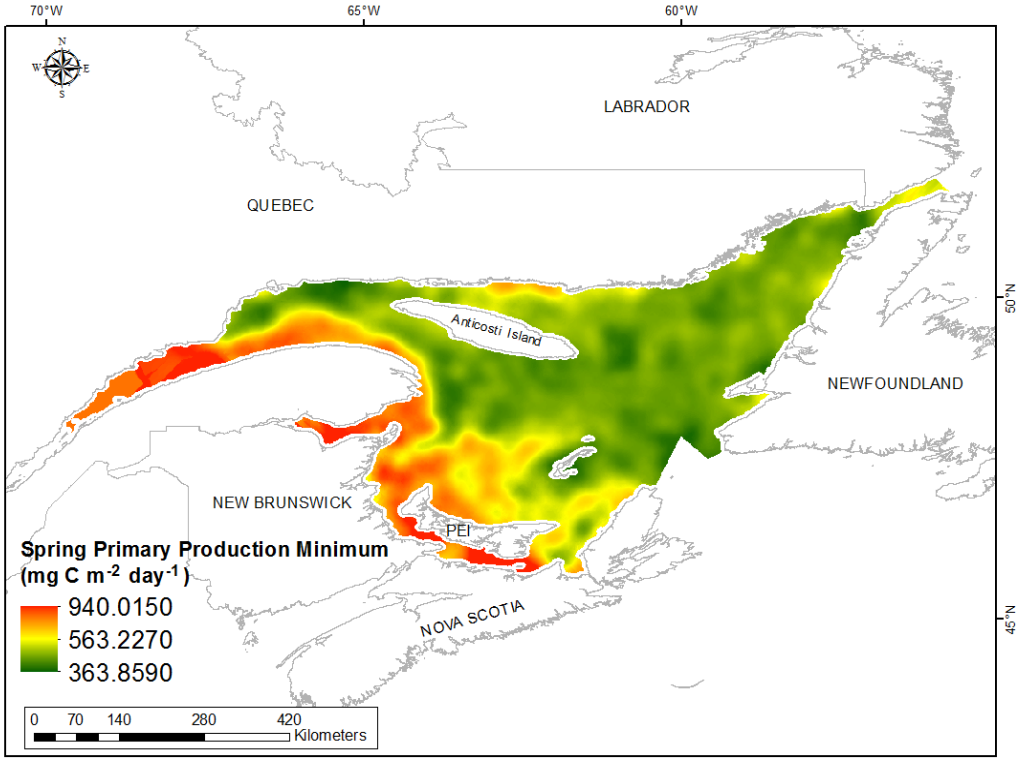

Fig. 460. Interpolated prediction surface of Spring Primary Production Minimum (mg C m^{-2} day^{-1}).

Spring Primary Production Maximum

This variable displayed a bell-shaped distribution with right-skewness (Table 185, Fig. 461). The data were higher than predicted by a normal distribution at low and high values however the mid-region followed the reference line well (Fig. 462). The areas of over- and under-prediction showed little spatial pattern over the spatial extent (Fig. 462).

The semivariogram showed moderate autocorrelation present in the data and the model showed a fair to poor fit between measured and predicted values (Fig. 463). Although the RMSPE and ASE were high, all other errors showed that the model was good at prediction (Table 186). The error map showed low error over the spatial extent but was slightly higher in the Gulf of St. Lawrence estuary, Chaleur Bay, and in the Strait of Belle Isle (Fig. 464). The kriged surface is presented in Fig. 465.

Table 185. Distributional properties of Spring Primary Production Maximum (mg C m^{-2} day^{-1}).

Property	Value
Number of Observations	2204
Minimum	473.910
Maximum	3071.800
Mean	1342.600
Median	1345.500
Standard Deviation	216.160
Skewness	0.686
Kurtosis	6.763

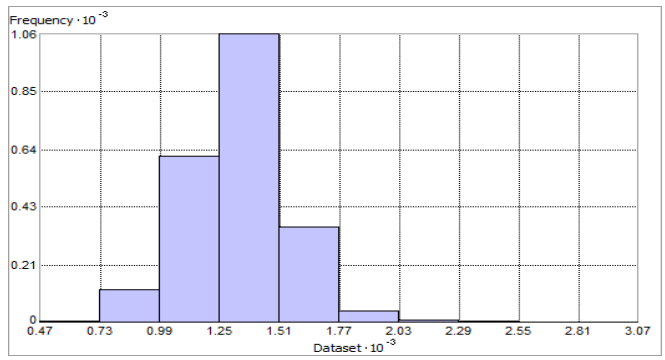

Fig. 461. Distribution of Spring Primary Production Maximum (mg C m^{-2} day^{-1}). Histogram was illustrated using 10 bins. X and Y axes shown at 10^{-3}.

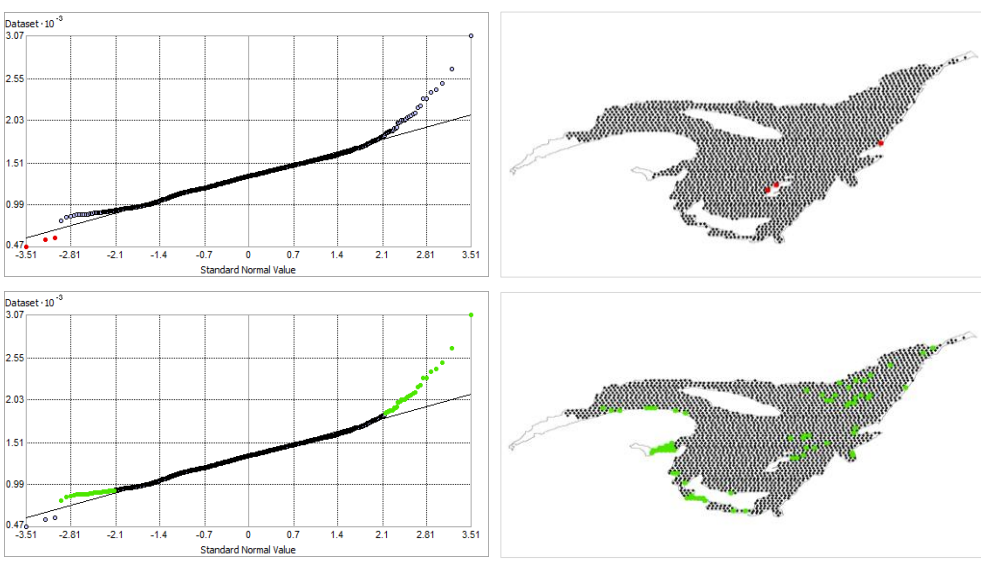

Fig. 462. Normal Q-Q plot for data values of Spring Primary Production Maximum (mg C m^{-2} day^{-1}). Points falling under (upper panel) and over (bottom panel) the reference line are mapped.

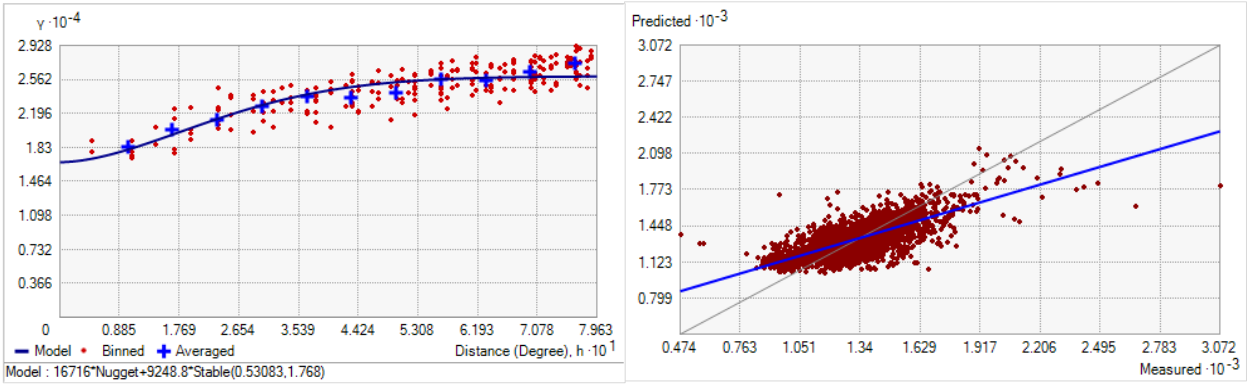

Fig. 463. Left panel: Semivariogram of Spring Primary Production Maximum (mg C m^{-2} day^{-1}). Binned values are shown as red dots; average points are shown as blue crosses; the model fit to the averaged values is shown as a blue line. Lag size: 0.066 degrees; number of lags: 12; Parameter: 1.768; Range: 0.531 degrees; Partial Sill: 9248.843. Right panel: Scatterplot of predicted values versus observed values for the model of Spring Primary Production Maximum (mg C m^{-2} day^{-1}).

Table 186. Results of cross-validation of the kriged model for the Spring Primary Production Maximum (mg C m^{-2} day^{-1}).

Prediction error	**Value**
Number of Observations	2204
Overall Mean Error	-0.839
Root Mean Square Prediction Error	148.473
Standardized Mean	-0.005
Standardized Root Mean Square Prediction Error	1.054
Average Standard Error	139.785

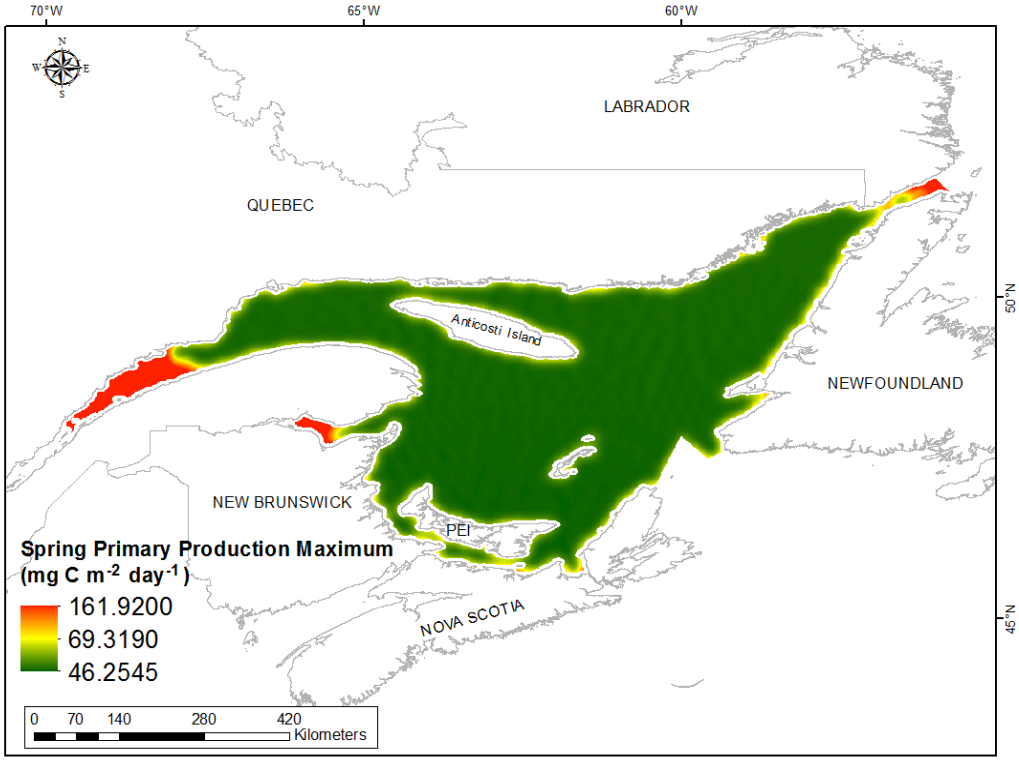

Fig. 464. Prediction standard error surface of Spring Primary Production Maximum (mg C m^{-2} day^{-1}).

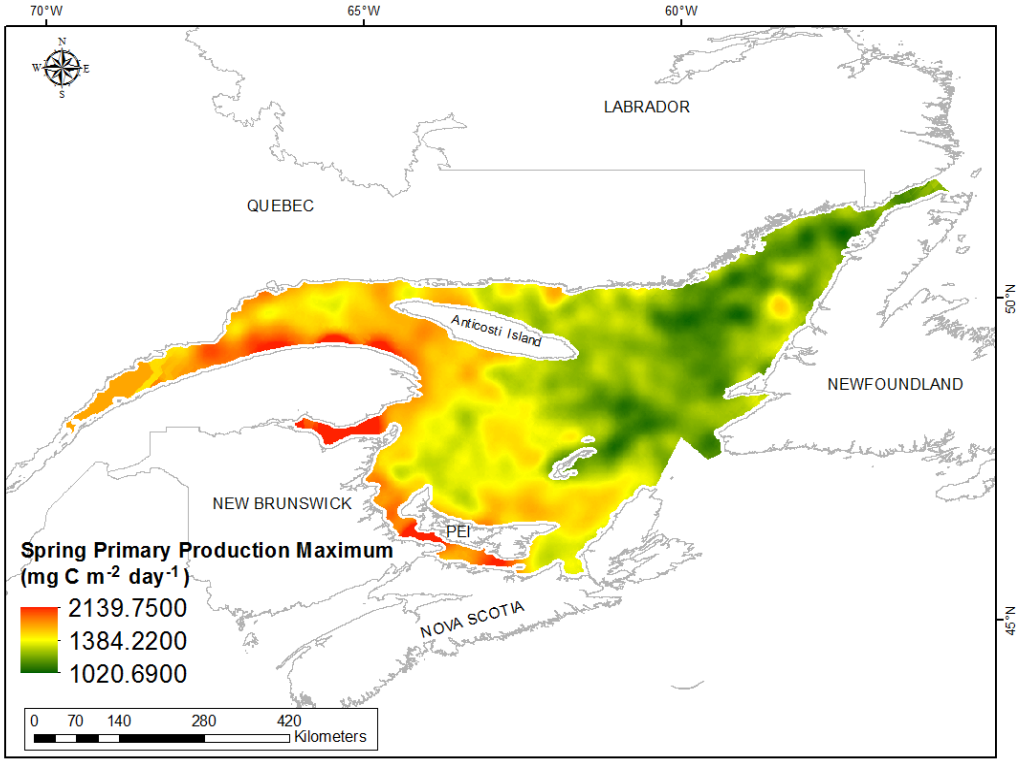

Fig. 465. Interpolated prediction surface of Spring Primary Production Maximum (mg C m^{-2} day^{-1}).

Spring Primary Production Range

This variable displayed a bell-shaped distribution with right-skewness with outlying data in the upper range (Table 187, Fig. 466). The data were higher than predicted by a normal distribution at low and high values however the mid-region was well-predicted (Fig. 467). No data points fell below the reference line. The areas of over-prediction showed no strong spatial pattern over the spatial extent (Fig. 467).

The semivariogram showed high autocorrelation present in the data and the model showed a fair to poor fit between measured and predicted values (Fig. 468). Although the RMSPE and ASE were high, all other errors showed that the model was good at prediction (Table 188). The error map showed moderate error across the study extent except at the exact location of data points where it was low (Fig. 469). Error was high in the Gulf of St. Lawrence estuary, Chaleur Bay, and in the Strait of Belle Isle. The kriged surface is presented in Fig. 470.

Table 187. Distributional properties of Spring Primary Production Range (mg C m^{-2} day^{-1}).

Property	Value
Number of Observations	2284
Minimum	0.000
Maximum	2528.600
Mean	832.810
Median	827.600
Standard Deviation	213.020
Skewness	0.700
Kurtosis	7.117

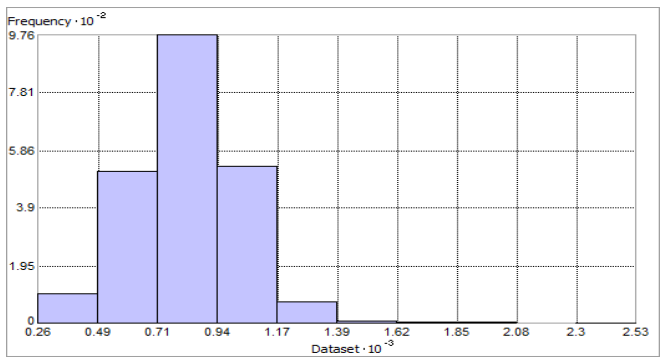

Fig. 466. Distribution of Spring Primary Production Range (mg C m^{-2} day^{-1}). Histogram was illustrated using 10 bins. X axis shown at 10^{-3}; Y axis at 10^{-2}.

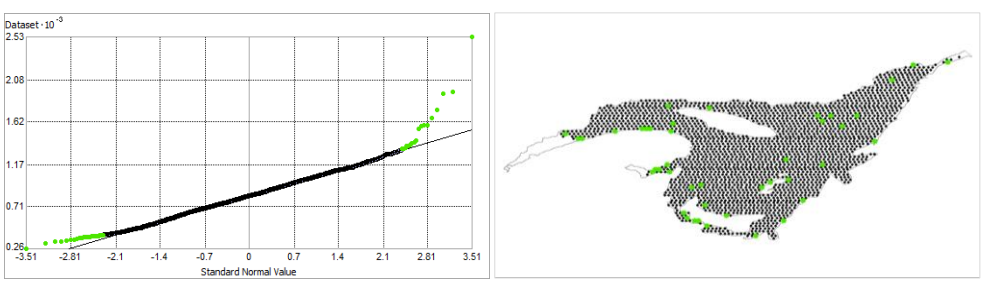

Fig. 467. Normal Q-Q plot for data values of Spring Primary Production Range (mg C m^{-2} day^{-1}). Points falling over the reference line are mapped; no points fall under the reference line.

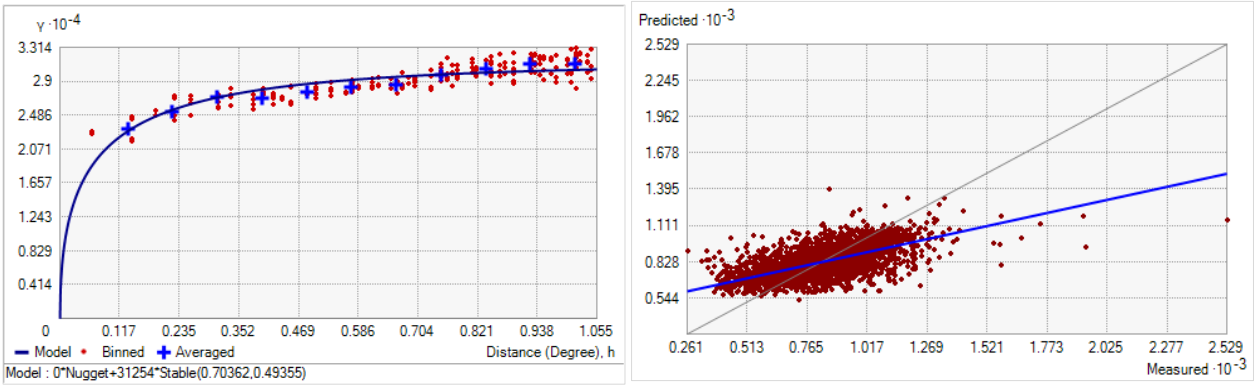

Fig. 468. Left panel: Semivariogram of Spring Primary Production Range (mg C m^{-2} day^{-1}). Binned values are shown as red dots; average points are shown as blue crosses; the model fit to the averaged values is shown as a blue line. Lag size: 0.088 degrees; number of lags: 12; Parameter: 0.494; Range: 0.704 degrees; Partial Sill: 31253.870. Right panel: Scatterplot of predicted values versus observed values for the model of Spring Primary Production Range (mg C m^{-2} day^{-1}).

Table 188. Results of cross-validation of the kriged model for Spring Primary Production Range (mg C m^{-2} day^{-1}).

Prediction error	**Value**
Number of Observations	2204
Overall Mean Error	-0.536
Root Mean Square Prediction Error	163.588
Standardized Mean	-0.003
Standardized Root Mean Square Prediction Error	1.059
Average Standard Error	153.431

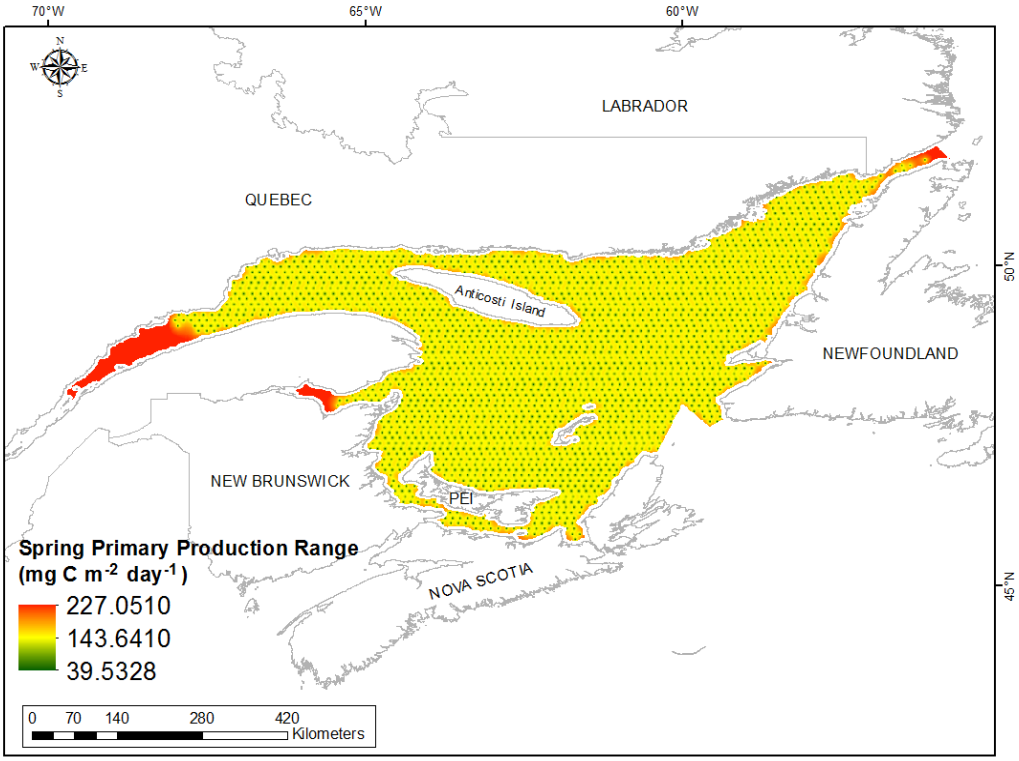

Fig. 469. Prediction standard error surface of Spring Primary Production Range (mg C m^{-2} day^{-1}).

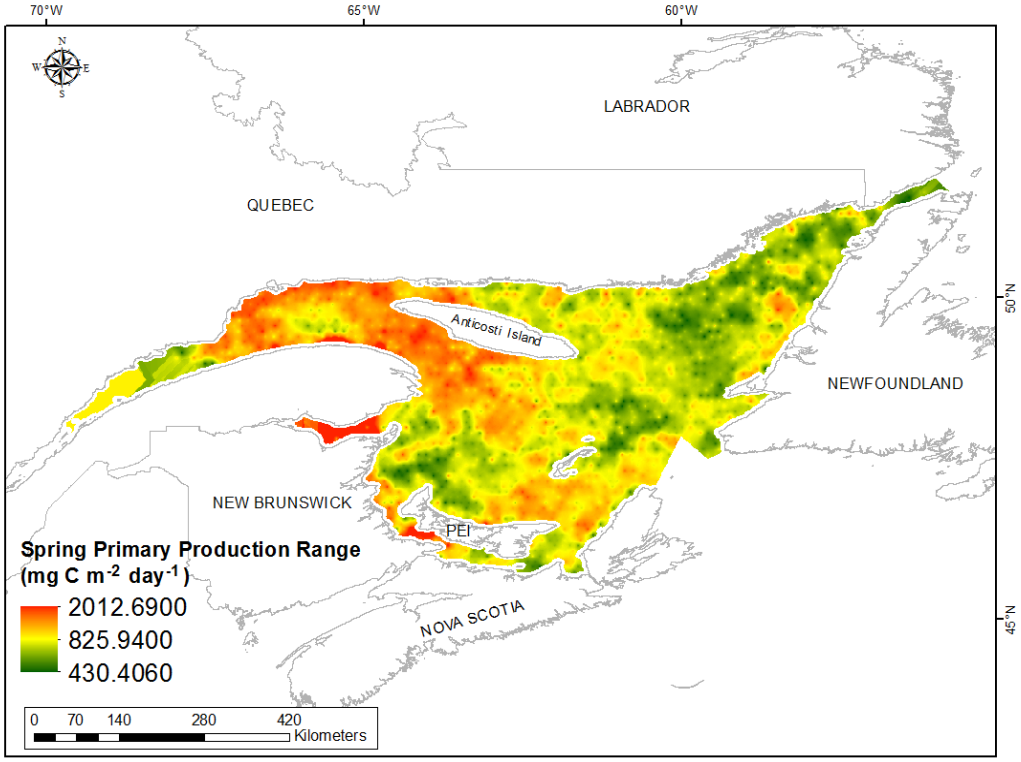

Fig. 470. Interpolated prediction surface of Spring Primary Production Range (mg C m^{-2} day^{-1}).

Spring Primary Production Average Minimum

This variable displayed a bell-shaped distribution with kurtosis prior to modeling (Table 189, Fig. 471). The data were higher than predicted by a normal distribution at low and high values however the mid-region was very well-predicted (Fig. 472). The areas of over- and under-prediction showed a spatial pattern over the spatial extent (Fig. 472).

The semivariogram showed moderate autocorrelation present in the data and the model showed a fair fit between measured and predicted values (Fig. 473). Although the RMSPE and ASE were high, all other errors showed that the model was good at prediction (Table 190). The error map showed low error over the spatial extent but was high in the Gulf of St. Lawrence estuary, Chaleur Bay, and in the Strait of Belle Isle (Fig. 474). The kriged surface is presented in Fig. 475.

Table 189. Distributional properties of Spring Primary Production Average Minimum (mg C m^{-2} day^{-1}).

Property	Value
Number of Observations	2204
Minimum	260.870
Maximum	2528.600
Mean	830.560
Median	827.600
Standard Deviation	200.820
Skewness	0.552
Kurtosis	6.042

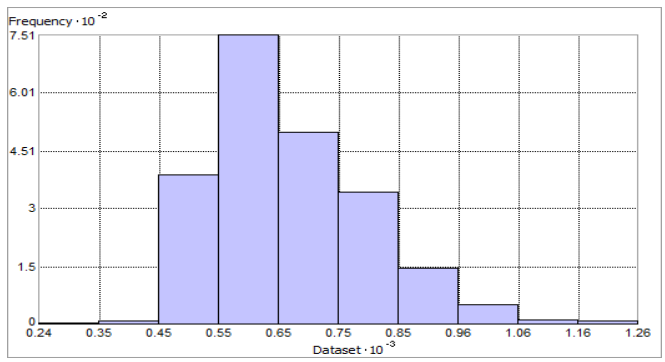

Fig. 471. Distribution of Spring Primary Production Average Minimum (mg C m^{-2} day^{-1}). Histogram was illustrated using 10 bins. X axis shown at 10^{-3}; Y axis at 10^{-2}.

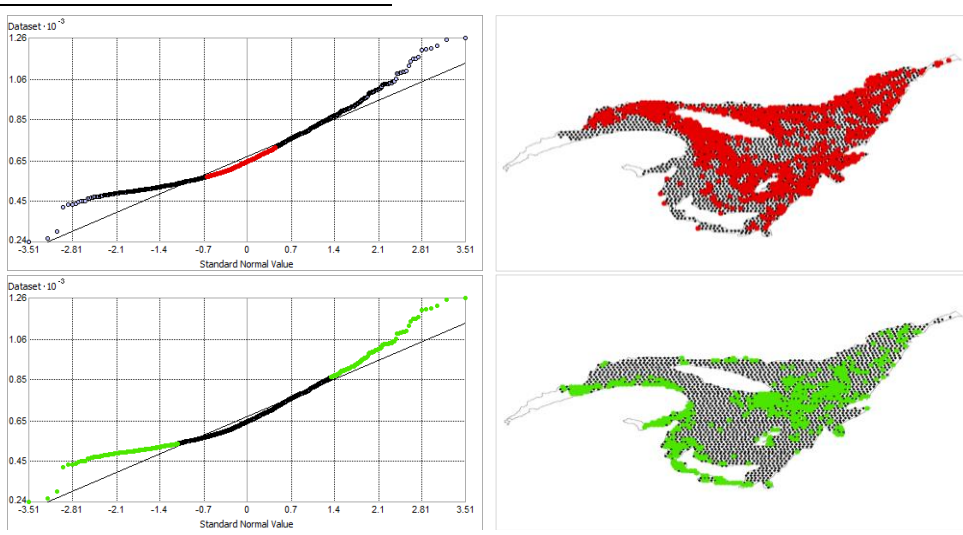

Fig. 467. Normal Q-Q plot for data values of Spring Primary Production Average Minimum (mg C m^{-2} day^{-1}). Points falling under (upper panel) and over (bottom panel) the reference line are mapped.

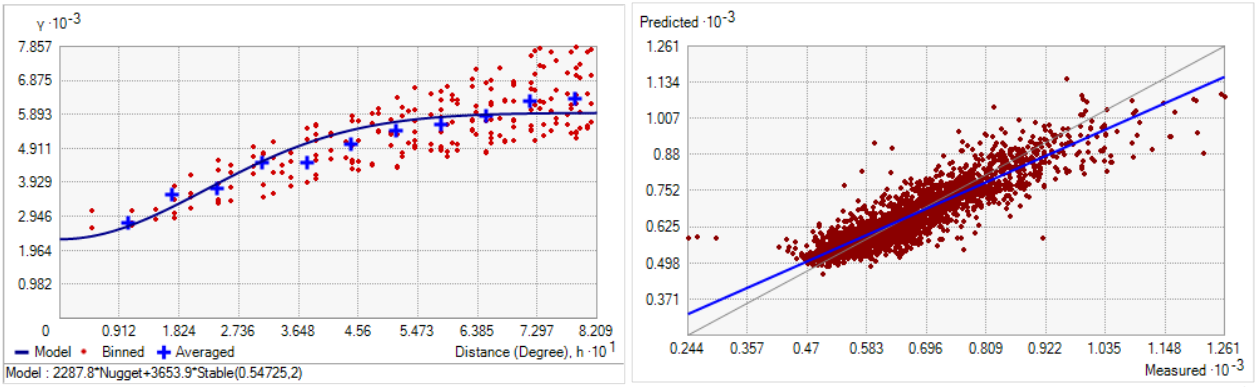

Fig. 473. Left panel: Semivariogram of Spring Primary Production Average Minimum (mg C m^{-2} day^{-1}). Binned values are shown as red dots; average points are shown as blue crosses; the model fit to the averaged values is shown as a blue line. Lag size: 0.068 degrees; number of lags: 12; Parameter: 2; Range: 0.547 degrees; Partial Sill: 3653.855. Right panel: Scatterplot of predicted values versus observed values for the model of Spring Primary Production Minimum (mg C m^{-2} day^{-1}).

Table 190. Results of cross-validation of the kriged model for Spring Primary Production Average Minimum (mg C m^{-2} day^{-1}).

Prediction error	**Value**
Number of Observations	2204
Overall Mean Error	-0.034
Root Mean Square Prediction Error	58.283
Standardized Mean	4.225×10^{-4}
Standardized Root Mean Square Prediction Error	1.089
Average Standard Error	52.450

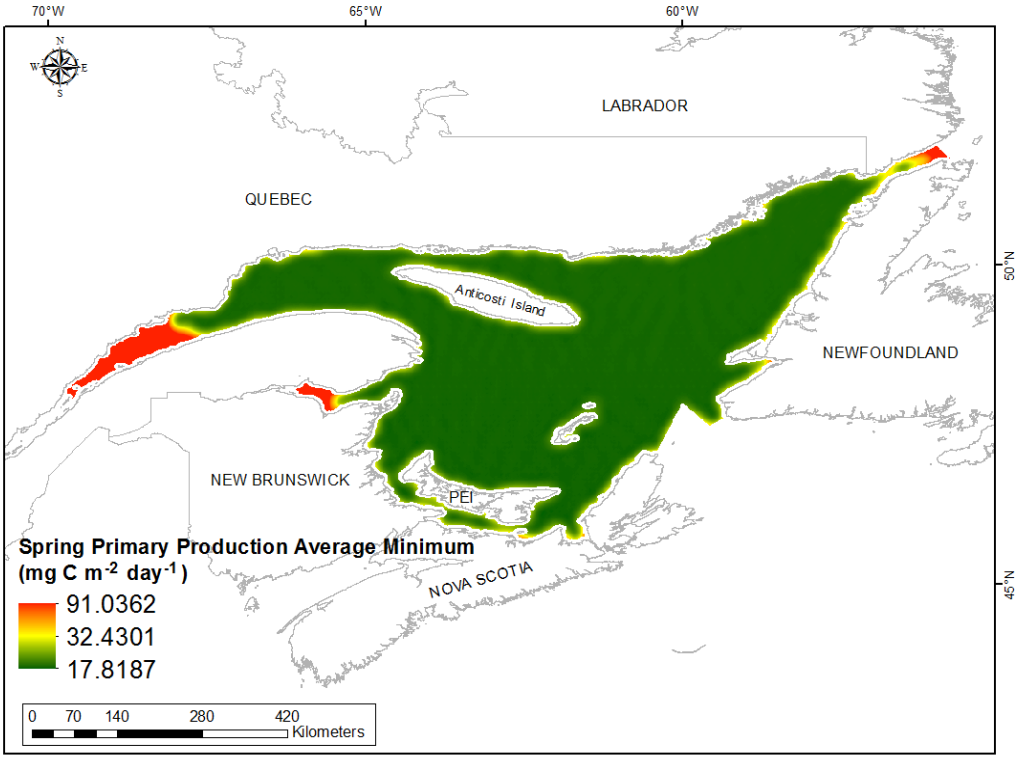

Fig. 474. Prediction standard error surface of Spring Primary Production Average Minimum (mg C m^{-2} day^{-1}).

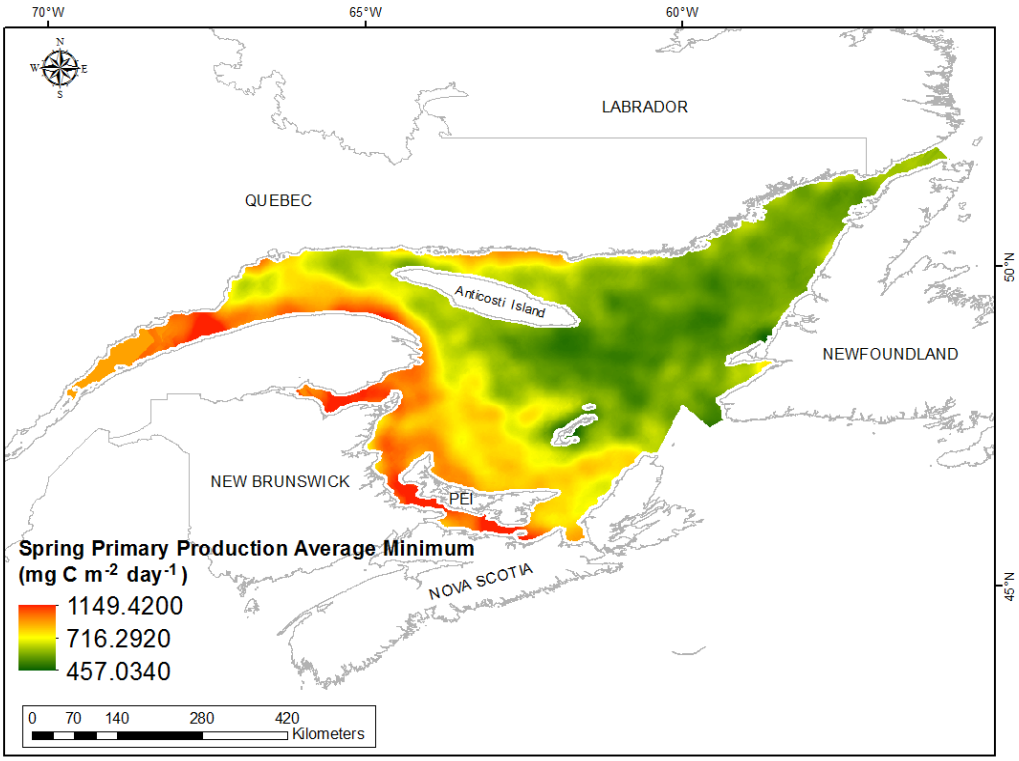

Fig. 475. Interpolated prediction surface of Spring Primary Production Average Minimum (mg C m^{-2} day^{-1}).

Spring Primary Production Average Maximum

This variable displayed a bell-shaped distribution with kurtosis prior to modeling (Table 191, Fig. 476). The data were higher than predicted by a normal distribution at high values however the mid-region was very well-predicted (Fig. 477). The areas of over-prediction showed a spatial pattern over the spatial extent (Fig. 477).

The semivariogram showed moderate autocorrelation present in the data and the model showed a fair fit between measured and predicted values (Fig. 478). Although the RMSPE and ASE were high, all other errors showed that the model was good at prediction (Table 192). The error map showed low error over the spatial extent but was slightly higher in the Gulf of St. Lawrence estuary, Chaleur Bay, and in the Strait of Belle Isle (Fig. 479). The kriged surface is presented in Fig. 480.

Table 191. Distributional properties of Spring Primary Production Average Maximum (mg C m^{-2} day^{-1}).

Property	Value
Number of Observations	2204
Minimum	434.050
Maximum	2123.700
Mean	1077.200
Median	1070.000
Standard Deviation	189.860
Skewness	0.602
Kurtosis	4.136

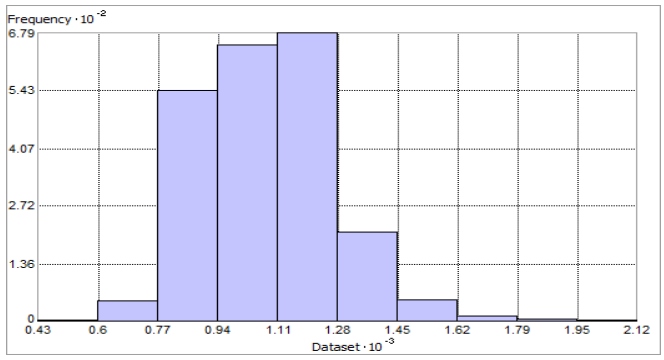

Fig. 476. Distribution of Spring Primary Production Average Maximum (mg C m^{-2} day^{-1}). Histogram was illustrated using 10 bins. X axis shown at 10^{-3}; Y axis at 10^{-2}.

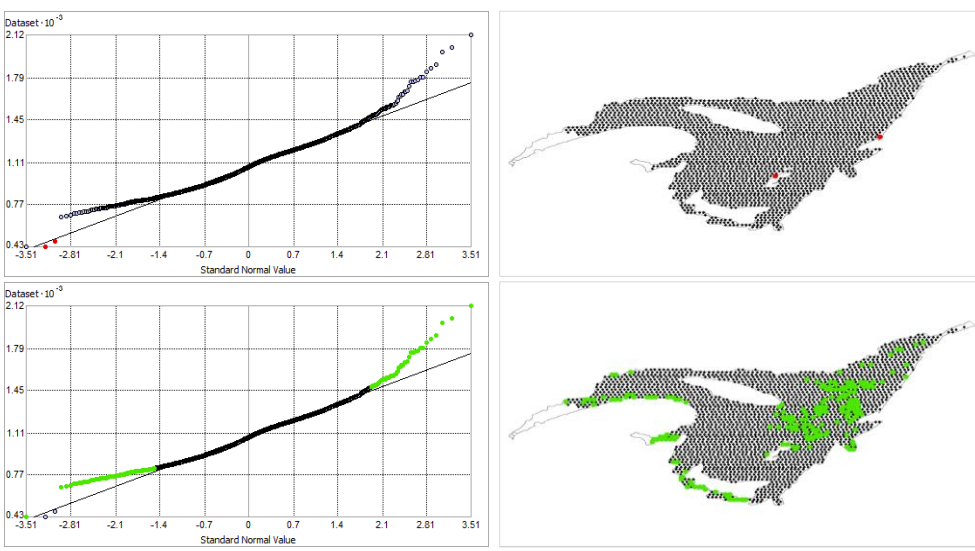

Fig. 477. Normal Q-Q plot for data values of Spring Primary Production Average Maximum (mg C m^{-2} day^{-1}). Points falling under (upper panel) and over (bottom panel) the reference line are mapped.

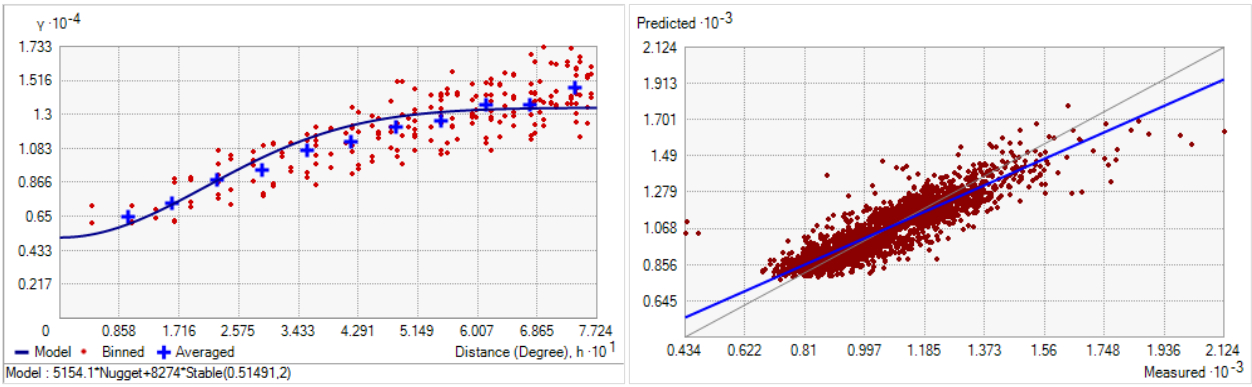

Fig 478. Left panel: Semivariogram of Spring Primary Production Average Maximum (mg C m^{-2} day^{-1}). Binned values are shown as red dots; average points are shown as blue crosses; the model fit to the averaged values is shown as a blue line. Lag size: 0.064 degrees; number of lags: 12; Parameter: 2; Range: 0.515 degrees; Partial Sill: 8273.963. Right panel: Scatterplot of predicted values versus observed values for the model of Spring Primary Production Maximum (mg C m^{-2} day^{-1}).

Table 192. Results of cross-validation of the kriged model for Spring Primary Production Average Maximum (mg C m^{-2} day^{-1}).

Prediction error	**Value**
Number of Observations	2204
Overall Mean Error	-0.110
Root Mean Square Prediction Error	87.614
Standardized Mean	2.367×10^{-4}
Standardized Root Mean Square Prediction Error	1.085
Average Standard Error	79.301

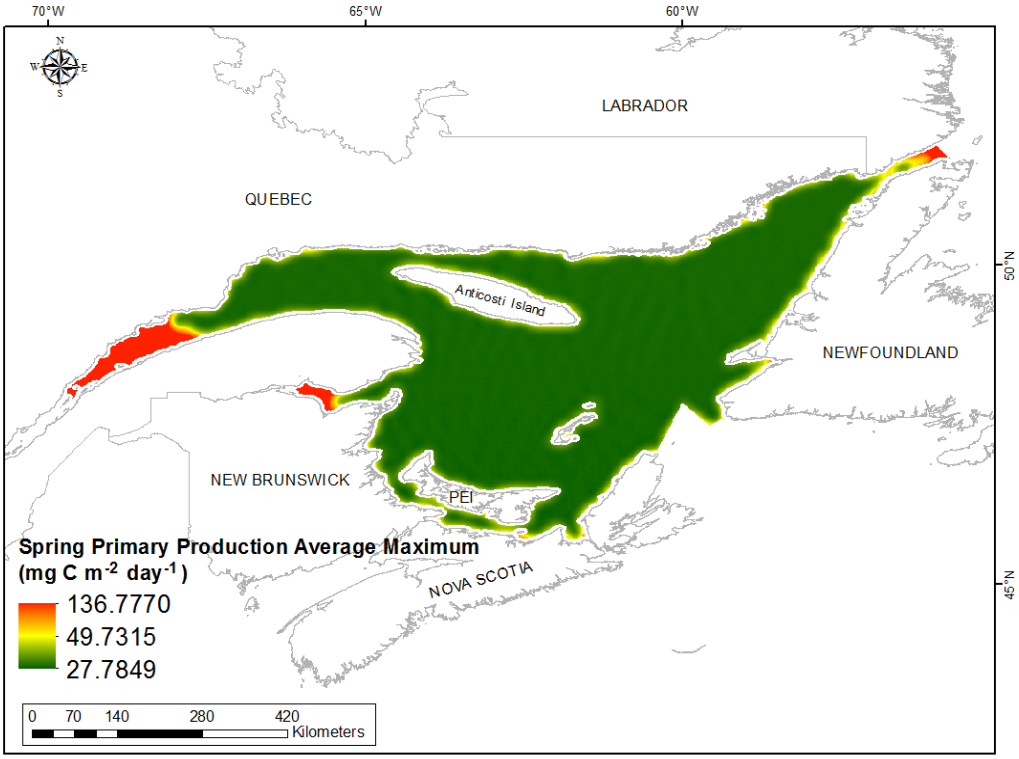

Fig. 479. Prediction standard error surface of Spring Primary Production Average Maximum (mg C m^{-2} day^{-1}).

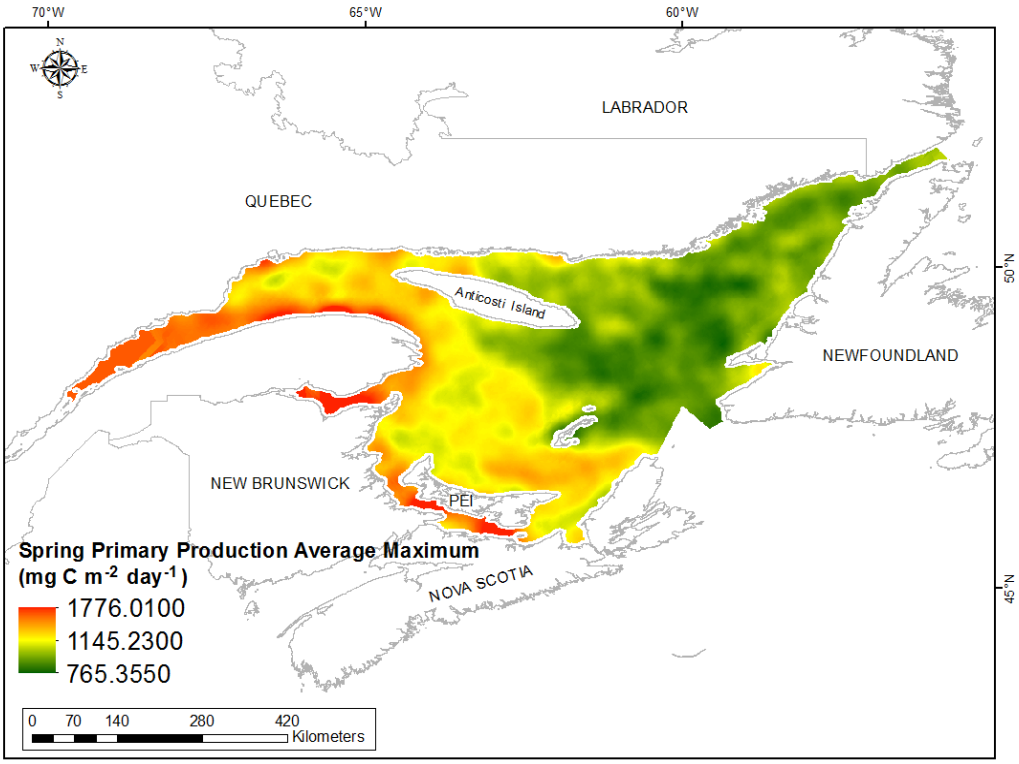

Fig. 480. Interpolated prediction surface of Spring Primary Production Average Maximum (mg C m^{-2} day^{-1}).

Spring Primary Production Average Range

This variable displayed a bell-shaped distribution with outlying data in the upper range (Table 193, Fig. 481). The data were higher than predicted by a normal distribution at low and high values however the mid-region was very well-predicted (Fig. 482). No data fell below the reference line. The areas of over-prediction showed no spatial pattern over the spatial extent (Fig. 482).

The semivariogram showed weak autocorrelation present in the data and the model showed a fair to poor fit between measured and predicted values (Fig. 483). Although the RMSPE and ASE were high, all other errors showed that the model was good at The error map showed low error over the spatial extent but was slightly higher in the Gulf of St. Lawrence estuary, Chaleur Bay, and in the Strait of Belle Isle (Fig. 484). The kriged surface is presented in Fig. 485.

Table 193. Distributional properties of Spring Primary Production Average Range (mg C m^{-2} day^{-1}).

Property	Value
Number of Observations	2204
Minimum	86.370
Maximum	1185.500
Mean	407.870
Median	401.850
Standard Deviation	120.960
Skewness	0.565
Kurtosis	4.408

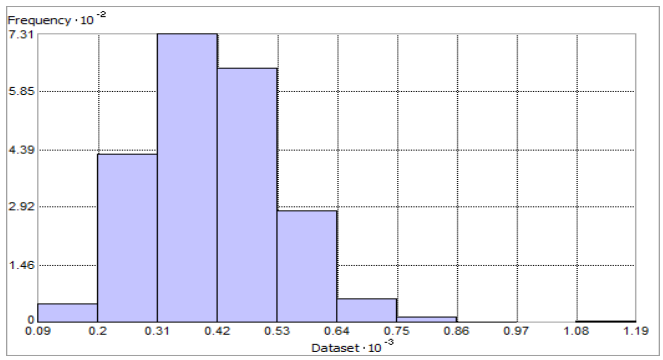

Fig. 481. Distribution of Spring Primary Production Average Range (mg C m^{-2} day^{-1}). Histogram was illustrated using 10 bins. X axis shown at 10^{-3}; Y axis at 10^{-2}.

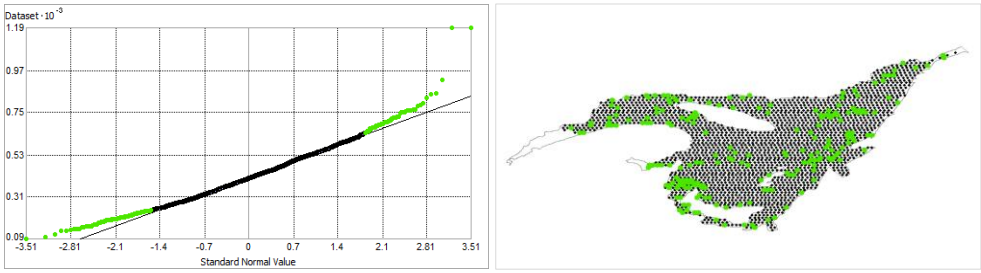

Fig. 482. Normal Q-Q plot for data values of Spring Primary Production Average Range (mg C m^{-2} day^{-1}). Points falling over the reference line are mapped; no points fall under the reference line.

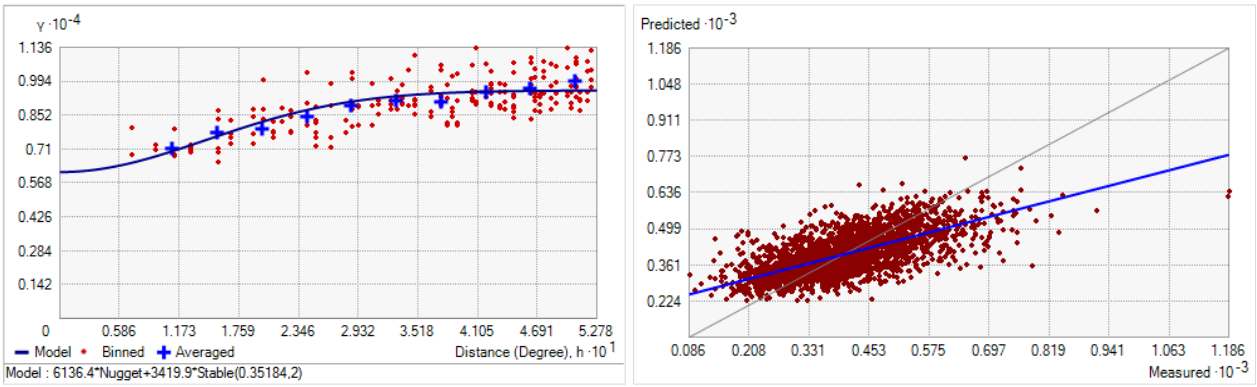

Fig 483. Left panel: Semivariogram of Spring Primary Production Average Range (mg C m^{-2} day^{-1}). Binned values are shown as red dots; average points are shown as blue crosses; the model fit to the averaged values is shown as a blue line. Lag size: 0.044 degrees; number of lags: 12; Parameter: 2; Range: 0.352 degrees; Partial Sill: 3419.920. Right panel: Scatterplot of predicted values versus observed values for the model of Spring Primary Production Range (mg C m^{-2} day^{-1}).

Table 194. Results of cross-validation of the kriged model for Spring Primary Production Average Range (mg C m^{-2} day^{-1}).

Prediction error	**Value**
Number of Observations	2204
Overall Mean Error	-0.404
Root Mean Square Prediction Error	90.875
Standardized Mean	-0.004
Standardized Root Mean Square Prediction Error	1.040
Average Standard Error	86.736

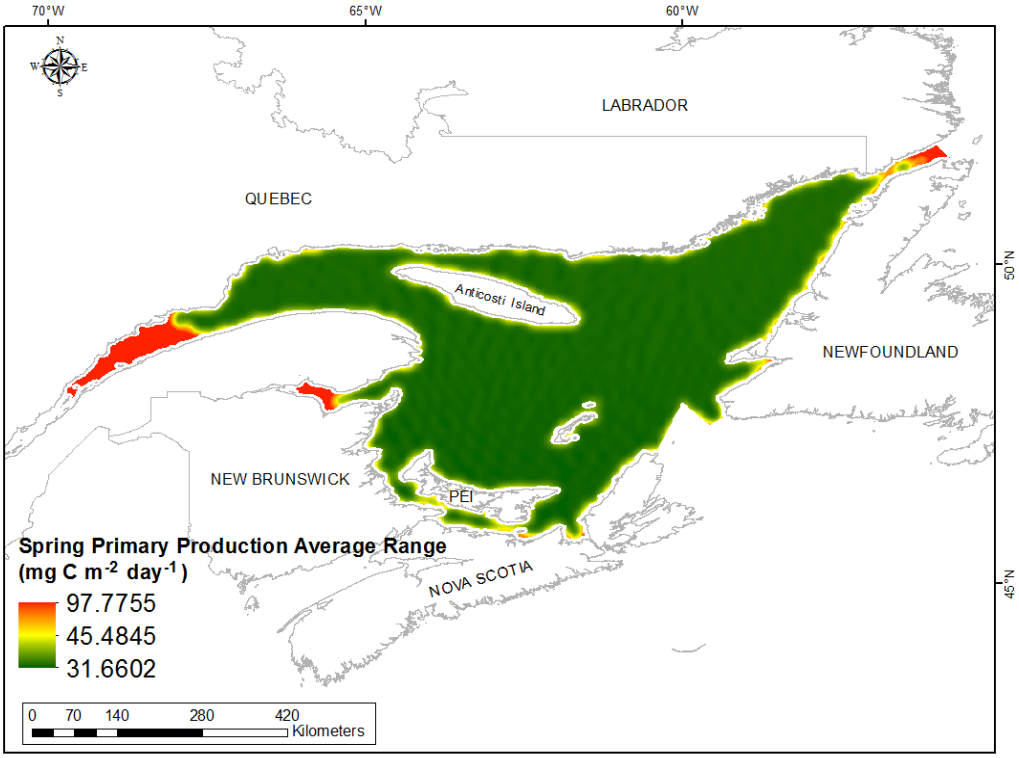

Fig. 484. Prediction standard error surface of Spring Primary Production Average Range (mg C m^{-2} day^{-1}).

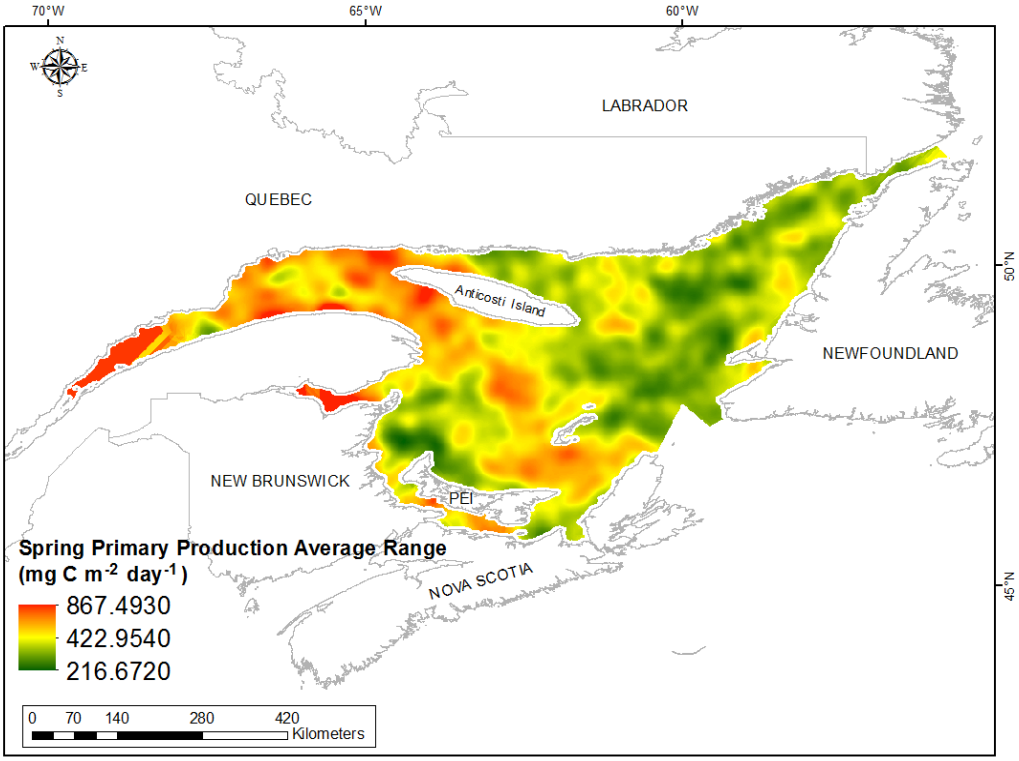

Fig. 485. Interpolated prediction surface of Spring Primary Production Average Range (mg C m^{-2} day^{-1}).

Summer Primary Production Mean

This variable displayed a bell-shaped distribution with high kurtosis (Table 195, Fig. 486). The data were higher than predicted by a normal distribution at low and high values however the mid-values deviated only slightly from the reference line (Fig. 487). The areas of under- and over-prediction showed a spatial pattern over the spatial extent (Fig. 487).

The semivariogram showed weak autocorrelation present in the data and the model showed a fair fit between measured and predicted values (Fig. 488). Although the RMSPE and ASE were high (Table 196), all other errors showed that the model was good at prediction. The error map showed low error over the study extent except for along the coast where it was high (Fig. 489). The kriged surface is presented in Fig. 490.

Table 195. Distributional properties of Summer Primary Production Mean (mg C m^{-2} day^{-1}).

Property	Value
Number of Observations	2273
Minimum	536.920
Maximum	1718.300
Mean	958.750
Median	947.280
Standard Deviation	106.060
Skewness	2.329
Kurtosis	13.717

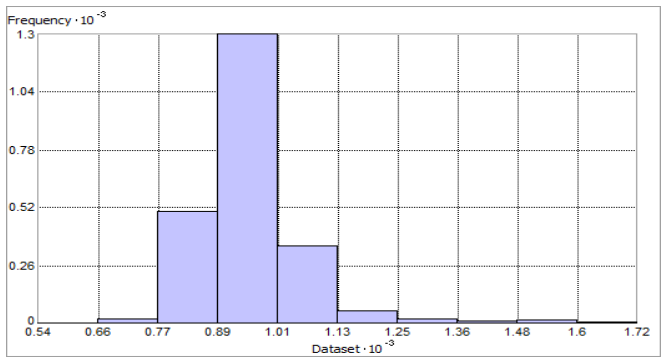

Fig. 486. Distribution of Summer Spring Primary Production Mean (mg C m^{-2} day^{-1}). Histogram was illustrated using 10 bins. X and Y axes shown at 10^{-3}.

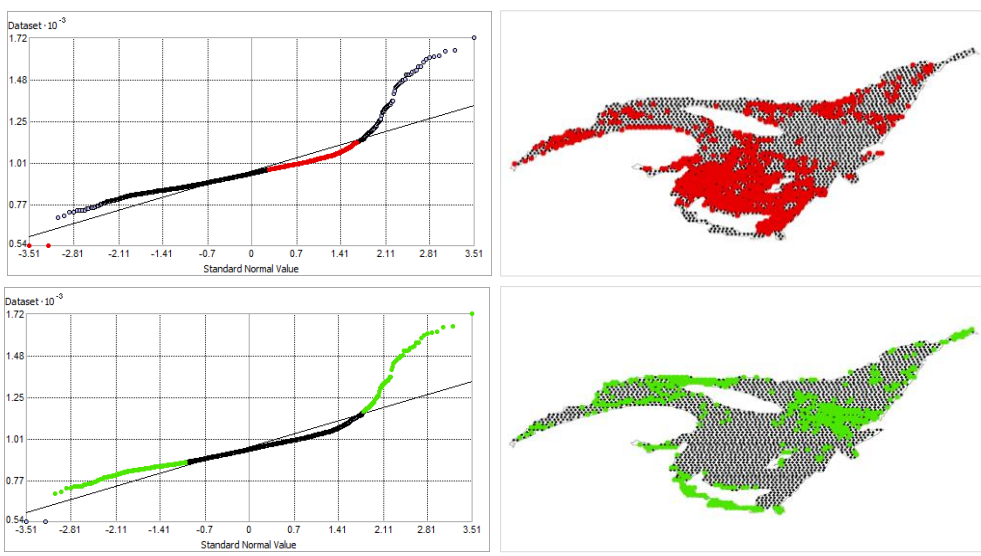

Fig. 487. Normal Q-Q plot for data values of Summer Primary Production Mean (mg C m^{-2} day^{-1}). Points falling under (upper panel) and over (bottom panel) the reference line are mapped.

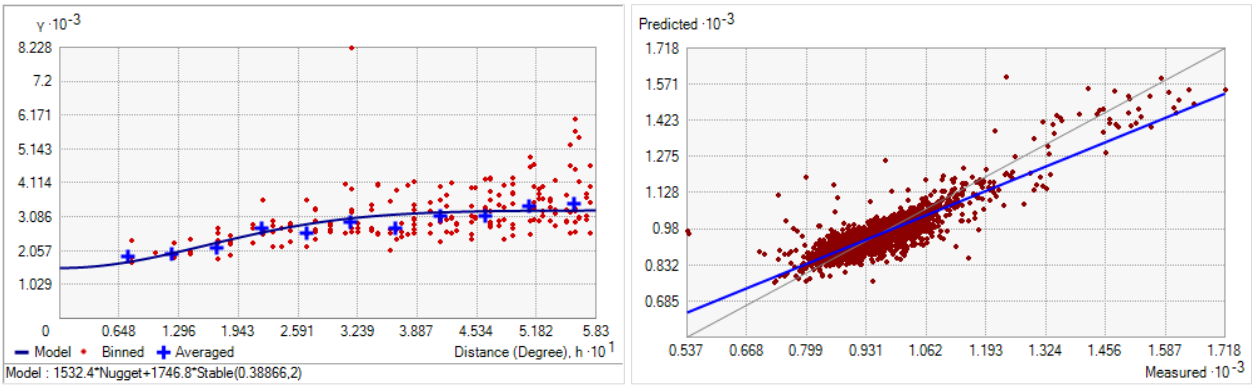

Fig. 488. Left panel: Semivariogram of Summer Primary Production Mean (mg C m^{-2} day^{-1}). Binned values are shown as red dots; average points are shown as blue crosses; the model fit to the averaged values is shown as a blue line. Lag size: 0.049 degrees; number of lags: 12; Parameter: 2; Range: 0.389 degrees; Partial Sill: 1746.816. Right panel: Scatterplot of predicted values versus observed values for the model of Summer Primary Production Mean (mg C m^{-2} day^{-1}).

Table 196. Results of cross-validation of the kriged model for Summer Primary Production Mean (mg C m^{-2} day^{-1}).

Prediction error	**Value**
Number of Observations	2273
Overall Mean Error	0.017
Root Mean Square Prediction Error	50.936
Standardized Mean	-7.890×10^{-4}
Standardized Root Mean Square Prediction Error	1.114
Average Standard Error	44.337

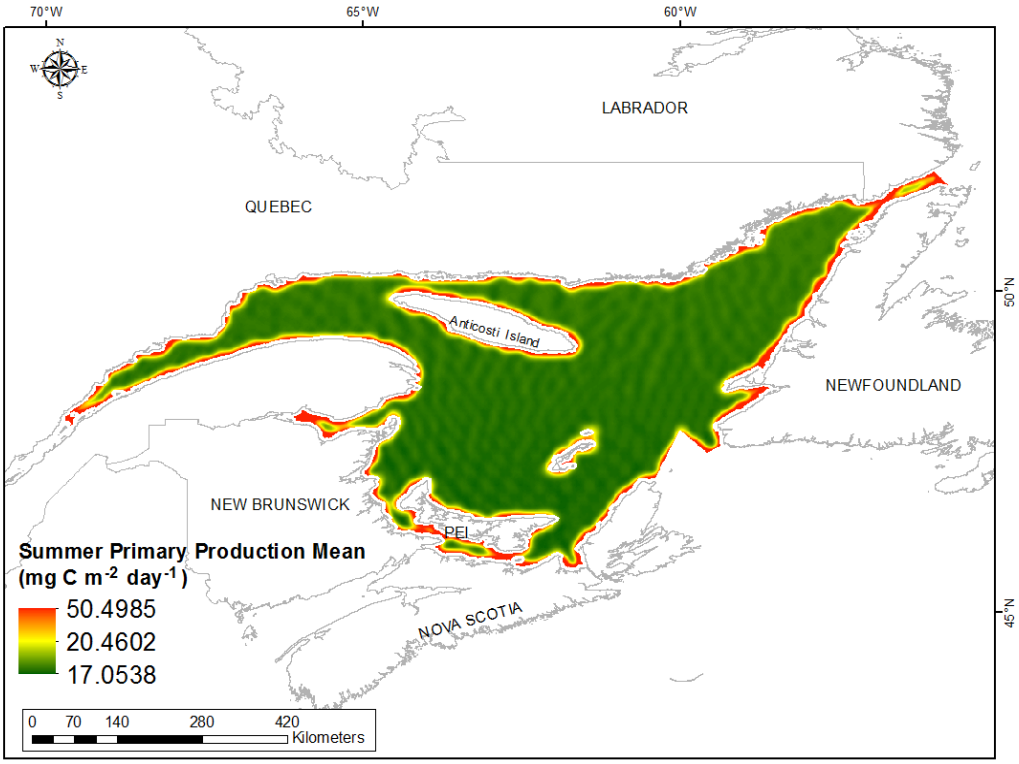

Fig. 489. Prediction standard error surface of Summer Primary Production Mean (mg C m^{-2} day^{-1}).

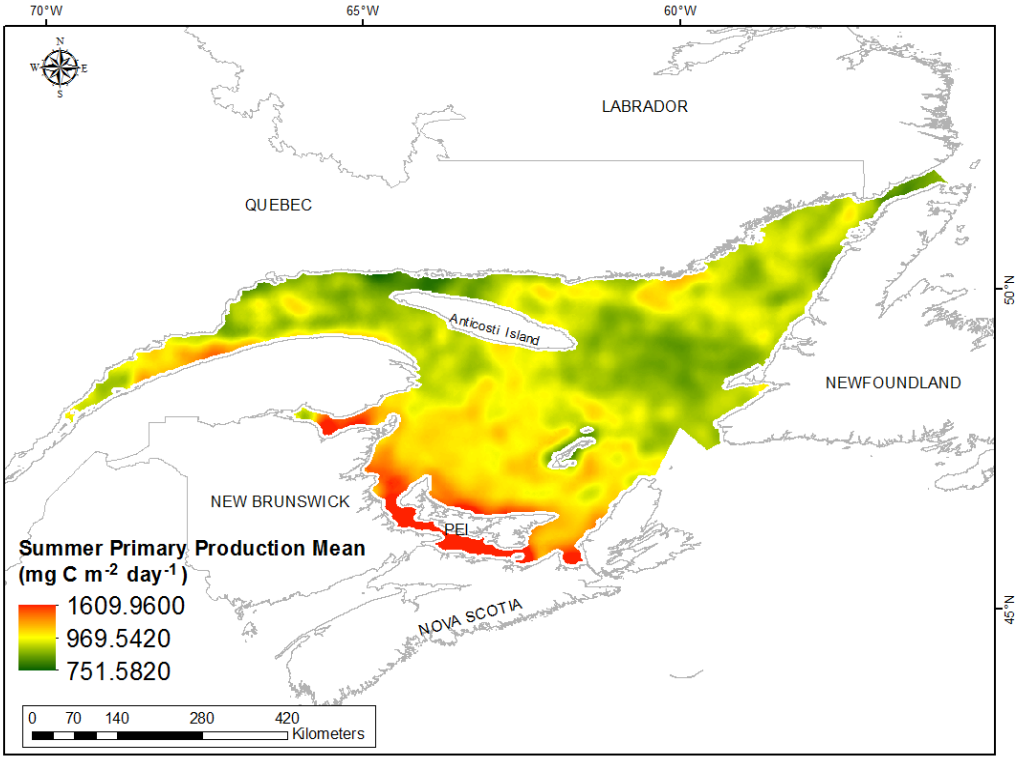

Fig. 490. Interpolated prediction surface of Summer Primary Production Mean (mg C m^{-2} day^{-1}).

Summer Primary Production Minimum

This variable displayed a bell-shaped distribution with right-skewness (Table 197, Fig. 491). The data were lower and higher than predicted by a normal distribution at low and high values, respectively, however the mid-values deviated only slightly from the reference line (Fig. 492). The areas of under- and over-prediction showed a spatial pattern over the spatial extent (Fig. 492).

The semivariogram showed moderate autocorrelation present in the data and the model showed a fair fit between measured and predicted values (Fig. 493). Although the RMSPE and ASE were high (Table 198), all other errors showed that the model was good at prediction. The error map showed moderate error across the study extent except at the exact location of data points where it was low (Fig. 494). The kriged surface is presented in Fig. 495.

Table 197. Distributional properties of Summer Primary Production Minimum (mg C m^{-2} day^{-1}).

Property	Value
Number of Observations	2273
Minimum	149.620
Maximum	1359.200
Mean	634.670
Median	641.240
Standard Deviation	129.890
Skewness	0.166
Kurtosis	6.225

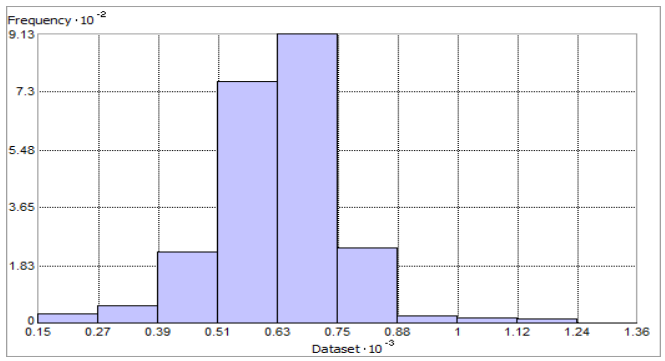

Fig. 491. Distribution of Summer Primary Production Minimum (mg C m^{-2} day^{-1}). Histogram was illustrated using 10 bins. X axis shown at 10^{-3}; Y axis shown at $10^{-2.}$

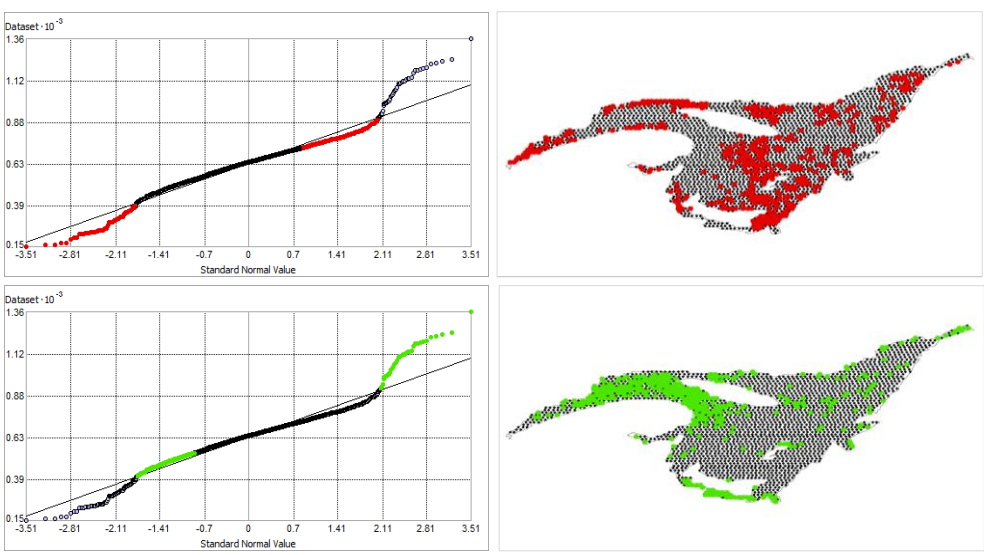

Fig. 492. Normal Q-Q plot for data values of Summer Primary Production Minimum (mg C m^{-2} day^{-1}). Points falling under (upper panel) and over (bottom panel) the reference line are mapped.

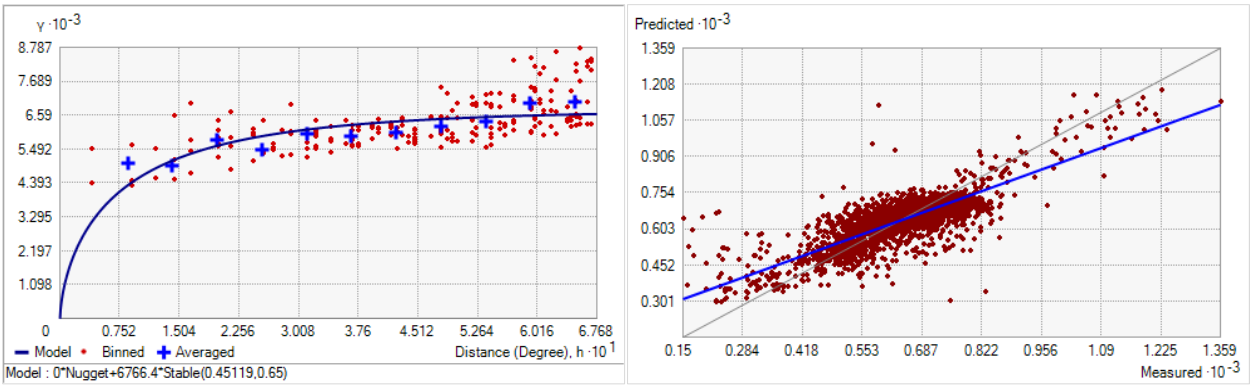

Fig. 493. Left panel: Semivariogram of Summer Primary Production Minimum (mg C m^{-2} day^{-1}). Binned values are shown as red dots; average points are shown as blue crosses; the model fit to the averaged values is shown as a blue line. Lag size: 0.056 degrees; number of lags: 12; Parameter: 0.650; Range: 0.451 degrees; Partial Sill: 6766.427. Right panel: Scatterplot of predicted values versus observed values for the model of Summer Primary Production Minimum (mg C m^{-2} day^{-1}).

Table 198. Results of cross-validation of the kriged model for Summer Primary Production Minimum (mg C m^{-2} day^{-1}).

Prediction error	**Value**
Number of Observations	2273
Overall Mean Error	0.379
Root Mean Square Prediction Error	77.130
Standardized Mean	0.004
Standardized Root Mean Square Prediction Error	1.070
Average Standard Error	71.204

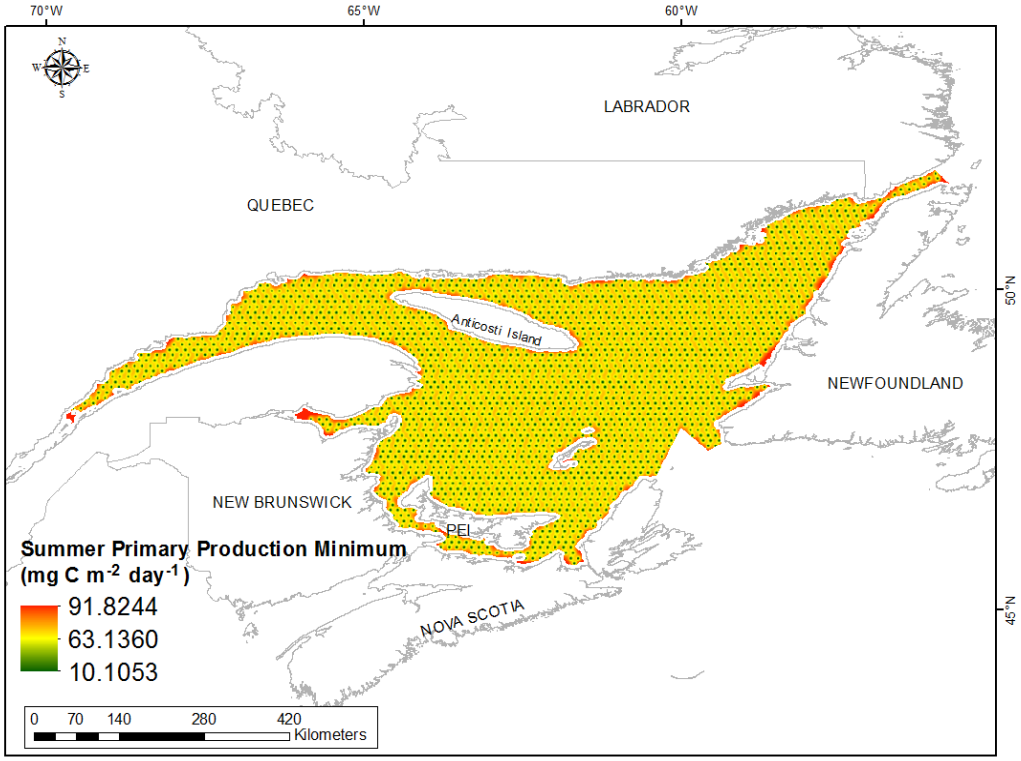

Fig. 494. Prediction standard error surface of Summer Primary Production Minimum (mg C m^{-2} day^{-1}).

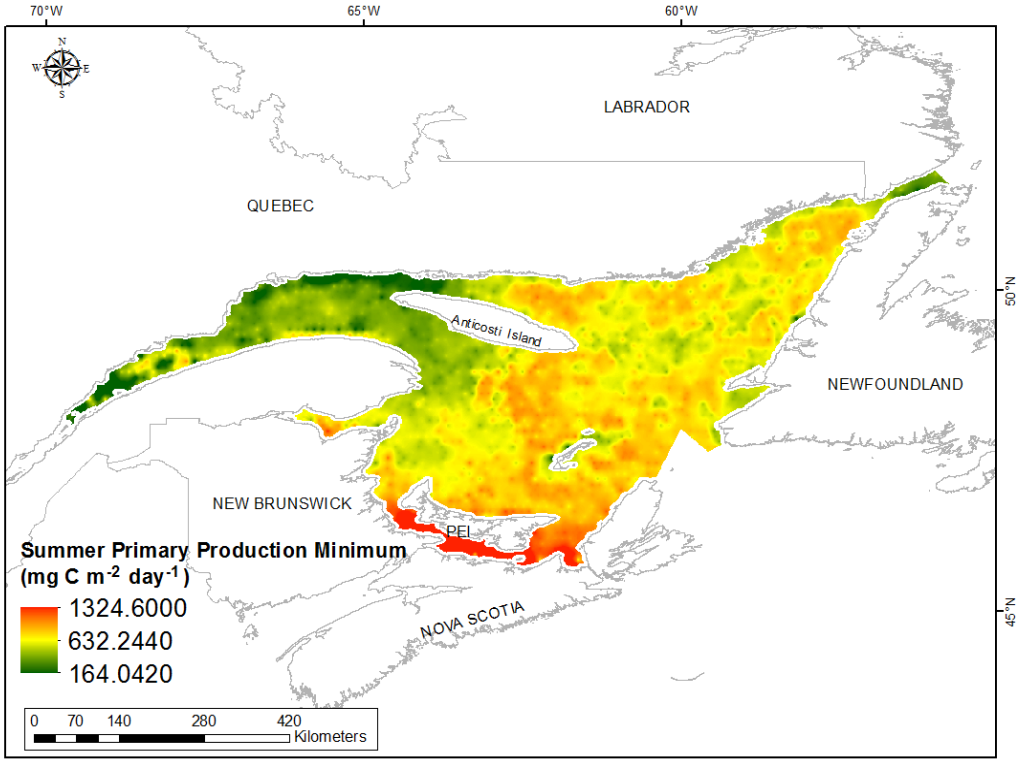

Fig. 495. Interpolated prediction surface of Summer Primary Production Minimum (mg C m^{-2} day^{-1}).

Summer Primary Production Maximum

This variable displayed a bell-shaped distribution with right-skewness (Table 199, Fig. 496). The data were higher than predicted by a normal distribution at low and high values, however mid-values deviated only slightly from the reference line (Fig. 497). The areas of under- and over-prediction showed no strong spatial pattern over the spatial extent (Fig. 497).

The semivariogram showed moderate autocorrelation present in the data and the model showed a fair fit between measured and predicted values (Fig. 498). Although the RMSPE and ASE were high (Table 200), all other errors showed that the model was good at prediction. The error map showed low error over the spatial extent but high error along the coast (Fig. 499). The kriged surface is presented in Fig. 500.

Table 199. Distributional properties of Summer Primary Production Maximum (mg C m^{-2} day^{-1}).

Property	Value
Number of Observations	2273
Minimum	735.830
Maximum	2810.100
Mean	1389.300
Median	1350.000
Standard Deviation	212.670
Skewness	1.025
Kurtosis	5.519

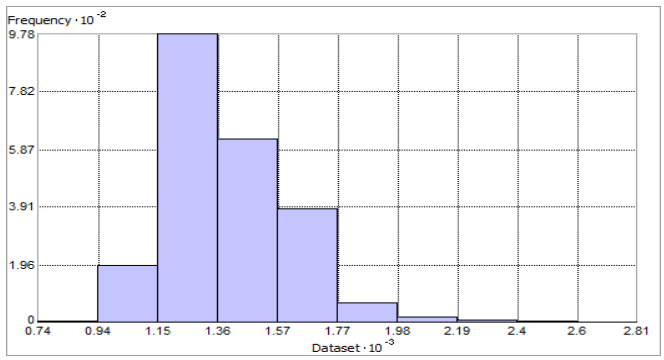

Fig. 496. Distribution of Summer Primary Production Maximum (mg C m^{-2} day^{-1}). Histogram was illustrated using 10 bins. X axis shown at 10^{-3}; Y axis shown at 10^{-2}.

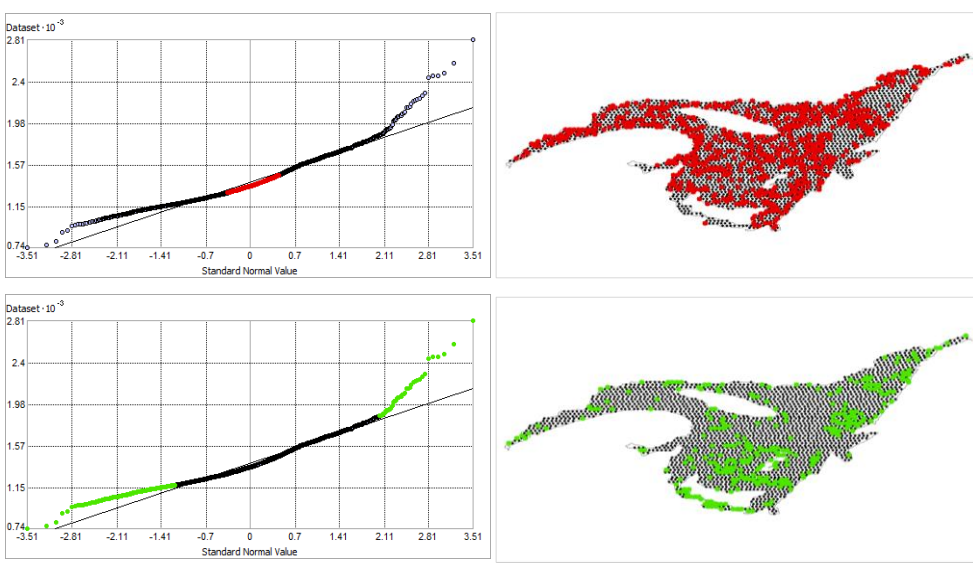

Fig. 497. Normal Q-Q plot for data values of Summer Primary Production Maximum (mg C m^{-2} day^{-1}). Points falling under (upper panel) and over (bottom panel) the reference line are mapped.

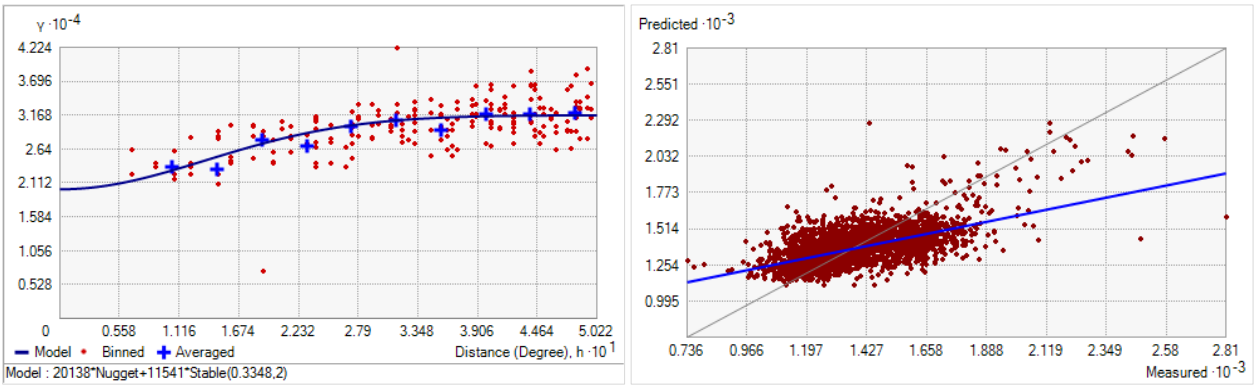

Fig. 498. Left panel: Semivariogram of Summer Primary Production Maximum (mg C m^{-2} day^{-1}). Binned values are shown as red dots; average points are shown as blue crosses; the model fit to the averaged values is shown as a blue line. Lag size: 0.042 degrees; number of lags: 12; Parameter: 2; Range: 0.335 degrees; Partial Sill: 11540.650. Right panel: Scatterplot of predicted values versus observed values for the model of Summer Primary Production Maximum (mg C m^{-2} day^{-1}).

Table 200. Results of cross-validation of the kriged model for Summer Primary Production Maximum (mg C m^{-2} day^{-1}).

Prediction error	**Value**
Number of Observations	2273
Overall Mean Error	-0.276
Root Mean Square Prediction Error	165.275
Standardized Mean	-0.002
Standardized Root Mean Square Prediction Error	1.034
Average Standard Error	158.403

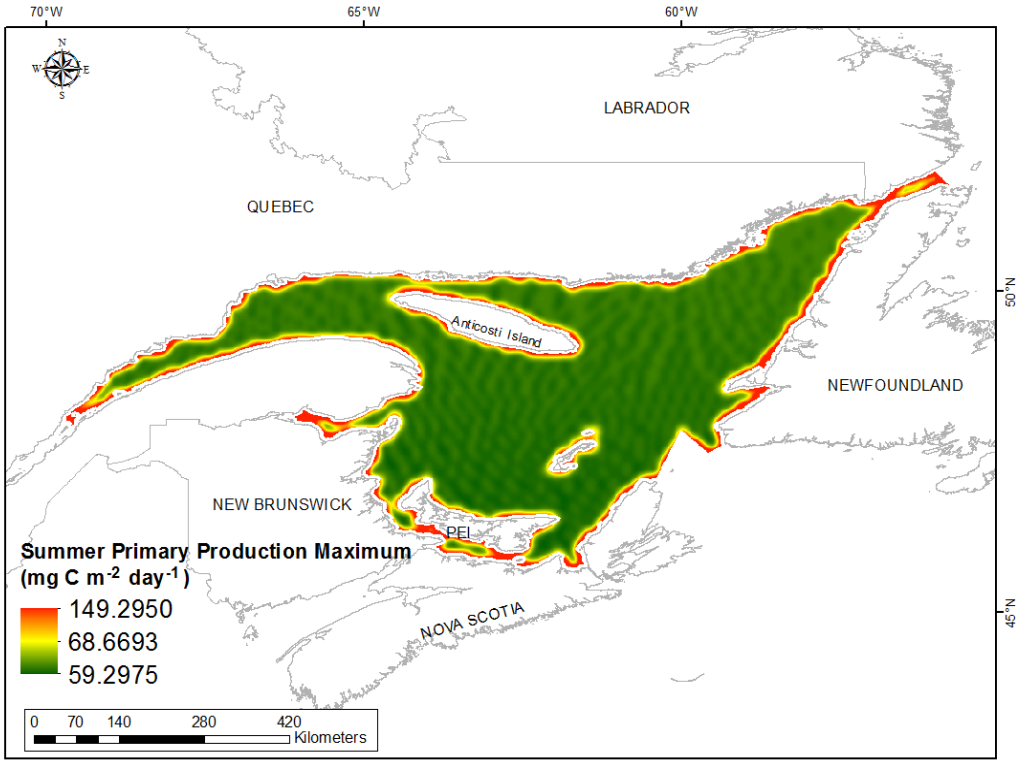

Fig. 499. Prediction standard error surface of Summer Primary Production Maximum (mg C m^{-2} day^{-1}).

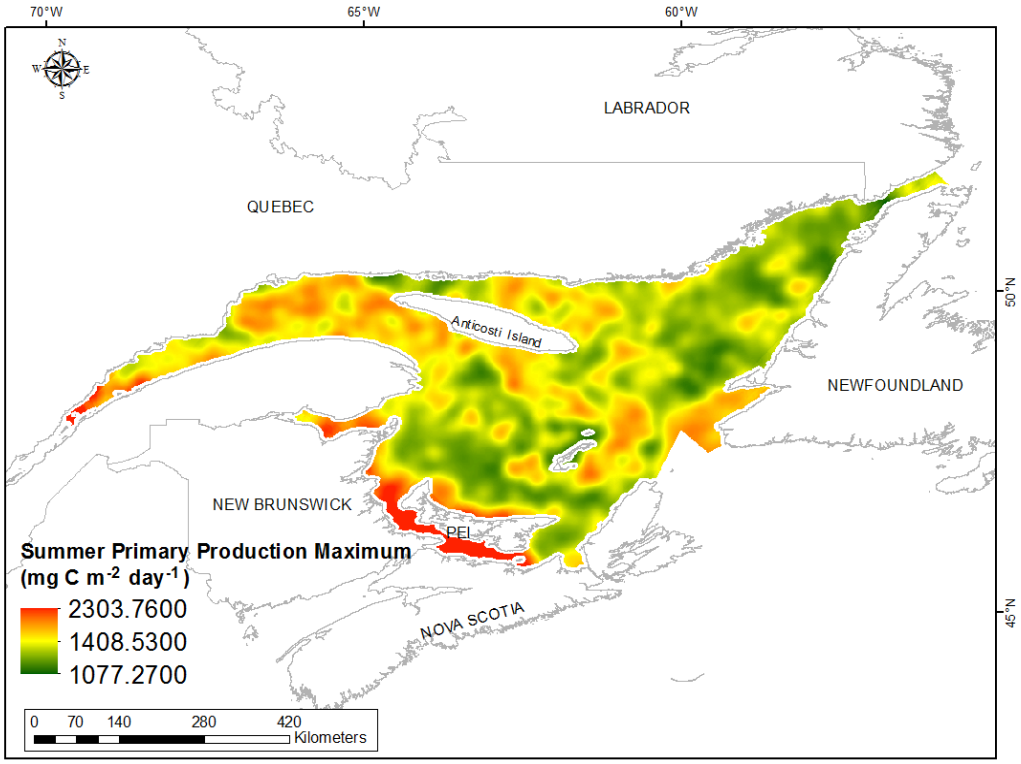

Fig. 500. Interpolated prediction surface of Summer Primary Production Maximum (mg C m^{-2} day^{-1}).

Summer Primary Production Range

This variable displayed a bell-shaped distribution with right-skewness with outlying data in the upper range (Table 201, Fig. 501). The data were higher than predicted by a normal distribution at low and high values but well predicted at mid-range values (Fig. 502). The areas of over-prediction showed no spatial pattern over the spatial extent (Fig. 502).

The semivariogram showed high autocorrelation present in the data and the model showed a poor fit between measured and predicted values, particularly at the upper range (Fig. 503). Although the RMSPE and ASE were high (Table 202), all other errors showed that the model was good at prediction. The error map showed moderate error across the study extent except at the exact location of data points where it was low (Fig. 504). The kriged surface is presented in Fig. 505.

Table 201. Distributional properties of Summer Primary Production Range (mg C m^{-2} day^{-1}).

Property	Value
Number of Observations	2273
Minimum	107.740
Maximum	2495.500
Mean	754.640
Median	719.370
Standard Deviation	236.630
Skewness	0.781
Kurtosis	4.922

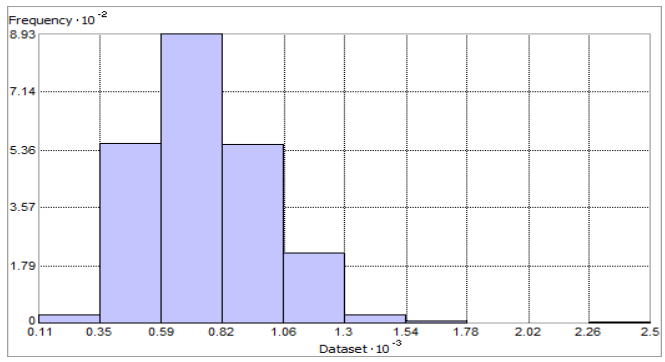

Fig. 501. Distribution of Summer Primary Production Range (mg C m^{-2} day^{-1}). Histogram was illustrated using 10 bins. X axis shown at 10^{-3}; Y axis shown at 10^{-2}.

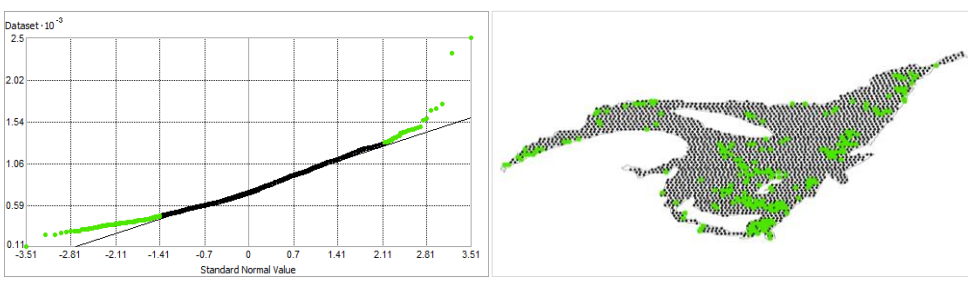

Fig. 502. Normal Q-Q plot for data values of Summer Primary Production Range (mg C m^{-2} day^{-1}). Points falling over bottom panel the reference line are mapped; no points fall below the reference line.

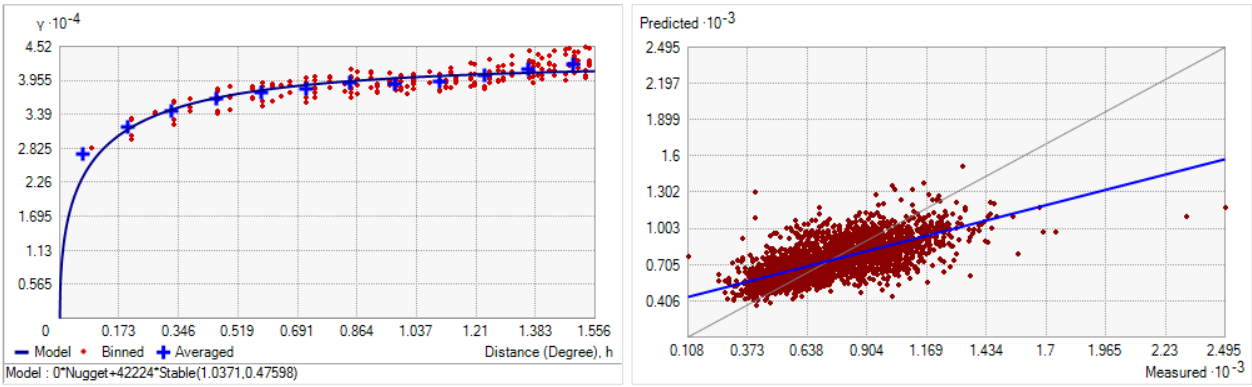

Fig. 503. Left panel: Semivariogram of Summer Primary Production Range (mg C m^{-2} day^{-1}). Binned values are shown as red dots; average points are shown as blue crosses; the model fit to the averaged values is shown as a blue line. Lag size: 0.130 degrees; number of lags: 12; Parameter: 0.476; Range: 1.037 degrees; Partial Sill: 42223.640. Right panel: Scatterplot of predicted values versus observed values for the model of Summer Primary Production Range (mg C m^{-2} day^{-1}).

Table 202. Results of cross-validation of the kriged model for Summer Primary Production Range (mg C m^{-2} day^{-1}).

Prediction error	**Value**
Number of Observations	2273
Overall Mean Error	-0.301
Root Mean Square Prediction Error	178.330
Standardized Mean	-0.001
Standardized Root Mean Square Prediction Error	1.035
Average Standard Error	170.971

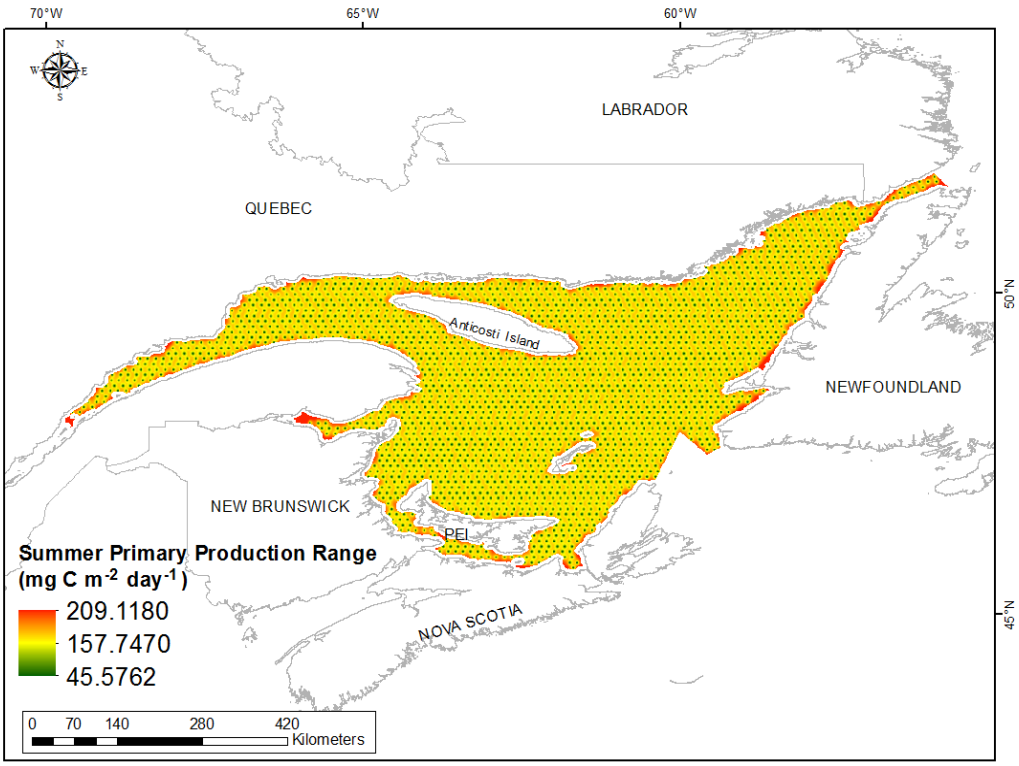

Fig. 504. Prediction standard error surface of Summer Primary Production Range (mg C m^{-2} day^{-1}).

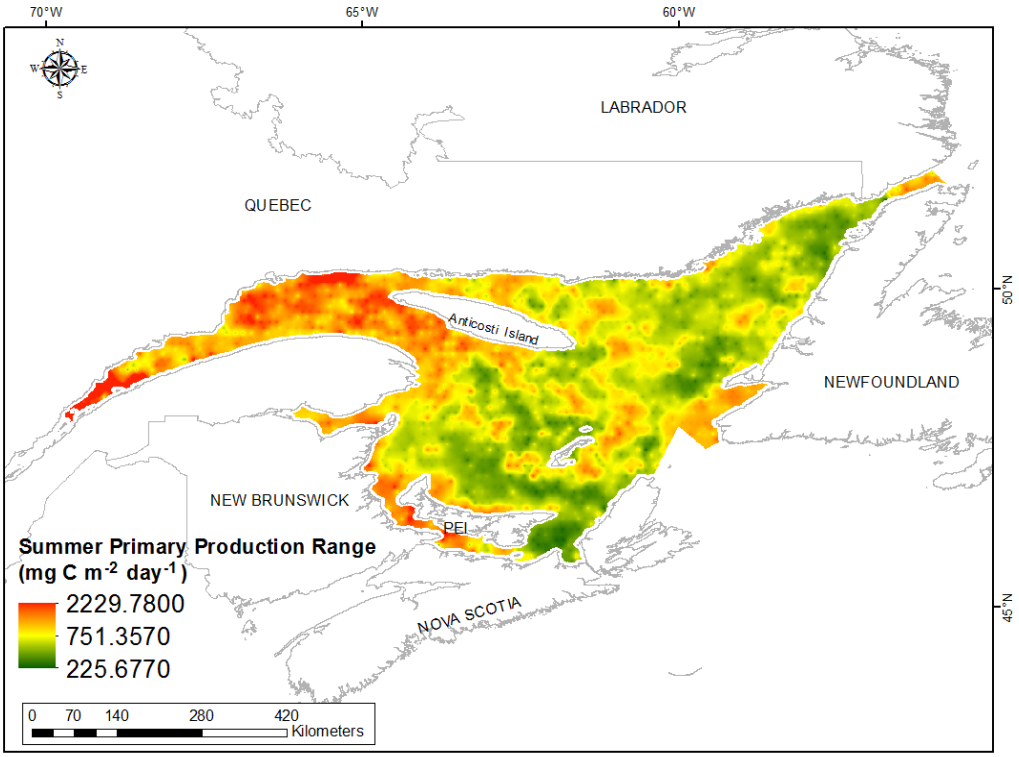

Fig. 505. Interpolated prediction surface of Summer Primary Production Range (mg C m^{-2} day^{-1}).

Summer Primary Production Average Minimum

This variable displayed a bell-shaped distribution with right skewness (Table 203, Fig. 506). The data were lower and higher than predicted by a normal distribution at low and high values, respectively, however mid-range values deviated only slightly from the reference line (Fig. 507). The areas of under- and over-prediction showed a strong spatial pattern over the study extent (Fig. 507).

The semivariogram showed moderate autocorrelation present in the data and the model showed a fair fit between measured and predicted values (Fig. 508). Although the RMSPE and ASE were high (Table 204), all other errors showed that the model was good at prediction. The error map showed low error over the study extent but high error around the coast (Fig. 509). The kriged surface is presented in Fig. 510.

Table 203. Distributional properties of Summer Primary Production Average Minimum (mg C m^{-2} day^{-1}).

Property	Value
Number of Observations	2273
Minimum	355.090
Maximum	1445.300
Mean	790.840
Median	791.240
Standard Deviation	108.860
Skewness	0.952
Kurtosis	8.209

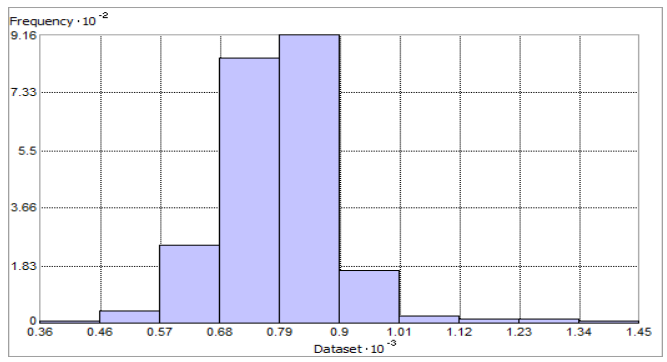

Fig. 506. Distribution of Summer Primary Production Average Minimum (mg C m^{-2} day^{-1}). Histogram was illustrated using 10 bins. X axis shown at 10^{-3}; Y axis shown at 10^{-2}.

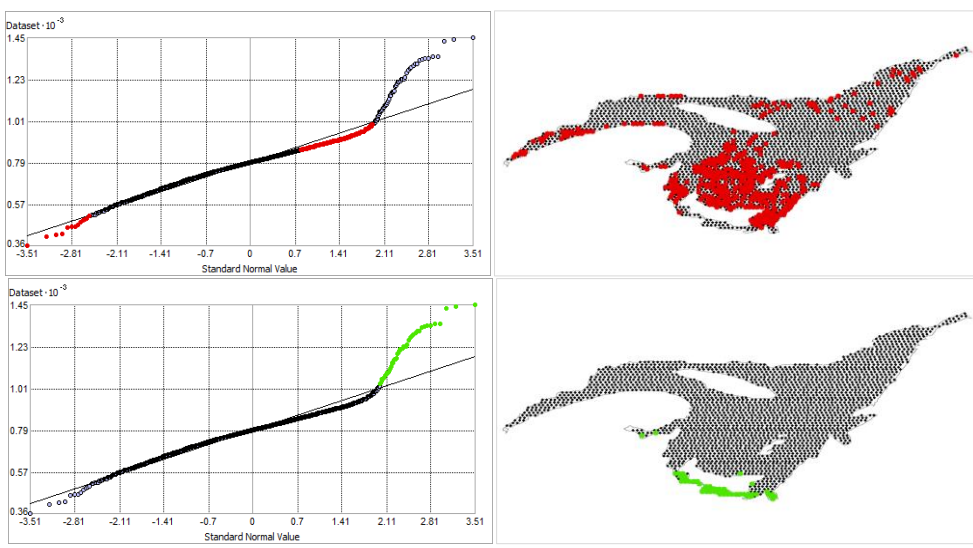

Fig. 507. Normal Q-Q plot for data values of Summer Primary Production Average Minimum (mg C m^{-2} day^{-1}). Points falling under (upper panel) and over (bottom panel) the reference line are mapped.

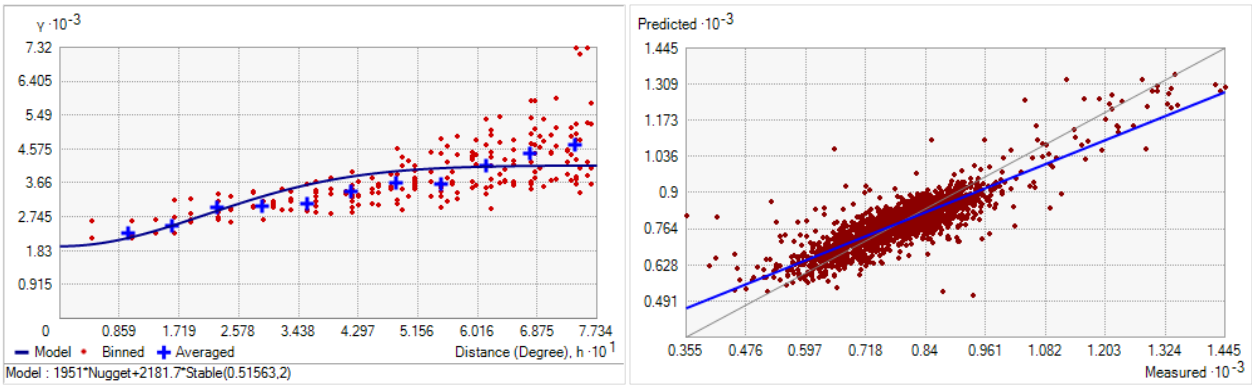

Fig. 508. Left panel: Semivariogram of Summer Primary Production Average Minimum (mg C m^{-2} day^{-1}). Binned values are shown as red dots; average points are shown as blue crosses; the model fit to the averaged values is shown as a blue line. Lag size: 0.064 degrees; number of lags: 12; Parameter: 2; Range: 0.516 degrees; Partial Sill: 2181.710. Right panel: Scatterplot of predicted values versus observed values for the model of Summer Primary Production Average Minimum (mg C m^{-2} day^{-1}).

Table 204. Results of cross-validation of the kriged model for Summer Primary Production Average Minimum (mg C m^{-2} day^{-1}).

Prediction error	**Value**
Number of Observations	2273
Overall Mean Error	0.143
Root Mean Square Prediction Error	55.667
Standardized Mean	0.001
Standardized Root Mean Square Prediction Error	1.129
Average Standard Error	48.195

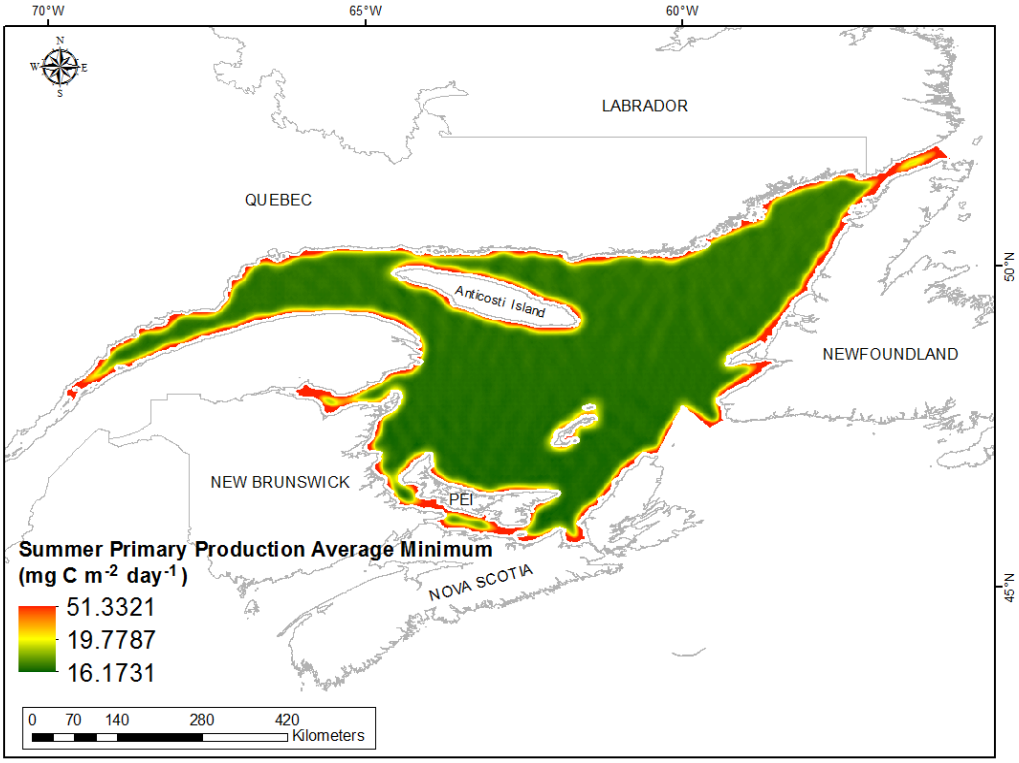

Fig. 509. Prediction standard error surface of Summer Primary Production Average Minimum (mg C m^{-2} day^{-1}).

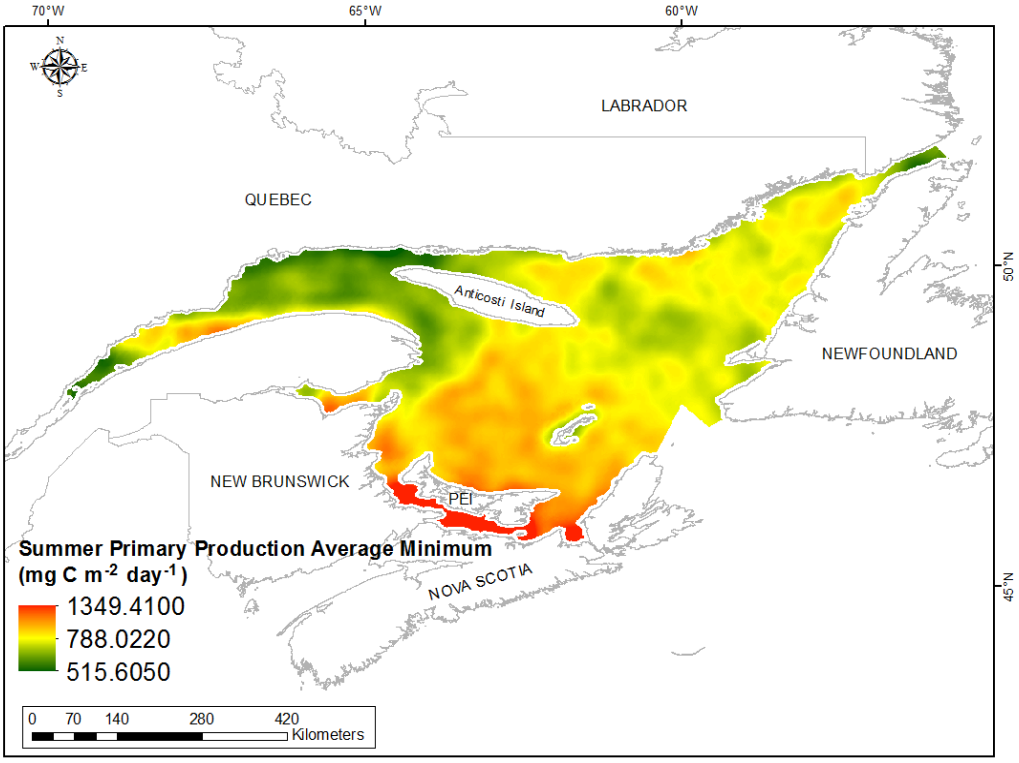

Fig. 510. Interpolated prediction surface of Summer Primary Production Average Minimum (mg C m^{-2} day^{-1}).

Summer Primary Production Average Maximum

This variable displayed a bell-shaped distribution with high kurtosis and right-skewness (Table 205, Fig. 511). The data were higher than predicted by a normal distribution at low and high values, however the mid-values deviated only slightly from the reference line (Fig. 512). The areas of under- and over-prediction showed a spatial pattern over the spatial extent (Fig. 512).

The semivariogram showed weak autocorrelation present in the data and the model showed a fair fit between measured and predicted values (Fig. 513). Although the RMSPE and ASE were high (Table 206), all other errors showed that the model was good at prediction. The error map showed low error across the spatial extent but was high along the coast (Fig. 514). The kriged surface is presented in Fig. 515.

Table 205. Distributional properties of Summer Primary Production Average Maximum (mg C m^{-2} day^{-1}).

Property	Value
Number of Observations	2273
Minimum	664.850
Maximum	1988.100
Mean	1132.600
Median	1114.700
Standard Deviation	131.990
Skewness	2.040
Kurtosis	11.004

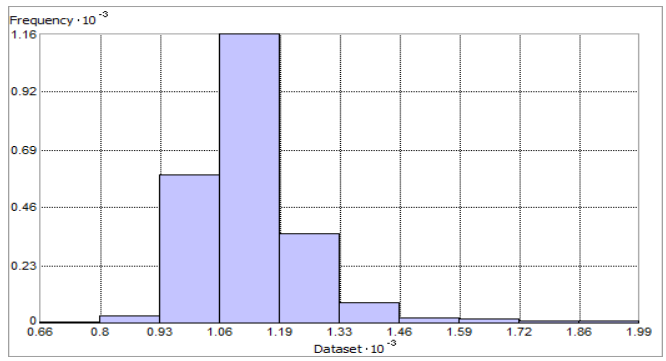

Fig. 511. Distribution of Summer Primary Production Average Maximum (mg C m^{-2} day^{-1}). Histogram was illustrated using 10 bins. X and Y axes shown at 10^{-3}.

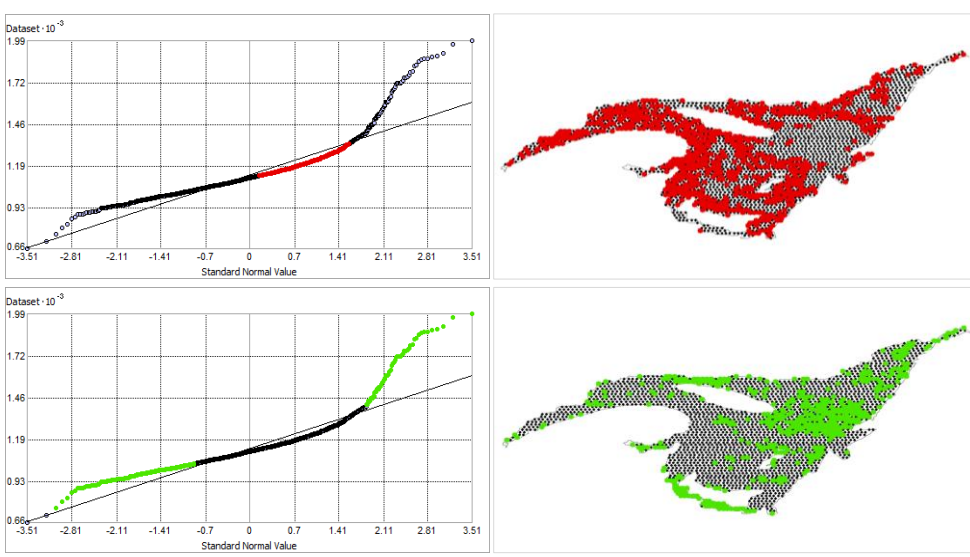

Fig. 512. Normal Q-Q plot for data values of Summer Primary Production Average Maximum (mg C m^{-2} day^{-1}). Points falling under (upper panel) and over (bottom panel) the reference line are mapped.

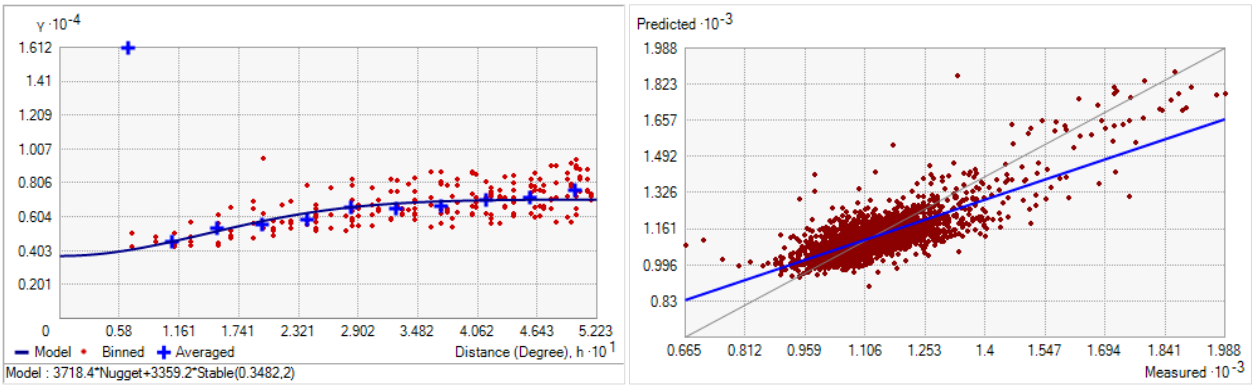

Fig. 513. Left panel: Semivariogram of Summer Primary Production Average Maximum (mg C m^{-2} day^{-1}). Binned values are shown as red dots; average points are shown as blue crosses; the model fit to the averaged values is shown as a blue line. Lag size: 0.044 degrees; number of lags: 12; Parameter: 2; Range: 0.348 degrees; Partial Sill: 3359.236. Right panel: Scatterplot of predicted values versus observed values for the model of Summer Primary Production Average Maximum (mg C m^{-2} day^{-1}).

Table 206. Results of cross-validation of the kriged model for Summer Primary Production Average Maximum (mg C m^{-2} day^{-1}).

Prediction error	**Value**
Number of Observations	2273
Overall Mean Error	-0.275
Root Mean Square Prediction Error	76.557
Standardized Mean	-0.003
Standardized Root Mean Square Prediction Error	1.079
Average Standard Error	69.413

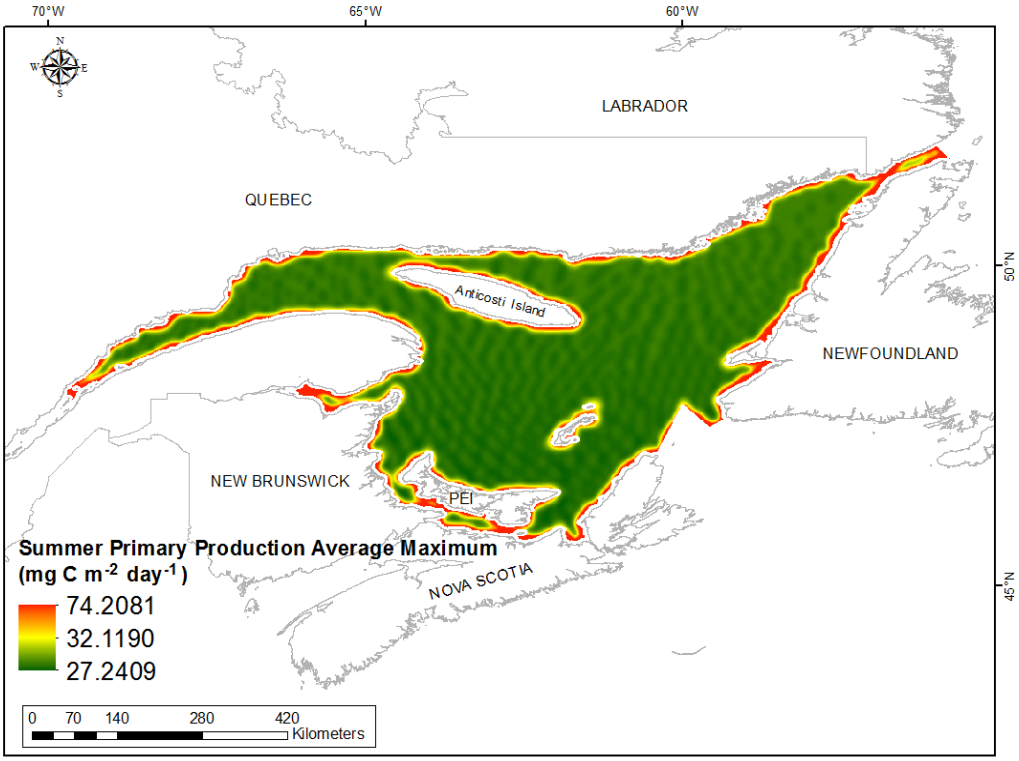

Fig. 514. Prediction standard error surface of Summer Primary Production Average Maximum (mg C m^{-2} day^{-1}).

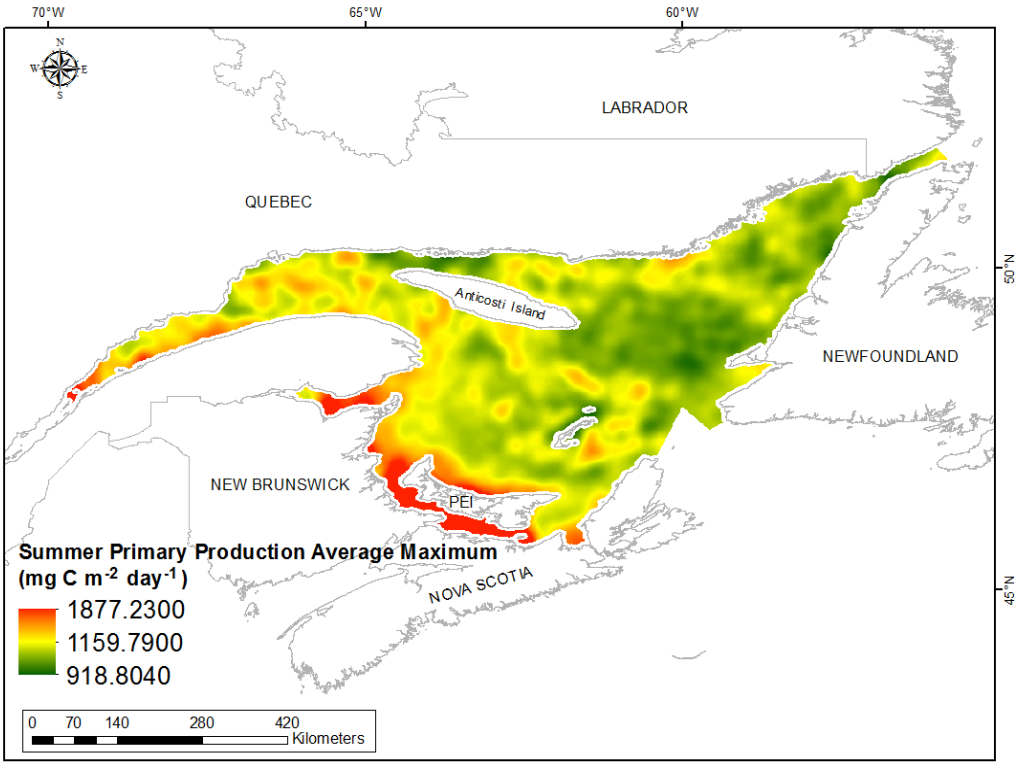

Fig. 515. Interpolated prediction surface of Summer Primary Production Average Maximum (mg C m^{-2} day^{-1}).

Summer Primary Production Average Range

This variable displayed right-skewness and high kurtosis (Table 207, Fig. 516). The data were higher than predicted by a normal distribution at low and high values, however mid-values deviated only slightly from the reference line (Fig. 517). The areas of under- and over-prediction showed no spatial pattern over the spatial extent (Fig. 517).

The semivariogram showed weak autocorrelation present in the data and the model showed a fair to poor fit between measured and predicted values (Fig. 518). Although the RMSPE and ASE were high (Table 208), all other errors showed that the model was good at prediction. The error map showed moderate error across the study extent except at the exact location of data points where it was low (Fig. 519). The kriged surface is presented in Fig. 520.

Table 207. Distributional properties of Summer Primary Production Average Range (mg C m^{-2} day^{-1}).

Property	Value
Number of Observations	2273
Minimum	91.120
Maximum	1190.700
Mean	341.730
Median	318.730
Standard Deviation	127.04
Skewness	1.078
Kurtosis	5.017

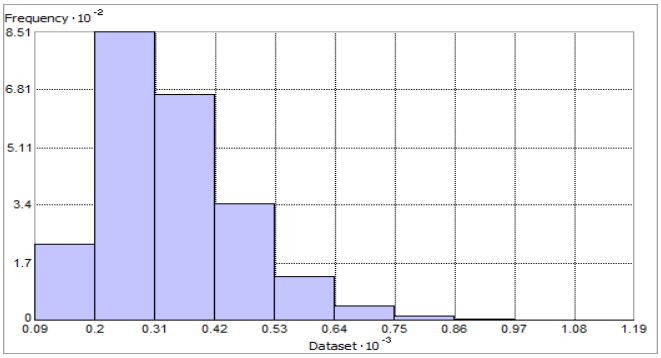

Fig. 516. Distribution of Summer Primary Production Average Range (mg C m^{-2} day^{-1}). Histogram was illustrated using 10 bins. X axis shown at 10^{-3}; Y axis shown at 10^{-2}.

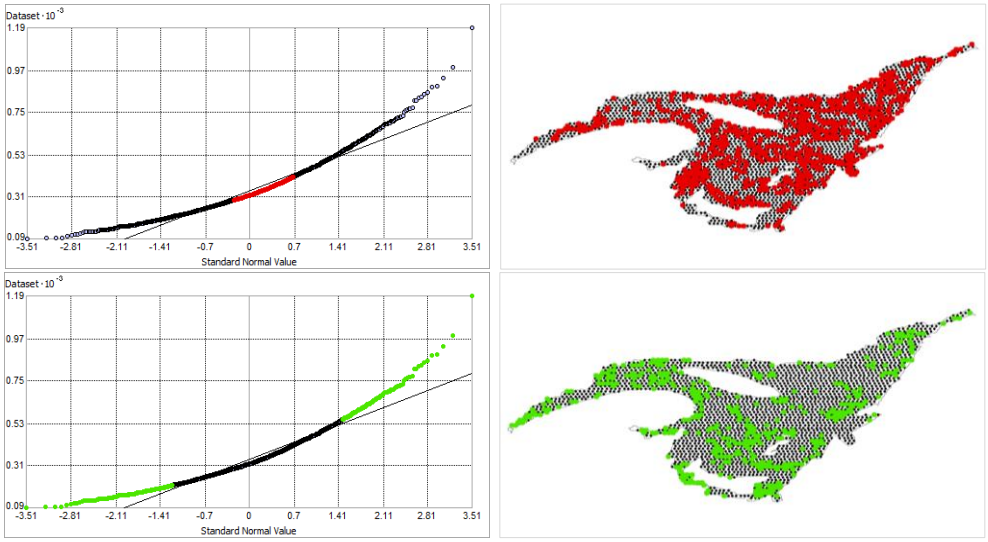

Fig. 517. Normal Q-Q plot for data values of Summer Primary Production Average Range (mg C m^{-2} day^{-1}). Points falling under (upper panel) and over (bottom panel) the reference line are mapped.

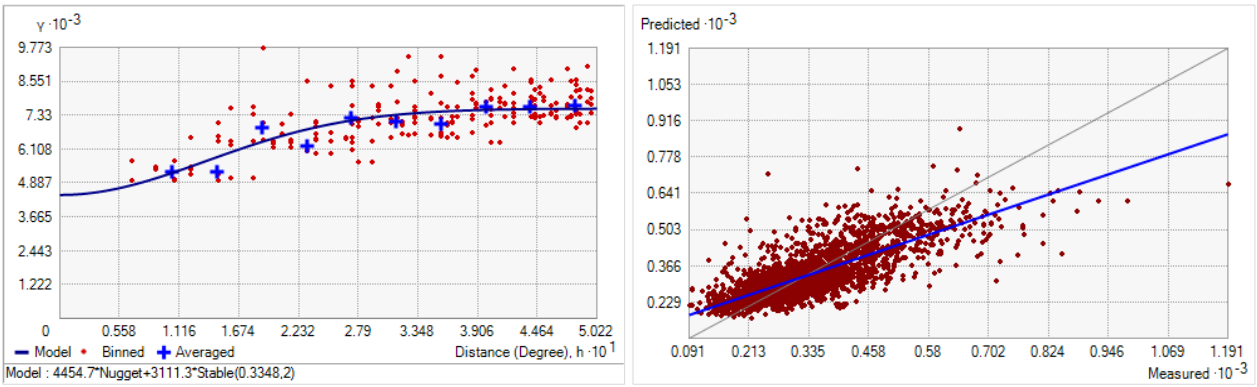

Fig. 518. Left panel: Semivariogram of Summer Primary Production Average Range (mg C m^{-2} day^{-1}). Binned values are shown as red dots; average points are shown as blue crosses; the model fit to the averaged values is shown as a blue line. Lag size: 0.042 degrees; number of lags: 12; Parameter: 2; Range: 0.335 degrees; Partial Sill: 3111.281. Right panel: Scatterplot of predicted values versus observed values for the model of Summer Primary Production Average Range (mg C m^{-2} day^{-1}).

Table 208. Results of cross-validation of the kriged model for Summer Primary Production Average Range (mg C m^{-2} day^{-1}).

Prediction error	**Value**
Number of Observations	2273
Overall Mean Error	-0.553
Root Mean Square Prediction Error	80.584
Standardized Mean	-0.006
Standardized Root Mean Square Prediction Error	1.054
Average Standard Error	75.316

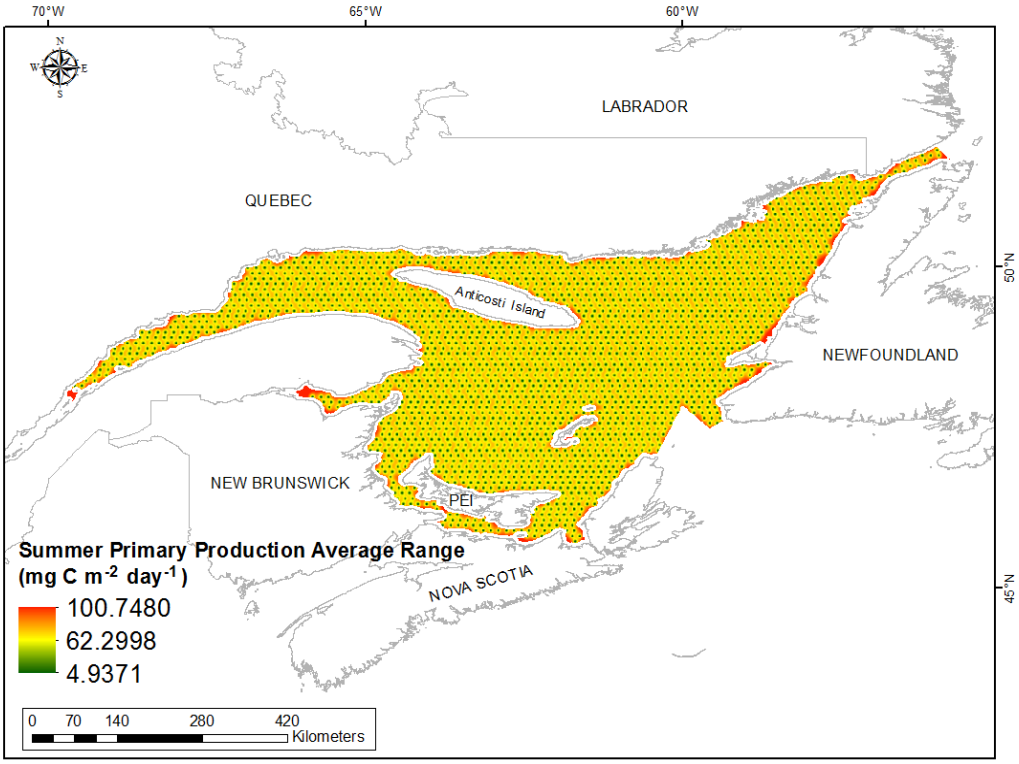

Fig. 519. Prediction standard error surface of Summer Primary Production Average Range (mg C m^{-2} day^{-1}).

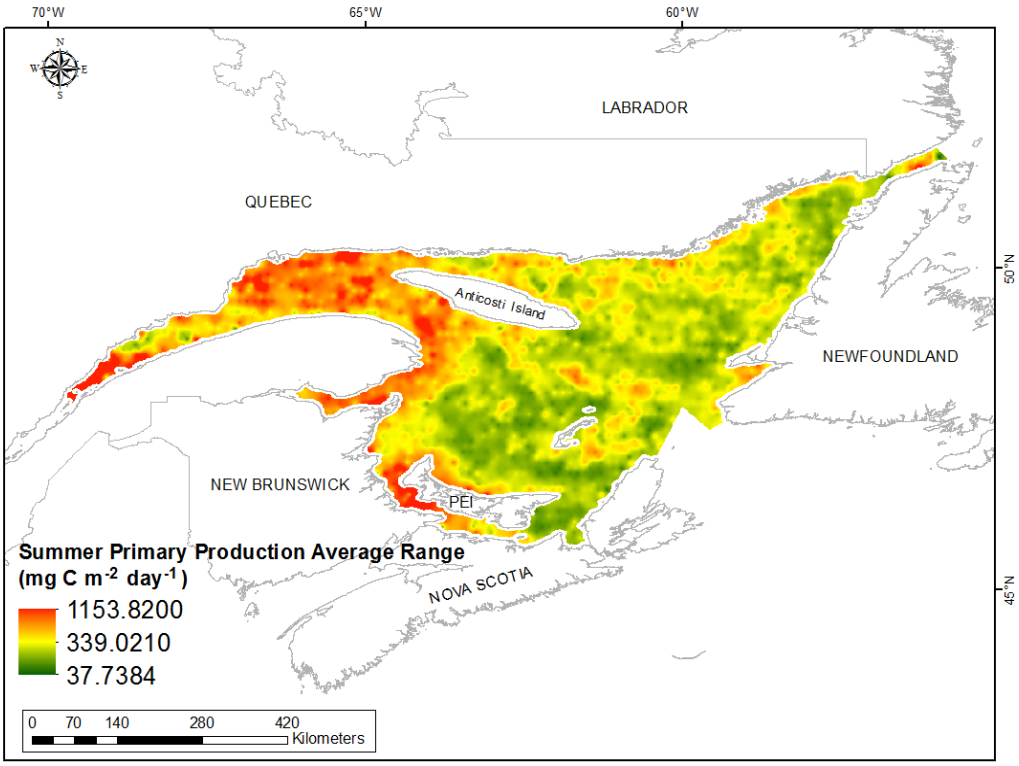

Fig. 520. Interpolated prediction surface of Summer Primary Production Average Range (mg C m^{-2} day^{-1}).

Annual Primary Production Mean

This variable displayed a bell-shaped distribution with high kurtosis (Table 209, Fig. 521). The data were higher than predicted by a normal distribution at low and high values, however the mid-values deviated only slightly from the reference line (Fig. 522). The areas of under- and over-prediction showed a spatial pattern over the spatial extent (Fig. 522).

The semivariogram showed moderate autocorrelation present in the data and the model showed a good fit between measured and predicted values (Fig. 523). Although the RMSPE and ASE were high (Table 210), all other errors showed that the model was good at prediction. The error map showed that error was low across the study extent but was high along the coast (Fig. 524). The kriged surface is presented in Fig. 525.

Table 209. Distributional properties of Annual Primary Production Mean (mg C m^{-2} day^{-1}).

Property	Value
Number of Observations	2284
Minimum	432.57
Maximum	1489.200
Mean	801.570
Median	777.910
Standard Deviation	107.720
Skewness	1.700
Kurtosis	8.301

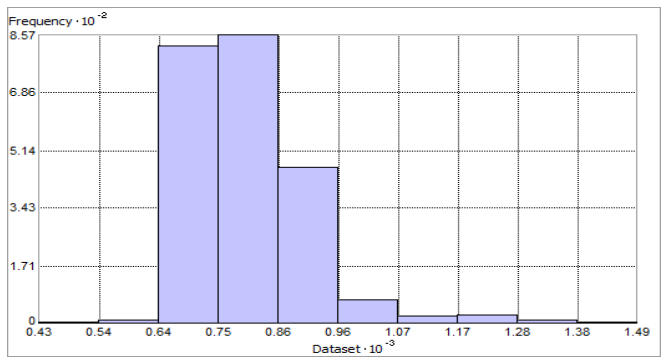

Fig. 521. Distribution of Annual Primary Production Mean (mg C m^{-2} day^{-1}). Histogram was illustrated using 10 bins. Y axis is shown at 10^{-2}; X axis at 10^{-3}.

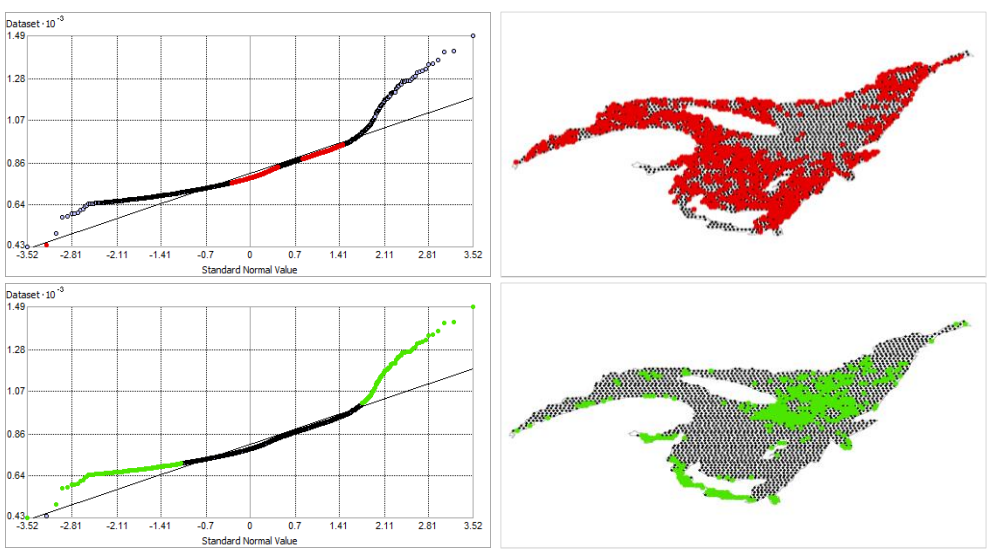

Fig. 522. Normal Q-Q plot for data values of Annual Primary Production Mean (mg C m^{-2} day^{-1}). Points falling under (upper panel) and over (bottom panel) the reference line are mapped.

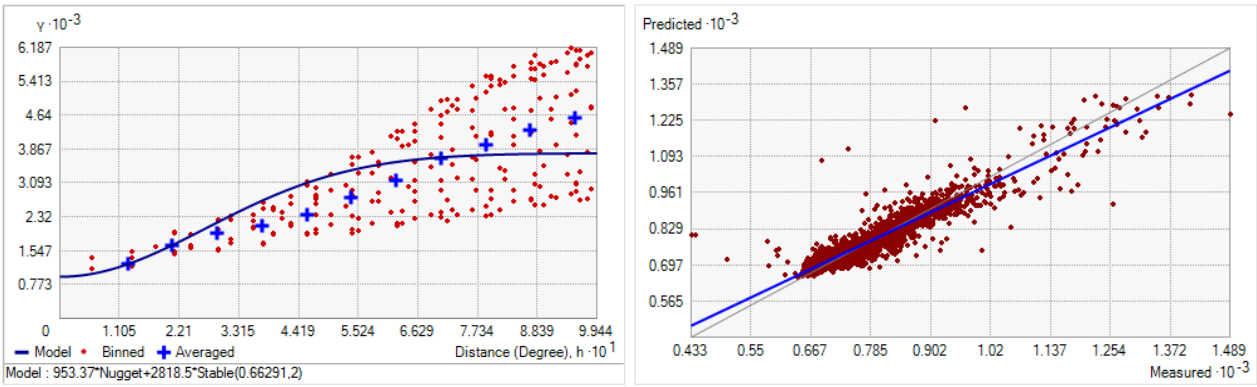

Fig. 523. Semivariogram of Annual Primary Production Mean (mg C m^{-2} day^{-1}). Binned values are shown as red dots; average points are shown as blue crosses; the model fit to the averaged values is shown as a blue line. Lag size: 0.083 degrees; number of lags: 12; Parameter: 2; Range: 0.663 degrees; Partial Sill: 2818.532. Right panel: Scatterplot of predicted values versus observed values for the model of Annual Primary Production Mean (mg C m^{-2} day^{-1}).

Table 210. Results of cross-validation of the kriged model for the Annual Primary Production Mean (mg C m^{-2} day^{-1}).

Prediction error	**Value**
Number of Observations	2284
Overall Mean Error	0.349
Root Mean Square Prediction Error	41.253
Standardized Mean	0.010
Standardized Root Mean Square Prediction Error	1.174
Average Standard Error	33.820

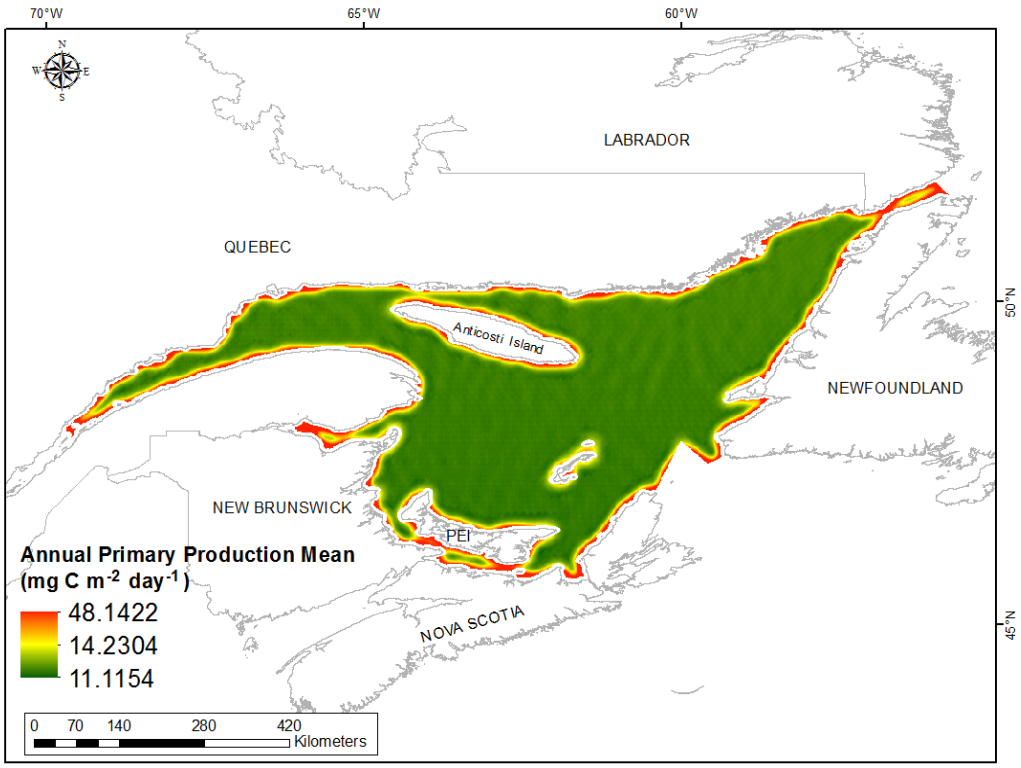

Fig. 524. Prediction standard error surface of Annual Primary Production Mean (mg C m^{-2} day^{-1}).

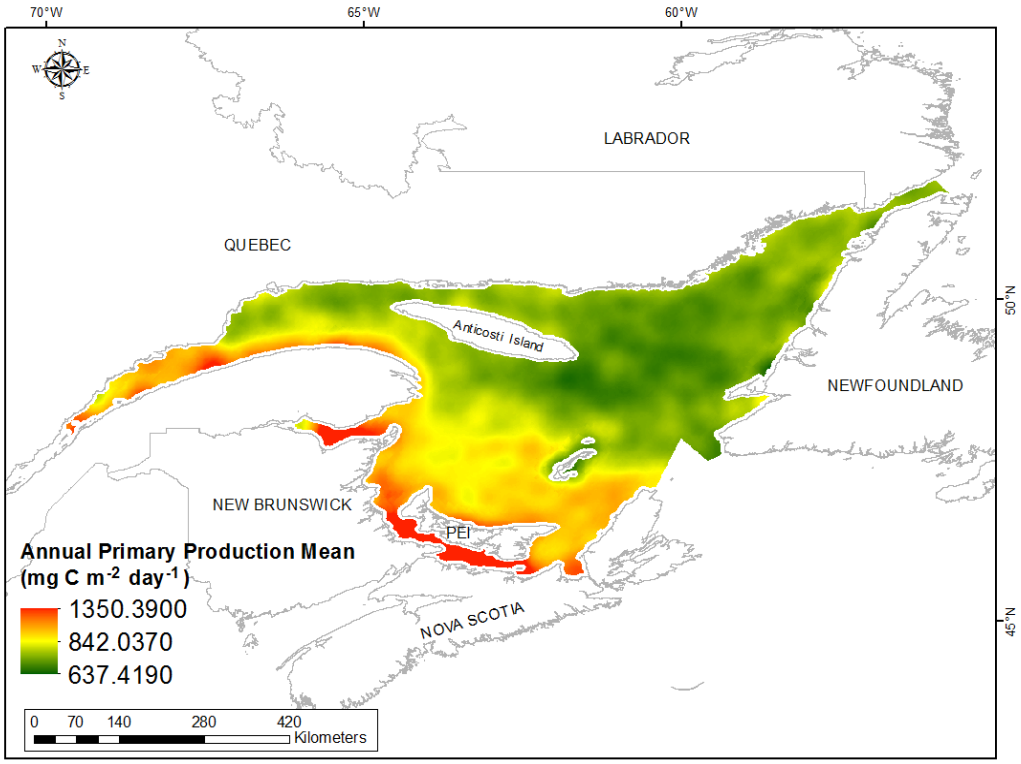

Fig. 525. Interpolated prediction surface of Annual Primary Production Mean (mg C m^{-2} day^{-1}).

Annual Primary Production Minimum

This variable displayed a highly right-skewed distribution (Table 211, Fig. 526). The data were higher than predicted by a normal distribution at low and high values, however the mid-values deviated only slightly from the reference line (Fig. 527). The areas of under- and over-prediction showed a weak spatial pattern over the spatial extent (Fig. 527).

The semivariogram showed little to no autocorrelation present in the data and the model showed a poor fit between measured and predicted values (Fig. 528). Although the RMSPE and ASE were high (Table 212), all other errors showed that the model was good at prediction. The error map showed moderate error across the study extent except at the exact location of data points where it was low (Fig. 529). High error was observed around the coast. The kriged surface is presented in Fig. 530.

Table 211. Distributional properties of Annual Primary Production Minimum (mg C m^{-2} day^{-1}).

Property	Value
Number of Observations	2284
Minimum	70.430
Maximum	676.610
Mean	203.680
Median	193.480
Standard Deviation	67.269
Skewness	1.904
Kurtosis	10.385

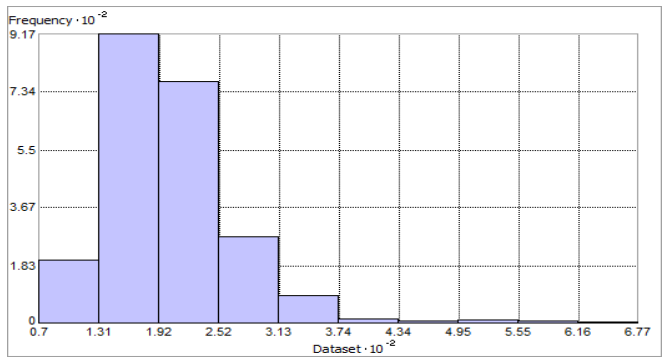

Fig. 526. Distribution of Annual Primary Production Minimum (mg C m^{-2} day^{-1}). Histogram was illustrated using 10 bins. X and Y axes shown 10^{-2}.

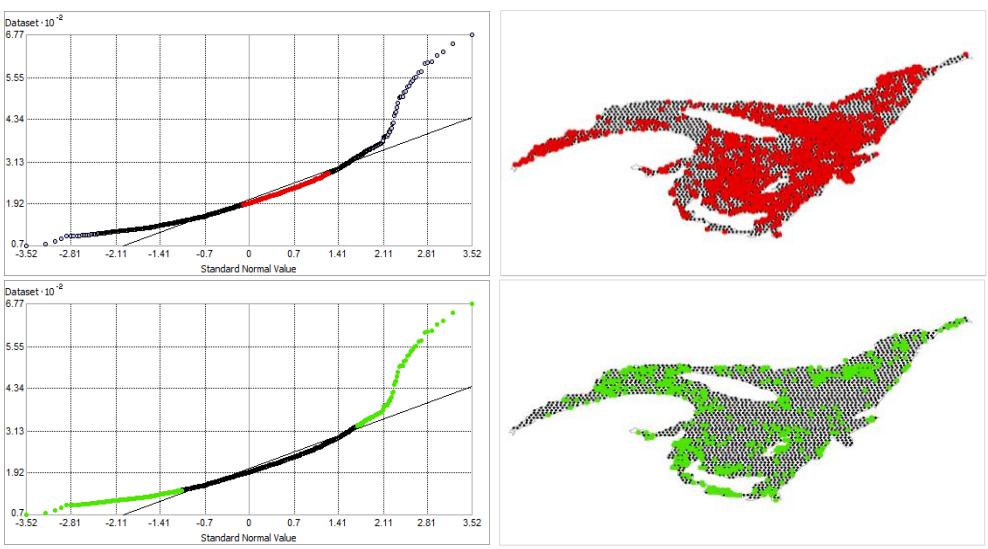

Fig. 527. Normal Q-Q plot for data values of Annual Primary Production Minimum (mg C m^{-2} day^{-1}). Points falling under (upper panel) and over (bottom panel) the reference line are mapped.

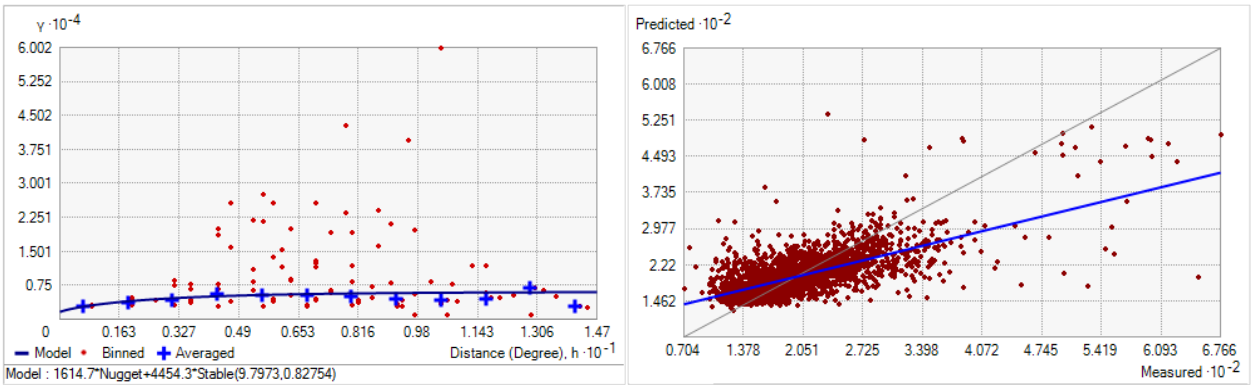

Fig. 528. Semivariogram of Annual Primary Production Minimum (mg C m^{-2} day^{-1}). Binned values are shown as red dots; average points are shown as blue crosses; the model fit to the averaged values is shown as a blue line. Lag size: 1.225 degrees; number of lags: 12; Parameter: 0.828; Range: 9.797 degrees; Partial Sill: 4454.340. Right panel: Scatterplot of predicted values versus observed values for the model of Annual Primary Production Minimum (mg C m^{-2} day^{-1}).

Table 212. Results of cross-validation of the kriged model for the Annual Primary Production Minimum (mg C m^{-2} day^{-1}).

Prediction error	**Value**
Number of Observations	2284
Overall Mean Error	-0.035
Root Mean Square Prediction Error	49.424
Standardized Mean	-1.858×10^{-4}
Standardized Root Mean Square Prediction Error	1.077
Average Standard Error	45.398

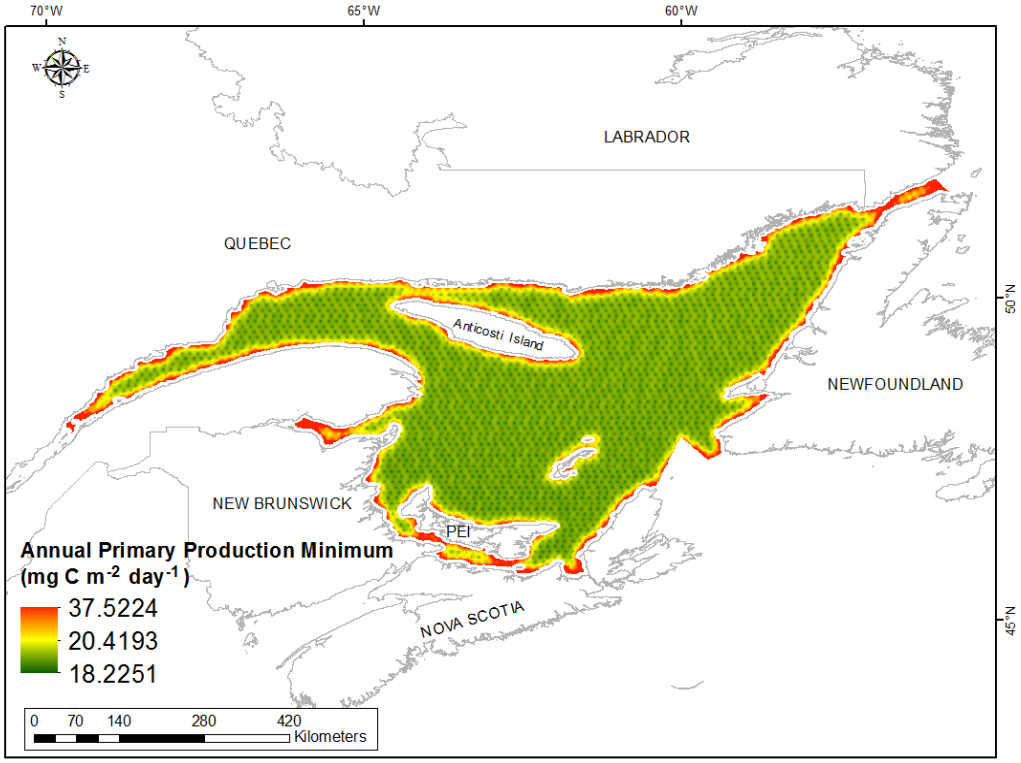

Fig. 529. Prediction standard error surface of Annual Primary Production Minimum (mg C m^{-2} day^{-1}).

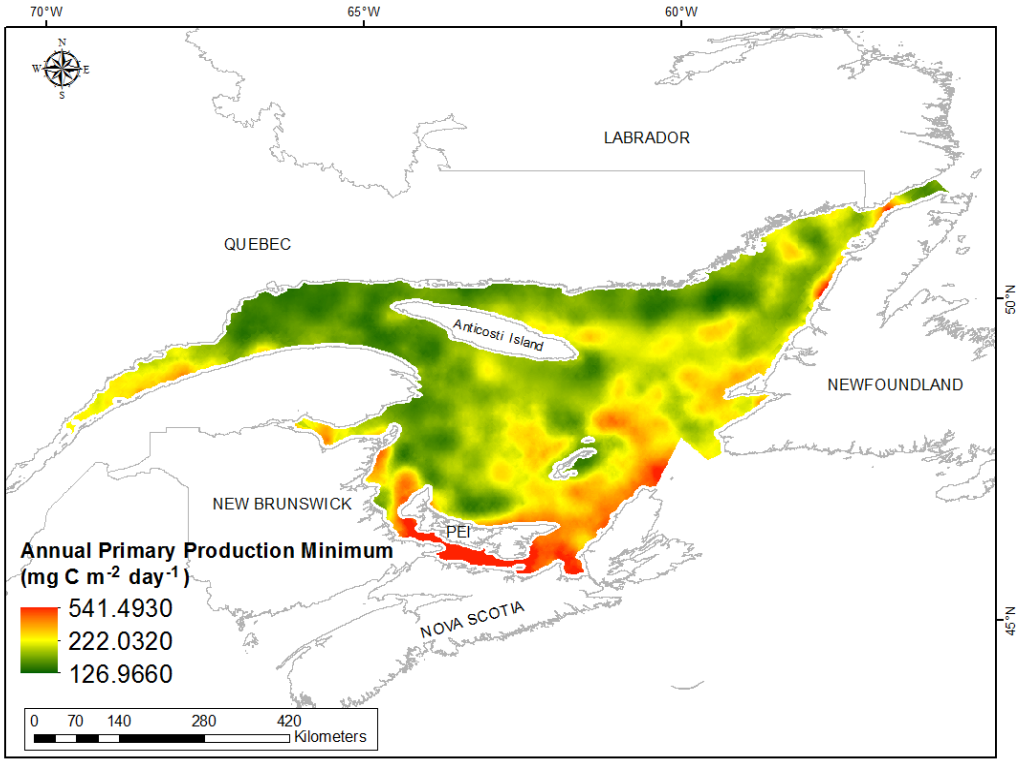

Fig. 530. Interpolated prediction surface of Annual Primary Production Minimum (mg C m^{-2} day^{-1}).

Annual Primary Production Maximum

This variable displayed a bell-shaped distribution with right-skewness and high kurtosis (Table 213, Fig. 531). The data were higher than predicted by a normal distribution at low and high values, however the mid-values deviated only slightly from the reference line (Fig. 532). The areas of under- and over-prediction showed a spatial pattern over the spatial extent (Fig. 532).

The semivariogram showed moderate autocorrelation present in the data and the model showed a fair to poor fit between measured and predicted values (Fig. 533). Although the RMSPE and ASE were high (Table 214), all other errors showed that the model was good at prediction. The error map showed that error was low across the study extent but was high along the coast (Fig. 534). The kriged surface is presented in Fig. 535.

Table 213. Distributional properties of Annual Primary Production Maximum (mg C m^{-2} day^{-1}).

Property	Value
Number of Observations	2284
Minimum	735.830
Maximum	3071.800
Mean	1480.300
Median	1455.900
Standard Deviation	216.250
Skewness	1.633
Kurtosis	10.166

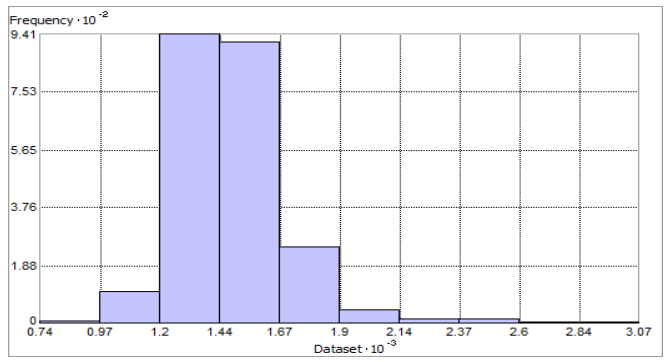

Fig. 531. Distribution of Annual Primary Production Maximum (mg C m^{-2} day^{-1}). Histogram was illustrated using 10 bins. X axis shown at 10^{-3}; Y axis shown at 10^{-2}.

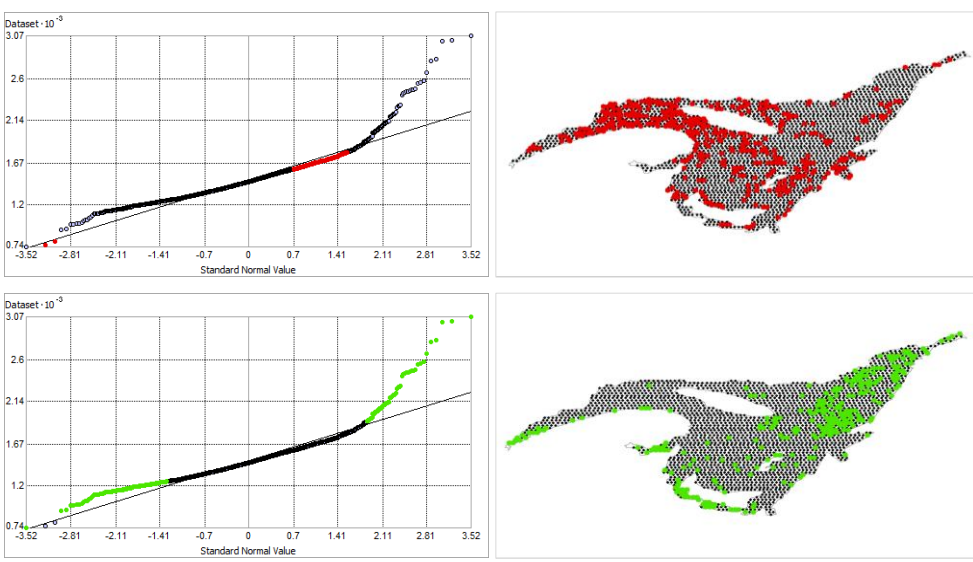

Fig. 532. Normal Q-Q plot for data values of Annual Primary Production Maximum (mg C m^{-2} day^{-1}). Points falling under (upper panel) and over (bottom panel) the reference line are mapped.

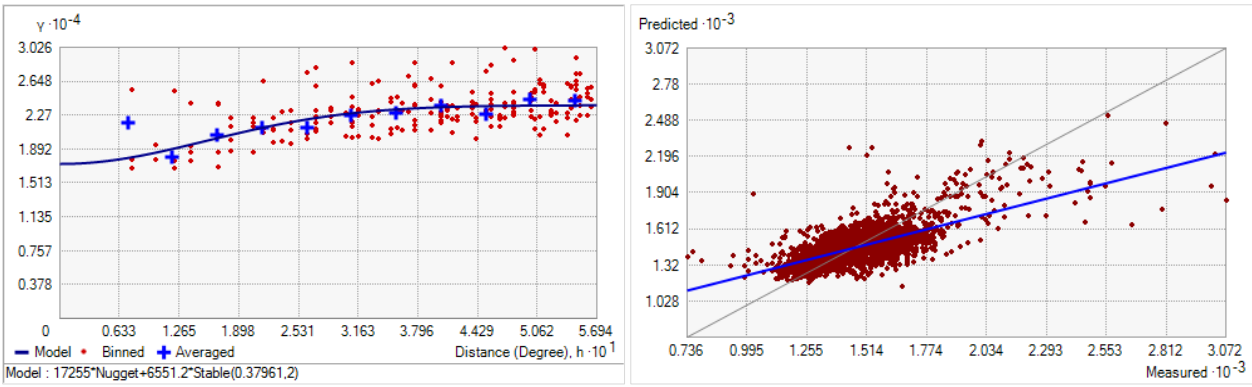

Fig. 533. Semivariogram of Annual Primary Production Maximum (mg C m^{-2} day^{-1}). Binned values are shown as red dots; average points are shown as blue crosses; the model fit to the averaged values is shown as a blue line. Lag size: 0.047 degrees; number of lags: 12; Parameter: 2; Range: 0.380 degrees; Partial Sill: 6551.199. Right panel: Scatterplot of predicted values versus observed values for the model of Annual Primary Production Maximum (mg C m^{-2} day^{-1}).

Table 214. Results of cross-validation of the kriged model for the Annual Primary Production Maximum (mg C m^{-2} day^{-1}).

Prediction error	**Value**
Number of Observations	2284
Overall Mean Error	-1.031
Root Mean Square Prediction Error	151.176
Standardized Mean	-0.006
Standardized Root Mean Square Prediction Error	1.055
Average Standard Error	142.061

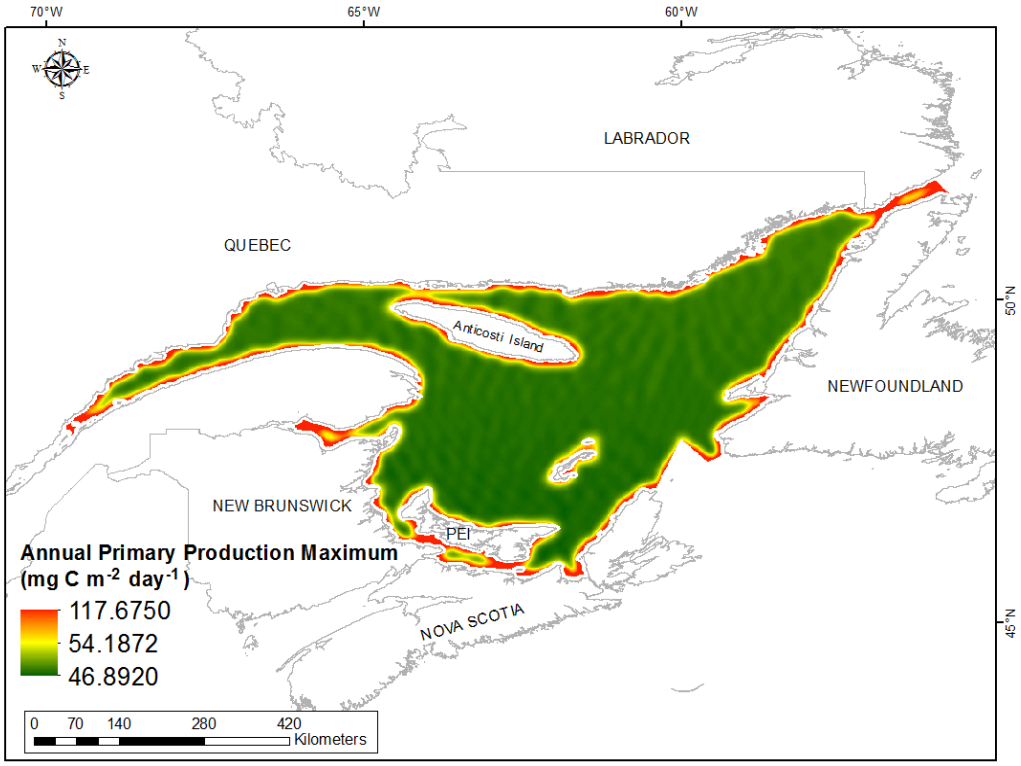

Fig. 534. Prediction standard error surface of Annual Primary Production Maximum (mg C m^{-2} day^{-1}).

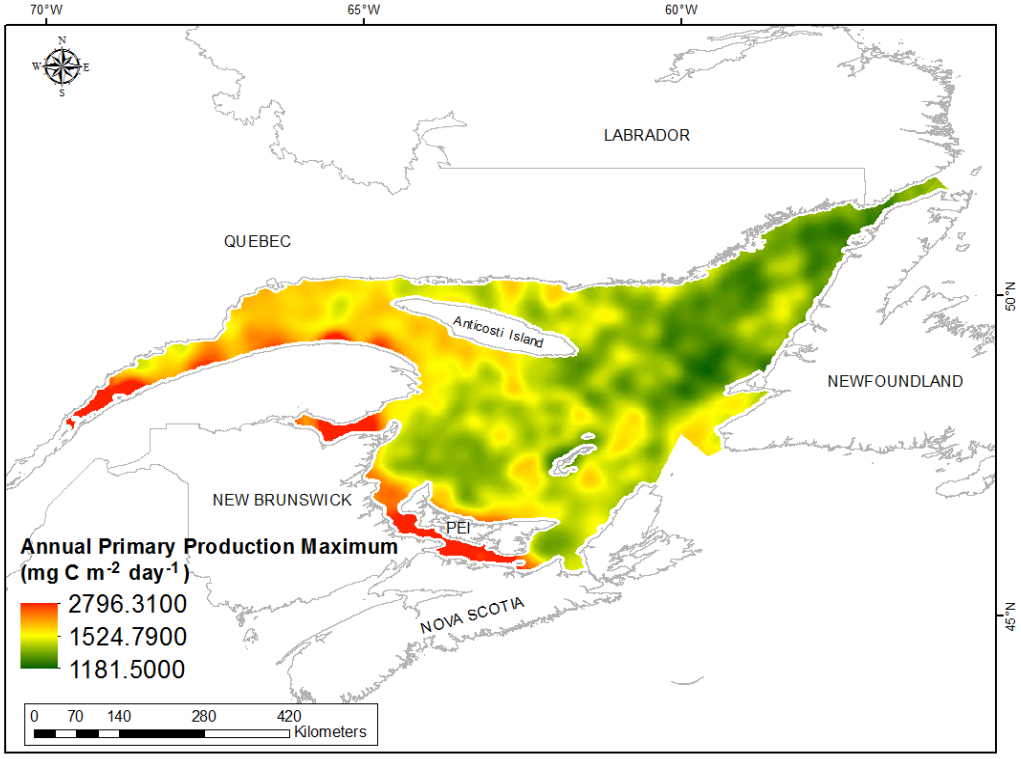

Fig. 535. Interpolated prediction surface of Annual Primary Production Maximum (mg C m^{-2} day^{-1}).

Annual Primary Production Range

This variable displayed a bell-shaped distribution with high kurtosis (Table 215, Fig. 536). The data were higher than predicted by a normal distribution at low and high values, however the mid-values deviated only slightly from the reference line (Fig. 537). The areas of under- and over-prediction showed a spatial pattern over the spatial extent (Fig. 537).

The semivariogram showed moderate autocorrelation present in the data and the model showed a fair to poor fit between measured and predicted values (Fig. 538). Although the RMSPE and ASE were high (Table 216), all other errors showed that the model was good at prediction. The error map showed that error was low across the study extent but was high along the coast (Fig. 539). The kriged surface is presented in Fig. 540.

Table 215. Distributional properties of Annual Primary Production Range (mg C m^{-2} day^{-1}).

Property	Value
Number of Observations	2284
Minimum	107.740
Maximum	2928.600
Mean	1276.6
Median	1253.700
Standard Deviation	218.310
Skewness	1.260
Kurtosis	9.438

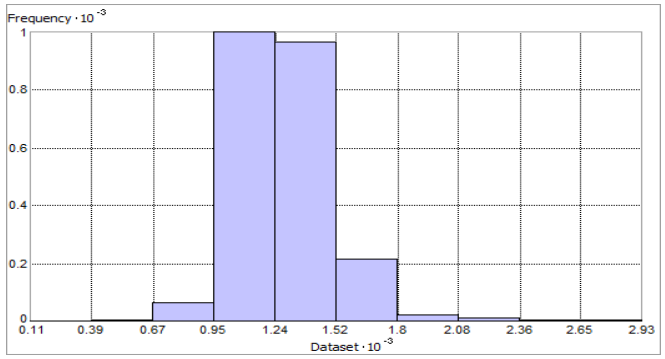

Fig. 536. Distribution of Annual Primary Production Range (mg C m^{-2} day^{-1}). Histogram was illustrated using 10 bins. X and Y axes shown at 10^{-3}.

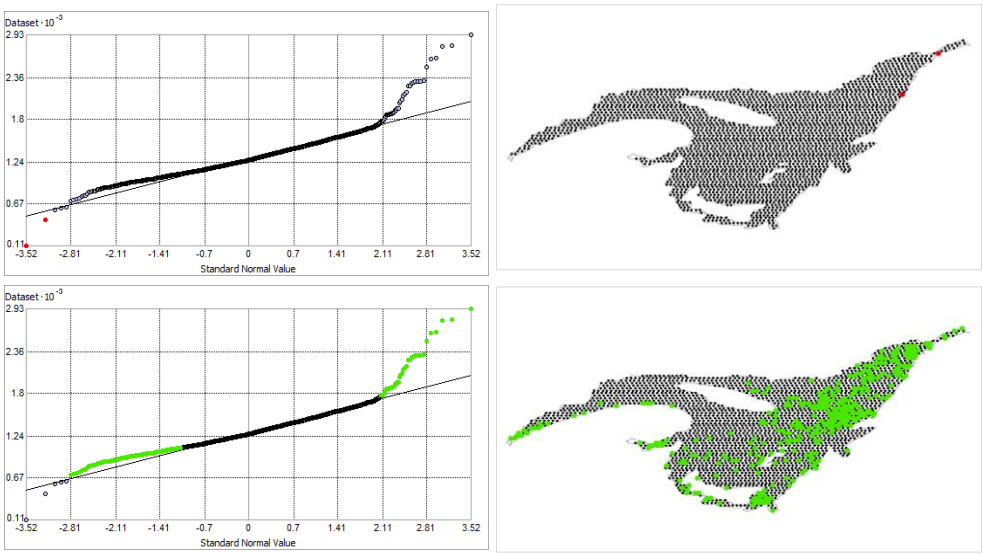

Fig. 537. Normal Q-Q plot for data values of Annual Primary Production Range (mg C m^{-2} day^{-1}). Points falling under (upper panel) and over (bottom panel) the reference line are mapped.

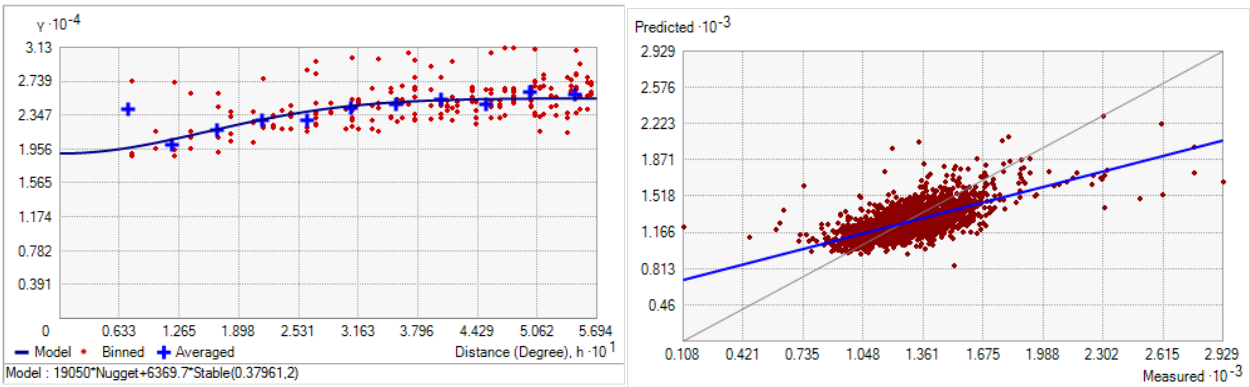

Fig. 538. Semivariogram of Annual Primary Production Range (mg C m^{-2} day^{-1}). Binned values are shown as red dots; average points are shown as blue crosses; the model fit to the averaged values is shown as a blue line. Lag size: 0.047 degrees; number of lags: 12; Parameter: 2; Range: 0.380 degrees; Partial Sill: 6369.708. Right panel: Scatterplot of predicted values versus observed values for the model of Annual Primary Production Range (mg C m^{-2} day^{-1}).

Table 216. Results of cross-validation of the kriged model for the Annual Primary Production Range (mg C m^{-2} day^{-1}).

Prediction error	**Value**
Number of Observations	2284
Overall Mean Error	-0.815
Root Mean Square Prediction Error	159.870
Standardized Mean	-0.005
Standardized Root Mean Square Prediction Error	1.066
Average Standard Error	148.598

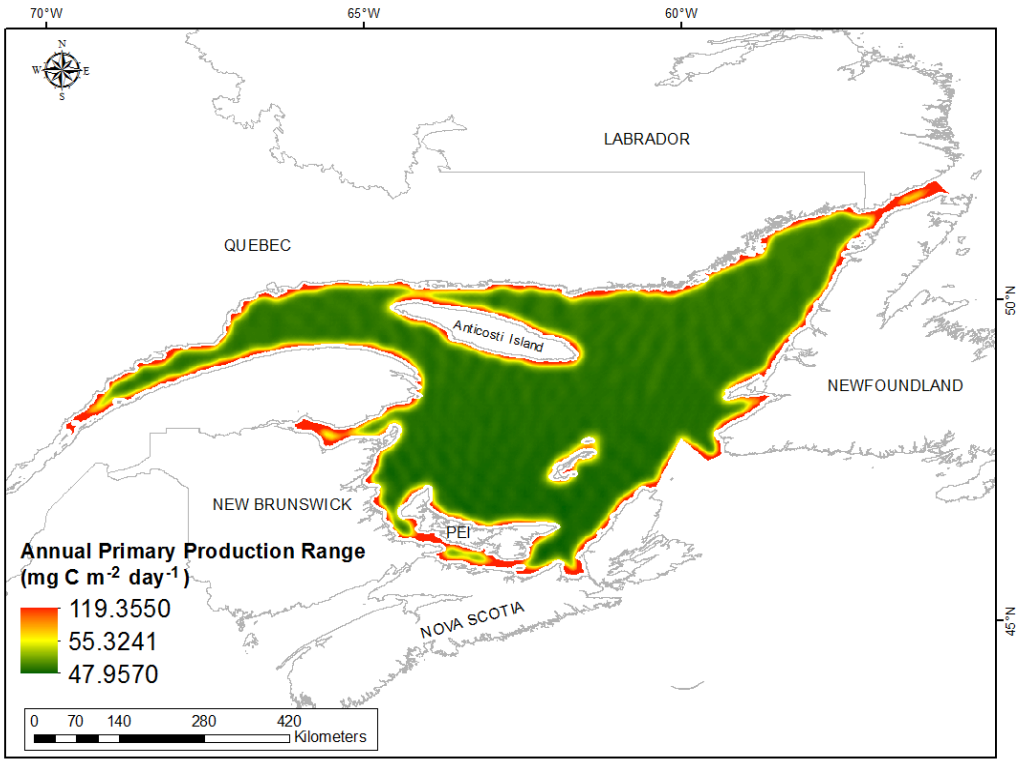

Fig. 539. Prediction standard error surface of Annual Primary Production Range (mg C m^{-2} day^{-1}).

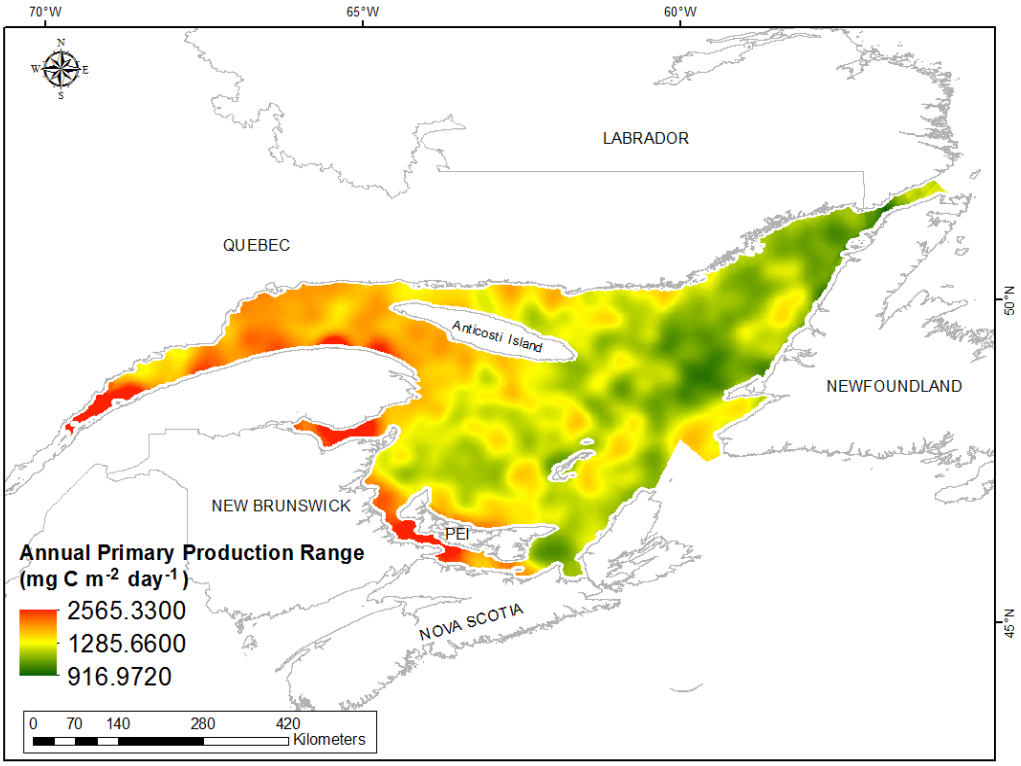

Fig. 540. Interpolated prediction surface of Annual Primary Production Range (mg C m^{-2} day^{-1}).

Annual Primary Production Average Minimum

This variable displayed a highly right-skewness distribution and high kurtosis (Table 217, Fig. 541). The data were higher than predicted by a normal distribution at low and high values, however the mid-values deviated only slightly from the reference line (Fig. 542). The areas of under- and over-prediction showed a spatial pattern over the spatial extent (Fig. 542).

The semivariogram showed moderate autocorrelation present in the data and the model showed a fair to poor fit between measured and predicted values (Fig. 543). Although the RMSPE and ASE were high (Table 218), all other errors showed that the model was good at prediction. The error map showed that error was low across the study extent but was high along the coast (Fig. 544). The kriged surface is presented in Fig. 545.

Table 217. Distributional properties of Annual Primary Production Average Minimum (mg C m^{-2} day^{-1}).

Property	Value
Number of Observations	2284
Minimum	208.040
Maximum	984.020
Mean	386.630
Median	370.900
Standard Deviation	96.100
Skewness	1.567
Kurtosis	7.414

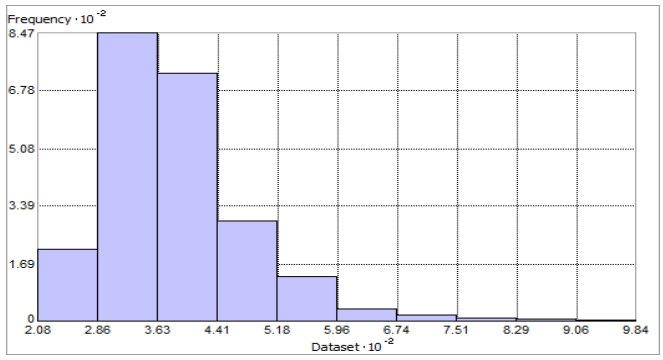

Fig. 541. Distribution of Annual Primary Production Average Minimum (mg C m^{-2} day^{-1}). Histogram was illustrated using 10 bins. X and Y axes shown at 10^{-2}.

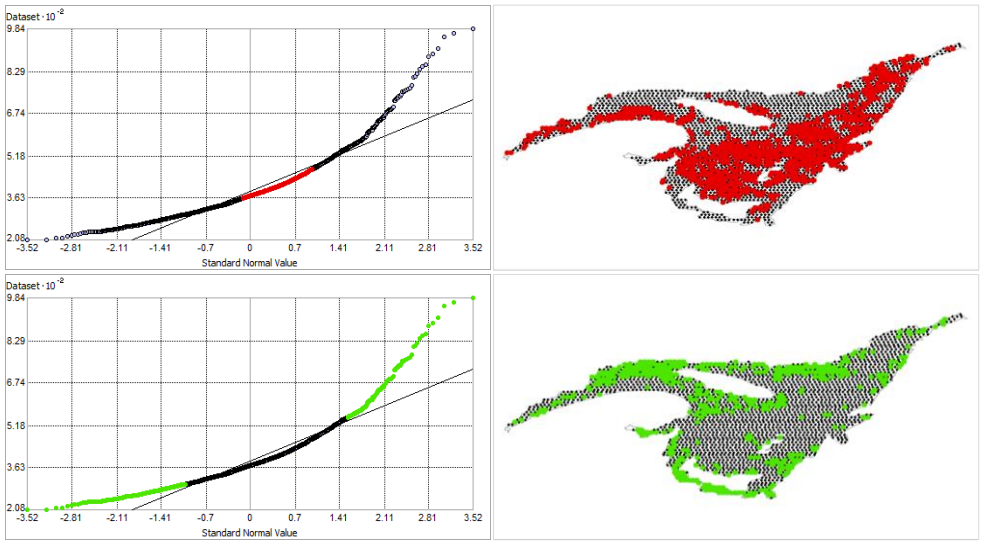

Fig. 542. Normal Q-Q plot for data values of Annual Primary Production Average Minimum (mg C m^{-2} day^{-1}). Points falling under (upper panel) and over (bottom panel) the reference line are mapped.

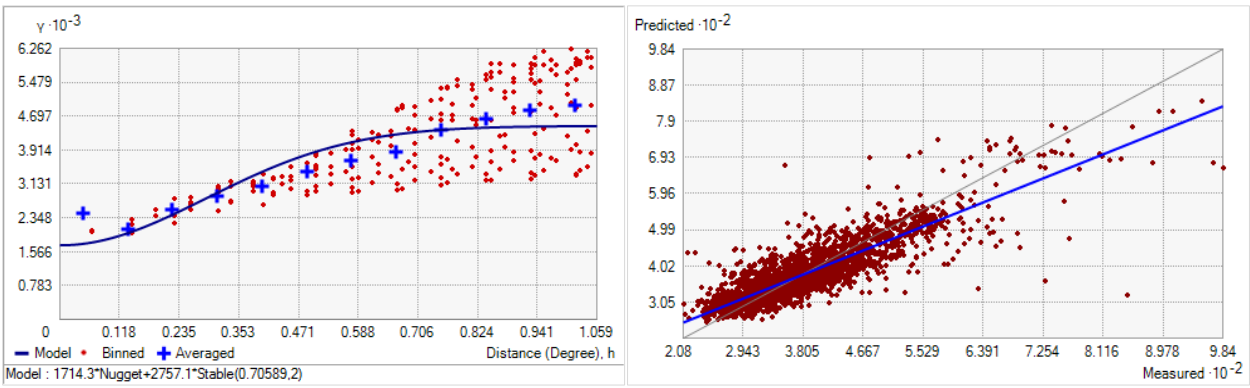

Fig. 543. Semivariogram of Annual Primary Production Average Minimum (mg C m^{-2} day^{-1}). Binned values are shown as red dots; average points are shown as blue crosses; the model fit to the averaged values is shown as a blue line. Lag size: 0.088 degrees; number of lags: 12; Parameter: 2; Range: 0.706 degrees; Partial Sill: 2757.125. Right panel: Scatterplot of predicted values versus observed values for the model of Annual Primary Production Average Minimum (mg C m^{-2} day^{-1}).

Table 218. Results of cross-validation of the kriged model for the Annual Primary Production Average Minimum (mg C m^{-2} day^{-1}).

Prediction error	**Value**
Number of Observations	2284
Overall Mean Error	0.073
Root Mean Square Prediction Error	49.965
Standardized Mean	0.003
Standardized Root Mean Square Prediction Error	1.106
Average Standard Error	44.333

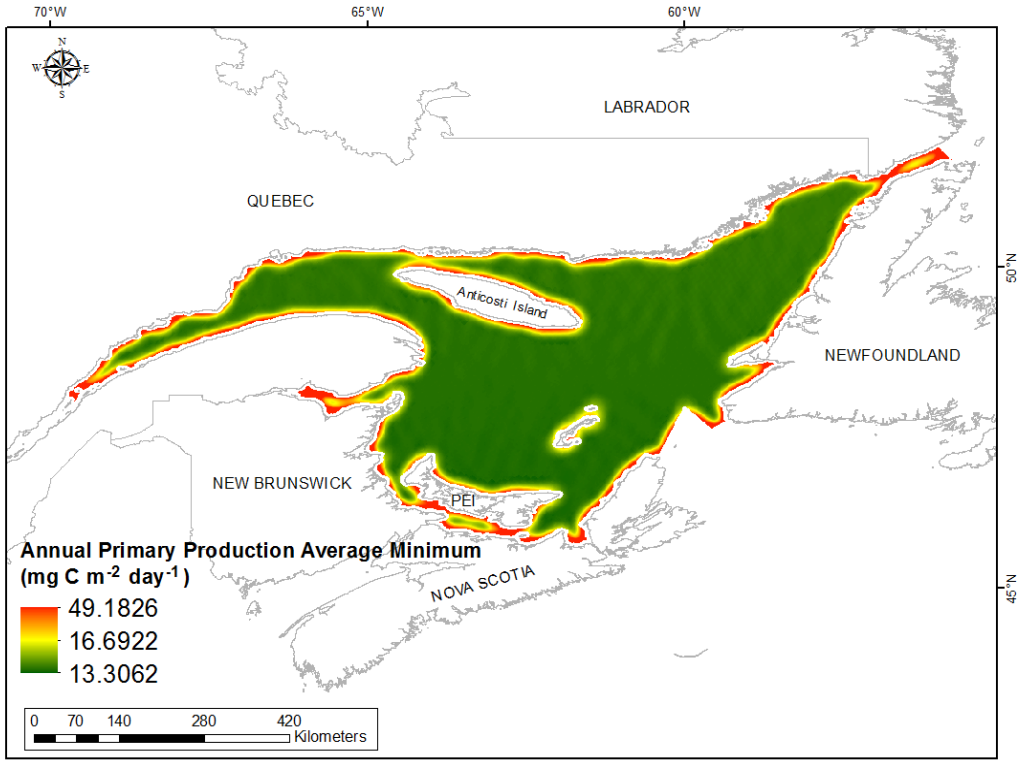

Fig. 544. Prediction standard error surface of Annual Primary Production Average Minimum (mg C m^{-2} day^{-1}).

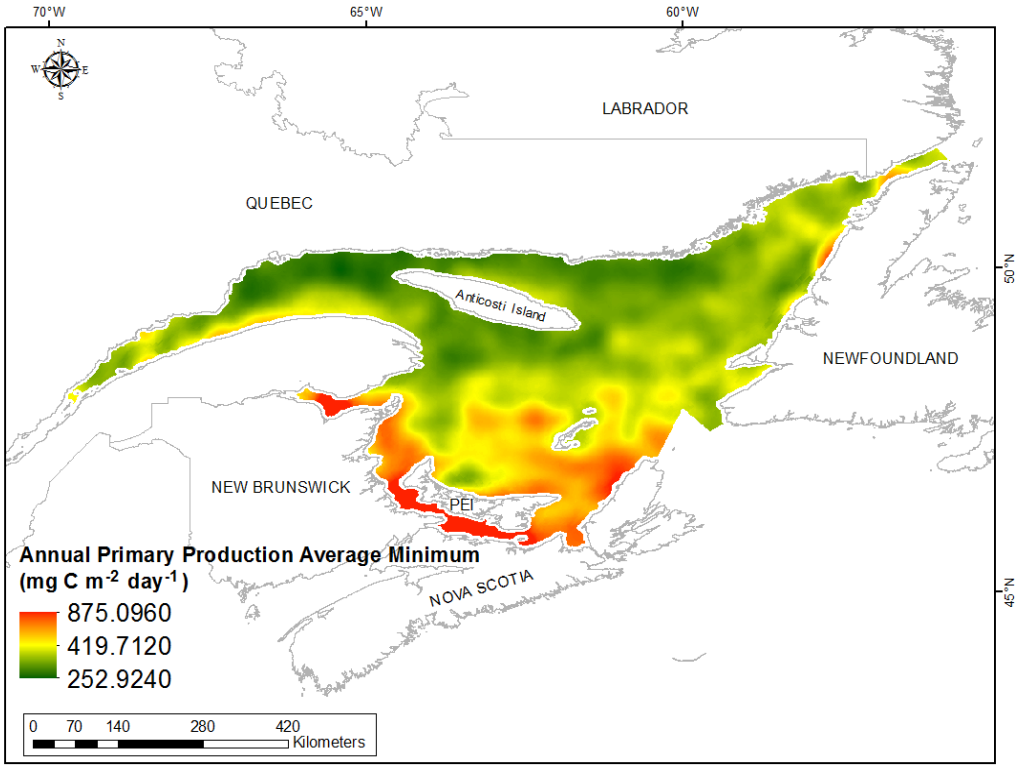

Fig. 545. Interpolated prediction surface of Annual Primary Production Average Minimum (mg C m^{-2} day^{-1}).

Annual Primary Production Average Maximum

This variable displayed a bell-shaped distribution with kurtosis prior to modeling (Table 219, Fig. 546). The data were higher than predicted by a normal distribution at low and high values, however the mid-values deviated only slightly from the reference line (Fig. 547). The lowest values fell under the reference line. The areas of under- and over-prediction showed a spatial pattern over the spatial extent (Fig. 547).

The semivariogram showed weak autocorrelation present in the data and the model showed a fair fit between measured and predicted values (Fig. 548). Although the RMSPE and ASE were high (Table 220), all other errors showed that the model was good at prediction. The error map showed that error was low across the study extent but was high along the coast (Fig. 549). The kriged surface is presented in Fig. 550.

Table 219. Distributional properties of Annual Primary Production Average Maximum (mg C m^{-2} day^{-1}).

Property	Value
Number of Observations	2284
Minimum	670.510
Maximum	2123.700
Mean	1231.400
Median	1215.400
Standard Deviation	154.410
Skewness	1.174
Kurtosis	6.584

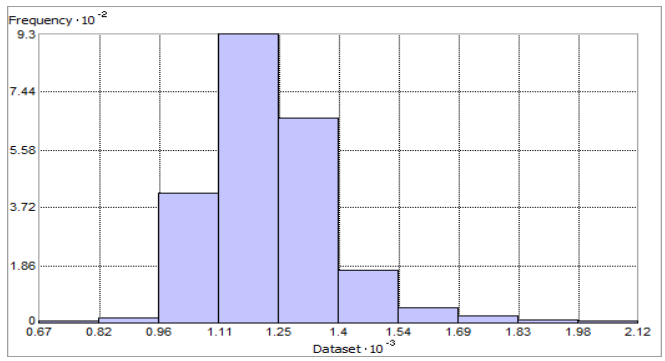

Fig. 546. Distribution of Annual Primary Production Average Maximum (mg C m^{-2} day^{-1}). Histogram was illustrated using 10 bins. X axis shown at 10^{-3}; Y axis at 10^{-2}.

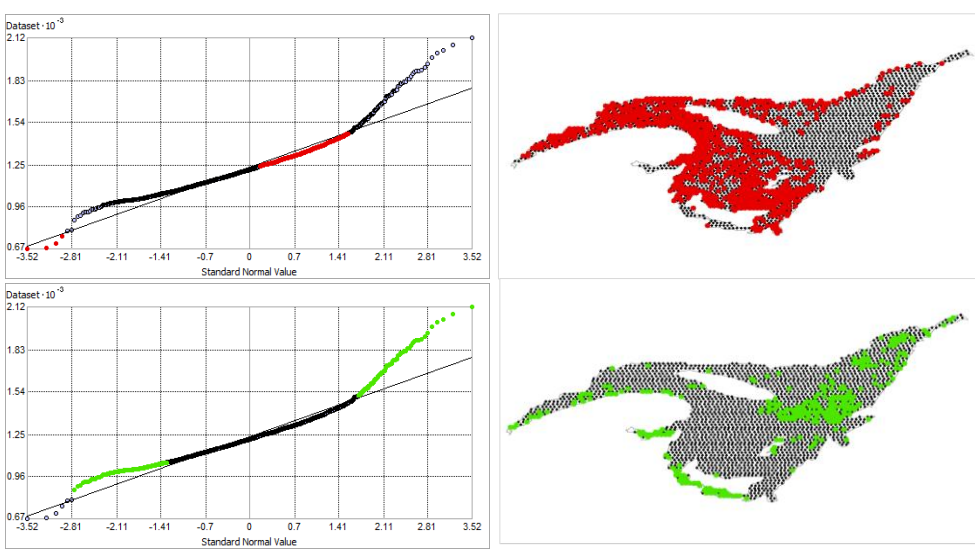

Fig. 547. Normal Q-Q plot for data values of Annual Primary Production Average Maximum (mg C m^{-2} day^{-1}). Points falling under (upper panel) and over (bottom panel) the reference line are mapped.

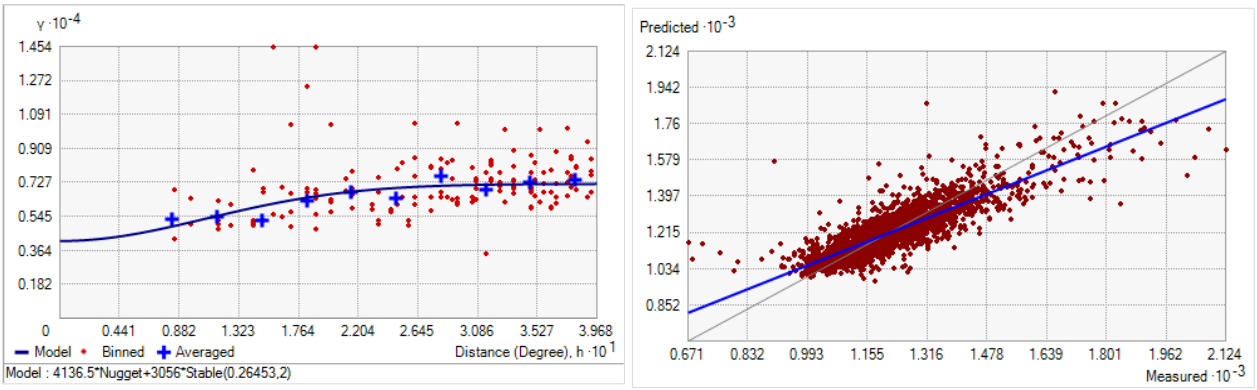

Fig. 548. Semivariogram of Annual Primary Production Average Maximum (mg C m^{-2} day^{-1}). Binned values are shown as red dots; average points are shown as blue crosses; the model fit to the averaged values is shown as a blue line. Lag size: 0.033 degrees; number of lags: 12; Parameter: 2; Range: 0.265 degrees; Partial Sill: 3056.025. Right panel: Scatterplot of predicted values versus observed values for the model of Annual Primary Production Average Maximum (mg C m^{-2} day^{-1}).

Table 220. Results of cross-validation of the kriged model for the Annual Primary Production Average Maximum (mg C m^{-2} day^{-1}).

Prediction error	**Value**
Number of Observations	2284
Overall Mean Error	-0.528
Root Mean Square Prediction Error	82.775
Standardized Mean	-0.006
Standardized Root Mean Square Prediction Error	1.072
Average Standard Error	75.837

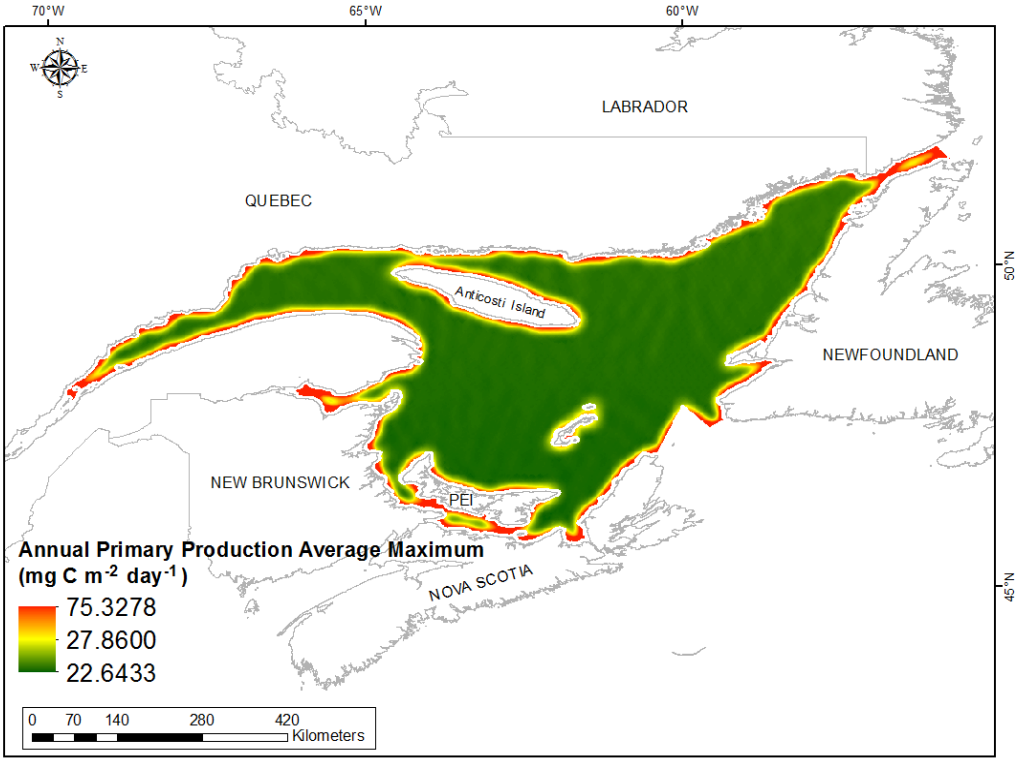

Fig. 549. Prediction standard error surface of Annual Primary Production Average Maximum (mg C m^{-2} day^{-1}).

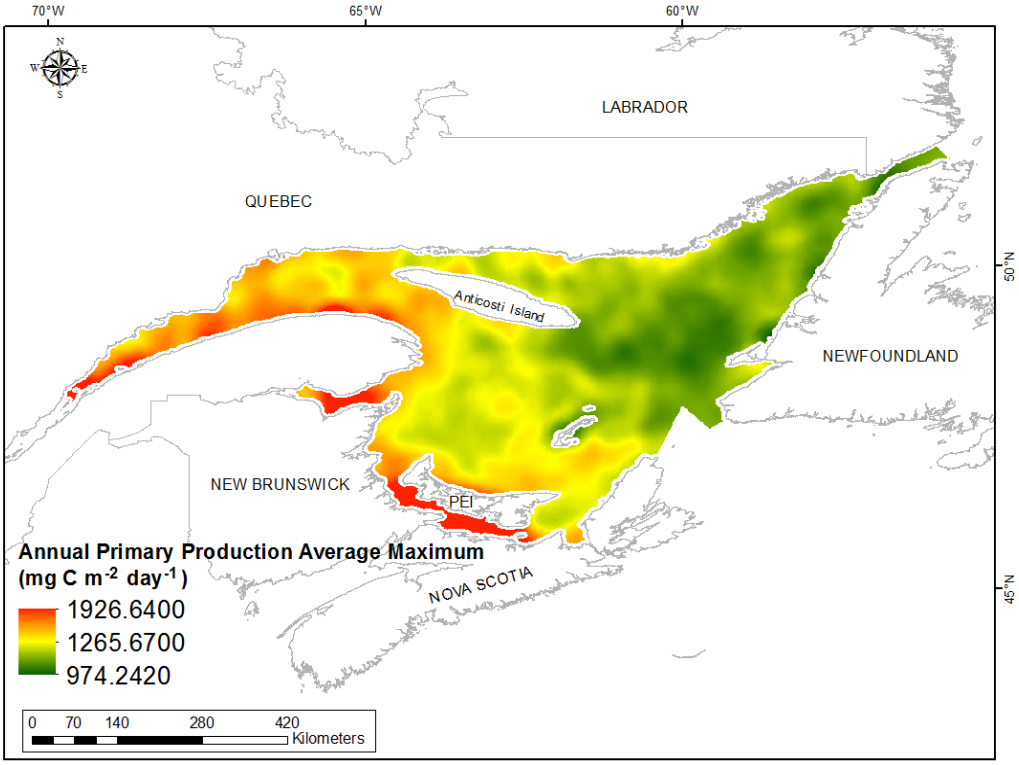

Fig. 550. Interpolated prediction surface of Annual Primary Production Average Maximum (mg C m^{-2} day^{-1}).

Annual Primary Production Average Range

This variable displayed a bell-shaped distribution with kurtosis prior to modeling (Table 221, Fig. 551). The data were higher than predicted by a normal distribution at low and high values, however the mid-values were well predicted (Fig. 552). The lowest values fell under the reference line. The areas of under- and over-prediction showed a spatial pattern over the spatial extent (Fig. 552).

The semivariogram showed moderate autocorrelation present in the data and the model showed a fair fit between measured and predicted values (Fig. 553). Although the RMSPE and ASE were high (Table 222), all other errors showed that the model was good at prediction. The error map showed moderate error across the study extent except at the exact location of data points where it was low (Fig. 554). The kriged surface is presented in Fig. 555.

Table 221. Distributional properties of Annual Primary Production Average Range (mg C m^{-2} day^{-1}).

Property	Value
Number of Observations	2284
Minimum	96.600
Maximum	1632.700
Mean	844.800
Median	827.610
Standard Deviation	153.100
Skewness	0.583
Kurtosis	4.670

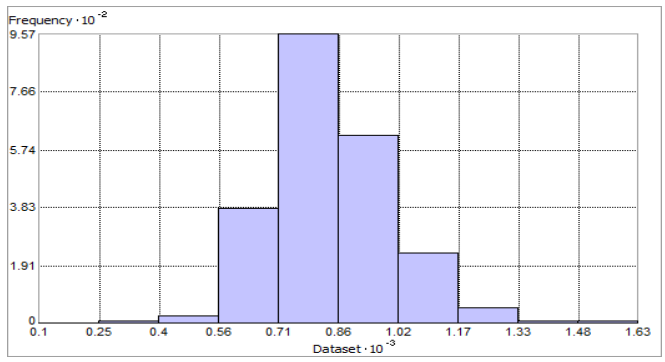

Fig. 551. Distribution of Annual Primary Production Average Range (mg C m^{-2} day^{-1}). Histogram was illustrated using 10 bins. X axis shown at 10^{-3}; Y axis at 10^{-2}.

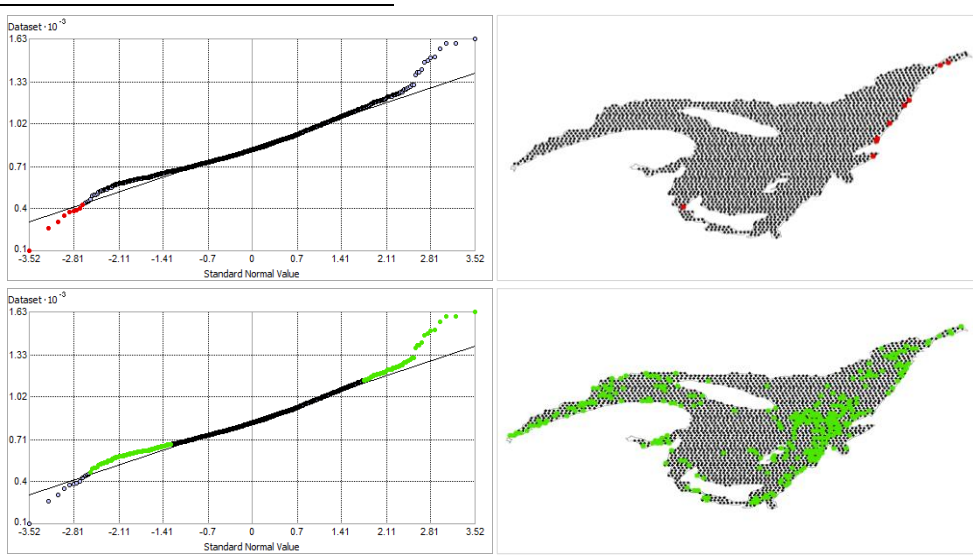

Fig. 552. Normal Q-Q plot for data values of Annual Primary Production Average Range (mg C m^{-2} day^{-1}). Points falling under (upper panel) and over (bottom panel) the reference line are mapped.

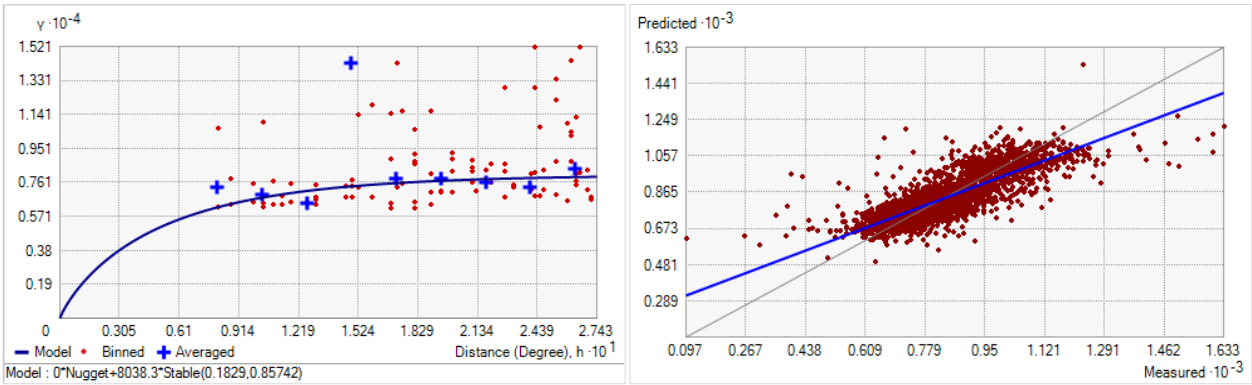

Fig. 553. Semivariogram of Annual Primary Production Average Range (mg C m^{-2} day^{-1}). Binned values are shown as red dots; average points are shown as blue crosses; the model fit to the averaged values is shown as a blue line. Lag size: 0.023 degrees; number of lags: 12; Parameter: 0.857; Range: 0.183 degrees; Partial Sill: 8038.335. Right panel: Scatterplot of predicted values versus observed values for the model of Annual Primary Production Average Range (mg C m^{-2} day^{-1}).

Table 222. Results of cross-validation of the kriged model for the Annual Primary Production Average Range (mg C m^{-2} day^{-1}).

Prediction error	**Value**
Number of Observations	2284
Overall Mean Error	-0.127
Root Mean Square Prediction Error	92.577
Standardized Mean	-0.002
Standardized Root Mean Square Prediction Error	1.051
Average Standard Error	87.021

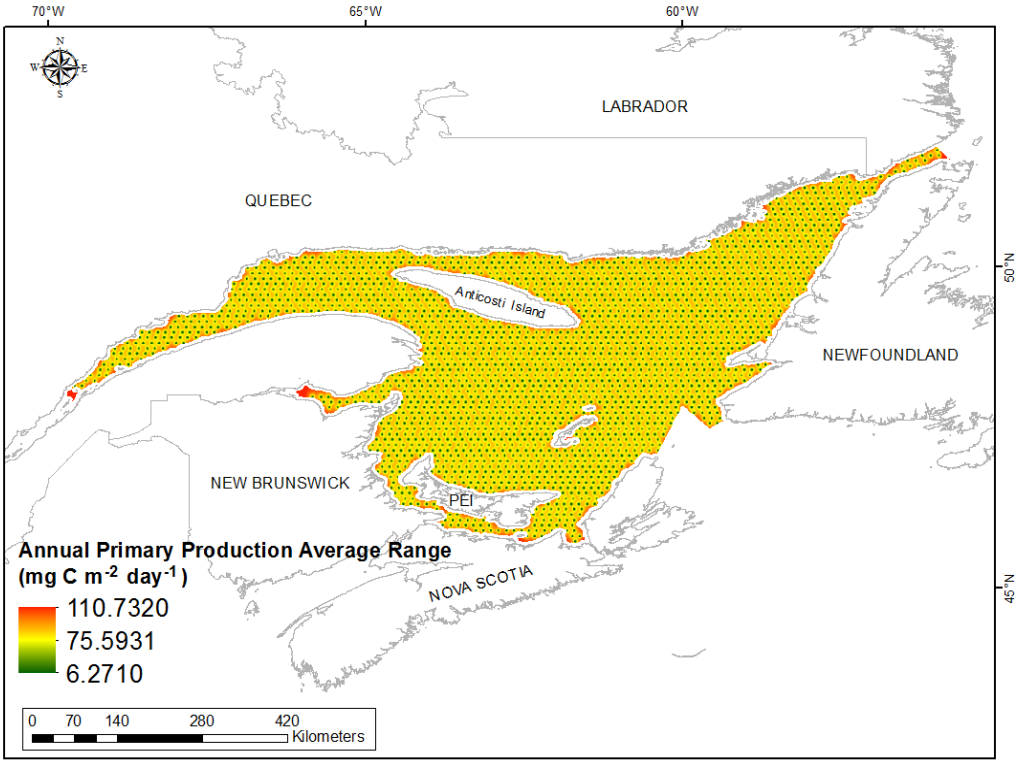

Fig. 554. Prediction standard error surface of Annual Primary Production Average Range (mg C m^{-2} day^{-1}).

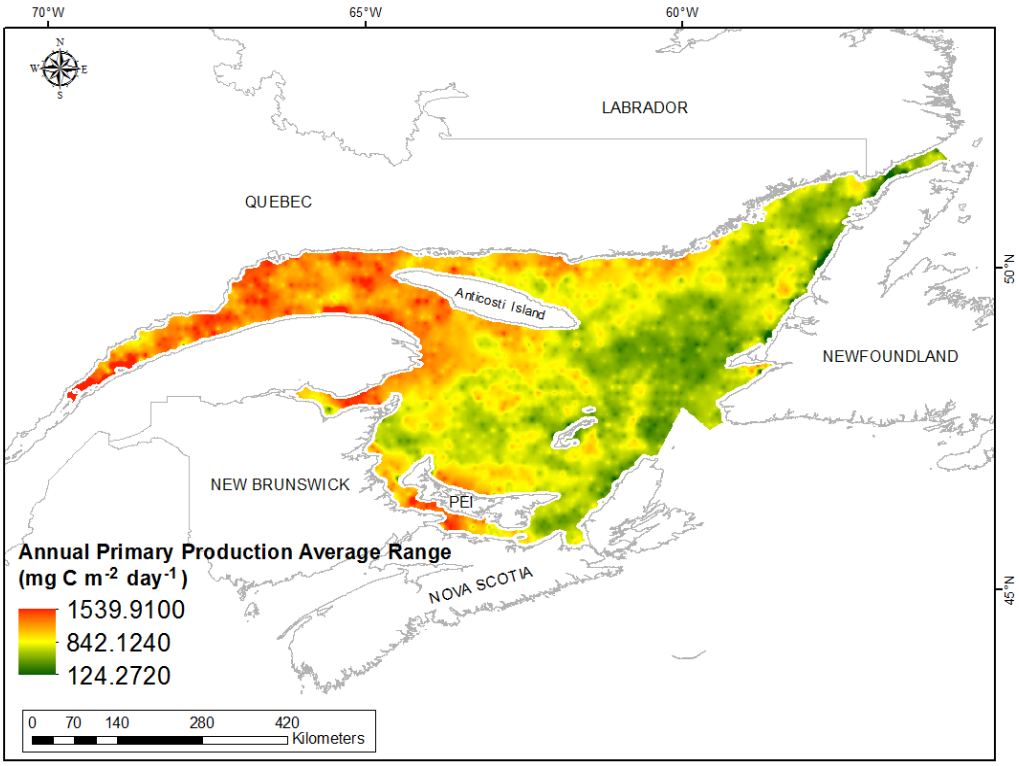

Fig. 555. Interpolated prediction surface of Annual Primary Production Average Range (mg C m^{-2} day^{-1}).

Dissolved Oxygen and Nutrients

Nutrients (e.g. nitrate, phosphate, silicate) are required for the growth of phytoplankton, and therefore directly influence chlorophyll *a* concentration and primary production in surface waters. Generally, as water stratification develops in the spring, nutrients are consumed and drawn down to deeper water by phytoplankton and remain low throughout the rest of the year, while dissolved oxygen decreases (Manasrah et al., 2006).

Dissolved Oxygen

This variable displayed a bimodal distribution (Table 223, Fig. 556). The data were higher than predicted by a normal distribution at low values, and oscillated about the reference line near mid values (Fig. 557). The areas of under- and over-prediction showed no spatial pattern over the spatial extent (Fig. 557).

The semivariogram showed weak autocorrelation present in the data and the model showed fair fit between measured and predicted values (Fig. 558). The model showed good cross-validation statistics (Table 224) indicating that the model was good at prediction. The error map showed a highly discontinuous and patchy pattern over the study extent with higher error along the coast (Fig. 559). Error was lower at the location of data points. The kriged surface is presented in Fig. 560.

Table 223. Distributional properties of Dissolved Oxygen (ml l^{-1}).

Property	Value
Number of Observations	1073
Minimum	4.211
Maximum	9.920
Mean	6.874
Median	6.949
Standard Deviation	0.845
Skewness	0.090
Kurtosis	2.150

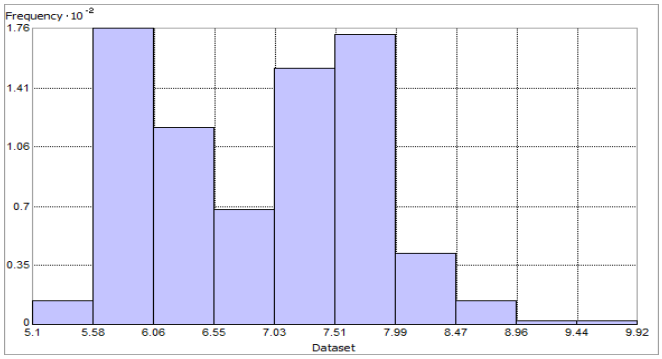

Fig. 556. Distribution of Dissolved Oxygen (ml l^{-1}). Histogram was illustrated using 10 bins. Y axis is shown at 10^{-4}.

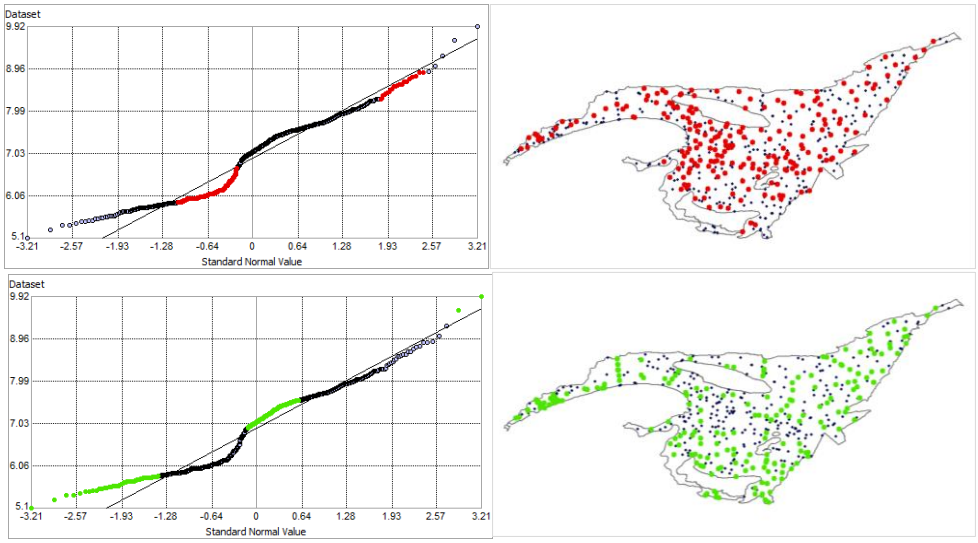

Fig. 557. Normal Q-Q plot for data values of Dissolved Oxygen (ml l^{-1}). Points falling under (upper panel) and over (bottom panel) the reference line are mapped.

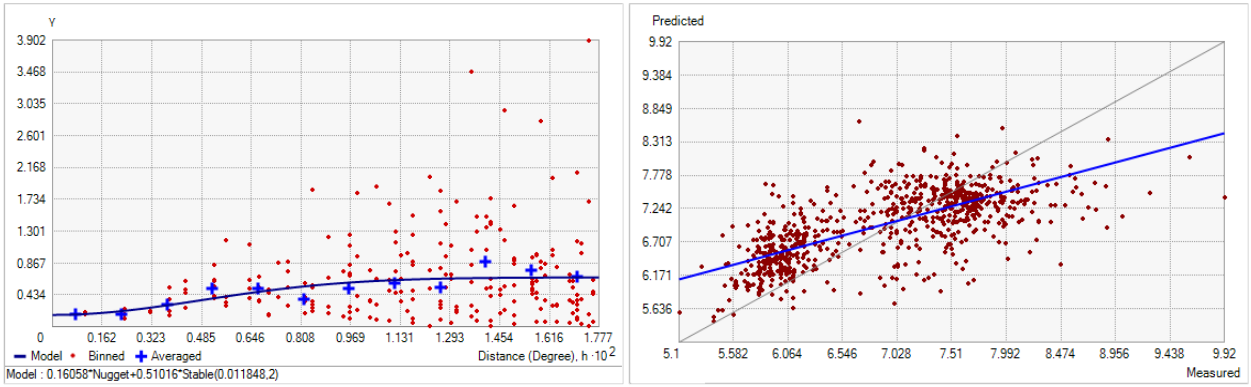

Fig. 558. Left panel: Semivariogram of Dissolved Oxygen (ml l^{-1}). Binned values are shown as red dots; average points are shown as blue crosses; the model fit to the averaged values is shown as a blue line. Lag size: 0.003 degrees; number of lags: 12; Parameter: 1.460; Range: 0.020 degrees; Partial Sill: 0.322. Right panel: Scatterplot of predicted values versus observed values for the variable Dissolved Oxygen (ml l^{-1}).

Table 224. Results of cross-validation of the kriged model for the Dissolved Oxygen (ml l^{-1}).

Prediction error	**Value**
Number of Observations	1073
Overall Mean Error	0.029
Root Mean Square Prediction Error	0.663
Standardized Mean	0.010
Standardized Root Mean Square Prediction Error	0.940
Average Standard Error	0.724

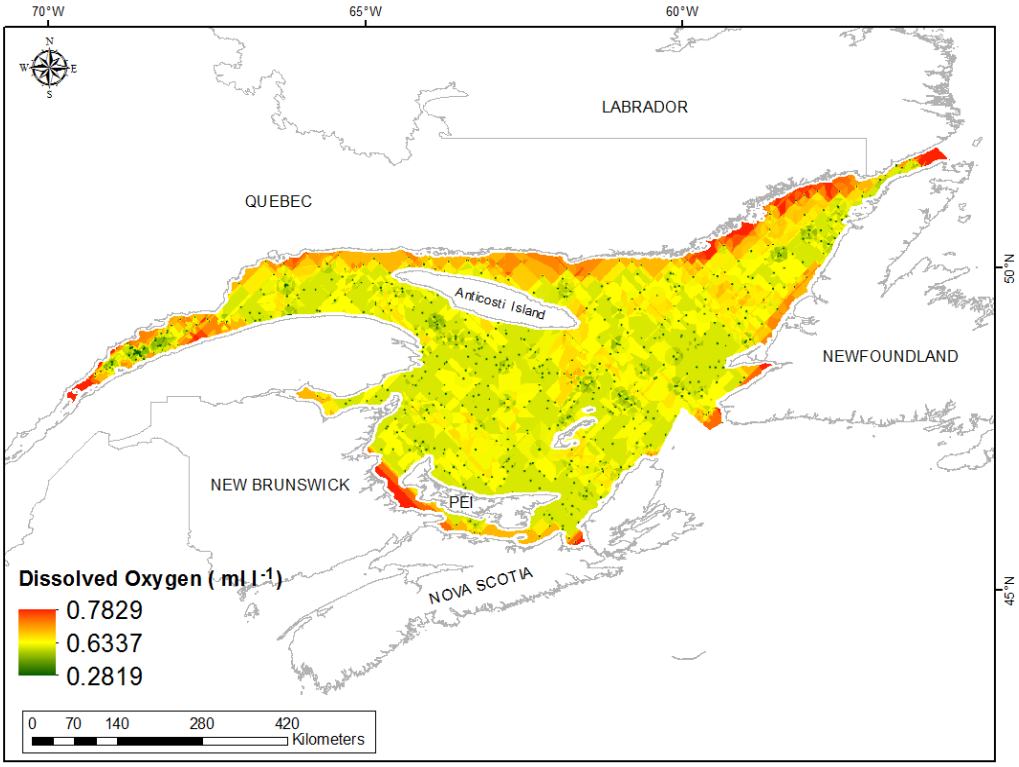

Fig. 559. Prediction standard error surface of Dissolved Oxygen (ml l^{-1}).

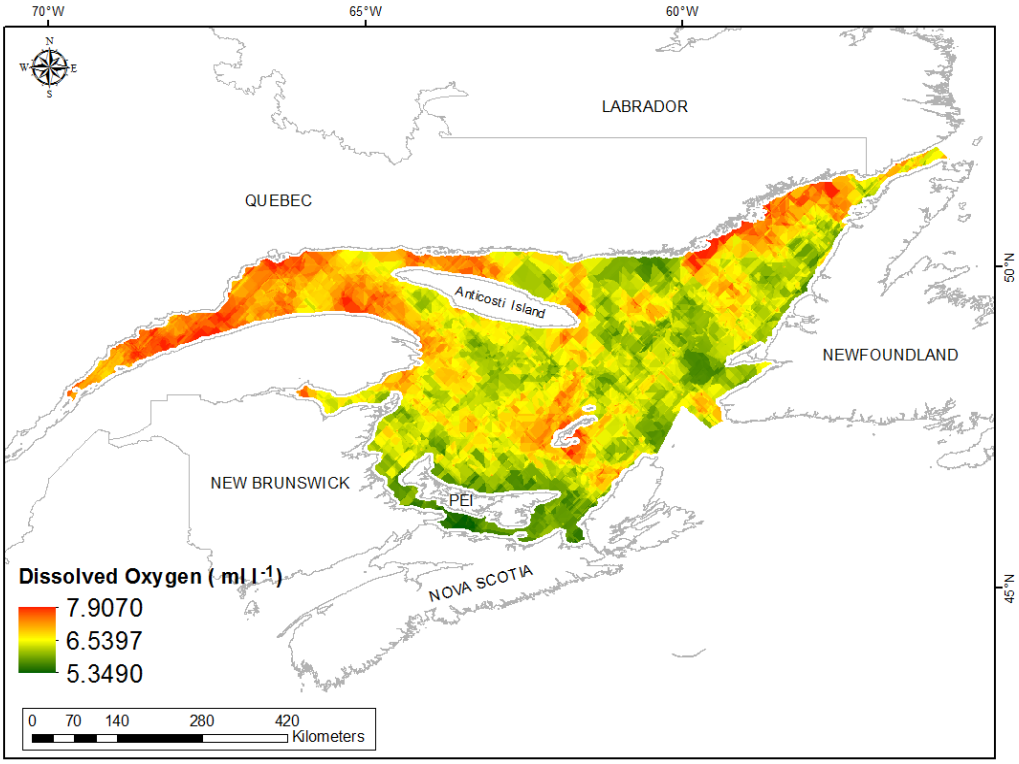

Fig. 560. Interpolated prediction surface of Dissolved Oxygen (ml l^{-1}).

Phosphate

This variable displayed a bimodal distribution (Table 228, Fig. 561). The data fit a normal distribution with deviation mainly in mid-range values (Fig. 562). The areas of under- and over-prediction showed no spatial pattern over the spatial extent (Fig. 562).

The semivariogram showed little autocorrelation present in the data and the model showed poor fit between measured and predicted values (Fig. 563). The model showed good cross-validation statistics (Table 226) indicating that the model was good at prediction. The error map showed a highly discontinuous and patchy pattern over the study extent with higher error along the coast (Fig. 564). Error was lower at the location of data points. The kriged surface is presented in Fig. 565.

Table 225. Distributional properties of Phosphate (µmol l^{-1}).

Property	Value
Number of Observations	982
Minimum	0.005
Maximum	1.295
Mean	0.431
Median	0.338
Standard Deviation	0.298
Skewness	0.622
Kurtosis	2.290

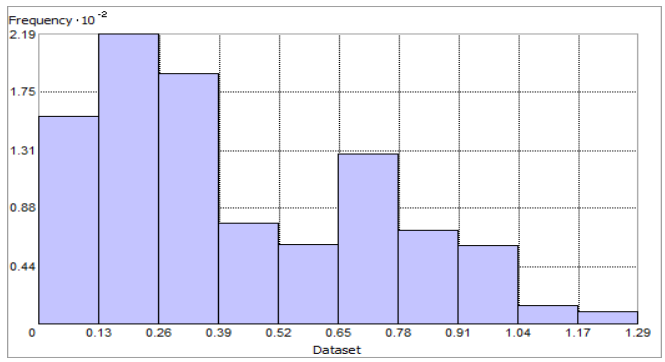

Fig. 561. Distribution of Phosphate (µmol l^{-1}). Histogram was illustrated using 10 bins. Y axis is shown at 10^{-4}.

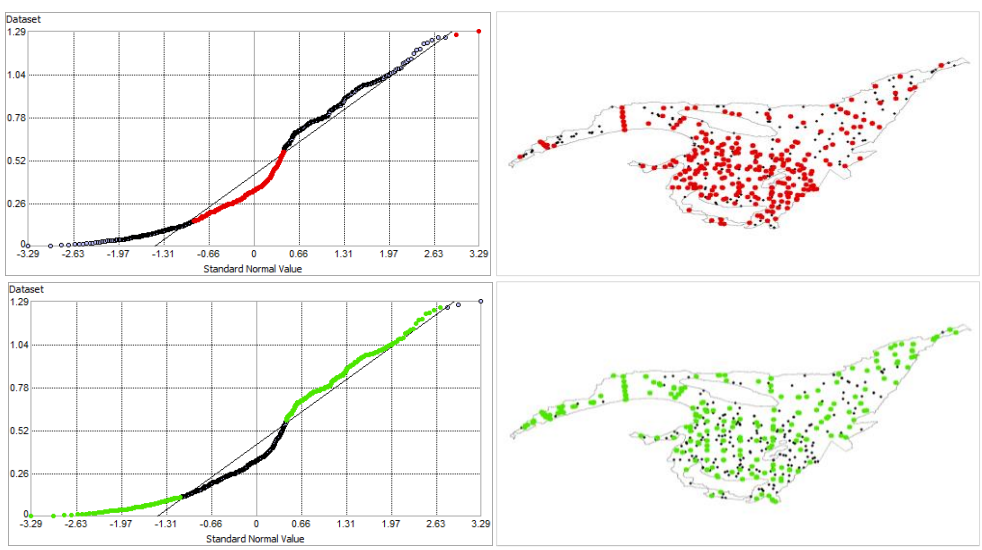

Fig. 562. Normal Q-Q plot for data values of Phosphate (µmol l^{-1}). Points falling under (upper panel) and over (bottom panel) the reference line are mapped.

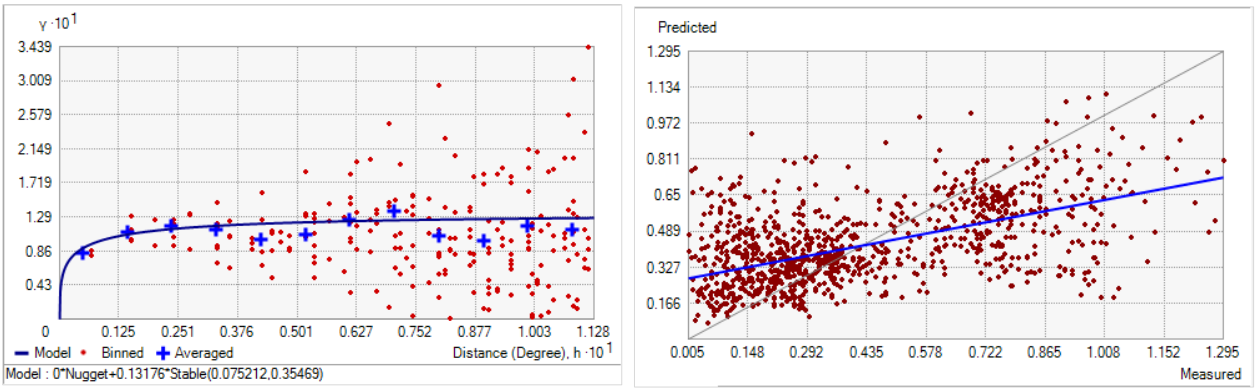

Fig. 563. Left panel: Semivariogram of Phosphate (µmol l^{-1}). Binned values are shown as red dots; average points are shown as blue crosses; the model fit to the averaged values is shown as a blue line. Lag size: 0.003 degrees; number of lags: 12; Parameter: 1.460; Range: 0.020 degrees; Partial Sill: 0.322. Right panel: Scatterplot of predicted values versus observed values for the variable Phosphate (µmol l^{-1}).

Table 226. Results of cross-validation of the kriged model for the Phosphate (µmol l^{-1}).

Prediction error	**Value**
Number of Observations	982
Overall Mean Error	0.007
Root Mean Square Prediction Error	0.254
Standardized Mean	0.011
Standardized Root Mean Square Prediction Error	0.807
Average Standard Error	0.329

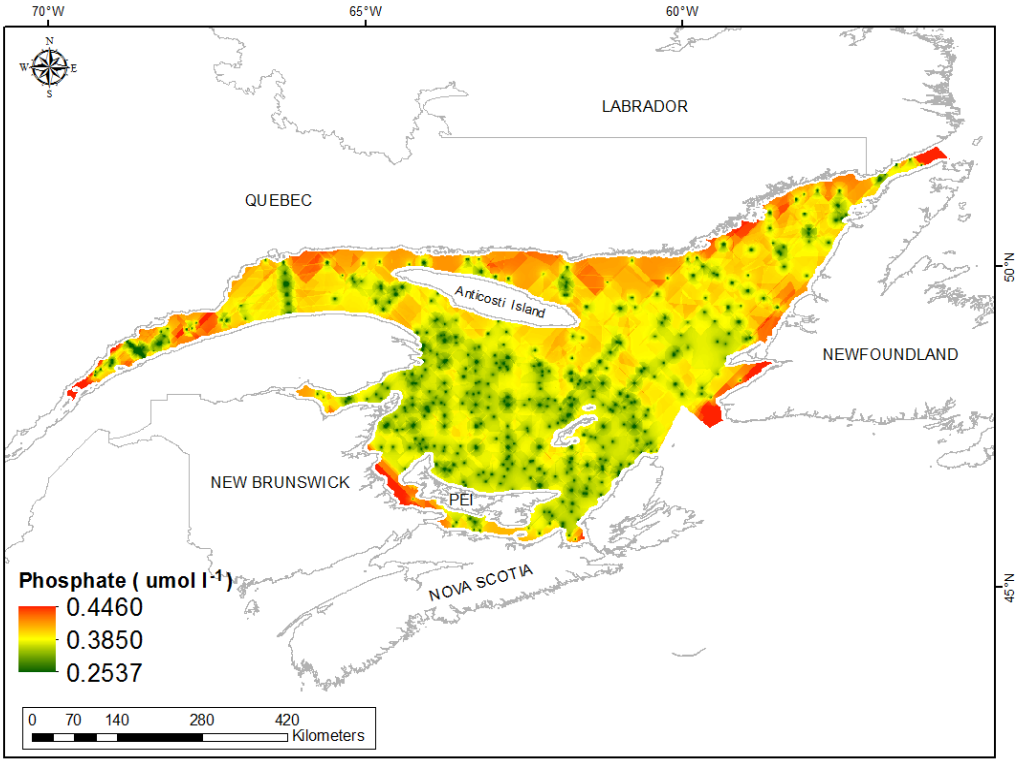

Fig. 564. Prediction standard error surface of Phosphate (µmol l^{-1}).

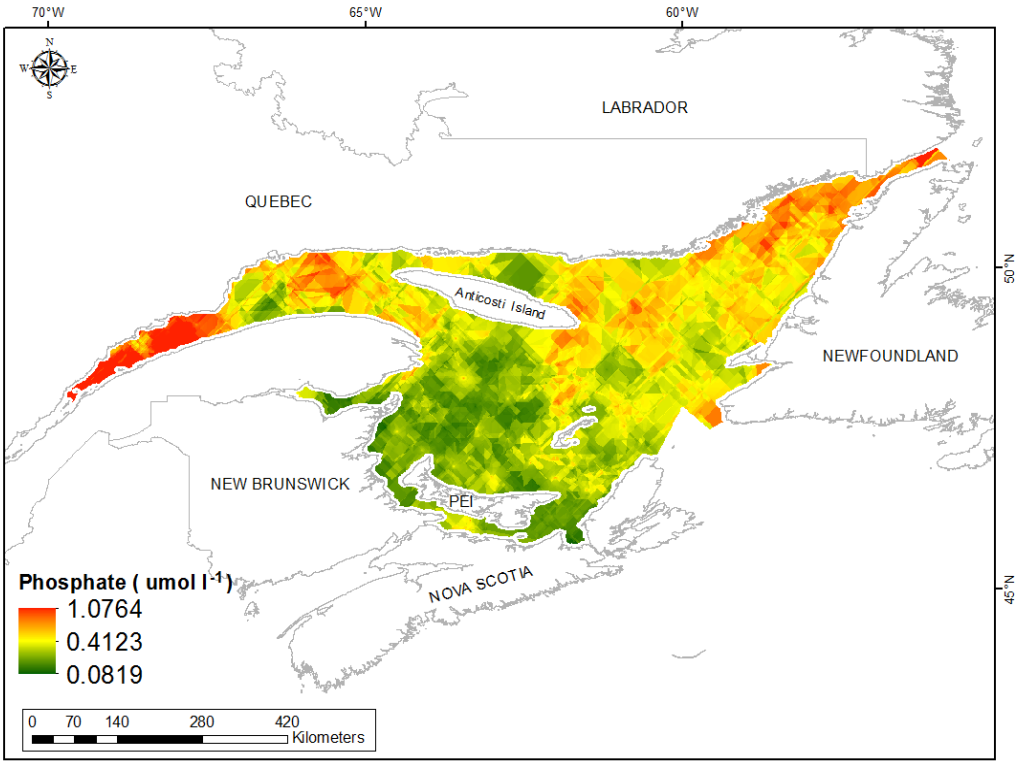

Fig. 565. Interpolated prediction surface of Phosphate (µmol l^{-1}).

Silicate

This variable displayed a right-skewed distribution with kurtosis prior to modeling (Table 227, Fig. 566). The data were higher than predicted by a normal distribution at upper values (Fig. 567). Mid-range values were slightly lower than the reference line. The areas of under- and over-prediction showed no spatial pattern over the spatial extent (Fig. 567).

The semivariogram showed little autocorrelation present in the data and the model showed poor fit between measured and predicted values (Fig. 568). The model showed poor cross-validation statistics (Table 228) with a standardized root mean square error less than 1, indicating that variability in the predictions has been overestimated. The error map showed a highly discontinuous and patchy pattern over the study extent with higher error along the coast (Fig. 569). Error was low at the location of data points. The kriged surface is presented in Fig. 570.

Table 227. Distributional properties of Silicate (µmol l^{-1}).

Property	Value
Number of Observations	985
Minimum	0.040
Maximum	30.185
Mean	4.995
Median	2.390
Standard Deviation	5.803
Skewness	1.759
Kurtosis	5.754

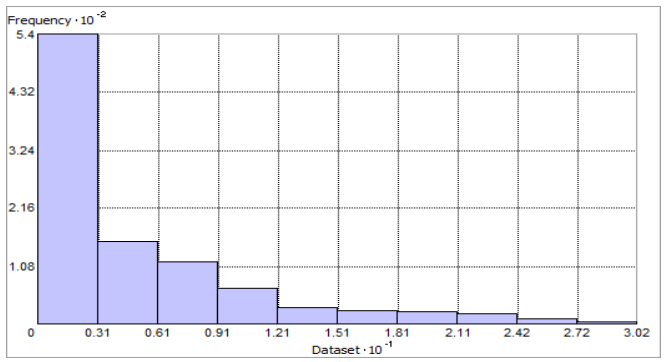

Fig. 566. Distribution of Silicate (µmol l^{-1}). Histogram was illustrated using 10 bins. Y axis is shown at 10^{-4}.

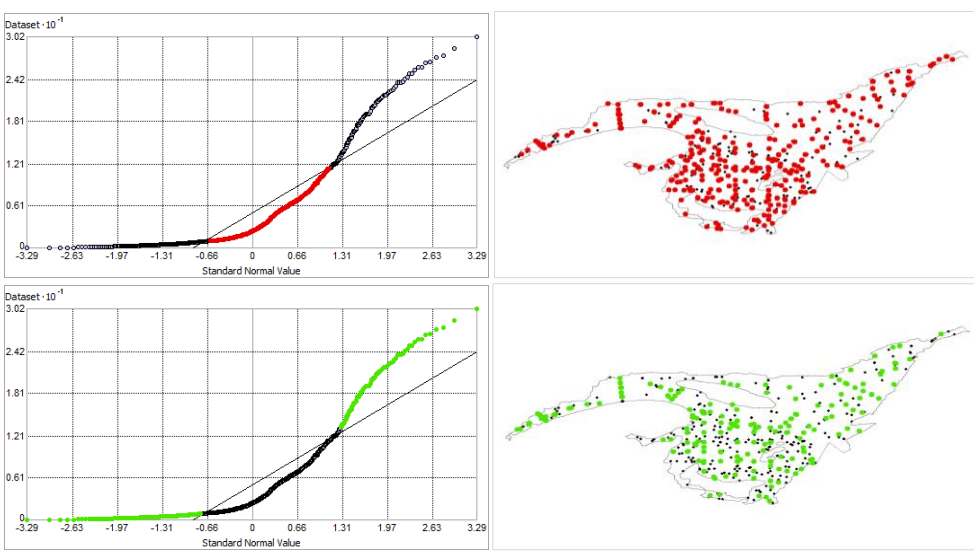

Fig. 567. Normal Q-Q plot for data values of Silicate (µmol l^{-1}). Points falling under (upper panel) and over (bottom panel) the reference line are mapped.

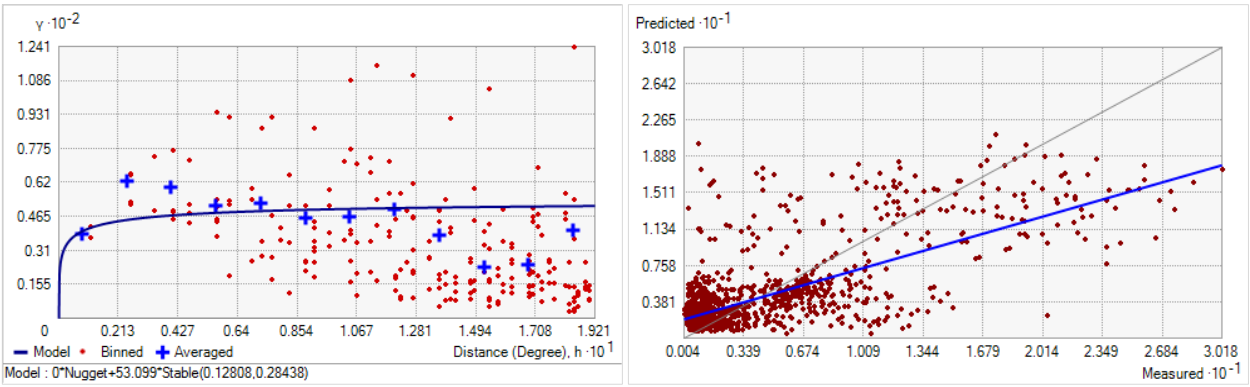

Fig. 568. Left panel: Semivariogram of Silicate (µmol l^{-1}). Binned values are shown as red dots; average points are shown as blue crosses; the model fit to the averaged values is shown as a blue line. Lag size: 0.003 degrees; number of lags: 12; Parameter: 1.460; Range: 0.020 degrees; Partial Sill: 0.322. Right panel: Scatterplot of predicted values versus observed values for the variable Silicate (µmol l^{-1}).

Table 228. Results of cross-validation of the kriged model for the Silicate (µmol l^{-1}).

Prediction error	**Value**
Number of Observations	985
Overall Mean Error	0.037
Root Mean Square Prediction Error	4.126
Standardized Mean	9.58×10^{-4}
Standardized Root Mean Square Prediction Error	0.648
Average Standard Error	6.682

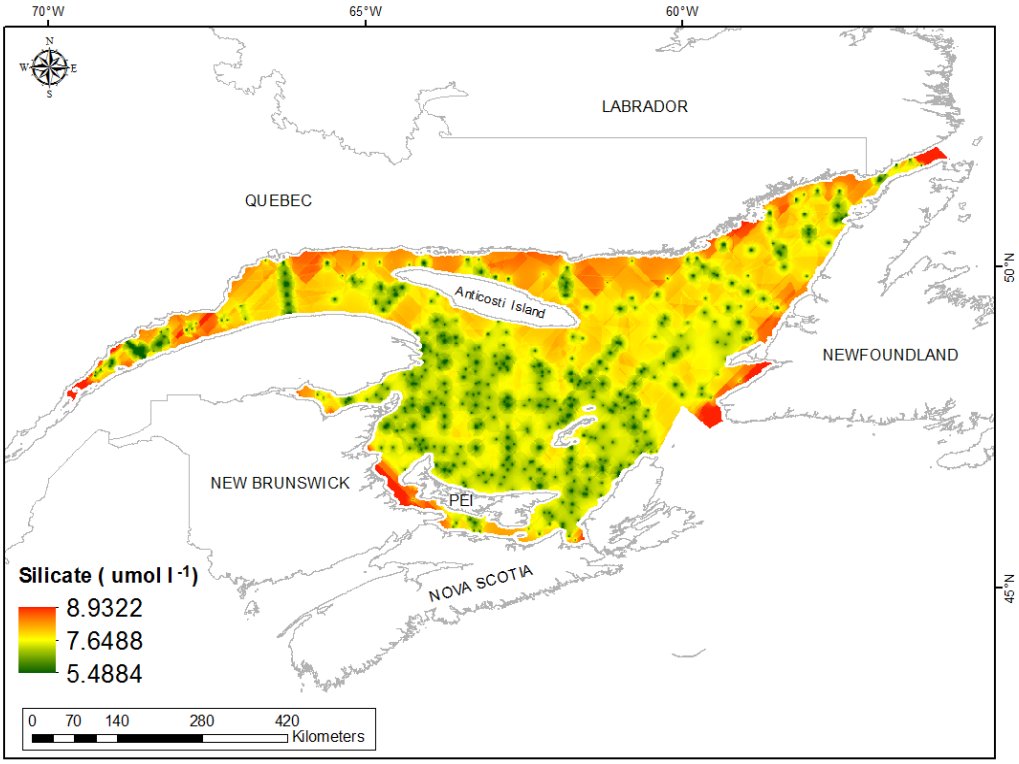

Fig. 569. Prediction standard error surface of Silicate (µmol l^{-1}).

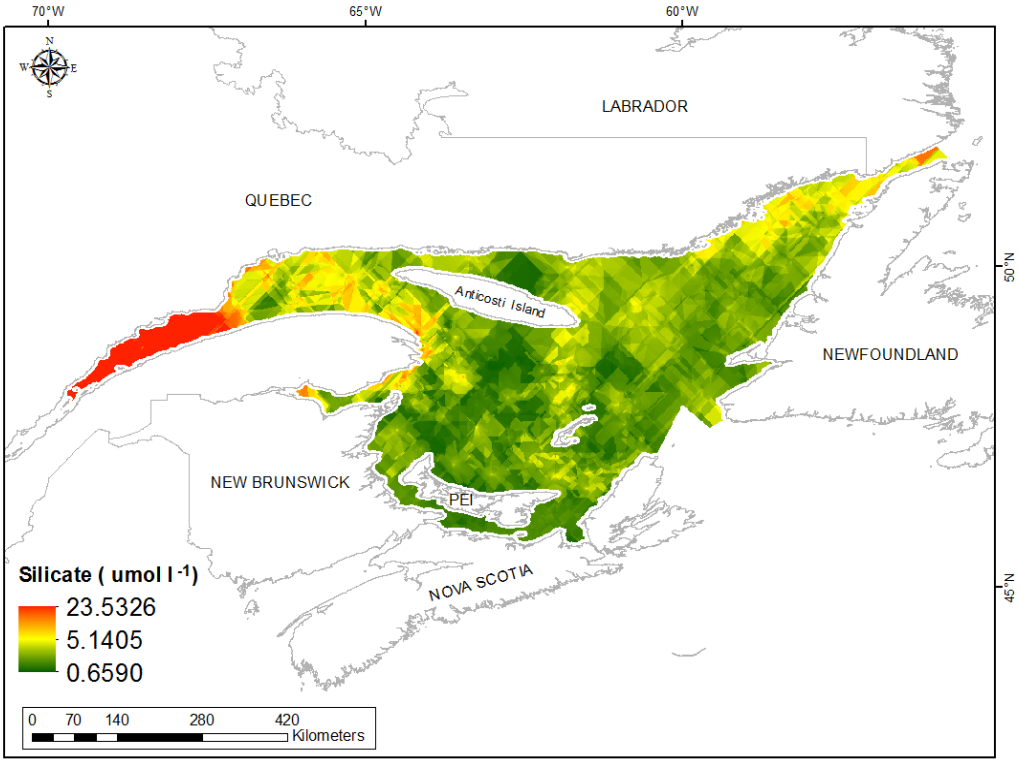

Fig. 570. Interpolated prediction surface of Silicate (µmol l^{-1}).

ACKNOWLEDGMENTS

Funding for this technical report was received from R. MacIsaac, Oceans Biologist, DFO, Gulf Region to E. Kenchington, and from a Strategic Program for Ecosystem-Based Research and Advice (SPERA) project to E. Kenchington. We thank C. Fuentes-Yaco and G. White of DFO, for providing the chlorophyll *a* and primary production layers, respectively. We thank L. Slaunwhite (DFO) for preparing the data for spatial interpolation. Finally, we thank F.J. Murillo and K. French, both of DFO, for their review and improvements to this report.

REFERENCES

Beazley, L.I., Kenchington, E.L., Murillo, F.J., Sacau, M. 2013. Deep-sea sponge grounds enhance diversity and abundance of epibenthic megafauna in the Northwest Atlantic. ICES J. Mar. Sci., 70: 1471–1490.

Bender, M., Grande, K., Johnson, K. 1987. A comparison of four methods for determining planktonic community production. Limnol. Oceanogr. 32: 1085-1098.

Boyer, T.P., Antonov, J.I., Baranova, O.K., and 12 others. 2013, World Ocean Database 2013. Sydney Levitus, Ed.; Alexey Mishonov, Technical Ed.; NOAA Atlas NESDIS 72, 209 pp.

Carney, R.S. 2005. Zonation of deep-sea biota on continental margins. Oceanogr. Mar. Biol. Annu. Rev., 43: 211–279.

Carstensen, J., Conley, D.J., Lophaven, S., Danielsson, A., Rahm, L., and Toompuu, A. 2002. Statistical Analysis and Modelling of Phytoplankton Dynamics: Exploitation of Data in the Nordic and Baltic Monitoring Programs, Nordic Council of Ministers.

Cheng, R.T., Ling, C-H, and Gartner, J.W. 1999. Estimates of bottom roughness length and bottom shear stress in South San Francisco Bay, California. J. Geophys. Res., 104: 7715-7728.

de Boyer Montégut, C., Madec, G., Fischer, A.S., Lazar, A., and Iudicone, D. 2004. Mixed layer depth over the global ocean: An examination of profile data and a profile-based climatology. J Geophys Res 109, C12003, doi:10.1029/2004JC002378.

De Vernal, A., St-Onge, G., and Gilbert, D. 2011. Oceanography and Quaternary geology of the St. Lawrence Estuary and the Saguenay Fjord. IOP Conf. Series: Earth and Environmental Science 14 (2011) 012004, doi:10.1088/1755-1315/14/1/012004, 10 pp.

Dufour, R., and Ouellet, P. 2007. Estuary and Gulf of St. Lawrence marine ecosystem overview and assessment report. Can. Tech. Rep. Fish. Aquat. Sci. 2744E: vii + 112 p.

Dutil, J.-D., Proulx, S., Chouinard, P.-M., and Borcard, D. 2011. A hierarchical classification of the seabed based on physiographic and oceanographic features in the St. Lawrence. Can. Tech. Rep. Fish. Aquat. Sci. 2916: vii + 72 p.

Feldman, G.C., and McClain, C.R. 2012. Ocean Color Web, SeaWiFS Reprocessing 2010.0, NASA Goddard Space Flight Centre. Eds. Kuring, N. and Bailey, S.W. June, 2012. http://oceancolor.gsfc.nasa.gov/

Ferry, N., Barnier, B., Garric, G., Haines, K., Masina, S., Parent, L., Storto, A., Valdivieso, M., Guinehut, S., and Mulet, S. 2012. NEMO: The modeling engine of global ocean reanalyses. Mercator Ocean Quarterly Newsletter #46. October 2012.

Fuentes-Yaco, C., Hanke, A., Caverhill, C., White, G., and Li, W. 2013. Phytoplankton blooms in the Gulf of St. Lawrence: a remote sensing approach. ACCESS 2013, Atlantic Canada Coastal and Estuarine Science Society, 9-11 May, 2013. Centre for Geographic Sciences, Nova Scotia Community College, Lawrencetown, N.S.

Goovaerts, P. 1997. Geostatistics for Natural Resources Evaluation. Oxford University Press. 483 pp.

Goovaerts, P. 2000. Geostatistical approaches for incorporating elevation into the spatial interpolation of rainfall. J. Hydrol., 228: 113–129.

Gunstra, M., and Van Auken, O.W. 2007. Using GIS to display complex soil salinity patterns in an inland salt marsh (Chapter 19). In: Developments in Environmental Sciences 5. Concepts and Applications in Environmental Geochemistry. pp 407-431.

Johnston, K., Ver Hoef, J.M., Krivoruchko, K., and Lucas, N. 2001. Using ArcGIS Geostatistical Analyst. ArcGIS User manual, ESRI. California, Redlands. 1-300 pp.

Knudby, A., Kenchington, E., Murillo, F.J. 2013. Modeling the distribution of *Geodia* sponges and sponge grounds in the northwest Atlantic Ocean. PLoS ONE 8(12): e82306. doi:10.1371/journal.pone.0082306.

Kravchenko, A., and Bullock, D.G. 1999. A comparative study of interpolation methods for mapping soil properties. Agron. J., 91: 393–400.

Krivoruchko, K. 2011. Spatial Statistical Data Analysis for GIS Users. ESRI Press, Redlands, CA. 928 pp.

Levin, L.A., Etter, R. J., Rex, M.A., Gooday, A.J., Smith, C. R., Pineda, J., Stuart, C. T., et al. 2001. Environmental influences on regional deep-sea species diversity. Annu. Rev. Ecol. Syst., 32: 51–93.

Li, J. and Heap, A.D. 2008. A Review of Spatial Interpolation Methods for Environmental Scientists. Geoscience Australia, Record 2008/23, 137 pp.

Lutz, M.J., Caldeira, K., Dunbar, R.B., Behrenfeld, M.J. 2007. Seasonal rhythms of net primary production and particulate organic carbon flux to depth describe the efficiency of biological pump in the global ocean. J Geophys Res-Oceans 112: C10011.

MacDonald, I. R., Bluhm, B. A., Iken, K., Gavaev, S., and Strong, S. 2010. Benthic macrofauna and megafauna assemblages in the Arctic Deep-Sea Canada Basin. Deep Sea Res. II, 57: 136–152.

Manasrah, R., Raheed, M., and Badran, M.I. 2006. Relationships between water temperature, nutrients and dissolved oxygen in the northern Gulf of Aqaba, Red Sea. Oceanologia, 48: 237-253.

Mercier, A., Hamel, J-F. 2011. Contrasting reproductive strategies in three deep- sea octocorals from eastern Canada: *Primnoa resedaeformis*, *Keratoisis ornata*, and *Anthomastus grandiflorus*. Coral Reefs, 30: 337–350.

Moses, W.J., Gitelson, A.A., and Povazhnyy, A. 2009. Estimation of chlorophyll-*a* concentration in case II waters using MODIS and MERIS data- successes and challenges. Environ. Res. Lett., 4, doi:10.1088/1748-9326/4/4/045005, 8 pp.

Papiol, V., Cartes, J. E., Fanelli, E., and Maynou, F. 2012. Influence of environmental variables on the spatio-temporal dynamics of the bentho-pelagic assemblages in the middle slope of the Balearic Basin (NW Mediterranean). Deep Sea Res. I, 61: 84–99.

Platt, T., Sathyendranath, S., Forget, M-H., White III, G.N., Caverhill, C., Bouman, H., Devred, E., Son, S. 2008. Operational estimation of primary production at large geographical scales. Remote Sens. Environ., 112: 3437-3448.

Polovina, J.J., Mitchum, G.T., and Evans, G.T. 1995. Decadal and basin-scale variation in mixed layer depth and the impact on biological production in the Central and North Pacific, 1960-88. Deep-Sea Res., 42: 1701-1716.

Robinson, T.P., and Metternicht, G. 2006. Testing the performance of spatial techniques for mapping soil properties. Comput. Electron. Agric., 50: 97-108.

Sibson, R. 1981. A brief description of natural neighbour interpolation. In: V. Barnett (Ed), Interpreting Multivariate Data. John Wiley and Sons, Chichester, pp. 21-36.

Shepard, D. 1968. A two-dimensional interpolation function for irregularly-spaced data. In: Proceedings of the 1968 23rd ACM national conference, Richard B Blue and Arthur M Rosenberg, eds., ACM, pp. 517–524.

Soltwedel, T., Jaeckisch, N., Ritter, N., Hasemann, C., Bergmann, M., and Klages, M. 2009. Bathymetric patterns of megafaunal assemblages from the arctic deep-sea observatory HAUSGARTEN. Deep Sea Res. I, 56: 1856–1872.

Spetland, F., Rapp, H.T., Hoffmann, F., and Tendal, O.S. 2007. Sexual reproduction of *Geodia barretti* Bowerbank 1858 (Porifera, Astrophorida) in two Scandinavian fjords. In: Custódio, M.R., Lôbo-Hajdu, G., Hajdu, E., and Muricy, G (eds). Porifera Research: Biodiversity, Innovation and Sustainability. Rio de Janeiro, Brazil: Museu. Nacional: 613-620.

Sun, Z., Hamel,J.-F., Edinger, E., Mercier, A. 2010a.Reproductive biology of the deep-sea octocoral *Drifa glomerata* in the Northwest Atlantic. Mar. Biol., 157: 863–873.

Sun, Z., Hamel, J.-F., Mercier, A. 2010b. Planulation periodicity, settlement preferences and growth of two deep-sea octocorals from the Northwest Atlantic. Mar. Ecol. Prog. Ser., 410: 71–87.

Sun, Z., Hamel, J.-F., Mercier, A. 2011.Planulation, larval biology, and early growth of the deep-sea soft corals *Gersemia fruticosa* and *Duva florida* (Octocorallia: Alcyonacea). Invert. Biol., 130: 91–99.

Sutherland, B.R., Barrett K.J. and Gingras, M.K. 2014. Clay settling in fresh and salt water. Environ. Fluid Mech., 15: 147-160.

Vance, R.R. 1973. On reproductive strategies in marine benthic invertebrates. Amer. Nat., 107: 339-352.

Yamamoto, J.K. 2007. On unbiased backtransform of lognormal kriging estimates. Comput. Geosci., 11: 219-234.